C and CP Violation in Light-Meson Decays

Dissertation
zur
Erlangung des Doktorgrades (Dr. rer. nat.)
der
Mathematisch-Naturwissenschaftlichen Fakultät
der
Rheinischen Friedrich-Wilhelms-Universität Bonn

vorgelegt von
Mehmet Hakan Akdag
aus
Neuwied

Bonn, September 2023

Angefertigt mit Genehmigung der Mathematisch-Naturwissenschaftlichen Fakultät der
Rheinischen Friedrich-Wilhelms-Universität Bonn.

Promotionskommission

Erstgutachter:	Priv.-Doz. Dr. Bastian Kubis
Zweitgutachter:	Priv.-Doz. Dr. Andreas Wirzba
Vorsitzender:	Prof. Dr. Klaus Desch
Fachfremdes Mitglied:	Prof. Dr. Jürgen Gall
Tag der Promotion:	26.09.2023
Erscheinungsjahr:	2023

If we knew what we were doing, it would not be called research, would it? – Albert Einstein

Abstract

This dissertation delves into the systematic parameterization of a *simultaneous* violation of C and CP in the light-meson sector, i.e., a source of CP violation that has been mostly disregarded over the past six decades. In order to uniquely identify these signals for new physics, which may, for instance, contribute to the matter–antimatter asymmetry, we focus on decays of the η meson. Throughout, we intuitively consider the Standard Model as an effective low-energy approximation of an unknown underlying theory at some high-energy scale Λ and rely on model-independent approaches of effective field theories and dispersion theory in analogy to their well-established applications in strong interactions, however, without making any assumption on possible new fundamental forces.

We start our analysis by revisiting fundamental neutrinoless quark-level operators in the spirit of Standard Model effective field theories up to and including mass dimension 8, which violate C and CP and conserve flavor, lepton-, and baryon-number. Providing the first complete set of these operators, we find that chirality-violating and -conserving ones are suppressed by v/Λ^4 or $1/\Lambda^4$, with Higgs vev v, respectively. Subsequently, we carefully translate these quark-level operators to chiral perturbation theory, relying on well-established spurion techniques, in order to access interactions in the light-meson sector and apply the thereby obtained new effective quantum field theory to more than 20 decays in total. As our key results, we present respective observables in explicit dependence on Λ and identify hierarchies in the chiral power counting as well as possible correlations.

We complement these findings with a dispersion-theoretical analysis of the C- and CP-violating decays that appear at lowest order in the chiral expansion and their correlations. The most promising candidates to find evidence for C and CP violation are the hadronic three-body decays $\eta^{(\prime)} \to \pi^+\pi^-\pi^0$ and $\eta' \to \eta\pi^+\pi^-$. Taking final-state interactions non-perturbatively into account, we study the asymmetries in the momentum distribution of the charged pions and determine the isoscalar and isotensor transitions in $\eta^{(\prime)} \to \pi^+\pi^-\pi^0$ and the isovector one in $\eta' \to \eta\pi^+\pi^-$, whose leading-order coupling constants are matched to the previously derived effective field theory. The remaining decays found to contribute at lowest chiral order are $\eta \to \pi^0\ell^+\ell^-$ and $\eta' \to \eta\ell^+\ell^-$. We approach these with dispersion theory, by using the hadronic three-body decays addressed above to predict hadronic contributions to the C- and CP-odd $\eta \to \pi^0\gamma^*$ and $\eta' \to \eta\gamma^*$ transition form factors. This strategy allows us to correlate C and CP violation in different decays in a non-perturbative manner. A combination of both of these measurements allows us to tighten the constraints on C and CP violation in $\eta \to \pi^+\pi^-\pi^0$.

With a variety of possible extensions, this thesis provides a dedicated theoretical framework to interpret hypothetical future findings, cf. the JEF or REDTOP collaborations, properly.

Several parts of this thesis have been published in

[1] H. Akdag, T. Isken, B. Kubis, "Patterns of C- and CP-violation in hadronic η and η' three-body decays",
JHEP 02 (2022) 137 [arXiv:2111.02417[hep-ph]],

[2] H. Akdag, B. Kubis, A. Wirzba, "C and CP violation in effective field theories",
JHEP 06 (2023) 154 [arXiv:2212.07794[hep-ph]],

[3] H. Akdag, B. Kubis, A. Wirzba, "Correlations of C and CP violation in $\eta \to \pi^0\ell^+\ell^-$ and $\eta' \to \eta\ell^+\ell^-$", arXiv:2307.02533[hep-ph], *under review*,

and in the proceeding

[4] H. Akdag, T. Isken, B. Kubis, "Dispersive representation of C- and CP-violation in η and η' decays", *PoS* (CD2021) 025, *under review*.

Additional projects with an important personal contribution that are not part of this thesis are

[5] D. Sadasivan, M. Mai, H. Akdag, M. Döring, "Dalitz plots and lineshape of $a_1(1260)$ from a relativistic three-body unitary approach",
Phys. Rev. D **101**, 094018 [arXiv:2002.12431[nucl-th]],

[6] D. Sadasivan, A. Alexandru, H. Akdag, et al., "Pole position of the $a_1(1260)$ resonance in a three-body unitary framework",
Phys. Rev. D **105**, 054020 [arXiv:2112.03355[hep-ph]].

Parts of the content of this thesis have been presented at the following conferences

- 19th International Conference on Hadron Spectroscopy and Structure (HADRON 2021), 26 July–1 August 2021. Mexico City, Mexico (C21-07-26.1),
- 10th International workshop on Chiral Dynamics (CD21), 15–19 November 2021. Beijing, China (C21-11-15.1),
- Fall 2022 Meeting of the APS Division of Nuclear Physics, 27–30 October 2022. New Orleans, Louisiana,
- 52. Arbeitstreffen Kernphysik, 23 February–2 March 2023. Schleching, Germany,
- ECT* workshop on "Precision Tests of Fundamental Physics with Light Mesons", 12–16 June 2023. Trento, Italy.

Contents

Chapter 1

Introduction

According to the current understanding of physics, nature can be described by four fundamental interactions. These are gravity, electromagnetism as well as strong and weak interactions. Except for gravity, these interactions can be summarized together with the fundamental building blocks of the universe, the elementary particles, in the so-called Standard Model of particle physics [7–12]. The latter is a quantum-field-theoretical model based on mathematical symmetries of nature. Generally, one distinguishes these symmetries between continuous and discrete ones, which differ in their number of symmetry operations, which are either infinite or finite, respectively. The most important discrete space-time symmetries are parity P (inversion of space coordinates), charge conjugation C (transformation between particles and antiparticles), and time inversion T. The fact that C, P, and T are mathematical constructs for quantum-mechanical systems raises the question whether the observable nature always preserves these symmetries. Indeed, a violation of certain combinations of discrete symmetries is considered as an essential prerequisite for our existence, i.e., the asymmetry between matter and antimatter, which cannot be explained by the latest state of the art.

In the following, we will get to know the Standard Model of particle physics (SM) on a purely qualitative level and list several open questions of modern physics driving the search for fundamental Beyond Standard Model (BSM) theories in Sect. 1.1. The incapability of the SM to explain the matter–antimatter asymmetry, which is introduced in Sect. 1.2, is shortly discussed in Sect. 1.3 by having a look at the violation of discrete space-time symmetries of the SM. Here we especially underline the relevance of the η meson, which serves as a suitable candidate to investigate one cause of this asymmetry, namely the violation of C and the successive operation of C and P, called CP. Section 1.4 emphasizes the importance of physical approaches from first principles at the example of strong interactions in the mesonic arena, i.e., for bound states of light quarks at energies below roughly 1 GeV. In this sense, Sect. 1.5 shortly introduces the—in the SM well-established—concepts of *dispersion theory* and *effective field theories* (EFTs) and differentiates their application to BSM physics from common high-energy BSM theories. A concise outline of this thesis is provided in Sect. 1.6.

1.1 | The Standard Model: an overview and open questions

The Standard Model of particle physics describes three fundamental physical interactions, i.e., electromagnetism, weak interactions, and strong interactions; while gravity currently eludes a verified quantum-field-theoretical description consistent with the former three. As

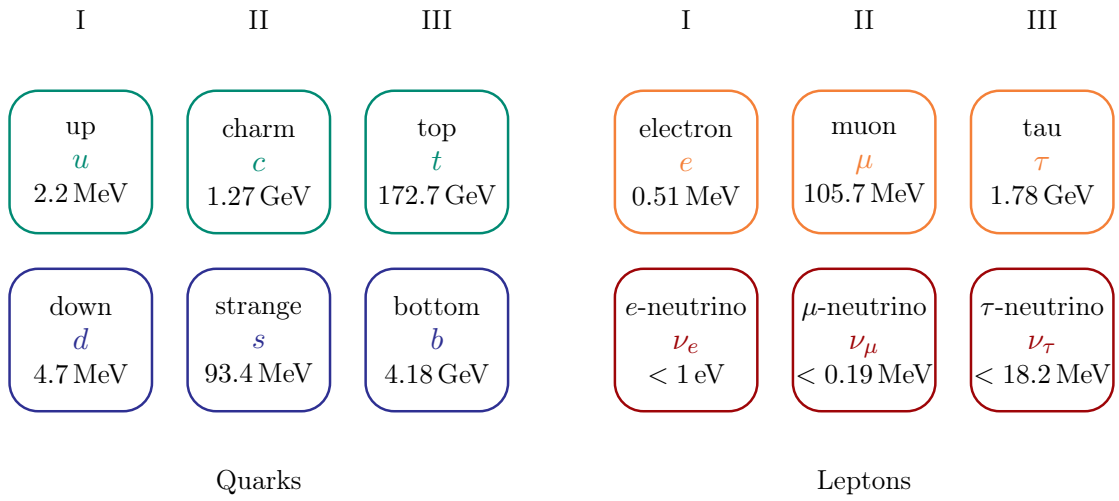

Figure 1.1: Fundamental fermions of the Standard Model of particle physics. Each fermion has spin 1/2. Quarks including their masses [13] are depicted on the left, while leptons are on the right. Each of these categories consists of three generations. The up-type quarks (green) carry the electromagnetic charge $+2/3$, the down-like quarks (blue) $-1/3$, leptons (orange) -1, and neutrinos (red) are chargeless.

a relativistic quantum field theory with the underlying gauge group

$$\mathrm{SU}(3)_C \times \mathrm{SU}(2)_L \times \mathrm{U}(1)_Y \,, \tag{1.1}$$

established in the 20$^{\text{th}}$ century and since then evolving, it describes the interaction of the known fundamental building blocks of our universe called elementary particles. These are subdivided according to their spin, i.e., a quantum mechanical quantity with the mathematical properties of an angular momentum giving rise to observable magnetic moments, into *fermions* (half-integer spin) and *bosons* (integer spin). The fermions are further classified as quarks (u, d, s, c, b, t) and leptons (e^-, τ^-, μ^-, ν_e, ν_τ, ν_μ), each of them containing six particles, which are grouped into three *generations* (sometimes also called *families*) including one pair of particles. The reasoning of this classification builds on the observation that each fermion has two siblings with the same quantum numbers, but different masses. The fermion pairs in each generation come with different electromagnetic charges. These fundamental fermions including their quantum numbers are summarized in Fig. 1.1. In addition, for each elementary fermion there exists an antifermion with exactly the same properties but an opposite charge. Note that only the ground states, i.e., the fermions in the first generations build atomic systems and are thus responsible for the stable matter content of our universe. Due to their larger masses, fermions of the second and third generation rather quickly decay into lower-lying energy states.

The fundamental interactions are mediated by the exchange of vector-bosons (spin-1) introduced to render the SM-Lagrange density, i.e., a hermitian and Poincaré-invariant function containing all information about the propagation and interaction of particles and their sym-

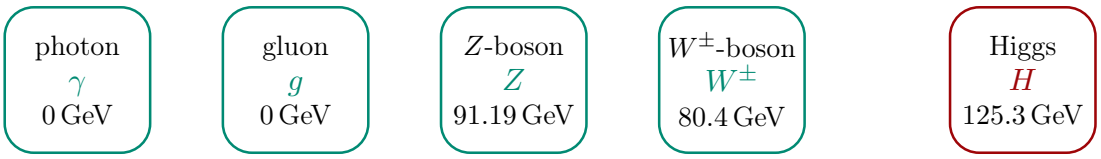

Figure 1.2: Fundamental bosons of the Standard Model of particle physics. The masses are taken from Ref. [13]. Gauge bosons (green) have spin-1, while the Higgs (red) is spinless.

metries, gauge invariant. The mediator of the electromagnetic interaction is the photon γ coupling to charged particles only. Gluons driving strong interactions couple to quarks, which are the only particles in the SM carrying color-charge. The mediators of the weak interaction are the Z- and $W^{\pm}$-bosons coupling to every known particle except gluons. Although gauge invariance demands all these particles to be massless, the Z- and $W^{\pm}$-bosons are even found to belong to the heaviest particles included in the SM. A possible explanation for this riddle was proposed by Higgs, Brout, and Englert in the 60's [9, 14]—and verified nearly six decades later with the ATLAS and CMS experiments at the Large Hadron Collider at CERN [15, 16]—who predicted a scalar field, known as the Higgs boson, responsible for the creation of particle masses. Their formalism follows the idea that the SM Lagrangian is invariant under gauge transformations, but the ground state is not. This allows the Higgs field to acquire a non-vanishing vacuum expectation value (vev) picked randomly by nature, which corresponds to a spontaneous breaking of the electroweak gauge group by means of

$$SU(2)_L \times U(1)_Y \to U(1)_Q \,. \tag{1.2}$$

Although gauge invariance does not seem to be manifest, it is still there and allows for this particular choice of vev. Therefore, one could say that gauge invariance is rather hidden than broken. The respective Higgs potential leads to the problem of kinematic mixing terms going along with non-invertable equations of motion. To circumvent this issue, a gauge fixing term (allowed by local gauge invariance) can be added, which cancels the kinematic mixing but introduces a mass term for the vector bosons. Hence, the Z- and $W^{\pm}$-bosons obtain their masses due to the interaction with the Higgs after electroweak symmetry is broken. As left- and right-handed fermions[1] transform differently in the SM, due to its gauge group $SU(2)_L \times U(1)_Y$, mass terms for fermions violate gauge invariance too. This problem can be resolved by introducing a Yukawa interaction, i.e., a coupling of two fermions with a scalar boson, between the massive SM fermions and the Higgs field, such that fermions obtain their masses when the Higgs acquires its vev. Despite the outstanding success of the SM to explain most phenomena in the electroweak and strong sector and to withstand countless high-precision experiments, this theory is still not the end of the story:

- The formulation of general relativity as a quantum theory, i.e., *quantum gravity*, is an ongoing endeavour of modern physics and may allow us to extend the SM by the inclusion of gravity.

[1] For more details refer to Sect. 2.2.1

- A still open question is whether the strong and electroweak interaction can be combined to a more fundamental *grand unified theory* (GUT). Although according theories exist, they could not be verified to date.

- Can quantum gravity, once it is formulated and approved, be further unified with GUTs leading to a *theory of everything*?

- The four interactions of nature act on different scales. Although their relative strengths are an important requirement to build the known stable matter, one may ask why the weak interaction for instance exceeds the strength of gravity by roughly a factor of 10^{24}. This observation, known as the *hierarchy problem*, can precisely be related to the question why the mass of the Higgs boson is so much smaller than the Plank mass, i.e., roughly 10^{18} GeV, as one would assume new physics at the heavy scale of the Higgs. This fact requires an extreme fine-tuning, ensuring that the quadratic divergences from radiative corrections and the Higgs bare mass cancel accordingly.

- Within the SM, neutrinos are massless. But the observed *neutrino oscillations* [17], i.e., processes allowing for a transition of neutrinos among their generations, require non-vanishing neutrino masses.

- Only about 5% of the universe is made of visible matter. The remaining energy content of the universe consists of *dark matter* (27%) and *dark energy* ($\approx$ 68%), which are responsible for the motion of visible matter in the cosmological Lambda-CDM model and the accelerated expansion of the universe, respectively.

- We observe a strong asymmetry between matter and antimatter in our universe. This requires a significant violation of symmetries that cannot be explained by the SM.

Of these physics puzzles, the latter is in the central scope of this dissertation and will be detailed in the proceeding section.

1.2 | Asymmetry between baryonic matter and antimatter

The most popular and so far best approved cosmological theory to describe the origin of matter and space-time is the Big Bang theory, cf. Ref. [18]. Elementary particles and antiparticles are supposed to have been created equally by the Big Bang. They are not only produced in pairs, but are also likely to annihilate when they meet, i.e., transitioning into pure energy and creating a thermal equilibrium. But the simple fact of our existence points towards an underlying mechanism prohibiting the steady annihilation of matter and antimatter, otherwise a formation of stable atomic systems would not be possible.[2] The assumption that the missing antimatter in our galaxy is just shifted to larger cosmological scales can be discarded, as this would induce a large amount of radiation that was never

[2]Whenever we speak about matter, we implicitly refer to baryons, a class of particles built from three valence quarks, like the proton or neutron.

observed. Therefore the most common modern, yet not verified, cosmological approach assumes the necessary asymmetry between matter and antimatter to be dynamically created during the baryogenesis. According to Sakharov [19] this origin of matter presupposes three conditions:

1. Trivially, we need a violation of the baryon number demanding an unequal amount of matter and antimatter.

2. Moreover, it has to be ensured that the symmetric amount of elementary particles and their antiparticles preferably form matter instead of antimatter, necessitating a violation of C. Furthermore, CP must be violated too, in order to maintain this asymmetry also between left(right)-handed baryons and right(left)-handed antibaryons. However, these two violations do in principle not have to originate from the same source.

3. The baryon asymmetry has to be conserved over time, which requires a violation of the thermal equilibrium. Otherwise, processes that increase and decrease the baryon number may compensate each other.

A possible new kind of interactions that simultaneously violate both C and CP, thus shedding a different light on the second Sakharov condition, is in the focus of this thesis.

1.3 | Violation of discrete space-time symmetries

The first violation of a discrete symmetry was observed by investigating the weakly induced β decay, which showed a maximal violation of parity [20]. This was followed by the discovery of the CP-violating decay $K_L \to 2\pi$ [21]. It has to be emphasized that these violations are only subject to the weak interaction. As far as the Standard Model is concerned, C, P, and T are separately conserved in the strong and electromagnetic interactions. In contrast, the weak interaction preserves only the combined application of all three operators, i.e., CPT. The latter must be preserved for any local quantum field theory respecting Lorentz invariance and hermiticity. This is known as the CPT theorem [22–24].
The idea that the conservation of discrete symmetries in the strong interactions does not have to be manifest first rose to prominence in the year 1950 with the work of Purcell and Ramsey [25], who proposed the violation of P and CP in the decay $\eta \to 2\pi$. Later, this idea was theoretically realized in a P- and CP-odd operator of dimension four in QCD, which is well-known as the θ-term. The latter induces, amongst others, an electric dipole moment (EDM) of the neutron. Rigorous experimental limits on EDMs imply corresponding theoretical limits on $\eta \to 2\pi$ [26–28], a link that can even be established without recourse to the θ-term as the fundamental mechanism [29–34]. Accordingly, no measurement so far could find evidence for this process, which is probably beyond experimental reach for the foreseeable future.
Given the dearth of experimental evidence for sources of CP violation beyond the Cabibbo–Kobayashi–Maskawa mechanism in the weak interactions of the Standard Model (SM), cf. Refs. [35, 36], it is worthwhile to investigate another category of CP-violating operators

that have gained much less attention so far: T-odd and P-even (ToPe) interactions, which in addition violate C according to the CPT theorem and hence enable the study of the second Sakharov condition from Sect. 1.2 in an appealing manner.
For the investigation of ToPe interactions, the $\eta^{(\prime)}$ meson is of particular interest. In general, decays of the $\eta^{(\prime)}$, most of which are suppressed at leading order in the SM, provide a somewhat unique playground for the search of BSM physics. The $\eta^{(\prime)}$ is an eigenstate of C and allows us to investigate ToPe forces in the absence of the weak interaction, such that the observation of a corresponding C-violating $\eta^{(\prime)}$ decay would automatically indicate physics beyond the Standard Model. Furthermore, the η provides an ideal stage to probe C and CP violation outside the nuclear arena (see the review [34] and references therein), which does not place rigorous bounds to constrain ToPe forces [37]. The new efforts of the REDTOP [38–40] and JEF [41–43] collaborations to search for rare $\eta^{(\prime)}$ decays underline the timeliness of model-independent C- and CP-violating operators in the η sector. This complements renewed recent interest in the feasibility to probe P- and CP-violating operators in η and η' decays [44–46], despite constraints from electric dipole moments.

1.4 | Intricacy of strong interactions at the mesonic level

The most successful theory so far describing strong interactions is Quantum Chromo Dynamics (QCD) relying on the $SU(3)_C$ gauge group. The elementary particles in this theory are quarks and the corresponding gauge bosons mediating the strong interaction are called gluons. The quarks can be subdivided according to their mass. The light quarks with masses far below 1 GeV are u, d, and s (up, down, strange), while the remaining heavy quarks are known as c, b, and t (charm, bottom, top), cf. Fig. 1.1.
A well-established tool in field theories to describe the interaction between its degrees of freedom is *perturbation theory*, i.e., a series expansion in terms of the respective coupling constant. Transition amplitudes can then be represented by a series of Feynman diagrams that can be truncated at higher orders if the coupling constant is small enough. The crucial fact that distinguishes QCD from perturbative theories as Quantum Electrodynamics (QED) is that gluons themselves carry the gauge theory's charge, called color, enabling them to interact with each other; other than photons in QED. This follows from the non-abelian structure of QCD. The consequence is a different running coupling constant than in abelian theories. While the coupling in QED stays in good approximation constant over a wide energy range, the strong coupling increases significantly with decreasing energies. It is exactly due to this attribute that QCD is only able to provide a perturbative description in the regime of *asymptotic freedom*, i.e., at energies large enough to ensure convergence of the series expansion,[3] but not for small energies in the confined regime. *Confinement* describes the fact that quarks and gluons form color-neutral objects, known as hadrons. The handling of confined states, for which a perturbative description is not applicable, is

[3]Here we ignore the fact that perturbation theory necessarily breaks down at a certain order. This is caused by the fact that at some point the suppression in the small expansion parameter is surpassed by the number of possible Feynman diagrams, which grows exponentially with the order of the expansion.

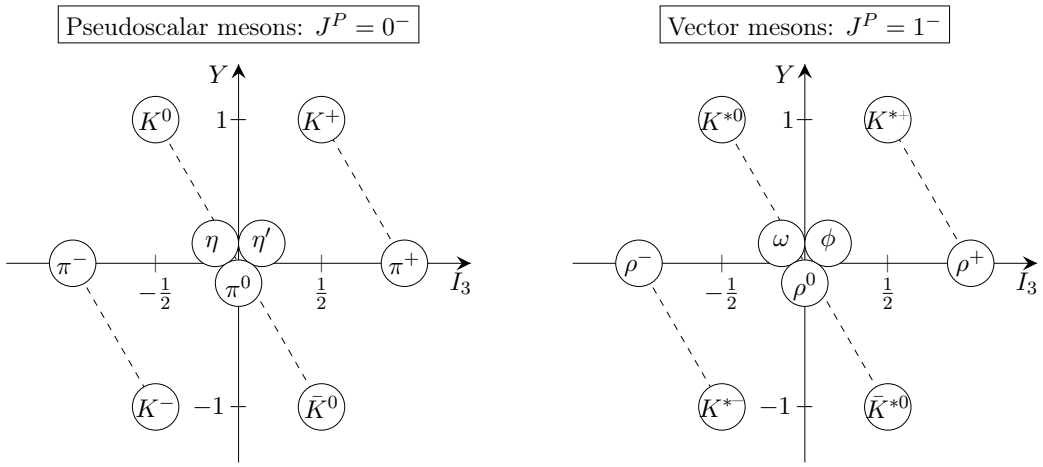

Figure 1.3: Nonets for light pseudoscalar and vector mesons, with total angular momentum $J = 0, 1$ respectively, in the plane of the isospin's third component I_3 and hypercharge $Y = 2(Q - I_3)$. Mesons along the dashed diagonal lines have the same charge Q. While uncharged pseudoscalars have the eigenvalue $C = +1$, uncharged vector mesons have $C = -1$.

one of the most challenging problems of strong interactions. The simplest examples are bound states of quarks and antiquarks, the so-called mesons. At low energies these mesons are the relevant degrees of freedom, and not quarks and gluons anymore. In this work we focus solely on light mesons, which consist of u, d, and s quarks.[4] A commonly used characteristics of mesons builds on the observation that u und d have very similar masses, leading to the concept of *isospin*, an inner approximate symmetry of strong interactions introduced in analogy to regular spin and explicitly broken by the quark-mass difference and electromagnetic interactions. The light mesons including their quantum numbers are depicted in Fig. 1.3.

1.5 | Methodology

To overcome the issues of investigating mesonic processes mentioned in the previous section, we approach them systematically by dispersion theory and EFTs. Throughout, we will use analogies of their applications to strong interactions, which have proven to be very successful, in order to access new sources of C and CP violation. However, we make no assumptions at any point in this thesis from which fundamental interactions ToPe forces may possibly originate. We solely suggest that additional C and CP violation arises from physics at some high-energy scale Λ and do not discuss the possibility of it being induced by light, extremely weakly coupled particles. Thus, we follow the quite intuitive ansatz that the SM itself, which is only below the unknown scale Λ, is just an effective approximation

[4] In many theories the attractive force between atomic nuclei is mediated by the ground states of light mesons, which thus play a crucial role in nuclear physics.

of a more fundamental theory. To access the underlying theory in a model-independent way, one can utilize an expansion in powers of $1/\Lambda$, indicating a hierarchy between the corresponding operators, which incorporate the same symmetries and degrees of freedom as the SM. After identifying these operators, the respective BSM effects can be accessed at the mesonic level with *chiral perturbation theory* (χPT), which also allows us to identify possible correlations between different C- and CP-odd decays. The corresponding operators in terms of mesonic degrees of freedom are ordered as a series, such that each successive term is suppressed by an increasing power of soft momenta and/or light-quark masses. With this power counting one can truncate the expansion analogously to perturbation theory in the usual sense. On the other hand, dispersion theory, which solely depends on the fundamental physical principals of causality and probability conservation, allows for a consistent non-perturbative summation of final-state rescattering effects. This means that dispersion theory goes beyond the leading order χPT and hence provides a high-precision analysis tool for observables from the theoretical side. We note that both of these frameworks act complementarily: products of linear combinations of the EFT's expansion coeffcients, in general known as *Wilson coefficients*, and the couplings in χPT, referred to as low-energy constants (LECs), can be matched to respective dispersive analyses.
The ansatz of investigating ToPe forces from first principles with the decay of light mesons has to be clearly distinguished from most of the common high-energy BSM theories, like *supersymmetry* [47], left-right symmetric models [48–56], and scenarios of composite Higgs fields [55–61]. Many of such BSM theories describe physics phenomena at scales of large energies, some of them far exceeding the capabilities of current experiments, or even at scales of yet unknown energies. The advantage of examining ToPe effects in mesonic interactions is that it enables the search of BSM signals at energies accessible with current experiments. In turn, these experiments require high accuracy and precision to be sensible to C- and CP-violating signals, probably even at a level that cannot be reached in the foreseeable future. The different ansätze of investigating BSM effects in the low- and high-energy regime do not necessarily contradict each other, but can rather act as supplementary theories describing the same underlying physics, just in a different range of validity. Moreover, probes on low-energy BSM physics (extracted by dispersion theory or χPT) can set more rigorous bounds on the high-energy scale Λ, or vice versa.

1.6 | Thesis outline

Part I of this thesis serves as introductory material and introduces the well-disposed reader to some basic physical and mathematical concepts that are elementary for the subsequent parts of this thesis. In Ch. 2 we provide an overview of the quantum-field-theoretical formulation of the Standard Model with the focus on the quantization of the (for this thesis) most important classes of elementary particles and their transformation under the discrete space-time symmetries C, P, and T. These considerations provide the basis for a description of ToPe effects with effective field theories and chiral perturbation theory. The foundations of dispersion theory are summarized in Ch. 3, which not only puts the

fundamental principles of probability conservation and causality in a rigorous mathematical framework but also includes the derivation of certain mesonic amplitudes including final-state interactions. Throughout this part, we highlight important equations with frames to help the reader keep an overview.

Part II includes the analysis of ToPe operators in effective field theories and starts with a short prologue in Ch. 4. We work out a complete set of fundamental C- and CP-violating quark-level operators in the spirit of Standard Model effective field theories that provides the leading underlying contributions to respective η physics in Ch. 5. These operators include information about the high-energy scale Λ. In Ch. 6 operators are matched carefully onto χPT and applied to more than 20 processes in the light-meson sector. As a central result of our analysis we quote corresponding observables in explicit dependence on Λ and identify hierarchies as well as possible correlations between them.

Part III investigates some of the most promising candidates to find signals of C and CP violation, according to the hierarchies in the chiral expansion worked out in the previous part, with dispersion theory. The latter is more precise from a theoretical point of view, because it consistently resums final-state interactions. Followed by a prologue in Ch. 7, we analyze—motivated by Ref. [62]—possible charge asymmetries in the momentum distribution of the hadronic three-body decays $\eta^{(\prime)} \to \pi^+\pi^-\pi^0$ and $\eta' \to \eta\pi^+\pi^-$ in Ch. 8. Furthermore, we extract coupling constants that can be matched with the EFT description of Ch. 6. Subsequently, Ch. 9 studies further correlations by using the aforementioned three-body decays as an input for the C- and CP-odd $\eta \to \pi^0\gamma^*$ and $\eta' \to \eta\gamma^*$ transition form factors. These results are used to place bounds on the respective semi-leptonic decays and to sharpen the constraints on ToPe effects in the three-body decays analysed in Ch. 8.

Part IV provides a summary of this thesis and discusses possible extensions for future analyses.

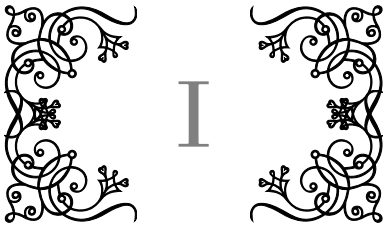

Foundations

Chapter 2

The Standard Model: fundamental fields & discrete space-time symmetries

To put the heuristic introduction to the Standard Model from Sect. 1.1 in a rigorous mathematical framework, we will shortly summarize its field theoretical description via a so-called Lagrange density, or simply *Lagrangian*. In general, a Lagrangian, whose relation to physical observables can be obtained from well-known "cooking recipes" called *Feynman rules*, is a compact description of all the information encoded in a quantum field theory. This information is concisely described by Weinberg's conjecture [63]:

> "Quantum field theory itself has no content beyond analyticity, unitarity, cluster decomposition, and symmetry. This can be put more precisely in the context of perturbation theory: if one writes down the most general possible Lagrangian, including all terms consistent with assumed symmetry principles, and then calculates matrix elements with this Lagrangian to any given order of perturbation theory, the result will simply be the most general possible S-matrix consistent with analyticity, perturbative unitarity, cluster decomposition and the assumed symmetry principles."

In this sense, the Lagrangian of the Standard Model of particle physics [7–12] in its full beauty before spontaneous symmetry breaking reads

$$\begin{aligned}\mathcal{L}^{(4)}_{\text{SM}} = &-\frac{1}{4}\big(W^i_{\mu\nu}W^{i\mu\nu} + G^a_{\mu\nu}G^{a\mu\nu} + B_{\mu\nu}B^{\mu\nu}\big) + \big(D_\mu\varphi\big)^\dagger\big(D^\mu\varphi\big) + m^2\varphi^\dagger\varphi - \lambda\big(\varphi^\dagger\varphi\big)^2 \\ &+ i\big(\bar{l}\not{D}l + \bar{e}\not{D}e + \bar{q}\not{D}q + \bar{u}\not{D}u + \bar{d}\not{D}d\big) - \big(\bar{l}\,Y_e e\varphi + \bar{q}\,Y_u u\tilde{\varphi} + \bar{q}\,Y_d d\varphi + \text{h.c.}\big)\,,\end{aligned} \tag{2.1}$$

where we indicated Yukawa couplings by $Y_{e,u,d}$ and used the abbreviations $l \equiv l^i_{Lp}$, $q \equiv q^{\alpha i}_{Lp}$, $e \equiv e_{Rp}$, $u \equiv u^\alpha_{Rp}$, $d \equiv d^\alpha_{Rp}$. The indices labeling fermions correspond to weak isospin ($i = 1, 2$), color ($\alpha = 1, 2, 3$), and generation ($p = 1, 2, 3$), respectively, whereas R and L denote the chirality. In vector notation, i picks one element of the left-handed doublets[1]

$$\big(q^\alpha_{Lp}\big)^i = \begin{pmatrix} u^\alpha_{Lp} \\ d^\alpha_{Lp} \end{pmatrix}^i \qquad \text{and} \qquad \big(l_{Lp}\big)^i = \begin{pmatrix} \nu_p \\ e_{Lp} \end{pmatrix}^i , \tag{2.2}$$

[1] Note that the SM only includes left-handed neutrinos and right-handed anti-neutrinos.

respectively. Analogously, p determines the concrete flavor in the triplets

$$\left(u^\alpha_{L,R}\right)_p = \begin{pmatrix} u^\alpha_{L,R} \\ c^\alpha_{L,R} \\ t^\alpha_{L,R} \end{pmatrix}_p , \qquad \left(d^\alpha_{L,R}\right)_p = \begin{pmatrix} d^\alpha_{L,R} \\ s^\alpha_{L,R} \\ b^\alpha_{L,R} \end{pmatrix}_p , \qquad \left(e_{L,R}\right)_p = \begin{pmatrix} e_{L,R} \\ \mu_{L,R} \\ \tau_{L,R} \end{pmatrix}_p . \tag{2.3}$$

To keep the notation simple, we may occasionally drop some of these indices throughout the course of this work. The interactions with gauge bosons are encoded in the covariant derivative, for which we choose the sign convention

$$D_\mu = \partial_\mu + ig_s T^a G^a_\mu + igS^i W^i_\mu + ig' Y B_\mu \,. \tag{2.4}$$

In this equation, $T^a \equiv \lambda^a/2$ includes the Gell-Mann matrices λ^a as $SU(3)_C$ generators, $S^i \equiv \tau^i/2$ includes the Pauli matrices τ^i as $SU(2)_L$ generators, and Y denotes the hypercharge. The gauge couplings corresponding to $SU(3)_C, SU(2)_L$, and $U(1)_Y$ are denoted by g_s, g, and g', respectively. The kinetic terms of the gauge bosons G^a_μ, W^i_μ, B_μ are encoded in the products of field strength tensors

$$\begin{aligned} G^a_{\mu\nu} &= \partial_\mu G^a_\nu - \partial_\nu G^a_\mu - g_s f^{abc} G^b_\mu A^c_\nu \,, \\ W^i_{\mu\nu} &= \partial_\mu W^i_\nu - \partial_\nu W^i_\mu - g\epsilon^{ijk} W^j_\mu W^k_\nu \,, \\ B_{\mu\nu} &= \partial_\mu B_\nu - \partial_\nu B_\mu \,, \end{aligned} \tag{2.5}$$

with f^{abc} and ϵ^{ijk} as the strucuture constants of $SU(3)$ and $SU(2)$, respectively.

The field φ, and similarly $\tilde{\varphi} \equiv i\tau^2\varphi^*$, is a scalar doublet, which can be written as

$$\varphi = \frac{1}{\sqrt{2}} U(x) \begin{pmatrix} 0 \\ v + h(x) \end{pmatrix} \quad \text{with} \quad v = \sqrt{m^2/\lambda} \,, \tag{2.6}$$

where h is the physical Higgs that represents fluctuations around the vacuum expectation value

$$\langle \varphi \rangle = \frac{1}{\sqrt{2}} \begin{pmatrix} 0 \\ v \end{pmatrix} \tag{2.7}$$

and $U(x) \in SU(2)$ contains the three Goldstone bosons W^i_μ of the gauge theory.[2] As the latter are no observable degrees of freedom, we can set $U(x) = \mathbb{1}$ in the so-called unitary gauge. This choice of gauge motivates the picture that the three degrees of freedom (one for each W^i_μ) manifest themselves as the longitudinal polarization of the three massive vector bosons after the electroweak symmetry is spontaneuosly broken. Loosely speaking, the Goldstone bosons are absorbed by the longitudinal polarization of the three massive vector bosons $W^\pm_\mu, Z_\mu$. These, together with the photon A_μ, are related to the Goldstone bosons

[2] According to Goldstone's theorem [64], there is a massless boson for each spontaneously broken global continuous symmetry.

and B_μ by

$$\begin{aligned} W_\mu^1 &= \frac{1}{\sqrt{2}}(W_\mu^+ + W_\mu^-)\,, & W_\mu^3 &= \sin\theta_w A_\mu + \cos\theta_w Z_\mu\,, \\ W_\mu^2 &= \frac{i}{\sqrt{2}}(W_\mu^+ - W_\mu^-)\,, & B_\mu &= \cos\theta_w A_\mu - \sin\theta_w Z_\mu\,, \end{aligned} \tag{2.8}$$

after the spontaneous breakdown of the electroweak symmetry. The weak mixing angle θ_w is related to g, g', and the QED coupling e by means of

$$\sin\theta_w = -\frac{e}{g}\,, \qquad \cos\theta_w = -\frac{e}{g'}\,. \tag{2.9}$$

Furthermore, the Yukawa interactions of the Higgs with the fermions give rise to fermion masses after spontaneous symmetry breaking. The quark mass matrix can be diagonalized with a unitary transformations acting on the quark triplets q. However, this comes along with a non-flavor-diagonal interaction of $W^\pm$ with quarks,[3] leading to additional flavor-dependent factors known as elements of the Cabibbo–Kobayashi–Maskawa (CKM) matrix. In total, the SM exhibits 19 free parameters which are not known a priori and have to be fixed by a comparison to experiments. This set of degrees of freedom consist of

- nine fermion masses originating from Yukawa couplings,
- the Higgs mass,
- the Higgs vev,
- three gauge couplings g_s, g , g',
- three angles of the CKM matrix,
- the CKM CP-violating phase,
- the QCD vacuum angle θ_{QCD}.[4]

In the following we discuss the quantization and the quantum-field-theoretical description of scalar fields in Sect. 2.1, fermions in Sect. 2.2, as well as abelian and non-abelian gauge bosons like photons and gluons in Sects. 2.3 and 2.4, respectively. Most of the aspects quoted in these sections can be found in standard QFT textbooks as Refs. [70–74], just to mention a few. Furthermore, we discuss the discrete space-time symmetries of each field based on the references above and Refs. [55, 75], to which we refer for further reading.

[3] A problem that does not occur for leptons.

[4] We did not include θ_{QCD} in the SM Lagrangian, as there is no strong (experimental) evidence for a value unequal to zero [65–68]. The QCD theta term [69] enters $\mathcal{L}_{\text{SM}}$ as $-\theta_{\text{QCD}} g_S^2\, G^{a\,\mu\nu}\tilde{G}^a_{\mu\nu}/32\pi^2$, with $\tilde{G}_{\mu\nu} \equiv \epsilon_{\alpha\beta\mu\nu}G^{\alpha\beta}/2$. In principle, similar θ-terms can be written down for the $SU(2)$ and $U(1)$ part of the SM, however these can be removed by chiral rotations and are thus unphysical [70].

2.1 | The scalar field

In this section we focus on the quantization of free scalar fields that applies for instance to the Higgs and (pseudo-)scalar mesons. First, we consider the corresponding equation of motion (eom), which is a relativistic formulation of the Schrödinger equation for spinless fields, i.e.,

$$\left(\partial_\mu \partial^\mu + m^2\right) \phi = 0\,. \tag{2.10}$$

This is known as the Klein–Gordon equation and can be derived from a field theoretical perspective applying the Euler–Lagrange equation

$$\frac{\partial \mathcal{L}}{\partial \varphi} - \partial_\mu \frac{\partial \mathcal{L}}{\partial(\partial_\mu \varphi)} = 0 \tag{2.11}$$

to the Lagrangian density for free charged Klein–Gordon fields

$$\mathcal{L}_{KG} = (\partial_\mu \phi)^\dagger \, \partial_\mu \phi - m^2 \phi^\dagger \phi\,. \tag{2.12}$$

Note that Eq. (2.11) holds for arbitrary Lagrangians $\mathcal{L}$ and fields φ at leading order in perturbation theory and is not restricted to scalar fields only. To obtain the eom as given in Eq. (2.10), the derivatives have to be taken with respect to $\varphi = \phi^\dagger$. Similarly, one has to use $\varphi = \phi$ to get the eom of the hermitian conjugate $\phi^\dagger$. The solution of the Klein–Gordon equation expressed in terms of Fourier modes are

$$\begin{aligned} \phi(t, \boldsymbol{x}) &= \int \frac{d^3p}{(2\pi)^3} \frac{1}{\sqrt{2E_p}} \left(a_p e^{-ipx} + b_p^\dagger e^{ipx}\right)\,, \\ \phi^\dagger(t, \boldsymbol{x}) &= \int \frac{d^3p}{(2\pi)^3} \frac{1}{\sqrt{2E_p}} \left(a_p^\dagger e^{ipx} + b_p e^{-ipx}\right)\,. \end{aligned} \tag{2.13}$$

While the ladder operator $a_p^\dagger$ (a_p) creates (annihilates) a scalar particle with momentum p, $b_p^\dagger$ (b_p) creates (annihilates) the respective antiparticle.[5] Hence, the scalar field ϕ includes information on both particle and antiparticle. Defining the canonical momentum $\pi(x) \equiv \partial_t \phi(x)$, the equal-time commutation relations read

$$\begin{aligned} \Big[\phi(t, \boldsymbol{x}), \pi(t, \boldsymbol{y})\Big] &= i\delta^{(3)}(\boldsymbol{x} - \boldsymbol{y})\,, \\ \Big[\phi(t, \boldsymbol{x}), \phi(t, \boldsymbol{y})\Big] &= \Big[\phi^\dagger(t, \boldsymbol{x}), \phi^\dagger(t, \boldsymbol{y})\Big] = 0\,, \end{aligned} \tag{2.14}$$

in accordance with Bose symmetry.

[5] When dealing with uncharged particles it suffices to consider just one field $\phi(t, \boldsymbol{x}) = \int \frac{d^3p}{(2\pi)^3} \frac{1}{\sqrt{2E_p}} \left(a_p e^{-ipx} + a_p^\dagger e^{ipx}\right)$ and set $\phi^\dagger = \phi$. In this case, the Klein–Gordon equation becomes $\mathcal{L}_{KG} = \frac{1}{2} (\partial_\mu \phi)^2 - \frac{m^2}{2} \phi^2$.

2.1.1 | Discrete symmetries

We now shortly state the transformation of the scalar field $\phi(t, \boldsymbol{x})$ and its hermitian conjugate $\phi^\dagger(t, \boldsymbol{x})$ under the discrete space time symmetries C, P, and T.
As charge conjugation interchanges particles and antiparticles, the creation and annihilation operators $a_p^{(\dagger)}$ change places with $b_p^{(\dagger)}$, giving rise to

$$\mathcal{C}\phi(t, \boldsymbol{x})\mathcal{C}^\dagger = e^{i\alpha_C}\phi^\dagger(t, \boldsymbol{x}) \quad \text{and} \quad \mathcal{C}\phi^\dagger(t, \boldsymbol{x})\mathcal{C}^\dagger = e^{-i\alpha_C}\phi(t, \boldsymbol{x})\,, \tag{2.15}$$

where α_C indicates an arbitrary phase. The transformations under parity yield

$$\mathcal{P}\phi(t, \boldsymbol{x})\mathcal{P}^\dagger = e^{i\alpha_\mathcal{P}}\phi(t, -\boldsymbol{x}) \quad \text{and} \quad \mathcal{P}\phi^\dagger(t, \boldsymbol{x})\mathcal{P}^\dagger = e^{-i\alpha_\mathcal{P}}\phi^\dagger(t, -\boldsymbol{x})\,, \tag{2.16}$$

with another phase α_P. And finally, time reversal acts as

$$\mathcal{T}\phi(t, \boldsymbol{x})\mathcal{T}^\dagger = e^{i\alpha_\mathcal{T}}\phi^\dagger(-t, \boldsymbol{x}) \quad \text{and} \quad \mathcal{T}\phi^\dagger(t, \boldsymbol{x})\mathcal{T}^\dagger = e^{-i\alpha_\mathcal{T}}\phi(-t, \boldsymbol{x})\,. \tag{2.17}$$

Given that the derivative transforms in the same manner as the space-time vector x_μ, i.e.,[6]

$$\mathcal{C}\partial_\mu\mathcal{C}^\dagger = \partial_\mu\,, \qquad \mathcal{P}\partial_\mu\mathcal{P}^\dagger = \varepsilon^\mu\partial_\mu\,, \qquad \mathcal{T}\partial_\mu\mathcal{T}^\dagger = -\varepsilon^\mu\partial_\mu\,, \tag{2.18}$$

with

$$\varepsilon^\mu = \begin{cases} +1\,, & \text{for } \mu = 0 \\ -1\,, & \text{for } \mu = 1, 2, 3 \end{cases}\,, \tag{2.19}$$

one can easily deduce that the Lagrangian in Eq. (2.12) preserves each discrete symmetry separately. Note that some literature uses $\mathcal{P}\partial_\mu\mathcal{P}^\dagger = \partial^\mu$ and $\mathcal{T}\partial_\mu\mathcal{T}^\dagger = -\partial^\mu$, which is somewhat inappropriate considering the correct Lorentz structure.

2.2 | The fermion field

We turn our attention to the quantization of fermions, which applies to all quarks, leptons, and their respective antiparticles in the Standard Model. As pioneered by Paul Dirac, the equation of motion for fermions is

$$(i\gamma^\mu\partial_\mu - m)\,\psi = 0, \tag{2.20}$$

or equivalently

$$\bar{\psi}\,(i\gamma^\mu\partial_\mu + m) = 0, \tag{2.21}$$

and known as the Dirac equation. This equation is linked to the free Dirac Lagrangian, which describes the propagation of fermions by

$$\mathcal{L}_D = \bar{\psi}\,(i\gamma^\mu\partial_\mu - m)\,\psi, \tag{2.22}$$

[6] Note that the Einstein sum convention does *not* apply to ε^μ.

with $\bar{\psi} = \psi^\dagger \gamma^0$, via Eq. (2.11). The Dirac matrices γ^μ are defined by the Clifford algebra

$$\{\gamma^\mu, \gamma^\nu\} \equiv \gamma^\mu \gamma^\nu + \gamma^\nu \gamma^\mu = 2g^{\mu\nu}, \tag{2.23}$$

with the Minkowski metric $g_{\mu\nu} = \text{diag}(1, -1, -1, -1)_{\mu\nu}$. This algebra does not define the Dirac matrices—which must have the dimension 4×4—uniquely.[7] One convenient representation for applications in the Standard Model, which we will use throughout, is the Weyl representation

$$\gamma^\mu = \begin{pmatrix} 0 & \sigma^\mu \\ \bar{\sigma}^\mu & 0 \end{pmatrix}, \quad \text{with} \quad \sigma^\mu \equiv (1, \boldsymbol{\sigma})^\mu \quad \text{and} \quad \bar{\sigma}^\mu \equiv (1, -\boldsymbol{\sigma})^\mu. \tag{2.24}$$

The vector $\boldsymbol{\sigma} = (\sigma^1\ \sigma^2\ \sigma^3\ )^T$ is determined by the Pauli matrices

$$\sigma^1 = \begin{pmatrix} 0 & 1 \\ 1 & 0 \end{pmatrix}, \quad \sigma^2 = \begin{pmatrix} 0 & -i \\ i & 0 \end{pmatrix}, \quad \sigma^3 = \begin{pmatrix} 1 & 0 \\ 0 & -1 \end{pmatrix}. \tag{2.25}$$

At this point it may be worth to interrupt the argument and take a look at a fundamental requirement $\mathcal{L}_D$ has to meet. A vital attribute of any Lagrangian, as especially fleshed out in Ch. 5, is hermiticity. The latter is required to yield real-valued, i.e., measurable, observables. However, it might not be obvious that $\mathcal{L}_D$ is hermitian if we use the well-known identity

$$\gamma_\mu^\dagger = \gamma_0 \gamma_\mu \gamma_0 \,. \tag{2.26}$$

To resolve this issue, consider that a Lagrange density is related to the action $S = \int \mathrm{d}^4x\, \mathcal{L}$. With this relation as well as the fact that basic quantum mechanics demands wave functions to vanish at infinity, we can conclude that *total derivatives* in $\mathcal{L}$ vanish after the integration—an additional principle crucial for Ch. 5 and 6—and can hence not affect the action. Thus, a partial integration allows us to write Eq. (2.22) in the manifestly hermitian form

$$\mathcal{L}_D = \bar{\psi}\Big[\frac{i}{2}\gamma^\mu(\vec{\partial}_\mu - \overleftarrow{\partial}_\mu) - m\Big]\psi\,, \tag{2.27}$$

where the arrows indicate the direction on which the derivatives act.
Returning to the quantization of fermion fields, we can express their Fourier representations by

$$\begin{aligned} \psi(t, \boldsymbol{x}) &= \sum_s \int \frac{d^3p}{(2\pi)^3} \frac{1}{\sqrt{2E_p}} \left(a_p^s u_p^s e^{-ipx} + b_p^{s\dagger} v_p^s e^{ipx} \right) , \\ \bar{\psi}(t, \boldsymbol{x}) &= \sum_s \int \frac{d^3p}{(2\pi)^3} \frac{1}{\sqrt{2E_p}} \left(a_p^{s\dagger} \bar{u}_p^s e^{ipx} + b_p^s \bar{v}_p^s e^{-ipx} \right) . \end{aligned} \tag{2.28}$$

[7] We used the most common, somewhat sloppy, notation for Dirac matrices. To be more rigorous about the correct matrix structure, consider spinor indices $\alpha, \beta, \gamma \in \{0, 1, 2, 3\}$. The product of γ-matrices hence reads $\gamma^\mu \gamma^\nu \equiv \gamma^\mu_{\alpha\gamma} \gamma^\nu_{\gamma\beta}$ and the Lagrangian is a scalar product in spinor space by means of $\mathcal{L}_D = \bar{\psi}_\alpha \left(i\gamma^\mu_{\alpha\beta} \partial_\mu - m\delta_{\alpha\beta} \right) \psi_\beta$.

According to the Pauli principle the spinor components obey the canonical anticommutation relations

$$\begin{aligned}\Big\{\psi_\alpha(t,\boldsymbol{x}),\psi^\dagger_\beta(t,\boldsymbol{y})\Big\} &= \delta_{\alpha\beta}\,\delta^{(3)}(\boldsymbol{x}-\boldsymbol{y})\,,\\ \Big\{\psi_\alpha(t,\boldsymbol{x}),\psi_\beta(t,\boldsymbol{y})\Big\} &= \Big\{\psi^\dagger_\alpha(t,\boldsymbol{x}),\psi^\dagger_\beta(t,\boldsymbol{y})\Big\} = 0\,,\end{aligned} \tag{2.29}$$

where we assumed the spinors to be evaluated at equal time. We can again physically interpret $a_p^{s\dagger}$ as the creation operator for particles, $b_p^{s\dagger}$ as the creation operator for antiparticles and a_p^s and b_p^s as the respective annihilation operators, each with momentum p and spin s. The Dirac spinors u_p^s and v_p^s themselves, whose the momentum dependence is indicated by the index p, obey the equations of motion

$$(\not{p}-m)u_p^s = 0 \quad \text{and} \quad (\not{p}+m)v_p^s = 0\,, \tag{2.30}$$

where we used the Feynman slash notation $\not{p} \equiv \gamma_\mu p^\mu$. Corresponding spinor solutions for a spin along arbitrary direction can be written in the compact form

$$u_p^s = \begin{pmatrix}\sqrt{p\cdot\sigma}\,\xi_s\\ \sqrt{p\cdot\bar\sigma}\,\xi_s\end{pmatrix}\,, \qquad v_p^s = \begin{pmatrix}\sqrt{p\cdot\sigma}\,\eta_s\\ -\sqrt{p\cdot\bar\sigma}\,\eta_s\end{pmatrix}\,, \tag{2.31}$$

where the square root over the matrix has to be understood as the positive square root over each respective eigenvalue. For the different spin combinations we have

$$\xi_{+1/2} = \begin{pmatrix}\cos\frac{\theta}{2}\\ \sin\frac{\theta}{2}e^{i\phi}\end{pmatrix}\,, \qquad \xi_{-1/2} = \begin{pmatrix}-\sin\frac{\theta}{2}e^{-i\phi}\\ \cos\frac{\theta}{2}\end{pmatrix}\,, \qquad \eta_s = \xi_{-s}\,. \tag{2.32}$$

A common phase convention is $\xi_{+1/2} = (1,\,0)^T$, $\xi_{-1/2} = (0,\,1)^T$. The spinor solutions are orthogonal by means of $\bar u^s u^{s'} = -\bar v^s v^{s'} = 2m\delta_{ss'}$ and $\bar u^s v^{s'} = 0$.

For convenience and later use, we introduce the following nomenclature for fermion bilinears

$$\begin{array}{llllll}\text{scalar}: & \bar\psi\psi\,, & \text{vector}: & \bar\psi\gamma^\mu\psi\,, & \text{tensor}: & \bar\psi\sigma^{\mu\nu}\psi\,,\\ \text{pseudoscalar}: & \bar\psi i\gamma_5\psi\,, & \text{axialvector}: & \bar\psi\gamma^\mu\gamma_5\psi\,, & \text{pseudotensor}: & \bar\psi i\sigma^{\mu\nu}\gamma_5\psi\,,\end{array} \tag{2.33}$$

where we use the short form for the commutator of Dirac matrices

$$\sigma^{\mu\nu} \equiv \frac{i}{2}[\gamma^\mu,\gamma^\nu] \tag{2.34}$$

as well as the fifth Dirac matrix

$$\gamma_5 \equiv i\gamma_0\gamma_1\gamma_2\gamma_3 = \gamma_5^\dagger, \quad \text{with} \quad (\gamma_5)^2 = \mathbb{1}_4 \quad \text{and} \quad \{\gamma_5,\gamma^\mu\} = 0\,. \tag{2.35}$$

Conventionally, imaginary units i are included in Eq. (2.33) to render each term hermitian.

2.2.1 | The chiral limit

An important case of $\mathcal{L}_D$ is the *chiral limit*, i.e., the limit in which fermion masses are set to zero. In this case it is appealing to write the spinor solution as

$$\psi = \begin{pmatrix} \zeta_L \\ \zeta_R \end{pmatrix} . \tag{2.36}$$

Note that the two component Weyl spinors ζ_R and ζ_L can easily be formulated in terms of ξ_s and η_s. Remaining in the Weyl basis, we conveniently introduce the chiral projectors

$$P_R \equiv \frac{1}{2}(1+\gamma_5) = \begin{pmatrix} 0 & 0 \\ 0 & \mathbb{1}_2 \end{pmatrix} = P_R^\dagger \quad \text{and} \quad P_L \equiv \frac{1}{2}(1-\gamma_5) = \begin{pmatrix} \mathbb{1}_2 & 0 \\ 0 & 0 \end{pmatrix} = P_L^\dagger , \tag{2.37}$$

for which the common relations of projection operators

$$P_R + P_L = 1 , \qquad P_{R,L}^2 = P_{R,L} , \quad \text{and} \quad P_R P_L = P_L P_R = 0 \tag{2.38}$$

hold. This allows us to divide the spinor ψ into its so-called *left-* and *right-handed* components by means of

$$\psi = \psi_R + \psi_L , \quad \text{with} \quad \psi_R \equiv P_R \psi = \begin{pmatrix} 0 \\ \zeta_R \end{pmatrix} \quad \text{and} \quad \psi_L \equiv P_L \psi = \begin{pmatrix} \zeta_L \\ 0 \end{pmatrix} . \tag{2.39}$$

Hence, the free Dirac Lagrangian can be written as

$$\mathcal{L}_D = \bar{\psi}_L i\gamma^\mu \partial_\mu \psi_L + \bar{\psi}_R i\gamma^\mu \partial_\mu \psi_R - m(\bar{\psi}_R \psi_L + \bar{\psi}_L \psi_R) , \tag{2.40}$$

from which we can read off that the fields of distinct chirality decouple in the chiral limit. In this case the Dirac equation translates (still using the Weyl representation) into the two independent Weyl equations

$$i\sigma^\mu \partial_\mu \zeta_R = 0 \quad \text{and} \quad i\bar{\sigma}^\mu \partial_\mu \zeta_L = 0 . \tag{2.41}$$

Although it may seem odd at first glance to speak of massless fermions, the chiral limit is manifest in the SM itself. Indeed, the SM Lagrangian describes a chiral theory of $SU(2)$ flavor doublets before the spontaneous breakdown of the electroweak symmetry, as is readily given in Eq. (2.1), and does not explicitly include fermion masses. As already explained previously, the latter are subject to a Yukawa coupling to the Higgs. Phrased differently, any operator that couples left- to right-handed fermions—and thus violates chirality—needs an insertion of the Higgs. This observation is of vital significance for Ch. 5.

Moreover, the chiral limit has important applications even after fermions acquired their masses, especially for the strong interactions. Having another glimpse at Fig. 1.1, one may notice the conspicuously small masses of the u, d, and s quarks, which are all well below

1 GeV. Treating them as approximately massless, we can summarize their free propagation, according to Eq. (2.40), by[8]

$$\mathcal{L}_D^\chi = \bar{q}_R i\gamma_\mu \partial^\mu q_R + \bar{q}_L i\gamma_\mu \partial^\mu q_L \,, \tag{2.42}$$

with left- and right-handed quark triplets q_L and q_R. This Lagrangian exhibits an accidental symmetry as it is invariant under global rotations in flavor space, which transform the triplets as [76, 77]

$$\begin{aligned} q_R = \begin{pmatrix} u_R \\ d_R \\ s_R \end{pmatrix} \quad &\mapsto \quad U_R \begin{pmatrix} u_R \\ d_R \\ s_R \end{pmatrix} \equiv \exp\left(-i\sum_{a=1}^{8} \theta_a^R \frac{\lambda_a}{2}\right) e^{-i\theta^R} \begin{pmatrix} u_R \\ d_R \\ s_R \end{pmatrix} \,, \\ q_L = \begin{pmatrix} u_L \\ d_L \\ s_L \end{pmatrix} \quad &\mapsto \quad U_L \begin{pmatrix} u_L \\ d_L \\ s_L \end{pmatrix} \equiv \exp\left(-i\sum_{a=1}^{8} \theta_a^L \frac{\lambda_a}{2}\right) e^{-i\theta^L} \begin{pmatrix} u_L \\ d_L \\ s_L \end{pmatrix} \,. \end{aligned} \tag{2.43}$$

In these transformations, the Gell-Mann matrices λ_a, which are explicitly given in Sect. 2.4, act in flavor space. The rotation matrices U_L and U_R are elements of two distinct unitary groups called $U(3)_L$ and $U(3)_R$. The corresponding overall symmetry group decomposes as

$$U(3)_L \times U(3)_R \to SU(3)_L \times SU(3)_R \times U(1)_V \times U(1)_A \,, \tag{2.44}$$

where $U(1)_V$ is related to baryon-number conservation and $U(1)_A$ corresponds to the chiral anomaly [78]. Therefore, we will henceforth consider the transformation matrices

$$R = \exp\left(-i\sum_{a=1}^{8} \theta_a^R \frac{\lambda_a}{2}\right) \in SU(3)_R \quad \text{and} \quad L = \exp\left(-i\sum_{a=1}^{8} \theta_a^L \frac{\lambda_a}{2}\right) \in SU(3)_L \,. \tag{2.45}$$

The transformation of quarks triplets under this $SU(3)_L \times SU(3)_R$ symmetry, i.e.,

$$\boxed{q_L \to L\, q_L \,, \qquad \bar{q}_L \to \bar{q}_L L^\dagger \,, \qquad q_R \to R\, q_R \,, \qquad \bar{q}_R \to \bar{q}_R R^\dagger \,,} \tag{2.46}$$

is the fundamental starting point when deriving mesonic interactions from underlying operators at the quark level, as detailed in Ch. 6.1.

[8] At this point it may be more rigorous to consider the full QCD Lagrangian. But for the sake of simplicity we will not include gluons at this stage of the discussion. However, this does not affect the validity of the chiral symmetry discussed in this section. We merely note that gluons, which are considered in Sect. 2.4, are invariant under chiral transformations.

2.2.2 | Discrete symmetries

An important ingredient for the derivation of the discrete space-time symmetries for Dirac structures is the observation that

$$\eta_s = -i\sigma_2(\xi_s)^*\,, \tag{2.47}$$

which relates the spinor solutions for fermions and antifermions by

$$u_p^s = -i\gamma_2(v_p^s)^*\,, \qquad v_p^s = -i\gamma_2(u_p^s)^*\,. \tag{2.48}$$

Consequently, the charge conjugates of the fields ψ and $\bar{\psi}$ are

$$\mathcal{C}\psi\mathcal{C}^\dagger = -ie^{i\beta_\mathcal{C}}(\bar{\psi}\gamma_0\gamma_2)^T \quad \text{and} \quad \mathcal{C}\bar{\psi}\mathcal{C}^\dagger = -ie^{-i\beta_\mathcal{C}}(\gamma_0\gamma_2\psi)^T\,, \tag{2.49}$$

where we dropped the dependencies on the space-time coordinates for simplicity and applied $i\gamma_2\psi^* = i(\psi^\dagger\gamma_2)^T = i(\bar{\psi}\gamma_0\gamma_2)^T$. In this intermediate step the identity $(\gamma_0)^2 = \mathbb{1}_4$ comes in handy.
Regarding spatial reflections, we first introduce $\bar{p} = (t, -\boldsymbol{x})$ as the parity transform of the four momentum p. Using the scalar products $\bar{p}\cdot\sigma = p\cdot\bar{\sigma}$ and $p\cdot\sigma = \bar{p}\cdot\bar{\sigma}$, we can easily derive

$$u_p^s = \gamma_0 u_{\bar{p}}^s\,, \qquad v_p^s = -\gamma_0 v_{\bar{p}}^s \tag{2.50}$$

from Eq. (2.31). Thus, the fermion fields transform according to

$$\mathcal{P}\psi\mathcal{P}^\dagger = e^{i\beta_\mathcal{P}}\gamma_0\psi \quad \text{and} \quad \mathcal{P}\bar{\psi}\mathcal{P}^\dagger = e^{-i\beta_\mathcal{P}}\bar{\psi}\gamma_0\,. \tag{2.51}$$

In general, time reversal is an anti-unitary operator, i.e., $\mathcal{T}c\mathcal{T}^\dagger = c^*$ for $c \in \mathbb{C}$. Hence, T is the only discrete symmetry directly affecting the Dirac matrices by flipping the sign of γ_2 and leaving the remaining ones unaffected. Its action on spinors can be deduced from the fact that T flips the spin and the three-momentum. Thus we need the relations

$$u_{\bar{p}}^{-s} = -\gamma_1\gamma_3(u_p^s)^*\,, \qquad v_{\bar{p}}^{-s} = -\gamma_1\gamma_3(v_p^s)^* \tag{2.52}$$

to derive

$$\mathcal{T}\psi\mathcal{T}^\dagger = e^{i\beta_\mathcal{T}}\gamma_1\gamma_3\psi \quad \text{and} \quad \mathcal{T}\bar{\psi}\mathcal{T}^\dagger = -e^{-i\beta_\mathcal{T}}\bar{\psi}\gamma_1\gamma_3\,. \tag{2.53}$$

Finally, we can most compactly summarize the transformation of fermion bilinears under the three discrete space-time symmetries as

$$\boxed{\begin{aligned} \mathcal{C}(\bar{\psi}\Gamma\chi)\mathcal{C}^\dagger &= -\bar{\chi}\gamma_0\gamma_2\Gamma^T\gamma_2\gamma_0\psi\,, \\ \mathcal{P}(\bar{\psi}\Gamma\chi)\mathcal{P}^\dagger &= \bar{\psi}\gamma_0\Gamma\gamma_0\chi\,, \\ \mathcal{T}(\bar{\psi}\Gamma\chi)\mathcal{T}^\dagger &= \bar{\psi}\gamma_1\gamma_3\Gamma^*\gamma_3\gamma_1\chi\,, \end{aligned}} \tag{2.54}$$

where Γ indicates an arbitrary combination of Dirac matrices. For convenience we kept the

result as general as possible and used two different fermion fields ψ and χ. This especially becomes relevant for the transformation under charge conjugation, which we derived by

$$\mathcal{C}(\bar{\psi}\Gamma\chi)\mathcal{C}^\dagger = -(\gamma_0\gamma_2\psi)^T\Gamma(\bar{\chi}\gamma_0\gamma_2)^T = \left[(\bar{\chi}\gamma_0\gamma_2)\Gamma^T(\gamma_0\gamma_2\psi)\right]^T = -(\bar{\chi}\gamma_0\gamma_2)\Gamma^T(\gamma_2\gamma_0\psi)\,. \tag{2.55}$$

While the sign-flip in the second step is due to the anticommutation of fermions, we get another sign-flip from anticommuting γ_0 and γ_2 in the third step. In the latter we additionally dropped the overall matrix transposition, as the whole expression is just a scalar. Another subtlety of C is that, although we anticommuted the fermion fields, the derivatives in Eq. (2.27) keep acting on the same field. Consequently, these derivatives have to act on the opposite direction, thus contributing with an additional negative sign.

With these findings and the properties of the γ-matrices fleshed out in the previous sections, one can compute the discrete symmetries of any Dirac structure and can especially show that the Dirac Lagrangian as given in Eq. (2.27) is invariant under C, P, and T separately.

2.3 | The photon field

We extend the discussion for the free Dirac Lagrangian from Sect. 2.2 and allow the fermions to couple to the electromagnetic field $A_\mu = (\Phi, \boldsymbol{A})_\mu$, with scalar potential Φ and vector potential $\boldsymbol{A}$. The corresponding abelian gauge theory, known as QED, is described by the Lagrangian

$$\mathcal{L}_{\text{QED}} = \bar{\psi}\gamma^\mu(i\partial_\mu - eA_\mu)\psi - \frac{1}{4}F_{\mu\nu}F^{\mu\nu}\,, \tag{2.56}$$

with the field strength tensor

$$F_{\mu\nu} \equiv \partial_\mu A_\nu - \partial_\nu A_\mu\,. \tag{2.57}$$

This theory is invariant under the local $U(1)$ gauge transformations

$$\psi(x) \to e^{i\alpha(x)}\psi(x)\,, \qquad A_\mu(x) \to A(x) - \frac{1}{e}\partial_\mu\alpha(x)\,. \tag{2.58}$$

The equation of motion of the photon field evaluates to

$$\partial_\mu F^{\mu\nu} = e\bar{\psi}\gamma^\nu\psi\,, \tag{2.59}$$

which corresponds to the inhomogenous Maxwell equations.

The Fourier representation of the quantized photon field with momentum p is

$$A_\mu(t,\boldsymbol{x}) = \int \frac{\mathrm{d}^3p}{(2\pi)^3}\frac{1}{\sqrt{2E_p}}\sum_{\lambda=1}^{2}\left(\epsilon_\mu^\lambda a_p^\lambda e^{-ipx} + \epsilon_\mu^{\lambda\dagger}a_p^{\lambda\dagger}e^{ipx}\right)\,, \tag{2.60}$$

where the index λ labels the polarization. Compared to the case of an uncharged scalar, the spin-1 case has additional polarization vectors ϵ_μ^λ. As the photon is massless, it does not have a longitudinal polarization. Considering an arbitrary direction of the photon's

momentum, the transverse polarization vectors read [79]

$$\epsilon^{\mu}_{\lambda=\pm1}(p) = \frac{1}{\sqrt{2}} e^{\mp i\delta} \left(0,\ \mp\cos\theta\,\cos\phi + i\sin\phi,\ \mp\cos\theta\,\sin\phi - i\cos\phi,\ \pm\sin\theta\right) , \tag{2.61}$$

with Euler angles ϕ, θ, and δ fixing the orientation of $\boldsymbol{p}$.[9] The ladder operators obey the equal-time commutation relations

$$\begin{aligned} \left[a_p^{\lambda}, (a_q^{\lambda'})^{\dagger}\right] &= -g_{\lambda\lambda'}(2\pi)^3\delta^{(3)}(\boldsymbol{p}-\boldsymbol{q})\,, \\ \left[a_p^{\lambda},\ a_q^{\lambda'}\ \right] &= \left[(a_p^{\lambda})^{\dagger}, (a_q^{\lambda'})^{\dagger}\right] = 0\,, \end{aligned} \tag{2.62}$$

which lead to

$$[A_\mu(t,\boldsymbol{x}), \pi_\nu(t,\boldsymbol{y})] = i g_{\mu\nu}\delta^{(3)}(\boldsymbol{x}-\boldsymbol{y}), \tag{2.63}$$

with $\pi_\nu \equiv \partial_t A_\nu$.

Finally we quote the two important identities

$$p_\mu p^\mu = 0\,, \qquad \epsilon_\mu p^\mu = 0\,, \tag{2.64}$$

which reflect the on-shell condition and gauge invariance, respectively.

2.3.1 | Discrete symmetries

The discrete symmetries of the photon field A_μ can be read off from Eq. (2.56) by noting that $\bar\psi\gamma^\mu e A_\mu\psi$ must transform in the same manner as $\bar\psi\gamma^\mu i\partial_\mu\psi$.[10] For the latter it is again convenient to consider the hermitian formulation as given in Eq. (2.27). In this sense, we obtain

$$\begin{aligned} \mathcal{C}A_\mu(t,\boldsymbol{x})\mathcal{C}^\dagger &= -A_\mu(t,\boldsymbol{x})\,, \\ \mathcal{P}A_\mu(t,\boldsymbol{x})\mathcal{P}^\dagger &= \varepsilon^\mu A_\mu(t,-\boldsymbol{x})\,, \\ \mathcal{T}A_\mu(t,\boldsymbol{x})\mathcal{T}^\dagger &= \varepsilon^\mu A_\mu(-t,\boldsymbol{x})\,, \end{aligned} \tag{2.65}$$

where we applied that time reversal flips the sign of the imaginary unit i and adapted the transformations given in Eq. (2.18). We additionally accounted for the minus sign from the term $(\vec\partial_\mu - \overleftarrow\partial_\mu)$ under charge conjugation, as already discussed at the end of Sect. 2.2.2. As each discrete symmetry is multiplicative, we can furthermore use Eq. (2.18) to derive

$$\boxed{\begin{aligned} \mathcal{C}F_{\mu\nu}(t,\boldsymbol{x})\mathcal{C}^\dagger &= -F_{\mu\nu}(t,\boldsymbol{x})\,, \\ \mathcal{P}F_{\mu\nu}(t,\boldsymbol{x})\mathcal{P}^\dagger &= \varepsilon^\mu\varepsilon^\nu F_{\mu\nu}(t,-\boldsymbol{x})\,, \\ \mathcal{T}F_{\mu\nu}(t,\boldsymbol{x})\mathcal{T}^\dagger &= -\varepsilon^\mu\varepsilon^\nu F_{\mu\nu}(-t,\boldsymbol{x})\,. \end{aligned}} \tag{2.66}$$

[9] Some more information about these angles can be found in Sect. B.1.

[10] In general, coupling constants like e are not assumed to transform under discrete space-time symmetries.

2.4 | The gluon field

The inclusion of gluons to the Dirac Lagrangian proceeds similarly to Sect. 2.3, except that we are now dealing with the non-abelian theory obeying the $SU(3)_C$ color gauge group. The QCD Lagrangian

$$\mathcal{L}_{\text{QCD}} = \sum_j \bar{q}_n^j \left[\delta_{nm}(i\gamma^\mu \partial_\mu - m_{q_j}) + g_s \gamma^\mu T^a_{nm} G^a_\mu\right] q_m^j - \frac{1}{4} G^a_{\mu\nu} G^{a\mu\nu} \tag{2.67}$$

applies to all quarks q_n^j with color n and flavor j. The pure quark terms of $\mathcal{L}_{\text{QCD}}$ always couples a certain color with its respective anticolor. In contrast, the matrix $T^a \equiv \lambda^a/2$ acting in color space, with the hermitian Gell-Mann matrices

$$\begin{aligned}
\lambda^1 &= \begin{pmatrix} 0 & 1 & 0 \\ 1 & 0 & 0 \\ 0 & 0 & 0 \end{pmatrix}, \quad \lambda^2 = \begin{pmatrix} 0 & -i & 0 \\ i & 0 & 0 \\ 0 & 0 & 0 \end{pmatrix}, \quad \lambda^3 = \begin{pmatrix} 1 & 0 & 0 \\ 0 & -1 & 0 \\ 0 & 0 & 0 \end{pmatrix}, \\
\lambda^4 &= \begin{pmatrix} 0 & 0 & 1 \\ 0 & 0 & 0 \\ 1 & 0 & 0 \end{pmatrix}, \quad \lambda^5 = \begin{pmatrix} 0 & 0 & -i \\ 0 & 0 & 0 \\ i & 0 & 0 \end{pmatrix}, \quad \lambda^6 = \begin{pmatrix} 0 & 0 & 0 \\ 0 & 0 & 1 \\ 0 & 1 & 0 \end{pmatrix}, \\
\lambda^7 &= \begin{pmatrix} 0 & 0 & 0 \\ 0 & 0 & -i \\ 0 & i & 0 \end{pmatrix}, \quad \lambda^8 = \frac{1}{\sqrt{3}} \begin{pmatrix} 1 & 0 & 0 \\ 0 & 1 & 0 \\ 0 & 0 & -2 \end{pmatrix},
\end{aligned} \tag{2.68}$$

as generators of $SU(3)$, allows for non-trivial color contractions of quarks and gluons G^a_μ. The dynamics of the latter is encoded in the gluonic field strength tensor

$$G^a_{\mu\nu} = \partial_\mu G^a_\nu - \partial_\nu G^a_\mu + g_s \, f_{abc} G^b_\mu G^c_\nu, \tag{2.69}$$

with the $SU(3)$ structure constants f_{abc} defined by

$$\left[T^a, T^b\right] = i f_{abc} T^c \,. \tag{2.70}$$

While the derivative character in $G^a_{\mu\nu}$ describes the propagation of massless gluons, the term $g_s \, f_{abc} G^b_\mu G^c_\nu$ is a consequence of the non-abelian gauge theory. This interaction gives rise to the self-coupling of gluons, with an accompanying running of the QCD coupling that causes confinement and asymptotic freedom, as already heuristically discussed in Sect. 1.4.[11]

[11] A rigorous mathematical prove of confinement is still an open endeavour and part of the *Millennium Problems* [80].

2.4.1 | Discrete symmetries

Comparing $\mathcal{L}_{\text{QCD}}$ with $\mathcal{L}_{\text{QED}}$, we observe that $G_\mu \equiv T^a G^a_\mu$ has to have the same discrete symmetries as the photon field A_μ in Eq. (2.65), i.e.,

$$\begin{aligned} \mathcal{C} G_\mu(t,\boldsymbol{x})\mathcal{C}^\dagger &= -\,G_\mu(t,\boldsymbol{x})\,, \\ \mathcal{P} G_\mu(t,\boldsymbol{x})\mathcal{P}^\dagger &= \varepsilon^\mu G_\mu(t,-\boldsymbol{x})\,, \\ \mathcal{T} G_\mu(t,\boldsymbol{x})\mathcal{T}^\dagger &= \varepsilon^\mu G_\mu(-t,\boldsymbol{x})\,. \end{aligned} \tag{2.71}$$

However, we need to decouple the contributions of T^a and G^a_μ in order to work out the symmetries of arbitrary color structures. As the matrix T^a can only occur inside a quark bilinear, we can apply the transformation in Eq. (2.54) analogously to $\bar\psi\Gamma T^a\chi$ upon replacing Γ by $(\Gamma\, T^a)$. We can simplify these transformations for $\bar\psi\Gamma T^a\chi$ using

$$(T^a)^T = (T^a)^* \equiv x^a T^a \quad \text{with} \quad x^a = \begin{cases} +1\,, & \text{for } a = 1,3,4,6,8 \\ -1\,, & \text{for } a = 2,5,7 \end{cases}\,, \tag{2.72}$$

which can be read off directly from Eq. (2.68). This finding combined with Eq. (2.71) gives rise to

$$\begin{aligned} \mathcal{C} G^a_\mu(t,\boldsymbol{x})\mathcal{C}^\dagger &= -\,x^a G^a_\mu(t,\boldsymbol{x})\,, \\ \mathcal{P} G^a_\mu(t,\boldsymbol{x})\mathcal{P}^\dagger &= \quad \varepsilon^\mu G^a_\mu(t,-\boldsymbol{x})\,, \\ \mathcal{T} G^a_\mu(t,\boldsymbol{x})\mathcal{T}^\dagger &= x^a\varepsilon^\mu G^a_\mu(-t,\boldsymbol{x})\,, \end{aligned} \tag{2.73}$$

and consequently

$$\boxed{\begin{aligned} \mathcal{C} G^a_{\mu\nu}(t,\boldsymbol{x})\mathcal{C}^\dagger &= -x^a G^a_{\mu\nu}(t,\boldsymbol{x})\,, \\ \mathcal{P} G^a_{\mu\nu}(t,\boldsymbol{x})\mathcal{P}^\dagger &= \varepsilon^\mu\varepsilon^\nu G^a_{\mu\nu}(t,-\boldsymbol{x})\,, \\ \mathcal{T} G^a_{\mu\nu}(t,\boldsymbol{x})\mathcal{T}^\dagger &= -x^a\varepsilon^\mu\varepsilon^\nu G^a_{\mu\nu}(-t,\boldsymbol{x})\,. \end{aligned}} \tag{2.74}$$

The only non-trivial color contractions left are the ones including the totally anti-symmetric and symmetric structure constants

$$f_{abc} = -\frac{i}{4}\text{Tr}\left(\lambda_a[\lambda_b\,,\lambda_c]\right)\,, \qquad d_{abc} = \frac{1}{4}\text{Tr}\left(\lambda_a\{\lambda_b\,,\lambda_c\}\right)\,, \tag{2.75}$$

which explicitly read

$$f_{123} = 1\,, \quad f_{147} = f_{246} = f_{257} = f_{345} = \frac{1}{2}\,, \quad f_{156} = f_{367} = -\frac{1}{2}\,, \quad f_{458} = f_{678} = \frac{\sqrt{3}}{2} \tag{2.76}$$

and

$$\begin{aligned} &d_{118} = d_{228} = d_{338} = \frac{1}{\sqrt{3}}, \qquad d_{888} = -\frac{1}{\sqrt{3}}, \qquad d_{247} = d_{366} = d_{377} = -\frac{1}{2}, \\ &d_{146} = d_{157} = d_{256} = d_{344} = d_{355} = \frac{1}{2}, \qquad\qquad d_{448} = d_{558} = d_{668} = d_{778} = -\frac{1}{2\sqrt{3}}\,, \end{aligned} \tag{2.77}$$

respectively. We observe that all non-vanishing values of f_{abc} (d_{abc}) contain an odd (even) number of indices 2, 5, 7. This indicates

$$x^a x^b x^c f_{abc} = -f_{abc}\,, \qquad x^a x^b x^c d_{abc} = d_{abc}\,, \tag{2.78}$$

and similar relations.

Chapter 3

An introduction to dispersion theory

This section provides an introduction to the model-independent description of scattering and decay amplitudes with dispersion relations. The latter allow for a non-perturbative resummation of final-state interactions, strictly relying on the fundamental physical principles of *unitarity* and *analyticity*. While unitarity is demanded by the conservation of probability, analyticity is a mathematical consequence of causality.

These principles are presented in Sect. 3.1 and 3.2, respectively. We continue with the analytic properties of four-point functions and set up corresponding dispersion relations in Sect. 3.3. Having provided these foundations, we apply dispersion theory to the prominent examples of the $\pi\pi$ scattering amplitude, the pion vector form factor, and to the inhomogeneous Omnès problem in Sect 3.4. A short overview of the kinematics of three- and four-point functions as well as the basics of partial-wave expansion, used throughout these sections, can be found in App. A and B.

We note that this chapter does not provide new insights into dispersion theory, but serves as a summary for its most important concepts used in the course of this thesis. The covered content is based on previous theses [81–89] and aims at the derivation of central results with immediate benefit for Part III.[1] For further reading about this topic we refer to Refs. [34, 90–95].

3.1 | Unitarity

We start our endeavor to find the implications of probability conservation with the quantum mechanical interaction picture, in which both states and operators are time dependent. A general Hamiltonian in this picture is decomposed as

$$H = H_0 + H_{\text{int}}, \tag{3.1}$$

where H_0 describes the free propagation of a particle and H_{int} encodes all information about the perturbation generated by interactions among particles. The corresponding Schrödinger equation

$$i\partial_t|\psi(t)\rangle = H_I(t)|\psi(t)\rangle\,, \qquad \text{with} \qquad H_I(t) = e^{iH_0t}H_{\text{int}}e^{-iH_0t}, \tag{3.2}$$

has the solution

$$|\psi(t)\rangle = U(t,t_0)|\psi(t_0)\rangle\,, \qquad \text{with} \qquad U(t,t_0) = \hat{T}e^{-i\int_{t_0}^{t}\mathrm{d}t'\,H_I(t')}\,, \tag{3.3}$$

[1] We note that especially Sects. 3.1, 3.2, and 3.3 are very close to the presentation of Ref. [87].

where $\hat{T}$ is the time-ordering operator and $U(t, t_0)$ is the time-evolution operator. Focusing on the latter, we may now regard the fact that the probabilities of every possible scattering event add up to 1. Imposing this seemingly trivial fact, we conclude that the norm of a state must be the same at any time, i.e.,

$$\langle\psi(t_0)|\psi(t_0)\rangle \stackrel{!}{=} \langle\psi(t)|\psi(t)\rangle = \langle\psi(t_0)|U^\dagger(t,t_0)U(t,t_0)|\psi(t_0)\rangle\,. \tag{3.4}$$

Thus, this constraint demands that the time-evolution operator is unitary. Hence, unitarity is a more elegant way to express that probability is conserved and serves as one of the most fundamental principles in physics. To investigate the consequence for general scattering amplitudes, introduce the S-matrix as the time-evolution operator for asymptotic states, i.e.,

$$S \equiv U(t_+, t_-)\,, \tag{3.5}$$

with $t_- = -\infty$ and $t_+ = +\infty$. Accordingly, probability conservation demands that the S-matrix is unitary, meaning

$$SS^\dagger = S^\dagger S = \mathbb{1}. \tag{3.6}$$

Using this unitarity relation, the time evolution of asymptotic momentum eigenstates with momenta k_x can be written as

$$|k_1, ..., k_n(t_+)\rangle = S^\dagger\,|k_1, ..., k_n(t_-)\rangle\,, \qquad |k_1, ..., k_n(t_-)\rangle = S\,|k_1, ..., k_n(t_+)\rangle\,, \tag{3.7}$$

or equivalently as

$$\langle k_1, ..., k_n(t_+)| = \langle k_1, ..., k_n(t_-)|\,S\,, \qquad \langle k_1, ..., k_n(t_-)| = \langle k_1, ..., k_n(t_+)|\,S^\dagger\,, \tag{3.8}$$

With these considerations we can describe the probability amplitude for the time evolution of an arbitrary number m of initial states, with momenta p_i, to a set of n final states, with momenta q_f, by the S-matrix element

$$S_{fi} \equiv \langle q_1, ..., q_n(t_+)|p_1, ..., p_m(t_-)\rangle = \langle q_1, ..., q_n(t_-)|S|p_1, ..., p_m(t_-)\rangle. \tag{3.9}$$

As the norm is conserved, we can drop the $t_\pm$ prescription within S-matrix elements for simplicity. Instead of directly computing these S-matrix elements, we first decompose S similarly to the Hamiltonian in the interaction picture. Conventionally, the S-matrix is split according to

$$S = \mathbb{1} + iT, \tag{3.10}$$

such that all information about interactions are shifted to the Lorentz-covariant *transfer matrix* T. In complete analogy to S_{fi}, the T-matrix element takes the form

$$(2\pi)^4\delta^4(Q_f - P_i)T_{fi} = \langle q_1, ..., q_n|T|p_1, ..., p_m\rangle, \tag{3.11}$$

where Q_f and P_i denote the total four-momenta of final and initial states, respectively, so that the delta distribution takes total four-momentum conservation into account. This T_{fi} is called *scattering amplitude* or simply *matrix element*.

It is important to notice that—other than S—the transfer matrix T is *not* unitary. The unitarity of the S-matrix rather dictates the condition[2]

$$T - T^\dagger = iT^\dagger T. \tag{3.12}$$

Embedding this expression between momentum eigenstates we find

$$\langle q_1, ..., q_n|T|p_1, ..., p_m\rangle - \langle q_1, ..., q_n|T^\dagger|p_1, ..., p_m\rangle = i\langle q_1, ..., q_n|TT^\dagger|p_1, ..., p_m\rangle. \tag{3.13}$$

If we subsequently insert a complete set of intermediate states, with total momenta K_n, on the right-hand side of this equation and apply the definition in Eq. (3.11) we arrive at

$$T_{fi} - T^*_{if} = i\sum_n \int \mathrm{d}\Pi_n (2\pi)^4 \delta^4\left(P_i - K_n\right) T^*_{nf} T_{ni}, \tag{3.14}$$

which is for historical reasons referred to as the *generalized optical theorem*. In this notation, n labels the different intermediates states, each consisting of an arbitrary number of single-particle states. Again, the distribution $\delta^4\left(P_i - K_n\right)$ ensures total four-momentum conservation and the integration measure

$$\mathrm{d}\Pi_n = \prod_{j\in n} \frac{\mathrm{d}^4 k_j}{(2\pi)^4}\, 2\pi\, \delta(k_j^2 - m_j^2)\, \theta(k_j^0) \tag{3.15}$$

sets the intermediate states on-shell, in a way consistent with Lorentz covariance. We furthermore only allow for positive-energy states using the Heaviside function. The index j counts single particles contributing to each intermediate multi-particle state n, while the quantities k_j and m_j denote their respective four-momenta and masses.

As a fundamental result in field theories, Olive [96] has shown that the conditions

$$T_{fi} \equiv \lim_{\epsilon\to 0} T_{fi}(s + i\epsilon)\,, \qquad T^*_{if} \equiv \lim_{\epsilon\to 0} T_{fi}(s - i\epsilon)\,, \tag{3.16}$$

where we only display the dependence on the variable s that is related to the available center-of-mass energy, hold in general and emerge from the CPT theorem. One can thus rewrite the left-hand side of the optical theorem as

$$T_{fi} - T^*_{if} = \mathrm{disc}\, T_{fi}\,, \tag{3.17}$$

[2]This relation arises from $S^\dagger S = \mathbb{1}$. Note that we could have as well used $SS^\dagger = \mathbb{1}$ to derive the expression $T - T^\dagger = iTT^\dagger$. Anyway, both formulations lead to equivalent physics.

where the *discontinuity* is defined as

$$\operatorname{disc} f(x) \equiv f(x+i\epsilon) - f(x-i\epsilon)\,, \tag{3.18}$$

with infinitesimal positive number ϵ. With this consideration we finally obtain the discontinuity relation

$$\boxed{\operatorname{disc} T_{fi} = i \sum_n \int \mathrm{d}\Pi_n (2\pi)^4 \delta^4 \left(P_i - K_n\right) T^*_{nf} T_{ni}\,,} \tag{3.19}$$

which provides a model-independent and non-perturbative starting point to evaluate matrix elements. Often the result in Eq. (3.17) is derived using time-reversal invariance for elastic scattering processes. However, the identities from Olive [96] are more general and hold for arbitrary processes with arbitrary discrete symmetries, as long as CPT is conserved. This underlines that unitarity does *not* require any other invariance principle to determine the discontinuity of a matrix element.

In many analyses one finds the unitarity relation of Eq. (3.19) expressed in terms of the imaginary part of T_{fi}. To link these formulations to the discontinuity, consider Schwarz' reflection principle, i.e.,

$$f^*(x) = f(x^*)\,, \tag{3.20}$$

which applies to continuous functions $f(x)$ that are holomorphic in the entire complex plane (up to branch cuts) and real for $x \in \mathbb{R}$ (below the branch point).[3] The discontinuity can thus be expressed in terms of the imaginary part using

$$\operatorname{disc} f(x) = 2i \operatorname{Im} f(x+i\epsilon), \tag{3.21}$$

so that the T-matrix element obeys[4]

$$2i \operatorname{Im} T_{fi} = \operatorname{disc} T_{fi}\,. \tag{3.22}$$

The discontinuity or imaginary part calculated in this manner takes all orders of perturbation theory into account and, once evaluated, can be inserted in dispersion relations, cf. Sect. 3.2, to obtain the full scattering amplitude.

Before doing so, however, it is worth discussing the meaning of the unitarity equation in Eq. (3.19), which is shown diagrammatically in Fig. 3.1, in more detail. The right-hand side describes a loop with all allowed intermediate states that can be set on-shell without violating energy-momentum conservation. An important observation, which can already be made at the level of Eq. (3.14), is that unitarity presupposes the necessity of loops, or

[3] More precisely, it suffices if $f(x)$ is real in a finite interval for $x \in \mathbb{R}$. This aspects is important when considering left-hand cuts in Sect. A.2.

[4] Note that Schwarz' reflection principle holds for instance for elastic two-body scattering, but does not apply if the corresponding amplitude is analytically continued to the respective three-body decay. We will encounter this fact at a later stage of this thesis. However, Eq. (3.19) still holds in general for the discontinuity.

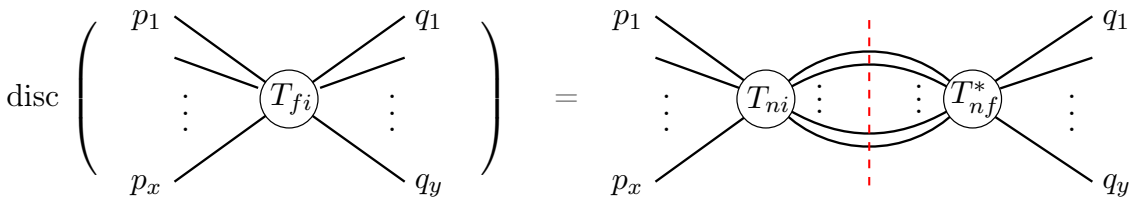

Figure 3.1: Qualitative illustration of the unitarity equation (3.19) for a T-matrix element describing the transition of an x-particle initial state to a y-particle final state. The depicted intermediate states are representative for the sum over all possible intermediate states. The unitarity cut is indicated by the red dashed line.

in other words, a field theory without loops does not conserve probability. The on-shell condition encoded in $\mathrm{d}\Pi_n$ is illustrated by the dashed *unitarity cut*. This last statement can be understood at the example of a scalar propagator, whose imaginary reads [70]

$$\mathrm{Im}\frac{1}{p^2 - m^2 + i\epsilon} = -\pi\,\delta(p^2 - m^2). \tag{3.23}$$

Thus, the propagator obtains a non-vanishing imaginary part only if the particle goes on-shell. Phrased differently, the imaginary part of a propagator is determined by its singularity. As an immediate consequence, unitarity, which demands intermediate states to be on-shell, implies poles setting in at the production threshold for the lowest-lying intermediate states. The resulting structure of singularities that generates the discontinuity of the scattering amplitude is called *branch cut*. If the total energy of the system is large enough, additional singularities occur for each new set of intermediate states.
Finally, we note that Eq. (3.19) can be proven analytically with the residue theorem. As shown by Cutkosky [97], the discontinuity of a loop can be evaluated by cutting through the diagram in each way that sets the propagators on-shell without violating four-momentum conservation. Replacing each cut propagator by

$$\frac{1}{p^2 - m^2 + i\epsilon} \to -2i\pi\,\delta(p^2 - m^2) \tag{3.24}$$

and summing over all possible cuts yields the discontinuity. This procedure is referred to as *cutting rule*. An illustration for such a cut is given in Fig. 3.1. Note that the word *cut* refers very efficiently to branch cuts, cutting rules, and Cutkosky's name at the same time.

3.2 | Analyticity

As a complement to unitarity, *analyticity* provides the second fundamental physical principle dispersive analyses are based on. We start with the physical motivation of analyticity as a mathematical consequence of causality. A constituent of the S-matrix, which we so far

paid little attention to, is the time ordering operator $\hat{T}$ introduced in Eq. (3.3). Noting that the time ordering of scattering events means that these events are causally related, we can directly build a bridge between causality and $\hat{T}$. To understand its crucial importance for the analytic properties of the scattering amplitude, consider its mathematical formulation in terms of the Heaviside step function. At hand of the example of two bosonic fields ϕ in position space, the time ordering operator reads

$$\hat{T}\{\phi_1(x)\phi_2(y)\} = \phi_1(x)\phi_2(y)\Theta(x^0 - y^0) + \phi_2(y)\phi_1(x)\Theta(y^0 - x^0)\,, \tag{3.25}$$

with the Minkowski four-vectors x and y. Applying the residue theorem, we can express the step function as

$$\Theta(x) = -\lim_{\epsilon\to 0}\frac{1}{2\pi i}\int_{-\infty}^{\infty}\frac{\mathrm{d}k}{k+i\epsilon}e^{-ikx}, \tag{3.26}$$

with $\epsilon > 0$, giving for instance rise to the Feynman propagator of freely propagating bosonic fields

$$D_f(x,y) = \left\langle 0|\hat{T}\{\phi_0(x)\phi_0(y)\}|0\right\rangle = \int\frac{\mathrm{d}^4k}{(2\pi)^4}\,\frac{i}{k^2 - m^2 + i\epsilon}\,e^{ik(x-y)}\,. \tag{3.27}$$

We note that the infinitesimal imaginary part ϵ in the Green's function is a direct consequence of causality. While in principle both signs $\pm i\epsilon$ are allowed, depending on the respective complex half-plane chosen to close the integration contour, only the positive one leads to a forward evolution in time. Thus, the argument of a scattering amplitude has to contain the $+i\epsilon$ prescription, which was already applied in the evaluation of the discontinuity of matrix elements in Sect. 3.1. In this referenced section we have seen that unitarity implies branch-cut singularities for the amplitude f. Assuming that only s-channel scattering is allowed, the amplitude $f(s + i\epsilon)$ is analytic, i.e., complex differentiable, throughout the entire complex plane; except along a branch cut for real s starting at the lowest-lying production threshold s_{th} of intermediate states. We note that only the branch point s_{th} is fixed, while aligning the branch cut with the real axis is just a choice. Often this convenient choice is made, because then the amplitude $f(s+i\epsilon)$ remains on the physical Riemann sheet as long as one does not cross the cut. Moreover, it is postulated that f contains no other singularities than the ones imposed by unitarity and crossing symmetry. This is known as the *principle of maximal analyticity*.

We now turn to the general description of analytic functions by invoking Cauchy's integral theorem. The latter states that every holomorphic function $f(s)$ evaluated in the complex argument s can be written as

$$f(s) = \frac{1}{2\pi i}\oint_{\mathcal{C}}\frac{f(x)}{x-s}\,\mathrm{d}x, \tag{3.28}$$

with $\mathcal{C}$ describing any closed integration contour in the complex plane that includes s but omits singularities. In order to apply Cauchy's theorem to the scattering amplitude, we choose a contour that does not cross the branch cut as depicted in Fig. 3.2. With this

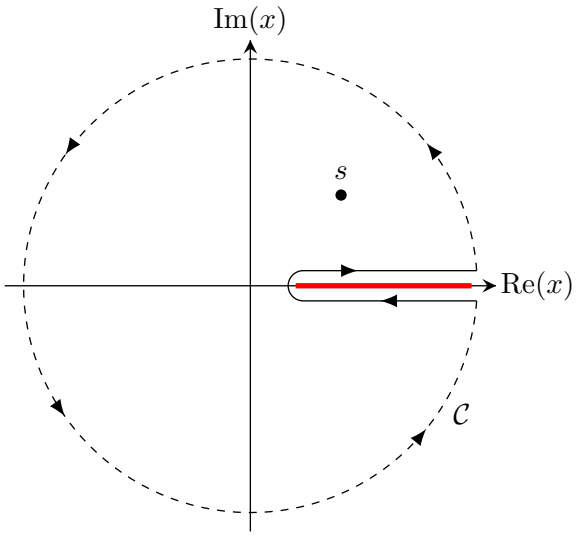

Figure 3.2: Integration contour in the complex plane chosen to evaluate Eq. (3.28) with the branch cut indicated in red. The vanishing integration over the arcs is indicated by dashed lines.

choice, we can rewrite Eq. (3.28) in terms of one integral that runs around the branch cut, i.e., around the line starting at s_{th} and extending to infinity, and one that includes a circle in the complex plane with infinitely large radius R. For $f(s)$ falling off fast enough for large arguments $|s| \to \infty$ we then obtain

$$\begin{aligned} f(s) &= \frac{1}{2\pi i} \int_{s_{\text{th}}}^{\infty} \frac{f(x+i\epsilon) - f(x-i\epsilon)}{x-s}\, \mathrm{d}x + \frac{1}{2\pi i} \int_{|x|=R} \frac{f(x)}{x-s} \mathrm{d}x \\ &= \frac{1}{2\pi i} \int_{s_{\text{th}}}^{\infty} \frac{f(x+i\epsilon) - f(x-i\epsilon)}{x-s}\, \mathrm{d}x, \end{aligned} \tag{3.29}$$

which is solely given by the integration around the branch cut. Mind the negative sign between $f(x+i\epsilon)$ and $f(x-i\epsilon)$ in the numerator that follows from the reversed orientation of integration in the lower half-plane. With these algebraic manipulations, we see that the expression in the numerator can be identified as the discontinuity of f along the branch cut. With the proper replacement $s \to s + i\epsilon$ motivated above, this finally results in the *dispersion relation*

$$\boxed{f(s+i\epsilon) = \frac{1}{2\pi i} \int_{s_{\text{th}}}^{\infty} \frac{\operatorname{disc} f(x)}{x-s-i\epsilon}\, \mathrm{d}x\,.} \tag{3.30}$$

Once more, we note that if $f(s)$ fulfills Schwarz' reflection principle, which is valid for functions that are analytic in the complex plane up to the branching cut at $s \geq s_{\text{th}}$ and real below the threshold s_{th}, the discontinuity can be replaced by $\operatorname{disc} f(s) = 2i \operatorname{Im} f(s+i\epsilon)$.

We would like to stress that we made an assumption about the asymptotic behaviour of f in Eq. (3.29) that may not necessarily hold for arbitrary functions. To resolve this issue,

we introduce so-called *subtractions* to achieve the desired asymptotics of $f(s)$ and thus a converging integral over the infinitely large circle. The idea behind subtractions is the simple fact that for a sufficiently large integer n we obtain $\lim_{x\to\infty} f(x)/x^n = 0$. Noting that for some $s_0 < s_{\text{th}} \in \mathbb{R}$ the discontinuity of $f(s_0)$ disappears, we can write

$$\frac{f(s)-f(s_0)}{s-s_0} = \frac{1}{2\pi i}\int_{s_{\text{th}}}^{\infty} \frac{\text{disc}\left(\frac{f(x)-f(s_0)}{x-s_0}\right)}{x-s}\,\mathrm{d}x = \frac{1}{2\pi i}\int_{s_{\text{th}}}^{\infty} \frac{\text{disc}f(x)}{(x-s)(x-s_0)}\mathrm{d}x \tag{3.31}$$

and thus obtain for the case $n = 1$ the once-subtracted dispersion relation

$$f(s) = f(s_0) + \frac{(s-s_0)}{2\pi i}\int_{s_{\text{th}}}^{\infty} \frac{\text{disc}f(x)}{(x-s)(x-s_0)}\mathrm{d}x\,. \tag{3.32}$$

The quantity $f(s_0)$, which is independent of s, is an undetermined constant and hence in general a free parameter of the amplitude. This degree of freedom can be matched to other theories or fixed by data regression. For simplicity, we choose the subtraction point $s_0 = 0$. Iterating Eq. (3.31) we can render any dispersion integral—with an arbitrary high-energy behaviour of f—finite by means of

$$\boxed{f(s) = P_{n-1}(s) + \frac{s^n}{2\pi i}\int_{s_{\text{th}}}^{\infty} \frac{\text{disc}f(x)}{x^n(x-s)}\mathrm{d}x,} \tag{3.33}$$

where P_{n-1} is a polynomial, known as *subtraction polynomial*, of order $n-1$ and all subtraction points are set to zero. The number of subtractions n fixes the asymptotics of $f(s)$, behaving as s^{n-1}, and sets the number of degrees of freedom to n.[5]
In summary, the virtue of dispersion relations is that the knowledge about the discontinuity suffices to reconstruct the whole scattering amplitude in a completely model-independent and non-perturbative manner, i.e., strictly relying on complex analysis. Information on the discontinuity of the scattering amplitude can be received from unitarity of the S-matrix. It should be noted, however, that the above derivation is only directly valid for amplitudes that depend on a single variable s.

3.3 | Dispersion relations for four-point functions

In this section we extend the dispersion relations introduced in the previous section to describe four-point functions, like in $2 \to 2$ scattering processes. A more rigorous mathematical derivation and in-depth discussion of this topic can for instance be found in Ref. [85]. In the following we conventionally choose the three Mandelstam variables s, t, and u as defined in App. A.2. Each of these variables describes a different scattering channel, all correlated by crossing symmetry. As described in App. A.2, only two Mandelstam variables

[5] In analogy to perturbative Lagrangian-based theories, the subtraction constants include a renormalization that cancels divergences in a similar manner as counter-terms. Compared to effective field theories, subtraction constants can be seen as analogs to low-energy constants.

are needed to describe the dynamics of a system with four external states. Therefore it suffices to write the matrix element $\mathcal{M}$ in terms of s and t only, i.e.,

$$\mathcal{M}(s,t) \equiv \mathcal{M}(s,t,u) = \mathcal{M}(s,t,3r-s-t), \tag{3.34}$$

where $3r = s+t+u$ as defined in Eq. (A.12). To simplify the study of the analytic structure of $\mathcal{M}(s,t)$, we fix t by a constant arbitrary real value t_0, so that the amplitude only depends on the variable s, i.e., $\mathcal{M}(s,t_0)$. If for $s \geq s_{\text{th}}^+$ a many-body intermediate state can be set on-shell without violating energy-momentum conservation, a branch cut arises in the region $[s_{\text{th}}, \infty)$. Such a right-hand cut has already been discussed in Sect. 3.2. The problem that complicates the treatment of four-point functions are additional singularities in the s-channel due to the contribution of crossed channels. These singularities occur when many-body intermediate states appear in the u-channel above threshold u_{th}, i.e., for

$$s \leq s_{\text{th}}^- \equiv 3r - t_0 - u_{\text{th}}\,. \tag{3.35}$$

This newly introduced branch cut is called *left-hand cut*. As we are now more familiar with the analytic structure of $\mathcal{M}(s,t_0)$, we can apply Cauchy's integral theorem to receive

$$\mathcal{M}(s,t_0) = \frac{1}{2\pi i}\oint_{\mathcal{C}} \mathrm{d}x\, \frac{\mathcal{M}(x,t_0)}{x-s}\,. \tag{3.36}$$

Avoiding branch cuts according to the complex integration contour shown in Fig. 3.3 and assuming that $\mathcal{M}(s,t_0)$ falls off fast enough for $x \to \pm\infty$, one is left with the integration along each cut. Similar to our previous considerations made in Sect. 3.2 we can hence write

$$\mathcal{M}(s,t_0) = \frac{1}{2\pi i}\int_{-\infty}^{s_{\text{th}}^-} \mathrm{d}x\, \frac{\mathrm{disc}_x \mathcal{M}(x,t_0)}{x-s} + \frac{1}{2\pi i}\int_{s_{\text{th}}^+}^{\infty} \mathrm{d}x\, \frac{\mathrm{disc}_x \mathcal{M}(x,t_0)}{x-s}\,, \tag{3.37}$$

where we for clarity use the notation disc_x to indicate the discontinuity in the variable x, i.e., $\mathrm{disc}_x \mathcal{M}(x,t) = \mathcal{M}(x+i\epsilon,t) - \mathcal{M}(x-i\epsilon,t)$. As the integration along the two arcs in the upper and lower complex half-plane does not vanish in general, we proceed with an n-times subtracted dispersion relation, which enforces the desired convergence. Thus, we consider the fixed-t dispersion relation

$$\mathcal{M}(s,t_0) = P_{n-1}^{t_0}(s) + \frac{Q_n(s)}{2\pi i}\int_{-\infty}^{s_{\text{th}}^-} \mathrm{d}x\, \frac{\mathrm{disc}_x \mathcal{M}(x,t_0)}{(x-s)Q_n(x)} + \frac{Q_n(s)}{2\pi i}\int_{s_{\text{th}}^+}^{\infty} \mathrm{d}x\, \frac{\mathrm{disc}_x \mathcal{M}(x,t_0)}{(x-s)Q_n(x)}\,, \tag{3.38}$$

where $P_{n-1}^{t_0}(s)$ is a subtraction polynomial in s of order $n-1$, with coefficients that could depend on t_0, and

$$Q_n(s) \equiv \prod_{i=1}^{n}(s-s_i)\,, \tag{3.39}$$

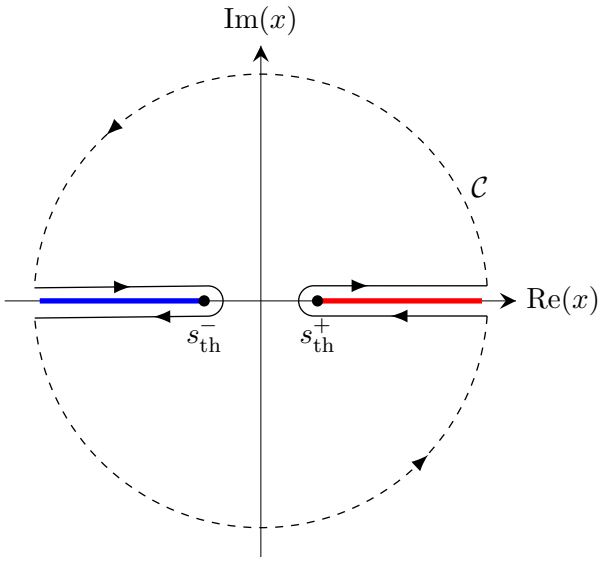

Figure 3.3: Integration contour $\mathcal{C}$ for $\mathcal{M}(s,t_0)$ in the complex plane, avoiding left-hand cuts (blue) and right-hand cuts (red). The fact that the integration along the arcs vanishes is indicated by the dashed lines. Note that in principle left- and right-hand cuts can overlap if s, t and u can become simultaneously larger than $4M_\pi^2$.

with subtraction points $s_i \in \mathbb{R}$. Although the derivation so far relies on the assumption that $t = t_0$ is fixed, we can restore the t-dependence, which may enter the subtraction polynomial P_{n-1}, the discontinuity of $\mathcal{M}$, and the threshold for the left-hand cut s_{th}^-, by

$$\mathcal{M}(s,t) = P_{n-1}^t(s) + \frac{Q_n(s)}{2\pi i}\int_{-\infty}^{s_{\text{th}}^-(t)} \mathrm{d}x\, \frac{\mathrm{disc}_x\mathcal{M}(x,t)}{(x-s)Q_n(x)} + \frac{Q_n(s)}{2\pi i}\int_{s_{\text{th}}^+}^{\infty} \mathrm{d}x\, \frac{\mathrm{disc}_x\mathcal{M}(x,t)}{(x-s)Q_n(x)}. \quad (3.40)$$

Applying crossing symmetry, we finally arrive at

$$\mathcal{M}(s,t) = P_{n-1}^t(s) + \frac{Q_n(s)}{2\pi i}\int_{s_{\text{th}}^+}^{\infty} \mathrm{d}x\, \frac{\mathrm{disc}_x\mathcal{M}(x,t)}{(x-s)Q_n(x)} + \frac{Q_n(u)}{2\pi i}\int_{u_{\text{th}}}^{\infty} \mathrm{d}x\, \frac{\mathrm{disc}_x\mathcal{M}(x,t)}{(x-u)Q_n(x)}. \quad (3.41)$$

Note that in this equation u and u_{th} are functions of s and t, as described in the beginning of this section. We additionally remark that the amplitude $\mathcal{M}(s,t)$ is by construction analytic in s. However, the fixed-t dispersion relation was derived for $t \in \mathbb{R}$ obeying Eq. (3.35). Hence, we cannot conclude that Eq. (3.41) applies for general $t \in \mathbb{C}$, leading to the caveat that this expression for $\mathcal{M}(s,t)$ is neither analytic in t nor in u. We will revise the n times subtracted fixed-t dispersion relation in the next section to solve these issues.

3.3.1 | Reconstruction theorems

A significant improvement to the attempt made in the previous section can be achieved with *reconstruction theorems* [98–101] that allow us to obtain an expression manifestly unitary

in all three Mandelstam variables. Reconstruction theorems state that the amplitude of a scalar $2 \to 2$ scattering process can—up to polynomial contributions in the Mandelstam variables—be decomposed into functions with definite angular momentum that depend on a single variable each. The derivation shown below was originally formulated by Ref. [88]. Here we merely sketch the main ideas.

In the following we make ample use of the decomposition of the matrix element into contributions with fixed partial wave. A short introduction into partial-wave analyses—especially with focus on the applications in this thesis—is presented in App. B. Let us differentiate between the partial-wave amplitudes for the three scattering channels in this section using f_ℓ^y with $y \in \{s,t,u\}$. Up to and including P-waves, the partial-wave expansion of $\mathcal{M}$ is

$$\operatorname{disc}_s \mathcal{M}(s,z_s) = \operatorname{disc} f_0^s(s) + z_s \kappa(s) \operatorname{disc} f_1^s(s)\,, \tag{3.42}$$

in accordance with Eq. (B.20).[6] Throughout, we will neglect the contributions of all higher partial waves without further notice. This allows us to write a fixed-t dispersion relation of the form

$$\begin{aligned}\mathcal{M}(s,t,u) = P_{n-1}^t(s) &+ \frac{Q_n(s)}{2\pi i}\int_{s_\text{th}}^\infty \mathrm{d}x\, \frac{\operatorname{disc} f_0^s(x) + [x\,(t-(s+u-x))+\Delta_s]\operatorname{disc} f_1^s(x)}{(x-s)Q_n(x)} \\ &+ \frac{Q_n(u)}{2\pi i}\int_{u_\text{th}}^\infty \mathrm{d}x\, \frac{\operatorname{disc} f_0^u(x) + [x\,((s+u-x)-t)+\Delta_u]\operatorname{disc} f_1^u(x)}{(x-u)Q_n(x)}\,,\end{aligned} \tag{3.43}$$

where $u = 3r - s - t$. The definitions of the kinematic functions $\Delta_{s,t,u}$ can be found in App. A.2. Absorbing polynomials in s and u of order $n-1$ in P_{n-1}^t we can rephrase our fixed-t channel dispersion relation as

$$\begin{aligned}\mathcal{M}(s,t,u) = P_{n-1}^t(s) &+ \frac{Q_n(s)}{2\pi i}\int_{s_\text{th}}^\infty \mathrm{d}x\, \frac{\operatorname{disc} f_0^s(x)}{(x-s)Q_n(x)} + \frac{Q_n(u)}{2\pi i}\int_{u_\text{th}}^\infty \mathrm{d}x\, \frac{\operatorname{disc} f_0^u(x)}{(x-u)Q_n(x)} \\ &+ [s\,(t-u)+\Delta_s]\frac{Q_{n-2}(s)}{2\pi i}\int_{s_\text{th}}^\infty \mathrm{d}x\, \frac{\operatorname{disc} f_1^s(x)}{(x-s)Q_{n-2}(x)} \\ &+ [u\,(s-t)+\Delta_u]\frac{Q_{n-2}(u)}{2\pi i}\int_{u_\text{th}}^\infty \mathrm{d}x\, \frac{\operatorname{disc} f_1^u(x)}{(x-u)Q_{n-2}(x)}\,.\end{aligned} \tag{3.44}$$

[6] Note that, in contrast to the previous section, we express the matrix element in this partial-wave expansion in terms of the cosine of the s-channel scattering angle z_s, i.e., we define $\mathcal{M}(s,z_s) \equiv \mathcal{M}(s,t,u)$.

In complete analogy we can write a fixed-u dispersion relation, with $s = 3r - t - u$, as

$$\begin{aligned}\mathcal{M}(s,t,u) = P^u_{n-1}(t) &+ \frac{Q_n(s)}{2\pi i}\int_{s_{\rm th}}^{\infty} \mathrm{d}x\, \frac{\mathrm{disc}\, f^s_0(x)}{(x-s)Q_n(x)} + \frac{Q_n(t)}{2\pi i}\int_{t_{\rm th}}^{\infty} \mathrm{d}x\, \frac{\mathrm{disc}\, f^t_0(x)}{(x-t)Q_n(x)} \\ &+ [s\,(t-u) + \Delta_s]\frac{Q_{n-2}(s)}{2\pi i}\int_{s_{\rm th}}^{\infty} \mathrm{d}x\, \frac{\mathrm{disc}\, f^s_1(x)}{(x-s)Q_{n-2}(x)} \\ &+ [t\,(u-s) + \Delta_t]\frac{Q_{n-2}(t)}{2\pi i}\int_{t_{\rm th}}^{\infty} \mathrm{d}x\, \frac{\mathrm{disc}\, f^t_1(x)}{(x-t)Q_{n-2}(x)}\,.\end{aligned} \tag{3.45}$$

Lastly, the fixed-s dispersion relation, with $t = 3r - s - u$, reads

$$\begin{aligned}\mathcal{M}(s,t,u) = P^s_{n-1}(u) &+ \frac{Q_n(t)}{2\pi i}\int_{t_{\rm th}}^{\infty} \mathrm{d}x\, \frac{\mathrm{disc}\, f^t_0(x)}{(x-t)Q_n(x)} + \frac{Q_n(u)}{2\pi i}\int_{u_{\rm th}}^{\infty} \mathrm{d}x\, \frac{\mathrm{disc}\, f^u_0(x)}{(x-u)Q_n(x)} \\ &+ [t\,(u-s) - \Delta_t]\frac{Q_{n-2}(t)}{2\pi i}\int_{t_{\rm th}}^{\infty} \mathrm{d}x\, \frac{\mathrm{disc}\, f^t_1(x)}{(x-t)Q_{n-2}(x)} \\ &+ [u\,(s-t) + \Delta_u]\frac{Q_{n-2}(u)}{2\pi i}\int_{u_{\rm th}}^{\infty} \mathrm{d}x\, \frac{\mathrm{disc}\, f^u_1(x)}{(x-u)Q_{n-2}(x)}\,.\end{aligned} \tag{3.46}$$

We can summarize Eqs. (3.46), (3.44), and (3.45) by

$$\begin{aligned}\mathcal{M}(s,t,u) = P_{n-1}(s,t,u) &+ \frac{Q_n(s)}{2\pi i}\int_{s_{\rm th}}^{\infty} \mathrm{d}x\, \frac{\mathrm{disc}\, f^s_0(x)}{(x-s)Q_n(x)} \\ &+ \frac{Q_n(t)}{2\pi i}\int_{t_{\rm th}}^{\infty} \mathrm{d}x\, \frac{\mathrm{disc}\, f^t_0(x)}{(x-t)Q_n(x)} + \frac{Q_n(u)}{2\pi i}\int_{u_{\rm th}}^{\infty} \mathrm{d}x\, \frac{\mathrm{disc}\, f^u_0(x)}{(x-u)Q_n(x)} \\ &+ [s\,(t-u) + \Delta_s]\frac{Q_{n-2}(s)}{2\pi i}\int_{s_{\rm th}}^{\infty} \mathrm{d}x\, \frac{\mathrm{disc}\, f^s_1(x)}{(x-s)Q_{n-2}(x)} \\ &+ [t\,(u-s) - \Delta_t]\frac{Q_{n-2}(t)}{2\pi i}\int_{t_{\rm th}}^{\infty} \mathrm{d}x\, \frac{\mathrm{disc}\, f^t_1(x)}{(x-t)Q_{n-2}(x)} \\ &+ [u\,(s-t) + \Delta_u]\frac{Q_{n-2}(u)}{2\pi i}\int_{u_{\rm th}}^{\infty} \mathrm{d}x\, \frac{\mathrm{disc}\, f^u_1(x)}{(x-u)Q_{n-2}(x)}\,,\end{aligned} \tag{3.47}$$

in which $P_{n-1}(s,t,u)$ indicates a simultaneous polynomial in s, t, and u. Noting that each dispersion integral depends on one Mandelstam variable only, we can write the reconstruction theorem in the convenient form

$$\boxed{\begin{aligned}\mathcal{M}(s,t,u) = \mathcal{F}^s_0(s) + \mathcal{F}^t_0(t) + \mathcal{F}^u_0(u) &+ [s\,(t-u) + \Delta_s]\mathcal{F}^s_1(s) \\ &+ [t\,(u-s) + \Delta_t]\mathcal{F}^t_1(t) + [u\,(s-t) + \Delta_u]\mathcal{F}^u_1(u)\,.\end{aligned}} \tag{3.48}$$

The thereby newly introduced *single-variable functions* are defined by

$$\mathcal{F}_\ell^y(y) = P^\ell_{n-(2\ell+1)}(y) + \frac{Q_{n-2\ell}(y)}{2\pi i}\int_{y_{\text{th}}}^\infty \mathrm{d}x\, \frac{\operatorname{disc} f_\ell^y(x)}{(x-y)Q_{n-2\ell}(x)}\,, \tag{3.49}$$

where the $P_m^\ell(y)$ are distinct polynomials of order m in y for each partial wave $\ell \in \{0,1\}$. In this derivation we absorbed several times polynomials in s, t, and u, respectively, by a redefinition of $P_m(y)$. As discussed in great detail in Ref. [88], the reconstruction theorem itself is invariant under certain polynomial shifts, while the single-variable functions are not. This is known as the *ambiguity* of this dispersive representation.

Finally, we remark that the number of subtractions necessary to render the dispersion integral finite can for example be determined with the Froissart bound [102]. The latter states that an amplitude for scalar $2 \to 2$ scattering grows asymptotically, i.e., for $s \to \infty$, not faster than $s\ln^2(s)$. The remaining missing information about the high-energy behaviour of the amplitude is encoded in the subtraction constants.

3.4 | Prominent applications

This section covers three common applications of dispersion relations to analyze mesonic interactions below the scale of about 1 GeV: the $\pi\pi$ scattering amplitude (Sect. 3.4.1), the pion vector form factor (Sect. 3.4.2), and the inhomogeneous Omnès problem (Sect. 3.4.3). Each of them is of vital importance for the dispersive analyses in Part III and requires knowledge about all previously presented concepts about dispersion theory.

3.4.1 | The $\pi\pi$ scattering amplitude

In all dispersive approaches presented in this thesis, we will make ample use of elastic $\pi\pi$ rescattering effects. Therefore, the aim of this section is to derive the well-known relation between the $\pi\pi$ phase shift and the $\pi\pi \to \pi\pi$ partial-wave amplitude for definite total isospin. In order to describe the latter we will choose the basis of cartesian pions, which are related to phyiscal pions and isospin states by

$$|\pi^\pm\rangle = \pm|1,\pm1\rangle = \frac{1}{\sqrt{2}}\big(|\pi^1\rangle \pm i|\pi^2\rangle\big)\,, \qquad |\pi^0\rangle = |1,0\rangle = |\pi^3\rangle\,. \tag{3.50}$$

This choice simplifies the decomposition into contributions of different isospin significantly. Throughout this section we will use the kinematic assignments of Sect. A.2 and assume isospin symmetry, i.e., neglect the mass difference between up and down quarks as well as electromagnetic effects. We start by defining the $\pi\pi$ scattering amplitude in cartesian basis as

$$\langle\pi^k(p_1)\pi^l(p_2)|T|\pi^i(q_1)\pi^j(q_2)\rangle = (2\pi)^4\delta^{(4)}\left(p_1+p_2-q_1-q_2\right)\mathcal{M}^{kl,ij}(s,t,u). \tag{3.51}$$

Employing isospin conservation, Bose statics, as well as crossing symmetry we can decompose the amplitude in terms of [103]

$$\mathcal{M}^{kl,ij}(s,t,u) = \delta^{ij}\delta^{kl}\mathcal{A}(s,t,u) + \delta^{ik}\delta^{jl}\mathcal{A}(t,u,s) + \delta^{il}\delta^{jk}\mathcal{A}(u,s,t)\,. \tag{3.52}$$

Moreover, the scalar function $\mathcal{A}$ is related to the three possible contributions of definite total isospin by

$$\begin{aligned}
\mathcal{T}^0(s,t,u) &= 3\mathcal{A}(s,t,u) + \mathcal{A}(t,u,s) + \mathcal{A}(u,s,t)\,,\\
\mathcal{T}^1(s,t,u) &= \mathcal{A}(t,u,s) - \mathcal{A}(u,s,t)\,,\\
\mathcal{T}^2(s,t,u) &= \mathcal{A}(t,u,s) + \mathcal{A}(u,s,t)\,.
\end{aligned} \tag{3.53}$$

A rigorous derivation for this isospin decomposition in all its particulars can be found in Ref. [81]. As stated in Ref. [76], the full $\pi\pi \to \pi\pi$ amplitude in terms of physical pions can be evaluated with the $\mathcal{T}^I$ using an appropriate Clebsch–Gordan series.

We now turn to the evaluation of the $\mathcal{T}^I$ with dispersion theory. Considering only elastic rescattering and absorbing a symmetry factor due to identical particles in a redefinition of $\mathcal{T}^I \to \frac{1}{2}\mathcal{T}^I$, the corresponding s-channel discontinuity in accordance with cutting rules reads[7]

$$\operatorname{disc}_s \mathcal{T}^I(s,z_s) = i\int \frac{\mathrm{d}^4k}{(2\pi)^4}\mathcal{T}^I(s,z_s')\mathcal{T}^{I*}(s,z_s'')(2\pi)\delta\big(k^2-M_\pi^2\big)\,(2\pi)\delta\big((l-k)^2-M_\pi^2\big)\,, \tag{3.54}$$

where $l = p_1+p_2$, $z_s = \cos\theta_s$, $z_s' = \cos\theta_s'$, and $z_s'' = \cos\theta_s''$. Here and in the following, the unprimed center-of-mass scattering angles correspond to the ones between the initial and final state momenta, the primed ones belong to the angles between the initial and intermediate state, and the double-primed quantities denote the angles between the intermediate and final state. The angular dependencies can be most conveniently worked out by choosing—without loss of generality—the initial state momenta to point in z-direction, the intermediate ones in arbitrary direction, and the final state momenta in the xz-plane. Accordingly, the spatial unit vectors read

$$\hat{p}_1 = (0,0,1)^T, \qquad \hat{q}_1 = (\sqrt{1-z_s^2},0,z_s)^T, \qquad \hat{k} = (\sqrt{1-z_s'^2}\cos\phi_s', \sqrt{1-z_s'^2}\sin\phi_s', z_s')^T\,. \tag{3.55}$$

By definition we have $z_s'' = \hat{k}\cdot\hat{q}_1$, such that

$$z_s'' = z_s z_s' + \sqrt{1-z_s^2}\sqrt{1-z_s'^2}\cos\phi_s'\,. \tag{3.56}$$

To simplify the integral in Eq. (3.54), it is advantageous to formulate the Dirac distributions in terms of k^0 and $|\boldsymbol{k}|$. This can be accomplished by the relation

$$\delta\big(f(x)\big) = \sum_{i=1}^{n}\frac{\delta(x-x_i)}{|f'(x_i)|}\,, \tag{3.57}$$

[7] One can alternatively also use the generalized optical theorem from Eq. (3.19).

with x_i as the simple roots of $f(x)$ and the prime denoting the first derivative. The occurring delta distributions can then be reduced to

$$\delta\big(|\boldsymbol{k}|^2 - M_\pi^2\big) = \frac{\delta\big(k^0 - \sqrt{|\boldsymbol{k}|^2 + M_\pi^2}\big)}{2\sqrt{|\boldsymbol{k}|^2 + M_\pi^2}} \qquad \text{and} \qquad \delta\big((l-k)^2 - M_\pi^2\big) = \frac{\delta\big(|\boldsymbol{k}| - \frac{\sqrt{s}}{2}\sigma_\pi(s)\big)}{2\sqrt{s}\,\sigma_\pi(s)}, \tag{3.58}$$

where the shortened notation $\sigma_\pi(s) = \sqrt{1 - 4M_\pi^2/s}$ was introduced. In the derivation of the second of the above listed delta distributions it comes in handy to use the fact that $|\boldsymbol{k}| = \sqrt{2}\sigma_\pi(s)/2$ in the center-of-mass frame. Using Eq. (3.58) we can now carry out the energy and momentum integration in $\mathrm{d}^4k = \mathrm{d}k^0\mathrm{d}|\boldsymbol{k}||\boldsymbol{k}|^2\mathrm{d}\Omega_k$ trivially. The unitarity relation becomes

$$\mathrm{disc}_s\,\mathcal{T}^I(s,z_s) = \frac{i}{32\pi^2}\sigma_\pi(s)\int \mathrm{d}\Omega_k \mathcal{T}^I(s,z_s')\mathcal{T}^{I*}(s,z_s''), \tag{3.59}$$

with $\mathrm{d}\Omega_k = \mathrm{d}z_s'\mathrm{d}\phi_s'$. The $\mathrm{d}z$ integration simplifies if we separate the angular part of $\mathcal{T}^I(s,z_s)$ using a partial-wave expansion, which reads

$$\mathcal{T}^I(s,z_s) = 16\pi\sum_{\ell=0}^{\infty}(2\ell+1)t_\ell^I(s)P_\ell(z_s)\ , \tag{3.60}$$

where in comparison to Eq. (B.16) a purely conventional constant was pulled out of the definition of the $\pi\pi$ partial-wave amplitude $t_\ell^I(s)$ with fixed isospin.[8] According to Eq. (B.16), the inverse transformation is given by

$$t_\ell^I(s) = \frac{1}{32\pi}\int_{-1}^{1}\mathrm{d}z_s\,P_\ell(z_s)\mathcal{T}^I(s,z_s). \tag{3.61}$$

With Eq. (3.60) we can separate the angular dependence and the one on s in the discontinuity relation of Eq. (3.59) by

$$\begin{aligned}&\sum_{\ell=0}^{\infty}(2\ell+1)P_\ell(z_s)\mathrm{disc}_s\ t_\ell^I(s)\\ &\quad= \frac{i}{2\pi}\sigma_\pi(s)\sum_{\ell,\ell'=0}^{\infty}(2\ell+1)(2\ell'+1)\int_{-1}^{1}\mathrm{d}z_s'\int_0^{2\pi}\mathrm{d}\phi_s' P_\ell(z_s')P_{\ell'}(z_s'')t_\ell^I(s)t_{\ell'}^{I*}(s).\end{aligned} \tag{3.62}$$

Next, employ the addition theorem for spherical harmonics

$$P_\ell(z_s'') = P_\ell(z_s)P_\ell(z_s') + 2\sum_{n=1}^{\ell}\frac{(\ell-n)!}{(\ell+n)!}P_\ell^n(z_s)P_\ell^n(z_s')\cos(n\phi_s'), \tag{3.63}$$

[8] The constant is chosen such that it cancels the constants that would later appear in the denominator of Eq. (3.69).

which applies for angles obeying Eq. (3.56). In this equation the $P_\ell^n(z)$ denote associated Legendre polynomials. Inserting this theorem in Eq. (3.62), the terms proportional to $\cos\phi_s'$ drop out after the integration over $\mathrm{d}\phi_s'$ and we obtain

$$\begin{aligned}&\sum_{\ell=0}^{\infty}(2\ell+1)P_\ell(z_s)\mathrm{disc}_s\ t_\ell^I(s)\\ &\qquad = i\sigma_\pi(s)\sum_{\ell,\ell'=0}^{\infty}(2\ell+1)(2\ell'+1)\int_{-1}^{1}\mathrm{d}z_s' P_\ell(z_s')P_{\ell'}(z_s')P_{\ell'}(z_s)t_\ell^I(s)t_{\ell'}^{I*}(s)\,.\end{aligned} \tag{3.64}$$

The integral on the right-hand side can now be carried out trivially with the orthogonality of Legendre polynomials

$$\int_{-1}^{1}\mathrm{d}z_s'\,P_\ell(z_s')P_{\ell'}(z_s') = \frac{2}{2\ell+1}\delta_{\ell\ell'}\,, \tag{3.65}$$

resulting in

$$\sum_{\ell=0}^{\infty}(2\ell+1)P_\ell(z_s)\mathrm{disc}_s\ t_\ell^I(s) = 2i\sigma_\pi(s)\sum_{\ell=0}^{\infty}(2\ell+1)P_\ell(z_s)t_\ell^I(s)t_\ell^{I*}(s) \tag{3.66}$$

and thus

$$\mathrm{disc}_s\ t_\ell^I(s) = 2i\sigma_\pi(s)|t_\ell^I(s)|^2. \tag{3.67}$$

With Schwarz' reflection principle we can write $\mathrm{disc}\, t_\ell^I = 2i\,\mathrm{Im}t_\ell^I$. Using that the imaginary part of any complex number x can be written as $\mathrm{Im}\,x = |x|\sin(\arg(x))\exp(-i\,\arg(x))$, which can be derived easily considering the Euler form of complex numbers, we obtain

$$|t_\ell^I(s)| = \frac{\sin\delta_\ell^I(s)}{\sigma_\pi(s)}, \tag{3.68}$$

where we introduced the $\pi\pi$ scattering phase shift $\delta_\ell^I(s) = \arg(t_\ell^I(s))$. Finally, we arrive at the $\pi\pi$-partial-wave amplitude

$$\boxed{t_\ell^I(s) = \frac{\sin\delta_\ell^I(s)\,e^{i\delta_\ell^I(s)}}{\sigma_\pi(s)}\,,} \tag{3.69}$$

which is solely determined by the phase input δ_ℓ^I. We note that Bose symmetry demands an odd (even) isospin of the $\pi\pi$ final state for an odd (even) relative angular momentum between the two pions.

3.4.2 | The pion vector form factor

We now introduce the Omnès function in order to parameterize $\pi\pi$ rescattering in a non-perturbative and model-independent manner. For this purpose, we consider the fundamen-

tal example of the pion vector form factor $F_\pi^V(s)$. The latter can be accessed via $\gamma^* \to \pi^+\pi^-$ and is physically motivated as the Fourier transform of the pion's spatial charge distribution. We choose the normalization $F_\pi^V(0) = 1$, ensuring that at low energies—or equivalently at large distances—one scatters off the pion as a homogenous structure, i.e., without resolving its composites.[9] For useful kinematic relations concerning the following calculations we refer to Sect. A.1.

To define the pion vector form factor we first consider

$$\langle \pi^+(p_+)\pi^-(p_-)|J^\mu(0)|0\rangle = p_+^\mu F_1 + p_-^\mu F_2\,, \tag{3.70}$$

with the isovector part of the electromagnetic current[10]

$$J_\mu = \frac{1}{2}\big(\bar{u}\gamma_\mu u - \bar{d}\gamma_\mu d\big)\,. \tag{3.71}$$

The decomposition into the unknown scalar functions $F_{1,2}$ follows from Poincaré invariance. Note that there is no explicit dependence on the photon momentum $q^\mu = (p_+ + p_-)^\mu$. On the one hand, the latter can be absorbed by $F_{1,2}$ using four-momentum conservation, on the other hand it neither contributes to the matrix element for on-shell photons, due to $\varepsilon_\mu q^\mu = 0$, nor for off-shell photons. The last statement directly follows from the fact that q^μ contracted with a conserved current vanishes.[11] Invoking gauge invariance, we find

$$0 \overset{!}{=} q_\mu \langle \pi^+(p_+)\pi^-(p_-)|J^\mu(0)|0\rangle = (M_\pi^2 + p_-p_+)(F_1 + F_2)\,, \tag{3.72}$$

where we set the pions on-shell by $p_-^2 = p_+^2 = M_\pi^2$. Thus, we can express the amplitude by only one of the two scalar functions and obtain

$$\langle \pi^+(p_+)\pi^-(p_-)|J_\mu(0)|0\rangle = (p_+ - p_-)_\mu F_\pi^V(s), \tag{3.73}$$

which is the defining equation for the pion vector form factor $F_\pi^V \equiv F_1 = -F_2$, with $s = q^2$. In the following, we restrict the calculation to elastic unitarity, meaning that we only allow for $\pi\pi$ intermediate states. Hence, the diagrammatic representation of Fig. 3.4 translates according to cutting rules into[12]

$$(p_+ - p_-)_\mu \mathrm{disc}_s\, F_\pi^V(s) = i\int \frac{\mathrm{d}^4k}{(2\pi)^2}\,\mathcal{T}^{I*}(s,z_s)(2k-q)_\mu F_\pi^V(s)\delta\left(k^2 - M_\pi^2\right)\delta\left((q-k)^2 - M_\pi^2\right)\,. \tag{3.74}$$

In the same manner as in section Sect. 3.4.1, we use Eq. (3.58) to carry out the integrals

[9] The case $F_\pi^V(s) = \text{const.}$ corresponds to a point-like pion.

[10] As noted in Ref. [95], G-parity forbids the coupling of the isoscalar part of the photon to two pions and can hence be neglected for the process at hand.

[11] This fact can be seen easily using the Dirac equation by means of $iq^\mu\bar{\psi}\gamma_\mu\psi = i(p_+ + p_-)^\mu\bar{\psi}\gamma_\mu\psi = \bar{\psi}\gamma_\mu(\overleftarrow{\partial}^\mu + \overrightarrow{\partial}^\mu)\psi = 0$.

[12] We again absorb the symmetry factor $1/2$ in the definition of $\mathcal{T}^I$.

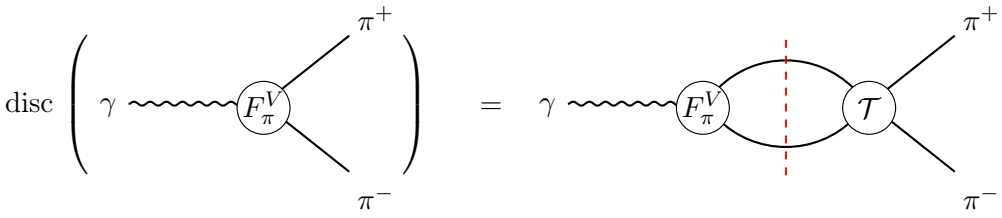

Figure 3.4: Diagrammatic representation of the discontinuity of the pion vector form factor F_π^V. The dashed line in red indicates the unitarity cut.

over $\mathrm{d}k^0$ and $\mathrm{d}|\boldsymbol{k}|$. The unitarity relation becomes

$$(p_+ - p_-)_\mu \mathrm{disc}_s\, F_\pi^V(s) = \frac{i}{32\pi^2}\sigma_\pi(s) F_\pi^V(s) \int \mathrm{d}\Omega_k\, \mathcal{T}^{I*}(s, z_s)(2k-q)_\mu\,, \tag{3.75}$$

where $|\boldsymbol{k}| = \sqrt{s}\,\sigma_\pi(s)/2$ and $k^0 = \sqrt{s}/2$ are fixed by the delta distributions. Next, we apply a common trick to get rid of the integrand's k_μ dependence and thereby simplify the angular integral. Again demanding Poincaré invariance, we can make the ansatz

$$\int \mathrm{d}\Omega_k\, \mathcal{T}^{I*}(s, z_k)(2k-q)_\mu \stackrel{!}{=} q_\mu I_1 + (p_+ - p_-)_\mu I_2, \tag{3.76}$$

with two yet unknown integrals $I_{1,2}$. Contracting each side of this equation with q^μ and $(p_+ - p_-)^\mu$ we obtain

$$0 = s\, I_1 \quad \text{and} \quad \int \mathrm{d}\Omega_k\, z_k\, \mathcal{T}^{I*}(s, z_k)(4M_\pi^2 - s) = (4M_\pi^2 - s)\, I_2. \tag{3.77}$$

Thus, Eq. (3.76) turns into

$$\int \mathrm{d}\Omega_k\, \mathcal{T}^{I*}(s, z_s)(2k-q)_\mu = (p_+ - p_-)_\mu \int \mathrm{d}\Omega_k\, z_k \mathcal{T}^{I*}(s, z_k)\,. \tag{3.78}$$

Upon insertion in Eq. (3.75), the discontinuity of F_π^V yields

$$\mathrm{disc}_s\, F_\pi^V(s) = \frac{i}{32\pi^2}\sigma_\pi(s) F_\pi^V(s) \int \mathrm{d}\Omega_k\, z_k \mathcal{T}^{I*}(s, z_s). \tag{3.79}$$

Regarding Eq. (3.61) and noting that $z_k = P_1(z_k)$, we have just projected out the P-wave of $\mathcal{T}^{I*}$, so that

$$\mathrm{disc}_s\, F_\pi^V(s) = 2i\,\sigma_\pi(s) F_\pi^V(s)\, t_1^{I*}(s). \tag{3.80}$$

As stated in Sect. 3.4.1, Bose symmetry demands that only $I = 1$ can contribute for $\ell = 1$. Inserting Eq. (3.69), we finally arrive at a unitarity relation consistent with Watson's final-state theorem [104]

$$\boxed{\mathrm{disc}_s\, F_\pi^V(s) = 2i\, F_\pi^V(s) \sin\delta_1^1(s) e^{-i\delta_1^1(s)} \theta(s - 4M_\pi^2)\,,} \tag{3.81}$$

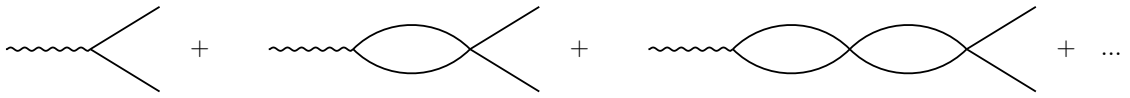

Figure 3.5: Resummation of two pion final-state interactions at the example of the pion vector form factor.

stating that the phase of F_π^V is the same as the phase shift of elastic $\pi\pi$ rescattering.

We now turn to the solution of the discontinuity relation for $F_\pi^V(s)$. Already in the late 1950s, Omnès [105] provided an analytic solution for equations of the type

$$\text{disc}_s\, \Omega_\ell^I(s) = 2i\Omega_\ell^I(s+i\epsilon)e^{-i\delta_\ell^I(s)} \sin\delta_\ell^I(s)\theta(s-s_{\text{th}})\,, \tag{3.82}$$

where $\Omega_\ell^I(s)$ is a complex-valued function that is supposed to be free of zeros. To emphasize that the following considerations hold for phase shifts with arbitrary I and ℓ, we keep the indices of δ_ℓ^I implicit. With Eq. (3.18) and the exponential form of the complex sine, the problem above can be formulated as

$$\Omega_\ell^I(s-i\epsilon) = \Omega_\ell^I(s+i\epsilon)e^{-2i\delta_\ell^I(s)}\theta(s-s_{\text{th}}), \tag{3.83}$$

resulting in

$$\text{disc}_s\left(\ln\Omega_\ell^I(s)\right) = 2i\delta_\ell^I(s)\theta(s-s_{\text{th}}). \tag{3.84}$$

As an advantage of this rephrasing, we can apply a dispersion relation to solve for $\ln\Omega_\ell^I(s)$. Expecting the scattering phase shift $\delta_\ell^I(s)$ to become constant for infinitely large s, we need a once subtracted dispersion relation, by means of

$$\ln\Omega_\ell^I(s+i\epsilon) = \ln\Omega_\ell^I(s_0) + \frac{s-s_0}{2\pi i}\int_{s_{\text{th}}}^\infty \mathrm{d}x\, \frac{\text{disc}_s\left(\ln\Omega_\ell^I(s)\right)}{(x-s_0)(x-s-i\epsilon)}\,, \tag{3.85}$$

to render the dispersion integral finite. With the subtraction point $s_0 = 0$ and the normalizing $\Omega(0) = 1$ we obtain

$$\boxed{\Omega_\ell^I(s+i\epsilon) = \exp\left(\frac{s}{\pi}\int_{s_{\text{th}}}^\infty \mathrm{d}x\, \frac{\delta_\ell^I(x)}{x(x-s-i\epsilon)}\right),} \tag{3.86}$$

which is known as the Omnès function [105]. A diagrammatic sketch of how the Omnès function resums elastic $\pi\pi$ final-state interactions, for which $s_{\text{th}} = 4M_\pi^2$, is given in Fig. 3.5. However, Eq. (3.86) does only provide one possible solution to Eq. (3.81). We can find the general solution by multiplying the Omnès function with a real-valued polynomial $P(s)$ without affecting the discontinuity. Hence, the general solution to the pion vector form

factor yields

$$\boxed{F_\pi^V(s) = P(s)\,\Omega_1^1(s)\,.} \tag{3.87}$$

3.4.3 | The inhomogeneous Omnès problem

The homogeneous Omnès problem presented in the previous section only applies to amplitudes depending on a single variable. Let us generalize the formalism by considering the scattering process $P_1P_2 \to P_3P_4$ with pseudoscalar mesons P_i of mass M_i. Unless otherwise stated, we assume that $M_i < \sum_{j=1,\,j\neq i}^{4} M_j$, i.e., energy-momentum conservation prohibits each particle to decay into the remaining ones. The complications arising when relaxing this constraint are discussed in Sect. 3.4.3.3.

In the following we derive a unitarity constraint for the s-channel partial-wave amplitude, while the derivations for the t- and u-channel amplitudes proceed in complete analogy. For simplicity and the sake of the argument, we restrict our analysis to the $P_1P_2 \to P_3P_4$ scattering amplitude with fixed isospin I. We define the corresponding amplitude by

$$\langle P_1(p_1)P_2(p_2)|T|P_3(p_3)P_4(p_4)\rangle^I = (2\pi)^4\delta^{(4)}\left(p_1+p_2-p_3-p_4\right)\mathcal{M}^I(s,t,u) \tag{3.88}$$

and choose the momentum assignment and the Mandelstam variables as given in Sect. A.2. Considering only elastic rescattering, as qualitatively depicted in Fig. 3.6, the s-channel discontinuity of $\mathcal{M}^I(s,z_s) \equiv \mathcal{M}^I(s,t,u)$ reads

$$\operatorname{disc}_s \mathcal{M}^I(s,z_s) = i\int \frac{\mathrm{d}^4k}{(2\pi)^2}\mathcal{M}^I(s,z_s')\mathcal{T}^{I*}(s,z_s'')\,\delta\big(k^2-M_\pi^2\big)\,\delta\big((l-k)^2-M_\pi^2\big)\,, \tag{3.89}$$

where $\mathcal{T}^I$ is the P_3P_4 scattering amplitude with definite total isospin I, $l = p_1+p_2$ and z_s, z_s', as well as z_s'' follow the respective definitions in Sect. 3.4.1. If we evaluate the Dirac distributions, as has been done several times in the previous sections, we find

$$\operatorname{disc}_s \mathcal{M}^I(s,z_s) = \frac{i}{32\pi^2}\frac{\lambda^{1/2}(s,M_3^2,M_4^2)}{s}\int \mathrm{d}\Omega_k\,\mathcal{M}^I(s,z_s')\,\mathcal{T}^{I*}(s,z_s''), \tag{3.90}$$

with $\mathrm{d}\Omega_k = \mathrm{d}z_s'\mathrm{d}\phi_s'$. To parameterize our amplitude in terms of the respective scattering phase shift, we repeat the derivation of Eq. (3.69), but this time allow for arbitrary masses of the particles in the final state and obtain

$$t_\ell^I(s) = \frac{s\,\sin\delta_\ell^I\,e^{i\delta_\ell^I}}{\lambda^{1/2}(s,M_3^2,M_4^2)}\,, \tag{3.91}$$

where $\delta_\ell^I \equiv \delta_\ell^I(s)$ is the phase shift of the P_3P_4 amplitude. Allow us to use the same convention for the partial-wave expansion of $\mathcal{T}^I$ as in Eq. (3.60), such that

$$\operatorname{disc}_s \mathcal{M}^I(s,z_s) = \frac{i}{2\pi}\sum_\ell (2\ell+1)\sin\delta_\ell^I\,e^{-i\delta_\ell^I}\int \mathrm{d}z_s'\mathrm{d}\phi_s'\mathcal{M}^I(s,z_s')P_\ell(z_s'')\,. \tag{3.92}$$

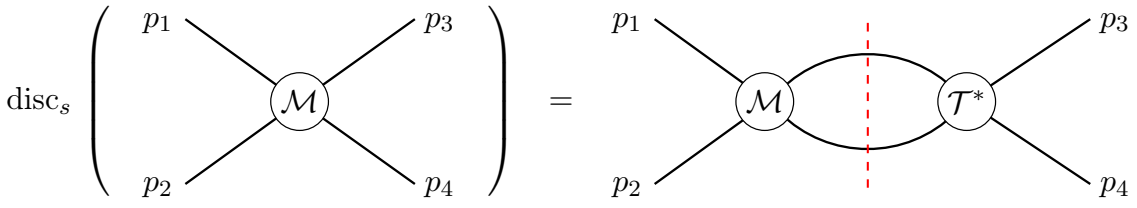

Figure 3.6: Illustration of the s-channel discontinuity of pseudoscalar $P_1P_2 \to P_3P_4$ scattering. The quantity $\mathcal{T}$ denotes the elastic P_3P_4 scattering amplitude. The unitarity cut is indicated in red.

Applying the redefined partial-wave expansion from Eq. (B.19) to $\mathcal{M}^I$, whose corresponding partial wave is denoted by f_ℓ^I, we obtain

$$\sum_\ell \kappa_s^\ell(s)\, P_\ell(z_s)\, \text{disc}_s\, f_\ell^I(s) = \frac{i}{2\pi} \sum_{\ell,\ell'} (2\ell+1) \sin\delta_\ell^I\, e^{-i\delta_\ell^I} \kappa_s^{\ell'}(s)\, f_{\ell'}^I(s) \int \mathrm{d}z_s' \mathrm{d}\phi_s' P_{\ell'}(z_s') P_\ell(z_s'')\,. \tag{3.93}$$

Note that due to our redefinition of the partial-wave amplitude f_ℓ^I, the term $\kappa_s^\ell(s)P_\ell(z_s)$ does not enter the discontinuity, cf. App. B.2.1.[13] Using the addition theorem for spherical harmonics, cf. Eqs. (3.63)–(3.66), the angular integrals can be carried out in a straightforward manner, yielding

$$\sum_\ell \kappa_s^\ell(s)\, P_\ell(z_s)\, \text{disc}_s\, f_\ell^I(s) = 2i \sum_\ell \kappa_s^\ell(s)\, P_\ell(z_s)\, \sin\delta_\ell^I\, e^{-i\delta_\ell^I}\, f_\ell^I(s)\,. \tag{3.94}$$

Finally, this leads us to the discontinuity equation for the s-channel partial-wave amplitude

$$\text{disc}_s\, f_\ell^I(s) = 2i\, \sin\delta_\ell^I\, e^{-i\delta_\ell^I}\, f_\ell^I(s)\, \theta(s-(M_3+M_4)^2)\,. \tag{3.95}$$

To relate this result to the full amplitude $\mathcal{M}^I(s,z_s)$, remember that the reconstruction theorem from Sect. 3.3.1 allows us to split $\mathcal{M}^I(s,z_s)$ into single-variable functions $\mathcal{A}_\ell^I(s)$. As the latter contain all information about the right-hand cut, we can set

$$\boxed{\text{disc}_s\, f_\ell^I(s) = \text{disc}_s\, \mathcal{A}_\ell^I(s) \qquad \text{and thus} \qquad f_\ell^I(s) = \mathcal{A}_\ell^I(s) + \hat{\mathcal{A}}_\ell^I(s)\,,} \tag{3.96}$$

where we introduced a function $\hat{\mathcal{A}}_\ell^I(s)$, which has a vanishing discontinuity along the right-hand cut in the complex s-plane, to obtain the most general solution. In the following, we will refer to $\hat{\mathcal{A}}_\ell^I(s)$ as the *inhomogeneity*. The resulting unitarity equation for the single-

[13] The shown evaluation becomes more intricate when taking higher partial waves into account, because for $\ell \geq 2$ the Legendre polynomials are not anti-proportional to κ_s^ℓ anymore. However, these contributions are often negligibly small with respect to the dominant S- and P-waves.

variable function $\mathcal{A}_\ell^I(s)$, i.e., the *inhomogeneous Omnès problem*, reads

$$\boxed{\text{disc}_s\, \mathcal{A}_\ell^I(s) = 2i\, \sin\delta_\ell^I(s) e^{-i\delta_\ell^I(s)} \left(\mathcal{A}_\ell^I(s) + \hat{\mathcal{A}}_\ell^I(s)\right) \theta\left(s - s_{\text{th}}\right)\,,} \tag{3.97}$$

with the two-particle threshold $s_{\text{th}} = (M_3 + M_4)^2$. The only, but crucial, aspect that distinguishes this unitarity relation from the one of the homogeneous Omnès problem is the newly introduced inhomogeneity $\hat{\mathcal{A}}_\ell^I$. The solution of the homogeneous part in Eq. (3.97) is given by the Omnès function and was already derived in section 3.4.2. The evaluation and physical meaning of $\hat{\mathcal{A}}_\ell^I$ will be discussed further below. Note that for elastic two-body scattering the discontinuity can be replaced by the imaginary part of $\mathcal{A}_\ell^I(s)$. In contrast, for a three-body decay, which is obtained by analytic continuation, the right-hand side of the unitarity equation above is not purely imaginary as $\hat{\mathcal{A}}_\ell^I(s)$ becomes complex and Schwarz' reflection principle is not applicable anymore. Therefore we solely refer to the discontinuity of $\mathcal{A}_\ell^I(s)$.

For a mathematically more rigorous treatment of the inhomogeneous Omnès problem we refer the reader to Refs. [85, 88].

3.4.3.1 | Solution

To solve Eq. (3.97) we proceed similarly to the treatment of inhomogeneous differential equations. Start with the solution of the homogeneous equation, i.e., the case where $\hat{\mathcal{A}}_\ell^I(s) = 0$, which is given by the Omnès function $\Omega_\ell^I(s)$ in Eq. (3.86). Hence, we can make the product ansatz

$$\mathcal{A}_\ell^I(s) = \Omega_\ell^I(s) \cdot \Psi_\ell^I(s)\,. \tag{3.98}$$

If we first rewrite Eq. (3.97) as

$$\mathcal{A}_\ell^I(s + i\epsilon) e^{-2i\delta_\ell^I} - \mathcal{A}_\ell^I(s - i\epsilon) = 2i\, \hat{\mathcal{A}}_\ell^I(s) \sin\delta_\ell^I(s) e^{-i\delta_\ell^I(s)} \theta(s - s_{\text{th}}) \tag{3.99}$$

and insert the product ansatz, we obtain

$$\left[\Psi_\ell^I(s + i\epsilon) - \Psi_\ell^I(s - i\epsilon)\right]\, |\Omega_\ell^I(s)| e^{-i\delta_\ell^I(s)} = 2i\, \hat{\mathcal{A}}_\ell^I(s) \sin\delta_\ell^I(s) e^{-i\delta_\ell^I(s)} \theta(s - s_{\text{th}})\,. \tag{3.100}$$

Here we used the fact that $\Omega_\ell^I(s \pm i\epsilon) = |\Omega_\ell^I(s)| e^{\pm i\delta_\ell^I(s)}$. Therefore, the discontinuity of Ψ reads

$$\text{disc}_s\, \Psi_\ell^I(s) = 2i\, \frac{\hat{\mathcal{A}}_\ell^I(s) \sin\delta_\ell^I(s)}{|\Omega_\ell^I(s)|} \theta(s - s_{\text{th}})\,. \tag{3.101}$$

With an n-times subtracted dispersion relation we obtain

$$\Psi_\ell^I(s) = P_{n-1}(s) + \frac{s^n}{\pi} \int_{s_{\text{th}}}^{\infty} \mathrm{d}x \frac{\sin\delta_\ell^I(x) \hat{\mathcal{A}}_\ell^I(x)}{|\Omega_\ell^I(x)|\, x^n (x - s)} \tag{3.102}$$

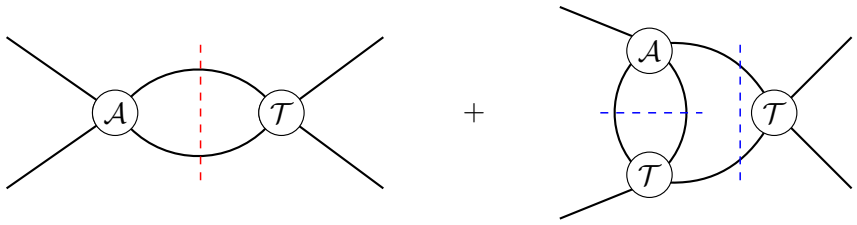

Figure 3.7: Schematic sketch of the right-hand side in Eq. (3.97) as the sum of single-variable function $\mathcal{A}_\ell^I(s)$ and inhomogeneity $\hat{\mathcal{A}}_\ell^I(s)$. The diagram on the left shows the homogeneous contribution with right-hand cut (red), while the diagram on the right indicates the inhomogeneous part including additional left-hand cuts (blue) in the crossed-channel.

and thus

$$\boxed{\mathcal{A}_\ell^I(s) = \Omega_\ell^I(s)\left(P_{n-1}(s) + \frac{s^n}{\pi}\int\limits_{s_\text{th}}^{\infty}\mathrm{d}x\,\frac{\sin\delta_\ell^I(x)\hat{\mathcal{A}}_\ell^I(x)}{|\Omega_\ell^I(x)|\,x^n(x-s)}\right),} \tag{3.103}$$

where P_{n-1} is a subtraction polynomial of order $n-1$. In the literature this is referred to as a Khuri–Treiman integral equation [106]. The great advantage over Eq. (3.49) is that the Omnès representation in Eq. (3.103) has a unique solution.

3.4.3.2 | Inhomogeneity

The corrections to the homogenous Omnès problem arise from left-hand-cut contributions to the partial wave. These are contained in the inhomogeneity $\hat{\mathcal{A}}_\ell^I$, which is—by its definition in Eq. (3.96)—given as

$$\boxed{\hat{\mathcal{A}}_\ell^I(s) = \frac{2\ell+1}{2\kappa_s^\ell(s)}\int_{-1}^{1}\mathrm{d}z_s P_\ell(z_s)\,\mathcal{M}^I(s,t,u) - \mathcal{A}_\ell^I(s)\,.} \tag{3.104}$$

Here we directly replaced the partial wave $f_\ell^I(s)$ by the corresponding expression from Eq. (B.19). For simplicity, we focus on the s-channel for now and restrict the calculation here and in the following to the case where $M_3 = M_4$. The evaluation of the angular integral proceeds in three steps:

1. Adapt the reconstruction theorem in Eq. (3.48) to the decay of interest and decompose $\mathcal{M}^I(s,t,u)$ in terms of single-variable functions $\mathcal{A}_\ell^I(s)$, $\mathcal{A}_\ell^I(t)$, and $\mathcal{A}_\ell^I(u)$.

2. Express all dependencies on t and u occurring in the reconstruction theorem in terms of the scattering angle z_s and κ_s as given in Eq. (A.15).

3. Use the symmetry $t(z_s) = u(-z_s)$, as demanded by Eq. (A.16) for $M_3 = M_4$, and

thus

$$\int \mathrm{d}z_s \, z_s^n \mathcal{A}_\ell^I(t) = (-1)^n \int \mathrm{d}z_s \, z_s^n \mathcal{A}_\ell^I(u) \tag{3.105}$$

to eliminate the u dependence and simplify the integrand.

Following these steps we can express the integral over every summand in the reconstruction theorem in terms of the *angular average*

$$\boxed{\langle z_s^n \mathcal{A}_\ell^I(s) \rangle \equiv \frac{1}{2} \int_{-1}^{1} \mathrm{d}z_s \, z_s^n \mathcal{A}_\ell^I(t) = \frac{1}{2} \int_{-1}^{1} \mathrm{d}z_s \, z_s^n \mathcal{A}_\ell^I\left(\frac{3r - s + z_s \kappa_s(s)}{2}\right).} \tag{3.106}$$

This equation shows that the inhomogeneity in the s-channel single-variable function is determined by contributions of the crossed-channels. Therefore, the unitarity relation for the s-channel single-variable function from Eq. (3.97) can be depicted as in Fig. 3.7. The derivation for the t- and u-channel inhomogeneities proceeds in a similar manner. For a crossed-channel amplitude, where we allow the intermediate state to include two particles of distinct mass, we can express the respective inhomogeneities via the angular averages

$$\boxed{\langle z_t^n \mathcal{A}(t) \rangle^{\pm} = \frac{1}{2} \int_{-1}^{1} \mathrm{d}z_t \, z_t^n \mathcal{A}\left(\frac{3r - t + z_t \kappa_t(t) \pm \Delta_t / t}{2}\right).} \tag{3.107}$$

3.4.3.3 | Analytic continuation

In the following we will shortly discuss the intricacies that arise when analytically continuing the occurring masses and Mandelstam variables from the assignment used in the two-particle scattering amplitude to the physical realm of the three-particle decay $P_1 \to P_2 P_3 P_4$, cf. Sect. A.2 for the explicit kinematic relations. It shall be underlined that one can in principle approach the three-body problem by directly evaluating three-particle unitarity cuts. However, this would be far more involved than the procedure explained in this section. Coming back to the analytic continuation, the first, somewhat trivial, observations we make is that the kinematically allowed domains for the Mandelstam variables are shifted according to Eqs. (A.22) and (A.23) and that energy conservation demands the involved masses to obey $M \equiv M_1 \geq \sum_{i=2}^{4} M_i$. The quantity M^2 is now equivalent to the available three-body center-of-mass energy and we should replace it by $M^2 + i\epsilon$ as noted by Refs. [107, 108]. The only dependence of the single-variable functions on M enters the angular averages in Eqs. (3.106) and (3.107) through r and $\kappa_{s,t}$. The kinematic functions $\kappa_{s,t}$, which are defined through square roots of Källén functions, can acquire non-vanishing imaginary parts for $M > \sum_{i=2}^{4} M_i$. As a consequence, a naive integration of the angular averages would cross the two-particle cut. This fact is characteristic for the emerging three-particle cuts as shown in Fig. 3.8. Consequently, the angular averages require a deformation of the integration contour in the complex plane. A suitable choice for this purpose is provided in App. E.2, which discusses the numerical implementation, at hand of the decays discussed

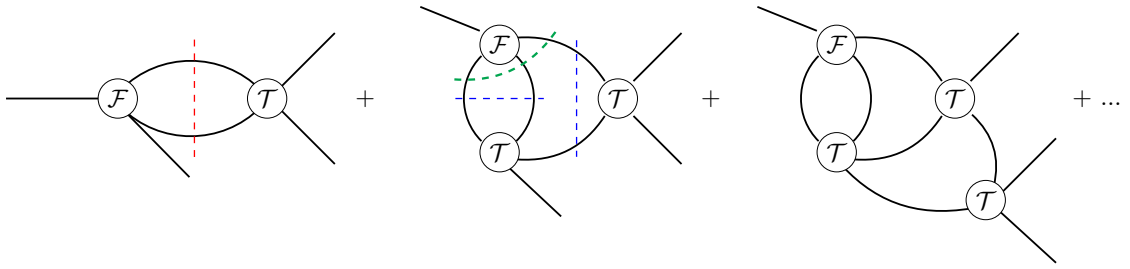

Figure 3.8: Qualitative illustration of rescattering effects in a three-body decay. The vertex $\mathcal{T}$ includes the resummation of elastic two-particle scattering, the left diagram corresponds to the homogeneous part of the single variable function $\mathcal{A}$ from Eq. (3.103) with right-hand cut (red). The remaining ones are contributions arising due to the inhomogeneity. The blue dashed lines indicate left-hand cuts in the crossed channels, while a three-particle cut is denoted by the green line. For simplicity none of the plenty of possible cuts is shown in the very last diagram.The infinite amount of contributing diagrams is obtained by expressing $\hat{\mathcal{A}}$ in terms of $\mathcal{A}$ and iterating Eq. (3.103).

in Ch. 8, in all its details. Note that the mentioned problems do not come up for $2 \to 2$ processes.

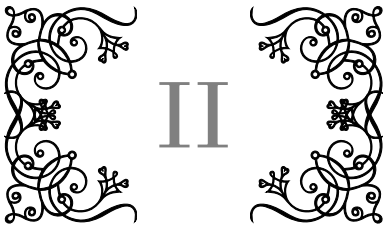

C and CP violation in effective field theories

Chapter 4

Prologue

Chapters 5 and 6 are based on the publication[1]

- H. Akdag, B. Kubis, A. Wirzba, "C and CP violation in effective field theories", *JHEP* 06 (2023) 154 [arXiv:2212.07794[hep-ph]].

The main motivation of this part of the thesis was to derive a C- and CP-odd χPT expression for the decay $\eta \to \pi^+\pi^-\pi^0$ that could be matched to the dispersive analysis presented at a later stage in Ch. 8. As a starting point, we first considered the C- and CP-odd operators at the quark level that were found at dimension 7 in Refs. [109–112]. As pointed out to us explicitly [113], but not mentioned in these references, these operators are chirality-violating and therefore have to implicitly include a Higgs, rendering them effectively to dimension 8 if the Higgs vacuum expectation value is considered in the dimensional counting. However, Refs. [109–112] provide no information on chirality-conserving operators at dimension 8. Beside this issue, we initially intended to extend the formalism of Ref. [114]. The latter derived P- and CP-violating operators in chiral perturbation theory starting from well-known quark-level operators at mass dimension six. However, it turned out that the extension of their group theoretical considerations on $SU(2)$ cannot be applied straightforwardly to the three-flavor case.

To tackle the first of these two problems, we considered the low-energy effective field theory (LEFT) in order to revisit fundamental flavor-conserving, lepton- and baryon-number-preserving, neutrinoless quark operators that violate C and CP in Ch. 5. After having verified that C- and CP-violating operators indeed first appear at dimension 7 we have also provided a corresponding complete list of dimension-8 operators. To overcome the second intricacy, we relied on the external source method of Gasser and Leutwyler [115, 116] and treated the genuine C- and CP-odd quark operators as spurions, in analogy to the chirality-breaking mass term included in standard χPT. It turned out that the decomposition into explicit irreducible representations of $SU(3)_L \times SU(3)_R$ in the spirit of Ref. [114] is not necessary for the construction of chirally invariant operators, if we account for the constraints imposed by discrete space-time symmetries. In this sense, the fundamental quark operators are matched to light-meson physics in Ch. 6. The latter additionally includes the extension to large-N_c and, in addition to the initially intended decay $\eta \to \pi^+\pi^-\pi^0$, the application to more than 20 decays in total. As central results of this analysis we provide the corresponding observables in explicit dependence on the underlying high-energy scale Λ for these possible effects of new physics.

[1] Parts of the introduction of this publication were reused in Ch. 1.

With the following paragraph we would like to clearly point out the contribution of the author of this thesis to the publication in question. The main author of this publication was responsible for most formulations, the technical development of the formalism, as well as for the analytic and numeric results. To be more precise, this includes the literature search; keeping the dialog with respective experts on this topic; the analytic reformulation of the complete sets of LEFT operators in order to obtain eigenstates of the discrete space-time symmetries; identifying the relevant C- and CP-odd operators and distinguishing the chirality violating operators at dimension 8 from the chirality preserving ones; extending the spurion technique to these quark operators; matching each of the latter onto χPT by writing down all possible corresponding chirally invariant traces; establishing a respective large-N_c expansion to describe the η'; proposing most of the presented applications; and evaluating the latter numerically with *Mathematica* [117]. All these steps were accompanied by continuous consultation of the co-authors Bastian Kubis and Andreas Wirzba, who also reviewed the analytic and numeric results and extended discussions in the manuscript. Without their experienced guidance this project would not have been possible.

Finally, we cannot let the support of the following people be unmentioned: we acknowledge the helpful discussions with Christopher Murphy, Yi Liao, Xiao-Dong Ma, Hao-Lin Wang, Susan Gardner, and Jun Shi and especially thank Peter Stoffer for his advices on the rigorous translation from LEFT operators to χPT. In addition, we are grateful for explanations about naive dimensional analysis by Jordy de Vries and for dicussions on related topics with Daniel Severt.

Chapter 5

Effective beyond Standard Model theories: fundamental C- and CP-violating operators

The efforts in search of new physics have reached a milestone with the observation of the Higgs boson at CERN's Large Hadron Collider [15, 16], one of the most important building blocks of the Standard Model of particle physics (SM). Until now, there is no evidence for new particles other than the ones contained in the SM, at least up to an energy scale of the order 1 TeV. However, physics beyond the Standard Model (BSM) can arise from heavy particles with masses above some unknown high-energy scale Λ exceeding the TeV range, which is out of experimental reach for the foreseeable future. It is commonly agreed on that—if such heavy degrees of freedom exist—the SM provides merely an effective description of the underlying beyond-Standard-Model theory. A convenient way to approach the effects of the latter below the scale Λ concerns the construction of effective field theories, providing a fundamental, model-independent framework. According to the Appelquist–Carazzone theorem [118] heavy particles decouple in a perturbative manner with (anomaly-free) interactions in the low-energy range. Hence the underlying BSM theory can be described by the *Standard Model effective field theory* (SMEFT), whose perturbative expansion in powers of the small parameter $1/\Lambda$ yields

$$\mathcal{L}_{\text{SMEFT}} = \mathcal{L}_{\text{SM}} + \frac{1}{\Lambda}\mathcal{L}_5 + \frac{1}{\Lambda^2}\mathcal{L}_6 + \frac{1}{\Lambda^3}\mathcal{L}_7 + \dots \quad \text{with} \quad \mathcal{L}_D \equiv \sum_i C_i^D Q_i^D \,. \tag{5.1}$$

In this operator-product-type of expansion the quantity $\mathcal{L}_{\text{SM}}$ denotes the renormalizable Lagrangian of the SM with mass dimension 4, the non-renormalizable Lagrangians $\mathcal{L}_D$ include operators Q_i^D with mass dimensions $D > 4$ that are suppressed by powers of $1/\Lambda$, and the C_i^D are the respective dimensionless coupling constants known as Wilson coefficients.

In general $\mathcal{L}_{\text{SMEFT}}$ is richer than $\mathcal{L}_{\text{SM}}$ itself, as the $\mathcal{L}_D$ are only restricted by Lorentz invariance, the same $SU(3)_C \times SU(2)_L \times U(1)_Y$ gauge group, and the same particle content as the SM. In the recent past, much effort has been devoted to the systematic construction of complete sets of operators contributing to the $\mathcal{L}_D$, which includes the classification and counting of all possible Q_i^D (cf. Ref. [119] for a short overview) as well as eliminating redundant operators with the aid of equations of motion, partial integration, and Fierz identities. The complete operator bases up to and including dimension 9 in SMEFT have been counted and/or computed in Refs. [119–128]. If we exclude the existence of, yet unobserved, hypothetical light degrees of freedom that couple extremely weakly to the SM particle content, such as axions and sterile neutrinos, SMEFT reduces to the SM in the limit

of small energies. An extension of SMEFT including new light particles can for instance be found in Refs. [129–135].

However, when going to even smaller energies, SMEFT may not be the most convenient theory to describe phenomena exclusively occurring below the electroweak scale $\Lambda_{\text{EW}} \lesssim v$, with v denoting the Higgs vacuum expectation value (vev). In this scenario, particles of the SM with masses larger than Λ_{EW} are no observable degrees of freedom anymore and the gauge group reduces to $SU(3)_C \times U(1)_Q$. This means that the top quark, the weak gauge bosons $W^\pm$ and Z^0, and the Higgs are integrated out and we are left with the dynamics of QCD and QED only, while effects of weak interactions are implicitly encoded in the constant Wilson coefficients, also giving rise to point-like interactions with neutrinos. Nevertheless, the construction of a consistent and complete basis of such a theory, without operator redundancies and terms of repeated flavors compositions, and its matching to SMEFT at larger energies is quite involved [136]. The appropriate theory to handle effects in this energy regime is known as *low-energy effective field theory* (LEFT), which is in principle a valid theory on its own, even without recourse to SMEFT. The continuation of LEFT to energies above Λ_{EW} may for instance as well be given by the *Higgs effective field theory* [137–144], which, in comparison to SMEFT, does not rely on the conjecture that the Higgs belongs to an electroweak doublet.[1] In either way, the operator product expansion of LEFT proceeds in analogy to Eq. (5.1) with a small expansion parameter that can be chosen as $1/v$. With its own Wilson coefficients $\tilde{C}_i^d$ and operators $\tilde{Q}_i^d$ of dimension d, the LEFT Lagrangian can be written as

$$\mathcal{L}_{\text{LEFT}} = v\tilde{\mathcal{L}}_3 + \mathcal{L}_{\nu\,\text{kin}} + \mathcal{L}_{\text{QCD+QED}} + \frac{1}{v}\tilde{\mathcal{L}}_5 + \frac{1}{v^2}\tilde{\mathcal{L}}_6 + \ldots \quad \text{with} \quad \tilde{\mathcal{L}}_d \equiv \sum_i \tilde{C}_i^d \tilde{Q}_i^d\,, \tag{5.2}$$

where the three-dimensional Lagrangian $\tilde{\mathcal{L}}_3$ refers to a mass term of a possible Majorana neutrino and the four-dimensional $\mathcal{L}_{\nu\text{kin}}$ includes the kinetic term for neutrinos. All other dependencies on the Higgs vev are hidden in the respective Wilson coefficients and do not contribute to the dimensional analysis, so that the different power counting schemes in SMEFT and in LEFT have to be clearly distinguished. However, assuming SMEFT to be the underlying theory of LEFT, we can account for the additional suppression in $1/\Lambda$ by redefining the Wilson coefficients of LEFT as [146]

$$\tilde{C}_i^d \to \left(\frac{v}{\Lambda}\right)^{\sum_j (D_j - 4)} \tilde{C}_i^d\,, \tag{5.3}$$

where the D_j denote the dimension of SMEFT operators that can be combined in one Feynman diagram to construct the desired LEFT operator. An overview of the considered effective field theories at different energy scales is shown in Fig. 5.1. The latter also includes χPT, which will be subject of Ch. 6.

Hitherto, the investigation of the complete basis in LEFT extends up to dimension 9 [136, 146–150], and the inclusion of axions or sterile neutrinos in LEFT can be found in Refs. [134,

[1] See Ref. [145] for a comprehensive review.

151–153]. A famous and maybe historically most important example of a LEFT operator is the Fermi theory of weak interactions [154, 155].

Our analysis aims at a rigorous derivation of C- and CP-violating sources in the mesonic sector arising from fundamental quark operators in LEFT.[2] These, due to the CPT theorem, T-odd and P-even (ToPe) contributions are of particular interest for cosmology, as they provide, according to the Sakharov conditions [19], one prerequisite (in addition to the T-odd, P-odd contributions) for the dynamical creation of the matter–antimatter asymmetry during the baryogenesis. On the other hand, theoretical work about this class of symmetry violation is severely lacking in contrast to the one for C-even and P-odd phenomena. First thoughts on the structure of these BSM operators, independent of which effective theory they could possibly belong to, were already made in the 1990s [158] and extended throughout that decade [109–112]. It was claimed that the first C- and CP-odd operators at low energies appear at dimension 7 and read[3]

$$\begin{aligned} &\bar{\psi}\overleftrightarrow{D}_\mu\gamma_5\psi\bar{\chi}\gamma^\mu\gamma_5\chi\,, \\ &\bar{\psi}\sigma_{\mu\nu}\lambda^a\psi F^{\mu\lambda}G^{a\nu}_\lambda\,, \\ &\bar{\psi}\sigma_{\mu\nu}\psi F^{\mu\lambda}Z^\nu_\lambda\,, \end{aligned} \tag{5.4}$$

for up to two fermion fields ψ and χ. An aspect withheld in these analyses is that the listed operators are chirality-violating and thus need to be equipped with an additional Higgs field. Therefore, according to a naive power counting, all these operators are of dimension 8 in SMEFT and of dimension 7 in LEFT. As the Higgs is integrated out in the latter theory, its vev, which is absorbed in the Wilson coefficients, does not contribute to the dimensional power. However, this leads to another unpleasant inconsistency: the heavy Z^0-boson is not integrated out although we are exclusively dealing with interactions at low energies. We have not yet specified chirality-conserving C- and CP-odd operators of dimension 8 in LEFT. These are a priori not suppressed with respect to the chirality-violating ones at dimension 7 in LEFT, as both can originate from operators of dimension 8 in SMEFT and thus have the same suppression in $1/\Lambda$. In a similar way this point was observed in nucleon EDM analyses [159–161], which found that T- and P-odd chirality-violating operators of dimension 5 in LEFT can effectively be of the same order of magnitude as chirality-conserving ones at dimension 6 in LEFT.

At the time the operators in Eq. (5.4) had been proposed, the rigorously derived complete operator basis in LEFT was not available.

In this chapter we thoroughly revisit the C- and CP-violating operators up to and including dimension 8 in LEFT and provide the first complete set of these operators. With focus on the application to ToPe forces in η decays, we restrict our analysis to flavor-conserving

[2] An alternative path for the C- and CP-violating sources could be realized in SMEFT at the W-scale, cf. Refs. [156, 157], and should yield a set of operators that is equivalent to the one considered and presented in this work.

[3] There are different formulations of the four-fermion operator in the cited literature, which are consistent with each other when using the Gordon identity.

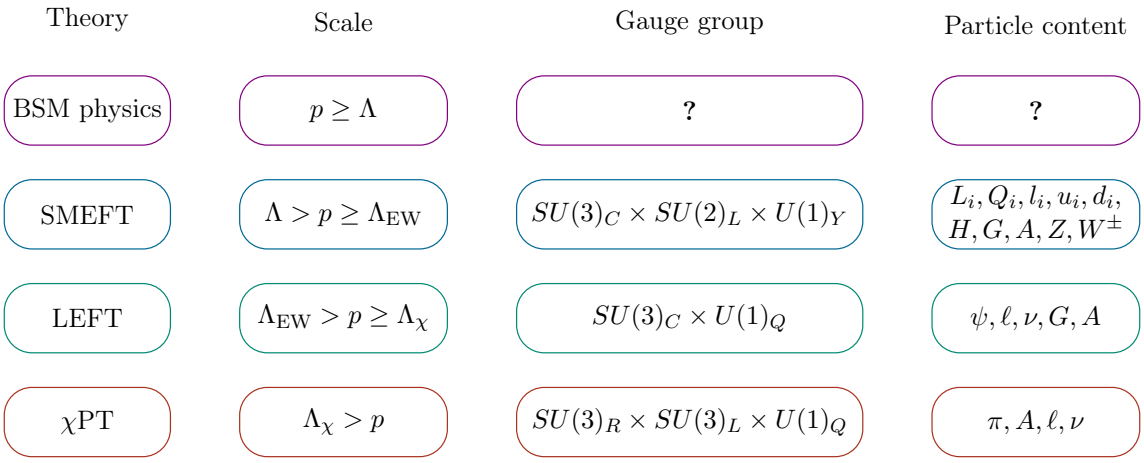

Figure 5.1: Comparison of effective field theories at different energy scales p.

quark operators (with couplings to the gluon and photon fields). Additionally we quote the corresponding semi-leptonic operators. A generalization to flavor-changing processes can be carried out in complete analogy and is left for future analyses, if the phenomenological interest in these operators is given. In Sect. 5.1 we introduce our notation and conventions, along with a short overview of the considered LEFT bases. We discuss the discrete space-time symmetries of building blocks of LEFT in Sect. 5.2. In Sect. 5.3 we summarize the list of ToPe operators, whose derivation from known LEFT bases is sketched in App. C. We close with a short conclusion in Sect. 5.4.

5.1 | LEFT: notations and conventions

Below the electroweak scale, the important degrees of freedom in the SM are two up-type and three down-type quarks, which we summarize by $\psi \in \{u, c, d, s, b\}$, three charged leptons $\ell \in \{e, \mu, \tau\}$, and the corresponding left-handed neutrinos $\nu_L \in \{\nu_L^e, \nu_L^\mu, \nu_L^\tau\}$. Except for the latter, these fermions are described by the QCD and QED Lagrangians by means of[4]

$$\mathcal{L}_{\rm QED+QCD} = -\frac{1}{4}F_{\mu\nu}F^{\mu\nu} - \frac{1}{4}G^a_{\mu\nu}G^{a\mu\nu} + \sum_\psi \bar{\psi}\big(i\not{D} - m_\psi\big)\psi + \sum_\ell \bar{\ell}\big(i\not{D} - m_\ell\big)\ell\,, \tag{5.5}$$

with photonic and gluonic field-strength tensors $F_{\mu\nu}, G^a_{\mu\nu}$. We denote the representations of these tensors in dual space by $\tilde{X}_{\mu\nu} = \frac{1}{2}\epsilon_{\mu\nu\alpha\beta}X^{\alpha\beta}$ with $X_{\mu\nu} \in \{F_{\mu\nu}, G^a_{\mu\nu}\}$. The gauge covariant derivative acting on quarks is chosen to be

$$\begin{aligned} D_\mu\psi &= \big(\vec{\partial}_\mu + ieQA_\mu + igT^aG^a_\mu\big)\psi\,, \\ D_\mu\bar{\psi} &= \bar{\psi}\big(\overleftarrow{\partial}_\mu - ieQA_\mu - igT^aG^a_\mu\big)\,, \end{aligned} \tag{5.6}$$

[4] One can in principle also include the QCD θ-term.

with $D_\mu\bar{\psi} \equiv (D_\mu\psi)^\dagger\gamma^0$. In this equation Q and $T^a = \frac{1}{2}\lambda^a$ are the generators of $U(1)_Q$ and $SU(3)_C$, respectively, where λ^a denote the Gell-Mann matrices obeying the relations

$$[T_a, T_b] = if_{abc}T_c\,, \qquad \{T_a, T_b\} = \frac{1}{3}\delta_{ab} + d_{abc}T_c\,. \tag{5.7}$$

The quantities f_{abc} and d_{abc} denote the totally antisymmetric and symmetric structure constants of $SU(3)$. The gauge covariant derivative acting on ℓ is defined analogously, but without a coupling to gluons. We will henceforth indicate the direction to which the derivative acts by arrows, i.e., $\bar{\psi}\vec{D}_\mu\psi = \bar{\psi}(D_\mu\psi)$ and $\bar{\psi}\overleftarrow{D}_\mu\psi = (D_\mu\bar{\psi})\psi$. It proves useful to introduce a hermitian version of the gauge covariant derivative by

$$\bar{\psi}i\overleftrightarrow{D}_\mu\psi \equiv \bar{\psi}i\vec{D}_\mu\psi - \bar{\psi}i\overleftarrow{D}_\mu\psi\,. \tag{5.8}$$

The remaining Lagrangian terms in the LEFT Lagrangian from Eq. (5.2) are built from the same degrees of freedom contained in Eq. (5.5) obeying the gauge group $SU(3)_c \times U(1)_{\text{em}}$. The choice of LEFT basis is not unique, we can for instance employ the Gordon identity, equations of motion, Fierz identities, as well as integration by parts to shift operators between the classes. In this work we consider the LEFT basis derived in Ref. [146] for operators with mass dimension $d \leq 6$ (5963 hermitian operators), Ref. [150] for operators of dimension 7 (5218 hermitian operators), and Ref. [136] for the ones at $d = 8$ (35058 hermitian operators).

To tackle the overwhelming amount of more than $45 \cdot 10^3$ operators up to dimension 8 in LEFT, we restrict our investigation to operators that may possibly contribute ToPe forces in η decays. Therefore we ignore operators including neutrinos,[5] drop all operators that violate lepton- and/or baryon-number conservation, and restrict the analysis to C- and CP-odd operators only that are at the same time flavor-conserving.[6] Still, we allow for chirality-conserving and -violating operators.

5.2 | Discrete space-time symmetries

In this section we shortly summarize the discrete symmetries of several quantities that constitute the respective LEFT operators, to pick the correct C- and CP-violating operators from the LEFT bases.

For any combination of Dirac matrices Γ, the well-known transformations of fermion bilin-

[5] The η decay listed as Γ_{20} in Ref. [13], $\eta \to \pi^+e^-\bar{\nu}_e$ + c.c., is in fact a C- and T-allowed decay.

[6] We note that the requirement of C and CP violation places a very selective constraint, reducing the amount of $45 \cdot 10^3$ operators tremendously.

ears under C, P, and T, cf., Sect. 2.2,[7] read

$$\begin{aligned} C: \quad \bar{\psi}\Gamma\chi \quad &\xrightarrow{C} \quad -\bar{\chi}\gamma_0\gamma_2\Gamma^T\gamma_2\gamma_0\psi\,, \\ P: \quad \bar{\psi}\Gamma\chi \quad &\xrightarrow{P} \quad \bar{\psi}\gamma_0\Gamma\gamma_0\chi\,, \\ T: \quad \bar{\psi}\Gamma\chi \quad &\xrightarrow{T} \quad \bar{\psi}\gamma_1\gamma_3\Gamma^*\gamma_3\gamma_1\chi\,, \end{aligned} \tag{5.9}$$

where Γ^T denotes the transposed of Γ, Γ^* is its complex conjugate, and the factor -1 in the first line arises from the anticommutation of fermion creation and annihilation operators. As the fermions in each bilinear change places under C, it may not be evident at first glance that the original covariant derivative $\vec{D}_\mu$ contributes to both eigenstates of C, in contrast to $\overleftrightarrow{D}_\mu$.[8]

The discrete symmetries of the gauge fields can be deduced from the requirement that their interaction with the quark currents implied by Eq. (5.5) preserves C, P, and T separately. The hermitian generators T_a of $SU(3)$ transform as $T_a \to T_a^T = T_a^*$ under C and T. Hence the discrete symmetries of all color structures can be derived with [55]

$$\begin{aligned} T_a \quad &\xrightarrow{C} \quad x_a T_a\,, & T_a \quad &\xrightarrow{P} \quad T_a\,, & T_a \quad &\xrightarrow{T} \quad x_a T_a\,, \\ G_a^\mu \quad &\xrightarrow{C} \quad -x_a G_a^\mu\,, & G_a^\mu \quad &\xrightarrow{P} \quad \varepsilon^\mu G_a^\mu\,, & G_a^\mu \quad &\xrightarrow{T} \quad x_a \varepsilon^\mu G_a^\mu\,, \\ G_a^{\mu\nu} \quad &\xrightarrow{C} \quad -x_a G_a^{\mu\nu}\,, & G_a^{\mu\nu} \quad &\xrightarrow{P} \quad \varepsilon^\mu\varepsilon^\nu G_a^{\mu\nu}\,, & G_a^{\mu\nu} \quad &\xrightarrow{T} \quad -x_a \varepsilon^\mu\varepsilon^\nu G_a^{\mu\nu}\,, \end{aligned} \tag{5.10}$$

where we used that ε^μ equals 1 for $\mu = 0$ and -1 for $\mu \in \{1,2,3\}$ and kept the notation short with $x_a = 1$ for $a \in \{1,3,4,6,8\}$ and $x_a = -1$ for $a \in \{2,5,7\}$. We already elaborated on these transformations in Sect. 2.4.1. To compile the discrete symmetries of operators including $SU(3)$ structure constants note that the non-vanishing values of f_{abc} (d_{abc}) contain an odd (even) number of indices picked from $\{2,5,7\}$. Let us illustrate this at a simple example: consider the C-transformation of the Weinberg-type term $f_{abc}G_\mu^{a\nu}G_\nu^{b\rho}G_\rho^{c\mu}$, which according to Eq. (5.10) has the eigenvalue $(-1)^3 x_a x_b x_c$. Due to the color contraction with f_{abc}, either one or all signs $x_{a,b,c}$ must be negative, such that the operator is C-even. In complete analogy, one can compute the discrete symmetries of arbitrary color contractions. We summarize the C, P, and T transformations of various quark bilinears, gauge fields, and color structures in Table 5.1, which comes in handy when searching for C- and CP-violating operators in LEFT.

5.3 | C- and CP-odd operators in LEFT

In this section we list our most convenient choice of linearly independent ToPe operators up to and including mass dimension 8 in LEFT, based on the operator bases in Refs. [136,

[7] In contrast to Sect. 2.2.2, we use a somewhat more synoptic notation to denote the transformation under discrete symmetries.

[8] For the standard derivative $\vec{D}$ one needs the decomposition $\bar{\psi}\vec{D}_\mu\psi = \frac{1}{2}\bar{\psi}\left[(\vec{D}_\mu + \vec{D}_\mu) - (\overleftarrow{D}_\mu - \vec{D}_\mu)\right]\psi$ to obtain (two distinct) C eigenstates.

	$\bar{\psi}\psi$	$\bar{\psi}i\gamma_5\psi$	$\bar{\psi}\gamma_\mu\psi$	$\bar{\psi}\gamma_\mu\gamma_5\psi$	$\bar{\psi}\sigma_{\mu\nu}\psi$	$\bar{\psi}i\sigma_{\mu\nu}\gamma_5\psi$	X_μ	$X_{\mu\nu}$	$f_{abc}G^{a\nu}_\mu G^{b\rho}_\nu G^{c\mu}_\rho$	$f_{abc}T^aG^b_{\mu\nu}G^{c\mu\nu}$	$f_{abc}T^aT^bG^c_{\mu\nu}$
C	$+$	$+$	$-$	$+$	$-$	$-$	$-$	$-$	$+$	$-$	$+$
P	$+$	$-$	ε^μ	$-\varepsilon^\mu$	$\varepsilon^\mu\varepsilon^\nu$	$-\varepsilon^\mu\varepsilon^\nu$	ε^μ	$\varepsilon^\mu\varepsilon^\nu$	$+$	$+$	$\varepsilon^\mu\varepsilon^\nu$
T	$+$	$-$	ε^μ	ε^μ	$-\varepsilon^\mu\varepsilon^\nu$	$\varepsilon^\mu\varepsilon^\nu$	ε^μ	$-\varepsilon^\mu\varepsilon^\nu$	$+$	$-$	$\varepsilon^\mu\varepsilon^\nu$

Table 5.1: Discrete space-time symmetries of quark bilinears with a single flavor and several gauge terms. In this simplified notation each $SU(3)$ color generator T_a is thought to be part of one quark bilinear. The sign ε^μ equals 1 for $\mu = 0$ and -1 for $\mu \in \{1,2,3\}$, $X_\mu \in \{A_\mu, T_aG^a_\mu\}$, and $X_{\mu\nu} \in \{F_{\mu\nu}, T_aG^a_{\mu\nu}\}$. Replacing any field-strength tensor by its representation in dual space $\tilde{X}_{\mu\nu}$, i.e., any contraction with the Levi-Civita symbol $\epsilon_{\alpha\beta\mu\nu}$, flips the signs of P and T. An exchange of the structure constants f_{abc} and d_{abc} changes signs of C and T. When multiplying each term with the imaginary unit i the sign of T flips, while the inclusion of $\vec{D}_\mu$ in a bilinear flips the signs of C and T. If necessary, factors of i are multiplied to render quark bilinears hermitian.

146, 150]. Details on the derivation of the full set of C- and CP-violating operators can be found in App. C, which also takes care of operators that are not hermitian in the first place.

At this point we shortly summarize the straightforward but, given the vast number of operators, quite tedious procedure. First, multiply each LEFT operator by a complex Wilson coefficient and add the hermitian conjugate. All LEFT bases under consideration are formulated in terms of left- and right-handed fermions, such that the resulting multilinears do not necessarily have definite eigenvalues under C, P, and T. To remedy this issue we decompose the chiral fields into their (pseudo)scalar, (axial)vector, and (pseudo)tensor contributions and compile their eigenvalues with the aid of Table 5.1 and similar relations for different color structures. Finally we have to identify chirality-conserving and -violating operators. If both appear at the same mass dimension of LEFT, we can ignore the latter, which is in some more detail discussed in Sect. 5.3.2.

While the identification of chirality-violating fermion bilinears is straightforward, special care has to be taken for quadrilinear quark operators. Some four-quark operators that are naively found to be chirality-breaking may be mediated by gauge-invariant BSM couplings of left-handed $W^\pm$ bosons to right-handed currents, induced via mixing of the $W^\pm$ bosons with their right-handed BSM counterparts. For instance, the dimension-6 P- and T-violating quadrilinear quark operator of Ng and Tulin [162]

$$i\frac{C_{\rm NT}}{\Lambda^2}\left\{(\bar{u}_R\gamma^\mu d_R)(\bar{d}_L\gamma_\mu u_L) - (\bar{d}_R\gamma^\mu u_R)(\bar{u}_L\gamma_\mu d_L)\right\} \tag{5.11}$$

(with Wilson coefficient $C_{\rm NT}$) can be traced back to the following gauge-invariant, manifestly chirally symmetric dimension-6 operator (resulting, e.g., in the reduction of minimal

left-right-symmetric models [163, 164]—a subclass of left-right models [48, 49])

$$\frac{C_{\rm LR}}{\Lambda^2}(i\tilde{H}^\dagger D_\mu H)(\bar{u}_R\gamma^\mu d_R) + \text{h.c.}\,. \tag{5.12}$$

Here H with $\tilde{H} \equiv i\tau_2 H^*$ is the Higgs doublet field, $D_\mu = \partial_\mu + igW^a\tau^a$, $a = 1, 2$, and $C_{\rm LR}$ the pertinent Wilson coefficient. This term yields, after electroweak symmetry breaking, in unitary gauge

$$-\frac{gv^2}{2\sqrt{2}}\left[\frac{C_{\rm LR}}{\Lambda^2}\bar{u}_R\gamma^\mu d_R W_\mu^\dagger + \text{h.c.}\right]\left(1+\frac{h}{v}\right)^2\,, \tag{5.13}$$

with h the lightest Higgs boson of the model, which corresponds to the physical Higgs boson, and v its vacuum expectation value. After integrating out the Higgs and $W^\pm$ bosons, we obtain, just below the $W^\pm$ mass, the four-quark operator (5.11) to leading order. Note that the Higgs vev v cancels against the mass of the $W^\pm$ bosons, as the coupling to the right-handed current involved the Higgs kinetic term and is therefore not of Yukawa nature. More details can be found in Refs. [165, 166], see also Ref. [167].

In accordance with this argument, the chirality-conserving operators can also be easily identified by the fact that they must appear at the same order in both LEFT and SMEFT, if a consistent operator basis is used.

To shorten the notation in the following subsections, we omit the ratio of scales v^4/Λ^4, which according to Eq. (5.3) is common to all our operators. Regarding Eq. (5.2), the suppression in terms of these heavy scales can explicitly be restored by multiplying each LEFT operator of dimension 7 by v/Λ^4 and the ones of dimension 8 by $1/\Lambda^4$.

5.3.1 | Dimension-7 operators

We show in App. C that there are indeed no ToPe operators below dimension 7 in LEFT as already implicitly claimed decades ago [158], but which was—to the best of our knowledge—not proven explicitly in the literature.[9] At dimension 7 we can confirm that exactly the operators already quoted in Eq. (5.4) contribute (except the one including the Z-boson, which obviously does not belong to LEFT), i.e.,

$$\begin{aligned}\mathcal{O}_{\psi\chi}^{(a)} &\equiv c_{\psi\chi}^{(a)}\,\bar{\psi}\overleftrightarrow{D}_\mu\gamma_5\psi\bar{\chi}\gamma^\mu\gamma_5\chi\,,\\ \mathcal{O}_{\psi}^{(b)} &\equiv c_{\psi}^{(b)}\,\bar{\psi}T^a\sigma^{\mu\nu}\psi F_{\mu\rho}G_\nu^{a\rho}\,,\end{aligned} \tag{5.14}$$

where $c_{\psi\chi}^{(a)}$ and $c_{\psi}^{(b)}$ denote *real*-valued Wilson coefficients with flavor indices ψ, χ combined with superscripts $(a), (b)$ serving as labels to classify operators unambiguously. The quadri-

[9] To consistently construct a C- and CP-odd operator from lower-dimensional ones, one could for instance include a T- and P-odd operator of dimension 6 of SMEFT in a C-violating electroweak loop. However, integrating out the weak gauge boson with mass dimension 1, i.e., replacing it by the quark current of dimension 3, effectively leads to a dimension-8 operator in LEFT. Due to the completeness of the LEFT operator bases used in this work, these contributions are automatically taken care of.

linear in this equation can in principle appear with two different color contractions.[10] In addition, we find the (semi-leptonic) operators containing quarks and charged leptons

$$\begin{aligned}\mathcal{O}^{(c)}_{\ell\psi} &\equiv c^{(c)}_{\ell\psi}\,\bar{\ell}\overleftrightarrow{D}_\mu\gamma_5\ell\bar{\psi}\gamma^\mu\gamma_5\psi\,,\\ \mathcal{O}^{(d)}_{\ell\psi} &\equiv c^{(d)}_{\ell\psi}\,\bar{\ell}\gamma^\mu\gamma_5\ell\bar{\psi}\overleftrightarrow{D}_\mu\gamma_5\psi\,.\end{aligned} \tag{5.15}$$

5.3.2 | Dimension-8 operators

As all terms in Sect. 5.3.1 are chirality-breaking, we can a priori not neglect chirality-conserving operators at dimension 8 in LEFT. Investigating the latter, we do not find any ToPe operators for pure gauge terms or terms including four fermions and two derivatives. For quark multilinears coupling to gluon field-strength tensors (henceforth called gluonic operators) we identify

$$\begin{aligned}\mathcal{O}^{(e)}_{\psi} &\equiv c^{(e)}_{\psi}\,f_{abc}\bar{\psi}\gamma^\mu i\overleftrightarrow{D}^\nu T^a\psi G^b_{\mu\rho}G^{c\,\rho}_{\nu}\,,\\ \mathcal{O}^{(f)}_{\psi\chi} &\equiv c^{(f)}_{\psi\chi}\,\bar{\psi}\gamma^\mu\psi\bar{\chi}\gamma^\nu T^a\chi G^a_{\mu\nu}\,,\\ \mathcal{O}^{(g)}_{\psi\chi} &\equiv c^{(g)}_{\psi\chi}\,\bar{\psi}\gamma^\mu\gamma_5\psi\bar{\chi}\gamma^\nu\gamma_5 T^a\chi G^a_{\mu\nu}\,,\\ \mathcal{O}^{(h)}_{\psi\chi} &\equiv c^{(h)}_{\psi\chi}\,f_{abc}\bar{\psi}\gamma^\mu\gamma_5 T^a\psi\bar{\chi}\gamma^\nu T^b\chi\tilde{G}^c_{\mu\nu}\,,\\ \mathcal{O}^{(i)}_{\psi\chi} &\equiv c^{(i)}_{\psi\chi}\,d_{abc}\bar{\psi}\gamma^\mu T^a\psi\bar{\chi}\gamma^\nu T^b\chi G^c_{\mu\nu}\,,\\ \mathcal{O}^{(j)}_{\psi\chi} &\equiv c^{(j)}_{\psi\chi}\,d_{abc}\bar{\psi}\gamma^\mu\gamma_5 T^a\psi\bar{\chi}\gamma^\nu\gamma_5 T^b\chi G^c_{\mu\nu}\,,\\ \mathcal{O}^{(k)}_{\psi\chi} &\equiv c^{(k)}_{\psi\chi}\,i\big[\bar{\psi}T^a\chi\bar{\chi}\sigma^{\mu\nu}\psi+\bar{\psi}\gamma_5 T^a\chi\bar{\chi}\sigma^{\mu\nu}\gamma_5\psi-(\psi\leftrightarrow\chi)\big]G^a_{\mu\nu}\,,\\ \mathcal{O}^{(l)}_{\psi\chi} &\equiv c^{(l)}_{\psi\chi}\,i\big[\bar{\psi}\chi\bar{\chi}\sigma^{\mu\nu}T^a\psi+\bar{\psi}\gamma_5\chi\bar{\chi}\sigma^{\mu\nu}\gamma_5 T^a\psi-(\psi\leftrightarrow\chi)\big]G^a_{\mu\nu}\,,\\ \mathcal{O}^{(m)}_{\psi\chi} &\equiv c^{(m)}_{\psi\chi}\,\big[\bar{\psi}\sigma^{\lambda\mu}T^a\chi\bar{\chi}\sigma_{\mu\nu}\psi+\bar{\psi}\sigma^{\lambda\mu}\gamma_5 T^a\chi\bar{\chi}\sigma_{\mu\nu}\gamma_5\psi+(\psi\leftrightarrow\chi)\big]G^{a\,\nu}_{\lambda}\,,\end{aligned} \tag{5.16}$$

as C- and CP-odd. Among these operators, $\mathcal{O}^{(i)}_{\psi\chi},\mathcal{O}^{(j)}_{\psi\chi},\mathcal{O}^{(k)}_{\psi\chi},\mathcal{O}^{(l)}_{\psi\chi}$ are antisymmetric under flavor interchange, while $\mathcal{O}^{(m)}_{\psi\chi}$ is symmetric.

Similar to the operators in Eq. (5.16) we find quark quadrilinears including photon field-

[10] We note that according to Refs. [161, 167], the four-quark operator in Eq. (5.14) should be valid just below the $W^\pm$ threshold. This means that one expects QCD corrections when running down to a scale μ, $1\,\text{GeV}\ll\mu\ll M_{W^\pm}$, such that the quadrilinear in Eq. (5.14) would mix with its corresponding different color contraction. These corrections are beyond the scope of our analysis and do not have any effect once the LEFT basis is matched onto χPT.

strength tensors (photonic operators), i.e.,

$$\begin{aligned}
\mathcal{O}^{(n)}_{\psi\chi} &\equiv c^{(n)}_{\psi\chi}\,\bar{\psi}\gamma^\mu\psi\bar{\chi}\gamma^\nu\chi F_{\mu\nu}\,,\\
\mathcal{O}^{(o)}_{\psi\chi} &\equiv c^{(o)}_{\psi\chi}\,\bar{\psi}\gamma^\mu\gamma_5\psi\bar{\chi}\gamma^\nu\gamma_5\chi F_{\mu\nu}\,,\\
\mathcal{O}^{(p)}_{\psi\chi} &\equiv c^{(p)}_{\psi\chi}\,\bar{\psi}\gamma^\mu T^a\psi\bar{\chi}\gamma^\nu T^a\chi F_{\mu\nu}\,,\\
\mathcal{O}^{(q)}_{\psi\chi} &\equiv c^{(q)}_{\psi\chi}\,\bar{\psi}\gamma^\mu\gamma_5 T^a\psi\bar{\chi}\gamma^\nu\gamma_5 T^a\chi F_{\mu\nu}\,,\\
\mathcal{O}^{(r)}_{\psi\chi} &\equiv c^{(r)}_{\psi\chi}\,i\big[\bar{\psi}\chi\bar{\chi}\sigma^{\mu\nu}\psi+\bar{\psi}\gamma_5\chi\bar{\chi}\sigma^{\mu\nu}\gamma_5\psi-(\psi\leftrightarrow\chi)\big]F_{\mu\nu}\,,
\end{aligned}\tag{5.17}$$

which, due to fewer possible color contractions, allow for fewer C- and CP-violating contributions than the gluonic operators. Each of these photonic operators is completely antisymmetric under interchange of quark flavors, up to the unknown Wilson coefficients. Therefore the operators $\mathcal{O}^{(z)}_{\chi\psi}$, with $z\in\{n,o,p,q,r\}$, can in principle always be absorbed by $\mathcal{O}^{(z)}_{\psi\chi}$ with an appropriate redefinition of the Wilson coefficients, leaving us with three independent flavor combinations to consider for the off-diagonal contributions, e.g., $\mathcal{O}^{(z)}_{ud},\mathcal{O}^{(z)}_{us}$, and $\mathcal{O}^{(z)}_{ds}$. Note that the diagonal elements $\mathcal{O}^{(z)}_{uu},\mathcal{O}^{(z)}_{dd}$, and $\mathcal{O}^{(z)}_{ss}$ vanish for all operators in Eq. (5.17).

There are only two ToPe operators in dimension 8 LEFT that contain quark bilinears, photons, and gluon field-strength tensors (photo-gluonic operators), which explicitly read

$$\begin{aligned}
\mathcal{O}^{(s)}_{\psi} &\equiv c^{(s)}_{\psi}\,\bar{\psi}\gamma^\mu i\overleftrightarrow{D}^\nu T^a\gamma_5\psi F_{\mu\rho}\tilde{G}^{a\,\rho}_{\nu}\,,\\
\mathcal{O}^{(t)}_{\psi} &\equiv c^{(t)}_{\psi}\,\bar{\psi}\gamma^\mu i\overleftrightarrow{D}^\nu T^a\gamma_5\psi F_{\nu\rho}\tilde{G}^{a\,\rho}_{\mu}\,.
\end{aligned}\tag{5.18}$$

Finally we quote our findings for semi-leptonic operators. The inclusion of leptonic bilinears reduces the amount of possible color contractions and hence the number of contributing ToPe operators enormously. Our results for gluonic operators at dimension 8 in LEFT read

$$\begin{aligned}
\mathcal{O}^{(u)}_{\ell\psi} &\equiv c^{(u)}_{\ell\psi}\,\bar{\ell}\gamma^\mu\ell\bar{\psi}\gamma^\nu T^a\psi G^a_{\mu\nu}\,,\\
\mathcal{O}^{(v)}_{\ell\psi} &\equiv c^{(v)}_{\ell\psi}\,\bar{\ell}\gamma^\mu\gamma_5\ell\bar{\psi}\gamma^\nu\gamma_5 T^a\psi G^a_{\mu\nu}\,,
\end{aligned}\tag{5.19}$$

while the ones for photonic terms are

$$\begin{aligned}
\mathcal{O}^{(w)}_{\ell\psi} &\equiv c^{(w)}_{\ell\psi}\,\bar{\ell}\gamma^\mu\ell\bar{\psi}\gamma^\nu\psi F_{\mu\nu}\,,\\
\mathcal{O}^{(x)}_{\ell\psi} &\equiv c^{(x)}_{\ell\psi}\,\bar{\ell}\gamma^\mu\gamma_5\ell\bar{\psi}\gamma^\nu\gamma_5\psi F_{\mu\nu}\,.
\end{aligned}\tag{5.20}$$

We list C- and CP-odd chirality-breaking quark quadrilinears in dimension 8 of LEFT, which do not gain any further consideration, in App. C.3.5. These can surely be neglected because, other than all the operators listed above, they do *not* arise from dimension 8 in SMEFT and thus originate from higher-dimensional operators in the SMEFT power counting, which implies a corresponding suppression due to additional inverse powers of

the BSM scale Λ.

5.4 | Conclusion

In this chapter, we provided a complete set of fundamental neutrinoless, flavor-preserving, lepton- and baryon-number-conserving C- and CP-odd quark-level operators in LEFT up to and including mass dimension 8. We have verified the operators from dimension-7 LEFT that were known before, but have also tackled the issue that these operators are chirality-violating, hence carefully taking chirality-conserving operators of mass dimension 8 into account. These may in principle be of the same numerical size as those of dimension 7, because both can arise from operators of dimension 8 of SMEFT; similar observations were made previously for dimension-5 and -6 operators in nucleon EDM analyses. As a consequence, every C- and CP-odd operator we identified is suppressed by $1/\Lambda^4$, with Λ indicating the new-physics scale.
Finally, we remark that by dropping the constraint of flavor-conservation, C- and CP-odd operators already appear at dimension 6 in LEFT, as similarly suggested in Ref. [156]. However, corresponding observables may not be distinguished easily from C or CP violation from the weak interaction.

Chapter 6

C- and CP-violating chiral perturbation theory

Some effort has been devoted to constructing chiral effective theories from underlying quark-level operators in SMEFT or LEFT, to access BSM phenomena including mesonic interactions below the hadronic scale of $\Lambda_\chi \approx 1.2\,\text{GeV}$. Most of these works rely (implicitly) on the spurion analysis introduced in the work of Gasser and Leutwyler [115, 116] and were for instance applied to neutrinoless double beta decays [168–171], baryon- and lepton-number-violating interactions [172–177], neutron–antineutron oscillation [178], CP violation in axion interactions [153], EDM analyses in the chiral $SU(2)$ case [114, 159, 160, 179], or in Lorentz- and CPT-violating extensions of the SM [180–182]. However, probably due to the missing set of ToPe operators on the quark level, a rigorous and complete derivation of C- and CP-violating mesonic operators is still missing in the literature. Thus, this chapter aims at the translation of the C- and CP-odd LEFT from Ch. 5 to mesonic operators and their applications. For this endeavor we rely on the well-established techniques from chiral perturbation theory (χPT).

At this point we would like to emphasize the importance of the effective field theory (EFT) approaches applied in this thesis. The breakdown of different energy scales in the EFT spirit is essential to incorporate the appropriate suppression of ToPe forces in terms of the BSM scale Λ, the Higgs vev v, and hadronic scale Λ_χ. Furthermore, given the unknown underlying mechanism above the scale Λ, the use of χPT in analogy to its usual application in the non-perturbative realm of QCD is inevitable. We will confirm in the following that ToPe operators necessarily are of higher dimension than, e.g., the lowest-dimensional T-odd and P-odd operators that can generate EDMs; EFT naturalness arguments, both in SMEFT and LEFT, therefore suggest the former to be further suppressed compared to the latter, and hence more difficult to detect. The motivation to undertake the present study at this point is clearly experiment-driven: the interpretation of new, improved limits on C- and CP-violating effects requires a dedicated theory framework, which we here provide. Even if new measurements continue to be essentially null tests, they can be viewed as tests of the SMEFT or LEFT picture of BSM physics, which is especially important when compared to similar EFT approaches in EDM analyses mentioned above.

In Sect. 6.1 we introduce the concepts of χPT in the SM and apply them to dimension-7 and -8 operators of the LEFT by introducing new sets sources fields. In Sect. 6.2 the ToPe chiral theory is taken to the large-N_c limit, allowing for a consistent description of the η'. Finally, we sketch the application of our formalism to various flavor-conserving decays of η and η' mesons in Sect. 6.3 and close with a brief summary in Sect. 6.4.

6.1 | Construction of effective C- and CP-violating chiral Lagrangians

In the following we summarize and extend the principles of matching between LEFT and χPT operators to obtain a model-independent effective $SU(3)$ theory for C and CP violation in flavor-conserving light-meson interactions, originating from the complete list of C- and CP-odd operators worked out in the previous chapter. We refer to this theory as T-odd, P-even chiral perturbation theory (ToPeχPT). In particular, we work out the non-trivial matching of quark multilinears with derivative character and couplings to gluons, which is in this sense not included in the current literature, while introducing the formalism in detail. Whenever possible, we restrict the matching to the leading order in the chiral power counting and C and CP violation.
For the sake of clarity, we outline this section as follows. We first introduce the our notation and conventions in Sect. 6.1.1 and summarize the discrete symmetries of each building block of χPT Sect. 6.1.2. Subsequently we explain the matching procedure between LEFT and χPT Sect. 6.1.3. Afterwards we illustrate the principles of matching in detail at the hand of the original dimension-7 operators in LEFT and furthermore translate the dimension-8 operators in Sects. 6.1.4 and 6.1.5, respectively. As a short intermediate summary we provide an overview of the corresponding overall C- and CP-violating Lagrangian in Sect. 6.1.6.

6.1.1 | Chiral perturbation theory: notation and conventions

According to Gasser and Leutwyler [115, 116], the massless QCD Lagrangian $\mathcal{L}^0_{\text{QCD}}$ can be extended by introducing external sources to obtain the most general non-kinetic quark operators, by means of

$$\mathcal{L} = \mathcal{L}^0_{\text{QCD}} + \bar{q}_L \gamma^\mu l_\mu q_L + \bar{q}_R \gamma^\mu r_\mu q_R - \bar{q}_R s q_L - \bar{q}_L s^\dagger q_R + \bar{q}_L \sigma^{\mu\nu} t_{\mu\nu} q_R + \bar{q}_R \sigma^{\mu\nu} t^\dagger_{\mu\nu} q_L \,, \quad (6.1)$$

with the light-quark triplet $q = (u, d, s)^T$, and external sources $r_\mu = r_\mu^\dagger$, $l_\mu = l_\mu^\dagger$, s, and $t_{\mu\nu}$, which are three-dimensional quadratic matrices in flavor space. The tensor source $t_{\mu\nu}$ was first introduced in Ref. [183]. The spontaneous breakdown of the $SU(3)_L \times SU(3)_R \times U(1)_V$ global and continuous gauge group of this theory results in an $SU(3)_V \times U(1)_V$ symmetry, thus generating eight Goldstone bosons ϕ_a as the relevant degrees of freedom. The Goldstone bosons are *not* massless as the chiral symmetry is in addition explicitly broken by the non-vanishing masses of up- and down-quarks.
The chiral theory (for reviews, see, e.g., Refs. [76, 77, 184]), which exhibits a certain power counting in terms of soft momenta and light quark masses, can then be described by the unitary matrix U defined as

$$U = \exp\left(\frac{i\Phi}{F_0}\right) \quad \text{with} \quad \Phi \equiv \lambda_a \phi^a = \begin{pmatrix} \pi^0 + \frac{1}{\sqrt{3}}\eta_8 & \sqrt{2}\pi^+ & \sqrt{2}K^+ \\ \sqrt{2}\pi^- & -\pi^0 + \frac{1}{\sqrt{3}}\eta_8 & \sqrt{2}K^0 \\ \sqrt{2}K^- & \sqrt{2}\bar{K}^0 & -\frac{2}{\sqrt{3}}\eta_8 \end{pmatrix} , \quad (6.2)$$

where $F_0 \lesssim F_\pi = 92.2\,\text{MeV}$ [13] is the pion decay constant in the chiral limit and η_8

the octet part of the η mesons. The matrix $\chi = 2B_0 s$ includes the scalar source and a low-energy coefficient B_0, and the field-strength tensors are given as

$$f_R^{\mu\nu} = \partial^\mu r^\nu - \partial^\nu r^\mu - i[r^\mu, r^\nu]\,, \qquad f_L^{\mu\nu} = \partial^\mu l^\nu - \partial^\nu l^\mu - i[l^\mu, l^\nu]\,. \tag{6.3}$$

The dynamics of the Goldstone bosons is driven by the gauge covariant derivative acting on U and $U^\dagger$ defined as[1]

$$D_\mu U \equiv \partial_\mu U - i r_\mu U + i U l_\mu\,, \qquad D_\mu U^\dagger \equiv \partial_\mu U^\dagger + i U^\dagger r_\mu - i l_\mu U^\dagger\,, \tag{6.4}$$

which is necessary to ensure invariance under local extension of the global gauge transformations.[2] In particular, note that the product rule applies to these derivatives [186], thereby—together with the unitarity of U—inducing the important identity $D_\mu U U^\dagger = -U D_\mu U^\dagger$. To keep the notation as simple as possible, we use the convention that the covariant derivative only acts on the object immediately to its right, by means of $D_\mu U U^\dagger \equiv (D_\mu U) U^\dagger$ and $D_\mu D_\nu U U^\dagger \equiv (D_\mu D_\nu U) U^\dagger$. We remark that the covariant derivative may in principle also act on any combination of chiral building blocks that transforms in the same manner as U or $U^\dagger$, respectively, for instance on $U f_L^{\mu\nu}$ or $U^\dagger f_R^{\mu\nu}$.
Our fundamental building blocks, ordered according to their power counting in soft momenta, transform under $SU(3)_L \times SU(3)_R$ group actions as

$$\begin{aligned}
\mathcal{O}(p^0): &\quad U &&\to R U L^\dagger\,, &\quad U^\dagger &\to L U^\dagger R^\dagger\,,\\
\mathcal{O}(p^1): &\quad D_\mu U &&\to R D_\mu U L^\dagger\,, &\quad D_\mu U^\dagger &\to L D_\mu U^\dagger R^\dagger\,,\\
\mathcal{O}(p^2): &\quad \chi &&\to R \chi L^\dagger\,, &\quad \chi^\dagger &\to L \chi^\dagger R^\dagger\,,\\
\mathcal{O}(p^2): &\quad f_R^{\mu\nu} &&\to R f_R^{\mu\nu} R^\dagger\,, &\quad f_L^{\mu\nu} &\to L f_L^{\mu\nu} L^\dagger\,,
\end{aligned} \tag{6.5}$$

where $L \in SU(3)_L$, $R \in SU(3)_R$ as explicitly given in Eq. (2.45). Any mesonic operator in Standard Model χPT (SMχPT) can be built by coupling these building blocks in all Lorentz-covariant ways that respect the conservation of discrete symmetries C, P, and T, and the invariance under $SU(3)_L \times SU(3)_R$ group actions. The latter condition demands the inclusion of traces in flavor space, which we indicate as $\langle \ldots \rangle$. The lowest-order SMχPT Lagrangian thus yields

$$\mathcal{L}_\chi^{(2)} = \frac{F_0^2}{4} \langle D_\mu U D^\mu U^\dagger \rangle + \frac{F_0^2}{4} \langle \chi U^\dagger + \chi^\dagger U \rangle\,. \tag{6.6}$$

To access mesonic interactions encoded in this Lagrangian, the matrix U can be expanded in a simple Taylor series according to

$$U = \mathbb{1} + \frac{i}{F_0}\Phi - \frac{1}{2F_0^2}\Phi^2 - \frac{i}{6F_0^3}\Phi^3 + \ldots\,. \tag{6.7}$$

[1] Confusion with the LEFT covariant derivative, which includes gluons, should be avoided by the context and the fact we only use the LEFT derivative $\vec{D}_\mu$ in vector notation.

[2] A *local* chiral symmetry is required to ensure that proper chiral Ward identities hold, cf. Ref. [185].

Once the chiral Lagrangian has been built, the external sources can be fixed to their physical values, i.e.,

$$s \mapsto M_q\,, \quad r_\mu \mapsto -eQA_\mu\,, \quad l_\mu \mapsto -eQA_\mu\,, \quad t_{\mu\nu} \mapsto 0\,, \tag{6.8}$$

with the matrices $M_q = \text{diag}(m_u, m_d, m_s)$ and $Q = \text{diag}(2/3, -1/3, -1/3)$. Finally, we quote the equation of motion to leading order [76, 77, 116, 184]

$$D^2UU^\dagger - UD^2U^\dagger - \chi U^\dagger + U\chi^\dagger + \frac{1}{3}\langle \chi U^\dagger - U\chi^\dagger\rangle = 0\,, \tag{6.9}$$

with $D^2 = D_\mu D^\mu$, which proves useful to remove redundancies.

6.1.2 | Discrete space-time symmetries

Similar to Sect. 5.2, we now discuss the transformation properties of the fundamental chiral building blocks under discrete space-time symmetries, which can be derived from those of the underlying quark currents and densities.

The discrete symmetries of the mesons matrix Φ and the external sources r_μ and l_μ are similar to the ones of the hermitian pseudoscalar quark density $i\bar{q}\gamma_5 q$ and the quark currents $\bar{q}_R\gamma_\mu q_R$ and $\bar{q}_L\gamma_\mu q_L$, respectively. This leads, upon suppressing the explicit dependencies on the space-time coordinates, to

$$\begin{aligned} &\Phi \overset{C}{\longleftrightarrow} \Phi^T\,, \quad &&\Phi \overset{P}{\longleftrightarrow} -\Phi\,, \quad &&\Phi \overset{T}{\longleftrightarrow} -\Phi\,, \\ &r_\mu \overset{C}{\longleftrightarrow} -l_\mu^T\,, \quad &&r_\mu \overset{P}{\longleftrightarrow} l^\mu\,, \quad &&r_\mu \overset{T}{\longleftrightarrow} r^\mu\,. \end{aligned} \tag{6.10}$$

To proceed, consider that T is an anti-unitary operator, such that $T : i \to -i$, and that the derivative transforms as $T : \partial_\mu \to -\partial^\mu$. Hence we can conclude from the defining equations of U and $f_{L/R}^{\mu\nu}$, as well as the fact that χ has to have the same discrete symmetries as U, the following transformation properties of our building blocks:[3]

$$\begin{aligned} &U \quad \overset{C}{\longleftrightarrow} U^T\,, \quad &&U \quad \overset{P}{\longleftrightarrow} U^\dagger\,, \quad &&U \quad \overset{T}{\longleftrightarrow} U\,, \\ &D_\mu U \overset{C}{\longleftrightarrow} D_\mu U^T\,, \quad &&D_\mu U \overset{P}{\longleftrightarrow} D^\mu U^\dagger\,, \quad &&D_\mu U \overset{T}{\longleftrightarrow} -D^\mu U\,, \\ &\chi \quad \overset{C}{\longleftrightarrow} \chi^T\,, \quad &&\chi \quad \overset{P}{\longleftrightarrow} \chi^\dagger\,, \quad &&\chi \quad \overset{T}{\longleftrightarrow} \chi\,, \\ &f_{L/R}^{\mu\nu} \overset{C}{\longleftrightarrow} -\left(f_{R/L}^{\mu\nu}\right)^T\,, \quad &&f_{L/R}^{\mu\nu} \overset{P}{\longleftrightarrow} f_{\mu\nu}^{R/L}\,, \quad &&f_{L/R}^{\mu\nu} \overset{T}{\longleftrightarrow} -f_{\mu\nu}^{L/R}\,. \end{aligned} \tag{6.11}$$

Here and in the following we use the definitions $D_\mu U^T \equiv (D_\mu U)^T$ and $D_\mu U^* \equiv (D_\mu U)^*$, respectively. Regarding products of chiral building blocks, these transformations apply to

[3] Literature about the T-transformation of the chiral building blocks is scarce, cf. Refs. [187, 188]. Unfortunately, Ref. [188] adapted the T transformation from Ref. [187] erroneously, by choosing $\Phi \overset{T}{\longleftrightarrow} \Phi$, which would imply that [according to Eq. (6.7)] U is no eigenstate of T. Moreover, Ref. [188] quotes the wrong time reversal of r_μ, l_μ, and $f_{L/R}^{\mu\nu}$, which should transform under T like the physical photon and the photonic field-strength tensor, respectively.

each matrix separately, while the algebraic properties of the trace play a vital role. For convenience we explicitly illustrate the transformation under discrete symmetries at the simple example of $\mathcal{L}_\chi^{(2)}$. Under charge conjugation the Lagrangian transforms as

$$\begin{aligned}\mathcal{L}_\chi^{(2)} \xrightarrow{C} \quad & \frac{F_0^2}{4}\langle D_\mu U^T D^\mu U^*\rangle + \frac{F_0^2}{4}\langle \chi^T U^* + \chi^* U^T\rangle \\ &= \frac{F_0^2}{4}\langle D^\mu U^\dagger D_\mu U\rangle + \frac{F_0^2}{4}\langle U^\dagger \chi + U\chi^\dagger\rangle \\ &= \frac{F_0^2}{4}\langle D_\mu U D^\mu U^\dagger\rangle + \frac{F_0^2}{4}\langle \chi U^\dagger + \chi^\dagger U\rangle\,,\end{aligned} \tag{6.12}$$

and is thus invariant. In the first equality we used that traces are invariant under matrix transposition, leading to the observation that for any operator consisting of the building blocks from Eq. (6.11) C merely reverses the order of the matrices (and flips sign and handedness of $f_{L/R}^{\mu\nu}$), whereas in the second equality we applied the cyclic property of the trace. Analogously, cyclicity renders $\mathcal{L}_\chi^{(2)}$ parity-invariant, while its T transformation is trivial. At this point, note that the terms $\chi U^\dagger$ and $\chi^\dagger U$ are summed without a relative factor to ensure that we have an eigenstate of P. We will make ample use of this observation in the following sections.

6.1.3 | Matching LEFT and χPT: building the chiral basis

Having provided the fundamental building blocks as well as their transformation under $SU(3)_L \times SU(3)_R$ group actions and discrete space-time symmetries C, P, and T, we may now match the C- and CP-violating LEFT operators from Sect. 5.3 onto χPT.

For this endeavour, we begin by regarding our LEFT operators as additional external sources, cf. Eq. (6.1). These sources can be written as general chiral irreducible representations, which for an arbitrary quark multilinear consisting of n bilinears takes the form

$$\mathcal{O} = T_{a_1 b_1 \ldots a_n b_n}(\bar{q}_{X_1}\Delta_1\Gamma_1\hat{\lambda}^1_{a_1 b_1} q_{Y_1})\ldots(\bar{q}_{X_n}\Delta_n\Gamma_n\hat{\lambda}^n_{a_n b_n} q_{Y_n})\,, \tag{6.13}$$

with $\hat{\lambda}^i_{a_i b_i}$ as 3×3 matrices (*not* single matrix elements) projecting out the flavor $a_i, b_i \in \{u, d, s\}$ of each quark bilinear, chiralities $X_i, Y_i \in \{L, R\}$, any combination of Dirac matrices Γ_i, arbitrary operators Δ_i that leave the chiral structure invariant (these may include derivatives acting on quark fields, leptonic terms, as well as photonic or gluonic field-strength tensors), and a coefficient tensor $T \equiv T_{a_1 b_1 \ldots a_n b_n}\hat{\lambda}^1_{a_1 b_1}\ldots\hat{\lambda}^n_{a_n b_n}$, which depends on the quark flavor and includes the Wilson coefficients of the respective LEFT operators. Upon treating the coefficents T of the external sources as spurions with well-defined transformation properties under $SU(3)_L \times SU(3)_R$ group actions, we can render the operators in Eq. (6.13), in which the quarks triplets transform as

$$q_L \to L\, q_L\,, \qquad \bar{q}_L \to \bar{q}_L L^\dagger\,, \qquad q_R \to R\, q_R\,, \qquad \bar{q}_R \to \bar{q}_R R^\dagger\,, \tag{6.14}$$

chirally invariant.[4] This procedure is completely analogous to the inclusion of quark masses using the building block χ.
The only terms in our LEFT operators, cf. Eq. (6.13), that survive (at lowest order in the QED coupling) the transition from energies above the chiral scale Λ_χ to the ones below it, are photonic field-strength tensors and leptonic bilinears encoded in the Δ_i and the spurion T. All other quantites are either too heavy (already accounted for in LEFT, like W- and Z-bosons) or no observable degrees of freedom due to color confinement, as quarks—therefore also derivatives acting on them—and gluons. However, although the latter do not appear as observable quantities in the effective theory, we still have to account for the information on their discrete symmetries and Lorentz structure when constructing the effective theory. For the explicit mapping of quark-level operators to the mesonic level we proceed as follows.

- First, rewrite each LEFT operator in terms of chiral irreps, cf. Eq. (6.13), and identify the spurions and their transformation properties under chiral group actions and C, P, and T.

- Next, attach chiral building blocks to the spurions, respect the initial Lorentz structure of quark–gluon terms (which, at leading order, only includes the contraction with the metric tensor $g_{\mu\nu}$, but at higher orders also with the Levi-Civita symbol $\epsilon_{\alpha\beta\mu\nu}$), and contract flavor indices to form chirally invariant traces in all possible ways at the lowest possible order in chiral power counting, cf. Eq. (6.5). This also includes the product of invariant flavor traces.

- Finally ensure hermiticity and the appropriate discrete symmetries by constraining respective coupling constants (multiplied, if needed, by a factor of i) to be equal up to a sign. These symmetries encode the remaining information from gluons, quark bilinears, and their derivatives that were all in some sense integrated out.

- In order to establish operators at higher chiral orders, one may repeat the above procedure with further insertions of D_μ, $\chi^{(\dagger)}$, and $f_{R,L}^{\mu\nu}$ to build chiral invariants or multiply other chirally invariant traces to the operators obtained at lower orders. In either way, one has to ensure throughout that hermiticity and proper transformations under the discrete symmetries are respected. In principle, higher-order operators can also arise from products of the spurion T [169] or loops of lower-order operators. We restrict the analysis to linear effects in the already strongly suppressed ToPe forces and only work at tree level.

- Make sure to constantly get rid of redundancies by identifying independent and non-vanishing operators.

We furthermore remark that there is no one-to-one correspondence between quark operators with those at the mesonic level and that, as usual when building chiral theories to higher orders, there is no way to know the number of possible operators a priori. One still has to

[4] The matrices L and R should not be mixed up with the chiral projection operators $P_{L,R} = (\mathbb{1} \pm \gamma_5)/2$.

keep in mind that, after building the chiral bases as described above for each LEFT operator, there still remains the question how these operators can be distinguished in experiment, if this is possible at all.
In the following we will denote the mesonic counterpart of any LEFT operator $\mathcal{O}_{\psi\chi}^{(z)}$ by $X_{\psi\chi}^{(z)}$.

6.1.4 | Matching dimension-7 LEFT operators

This section is devoted to providing a detailed discussion of the χPT Lagrangian arising from the C- and CP-odd dimension-7 LEFT quark operators listed in Eq. (5.14) and the semi-leptonic ones from Eq. (5.15).

6.1.4.1 | The quark quadrilinear operator

First we investigate the operator

$$\mathcal{O}_{\psi\chi}^{(a)} = \; c_{\psi\chi}^{(a)}\, \bar{\psi}\overleftrightarrow{D}_\mu\gamma_5\psi\bar{\chi}\gamma^\mu\gamma_5\chi\,. \tag{6.15}$$

In terms of chiral irreps, this operator can analytically be rewritten as

$$\begin{aligned}\mathcal{O}_{\psi\chi}^{(a)} = c_{\psi\chi}^{(a)}\big[&(\bar{q}_L\overleftrightarrow{D}_\mu\lambda^\dagger q_R)(\bar{q}_R\gamma^\mu\lambda_R q_R) - (\bar{q}_R\overleftrightarrow{D}_\mu\lambda q_L)(\bar{q}_R\gamma^\mu\lambda_R q_R)\\ &+ (\bar{q}_R\overleftrightarrow{D}_\mu\lambda q_L)(\bar{q}_L\gamma^\mu\lambda_L q_L) - (\bar{q}_L\overleftrightarrow{D}_\mu\lambda^\dagger q_R)(\bar{q}_L\gamma^\mu\lambda_L q_L)\big]\,,\end{aligned} \tag{6.16}$$

where, compared to Eq. (6.13), we use the abbreviations $\hat{\lambda}_{\psi\psi}^{(\dagger)} \equiv \lambda^{(\dagger)}$, $\hat{\lambda}_{L/R}^{\chi\chi} \equiv \lambda_{L/R}$ and hence keep the dependence on the quark flavor implicit. For convenience we have chosen a notation such that the spurions—which do in our case not contribute to the chiral power counting—transform analogously to the building blocks from Eq. (6.5), i.e.,

$$\begin{aligned}\mathcal{O}(p^0):&\quad \lambda \;\to R\lambda L^\dagger\,, &&\qquad \lambda^\dagger \to L\lambda^\dagger R^\dagger\,,\\ \mathcal{O}(p^0):&\quad \lambda_R \to R\lambda_R R^\dagger\,, &&\qquad \lambda_L \to L\lambda_L L^\dagger\,,\end{aligned} \tag{6.17}$$

such that $\mathcal{O}_{\psi\chi}^{(a)}$ is a chiral invariant. In fact, λ transforms analogously to U or χ, while λ_R transforms, e.g., as $U\lambda^\dagger$ (or as $\lambda U^\dagger$) and λ_L as $\lambda^\dagger U$ (or as $U^\dagger\lambda$).
The discrete symmetries of the λ yield

$$\begin{aligned}&\lambda \;\overset{C}{\longleftrightarrow} \lambda^T\,, && \lambda \;\overset{P}{\longleftrightarrow} \lambda^\dagger\,, && \lambda \;\overset{T}{\longleftrightarrow} \lambda\,,\\ &\lambda_R \overset{C}{\longleftrightarrow} \lambda_L^T\,, && \lambda_R \overset{P}{\longleftrightarrow} \lambda_L\,, && \lambda_R \overset{T}{\longleftrightarrow} \lambda_R\,,\\ &\lambda_L \overset{C}{\longleftrightarrow} \lambda_R^T\,, && \lambda_L \overset{P}{\longleftrightarrow} \lambda_R\,, && \lambda_L \overset{T}{\longleftrightarrow} \lambda_L\,.\end{aligned} \tag{6.18}$$

Once the chiral operator basis is established, each spurion can be set to its physical value, i.e., the respective 3×3 matrix projecting out the correct flavor in each bilinear, or more explicitly $\lambda^{(\dagger)}, \lambda_{L/R} \in \{\mathrm{diag}(1,0,0), \mathrm{diag}(0,1,0), \mathrm{diag}(0,0,1)\}$. This gives rise to the conditions $\lambda = \lambda^\dagger$, $\lambda_L = \lambda_R$, and, for the case $\psi = \chi$, $\lambda = \lambda_L$. Furthermore, note that

$\lambda\lambda_L = \lambda^2 = \lambda$ for $\psi = \chi$ and $\lambda\lambda_L = 0$ for $\psi \neq \chi$.

Assigning the chiral irreps to each of the four summands in Eq. (6.16), we can symbolically write

$$\mathcal{O}^{(a)}_{\psi\chi} = \bar{3}_L \otimes (15_R \oplus 3_R) - 3_L \otimes (\bar{15}_R \oplus \bar{3}_R) + (15_L \oplus 3_L) \otimes \bar{3}_R - (\bar{15}_L \oplus \bar{3}_L) \otimes 3_R \,. \quad (6.19)$$

The group-theoretical derivation of such decompositions into chiral irreps is sketched in App. D. At the mesonic level, these irreps come (a priori) with independent coupling constants, called low-energy constants (LECs), which encode all information about the involved non-perturbative QCD effects. The first summand in the equation above has, for instance, the LEC $g_{\bar{3}_L\otimes(15_R\oplus 3_R)} \equiv g_{\bar{3}_L\otimes 15_R} + g_{\bar{3}_L\otimes 3_R}$. Each of these unknown LECs is common to all χPT operators arising from the same irrep operator of Eq. (6.19). However, chiral symmetry does not fix the relative size of mesonic operators in each single irrep, thus generating additional LECs that have to be determined by external input.

We may now move on to the χPT operator basis and consider only the dominant linear effects in the spurions as higher orders in λ would imply an additional suppression by the small expansion parameter of LEFT.[5] Let us start with the lowest possible order p^0, which only allows for $\lambda^{(\dagger)}$, $\lambda_{L/R}$, and U to occur in the traces. There are two possible ways of arranging the λ: either $\lambda^{(\dagger)}$ and $\lambda_{L/R}$ are part of the same trace, or of two different traces. We cannot multiply by any other traces, as there is no non-constant chirally invariant trace solely consisting of U and $U^\dagger$.[6]

Due to the unitarity of U, the only invariant traces that can be built in the first of the two cases are

$$\begin{aligned} &g^{(a)}_{(15_L\oplus 3_L)\otimes\bar{3}_R} g_0^{(a)} \langle \lambda\lambda_L U^\dagger \rangle \,, \quad g^{(a)}_{\bar{3}_L\otimes(15_R\oplus 3_R)} \hat{g}_0^{(a)} \langle \lambda^\dagger \lambda_R U \rangle \,, \\ &g^{(a)}_{(\bar{15}_L\oplus \bar{3}_L)\otimes 3_R} \tilde{g}_0^{(a)} \langle \lambda_L \lambda^\dagger U \rangle \,, \quad g^{(a)}_{3_L\otimes(\bar{15}_R\oplus \bar{3}_R)} \breve{g}_0^{(a)} \langle \lambda_R \lambda U^\dagger \rangle \,, \end{aligned} \quad (6.20)$$

where $g_0^{(a)}, \tilde{g}_0^{(a)}, \hat{g}_0^{(a)}, \breve{g}_0^{(a)}$ denote LECs, and the superscripts like $g^{(a)}_{(15_L\oplus 3_L)\otimes\bar{3}_R}$ are introduced to distinguish LECs that correspond to the same irrep, but may in principle be different when they are derived from other operators of LEFT. Any linear combination of these traces gives a chiral term consistent with the $SU(3)_L \times SU(3)_R$ symmetry of the underlying LEFT operator, yet still does not account for the discrete space-time symmetries. The inclusion of the correct C, P, and T transformations in the chiral operator implies an appropriate linear combination of these four traces, while the LECs are constrained to be the same up to a sign (multiplied by a factor of i if necessary), as already done for the mass term

[5] Translating each quark bilinear separately from LEFT to χPT has hidden complications. In Ref. [156] this was done to illustrate examples of operators in χPT. In general there is no guarantee for the completeness of the operator basis, neither for the correct assignment of independent LECs nor for finding the lowest contributing order. We thank Peter Stoffer for pointing this out to us. The last of these aspects is also mentioned in Ref. [175]. Moreover, the translation of separate bilinears is doomed to fail if non-trivial color structures occur, as we can only translate color-neutral objects to χPT.

[6] In general, one can neither multiply any additional chirally invariant trace that contains only fields U and less than two derivatives, as all such traces can be brought to the form $\langle D_\mu U U^\dagger \rangle = 0$ using the unitarity of U and the cyclic property of the trace.

$\langle \chi U^\dagger + \chi^\dagger U \rangle$ in the original work of Ref. [115]. Hence the corresponding C- and CP-odd operator takes the form

$$i\big\langle (\lambda\lambda_L U^\dagger + \lambda^\dagger \lambda_R U) - (\lambda_L \lambda^\dagger U + \lambda_R \lambda U^\dagger)\big\rangle\,, \tag{6.21}$$

with only one overall LEC that can conventionally be chosen to be $g^{(a)}_{(15_L\oplus 3_L)\otimes\bar{3}_R} g^{(a)}_0$ or any of the four combination of LECs listed in Eq. (6.20).[7] The expression in each parenthesis is parity-invariant on its own, while the relative minus sign ensures C violation. An imaginary unit in front of the trace is required by hermiticity and the T-odd nature of the initial LEFT operator.[8] Analogously, we find the operator

$$i\langle \lambda U^\dagger - \lambda^\dagger U\rangle\langle \lambda_L - \lambda_R\rangle \tag{6.22}$$

for the case where the spurions appear in two different traces. Unfortunately, both of the operators in Eqs. (6.21) and (6.22) vanish once the spurions are set to their physical values described previously. Hence, we must move to the next higher order $\mathcal{O}(p^2)$ and proceed in the same manner. This order is obviously more intricate, as we have to consider more chiral building blocks from Eq. (6.5). Since the strategy should be clear by now, we directly write down our results for all independent traces of combinations of spurions and chiral building blocks that form hermitian C-, CP-, and T-odd operators that are at the same time chiral and Lorentz invariants and do not vanish after the spurions acquire their physical realizations. Henceforth we will drop all LECs belonging to chiral irreps, like $g^{(a)}_{3_L\otimes(\bar{15}_R\oplus\bar{3}_R)}$, as they can always be absorbed by the relative LECs between each operator. Up to $\mathcal{O}(p^2)$ we obtain:

$$\begin{aligned}
X^{(a)}_{\psi\chi} = \frac{v}{\Lambda^4} c^{(a)}_{\psi\chi}\big[\quad & i g^{(a)}_1 \langle \lambda D_\mu U^\dagger + \lambda^\dagger D_\mu U\rangle\langle \lambda_L D^\mu U^\dagger U + \lambda_R D^\mu U U^\dagger\rangle \\
& + i g^{(a)}_2 \big\langle (\lambda D^2 U^\dagger U \lambda_L U^\dagger + \lambda^\dagger D^2 U U^\dagger \lambda_R U) \\
& \qquad\qquad - (\lambda^\dagger U \lambda_L D^2 U^\dagger U + \lambda U^\dagger \lambda_R D^2 U U^\dagger)\big\rangle \\
& + i g^{(a)}_3 \big\langle (\lambda D_\mu U^\dagger D^\mu U \lambda_L U^\dagger + \lambda^\dagger D^\mu U D_\mu U^\dagger \lambda_R U) \\
& \qquad\qquad - (\lambda^\dagger U \lambda_L D_\mu U^\dagger D^\mu U + \lambda U^\dagger \lambda_R D^\mu U D_\mu U^\dagger)\big\rangle \\
& + i g^{(a)}_4 \big\langle (\lambda D_\mu U^\dagger U \lambda_L D^\mu U^\dagger + \lambda^\dagger D^\mu U U^\dagger \lambda_R D_\mu U) \\
& \qquad\qquad - (\lambda^\dagger D_\mu U \lambda_L U^\dagger D^\mu U + \lambda D^\mu U^\dagger \lambda_R U D_\mu U^\dagger)\big\rangle \\
& + \mathcal{O}(p^4)\big]\,.
\end{aligned} \tag{6.23}$$

[7] In the literature one often introduces a set of (anti-)hermitian chiral building blocks, cf. for instance Refs. [76, 77, 183, 184], which make it easier to get rid of redundancies in higher-order operators. These building blocks are eigenstates of the discrete symmetries and thus already have constraints imposed on the LECs, at least to some extent, built in. However, as we are interested in leading contributions of C- and CP-violating effects, the more historic building blocks quoted in Eq. (6.5) do not have any major disadvantage.

[8] The constraints of hermiticity and the correct T transformation are often correlated.

Keeping the implicit dependence of $\lambda_{L/R}$ and $\lambda^{(\dagger)}$ on the flavor ψ, χ in mind, each of the for summands proportional to the $g_i^{(a)}$ gives in principle rise to nine operators, i.e., one for each combination of flavor indices.
There is also another color contraction for the underlying LEFT operator $\mathcal{O}_{\psi\chi}^{(a)}$; as stated in Ref. [173] this leads to the same operator basis but merely with different LECs. However the latter can always be absorbed by redefining the LECs in Eq. (6.23).

6.1.4.2 | The quark bilinear operator

The matching of

$$\mathcal{O}_{\psi}^{(b)} = c_{\psi}^{(b)} \, \bar{\psi} T^a \sigma^{\mu\nu} \psi F_{\mu\rho} G_{\nu}^{a\rho} \,, \tag{6.24}$$

proceeds in the same manner, but includes further subtleties due to the presence of the photonic and gluonic field-strength tensor. Once more we start with the decomposition in chiral irreps by

$$\mathcal{O}_{\psi}^{(b)} = c_{\psi}^{(b)} \left[\bar{q}_R \Delta_{\mu\nu}^{(b)} \sigma^{\mu\nu} \lambda q_L + \bar{q}_L \Delta_{\mu\nu}^{(b)} \sigma^{\mu\nu} \lambda^\dagger q_R \right] \tag{6.25}$$

with $\Delta_{\mu\nu}^{(b)} \equiv T^a G_{\nu}^{a\rho} F_{\mu\rho}$, $\hat{\lambda}_{\psi\psi}^{(\dagger)} \equiv \lambda^{(\dagger)}$ with the same transformations under the gauge group action and discrete symmetries as quoted in Eqs. (6.17) and (6.18). Again, when setting the spurions to their physical values we can apply $\lambda = \lambda^\dagger$.
The quark–gluon structure of this operator is a Lorentz tensor coupling to the photonic field-strength tensor $F_{\mu\nu}$. If we allow for further interactions of the photon with quarks, $F_{\mu\nu}$ has to be treated in the same manner as $G_{\mu\nu}$ in the course of our matching procedure. However, these contributions are suppressed by the QED coupling α. Working at lowest order in α, $F_{\mu\nu}$ on its own cannot contribute to hadronic states and can thus be considered a fixed external source. In this case the corresponding χPT operator for $\mathcal{O}_{\psi}^{(b)}$ has to take the form

$$X_{\psi}^{(b)} = \frac{v}{\Lambda^4} c_{\psi}^{(b)} \left(X_{\psi}^{(b)}\right)^{\mu\nu} F_{\mu\nu} \,, \tag{6.26}$$

with a mesonic Lorentz tensor $\left(X_{\psi}^{(b)}\right)^{\mu\nu}$ that includes the traces over spurions and chiral building blocks.[9] As a consequence $\left(X_{\psi}^{(b)}\right)^{\mu\nu}$ must not be symmetric under $\mu \leftrightarrow \nu$ and $X_{\psi}^{(b)}$ has to be at least of chiral order p^4.[10] In accordance with Ref. [189], the gluon in Eq. (6.24), which is a chiral singlet, merely enters $X_{\psi}^{(b)}$ as an overall constant that can—together with all unknown non-perturbative QCD effects—be absorbed in the LECs. Apart from this, the external source $F_{\mu\nu}$ already reproduces the correct discrete symmetries of the operator $\mathcal{O}_{\psi}^{(b)}$, such that $\left(X_{\psi}^{(b)}\right)^{\mu\nu}$ has to be matched to an operator that preserves C, P, and T separately. As we search for a Lorentz tensor at lowest possible order, we either have to build the chiral operator with two derivatives acting on matrices $U^{(\dagger)}$ or one field-strength tensor $f_{L/R}^{\mu\nu}$. In the first of these cases both derivatives have to enter the same trace, as a trace without

[9] As for any external source one can in general take derivatives of $F_{\mu\nu}$. However, these derivatives can be shifted into the hadronic part of $X_{\psi}^{(b)}$ by partial integration.

[10] We need at least two Lorentz indices, which according to Eq. (6.5) result in one power in the chiral counting each, to build $\left(X_{\psi}^{(b)}\right)^{\mu\nu}$. Moreover, we know that $F_{\mu\nu}$ is of order p^2.

spurions and only one derivative, i.e., $\langle D^\mu U U^\dagger \rangle$, vanishes. However, as we have only one spurion, these single traces are always symmetric under the exchange $\mu \leftrightarrow \nu$, which can easily be seen using $D^\mu U D^\nu U^\dagger = -(U D^\mu U^\dagger)(U D^\nu U^\dagger)$. For the remaining option with $f_{L/R}^{\mu\nu}$ the relative signs within each trace are fixed by the correct C transformation. These relative signs lead to a cancellation of the respective traces, since $\lambda^{(\dagger)}$ and $f_{L/R}^{\mu\nu}$ are diagonal and therefore commute, and furthermore for physical values $\lambda = \lambda^\dagger$ and $f_L^{\mu\nu} = f_R^{\mu\nu}$. Hence, there is no non-vanishing contribution to $X_\psi^{(b)}$ at order p^4. To find chiral analogs of the LEFT operator $\mathcal{O}_\psi^{(b)}$ we must extend our search to operators at order p^6. However, the derivation of the complete operator set at this order is beyond the scope of our analysis. Although $X_\psi^{(b)}$ is suppressed in the chiral power counting compared to the one found in Eq. (6.23), it may still be of relevance for physical applications, as it can contribute with a different field content and different quantum numbers, e.g., partial waves.
Remember, throughout we will, for *all* operators, work at the lowest order in α and hence treat $F_{\mu\nu}$[11] and semi-leptonic bilinears as fixed external sources.

6.1.4.3 | Semi-leptonic operators

Starting with $\mathcal{O}_{\ell\psi}^{(c)}$, we can in this case match the quark–gluon structure, which is simply given by the axialvector current $\bar\psi\gamma^\mu\gamma_5\psi$, onto χPT by identifying traces built from the spurions $\lambda_{L/R}$ that are Lorentz vectors and have the signature $CPT = +-+$. The operator complying with these requirements is

$$X_{\ell\psi}^{(c)} = \frac{v}{\Lambda^4} c_{\ell\psi}^{(c)} g_1^{(c)} \left(\bar\ell \overleftrightarrow{D}_\mu \gamma_5 \ell\right) i\langle \lambda_L D^\mu U^\dagger U - \lambda_R D^\mu U U^\dagger \rangle + \mathcal{O}(p^4)\,. \tag{6.27}$$

Regarding the mesonic analog of $\mathcal{O}_{\ell\psi}^{(d)}$, it can be easily checked that there is no contribution to $X_{\ell\psi}^{(d)}$ at $\mathcal{O}(p^2)$.

6.1.5 | Matching dimension-8 LEFT operators

In this section we quote our results for the χPT expressions derived from the dimension-8 quark level in LEFT. Again we restrict the chiral basis to linear contributions in $1/\Lambda^4$, lowest order in α, as well as to $\mathcal{O}(p^2)$ for gluonic operators and $\mathcal{O}(p^4)$ for photonic and photo-gluonic ones, or in other words the lowest order for each contribution.

6.1.5.1 | Gluonic operators

There is only one leading-order contribution to $X_\psi^{(e)}$

$$\frac{c_\psi^{(e)}}{\Lambda^4} i\langle \left(\lambda_L D^2 U^\dagger U + \lambda_R D^2 U U^\dagger\right) - \left(\lambda_L U^\dagger D^2 U + \lambda_R U D^2 U^\dagger\right)\rangle + \mathcal{O}(p^4), \tag{6.28}$$

[11] If we allow $F_{\mu\nu}$ to hadronize, every of our remaining LEFT operators with a photonic field-strength tensor maps onto the same χPT expression as a corresponding gluonic one, but with different LECs and an additional suppression in α.

which vanishes for physical values of the spurions as demanded by the equations of motion (6.9). Thus $X_\psi^{(e)}$ starts at the next higher order. We refrain from deriving the numerous contributions of higher orders at this early stage in the analysis of ToPe operators and proceed similarly for all other operators.
The LEFT operators $\mathcal{O}^{(f,g,h,i,j)}$ differ only in their color contractions and their vector or axialvector Dirac structure and therefore map to the same χPT operator, but with different LECs. They cannot be distinguished at the mesonic level and give rise to the operator

$$\begin{aligned} X_{\psi\chi}^{(f,g,h,i,j)} =& \frac{1}{\Lambda^4} c_{\psi\chi}^{(f,g,h,i,j)} \\ &\times \Big[i g_1^{(f,g,h,i,j)} \big\langle \big(\lambda_L U^\dagger D^2 U U^\dagger \tilde\lambda_R U + \lambda_R U D^2 U^\dagger U \tilde\lambda_L U^\dagger\big) \\ &\qquad - \big(\tilde\lambda_R U D^2 U^\dagger U \lambda_L U^\dagger + \tilde\lambda_L U^\dagger D^2 U U^\dagger \lambda_R U\big)\big\rangle \\ &+ i g_2^{(f,g,h,i,j)} \big\langle \big(\lambda_L D_\mu U^\dagger U D^\mu U^\dagger \tilde\lambda_R U + \lambda_R D_\mu U U^\dagger D^\mu U \tilde\lambda_L U^\dagger\big) \\ &\qquad - \big(\lambda_L U^\dagger \tilde\lambda_R D_\mu U U^\dagger D^\mu U + \lambda_R U \tilde\lambda_L D_\mu U^\dagger U D^\mu U^\dagger\big)\big\rangle \\ &+ i g_3^{(f,g,h,i,j)} \big\langle \big(\lambda_L D^2 U^\dagger \tilde\lambda_R U + \lambda_R D^2 U \tilde\lambda_L U^\dagger\big) \\ &\qquad - \big(\tilde\lambda_R D^2 U \lambda_L U^\dagger + \tilde\lambda_L D^2 U^\dagger \lambda_R U\big)\big\rangle \\ &+ i g_4^{(f,g,h,i,j)} \big\langle \lambda_L U^\dagger \tilde\lambda_R U - \lambda_R U \tilde\lambda_L U^\dagger\big\rangle \big\langle \chi^\dagger U - \chi U^\dagger\big\rangle \\ &+ \mathcal{O}(p^4)\Big], \end{aligned} \tag{6.29}$$

where we defined the products of Wilson coefficients and LECs by $c_{\psi\chi}^{(f,g,h,i,j)} g_i^{(f,g,h,i,j)} \equiv \sum_{z=f,g,h,i,j} c_{\psi\chi}^{(z)} g_i^{(z)}$. We will use this notation throughout for any combination of indices. The diagonal matrices $\lambda_{L/R}(\tilde\lambda_{L/R})$ project out the flavor $\psi(\chi)$ in complete analogy to the definitions in the previous sections. Some terms can be discarded using $\big\langle D^2 U U^\dagger - D^2 U^\dagger U\big\rangle = D_\mu\big(\big\langle D^\mu U U^\dagger - D^\mu U^\dagger U\big\rangle\big) = 0$, which can also easily be deduced from Eq. (6.9). Analogously, $\mathcal{O}^{(k)}$ and $\mathcal{O}^{(l)}$ can be projected onto one single mesonic operator. The peculiarity of these quadrilinears is that the physical values of their spurions, let us call them $\hat\lambda_{\psi\chi} \equiv \lambda$ and $\hat\lambda_{\chi\psi} \equiv \tilde\lambda$, appearing in the two contributing bilinears are no eigenstates of hermitian conjugation. To simplify the evaluation we introduce the hermitian and antihermitian combinations $\lambda_\pm = \lambda \pm \tilde\lambda$.[12] When the spurions acquire their physical values, we can set $\lambda_+^\dagger = \lambda_+$, $\lambda_-^\dagger = -\lambda_-$, $\lambda_\pm \lambda_\pm^\dagger = \mathbb{1}$, and $\lambda_+\lambda_- = -\lambda_-\lambda_+$, independently of their explicit flavor indices. Moreover, the $\lambda_\pm$ are real and thus $\lambda_\pm^T = \lambda_\pm^\dagger$. As λ and $\tilde\lambda$ transform according to the first line in Eq. (6.18), the discrete symmetries of $\lambda_\pm$ become

$$\lambda_\pm \xleftrightarrow{C} \lambda_\pm^T, \qquad \lambda_\pm \xleftrightarrow{P} \pm\lambda_\pm^\dagger, \qquad \lambda_\pm \xleftrightarrow{T} \lambda_\pm. \tag{6.30}$$

The minus sign for the parity transform of λ_- may be unintuitive, but compensates for the fact that λ_- is anti-hermitian, i.e., after inserting the physical values λ_- is invariant under parity as it should. With this new set of spurions—and noting that the antisymmetry of

[12] Going back to the irreducible representation of a general quark multilinear from Eq. (6.13), this redefinition of the spurions merely leads to another redefinition of the LECs.

the LEFT operator under $\psi \leftrightarrow \chi$ demands that one bilinear includes $\lambda_+^{(\dagger)}$ while the other one has to contain $\lambda_-^{(\dagger)}$—we can evaluate the χPT analogs of $\mathcal{O}_{\psi\chi}^{(k,l)}$ in the familiar way. However, we do not find any operator at chiral order p^2 and hence ignore the contribution of $X_{\psi\chi}^{(k,l)}$ for now.
Analogously, the symmetry of the operator $\mathcal{O}_{\psi\chi}^{(m)}$ under $\psi \leftrightarrow \chi$ demands that either both quark bilinears include all possible combinations of the spurions $\lambda_-^{(\dagger)}\lambda_-^{(\dagger)}$ or of $\lambda_+^{(\dagger)}\lambda_+^{(\dagger)}$. Again there is no non-vanishing C- and CP-odd mesonic operator at leading order.

6.1.5.2 | Photonic operators

As previously seen for the gluonic operators, we can again match several photonic operators from LEFT to the same χPT operator upon redefining the LECs. Hence the mesonic counterpart of the operator $\mathcal{O}_{\psi\chi}^{(n,o,p,q)}$ yields to lowest order

$$\begin{aligned} X_{\psi\chi}^{(n,o,p,q)} =& \frac{1}{\Lambda^4} c_{\psi\chi}^{(n,o,p,q)} \\ & \Big[g_1^{(n,o,p,q)} \epsilon_{\alpha\beta\mu\nu} \big\langle \big(\lambda_L U^\dagger \tilde{\lambda}_R f_R^{\alpha\beta} U - \lambda_R U \tilde{\lambda}_L f_L^{\alpha\beta} U^\dagger \big) \\ & \qquad + \big(\tilde{\lambda}_R U \lambda_L U^\dagger f_R^{\alpha\beta} - \tilde{\lambda}_L U^\dagger \lambda_R U f_L^{\alpha\beta} \big) \big\rangle \\ & + g_2^{(n,o,p,q)} \big\langle \lambda_L D_\mu U^\dagger U + \lambda_R D_\mu U U^\dagger \big\rangle \big\langle \tilde{\lambda}_L D_\nu U^\dagger U + \tilde{\lambda}_R D_\nu U U^\dagger \big\rangle \\ & + g_3^{(n,o,p,q)} \big\langle \lambda_L D_\mu U^\dagger U - \lambda_R D_\mu U U^\dagger \big\rangle \big\langle \tilde{\lambda}_L D_\nu U^\dagger U - \tilde{\lambda}_R D_\nu U U^\dagger \big\rangle \Big] \\ & \times F^{\mu\nu} + \mathcal{O}(p^6) \,. \end{aligned} \tag{6.31}$$

Note that the ϵ-tensor flips sign under P and T. The photonic LEFT quadrilinear $\mathcal{O}_{\psi\chi}^{(r)}$, mixing quark flavors in each bilinear, can again be conveniently matched using the (anti-) hermitian spurions $\lambda_\pm^{(\dagger)}$. But once more, we do not find any operator up to and including chiral order p^4.

6.1.5.3 | Photo-gluonic operators

Both photo-gluonic operators $\mathcal{O}_\psi^{(s,t)}$ map onto the same χPT expression

$$X_\psi^{(s,t)} = \frac{1}{\Lambda^4} c_\psi^{(s,t)} g_1^{(s,t)} \epsilon_{\alpha\beta\mu\nu} \big\langle \lambda_L U^\dagger f_R^{\alpha\beta} U - \lambda_R U f_L^{\alpha\beta} U^\dagger \big\rangle F^{\mu\nu} + \mathcal{O}(p^6) \,. \tag{6.32}$$

6.1.5.4 | Semi-leptonic operators

We find that the C- and CP-violating contributions from the gluonic semi-leptonic operators $\mathcal{O}_{\ell\psi}^{(u)}$, $\mathcal{O}_{\ell\psi}^{(v)}$ vanish at $\mathcal{O}(p^2)$, while the photonic ones $\mathcal{O}_{\ell\psi}^{(w)}$, $\mathcal{O}_{\ell\psi}^{(x)}$ give rise to

$$X_{\ell\psi}^{(w)} = \frac{1}{\Lambda^4} c_{\ell\psi}^{(w)} g_1^{(w)} \, i \big\langle \lambda_L D_\nu U^\dagger U + \lambda_R D_\nu U U^\dagger \big\rangle \bar{\ell} \gamma_\mu \ell F^{\mu\nu} + \mathcal{O}(p^6) \tag{6.33}$$

and

$$X^{(x)}_{\ell\psi} = \frac{1}{\Lambda^4} g_1^{(x)} c^{(x)}_{\ell\psi}\, i\langle \lambda_L D_\nu U^\dagger U - \lambda_R D_\nu U U^\dagger\rangle \bar{\ell}\gamma_\mu\gamma_5\ell F^{\mu\nu} + \mathcal{O}(p^6)\,, \tag{6.34}$$

respectively.

6.1.6 | Summary of the effective C- and CP-odd Lagrangian

In the preceding sections we derived the lowest possible contributing order of mesonic operators for all flavor-conserving, neutrinoless C- and CP-violating sources (except purely leptonic ones) that preserve baryon and lepton number up to dimension 8 in LEFT. Working to lowest order in the QED coupling α, i.e., treating photons and leptons as fixed external sources, these contributions start at $\mathcal{O}(p^2)$ for gluonic and semi-leptonic operators and at $\mathcal{O}(p^4)$ for photonic ones. We identified that the 24 LEFT operators $\mathcal{O}^{(a)}_{\psi\chi}, \ldots, \mathcal{O}^{(x)}_{\ell\chi}$ (without counting different flavor combinations) listed in Eqs. (5.14)–(5.19) give in general rise to 15 different groups of operators $X^{(z)}$ on the mesonic level, which build the full chiral Lagrangian

$$\begin{aligned}\mathcal{L}_{\not{C}P\not{T}} = \sum_{\psi,\chi,\ell} \Big[& X^{(a)}_{\psi\chi} + X^{(b)}_{\psi} + X^{(c)}_{\ell\psi} + X^{(d)}_{\ell\psi} + X^{(e)}_{\psi\chi} + X^{(f,g,h,i,j)}_{\psi\chi} + X^{(k,l)}_{\psi\chi} + X^{(m)}_{\psi\chi} \\ & + X^{(n,o,p,q)}_{\psi\chi} + X^{(r)}_{\psi\chi} + X^{(s,t)}_{\psi} + X^{(u)}_{\ell\psi} + X^{(v)}_{\ell\psi} + X^{(w)}_{\ell\psi} + X^{(x)}_{\ell\psi} \Big]\,.\end{aligned} \tag{6.35}$$

In this Lagrange density, the terms $X^{(a)}_{\psi\chi}$, $X^{(b)}_{\psi}$, $X^{(c)}_{\ell\psi}$, $X^{(d)}_{\ell\psi}$ originate from dimension 7 of LEFT, the rest from dimension 8. The contributions of order p^2 for the gluonic operators $X^{(a)}_{\psi\chi}$, $X^{(f,g,h,i,j)}_{\psi\chi}$ can be found in Eqs. (6.23) and (6.29), respectively, while $X^{(e)}_{\psi\chi}$, $X^{(k,l)}_{\psi\chi}$, $X^{(m)}_{\psi\chi}$ start at higher orders. The photonic operator $X^{(n,o,p,q)}_{\psi\chi}$ is mapped to its lowest possible order p^4 in Eq. (6.31), whereas $X^{(r)}_{\psi\chi}$ first appears at $\mathcal{O}(p^6)$. For the photo-gluonic operators we find that $X^{(b)}_{\psi}$ only starts at $\mathcal{O}(p^6)$, and $X^{(s,t)}_{\psi}$ at $\mathcal{O}(p^4)$ is given in Eq. (6.32). Finally, the lowest possible contribution at $\mathcal{O}(p^2)$ to the semi-leptonic operators $X^{(c)}_{\ell\psi}$, $X^{(w)}_{\ell\psi}$, $X^{(x)}_{\ell\psi}$ are listed in Eqs. (6.27), (6.33), and (6.34), while $X^{(d)}_{\ell\psi}$, $X^{(u)}_{\ell\psi}$, $X^{(v)}_{\ell\psi}$ start at higher orders.

6.2 | The large-N_c extension

So far, the framework of ToPeχPT covers the sector of the meson octet. It can, however, be generalized to include the singlet η', whose mass $M_{\eta'}$ remains non-vanishing in the chiral limit due to the $U(1)_A$ anomaly, in a straightforward manner. Taking the number of colors N_c to be large, this anomaly is suppressed, so that the η' is rendered massless and takes the role of the ninth Goldstone boson.

As a consequence for the perturbative treatment in the effective low-energy theory, not only the momentum p but also $M_{\eta'}$ needs to be considered as small. This can be achieved by simultaneously expanding the chiral Lagrangian in soft momenta, light quark masses, and powers of $1/N_c$. One hence introduces a small counting parameter δ and uses

$$p = \mathcal{O}(\sqrt{\delta})\,, \qquad m = \mathcal{O}(\delta)\,, \qquad 1/N_c = \mathcal{O}(\delta)\,. \tag{6.36}$$

The large-N_c extension of SMχPT has been subject to many previous analyses, see for instance Refs. [190–198] and the numerous references therein. As these considerations rely on general gluon dynamics, we can apply the large-N_c extension in this section to ToPeχPT without much trouble, and refer to the abovementioned works for further details.

To include the singlet in our formalism at the level of the general Lagrangian from Eq. (6.1), we add the term $\mathcal{L}_{N_c} \equiv \theta\omega$ with a new external source θ, whose physical value is the QCD vacuum angle θ_{QCD}, and the winding number density $\omega = g^2/(32\pi^2) G^a_{\mu\nu}\tilde{G}^{a\,\mu\nu}$.[13] The first modifications we have to make in order to enhance the $SU(3)_L \times SU(3)_R$ symmetry to $U(3)_L \times U(3)_R$ is to replace

$$U \mapsto \bar{U} = e^{i\varphi} U \,, \tag{6.37}$$

where $\varphi \equiv \sqrt{2/3}\,\eta_0/F_0$, and the new chiral transformation reads $\bar{U} \to R\bar{U}L^\dagger$ with $L \in U(3)_L$ and $R \in U(3)_R$. The remaining chiral building blocks stay unchanged, except that they transform with L, R as elements of $U(3)_{L,R}$ instead of $SU(3)_{L,R}$. We shall not introduce a new notation for the large-N_c case of these building blocks, which is unambiguously fixed by the use of either U or $\bar{U}$ in each operator. At leading order, the octet and singlet components η_8 and η_0 are related to the physical mass eigenstates by the single-angle mixing scheme

$$\begin{pmatrix} \eta_8 \\ \eta_0 \end{pmatrix} = \begin{pmatrix} \cos\theta & \sin\theta \\ -\sin\theta & \cos\theta \end{pmatrix} \begin{pmatrix} \eta \\ \eta' \end{pmatrix} . \tag{6.38}$$

Henceforth we work with the ideal mixing angle $\theta = \arcsin(-1/3)$, so that

$$\bar{U} = \exp\left(\frac{i\bar{\Phi}}{F_0}\right) \quad \text{with} \quad \bar{\Phi} = \begin{pmatrix} \frac{1}{\sqrt{3}}\eta' + \sqrt{\frac{2}{3}}\eta + \pi^0 & \sqrt{2}\pi^+ & \sqrt{2}K^+ \\ \sqrt{2}\pi^- & \frac{1}{\sqrt{3}}\eta' + \sqrt{\frac{2}{3}}\eta - \pi^0 & \sqrt{2}K^0 \\ \sqrt{2}K^- & \sqrt{2}\bar{K}^0 & \frac{2}{\sqrt{3}}\eta' - \sqrt{\frac{2}{3}}\eta \end{pmatrix} . \tag{6.39}$$

For convenience and later use we quote φ in terms of the physical η and η' fields, i.e.,

$$\varphi = \frac{\sqrt{2}}{3\sqrt{3}F_0}\,\eta + \frac{4}{3\sqrt{3}F_0}\,\eta' \,. \tag{6.40}$$

We have to introduce new building blocks from the pure singlet contribution, which are

$$(\varphi + \theta) \to (\varphi + \theta) \,, \qquad D_\mu\varphi \to D_\mu\varphi \,, \qquad D_\mu\theta \to D_\mu\theta \,, \tag{6.41}$$

with

$$D_\mu\varphi \equiv \partial_\mu\varphi - 2\langle a_\mu\rangle \quad \text{and} \quad D_\mu\theta \equiv \partial_\mu\theta + 2\langle a_\mu\rangle \,, \tag{6.42}$$

where $2\langle a_\mu\rangle = \langle r_\mu - l_\mu\rangle$ is the singlet axial current discussed in more detail in Ref. [197].[14]

[13] Note that none of the LEFT operators considered in this work can contribute to a singlet under $SU(3)_L \times SU(3)_R$, so that $\mathcal{L}_{N_c}$, which arises naturally from QCD, is indeed the only external source with the desired transformation property we can add to Eq. (6.1).

[14] More precisely, we have $\varphi \to \varphi - i\ln(\det R) + i\ln(\det L)$ and $\theta \to \theta + i\ln(\det R) - i\ln(\det L)$, so that

With these new building blocks we cannot only construct completely new operators, e.g., by contracting a vector operator with $D_\mu\varphi$ or $D_\mu\theta$, but can also multiply any Lorentz - invariant combination of them to any operator without affecting the transformation under $U(3)_L \times U(3)_R$. As φ and θ transform as $CPT = + - -$ [196], odd powers of them will change the discrete symmetries of the overall operator.

However, we do not have to consider the infinite amount of all new operators that arise from insertions of the elements in Eq. (6.41), as the latter affect the power counting in δ, which can be summarized as follows. Traceless operators are subject to purely gluonic interactions, which scale at leading order as N_c^2. Each trace in flavor space originates from one quark loop, leading to a suppression of $1/N_c$. Moreover each φ and θ counts as another factor $1/N_c$. Hence the generalized power counting in large-N_c χPT, i.e., the order of δ, can be understood as

$$\mathcal{O}_\delta = -2 + N_{\text{tr}} + \frac{1}{2}N_\chi + N_\varphi\,, \tag{6.43}$$

where N_{tr} denotes the number of traces, N_φ indicates the power of φ and θ, and $N_\chi \equiv N_p + 2N_m$ is the power counting in standard χPT as described in Sect. 6.1.1, which keeps track of the power of soft momenta N_p and the power of light quark masses N_m. This power counting allows for four different contributions at order δ^0, namely $(N_{\text{tr}}, N_\chi, N_\varphi) \in \{(2,0,0),(1,2,0),(1,0,1),(0,0,2)\}$, out of which only $(1,2,0)$ can contribute to a C-odd operator. Hence the leading contribution to all gluonic operators at large N_c can directly be read off the respective contributions in standard ToPeχPT, which consist of one single trace. Similarly, all photonic and photo-gluonic operators start at $\mathcal{O}(\delta)$ in large-N_c, as they require $N_\chi \geq 4$ and can thus be obtained by the corresponding ToPeχPT operators with $N_{\text{tr}} = 1$, $N_\varphi = 0$. Considering the matching of LEFT operators that initially had no chiral counterpart at $\mathcal{O}(p^2)$ for $N_c = 3$, the chiral singlets from Eq. (6.41) allow for new chirally invariant operators in the large-N_c limit, so that these LEFT sources may indeed show up at $\mathcal{O}(p^2)$ but at higher order in δ.

φ and θ are not invariant on their own. However, $D_\mu\varphi$ and $D_\mu\theta$ are still invariant as separate quantities.

For convenience we quote the order δ^0 analog to Eq. (6.35) in the large-N_c limit as

$$\begin{aligned}\bar{\mathcal{L}}_{\not C P \not T} = \frac{iv}{\Lambda^4}\sum_{\psi,\chi,\ell}\Big[\quad & c^{(a)}_{\psi\chi}\bar{g}^{(a)}_2\big\langle(\lambda D^2\bar{U}^\dagger\bar{U}\lambda_L\bar{U}^\dagger+\lambda^\dagger D^2\bar{U}\bar{U}^\dagger\lambda_R\bar{U})-\text{h.c.}\big\rangle\\ &+c^{(a)}_{\psi\chi}\bar{g}^{(a)}_3\big\langle(\lambda D_\mu\bar{U}^\dagger D^\mu\bar{U}\lambda_L\bar{U}^\dagger+\lambda^\dagger D^\mu\bar{U}D_\mu\bar{U}^\dagger\lambda_R\bar{U})-\text{h.c.}\big\rangle\\ &+c^{(a)}_{\psi\chi}\bar{g}^{(a)}_4\big\langle(\lambda D_\mu\bar{U}^\dagger\bar{U}\lambda_L D^\mu\bar{U}^\dagger+\lambda^\dagger D^\mu\bar{U}\bar{U}^\dagger\lambda_R D_\mu\bar{U})-\text{h.c.}\big\rangle\\ &+c^{(c)}_{\ell\psi}\bar{g}^{(c)}_1\,\bar{\ell}\overleftrightarrow{D}_\mu\gamma_5\ell\big\langle\lambda_L D^\mu\bar{U}^\dagger\bar{U}-\lambda_R D^\mu\bar{U}\bar{U}^\dagger\big\rangle\\ &+\frac{1}{v}c^{(f,g,h,i,j)}_{\psi\chi}\bar{g}^{(f,g,h,i,j)}_1\big\langle\big(\lambda_L\bar{U}^\dagger D^2\bar{U}\bar{U}^\dagger\tilde{\lambda}_R\bar{U}+\lambda_R\bar{U}D^2\bar{U}^\dagger\bar{U}\tilde{\lambda}_L\bar{U}^\dagger\big)-\text{h.c.}\big\rangle\\ &+\frac{1}{v}c^{(f,g,h,i,j)}_{\psi\chi}\bar{g}^{(f,g,h,i,j)}_2\big\langle\big(\lambda_L D_\mu\bar{U}^\dagger\bar{U}D^\mu\bar{U}^\dagger\tilde{\lambda}_R\bar{U}+\lambda_R D_\mu\bar{U}\bar{U}^\dagger D^\mu\bar{U}\tilde{\lambda}_L\bar{U}^\dagger\big)-\text{h.c.}\big\rangle\\ &+\frac{1}{v}c^{(f,g,h,i,j)}_{\psi\chi}\bar{g}^{(f,g,h,i,j)}_3\big\langle\big(\lambda_L D^2\bar{U}^\dagger\tilde{\lambda}_R\bar{U}+\lambda_R D^2\bar{U}\tilde{\lambda}_L\bar{U}^\dagger\big)-\text{h.c.}\big\rangle\\ &+\mathcal{O}(\delta)\Big]\,.\end{aligned} \tag{6.44}$$

Interactions at higher order in δ can be obtained by the procedure described above. In the following sections we will refer to the large-N_c limit of a ToPeχPT operator $X^{(z)}_{\psi\chi}$ as $\bar{X}^{(z)}_{\psi\chi}$. As a final remark, all operators in ToPeχPT and its large-N_c extension that only differ by the shift $U\to\bar{U}$ carry the same LECs at leading order, as is the case for the leading order in large-N_c SMχPT [197]. Nevertheless, we will still denote the LECs in the large-N_c theory by $\bar{g}^{(z)}_i$ to be as general as possible.

6.3 | Application to C- and CP-violating decays

Up to now, various experiments have actively searched for C violation in η decays (in the following we will use the abbreviation $\eta^{(\prime)}$ to refer to both η and η'), as in $\eta^{(\prime)}\to 3\gamma$ [199–201], $\eta\to\pi^0\gamma$ [202], $\eta^{(\prime)}\to\pi^0\ell^+\ell^-$ [203–205] and $\eta'\to\eta\ell^+\ell^-$ [204, 205] driven by a single virtual photon, $\eta\to\pi^+\pi^-\gamma$ [206–208], $\eta\to 2\pi^0\gamma$ [201, 209], $\eta\to 3\pi^0\gamma$ [201, 209], and in $\pi^0\to 3\gamma$ [210], without strong empirical evidence for this kind of BSM physics.[15] However, in the foreseeable future the new experimental setups from the REDTOP [38–40] and JEF [41–43] collaborations will search for rare $\eta^{(\prime)}$ decays with an increased accuracy that may allow us to set more stringent bounds on ToPe forces.

The model-independent effective theory derived in the previous sections provides the theoretical foundation to identify the most promising decays to observe and to figure out any, as yet unknown, correlation between different C- and CP-violating transitions. As the sources of the latter are rigorously worked out on the quark level, we can provide the explicit de-

[15] Some of the listed decays may in principle also be driven by C- and P-odd operators, which are not covered by our framework. These contributions have less physical motivation, as they conserve CP, and are beyond the scope of this work. Therefore we assume all decay widths of C-violating amplitudes to originate solely from sources with additional T violation and ignore possible P-violating effects at this stage.

pendence of C- and CP-odd observables on the new-physics scale Λ. To this end, we not only restrict our analysis to pure BSM processes, but also investigate the interference of SM and C-violating contributions for suitable candidates. A list of all decays considered in this work is contained in Table 6.1, which summarizes our results in a compact way. Each C- and CP-odd contribution to these decays, except for $\eta \to 3\pi^0\gamma$, exhibits a unique representation in terms of mesonic degrees of freedom. Identifying these mesonic operators first eases the search for a corresponding ToPeχPT operator that generates the desired transition. These chiral operators in turn can be related to the underlying quark operators. For a consistent treatment of η and η' decays, we will work with ToPeχPT in the large-N_c limit with generalized power counting in δ throughout, as explained in Sect. 6.2. However, we may still quote the power counting in soft momenta p, because it is directly visible in the operators at the mesonic level. As central numeric results of this work we give the theoretical estimates of observables in dependence on Λ (explained in more detail below), while the limits that can be set on Λ with the currently most precise measurements are quoted in the respective sections. In the rest of this manuscript we explain in detail the assumptions and simplifications entering Table 6.1.

First of all, we need to emphasize that the computation of most of the considered decays with ToPeχPT is rather meant to be a proof of principle. As we will see in the following, a rigorous evaluation would require the complete construction of the chiral basis for all C- and CP-odd LEFT operators also including higher orders in ToPeχPT, which leads to a large number of free LECs that cannot be fixed at the present stage. Therefore we do not investigate each single ToPeχPT operator. Instead, we focus on one set of operators that stands out, namely the ones derived from the LEFT source

$$\mathcal{O}^{(a)}_{\psi\chi} = \frac{v}{\Lambda^4}\, c^{(a)}_{\psi\chi}\, \bar{\psi}\overleftrightarrow{D}_\mu \gamma_5 \psi \bar{\chi}\gamma^\mu\gamma_5\chi\,, \tag{6.45}$$

for which, in comparison to Eq. (5.14), we restored the explicit dependence on the EFT scale. This is the *only* LEFT operator able to generate the C- and CP-violating contributions to *all* mesonic decays listed in Table 6.1 at the corresponding leading orders in p. The special feature that makes this operator unique in our analysis and allows us to in particular generate $\eta^{(\prime)} \to \pi^0\pi^+\pi^-$ at lowest order is its compositeness of both spurions $\lambda^{(\dagger)}$ and $\lambda_{L,R}$. These are the only decays, according to the third row in Table 6.1, that occur at lowest order in δ and p.[16]

Comparing the fourth and fifth columns of Table 6.1 we see that in order to set a realistic lower limit on Λ in the TeV range, the biggest chance to find evidence for ToPe forces in future experiments is given by processes including an interference of SM and BSM contributions. This is no surprising result, as the respective observables scale linearly with BSM physics [62], i.e., with $1/\Lambda^4$, as opposed to purely C-odd decays that can only be observed by quadratic effects scaling with $1/\Lambda^8$. Still, one can judge from our numerical results which pure BSM processes are more suitable candidates for experimental setups than others, e.g.,

[16] The remaining non-vanishing terms in the leading-order Lagrangian from Eq. (6.44) contribute either to interactions of the type $\eta'\eta(\pi^+\partial^\mu\pi^- + \pi^-\partial^\mu\pi^+)A_\mu$ or to operators with a larger number of mesons.

Decay	Mesonic operator	Lowest order	Current measurement	Theoretical estimate	Section
$\eta^{(\prime)} \to \pi^0\pi^+\pi^-$	$i\,\eta^{(\prime)}\partial^\mu\pi^0(\pi^+\partial_\mu\pi^- - \pi^-\partial_\mu\pi^+)$	$p^2\,(\delta^0)$	$g_2 = -9.3(4.5)\cdot 10^3/\text{TeV}^2$ [1]	$\lvert g_2\rvert \sim 3\cdot 10^{-4}\,\text{TeV}^2/\Lambda^4$	6.3.1
$\eta' \to \eta\pi^+\pi^-$	$i\,\eta'\partial^\mu\eta(\pi^+\partial_\mu\pi^- - \pi^-\partial_\mu\pi^+)$	$p^2\,(\delta^1)$	$g_1 = 0.7(1.0)\cdot 10^6/\text{TeV}^2$ [1]	$\lvert g_1\rvert \sim 3\cdot 10^{-4}\,\text{TeV}^2/\Lambda^4$	6.3.2
$\eta^{(\prime)} \to \pi^0\gamma^*$	$\partial_\mu\eta^{(\prime)}\,\partial_\nu\pi^0 F^{\mu\nu}$	$p^4\,(\delta^2)$	–	–	6.3.3
$\eta' \to \eta\gamma^*$	$\partial_\mu\eta'\,\partial_\nu\eta F^{\mu\nu}$	$p^4\,(\delta^2)$	–	–	6.3.3
$\eta \to \pi^0 e^+e^-$	$\eta\partial_\mu\pi^0\,\bar{e}\gamma^\mu e$	$p^2\,(\delta^1)$	$\text{BR} < 7.5\cdot 10^{-6}$ [203]	$\text{BR} \sim 7\cdot 10^{-27}\,\text{TeV}^8/\Lambda^8$	6.3.4
$\eta \to \pi^0\mu^+\mu^-$	$\eta\partial_\mu\pi^0\,\bar{\mu}\gamma^\mu\mu$	$p^2\,(\delta^1)$	$\text{BR} < 5\cdot 10^{-6}$ [205]	$\text{BR} \sim 2\cdot 10^{-27}\,\text{TeV}^8/\Lambda^8$	6.3.4
$\eta' \to \pi^0 e^+e^-$	$\eta'\partial_\mu\pi^0\,\bar{e}\gamma^\mu e$	$p^2\,(\delta^1)$	$\text{BR} < 1.4\cdot 10^{-3}$ [204]	$\text{BR} \sim 9\cdot 10^{-28}\,\text{TeV}^8/\Lambda^8$	6.3.4
$\eta' \to \pi^0\mu^+\mu^-$	$\eta'\partial_\mu\pi^0\,\bar{\mu}\gamma^\mu\mu$	$p^2\,(\delta^1)$	$\text{BR} < 6\cdot 10^{-5}$ [205]	$\text{BR} \sim 6\cdot 10^{-28}\,\text{TeV}^8/\Lambda^8$	6.3.4
$\eta' \to \eta e^+e^-$	$\eta'\partial_\mu\eta\,\bar{e}\gamma^\mu e$	$p^2\,(\delta^1)$	$\text{BR} < 2.4\cdot 10^{-3}$ [204]	$\text{BR} \sim 9\cdot 10^{-29}\,\text{TeV}^8/\Lambda^8$	6.3.4
$\eta' \to \eta\mu^+\mu^-$	$\eta'\partial_\mu\eta\,\bar{\mu}\gamma^\mu\mu$	$p^2\,(\delta^1)$	$\text{BR} < 1.5\cdot 10^{-5}$ [205]	$\text{BR} \sim 3\cdot 10^{-29}\,\text{TeV}^8/\Lambda^8$	6.3.4
$\eta \to \pi^+\pi^-\gamma$	$\epsilon_{\alpha\beta\mu\nu}\,\eta\big(\partial^\nu\pi^+\partial^\rho\partial^\mu\pi^- + \partial^\nu\pi^-\partial^\rho\partial^\mu\pi^+\big)\partial_\rho F^{\alpha\beta}$	$p^6\,(\delta^2)$	$A_{LR} = 0.009(4)$ [13]	$\lvert A_{LR}\rvert \sim 5\cdot 10^{-16}\,\text{TeV}^4/\Lambda^4$	6.3.5
$\eta' \to \pi^+\pi^-\gamma$	$\epsilon_{\alpha\beta\mu\nu}\,\eta'\big(\partial^\nu\pi^+\partial^\rho\partial^\mu\pi^- + \partial^\nu\pi^-\partial^\rho\partial^\mu\pi^+\big)\partial_\rho F^{\alpha\beta}$	$p^6\,(\delta^2)$	$A_{LR} = 0.03(4)$ [13]	$\lvert A_{LR}\rvert \sim 1\cdot 10^{-14}\,\text{TeV}^4/\Lambda^4$	6.3.5
$\eta \to \pi^0\pi^0\gamma$	$\epsilon_{\alpha\beta\mu\nu}\,\eta\big(\partial^\nu\pi^0\partial^\rho\partial^\mu\pi^0 + \partial^\nu\pi^0\partial^\rho\partial^\mu\pi^0\big)\partial_\rho F^{\alpha\beta}$	$p^6\,(\delta^3)$	$\text{BR} < 5\cdot 10^{-4}$ [209]	$\text{BR} \sim 1\cdot 10^{-29}\,\text{TeV}^8/\Lambda^8$	6.3.6
$\eta' \to \pi^0\pi^0\gamma$	$\epsilon_{\alpha\beta\mu\nu}\,\eta'\big(\partial^\nu\pi^0\partial^\rho\partial^\mu\pi^0 + \partial^\nu\pi^0\partial^\rho\partial^\mu\pi^0\big)\partial_\rho F^{\alpha\beta}$	$p^6\,(\delta^3)$	–	$\text{BR} \sim 2\cdot 10^{-28}\,\text{TeV}^8/\Lambda^8$	6.3.6
$\eta' \to \eta\pi^0\gamma$	$\epsilon_{\alpha\beta\mu\nu}\,\eta'\partial^\mu\eta\partial^\nu\pi^0 F^{\alpha\beta}$	$p^4\,(\delta^3)$	–	$\text{BR} \sim 2\cdot 10^{-28}\,\text{TeV}^8/\Lambda^8$	6.3.7
$\eta' \to \eta\pi^0\pi^0\gamma$	$\eta'\partial_\mu\eta\pi^0\partial_\nu\pi^0 F^{\mu\nu}$	$p^4\,(\delta^2)$	–	$\text{BR} \sim 2\cdot 10^{-32}\,\text{TeV}^8/\Lambda^8$	6.3.8
$\eta \to 3\pi^0\gamma$	$\partial_\mu\eta\partial_\nu\pi^0\partial_\alpha\pi^0\pi^0\partial^\alpha F^{\mu\nu}$	$p^6\,(\delta^3)$	$\text{BR} < 6\cdot 10^{-5}$ [209]	$\text{BR} \sim 1\cdot 10^{-35}\,\text{TeV}^8/\Lambda^8$	6.3.9
$\eta' \to 3\gamma$	$\epsilon^{\mu\nu\rho\sigma}\partial_\alpha\eta'(\partial^\gamma F^{\alpha\beta})(\partial_\gamma\partial_\beta F_{\rho\sigma})F_{\mu\nu}$	$p^{10}\,(\delta^4)$	$\text{BR} < 1\cdot 10^{-4}$ [199]	$\text{BR} \sim 3\cdot 10^{-35}\,\text{TeV}^8/\Lambda^8$	6.3.10
$\eta \to 3\gamma$	$\epsilon^{\mu\nu\rho\sigma}\partial_\alpha\eta(\partial^\gamma F^{\alpha\beta})(\partial_\gamma\partial_\beta F_{\rho\sigma})F_{\mu\nu}$	$p^{10}\,(\delta^4)$	$\text{BR} < 4\cdot 10^{-5}$ [202]	$\text{BR} \sim 1\cdot 10^{-36}\,\text{TeV}^8/\Lambda^8$	6.3.10
$\pi^0 \to 3\gamma$	$\epsilon^{\mu\nu\rho\sigma}\partial_\alpha\pi^0(\partial^\gamma F^{\alpha\beta})(\partial_\gamma\partial_\beta F_{\rho\sigma})F_{\mu\nu}$	$p^{10}\,(\delta^4)$	$\text{BR} < 3.1\cdot 10^{-8}$ [210]	$\text{BR} \sim 2\cdot 10^{-43}\,\text{TeV}^8/\Lambda^8$	6.3.10

Table 6.1: Overview of C- and CP-odd decays analyzed in this work. At the lowest possible order in soft momenta p, each process exhibits a unique representation in terms of mesonic degrees of freedom (up to overall normalizations and partial integration) as quoted in the second column, except for the decay $\eta \to 3\pi^0\gamma$, for which we list only one possible momentum assignment. Each operator can be seen as part of a Lagrangian once multiplied with a real-valued coupling constant. The decays are ordered according to increasing number of photons (the dilepton decays are assumed to proceed via single virtual photons), and furthermore according to increasing number of mesons involved. As numerical results we quote the explicit dependence on the BSM scale Λ derived from the dimension 7 LEFT quadrilinear, cf. Eq. (5.14), in the fifth column. The assumptions and simplifications these results (i.e., coupling constants $g_{1,2}$, left-right asymmetries A_{LR}, and branching ratios BR) rely on, can be found in the main text and referenced sections.

$\pi^0 \to 3\gamma$ is the least suitable one since a realistic limit on $\Lambda \sim 1\,\text{TeV}$ would require the experiment to measure a branching ratio that is roughly 10^{35} times smaller than the currently most stringent limit.

In each section referenced in the sixth column of Table 6.1 we additionally quote the bound on Λ that can be set by current experiments and find for all considered decays that $\Lambda \gtrsim 1\,\text{GeV}$. These can, for instance, be compared to indirect constraints on ToPe forces that have been set with elementary fermion EDMs in Ref. [111, 112]. In these analyses a Z^0 loop consistent with SM symmetries was attached on top of ToPe operators at fermion level, so that the interference of the vector and axialvector contribution of the two occurring Z^0

vertices flips C and P and hence converts the initial ToPe operator into a contribution to elementary fermion EDMs. With this procedure, the aforementioned references found a far more restrictive value of $\Lambda \gtrsim 50\,\text{TeV}$.[17] However, these works made the somewhat inappropriate assumption that their C- and CP-odd dimension-7 operators scale as $1/\Lambda^3$. We have shown in Ch. 5 that the scaling in the spirit of SMEFT and LEFT should rather be v/Λ^4. Naively matching their result with this more appropriate dependence on Λ yields roughly $\Lambda \gtrsim 13\,\text{TeV}$, which is a more realistic scenario for future high-energy experiments. In order to compete with these limits from EDMs, which are according to our NDA estimates roughly three orders of magnitude more stringent, future experiments have to increase their sensitivity in respective light-meson decays significantly. However, as noted in Ref. [34], we cannot judge the presence of ToPe forces from non-vanishing EDMs. In contrast, finding evidence for non-vanishing signals of the observables listed in Tab. 6.1 would provide strong evidence for ToPe effects.

Before investigating each decay appearing in Tab. 6.1 in detail, we would like to comment on the method we use to estimate the included coupling constants. As a rough order-of-magnitude estimate we rely on naive dimensional analysis (NDA) [61, 211–214]. The latter describes a method to estimate the scale of coupling constants of an effective field theory by simply counting powers of the mass dimension and keeping track of factors of 4π in each operator. This simple kind of power counting already proved to be very successful when estimating the order of magnitude of the LECs at $\mathcal{O}(p^4)$ in SMχPT, as illustrated in Ref. [214]. To properly account for the matching of LEFT and ToPeχPT at the renormalization scale $\Lambda_\chi = 4\pi F_0$ we pursue the following strategy: for a generic coupling g in any of our EFTs we introduce, in accordance to Weinberg's power counting scheme [61], a reduced coupling constant

$$\tilde{g} \equiv (4\pi)^{2-n}\Lambda_\chi^{d-4} g\,, \tag{6.46}$$

where n indicates the number of involved fields and d is the canonical dimension of the operator, i.e., the overall mass dimension of fields and derivatives but without counting couplings. This procedure renders the reduced coupling $\tilde{g}$ dimensionless and approximately of order unity. We first consider the case without dynamical photons and apply the rescaling to the coupling constant $C_{\psi\chi}^{(a)} \equiv \frac{v}{\Lambda^4} c_{\psi\chi}^{(a)}$ in Eq. (6.45), yielding

$$C_{\psi\chi}^{(a)} \bar{\psi}(\vec{\partial}_\mu - \overleftarrow{\partial}_\mu)\gamma_5 \psi \bar{\chi}\gamma^\mu\gamma_5\chi = \frac{(4\pi)^2}{\Lambda_\chi^3}\tilde{C}_{\psi\chi}^{(a)} \bar{\psi}(\vec{\partial}_\mu - \overleftarrow{\partial}_\mu)\gamma_5 \psi \bar{\chi}\gamma^\mu\gamma_5\chi\,, \tag{6.47}$$

where we obtained $\tilde{C}_{\psi\chi}^{(a)} = C_{\psi\chi}^{(a)}\Lambda_\chi^3/(4\pi)^2 \sim \mathcal{O}(1)$ from Eq. (6.46) with $n = 4$ and $d = 7$. When matching to a ToPeχPT operator with m photons, we have to include additional factors of the reduced QED coupling, i.e., multiply the LEFT operator by $e^m/(4\pi)^m$.[18] In

[17] Here we ignore the limits that have been set by Ref. [112] with the operator including the weak gauge boson in Eq. (5.4), as it does not appear in the considered LEFT bases.

[18] This statement is consistent with Weinberg's power counting. If we take for instance the minimal coupling of a photon via the covariant derivative, i.e., the part left out in Eq. (6.47), the NDA rule demands

this way we continuously keep track of what causes the χPT operator to occur, as necessary for a consistent description by NDA. At the level of ToPeχPT we proceed analogously for any given operator that is derived from this LEFT source and relate the LECs ($\bar{g}_i^{(a)}$) to reduced ones ($\tilde{g}_i^{(a)}$). To connect the corresponding reduced LECs $\tilde{g}_i^{(a)} \sim \mathcal{O}(1)$ to LEFT as the underlying theory we can set $\tilde{g}_i^{(a)} \sim \tilde{C}_{\psi\chi}^{(a)}$ for mesonic operators without dynamical photons (and similarly for ToPeχPT operators with additional photons). This is justified as NDA merely provides an order of magnitude estimate for coupling constants, which may well differ by a factor of a few. With this matching between reduced couplings in LEFT and ToPeχPT we can read off the approximate order of magnitude for the LECs $\bar{g}_i^{(a)}$, which can be used as a numerical input for the chiral theory.

6.3.1 | $\eta^{(\prime)} \to \pi^0\pi^+\pi^-$

In this section we investigate possible C- and CP-violating contributions to the three-body decay $\eta^{(\prime)} \to \pi^0\pi^+\pi^-$ with ToPeχPT. As already pointed out in Refs. [1, 62] these BSM contributions are driven by transitions of total isospin $I = 0$ and $I = 2$. Hence the amplitude can be decomposed as

$$\mathcal{M}^{\not C}(s,t,u) = \mathcal{M}_0^{\not C}(s,t,u) + \mathcal{M}_2^{\not C}(s,t,u)\,. \tag{6.48}$$

These contributions were constructed in Ref. [1] using dispersion-theoretical methods. Regression to the respective Dalitz-plot distribution [215] resulted in limits on the BSM coupling constants $g_0, g_2 \in \mathbb{R}$ defined via

$$\begin{aligned} \mathcal{M}_0^{\not C}(s,t,u) &\approx i g_0 (s-t)(t-u)(u-s)\,, \\ \mathcal{M}_2^{\not C}(s,t,u) &\approx i g_2 (t-u)\,. \end{aligned} \tag{6.49}$$

While T violation arises naturally by the imaginary unit i, C violation is encoded in the antisymmetry in the Mandelstam variables. In the following we investigate how to reconstruct these amplitudes with ToPeχPT, so that g_0 and g_2 serve as input for this effective theory allowing us to set limits on the BSM scale Λ.

6.3.1.1 | Kinematics and isospin projections

We define the C- and CP-odd contribution to the T-matrix element of $\eta^{(\prime)} \to \pi^+\pi^-\pi^0$ by

$$\left\langle \pi^+(p_+)\,\pi^-(p_-)\,\pi^0(p_0)\middle| iT \middle|\eta^{(\prime)}(P_{\eta^{(\prime)}})\right\rangle = (2\pi)^4\,\delta^{(4)}(P_{\eta^{(\prime)}} - p_+ - p_- - p_0)\,i\mathcal{M}^{\not C}(s,t,u) \tag{6.50}$$

and work in the isospin limit, i.e., $M_\pi \equiv M_{\pi^\pm} = M_{\pi^0}$. The Mandelstam variables are chosen to be

$$s = (P_{\eta^{(\prime)}} - p_0)^2\,, \qquad t = (P_{\eta^{(\prime)}} - p_+)^2\,, \qquad u = (P_{\eta^{(\prime)}} - p_-)^2\,, \tag{6.51}$$

the reduced coupling $e\tilde{C}_{\psi\chi}^{(a)} = eC_{\psi\chi}^{(a)}\Lambda_\chi^3/(4\pi)^3 \sim \mathcal{O}(1)$, as $n = 5$ and $d = 7$.

which are related to each other by

$$s+t+u = M_{\eta^{(\prime)}}^2 + 3M_\pi^2 \equiv 3r\,. \tag{6.52}$$

The isospin decomposition of the isoscalar and isotensor three-pion final states, i.e., $|I=0\rangle$ and $|I=2\rangle$ respectively, are given by [216]

$$\begin{aligned}
|2(2)\rangle &= \frac{1}{2}\Big[\big(|\pi^+\pi^0\pi^-\rangle - |\pi^-\pi^0\pi^+\rangle\big) + \big(|\pi^0\pi^+\pi^-\rangle - |\pi^0\pi^-\pi^+\rangle\big)\Big],\\
|2(1)\rangle &= \frac{1}{2\sqrt{3}}\Big[\big(|\pi^0\pi^-\pi^+\rangle - |\pi^0\pi^+\pi^-\rangle\big) - 2\big(|\pi^-\pi^+\pi^0\rangle - |\pi^+\pi^-\pi^0\rangle\big)\\
&\qquad + \big(|\pi^+\pi^0\pi^-\rangle - |\pi^-\pi^0\pi^+\rangle\big)\Big]\,,\\
|0(1)\rangle &= \frac{1}{\sqrt{6}}\Big[\big(|\pi^0\pi^-\pi^+\rangle - |\pi^0\pi^+\pi^-\rangle\big) + \big(|\pi^-\pi^+\pi^0\rangle - |\pi^+\pi^-\pi^0\rangle\big)\\
&\qquad + \big(|\pi^+\pi^0\pi^-\rangle - |\pi^-\pi^0\pi^+\rangle\big)\Big]\,,
\end{aligned} \tag{6.53}$$

where the integer in parenthesis denote the isospin of the first two pions. From this Clebsch–Gordan series one can already judge that the isoscalar and isotensor contributions are antisymmetric under exchange of the charged pions and thus C-violating (the $|0\rangle$ state has also an enhanced symmetry under exchange of any two pions). Hence each ToPeχPT operator that contributes to $\eta^{(\prime)} \to \pi^0\pi^+\pi^-$ can for instance be associated with an isospin state of the form $|\pi^-\pi^+\pi^0\rangle - |\pi^+\pi^-\pi^0\rangle$. With Eq. (6.53) we can project out the single isospin contributions by means of[19]

$$|\pi^-\pi^+\pi^0\rangle - |\pi^+\pi^-\pi^0\rangle = \frac{1}{\sqrt{3}}\big(\sqrt{2}\,|0(1)\rangle - 2\,|2(1)\rangle\big)\,. \tag{6.54}$$

6.3.1.2 | Limits on the BSM physics scale

Starting from the large-N_c Lagrangian at leading order δ^0, cf. Eq. (6.44), we can evaluate the matrix element $\mathcal{M}^{\not C}$ upon expanding $\bar{U}$ up to second order in $\bar{\Phi}$ and neglecting photons. We will first investigate the decay of the η meson and discuss the η' at the end of this section. Whenever possible, we conventionally eliminate derivatives acting on the decay particle by partial integration, helping us to find a more compact notation of our operators. The operator generating the C- and CP-odd contributions to the desired decay is

$$\bar{\mathcal{L}}_{\not C P \not T} = i\frac{v}{\Lambda^4 F_0^4}\,2\mathcal{N}_{\eta\to 3\pi}\,\eta\partial^\mu\pi^0(\pi^+\partial_\mu\pi^- - \pi^-\partial_\mu\pi^+) + \dots\,, \tag{6.55}$$

[19] One could as well use $|\pi^+\pi^0\pi^-\rangle - |\pi^-\pi^0\pi^+\rangle = \frac{1}{\sqrt{3}}(\sqrt{2}|0(1)\rangle + |2(1)\rangle + \sqrt{3}|2(2)\rangle)$ or the order $|\pi^0\pi^-\pi^+\rangle - |\pi^0\pi^+\pi^-\rangle = \frac{1}{\sqrt{3}}(\sqrt{2}|0(1)\rangle + |2(1)\rangle - \sqrt{3}|2(2)\rangle)$. As we cannot distinguish between the states $|2(1)\rangle$ and $|2(2)\rangle$ we can only make a statement for the overall isospin 2 contribution. The latter, as well as the overall isoscalar contribution, is the same for all of the three sequences $|\pi^-\pi^+\pi^0\rangle - |\pi^+\pi^-\pi^0\rangle$, $|\pi^+\pi^0\pi^-\rangle - |\pi^-\pi^0\pi^+\rangle$, and $|\pi^0\pi^-\pi^+\rangle - |\pi^0\pi^+\pi^-\rangle$, as long as we stay consistent in notation. Hence, it does not matter which order we choose for the pions in the isospin state for our ToPeχPT operators.

where the ellipsis includes operators that cannot generate the desired transition at $\mathcal{O}(\delta^0)$ and the normalization, given as a linear combinations of Wilson coefficients and LECs, reads

$$\mathcal{N}_{\eta\to 3\pi} = 4\sqrt{\frac{2}{3}}\big(c_{uu}^{(a)} - c_{ud}^{(a)} - c_{du}^{(a)} + c_{dd}^{(a)}\big)\big(\bar{g}_3^{(a)} - \bar{g}_2^{(a)}\big)\,. \tag{6.56}$$

We see that the leading-order contributions to $\eta \to \pi^0\pi^+\pi^-$ arises solely from $\bar{X}_{\psi\chi}^{(a)}$ and furthermore note that all contributions proportional to $c_{\psi\chi}^{(a)}$ with $\psi = s$ and/or $\chi = s$ vanish. The evaluation of the corresponding amplitude $\mathcal{M}^{\not C}$ yields

$$\mathcal{M}^{\not C} = i\frac{v}{\Lambda^4 F_0^4} 2\mathcal{N}_{\eta\to 3\pi}\, p_0(p_- - p_+) = i\frac{v}{\Lambda^4 F_0^4}\mathcal{N}_{\eta\to 3\pi}\,(t-u)\,. \tag{6.57}$$

In order to match the included coupling constants to known observables, we first have to separate the different isospin contributions to this matrix element. According to Eq. (6.54), $\mathcal{M}^{\not C}$ decomposes into[20]

$$\mathcal{M}^{\not C} = \frac{1}{\sqrt{3}}\big(\sqrt{2}\mathcal{M}_0^{\not C} - 2\mathcal{M}_2^{\not C}\big)\,. \tag{6.58}$$

The isoscalar and isotensor contributions in this equation can be evaluated in compliance with Eq. (6.53) by taking the appropriate linear combinations with interchange of pions. Noting that under $\pi^+ \leftrightarrow \pi^-$ ($\pi^+ \leftrightarrow \pi^0$, $\pi^- \leftrightarrow \pi^0$) the Mandelstam variables exchange as $t \leftrightarrow u$, ($t \leftrightarrow s$, $s \leftrightarrow u$), the amplitudes $\mathcal{M}_{0,2}^{\not C}$ become

$$\begin{aligned}
\mathcal{M}_0^{\not C} &= i\mathcal{N}_{\eta\to 3\pi}\frac{v}{\Lambda^4 F_0^4}\frac{1}{\sqrt{6}}\big[(s-t)+(t-u)+(u-s)\big] = 0\,,\\
\mathcal{M}_2^{\not C} &= i\mathcal{N}_{\eta\to 3\pi}\frac{v}{\Lambda^4 F_0^4}\frac{1}{2\sqrt{3}}\big[(s-t)-2(t-u)-(s-u)\big] = -i\mathcal{N}_{\eta\to 3\pi}\frac{v}{\Lambda^4 F_0^4}\frac{\sqrt{3}}{2}(t-u)\,,
\end{aligned} \tag{6.59}$$

and hence $\mathcal{M}^{\not C} = -2/\sqrt{3}\,\mathcal{M}_2^{\not C}$ at chiral order δ^0.

Similarly, all contributions of $\mathcal{M}_0^{\not C}$ vanish in the isospin limit up to $\mathcal{O}(\delta)$ and we thus need at least six derivatives to have enough freedom to reproduce the totally antisymmetric behaviour of the isospin 0 state. This fact was already known decades ago, cf. Ref. [217]. Hence, to evaluate a possible contribution of $\mathcal{M}_0^{\not C}$ we have to construct the contributions to $X_{\chi\psi}^{(a)}$ at order δ^2. Unfortunately this involves the construction of an overwhelming amount of operators with independent free parameters to fix the already strongly suppressed amplitude $\mathcal{M}_0^{\not C}$. One can bring all of these numerous operators to the form of Eq. (6.49) and effectively fix one overall normalization that would correspond to g_0. However, this would not provide new physical insights, because these operators at order δ^2 are less likely to contribute to any other process in a meaningful way and the theory does thus not gain any predictive power by fixing this normalization. Nevertheless, we give one arbitrarily chosen example

[20] The decomposition in Eq. (6.48), used for the dispersive approach in Ref. [1], absorbs the relative factors $\sqrt{2/3}$ and $2/\sqrt{3}$ directly in the coupling constants g_0 and g_2, respectively.

how the $I = 0$ contribution arises from $\bar{X}^{(a)}_{\psi\chi}$, i.e.,

$$\bar{X}^{(a)}_{\psi\chi} \supset \frac{v}{\Lambda^4} c^{(a)}_{\psi\chi} \bar{g}^{(a)}_0 i\big\langle \big(\lambda\lambda_L \partial_\mu\partial_\nu\partial_\alpha \bar{U}^\dagger \partial^\mu\partial^\nu \bar{U} \partial^\alpha \bar{U}^\dagger + \lambda^\dagger\lambda_R \partial_\mu\partial_\nu\partial_\alpha \bar{U} \partial^\mu\partial^\nu \bar{U}^\dagger \partial^\alpha \bar{U}\big) - \text{h.c.}\big\rangle\,, \tag{6.60}$$

as a proof of concept.
However, as we control the dominant isotensor contribution, we can use the result of Ref. [1], i.e., $g_2 = -0.0093(46)\,\text{GeV}^{-2}$, to place bounds on the BSM scale Λ. For simplicity, we first consider the NDA estimate of a generic meson operator included in Eq. (6.55) like

$$i\frac{v}{\Lambda^4 F_0^4} c^{(a)}_{\psi\chi} \bar{g}^{(a)}_i \eta \partial_\mu\pi^0 (\pi^+\partial_\mu\pi^- - \pi^-\partial_\mu\pi^+)\,. \tag{6.61}$$

According to Weinberg's power counting from Eq. (6.46) the reduced coupling for this generic operator with $n = 4$ and $d = 6$ reads

$$\tilde{G}^{(a)}_i \equiv \frac{v}{\Lambda^4 F_0^4} c^{(a)}_{\psi\chi} \bar{g}^{(a)}_i \frac{\Lambda_\chi^2}{(4\pi)^2} \sim \mathcal{O}(1)\,. \tag{6.62}$$

On the other side, we have already seen in Eq. (6.47) that the reduced coupling for the underlying LEFT operator $\bar{X}^{(a)}_{\psi\chi}$, with $n = 4$ and $d = 7$, is

$$\tilde{C}^{(a)}_{\psi\chi} \equiv \frac{v}{\Lambda^4} c^{(a)}_{\psi\chi} \frac{\Lambda_\chi^3}{(4\pi)^2} \sim \mathcal{O}(1)\,. \tag{6.63}$$

As both couplings are by construction of the same order of magnitude, we can set $\tilde{C}^{(a)}_{\psi\chi} \sim \tilde{G}^{(a)}_i$ to obtain $\bar{g}^{(a)}_i \sim \Lambda_\chi F_0^4$. As long as there is no unexpected fine tuning of the Wilson coefficients or LECs, we can apply the same NDA estimate to their linear combination encoded in the normalization $\mathcal{N}_{\eta\to3\pi}$ and therefore obtain $\mathcal{N}_{\eta\to3\pi} \sim \Lambda_\chi F_0^4$. Combining this estimate with the external input for the isotensor coupling (for simplicity we will only consider the respective central value) by means of

$$\mathcal{M}^{\not{C}} = i\frac{v}{\Lambda^4 F_0^4} \mathcal{N}_{\eta\to3\pi}(t-u) \stackrel{!}{=} i g_2 (t-u)\,, \tag{6.64}$$

the currently best experimental precision for the $\eta \to \pi^0\pi^+\pi^-$ Dalitz plot [215] can merely set

$$\Lambda \sim \left(\frac{v}{|g_2|}\Lambda_\chi\right)^{1/4} > 13\,\text{GeV} \tag{6.65}$$

as the lower limit on the BSM scale Λ.[21] This result depends of course strongly on the validity of NDA, but should give a reasonable approximation for the order of magnitude. If we were to estimate a more realistic limit on Λ, i.e., a value in the TeV range, one should expect an increase by a factor of 10^2 (staying in the framework of naive dimensional

[21] Note that NDA does not fix the sign of the normalization $\mathcal{N}_{\eta\to3\pi}$. In order to pick the correct sign of the latter and thereby ensure that $\Lambda \in \mathbb{R}$ we take the absolute value of g_2.

analysis). Hence, to set a reasonable limit on Λ, let us take for instance $\Lambda \sim 1\,\text{TeV}$, the charge asymmetry in the $\eta \to \pi^0\pi^+\pi^-$ Dalitz-plot distribution, which is proportional to g_2, has to be roughly 10^8 times smaller than the current value of Ref. [215], which can be readily obtained from Eq. (6.65):[22]

$$|g_2| \sim \frac{v}{\Lambda^4}\Lambda_\chi \approx 3 \cdot 10^{-4}\,\text{TeV}^2/\Lambda^4\,. \tag{6.66}$$

We now turn the focus on the decay amplitude $\eta' \to \pi^0\pi^+\pi^-$ that can be computed with the same Lagrangian of Eq. (6.44) and reads

$$\mathcal{M}^{\not C} = i\frac{v}{\Lambda^4 F_0^4}\mathcal{N}_{\eta'\to 3\pi}(t-u)\,, \tag{6.67}$$

where $\mathcal{N}_{\eta'\to 3\pi} = \mathcal{N}_{\eta\to 3\pi}/\sqrt{2}$. Hence, the C- and CP-violating contributions to the decays $\eta \to \pi^0\pi^+\pi^-$ and $\eta' \to \pi^0\pi^+\pi^-$ are maximally correlated at leading order in large-N_c. They merely differ by their available phase space and an overall factor $\sqrt{2}$. Unfortunately, the current data situation [218] does not allow for a rigorous regression to the respective Dalitz-plot distribution, cf. Ref. [1]. Therefore we can at this point not cross-check the limit on g_2 set above.

6.3.2 | $\eta' \to \eta\pi^+\pi^-$

In this section we focus on another interference of SM contributions and ToPe forces. The decay $\eta' \to \eta\pi^+\pi^-$ is driven by a transition of total isospin $I = 1$ and is at leading order of the form

$$\mathcal{M}_1^{\not C}(s,t,u) = ig_1(t-u)\,, \tag{6.68}$$

with the same reasoning as for $\eta^{(\prime)} \to \pi^0\pi^+\pi^-$. A result for the isovector coupling g_1 (within the scope of current experimental precision) can again be found in Ref. [1]. In the following we use the same kinematics as in the previous chapter but replace $p_0 \to P_\eta$ and $P_{\eta^{(\prime)}} \to P_{\eta'}$.

There is no leading-order contribution from Eq. (6.44) that does not vanish after partial integration. Non-vanishing contributions could be generated at subleading order in δ, i.e., in the N_c counting; at higher orders in the chiral expansion, which, given that we look for the exact energy dependence of Eq. (6.68), would amount to quark-mass suppression; or via isospin-breaking mixing of π^0 and $\eta^{(\prime)}$, surely the smallest and most negligible effect. We thus consider operators at $\mathcal{O}(\delta^1)$ but with $\mathcal{O}(p^2)$ and use the freedom of the large-N_c expansion to include the η' via the chiral singlet $(\varphi + \theta)$. Henceforth we will directly drop the contribution of θ entering this chiral building block. Note that φ includes a linear combination of η and η'. There are only a couple of operators that generate the desired

[22] Similarly, the more suppressed isoscalar coupling would have to take a value $g_0 \sim \Lambda_\chi^4 g_2$ as demanded by NDA.

transition at the given order, as for instance

$$\bar{X}^{(a)}_{\psi\chi} \supset \frac{v}{\Lambda^4} c^{(a)}_{\psi\chi} \bar{g}^{(a)}_5 \cdot \varphi \left\langle \left(\lambda \bar{U}^\dagger \lambda_R \partial_\mu \bar{U} \partial^\mu \bar{U}^\dagger - \lambda^\dagger \bar{U} \lambda_L \partial_\mu \bar{U}^\dagger \partial^\mu \bar{U}\right) + \text{h.c.} \right\rangle , \tag{6.69}$$

which gives rise to

$$\sum_{\psi,\chi} \bar{X}^{(a)}_{\psi\chi} \supset i \frac{v}{\Lambda^4 F_0^4} 2\mathcal{N}_{\eta'\to\eta\pi\pi}\, \eta' \partial_\mu \eta (\pi^+ \partial_\mu \pi^- - \pi^- \partial_\mu \pi^+) . \tag{6.70}$$

The normalization of this operator is

$$\mathcal{N}_{\eta'\to\eta\pi\pi} = 4\frac{\sqrt{2}}{3}\left(c^{(a)}_{uu} - c^{(a)}_{ud} + c^{(a)}_{du} - c^{(a)}_{dd}\right)\bar{g}^{(a)}_5 . \tag{6.71}$$

We note that every other operator able to generate $\eta' \to \eta\pi^+\pi^-$ at $\mathcal{O}(p^2)$, which can be obtained by letting one of the two derivatives in Eq. (6.69) act on another chiral buildung block, can analytically be written in this form and absorbed by a shift in the normalization. The respective matrix element reads

$$\mathcal{M}_1^{\not C} = i\frac{v}{\Lambda^4 F_0^4} 2\mathcal{N}_{\eta'\to\eta\pi\pi}\, P_\eta (p_- - p_+) = i\frac{v}{\Lambda^4 F_0^4}\mathcal{N}_{\eta'\to\eta\pi\pi}(t-u) . \tag{6.72}$$

With the NDA prediction $\mathcal{N}_{\eta'\to\eta\pi\pi} \sim \Lambda_\chi F_0^4$, this result can be compared to the isovector coupling $g_1 = 0.7(1.0)\,\text{GeV}^{-2}$ of Ref. [1]. This reveals that the current experimental limit on the Dalitz-plot asymmetries [219] constrains the new-physics scale roughly as

$$\Lambda \sim \left(\frac{v}{g_1}\Lambda_\chi\right)^{1/4} > 4\,\text{GeV} , \tag{6.73}$$

where we applied the central value of g_1. A scale $\Lambda \sim 1\,\text{TeV}$ could be tested if the experiment restricted the isovector coupling g_1 and thus the corresponding mirror asymmetry to a value that is approximately 10^{-8} times the current value.

6.3.3 | $\eta^{(\prime)} \to \pi^0\gamma^*$ and $\eta' \to \eta\gamma^*$

In this section we consider the simplest C-violating decays of the $\eta^{(\prime)}$ into an odd number of photons. To shorten the notation we will refer to $\eta^{(\prime)} \to \pi^0\gamma^*$ and $\eta' \to \eta\gamma^*$ by $X \to Y\gamma^*$ and ignore the decay into a real photon, as it has to either violate gauge invariance or does not preserve angular momentum [34, 220]. The latter enforces a relative P-wave between the pion and photon, which moreover demands that parity is conserved and hence CP is violated. Already in the 1960s it was proposed that the Lagrangian driving the $\eta \to \pi^0\gamma^*$ transition starts at chiral order p^4 [221], by means of

$$\mathcal{L}_{\eta\to\pi^0\gamma^*} \propto \partial_\mu \eta\, \partial_\nu \pi^0 F^{\mu\nu} + \mathcal{O}(p^6) . \tag{6.74}$$

This manifestation of gauge invariance was also applied in the SM contributions to kaon decays [222, 223] and holds similarly for all processes $X \to Y\gamma^*$ with pseudoscalars X, Y. Without deriving the full set of mesonic operators for $\bar{X}^{(a)}_{\psi\chi}$ at next-to-leading order, we just give one example of how this operator contributes to $X \to Y\gamma^*$. As similarly argued in Sect. 6.1.4.2, a single-trace operator with the correct discrete symmetries that includes both derivatives vanishes due to the antisymmetry of $F^{\mu\nu}$. Therefore we have to increase the order of δ by either using $\partial_\mu\varphi$, i.e., the derivative of the chiral singlet, or simply writing down a double-trace operator. To recover the form of Eq. (6.74) we stick to the latter strategy and obtain

$$\bar{X}^{(a)}_{\psi\chi} \supset \frac{v}{\Lambda^4} c^{(a)}_{\psi\chi} \bar{g}^{(a)}_6 \big\langle \big(\lambda f_L^{\mu\nu} \partial_\mu \bar{U}^\dagger - \lambda^\dagger f_R^{\mu\nu} \partial_\mu \bar{U}\big) - \text{h.c.}\big\rangle \big\langle \lambda_L \partial_\nu \bar{U}^\dagger \bar{U} - \lambda_R \partial_\nu \bar{U} \bar{U}^\dagger \big\rangle \tag{6.75}$$

at $\mathcal{O}(\delta^2)$, yielding

$$\sum_{\psi,\chi} \bar{X}^{(a)}_{\psi\chi} \supset e \frac{v}{\Lambda^4 F_0^2} \mathcal{N}_{X\to Y\gamma^*} \partial_\mu X \, \partial_\nu Y F^{\mu\nu} \equiv \mathcal{L}_{X\to Y\gamma^*} \,, \tag{6.76}$$

with

$$\begin{aligned}
\mathcal{N}_{\eta\to\pi^0\gamma^*} &= \bar{g}^{(a)}_6 \frac{8}{3}\sqrt{\frac{2}{3}}\Big(-4c^{(a)}_{ud} + 2c^{(a)}_{us} - 2c^{(a)}_{du} + c^{(a)}_{ds} + c^{(a)}_{su} - c^{(a)}_{sd}\Big) \,, \\
\mathcal{N}_{\eta'\to\pi^0\gamma^*} &= -\bar{g}^{(a)}_6 \frac{16}{3\sqrt{3}}\Big(2c^{(a)}_{ud} + 2c^{(a)}_{us} + c^{(a)}_{du} + c^{(a)}_{ds} + c^{(a)}_{su} - c^{(a)}_{sd}\Big) \,, \\
\mathcal{N}_{\eta'\to\eta\gamma^*} &= \bar{g}^{(a)}_6 \frac{8\sqrt{2}}{3}\Big(-2c^{(a)}_{us} + c^{(a)}_{ds} - c^{(a)}_{su} - c^{(a)}_{sd}\Big) \,.
\end{aligned} \tag{6.77}$$

One has to keep in mind that each of our LEFT operators, once taken to $\mathcal{O}(\delta^2)$, may in principle also contribute at the same order of magnitude as $\bar{X}^{(a)}_{\psi\chi}$. But again, the full set of NLO expression derived from all C- and CP-violating LEFT operators is beyond the scope of this work. However, we already proved at this point that the decays at hand provide orthogonal probes of ToPe forces as their normalizations in Eq. (6.77) are linearly independent.

Still, we would like to comment on the contribution of the second original dimension-7 LEFT operator from Eq. (5.14), i.e., the bilinear $\mathcal{O}^{(b)}_\psi$. We note that the leading-order contribution of the latter in the $SU(3)$ case does not contribute to the desired decays of order p^4. However, we can still consider the $U(3)$ version of this operator by including φ using

$$\bar{X}^{(b)}_\psi \supset i \frac{v}{\Lambda^4} c^{(b)}_\psi \bar{g}^{(b)}_2 \, (\partial_\mu\varphi) \big\langle \lambda \partial_\nu \bar{U}^\dagger - \lambda^\dagger \partial_\nu \bar{U} \big\rangle F^{\mu\nu} \,, \tag{6.78}$$

which involves only one trace and is therefore of the order $\mathcal{O}(\delta^2)$ and $\mathcal{O}(p^4)$.

We continue with $\mathcal{L}_{X\to Y\gamma^*}$ from Eq. (6.76) and consider the decay of the virtual photon in Sect. 6.3.4 to extract physical observables. To this end, we quote the normalization according to NDA as similarly derived in Sect. 6.3.1.2, i.e., $\mathcal{N}_{X\to Y\gamma^*} \sim F_0^4/\Lambda_\chi$, and remark that any other leading-order contribution derived from $\mathcal{O}^{(a)}_{\psi\chi}$ just leads to additional linear

combinations of LECs and Wilson coefficients, which can be absorbed by a redefinition of $\mathcal{N}_{X\to Y\gamma^*}$ but do not affect the naive power counting. For further calculations it is convenient to describe the decay $X \to Y\gamma^*$ in terms of a singularity-free electromagnetic transition form factor $F_{XY}(s)$. Using Poincaré invariance and current conservation, the amplitude can be decomposed as [223, 224]

$$\langle Y(p)|J_\mu^{em}(0)|X(P)\rangle = -i\left[s(P+p)_\mu - (P^2-p^2)q_\mu\right] F_{XY}(s), \tag{6.79}$$

with electromagnetic current J_μ^{em}, $q_\mu = (P-p)_\mu$, and $s = q^2$.

6.3.4 | $\eta^{(\prime)} \to \pi^0\ell^+\ell^-$ and $\eta' \to \eta\ell^+\ell^-$

The framework presented in this paper allows us to consider the decays $\eta^{(\prime)} \to \pi^0\ell^+\ell^-$ and $\eta' \to \eta\ell^+\ell^-$ (abbreviated with $X \to Y\ell^+\ell^-$) in two ways: we can either compute the decay chain $X \to Y\gamma^* \to Y\ell^+\ell^-$ or even directly access it as a point interaction originating from semi-leptonic operators. Note that in the decay chain the photon pole $1/q^2$ cancels against a necessary q^2 term in the numerator if the coupling to $\ell^+\ell^-$ respects gauge invariance. As a consequence, the single-photon and the direct amplitude cannot be separated by searching for a photon pole [221, 224, 225]. Note that within the SM, these decays can be generated via two-photon intermediate states [226–228].

The operator from Eq. (6.76) coupling to a conserved lepton current gives a dominant contribution to $X \to Y\ell^+\ell^-$ if the underlying C- and CP-violating mechanism is driven by a one-photon exchange. The only semi-leptonic operator at order δ^0 is the one from Eq. (6.44), which does not generate the desired transition. Instead of deriving the full set of operators at $\mathcal{O}(\delta)$ for all six semi-leptonic LEFT sources, we can easily discard most of them with the following considerations. First of all, the photonic semi-leptonic operators are obviously not involved at lowest order in α as we have no photon in the initial or final state. Moreover, operators including a pseudoscalar or axialvector lepton bilinear must couple to an hadronic operator that is P-odd to preserve parity. On the hadronic level, a P-odd operator that involves an even number of pseudoscalars (in our case $\eta^{(\prime)}, \pi^0$) requires a contraction with the Levi-Civita symbol, as explained in more detail in Sect. 6.3.5. The only Lorentz structure left that can contract with the ϵ-tensor includes three derivatives, which have to act on different $U^{(\dagger)}$ to generate a non-vanishing operator. However, this goes along with an interaction containing at least three pseudoscalars. Hence, the only LEFT operator that can contribute to $X \to Y\ell^+\ell^-$ at lowest order is the one involving the P-even lepton bilinear, i.e., $\mathcal{O}_{\ell\psi}^{(u)}$. Using partial integration and the Dirac equation for the leptons, one can pin down the requested leading-order semi-leptonic four-point interaction to only one operator at $\mathcal{O}(\delta)$ and $\mathcal{O}(p^2)$:

$$\bar{X}_{\ell\psi}^{(u)} \supset \frac{c_{\ell\psi}^{(u)}}{\Lambda^4}\,\bar{g}_1^{(u)}\, i\varphi\langle\lambda_L\partial_\mu\bar{U}^\dagger\bar{U} - \lambda_R\partial_\mu\bar{U}\bar{U}^\dagger\rangle\bar{\ell}\gamma^\mu\ell\,. \tag{6.80}$$

This chiral operator gives rise to an expression of the form

$$(X\partial_\mu Y)\bar{\ell}\gamma^\mu\ell\,. \tag{6.81}$$

For now we continue with the one-photon exchange driven by the LEFT operator $\mathcal{O}^{(a)}_{\psi\chi}$ in focus of this chapter and define the corresponding T-matrix element as

$$\langle Y(p)\ell^+(p_{\ell^+})\ell^-(p_{\ell^-})|iT|X(P)\rangle \equiv (2\pi)^4\delta^{(4)}(P-p-p_{\ell^+}-p_{\ell^-})i\mathcal{M}(s,t,u)\,, \tag{6.82}$$

where the amplitude $\mathcal{M}$ depends on the three Mandelstam variables

$$s=(P-p)^2\,,\qquad t_\ell=(P-p_{\ell^+})^2\,,\qquad u_\ell=(P-p_{\ell^-})^2\,, \tag{6.83}$$

which obey $s+t+u=M_X^2+M_Y^2+2m_\ell^2$. Starting from Eq. (6.76) we allow the photon with momentum $q\equiv p_{\ell^+}+p_{\ell^-}$ to decay into a lepton pair, so that the amplitude becomes[23]

$$\begin{aligned} i\mathcal{M}(s,t,u) &= \frac{v}{\Lambda^4F_0^2}e^2\mathcal{N}_{X\to Y\gamma^*}\frac{1}{s}\,(P_\mu p_\nu - P_\nu p_\mu)q^\mu\,\bar{u}_r(p_{\ell^-})\gamma^\nu v_{r'}(p_{\ell^+}) \\ &= \frac{v}{\Lambda^4F_0^2}e^2\mathcal{N}_{X\to Y\gamma^*}\,P_\nu\,\bar{u}_r(p_{\ell^-})\gamma^\nu v_{r'}(p_{\ell^+}) \\ &= e^2(P+p)_\nu F_{XY}(s)\,\bar{u}_r(p_{\ell^-})\gamma^\nu v_{r'}(p_{\ell^+})\,. \end{aligned} \tag{6.84}$$

In the second line we simplified the expression using $q^2=s$ and the fact that q_ν contracted with the lepton current vanishes as demanded by the Dirac equation. As a consistency check, we expressed the amplitude in terms of the transition form factor $F_{XY}(s)=v\mathcal{N}_{X\to Y\gamma^*}/(2e\Lambda^4F_0^2)$ from Eq. (9.6). We observe that the form factor is a constant at leading chiral order, which meets our expectations. Note that the second line in Eq. (6.84), which comes from a LEFT operator of dimension 7, gives the same structure as the chiral operator (6.80), which comes from an LEFT operator of dimension 8.
In analogy to Ref. [229], the doubly differential decay width reads

$$\frac{\mathrm{d}\Gamma_{X\to Y\ell^+\ell^-}}{\mathrm{d}s\,\mathrm{d}\tau}=\left(\frac{v}{\Lambda^4F_0^2}\right)^2\frac{\alpha^2}{64\pi M_X^3}\mathcal{N}^2_{X\to Y\gamma^*}\,\left(\lambda(s,M_X^2,M_Y^2)-\tau^2\right), \tag{6.85}$$

with the electromagnetic fine structure constant $\alpha=e^2/4\pi$, the Källén function $\lambda(x,y,z)=x^2+y^2+z^2-2(xy+xz+yz)$, and the Lorentz -invariant $\tau=t_\ell-u_\ell$. An analytic integration over τ yields

$$\frac{\mathrm{d}\Gamma_{X\to Y\ell^+\ell^-}}{\mathrm{d}s}=\left(\frac{v}{\Lambda^4F_0^2}\right)^2\frac{\alpha^2}{32\pi M_X^3}\mathcal{N}^2_{X\to Y\gamma^*}\,\lambda^{3/2}(s,M_X^2,M_Y^2)\,\sigma_\ell(s)\left(1-\frac{\sigma_\ell^2(s)}{3}\right), \tag{6.86}$$

where $\sigma_\ell(s)=\sqrt{1-4m_\ell^2/s}$ and the physical range is restricted to $4m_\ell^2\le s\le(M_X-M_Y)^2$. After an additional numeric integration over s we can investigate how rigorously the bounds

[23] Note that the photon propagator reduces the power counting in soft momenta by 2.

on the new-physics scale Λ can be placed with measurements of the electronic and muonic decay channels. With the shorthand notation

$$\tilde{\Lambda}_{X\to Y\ell^+\ell^-} \equiv \frac{v^2}{F_0^4\,\Gamma_{X\to Y\ell^+\ell^-}}\frac{\alpha^2}{32\pi M_X^3}\mathcal{N}^2_{X\to Y\gamma^*}\cdot 10^{-2}\text{GeV}^8 \tag{6.87}$$

we obtain the limits

$$\begin{aligned}
&\Lambda \sim (0.087\,\tilde{\Lambda}_{\eta\to\pi^0 e^+e^-})^{1/8} > 2.3\,\text{GeV}\,, && \Lambda \sim (0.027\,\tilde{\Lambda}_{\eta\to\pi^0\mu^+\mu^-})^{1/8} > 2.1\,\text{GeV}\,,\\
&\Lambda \sim (10.1\,\tilde{\Lambda}_{\eta'\to\pi^0 e^+e^-})^{1/8} > 3.5\,\text{GeV}\,, && \Lambda \sim (7.4\,\tilde{\Lambda}_{\eta'\to\pi^0\mu^+\mu^-})^{1/8} > 3.5\,\text{GeV}\,,\\
&\Lambda \sim (1.0\,\tilde{\Lambda}_{\eta'\to\eta e^+e^-})^{1/8} > 0.7\,\text{GeV}\,, && \Lambda \sim (0.3\,\tilde{\Lambda}_{\eta'\to\eta\mu^+\mu^-})^{1/8} > 1.1\,\text{GeV}\,,
\end{aligned} \tag{6.88}$$

where we applied the NDA estimate $\mathcal{N}_{\eta\to\pi^0\gamma^*} \sim F_0^4/\Lambda_\chi$, used $M_\eta = 547.86\,\text{MeV}$, $M_{\pi^0} = 134.98\,\text{MeV}$, $m_e = 0.51\,\text{MeV}$, $m_\mu = 105.67\,\text{MeV}$ [13], neglected their errors with respect to the dominating uncertainty from NDA, and inserted the branching ratios from Table 6.1. We can again reverse this argument, i.e., the semi-leptonic branching ratios in explict dependence of Λ read

$$\begin{aligned}
&\text{BR}_{\eta\to\pi^0 e^+e^-} \sim 7\cdot 10^{-27}\,\text{TeV}^8/\Lambda^8\,, && \text{BR}_{\eta\to\pi^0\mu^+\mu^-} \sim 2\cdot 10^{-27}\,\text{TeV}^8/\Lambda^8\,,\\
&\text{BR}_{\eta'\to\pi^0 e^+e^-} \sim 9\cdot 10^{-28}\,\text{TeV}^8/\Lambda^8\,, && \text{BR}_{\eta'\to\pi^0\mu^+\mu^-} \sim 6\cdot 10^{-28}\,\text{TeV}^8/\Lambda^8\,,\\
&\text{BR}_{\eta'\to\eta e^+e^-} \sim 9\cdot 10^{-29}\,\text{TeV}^8/\Lambda^8\,, && \text{BR}_{\eta'\to\eta\mu^+\mu^-} \sim 3\cdot 10^{-29}\,\text{TeV}^8/\Lambda^8\,,
\end{aligned} \tag{6.89}$$

respectively.[24] At this point we once more underline that these estimates are only valid for the mechanism $X \to Y\gamma^* \to Y\ell^+\ell^-$ driven by $\mathcal{O}^{(a)}_{\psi\chi}$. A more thorough investigation of $X \to Y\ell^+\ell^-$ including the remaining LEFT sources, semi-leptonic four-point interactions, as well as hadronic contributions to the $X \to Y\gamma^*$ form factor is left for future work.

6.3.5 | $\eta^{(\prime)} \to \pi^+\pi^-\gamma$

While the SM contribution to the anomalous decay $\eta^{(\prime)} \to \pi^+\pi^-\gamma$ is well known and has been studied extensively in particular using dispersion-theoretical approaches [230–235], the considerations of C violation in $\eta \to \pi^+\pi^-\gamma$ date back to the 1960s [224, 236] and 1970s [206–208]. Let us define the respective matrix element by

$$\langle\pi^+(p_+)\pi^-(p_-)\gamma(q)|iT|\eta^{(\prime)}(P)\rangle = (2\pi)^4\delta^{(4)}(P-p_+-p_--q)i\mathcal{M}_c(s,t_c,u_c)\,, \tag{6.90}$$

with Mandelstam variables

$$s = (P-q)^2\,,\quad t_c = (P-p_+)^2\,,\quad u_c = (P-p_-)^2 \tag{6.91}$$

[24] Note that, here and henceforth, we use the total decay width $\Gamma_{\eta'} = 0.23\,\text{MeV}$ indicated as *PDG average* in Ref. [13].

obeying $s + t_c + u_c = M_{\eta^{(\prime)}}^2 + 2M_\pi^2$. Unless otherwise stated, we work in the isospin limit. We begin our discussion by relaxing the constraint of C-invariance and split the amplitude according to

$$i\mathcal{M}_c(s,t_c,u_c) \equiv \mathcal{M}_c^C(s,t_c,u_c) + \mathcal{M}_c^{\not C}(s,t_c,u_c)\,. \tag{6.92}$$

The SM contribution $\mathcal{M}_c^C(s,t_c,u_c)$ is, at leading order, given by the Wess–Zumino–Witten (WZW) term [237, 238] and can be described by

$$\mathcal{M}_c^C(s,t_c,u_c) = i\epsilon_{\alpha\beta\mu\nu}\varepsilon^{*\,\alpha}q^\beta p_+^\mu p_-^\nu F_c^C(s,t_c,u_c)\,. \tag{6.93}$$

The invariant function F_c^C can be expanded in terms of pion–pion partial waves according to to [239]

$$F_c^C(s,t_c,u_c) = \sum_\ell P_\ell'(z_s) f_\ell(s)\,, \qquad z_s = \frac{s(t-u) + (M_1^2 - M_2^2)M_{\eta^{(\prime)}}^2}{\lambda^{1/2}(s,M_1^2,M_2^2)(M_{\eta^{(\prime)}}^2 - s)}\,, \tag{6.94}$$

where z_s is the cosine of the scattering angle, $P_\ell'(z_s)$ refers to the first derivatives of the Legendre polynomials, and for convenience and later use we keep the dependence on the masses of the two mesons in the final state explicit. For the application at hand we can simply set $M_1 = M_2 = M_\pi$. For the C-even SM amplitude, only partial waves of odd ℓ contribute. Accounting for s-channel final-state rescattering and restricting the calculation to the dominant P-wave, the scalar function F_c^C becomes

$$F_c^C(s,t_c,u_c) = P(s)\,\Omega(s)\,, \qquad \Omega(s) = \exp\left(\frac{s}{\pi}\int_{4M_\pi^2}^\infty \mathrm{d}x\,\frac{\delta(x)}{x(x-s)}\right)\,, \tag{6.95}$$

where $\Omega(s)$ is the Omnès function [105], $\delta(s)$ is the $\pi\pi$ P-wave phase shift, for which we employ the parameterization of Ref. [240], and $P(s)$ is a real-valued subtraction polynomial, for which we employ $P(s) = 5.09/\mathrm{GeV}^3(1+2.40s/\mathrm{GeV}^2 - 2.42s^2/\mathrm{GeV}^4)$ for the decay of the η and $P(s) = 5.05/\mathrm{GeV}^3(1+0.99s/\mathrm{GeV}^2 - 0.55s^2/\mathrm{GeV}^4)$ for the η' [241]. For our purposes we can neglect all parameter uncertainties, left-hand cuts, and higher partial waves.

In contrast, we only work at leading order for the χPT analog of the C-violating contribution $\mathcal{M}_c^{\not C}(s,t_c,u_c)$, which was found in Ref. [236] to be $\mathcal{O}(p^6)$. It is commonly known that an interaction with an odd number of pseudoscalars requires an ϵ-tensor to render the Lagrangian invariant under parity.[25] Thus we naively start at $\mathcal{O}(p^4)$ like the WZW term. To furthermore violate C the dipion system must have an even orbital angular momentum l. Hence, when interchanging the pions, we find $|\pi^+\pi^-\rangle = (-1)^l|\pi^-\pi^+\rangle = |\pi^-\pi^+\rangle$. Finally

[25] This statement is also manifest in the construction of chirally invariant traces: a parity-violating trace, i.e., a trace with a relative minus sign between its parity transformed as for instance $\langle \lambda U^\dagger - \lambda^\dagger U\rangle$, always includes an odd number of pseudoscalars according to Eq. (6.7). The only freedom we have in the construction of χPT operators to restore parity invariance without flipping this relative sign or multiplying other parity-violating traces (which both lead to an overall even number of pseudoscalars) is the inclusion of an ϵ-tensor. We remark that this argument does not hold for semi-leptonic interactions, as the multiplication with a parity-flipping lepton current or density does not change the number of mesons.

demanding Bose statistics, i.e., symmetrizing under interchange of the pions, the amplitude at $\mathcal{O}(p^4)$ vanishes due to contraction with the ϵ-tensor. Thus we need to equip the matrix element by another momentum configuration that is antisymmetric under $\pi^+ \leftrightarrow \pi^-$, which leads to

$$\mathcal{M}_c^{\not C}(s,t_c,u_c) \sim \epsilon_{\alpha\beta\mu\nu}\varepsilon^{*\,\alpha} q^\beta p_+^\mu p_-^\nu q_\rho (p_-^\rho - p_+^\rho) \tag{6.96}$$

in consistency with Ref. [236]. Note that this matrix element also differs from the WZW term by a relative factor i, ensuring T violation and hence CPT-invariance. For better comparability of Eq. (6.96) with the SM amplitude in Eq. (6.93), we can also define a scalar function in the C-violating case, i.e.,

$$F_c^{\not C}(s,t_c,u_c) \equiv q_\rho(p_-^\rho - p_+^\rho) + \ldots = (t_c - u_c)/2 + \ldots\,, \tag{6.97}$$

where the ellipsis denotes higher-order terms in the chiral expansion. Comparing to Eq. (6.94), we see that the amplitude (6.97) indeed corresponds to the leading C-odd partial wave, a D-wave.

We now wish to reconstruct Eq. (6.96) with ToPeχPT and again pick one arbitrary operator that may generate this matrix element at lowest order. One contribution at $\mathcal{O}(\delta^2)$ originates from

$$\bar{X}_{\psi\chi}^{(a)} \supset i\frac{v}{\Lambda^4} c_{\psi\chi}^{(a)} \bar{g}_7^{(a)} \epsilon_{\alpha\beta\mu\nu} \Big\langle \big(\lambda\lambda_L \partial^\nu \bar{U}^\dagger \partial_\rho f_R^{\alpha\beta} \partial^\mu \bar{U} \partial^\rho \bar{U}^\dagger - \lambda^\dagger \lambda_R \partial^\nu \bar{U} \partial_\rho f_L^{\alpha\beta} \partial^\mu \bar{U}^\dagger \partial^\rho \bar{U}\big) - \text{h.c.}\Big\rangle\,. \tag{6.98}$$

If we only consider contributions to $\eta \to \pi^+\pi^-\gamma$, use partial integration, and make use of the amplitude's symmetry, this operator evaluates to the compact expression

$$\sum_{\psi,\chi} \bar{X}_{\psi\chi}^{(a)} \supset e\frac{v}{\Lambda^4 F_0^3} \mathcal{N}_{\eta^{(\prime)}\to\pi^+\pi^-\gamma}\, \epsilon_{\alpha\beta\mu\nu}\, \eta^{(\prime)} (\partial^\nu \pi^+ \partial^\rho \partial^\mu \pi^- + \partial^\nu \pi^- \partial^\rho \partial^\mu \pi^+) \partial_\rho F^{\alpha\beta}\,. \tag{6.99}$$

The constants

$$\mathcal{N}_{\eta\to\pi^+\pi^-\gamma} = \sqrt{2}\mathcal{N}_{\eta'\to\pi^+\pi^-\gamma}\,, \qquad \mathcal{N}_{\eta'\to\pi^+\pi^-\gamma} \equiv -\frac{4}{\sqrt{3}}\bar{g}_7^{(a)}\big(c_{uu}^{(a)} - c_{dd}^{(a)}\big) \tag{6.100}$$

serve as the normalizations. We cannot claim at hand of this single example that $\eta \to \pi^+\pi^-\gamma$ and $\eta' \to \pi^+\pi^-\gamma$ are maximally correlated. From this operator we can compute the matrix element

$$\mathcal{M}_c^{\not C}(s,t_c,u_c) = e\frac{v}{\Lambda^4 F_0^3} \mathcal{N}_{\eta^{(\prime)}\to\pi^+\pi^-\gamma}\, \epsilon_{\alpha\beta\mu\nu}\, \varepsilon^{*\,\alpha} q^\beta p_+^\mu p_-^\nu (t_c - u_c) \tag{6.101}$$

in consistency with the previous considerations. The respective NDA estimate yields $\mathcal{N}_{\eta^{(\prime)}\to\pi^+\pi^-\gamma} \sim F_0^4/\Lambda_\chi^3$.

The interference of the SM and BSM amplitudes M_c^C and $M_c^{\not C}$ gives rise to an asymmetry in the distribution of charged pion momenta. To quantify this so-called left–right asymmetry,

we introduce the ratio

$$A_{LR} \equiv \frac{\Gamma(t_c > u_c) - \Gamma(u_c > t_c)}{\Gamma_{\eta^{(\prime)}\to\pi^+\pi^-\gamma}}\,, \tag{6.102}$$

where the Γ denote the phase space integrals over $|\mathcal{M}_c(s,t_c,u_c)|^2$ for $t_c > u_c$, $u_c > t_c$, and the full range, respectively. These integrals are explicitly defined by

$$\Gamma = \int_{4M_\pi^2}^{M_{\eta^{(\prime)}}^2} \mathrm{d}s\, \Gamma_0(s) \int_{z_s^{\min}}^{z_s^{\max}} \mathrm{d}z_s\, (1-z_s^2)\, |iF_c^C(s,t_c,u_c) + F_c^{\not C}(s,t_c,u_c)|^2\,, \tag{6.103}$$

with

$$\Gamma_0(s) \equiv \frac{(M_{\eta^{(\prime)}}^2 - s)^3 \lambda^{3/2}(s, M_1^2, M_2^2)}{16(8\pi M_{\eta^{(\prime)}})^3 s^2}\,, \tag{6.104}$$

again keeping the final-state masses M_1 and M_2 general for generalization in the coming sections. The limits of the angular integration $z_s^{\min}$, $z_s^{\max}$ are fixed by $0 \le z_s \le 1$ for $\Gamma(t_c > u_c)$, $-1 \le z_s \le 0$ for $\Gamma(u_c > t_c)$, and $-1 \le z_s \le 1$ for $\Gamma_{\eta^{(\prime)}\to\pi^+\pi^-\gamma}$. Note that only the contribution of the interference term, i.e.,

$$2\mathrm{Re}\left[iF_c^C(s,t_c,u_c)\left(F_c^{\not C}(s,t_c,u_c)\right)^*\right] \subset \left|iF_c^C(s,t_c,u_c) + F_c^{\not C}(s,t_c,u_c)\right|^2\,, \tag{6.105}$$

survives in the numerator of A_{LR}, while the denominator is dominated by the SM part. We can now express $F_c^{\not C}(s,t_c,u_c)$ in terms of z_s and carry out the $\mathrm{d}z_s$ integral analytically, yielding

$$\Gamma(t_c > u_c) - \Gamma(u_c > t_c) = -\frac{e\,v\,\mathcal{N}_{\eta\to\pi^+\pi^-\gamma}}{2\Lambda^4 F_0^3} \int_{4M_\pi^2}^{M_\eta^2} \mathrm{d}s\, \Gamma_0(s)\sigma(s)\big(M_{\eta^{(\prime)}}^2 - s\big)P(s)\mathrm{Im}\left(\Omega(s)\right)\,. \tag{6.106}$$

The last factor demonstrates a crucial aspect about the C-odd asymmetry: due to the relative factor of i between C-conserving and C-violating amplitude, their interference would actually vanish, were it not for strong rescattering phases. For the two different decays of the η and η' we obtain

$$\begin{aligned}
\Gamma(t_c > u_c) - \Gamma(u_c > t_c)\big|_{\eta\to\pi^+\pi^-\gamma} &= -6.6\cdot 10^{-12}\,\mathrm{GeV}^6 \times e\frac{v}{\Lambda^4 F_0^3}\mathcal{N}_{\eta\to\pi^+\pi^-\gamma}\,,\\
\Gamma(t_c > u_c) - \Gamma(u_c > t_c)\big|_{\eta'\to\pi^+\pi^-\gamma} &= -1.5\cdot 10^{-7}\,\mathrm{GeV}^6 \times e\frac{v}{\Lambda^4 F_0^3}\mathcal{N}_{\eta'\to\pi^+\pi^-\gamma}\,,
\end{aligned} \tag{6.107}$$

respectively. The polynomial $P(s)$ is already normalized such that the integral over the full decay range reproduces the experimental decay width, i.e., $\Gamma_{\eta\to\pi^+\pi^-\gamma} \approx 55\,\mathrm{eV}$ and $\Gamma_{\eta'\to\pi^+\pi^-\gamma} \approx 56\,\mathrm{keV}$, respectively. Finally, the lower bound on the new-physics scale as a function of $A_{LR} = 0.009(4)$ [13] for the decay of the η and $A_{LR} = 0.03(4)$ [13] for the η'

under the abovementioned NDA approximation becomes

$$\begin{aligned}\Lambda|_{\eta\to\pi^+\pi^-\gamma} &\sim \left(1.2\cdot 10^{-4}\,\text{GeV}^5\, e\frac{v}{A_{LR}\Lambda_\chi^3}F_0\right)^{1/4} > 0.5\,\text{GeV}\,,\\ \Lambda|_{\eta'\to\pi^+\pi^-\gamma} &\sim \left(1\cdot 10^{-7}\,\text{GeV}^5\, e\frac{v}{A_{LR}\Lambda_\chi^3}F_0\right)^{1/4} > 0.8\,\text{GeV}\,.\end{aligned} \tag{6.108}$$

Both results were computed with the central values of the empirical asymmetries. In terms of the BSM scale, the left-right asymmetries become

$$\begin{aligned}|A_{LR}|_{\eta\to\pi^+\pi^-\gamma} &\sim 5\cdot 10^{-16}\,\text{TeV}^4/\Lambda^4\,,\\ |A_{LR}|_{\eta'\to\pi^+\pi^-\gamma} &\sim 1\cdot 10^{-14}\,\text{TeV}^4/\Lambda^4\,,\end{aligned} \tag{6.109}$$

respectively. The significantly larger asymmetry in the η' decay is mainly due to the fact that the phase space covers the whole region of the $\rho(770)$ resonance in the $\pi^+\pi^-$ invariant mass, with its associated phase motion and peaking imaginary part. — In principle, the D-wave phase motion of the C-violating amplitude would induce another contribution to the asymmetry, which we have neglected in the above. However, this is strongly suppressed relative to the P-wave in the near-threshold region covered in the η decay, staying well below 1°, while it rises only up to about 10° at the η' mass [240], where it competes with the resonating P-wave. Neither effect is relevant at the present level of accuracy.

6.3.6 | $\eta^{(\prime)} \to \pi^0\pi^0\gamma$

In full analogy to the charged $\pi^+\pi^-\gamma$ final state from the previous section, we will investigate C violation via the neutral one $\eta \to \pi^0\pi^0\gamma$, as was suggested by Refs. [242, 243], and furthermore extend the analysis straightforwardly to $\eta' \to \pi^0\pi^0\gamma$. The T-matrix element

$$\langle\pi^0(p_1)\pi^0(p_2)\gamma(q)|iT|\eta^{(\prime)}(P)\rangle = (2\pi)^4\delta^{(4)}(P-p_1-p_2-q)i\mathcal{M}_n(s,t_n,u_n) \tag{6.110}$$

is described by the Mandelstam variables

$$s=(P-q)^2\,,\quad t_n=(P-p_1)^2\,,\quad u_n=(P-p_2)^2\,, \tag{6.111}$$

fulfilling the relation $s+t_n+u_n = M_\eta^2+2M_{\pi^0}^2$. The matrix element $\mathcal{M}_n$ has the same structure as given in Eq. (6.96). The ToPeχPT operator from Eq. (6.98) we found in the charged channel is not able to generate non-vanishing contributions to the uncharged one. This is rooted in the fact that all interactions in which no charged mesons participate are located in the diagonal entries of matrices $U^{(\dagger)}$. Hence, any product of the latter commutes with the spurions and $f_{L,R}^{\mu\nu}$ upon setting all charged mesons to zero. This fact rules out single-trace operators at $\mathcal{O}(\delta^2)$ derived from $\bar{X}_{\psi\chi}^{(a)}$. Thus we once more consider a double-trace operator (although the chiral singlet $\partial_\mu\varphi$ multiplied with a single trace might work

as well), so that the lowest-order operator we find occurs at $\mathcal{O}(\delta^3)$ and reads[26]

$$\bar{X}^{(a)}_{\psi\chi} = i\frac{v}{\Lambda^4}c^{(a)}_{\psi\chi}\bar{g}^{(a)}_8\epsilon_{\alpha\beta\mu\nu}\left\langle \bar{U}\partial^\gamma\partial^\mu\bar{U}^\dagger + \bar{U}^\dagger\partial^\gamma\partial^\mu\bar{U}\right\rangle\left\langle\left(\lambda\lambda_L\partial_\gamma f_L^{\alpha\beta}\partial^\nu\bar{U}^\dagger - \lambda^\dagger\lambda_R\partial_\gamma f_R^{\alpha\beta}\partial^\nu\bar{U}\right) - \text{h.c.}\right\rangle \tag{6.112}$$

which yields

$$\sum_{\psi,\chi}\bar{X}^{(a)}_{\psi\chi} \supset e\frac{v}{\Lambda^4 F_0^3}\mathcal{N}_{\eta^{(\prime)}\to\pi^0\pi^0\gamma}\epsilon_{\alpha\beta\mu\nu}\,\eta^{(\prime)}\partial^\nu\pi^0\partial^\rho\partial^\mu\pi^0\partial_\rho F^{\alpha\beta}\,. \tag{6.113}$$

The normalizations

$$\mathcal{N}_{\eta\to\pi^0\pi^0\gamma} = \frac{16}{3}\sqrt{\frac{2}{3}}\bar{g}^{(a)}_8\left(2c^{(a)}_{uu} - c^{(a)}_{dd} + c^{(a)}_{ss}\right), \quad \mathcal{N}_{\eta'\to\pi^0\pi^0\gamma} = \frac{16}{3\sqrt{3}}\bar{g}^{(a)}_8\left(2c^{(a)}_{uu} - c^{(a)}_{dd} - 2c^{(a)}_{ss}\right) \tag{6.114}$$

show that both decays are uncorrelated. In particular, as the LECs involved differ from the ones relevant for the $\pi^+\pi^-\gamma$ final state studied in the previous section, we note that the C-violating operators do not relate to pion pairs of definite isospin. Finally, the decay amplitude of the neutral channel becomes

$$\mathcal{M}_n(s,t_n,u_n) = e\frac{v}{\Lambda^4 F_0^3}\mathcal{N}_{X\to Y\pi^0\gamma}\epsilon_{\alpha\beta\mu\nu}\varepsilon^{*\,\alpha}q^\beta p_1^\mu p_2^\nu(t_n - u_n)\,, \tag{6.115}$$

where NDA presumes that $\mathcal{N}_{\eta^{(\prime)}\to\pi^0\pi^0\gamma} \sim F_0^4/\Lambda_\chi^3$. As in Eq. (6.97), this corresponds to a D-wave amplitude: for two identical neutral pions, only even partial waves are allowed, the odd ones are forbidden by Bose symmetry.

As the decay at hand has no contribution by SM physics, the relevant observable is the full decay width

$$\begin{aligned}\Gamma_{\eta^{(\prime)}\to\pi^0\pi^0\gamma} &= \frac{1}{2}\left(e\frac{v}{\Lambda^4 F_0^3}\mathcal{N}_{\eta^{(\prime)}\to\pi^0\pi^0\gamma}\right)^2\int_{4M_{\pi^0}^2}^{M_X^2}\mathrm{d}s\,\Gamma_0(s)\int_{-1}^{1}\mathrm{d}z_s\,(1-z_s^2)(t_n-u_n)^2 \\ &= \frac{2}{15}\left(e\frac{v}{\Lambda^4 F_0^3}\mathcal{N}_{\eta^{(\prime)}\to\pi^0\pi^0\gamma}\right)^2\int_{4M_{\pi^0}^2}^{M_X^2}\mathrm{d}s\,\Gamma_0(s)\frac{(M_X^2-s)^2(s-4M_{\pi^0}^2)}{s}\,,\end{aligned} \tag{6.116}$$

where the kinematical functions can be adapted from Eq. (6.104) and the additional factor $1/2$ accounts for Bose symmetry as we have two identical particles in the final state. The numeric values of the phase space integrals yield

$$\begin{aligned}\Gamma_{\eta\to\pi^0\pi^0\gamma} &= \left(e\frac{v}{\Lambda^4 F_0^3}\mathcal{N}_{\eta\to\pi^0\pi^0\gamma}\right)^2 \times 6.4\cdot 10^{-13}\,\text{GeV}^{11}\,, \\ \Gamma_{\eta'\to\pi^0\pi^0\gamma} &= \left(e\frac{v}{\Lambda^4 F_0^3}\mathcal{N}_{\eta'\to\pi^0\pi^0\gamma}\right)^2 \times 2.5\cdot 10^{-9}\,\text{GeV}^{11}\,.\end{aligned} \tag{6.117}$$

[26] Note we have not explicitly checked whether a contribution at lower order in δ can be derived from one of the other numerous C- and CP-odd LEFT operators. However, the lowest possible order in soft momenta must still be p^6.

With the NDA estimate quoted above, the current experimental measurements of the decay widths listed in Table 6.1 set the limits

$$\Lambda \sim \left(\frac{6.4\cdot 10^{-13}\,\text{GeV}^{11}}{\Gamma_{\eta\to\pi^0\pi^0\gamma}}\alpha v^2\frac{F_0}{\Lambda_\chi^5}\right)^{1/8} > 0.6\,\text{GeV}\,, \tag{6.118}$$

while no search has been performed for $\eta'\to\pi^0\pi^0\gamma$ to date. For arbitrary Λ the respective branching ratios behave as

$$\begin{aligned}\text{BR}_{\eta\to\pi^0\pi^0\gamma} &\sim 1\cdot 10^{-29}\,\text{TeV}^8/\Lambda^8\,,\\ \text{BR}_{\eta'\to\pi^0\pi^0\gamma} &\sim 2\cdot 10^{-28}\,\text{TeV}^8/\Lambda^8\,.\end{aligned} \tag{6.119}$$

This tremendous suppression is due to the Λ^{-8} dependence of the decay width and underlines that decays allowing for an interference of SM and BSM amplitudes—as the charged channel $\eta\to\pi^+\pi^-\gamma$—are much more suitable to search for this kind of new physics, as they scale with Λ^{-4}.

6.3.7 | $\eta'\to\eta\pi^0\gamma$

In this section we focus on the decay $\eta'\to\eta\pi^0\gamma$, for which no measurement has been recorded so far. We define the corresponding matrix element via

$$\langle\eta(p_1)\pi^0(p_2)\gamma(q)|iT|\eta^{(\prime)}(P)\rangle = (2\pi)^4\delta^{(4)}(P-p_1-p_2-q)i\mathcal{M}(s,t,u)\,, \tag{6.120}$$

with Mandelstam variables

$$s=(P-q)^2\,,\quad t=(P-p_1)^2\,,\quad u=(P-p_2)^2\,, \tag{6.121}$$

obeying $s+t+u=M_{\eta'}^2+M_\eta^2+M_{\pi^0}^2$. At the mesonic level, the driving operator must have the form

$$\epsilon_{\alpha\beta\mu\nu}\,\eta'\partial^\mu\eta\partial^\nu\pi^0F^{\alpha\beta} \tag{6.122}$$

in compliance with Sect. 6.3.5. Similar to the arguments given in Sect. 6.3.6 we cannot build an operator at $\mathcal{O}(\delta^1)$. The lowest order contribution we find is

$$\bar{X}^{(a)}_{\psi\chi} = \frac{v}{\Lambda^4}c^{(a)}_{\psi\chi}\bar{g}^{(a)}_9\,\epsilon_{\alpha\beta\mu\nu}\,\varphi\left\langle\left(\lambda_L f_L^{\alpha\beta}\partial^\mu\bar{U}^\dagger\bar{U}-\lambda_R f_R^{\alpha\beta}\partial^\mu\bar{U}\bar{U}^\dagger\right)-\text{h.c.}\right\rangle\left\langle\lambda\partial^\nu\bar{U}^\dagger-\lambda^\dagger\partial^\nu\bar{U}\right\rangle \tag{6.123}$$

at $\mathcal{O}(\delta^3)$.[27] The corresponding Lagrangian

$$\sum_{\psi,\chi}\bar{X}^{(a)}_{\psi\chi}\supset e\frac{v}{\Lambda^4F_0^3}\frac{1}{2}\mathcal{N}_{\eta'\to\eta\pi^0\gamma}\,\epsilon_{\alpha\beta\mu\nu}\,\eta'\partial^\mu\eta\partial^\nu\pi^0F^{\alpha\beta}\,, \tag{6.124}$$

[27] We have not explicitly checked whether any of the remaining LEFT operators can generate $\eta'\to\eta\pi^0\gamma$ at $\mathcal{O}(\delta^1)$ or $\mathcal{O}(\delta^2)$.

with normalization

$$\mathcal{N}_{\eta'\to\eta\pi^0\gamma} = \frac{32\sqrt{2}}{9}\big(-c_{ud}^{(a)} + c_{us}^{(a)} - 2c_{du}^{(a)} - c_{ds}^{(a)} + 2c_{su}^{(a)} + c_{sd}^{(a)}\big)\,\bar{g}_9^{(a)}\,, \tag{6.125}$$

results in the matrix element

$$i\mathcal{M} = e\frac{v}{\Lambda^4 F_0^3}\mathcal{N}_{\eta'\to\eta\pi^0\gamma}\,\epsilon_{\alpha\beta\mu\nu}\,p_1^\mu p_2^\nu q^\alpha \epsilon^\beta\,. \tag{6.126}$$

The lower number of derivatives/momenta involved in this amplitude as compared to the decays $\eta^{(\prime)}\to\pi^0\pi^0\gamma$ discussed in the previous section can again be understood in terms of the contributing leading partial waves: while all of these decays violate C and do not allow for a SM decay amplitude as the similar ones with a $\pi^+\pi^-$ pair in the final state, there are no restrictions from Bose symmetry on the $\eta\pi^0$ final state, and hence the leading contribution (6.126) is a P-, not a D-wave; note how the $\eta\pi$ P-wave combines to J^{PC} quantum numbers 1^{-+}. The respective decay width can be evaluated in the same manner as in the previous sections and becomes

$$\Gamma_{\eta'\to\eta\pi^0\gamma} = \left(e\frac{v}{\Lambda^4 F_0^3}\mathcal{N}_{\eta'\to\eta\pi^0\gamma}\right)^2 \frac{4}{3}\int_{M_{\text{min}}^2}^{M_{\eta'}^2} \mathrm{d}s\,\Gamma_0(s)\,, \tag{6.127}$$

with $M_{\text{min}}\equiv M_\eta + M_{\pi^0}$. A numeric integration yields

$$\Gamma_{\eta'\to\eta\pi^0\gamma} = \left(e\frac{v}{\Lambda^4 F_0^3}\mathcal{N}_{\eta'\to\eta\pi^0\gamma}\right)^2 \times 1.6\cdot 10^{-9}\,\text{GeV}^7\,, \tag{6.128}$$

so that the NDA estimate $\mathcal{N}_{\eta'\to\eta\pi^0\gamma}\sim F_0^4/\Lambda_\chi$ finally results in

$$\text{BR}_{\eta'\to\eta\pi^0\gamma}\sim 2\cdot 10^{-28}\,\text{TeV}^8/\Lambda^8\,. \tag{6.129}$$

6.3.8 | $\eta'\to\eta\pi^0\pi^0\gamma$

Another C-violating decay that has not yet been searched for is $\eta'\to\eta\pi^0\pi^0\gamma$. Let us define the corresponding T-matrix element as

$$\langle\pi^0(p_1)\pi^0(p_2)\eta(p_3)\gamma(p_4)|iT|\eta'(P)\rangle \equiv (2\pi)^4\delta^{(4)}(P-p_1-p_2-p_3-p_4)i\mathcal{M}(p_1,p_2,p_3,p_4)\,. \tag{6.130}$$

On the mesonic level this decay requires an operator coupling uncharged pseudoscalars to a photon. As the covariant derivative only couples the photon to charged mesons, the desired operator has to include one $F_{\mu\nu}$, similar to the Lagrangian in Eq. (6.74). This leaves us with

$$\eta'\partial_\mu\eta\pi^0\partial_\nu\pi^0 F^{\mu\nu} \tag{6.131}$$

as the only possible assignment of derivatives that does not vanish for an on-shell photon respecting gauge invariance, i.e., upon setting $q^2=0$ and $q^\mu\varepsilon_\mu=0$. Any operator with

a derivative acting on η' can be brought to the same form as the one above using partial integration.

We thus arbitrarily choose the chiral operator

$$\bar{X}^{(a)}_{\psi\chi} \supset \frac{v}{\Lambda^4} c^{(a)}_{\psi\chi} \bar{g}^{(a)}_{10}\, i(\partial_\mu\varphi)\big\langle(\lambda\lambda_L f_L^{\mu\nu}\partial_\nu\bar{U}^\dagger - \lambda^\dagger\lambda_R f_R^{\mu\nu}\partial_\nu\bar{U}) - \text{h.c.}\big\rangle \tag{6.132}$$

as a contribution at lowest possible order. Only keeping non-vanishing terms, the corresponding Lagrangian at $\mathcal{O}(\delta^2)$ in mesonic degrees of freedom reads

$$\sum_{\psi,\chi} \bar{X}^{(a)}_{\psi\chi} \supset e\frac{v}{\Lambda^4 F_0^4}\mathcal{N}_{\eta'\to\eta\pi^0\pi^0\gamma}\,\eta'\partial_\mu\eta\pi^0\partial_\nu\pi^0 F^{\mu\nu}\,, \tag{6.133}$$

with

$$\mathcal{N}_{\eta'\to\eta\pi^0\pi^0\gamma} \equiv -\frac{4\sqrt{2}}{9}\bar{g}^{(a)}_{10}\big(2c^{(a)}_{uu} - c^{(a)}_{dd}\big)\,. \tag{6.134}$$

The resulting matrix element evaluates to

$$i\mathcal{M}(p_1,p_2,p_3,p_4) = e\frac{v}{\Lambda^4 F_0^4}\mathcal{N}_{\eta'\to\eta\pi^0\pi^0\gamma}(p_3^\mu(p_1^\nu+p_2^\nu) - p_3^\nu(p_1^\mu+p_2^\mu))p_{4\mu}\epsilon^*_\nu\,, \tag{6.135}$$

and is related to the decay width by

$$\Gamma_{\eta'\to\eta\pi^0\pi^0\gamma} = (2\pi)^4\frac{S}{2M}\int \mathrm{d}\Phi_4 \sum_{\text{pol.}} |\mathcal{M}(p_1,p_2,p_3,p_4)|^2\,. \tag{6.136}$$

Here $\mathrm{d}\Phi_4$ is the four-body phase space, M is the mass of the decaying particle, and we explicitly accounted for a symmetry factor S. We now turn the focus on the computation of the four-body phase space and divide the final state into the two-body subsystems, with momenta $q = p_1+p_2$ and $k = p_3+p_4$. At this point we will keep the mass assignments of the particles as general as possible in order to be able to re-use the calculation at a later stage. Introducing $s_{12} = q^2$ and $s_{34} = k^2$, the absolute values of the occurring three-momenta read

$$|\boldsymbol{q}| = \frac{\lambda^{1/2}(M^2,s_{12},s_{34})}{2M}\,,\quad |\boldsymbol{p}_1^{12}| = \frac{\lambda^{1/2}(s_{12},m_1^2,m_2^2)}{2\sqrt{s_{12}}}\,,\quad |\boldsymbol{p}_3^{34}| = \frac{\lambda^{1/2}(s_{34},m_3^2,m_4^2)}{2\sqrt{s_{34}}}\,, \tag{6.137}$$

where the additional indices 12 and 34 indicate the respective center-of-mass systems chosen for the evaluation and $\boldsymbol{q}$ is taken in the rest frame of the decaying particle. The explicit

expressions for the four-momenta are

$$\begin{aligned}
p_1 &= \Big(\gamma_{12}(E_1^{12} + \beta_{12}|\boldsymbol{p}_1^{12}|\cos\theta_{12})\,,\quad |\boldsymbol{p}_1^{12}|\sin\theta_{12}\,,\ 0\,,\ \gamma_{12}(\beta_{12}E_1^{12} + |\boldsymbol{p}_1^{12}|\cos\theta_{12})\Big)^T\,,\\
p_2 &= \Big(\gamma_{12}(E_2^{12} - \beta_{12}|\boldsymbol{p}_1^{12}|\cos\theta_{12})\,,\ -|\boldsymbol{p}_1^{12}|\sin\theta_{12}\,,\ 0\,,\ \gamma_{12}(\beta_{12}E_2^{12} - |\boldsymbol{p}_1^{12}|\cos\theta_{12})\Big)^T\,,\\
p_3 &= \Big(\gamma_{34}(E_3^{34} + \beta_{34}|\boldsymbol{p}_3^{34}|\cos\theta_{34})\,,\ -|\boldsymbol{p}_3^{34}|\sin\theta_{34}\cos\phi_{34}\,,\ -|\boldsymbol{p}_3^{34}|\sin\theta_{34}\sin\phi_{34}\,,\\
&\qquad \gamma_{34}(-\beta_{34}E_3^{34} - |\boldsymbol{p}_3^{34}|\cos\theta_{34})\Big)^T\,,\\
p_4 &= \Big(\gamma_{34}(E_4^{34} - \beta_{34}|\boldsymbol{p}_3^{34}|\cos\theta_{34})\,,\quad |\boldsymbol{p}_3^{34}|\sin\theta_{34}\cos\phi_{34}\,,\quad |\boldsymbol{p}_3^{34}|\sin\theta_{34}\sin\phi_{34}\,,\\
&\qquad \gamma_{34}(-\beta_{34}E_4^{34} + |\boldsymbol{p}_3^{34}|\cos\theta_{34})\Big)^T\,,
\end{aligned} \tag{6.138}$$

with $E_n^{ij} = \sqrt{m_n^2 + |\boldsymbol{p}_n^{ij}|^2}$, $\beta_{12} = |\boldsymbol{q}|/E_q$, $\beta_{34} = |\boldsymbol{k}|/E_k$, $E_q^2 = |\boldsymbol{q}|^2 + s_{12}$, $E_k^2 = |\boldsymbol{k}|^2 + s_{34}$, and $\gamma_{ij} = 1/\sqrt{1-\beta_{ij}^2}$. The four-body phase space in terms of the five independent variables reads

$$\mathrm{d}\Phi_4 = \frac{1}{32(2\pi)^{10}}\mathrm{d}s_{12}\,\mathrm{d}s_{34}\,\mathrm{d}\theta_{12}\,\mathrm{d}\theta_{34}\,\mathrm{d}\phi_{34}\frac{|\boldsymbol{q}|}{M}\frac{|\boldsymbol{p}_1^{12}|}{\sqrt{s_{12}}}\frac{|\boldsymbol{p}_3^{34}|}{\sqrt{s_{34}}}\sin\theta_{12}\sin\theta_{34}\,, \tag{6.139}$$

where the non-trivial integration limits are

$$(m_1+m_2)^2 \le s_{12} \le (M-m_3-m_4)^2\,, \qquad (m_3+m_4)^2 \le s_{34} \le (M-\sqrt{s_{12}})^2\,. \tag{6.140}$$

For the remaining details regarding the kinematics we refer to Ref. [244], while equivalent formulations can be found in Refs. [245–247].

Inserting the explicit masses of the contributing particles and applying $S = 1/2$, we finally find with the NDA estimate $\mathcal{N}_{\eta'\to\eta\pi^0\pi^0\gamma} \sim F_0^4/\Lambda_\chi$ that the branching ratio yields

$$\mathrm{BR}_{\eta'\to\eta\pi^0\pi^0\gamma} \sim 4\pi\alpha\frac{v^2}{\Gamma_{\eta'}\Lambda_\chi^2\Lambda^8}\cdot 1\cdot 10^{-15} \approx 2\cdot 10^{-32}\,\mathrm{TeV}^8/\Lambda^8\,. \tag{6.141}$$

6.3.9 | $\eta \to 3\pi^0\gamma$

In complete analogy to Sect. 6.3.8, we can derive the transition $\eta \to 3\pi^0\gamma$ by appropriately replacing the four-momenta and masses of η' and η by the ones for η and π^0.[28] However, the enhanced symmetry of this process prohibits any operator whose derivatives on pion fields contract with the field-strength tensor. Thus, we require a term with at least four

[28] We do not consider the decay $\eta' \to 3\pi^0\gamma$ here, as the increased phase space allows for an ω in the intermediate state. As a consequence, we would expect this to rather test the C-violating vector-meson decay $\omega \to 3\pi^0$, analogously to how $\eta' \to \pi^+\pi^-\pi^0\gamma$ is dominated by $\eta' \to \omega\gamma$ in the Standard Model.

derivatives that does not lead to mass terms, as for instance

$$\partial_\mu\eta\partial_\nu\pi^0\partial_\alpha\pi^0\pi^0\partial^\alpha F^{\mu\nu}\,, \tag{6.142}$$

which we consider as an example for this decay. The corresponding chiral Lagrangian from $\bar{X}^{(a)}_{\psi\chi}$ at lowest order (i.e., δ^3) obtains a contribution from[29]

$$\bar{X}^{(a)}_{\psi\chi} \supset \frac{v}{\Lambda^4}c^{(a)}_{\psi\chi}\,\bar{g}_{11}\,i(\partial_\mu\varphi)\big\langle(\lambda\lambda_L\partial^\alpha f_L^{\mu\nu}\partial_\alpha\bar{U}^\dagger\bar{U}\partial_\nu\bar{U}^\dagger-\lambda^\dagger\lambda_R\partial^\alpha f_R^{\mu\nu}\partial_\alpha\bar{U}\bar{U}^\dagger\partial_\nu\bar{U})-\text{h.c.}\big\rangle\,, \tag{6.143}$$

leading to the operator

$$\sum_{\psi\chi}\bar{X}^{(a)}_{\psi\chi} \supset e\frac{v}{\Lambda^4F_0^4}\mathcal{N}_{\eta\to3\pi^0\gamma}\,\partial_\mu\eta\partial_\nu\pi^0\partial_\alpha\pi^0\pi^0\partial^\alpha F^{\mu\nu}\,, \tag{6.144}$$

with the normalization

$$\mathcal{N}_{\eta\to3\pi^0\gamma} \equiv -\frac{4}{3}\sqrt{\frac{2}{3}}\,\bar{g}^{(a)}_{11}(2c^{(a)}_{uu}+c^{(a)}_{dd})\,. \tag{6.145}$$

Accordingly, the overall matrix element becomes

$$\begin{aligned}i\mathcal{M}(p_1,p_2,p_3,p_4) = e\frac{v}{\Lambda^4F_0^4}\mathcal{N}_{\eta\to3\pi^0\gamma}\,P^\mu\big(&p_1^\nu p_2^\alpha+p_2^\nu p_1^\alpha+p_1^\nu p_3^\alpha+p_3^\nu p_1^\alpha+p_2^\nu p_3^\alpha+p_3^\nu p_2^\alpha\big)\\ &\times p_{4\alpha}\big(p_{4\mu}\epsilon^*_\nu-p_{4\nu}\epsilon^*_\mu\big)\,.\end{aligned} \tag{6.146}$$

With the same four-body phase space as in Sect. 6.3.8, but with appropriately re-assigned masses, a symmetry factor $S=1/6$, the NDA prediction $\mathcal{N}_{\eta\to3\pi^0\gamma}\sim F_0^4/\Lambda_\chi^3$, and the experimental width $\Gamma_{\eta\to3\pi^0\gamma}$ listed in Table 6.1 we find the lower limit

$$\Lambda \sim \left(4\pi\alpha\frac{v^2}{\Gamma_{\eta\to3\pi^0\gamma}\Lambda_\chi^6}\cdot6\cdot10^{-21}\,\text{GeV}^{13}\right)^{1/8} > 140\,\text{MeV} \tag{6.147}$$

or

$$\text{BR}_{\eta\to3\pi^0\gamma}\sim1\cdot10^{-35}\,\text{TeV}^8/\Lambda^8 \tag{6.148}$$

for the theoretically estimated branching ratio, respectively.

6.3.10 | $\eta^{(\prime)}\to3\gamma$ and $\pi^0\to3\gamma$

In this section we investigate the CP-odd contributions of the C-violating decays $\eta^{(\prime)}\to3\gamma$ and $\pi^0\to3\gamma$, which have been considered in Refs. [243, 248, 249] while possible C- and P-violating contributions through weak interactions (in the case of π^0) have been discussed in Ref. [250]. For this purpose we introduce the T-matrix element

$$\langle\gamma(q_1)\gamma(q_2)\gamma(q_3)|iT|X(P)\rangle = (2\pi)^4\delta^{(4)}(P-q_1-q_2-q_3)i\mathcal{M}(s,t,u) \tag{6.149}$$

[29] Again, we have not considered other LEFT operators that may contribute at order δ^2.

with $X = \eta', \eta, \pi^0$ and define the Mandelstam variables

$$s = (P - q_1)^2\,, \quad t = (P - q_2)^2\,, \quad u = (P - q_3)^2\,, \tag{6.150}$$

with $s + t + u = M_X^2$. The three-photon final state sets demanding constraints on the amplitude. First of all, the covariant derivative only couples charged mesons to the photon, thus we need exactly three field-strength tensors picked from $f_L^{\mu\nu}, f_R^{\mu\nu}, F_{\mu\nu}$ to generate the 3γ final state and can use ∂_μ instead of D_μ. Since we have an odd number of pseudoscalars, a Levi-Civita symbol has to be involved when contracting the Lorentz indices to respect parity invariance. Moreover Bose statistics demands a symmetrized 3γ final state, so that non-vanishing operators require at least four additional derivatives [248]. Finally, to obtain a coupling with a single meson (multiple) derivatives can only act on one single U or $U^\dagger$ at a time. We can now pick one ToPeχPT operator that meets all these requirements (which demand an operator starting at $\mathcal{O}(\delta^4)$) and arbitrarily choose

$$\bar{X}^{(a)}_{\psi\chi} \supset \frac{v\bar{g}^{(a)}_{12}c^{(a)}_{\psi\chi}}{\Lambda^4 F_0} i\epsilon^{\mu\nu\rho\sigma}\big\langle(\lambda\lambda_L f^L_{\mu\nu}\partial^\gamma f_L^{\alpha\beta}\partial_\gamma\partial_\beta f^L_{\rho\sigma}\partial_\alpha\bar{U}^\dagger - \lambda^\dagger\lambda_R f^R_{\mu\nu}\partial^\gamma f_R^{\alpha\beta}\partial_\gamma\partial_\beta f^R_{\rho\sigma}\partial_\alpha\bar{U}) - \text{h.c.}\big\rangle\,, \tag{6.151}$$

giving rise to

$$\sum_{\psi,\chi}\bar{X}^{(a)}_{\psi\chi} \supset e^3\frac{v}{\Lambda^4 F_0}2\mathcal{N}_{X\to3\gamma}\,\epsilon^{\mu\nu\rho\sigma}\partial_\alpha X(\partial^\gamma F^{\alpha\beta})(\partial_\gamma\partial_\beta F_{\rho\sigma})F_{\mu\nu}\,, \tag{6.152}$$

with

$$\begin{aligned}\mathcal{N}_{\pi^0\to3\gamma} &= \bar{g}^{(a)}_{12}\frac{2}{27}\big(-8c^{(a)}_{uu} - c^{(a)}_{dd}\big)\,, \qquad \mathcal{N}_{\eta\to3\gamma} = \bar{g}^{(a)}_{12}\frac{2}{27}\sqrt{\frac{2}{3}}\big(-8c^{(a)}_{uu} + c^{(a)}_{dd} - c^{(a)}_{ss}\big)\,,\\ \mathcal{N}_{\eta'\to3\gamma} &= \bar{g}^{(a)}_{12}\frac{2}{27\sqrt{3}}\big(-8c^{(a)}_{uu} + c^{(a)}_{dd} + 2c^{(a)}_{ss}\big)\,.\end{aligned} \tag{6.153}$$

This result is consistent with Refs. [243, 248] who claimed that the only contribution to $X \to 3\gamma$ arises at order p^{10} in soft momenta.

Although the derivation of the full set of ToPeχPT operators up to chiral order p^{10} is far beyond the scope of this work, every operator that contributes to $X \to 3\gamma$ at this order has to have the same functional form as in Eq. (6.152), modulo partial integrations, so that all contributions from the genuine LEFT operator $\mathcal{O}^{(a)}_{\psi\chi}$ lead to the same NDA estimate. We

continue the computation of the matrix element following Ref. [248] and write

$$\begin{aligned}\sum_{\text{pol}} |\mathcal{M}(s,t,u)|^2 &= \left(e^3 \frac{v}{\Lambda^4 F_0} 2\mathcal{N}_{X\to 3\gamma}\right)^2 32\,(q_1q_2)(q_2q_3)(q_3q_1) \\ &\quad \times \left[(q_1q_2)^2\,(q_1q_3-q_2q_3)^2 + (q_1q_3)^2\,(q_1q_2-q_3q_2)^2 + (q_2q_3)^2\,(q_2q_1-q_3q_1)^2\right] \\ &= \left(e^3 \frac{v}{\Lambda^4 F_0} \mathcal{N}_{X\to 3\gamma}\right)^2 s\,t\,u\left[u^2\,(t-s)^2 + t^2\,(u-s)^2 + s^2\,(u-t)^2\right] .\end{aligned} \tag{6.154}$$

Inserting this result in the decay width

$$\Gamma_{X\to 3\gamma} = \frac{S}{256\pi^3 M_X^3} \int_0^{M_X^2} \mathrm{d}s \int_0^{M_X^2-s} \mathrm{d}t \sum_{\text{pol}} |\mathcal{M}(s,t,u)|^2 \tag{6.155}$$

with symmetry factor $S = 1/6$ and carrying out the integrals over s and t analytically, we obtain

$$\Gamma_{X\to 3\gamma} = \frac{\alpha^3 M_X^{15}}{24} \frac{1}{5040} \left(\frac{v}{\Lambda^4 F_0} \mathcal{N}_{X\to 3\gamma}\right)^2 . \tag{6.156}$$

With the NDA estimate $\mathcal{N}_{X\to 3\gamma} \sim \Lambda_\chi^{-3}(4\pi)^{-4}$, the experimental decay widths, cf. Table 6.1, and the abbreviation

$$\tilde{\Lambda}_{3\gamma} \equiv \frac{1}{5040} \frac{v^2\alpha^3}{24 F_0^2 \Lambda_\chi^6 (4\pi)^8} , \tag{6.157}$$

we set the following lower limits on Λ:

$$\begin{aligned}\Lambda &\sim \left[\frac{M_{\eta'}^{15}}{\Gamma_{\eta'\to 3\gamma}} \tilde{\Lambda}_{3\gamma}\right]^{1/8} > 160\,\text{MeV} , \\ \Lambda &\sim \left[\frac{M_{\eta}^{15}}{\Gamma_{\eta\to 3\gamma}} \tilde{\Lambda}_{3\gamma}\right]^{1/8} > 120\,\text{MeV} , \\ \Lambda &\sim \left[\frac{M_{\pi^0}^{15}}{\Gamma_{\pi^0\to 3\gamma}} \tilde{\Lambda}_{3\gamma}\right]^{1/8} > 40\,\text{MeV} .\end{aligned} \tag{6.158}$$

Reversing the argument, the branching ratios as functions of Λ are

$$\begin{aligned}\text{BR}_{\eta'\to 3\gamma} &\sim 3\cdot 10^{-35}\,\text{TeV}^8/\Lambda^8 , \\ \text{BR}_{\eta\to 3\gamma} &\sim 1\cdot 10^{-36}\,\text{TeV}^8/\Lambda^8 , \\ \text{BR}_{\pi^0\to 3\gamma} &\sim 2\cdot 10^{-43}\,\text{TeV}^8/\Lambda^8 .\end{aligned} \tag{6.159}$$

6.4 | Summary and outlook

By matching the fundamental C- and CP-violating LEFT operators from Ch. 5 thoroughly onto χPT we established a new rigorous and model-independent framework to access possible C- and CP-violating effects in flavor-conserving decays of η, η', and π^0, which solely

relies on the conjecture that these BSM effects arise from phenomena at scales of yet unknown high energies, for which the Standard Model provides an appropriate low-energy approximation. In this context, novel 3×3 spurion matrices were applied to ensure the transfer of the u, d, s flavor degrees of freedom and chirality structure of the quark bilinears from the SMEFT and LEFT levels to chiral operators at the χPT level. Knowing the underlying mechanisms at the level of LEFT and χPT, we derived mesonic operators, amplitudes, and observables for more than 20 decays in total.

Furthermore, we estimated that the currently most precise experiments searching for C and CP violation in the light-meson sector can merely restrict Λ to the few GeV range. Due to the lack of sufficient input to fix the numerous low-energy constants and Wilson coefficients entering the effective chiral theory, these estimates are based on naive dimensional analysis, which does not only require knowledge about the mesonic operators (some of them were already known in the 1960s) but also about the particular sources of these operators on the quark level. These estimates are roughly three orders of magnitude less rigorous compared to indirect limits on ToPe forces set in Ref. [112] from elementary fermion EDMs, which we adapted to the more appropriate suppression in the sense of SMEFT and LEFT.

As the central numerical results of our analysis we reversed the argument above and expressed the observable branching ratios for pure BSM processes as well as asymmetry parameters for interferences of SM and BSM contributions in terms of the new-physics scale. While the former scale with $1/\Lambda^8$, the interference effects are proportional to $1/\Lambda^4$ and are thus more suitable candidates for experimental searches. Hence, the most promising of our investigated decays to find evidence for ToPe forces are $\eta^{(\prime)} \to \pi^0\pi^+\pi^-$, $\eta' \to \eta\pi^+\pi^-$, and $\eta^{(\prime)} \to \pi^+\pi^-\gamma$. In addition, our estimates for the pure C-violating decays allow us to weed out those that require significantly higher experimental precision than others.

We find that the currently most rigorous experimental limits on ToPe forces in the light-meson sector must become more stringent by roughly a factor of 10^7 in order to test this scenario for a BSM scale of $\Lambda \sim 1\,\text{TeV}$. Although these theoretical bounds cannot be reached by experiments in the near future, the search for the decays proposed in this work—prospectively conducted, for instance, by the REDTOP [38–40] and JEF [41–43] collaborations—can still provide important insights to understand the sources of possible C and CP violation. Any experimental evidence for these decays could imply, for instance, that a simultaneous violation of C and CP violation originates from (weakly coupled) light degrees of freedom, or that the SMEFT and/or LEFT power counting is bypassed by another, yet unknown mechanism.

Obviously, this casts doubt at the possibility to interpret any observable C- and CP-odd signals in terms of SMEFT. However, we can relax the constraints obtained here to some extent by concentrating on LEFT without any reference to SMEFT at all; this would effectively replace the TeV scale Λ by an electroweak scale of the order of 100 GeV, and therefore reduce the discrepancy between our theoretical expectation and current experimental sensitivity by a factor of about $1/4 \times 10^3$ – 10^4 for interferences with SM amplitudes and 10^5 – 10^8 for pure BSM transitions.

Our analysis opens a new window to model-independent theoretical analyses of C and CP violation with a vast number of possible future extensions. These are not only restricted to applications to meson scattering and decays not covered in this work, especially to ones that include interferences of SM and BSM physics, but also to extensions to flavor-violating transitions (once the LEFT basis of Ch. 5 is extended accordingly), to heavy-quark physics, to processes in the baryon or nuclear sector [251–256], and cross-relations to EDMs [257].

III

Dispersive analysis of C and CP violation in $\eta^{(\prime)}$ decays

Chapter 7

Prologue

This part covers two chapters that are subject to separate publications.
First, we comment on Ch. 8, which is based on

- H. Akdag, T. Isken, B. Kubis, "Patterns of C- and CP-violation in hadronic η and η' three-body decays", *JHEP* 02 (2022) 137 [arXiv:2111.02417[hep-ph]].[1]

The motivation of this article was to embed the idea of Ref. [62], who investigated C and CP violation arising from isoscalar and isotensor transitions in $\eta \to \pi^+\pi^-\pi^0$, in the framework of dispersion theory and hence to investigate the Dalitz-plot asymmetries originating from the interference with the SM contribution more precisely. For this purpose, we construct the amplitude of the three-body decay in a non-perturbative and model-independent manner, relying on the fundamental principles of analyticity and unitarity. The underlying concepts are explained in detail in Ch. 3. We furthermore extend these considerations to $\eta' \to \pi^+\pi^-\pi^0$, by merely increasing the available phase space, and $\eta' \to \eta\pi^+\pi^-$, whose ToPe effects are driven by an isovector transition. The importance of these three decays has already been proven in Sect. 6.3: they correspond to the few decays that contribute to lowest order in soft momenta p, they allow for observables that are linear in ToPe forces, i.e., have a suppression of $1/\Lambda^4$ in the BSM scale, and they are of experimental significance as they do not include photons in the final states.
Ensuring that the high-energy behaviour of the single-variable functions, which enter the overall matrix elements in the spirit of reconstruction theorems, meet various constraints imposed by the well-investigated SM contribution, we apply the same justified asymptotics for the single-variable functions of the BSM amplitudes. This allows us to fix our dispersive representations of the isoscalar and isotensor transitions in $\eta^{(\prime)} \to \pi^+\pi^-\pi^0$ by only one complex subtraction constant each and the isovector contribution to $\eta' \to \eta\pi^+\pi^-$ by two subtraction constants. However, hermiticity and CPT-invariance demand that the underlying effective BSM coupling constants, which can be extracted by Taylor expansions of our decay amplitudes, are purely imaginary (cf. Sects. 6.3.1 and 6.3.2). These couplings in turn fix the phases of the subtraction constants. Hence, the isoscalar and isotensor transitions in $\eta^{(\prime)} \to \pi^+\pi^-\pi^0$ are determined by one *real* degree of freedom each, while the isovector contribution to $\eta' \to \eta\pi^+\pi^-$ includes two *real* free parameters.
A comparison with the respective Dalitz-plot distributions measured by the KLOE-2 [215] and BESIII [219] collaborations shows that all signals for ToPe effects can be excluded within at most 2σ. Furthermore, we observe that the current experimental precision restricts these BSM contributions to the relative per mille level. The results of the effective

[1] Parts of the introduction of this publication were reused in Ch. 1.

C- and CP-odd coupling constants were already used in Sects. 6.3.1 and 6.3.2 to match the respective low-energy coefficients in ToPeχPT. The dispersive amplitudes are reconsidered in Ch. 9 to investigate other C- and CP-odd signals and also will also be provided to the REDTOP collaboration [40] for future high-precision analyses.

In the following we point out how the author of this thesis contributed to the publication at hand. First of all, it has to be emphasized that a preliminary version of the analysis of C and CP violation in $\eta \to 3\pi$ as presented in Sect. 8.1 and especially Figs. 8.1, 8.2, and 8.4 were already part of a previous thesis [88]. The main results of the latter were reconstructed and verified by the author of the thesis at hand, who carried out an independent computation with Mathematica [117]; implemented a generalized algorithm to solve the system of coupled-integration equations, giving rise to the single-variable functions, from scratch that runs on all common operating systems and current compiler versions for C++; extended the dispersive framework to analyze C- and CP-violation in the decays $\eta' \to \pi^+\pi^-\pi^0$ and $\eta' \to \eta\pi^+\pi^-$ and evaluated the numeric results for them; made the observation of the incorrectly granted phase freedom between SM and BSM amplitudes, not least due to the progress made in Ref. [2] or Ch. 6, respectively; and finally contributed—as the main author of the publication above—most formulations, which are especially in Sect. 8.1 partly adapted from Ref. [88].

Lastly, we would like to make the following acknowledgments: We are grateful to Susan Gardner, Martin Hoferichter, and Peter Stoffer for very helpful discussions. We thank Andrzej Kupść for his support with the data from Ref. [219], Bachir Moussallam for providing the $\eta\pi$ phase shift of Ref. [258], and Malwin Niehus for his support in the development of the numerical algorithm for the solution of the Khuri–Treiman equations.

Now we focus on Ch. 9, which is based on the publication

[3] H. Akdag, B. Kubis, A. Wirzba, "Correlations of C and CP violation in $\eta \to \pi^0\ell^+\ell^-$ and $\eta' \to \eta\ell^+\ell^-$", arXiv:2307.02533[hep-ph], *under review*.

The aim of this work is to study the correlation of C- and CP-violating signals between *different* decays in more detail. To this end we reconsider the decays that appear, according to Tab. 6.1, at lowest order in the chiral expansion, i.e., $\eta \to \pi^+\pi^-\pi^0$, $\eta' \to \eta\pi^+\pi^-$, $\eta \to \pi^0\ell^+\ell^-$, and $\eta' \to \eta\ell^+\ell^-$. Note that the SM contributions to the latter two are driven by a two-photon exchange, which is still subject of current investigations [226, 228, 259–261], while we have already discussed the comparatively poor theoretical work on the C-violating one-photon exchange at least to some extent in Sect. 6.3.4. Extending the considerations to the latter, we use the rigorous parameterization of C and CP violation in the dominant hadronic three-body decays obtained in Ch. 8 in order to *predict* the isovector part in the hadronic long-distance contributions to the transition form factors $\eta \to \pi^0\gamma^*$ and $\eta' \to \eta\gamma^*$. These predictions solely use the $\pi\pi$ scattering phase shift and the asymmetries of the hadronic Dalitz plots as input. The form factors are again computed non-perturbatively in a dispersive framework, by cutting the respective dipion intermediate states in $\eta \to \pi^+\pi^-\pi^0 \to \pi^0\gamma^*$ and $\eta' \to \eta\pi^+\pi^- \to \eta\gamma^*$. This procedure is inspired by Ref. [262], which similarly derived the decays $\omega/\phi \to \pi^0\gamma^*$ that are compatible with Standard Model symmetries. Using that the dispersive representations in Ch. 8 are linear in the subtraction constants, we can parameterize their contribution to the transition form factors in explicit dependence on the leading order isoscalar and isotensor BSM coupling constants that enter $\eta \to \pi^+\pi^-\pi^0$, and the isovector coupling entering $\eta' \to \eta\pi^-\pi^0$. On the other hand, we estimate the size of possible isoscalar contributions to the transition form factor by a symmetry-driven vector-meson dominance (VMD) approach. To this end, we first extract ρ-meson couplings by an analytic continuation of $\eta \to \pi^+\pi^-\pi^0$ and $\eta' \to \eta\pi^+\pi^-$ to the second Riemann sheet and relate them to the couplings with same total isospin in the VMD amplitude with $SU(3)$ symmetry arguments and naive dimensional analysis. This procedure requires an extension of operators in ToPeχPT to describe the dynamics of vector-meson interactions. We furthermore argue how long-distance contributions from C- and CP-odd photon-hadron couplings or short-range semi-leptonic four-point interactions, cf. Sect. 6.3.4 for their description with ToPeχPT, could enter our results, but keep the focus on the conceptually more insightful hadronic long-range effects mentioned above. With this theory apparatus we calculate limits on the branching ratios for $\eta \to \pi^0\ell^+\ell^-$ and $\eta' \to \eta\ell^+\ell^-$ for the case that these transitions are driven by ToPe forces. We find that for both decays the prediction of our dispersive representation yields upper limits that are of the same order of magnitude as the experimental findings [203–205]. Moreover, we find the experimental of $\eta \to \pi^0\ell^+\ell^-$ to be more restrictive than our theoretical result and hence use the experimental ones for $\eta \to \pi^0\ell^+\ell^-$ to refine the isoscalar coupling constant entering the C- and CP-odd contribution of $\eta \to \pi^+\pi^-\pi^0$, which was found in Ch. 8 to be less rigorously constrained by the experiment than the respective isotensor coupling.
The author of this thesis carried out all numeric and analytic calculations in the concerning

publication. This especially includes the analytic derivation of a dispersion relation for the transition form factors; the non-trivial implementation of dispersion integrals as explained in detail in App. E; the inclusion of vector mesons in the formalism of ToPeχPT with corresponding applications to the required vector-meson interactions; the analytic continuation of the C-violating P-waves in $\eta \to \pi^+\pi^-\pi^0$ and $\eta' \to \eta\pi^+\pi^-$ to the pole position on the second Riemann sheet, allowing to extract the effective coupling constants which enter the respective isoscalar contribution; and an improved refit of the $\eta \to \pi^+\pi^-\pi^0$ Dalitz plot that incorporates the constraint of the upper experimental limits on $\eta \to \pi^0\ell^+\ell^-$. The co-authors Bastian Kubis and Andreas Wirzba contributed with invaluable discussions on this topic, with driving ideas throughout the working process, and with a critical review of all results and formulations.

Chapter 8

Patterns of C and CP violation in hadronic η and η' three-body decays

Studying the charge asymmetry of the $\eta \to \pi^+\pi^-\pi^0$ Dalitz-plot distribution offers an ideal stage in the search for ToPe forces. As pointed out in Ref. [62], in contrast to other C-violating processes such as $\eta^{(\prime)} \to 3\gamma$, $\eta^{(\prime)} \to \pi^0\gamma^*$, etc., the breaking of mirror symmetry in $\eta \to \pi^+\pi^-\pi^0$ is linear in these BSM operators, as it is generated through interference with the SM mechanism. Moreover, in Sect. 6.3 we have shown that $\eta \to \pi^+\pi^-\pi^0$ appears at the lowest possible order in the chiral power counting and is thus one of the most suitable candidates in order to investigate ToPe forces. The simplest observable that can be probed experimentally is the left-right asymmetry A_{LR} that compares the two halves of the Dalitz-plot distribution divided along the $\pi^+ \leftrightarrow \pi^-$ line of reflection [263]. It is also possible to construct more sophisticated quadrant and sextant asymmetry parameters A_Q and A_S that allow us to disentangle the contributions of the BSM $\Delta I = 0, 2$ operators, respectively [263–265]. The KLOE-2 collaboration, in the most precise measurement of the $\eta \to \pi^+\pi^-\pi^0$ Dalitz plot to date, reports all three asymmetry parameters to be consistent with zero [215], superseding many earlier experimental investigations [207, 263, 266–270]. Alternatively, C violation in the phenomenological expansion of the Dalitz-plot distribution, i.e., a two-dimensional Taylor series around its center, can be studied by allowing for both C-conserving and C-violating terms. Until now the KLOE-2 collaboration has probed the first four C-violating terms of this parameterization, which again are all consistent with zero [215]. Thus, experimentally there is no evidence found for C violation in $\eta \to \pi^+\pi^-\pi^0$. Theoretical studies of C violation in $\eta \to \pi^+\pi^-\pi^0$ first came to prominence [263–265] after the discovery of CP-violating $K_L^0 \to \pi\pi$ decays in the 1960s [21, 271]. Already at this time it was claimed that $\eta \to \pi^+\pi^-\pi^0$ is far more sensitive to isotensor $\Delta I = 2$ than to isoscalar $\Delta I = 0$ transitions, since the latter is suppressed by a large angular momentum barrier [217]. Chiral BSM Lagrangians from which we can deduce the effective mesonic operators $X_I^{\not C}$ for $\eta \to \pi^+\pi^-\pi^0$ were already discussed in Sect. 6.3.1. We have seen that both isoscalar and isotensor transitions can be generated without mass terms and correspond to operators of order p^6 and p^2, respectively. To shorten the notation, especially for the isoscalar operator, we quote the operators in cartesian basis, cf. Eq. (3.50), as

$$\begin{aligned} X_0^{\not C} &\sim \epsilon_{ijk}\,(\partial_\mu\partial_\nu\partial_\lambda\pi^i)(\partial^\mu\partial^\nu\pi^j)(\partial^\lambda\pi^k)\,\eta\,, \\ X_2^{\not C} &\sim \epsilon_{ij3}\,\pi^i\,(\partial_\mu\pi^j)(\partial^\mu\pi^3)\,\eta\,. \end{aligned} \tag{8.1}$$

Note that both operators in this basis have to be multiplied by a *real*-valued LEC to obtain

the desired T-odd attribute. This can be understood from the fact that under T both π^1 and π^3 are invariant and π^2 flips its sign, otherwise the charged pions in Eq. (3.50) would not transform as T-odd quantities (as they should according to Sect. 6.1.2). Furthermore, note that in contrast to the Levi-Civita symbol $\epsilon_{\alpha\beta\mu\nu}$ with Lorentz indices, the three-dimensional ϵ_{ijk} acts in isospin space and is thus unaffected by T. The above operators imply a strong kinematic suppression of the $\Delta I = 0$ transition compared to $\Delta I = 2$ across the Dalitz plot, given the small available phase space in $\eta \to \pi^+\pi^-\pi^0$, as long as the respective coupling strengths of both operators, i.e., g_0 and g_2, are of similar size. So far we only have the NDA estimate $g_0 \sim \Lambda_\chi^4 g_2 \approx 2\,\text{GeV}^4 \cdot g_2$ from Sect. 6.3.1.2, which may be verified or corrected—according to the current experimental precision—in the course of this chapter.

Since the 1960s C violation in this decay has been mostly neglected by theory until recently a new theoretical formalism was proposed in Ref. [62]. In this framework the decay amplitude is decomposed into three contributions that can be associated with operators describing the isospin transitions $\Delta I = 0, 1, 2$. While the Standard-Model contribution is driven almost exclusively by the $\Delta I = 1$ contribution (ignoring isospin breaking of higher order that is known to have only tiny effects [272, 273]), the additional BSM amplitudes arise from $\Delta I = 0, 2$ transitions. The individual strengths of the latter are given by two complex-valued normalizations.[1] Physically this approach is more meaningful compared to simple phenomenological (i.e., polynomial) parameterizations, as it allows for a direct extraction of the coupling strengths that may subsequently be matched to underlying BSM operators. The energy dependence of the C-violating amplitudes in Ref. [62] is based on the well-known one-loop representation of the SM decay in chiral perturbation theory (χPT) [274]. The authors find the BSM normalization of the $\Delta I = 0$ amplitude to be between two and four orders of magnitude less rigorously constrained than the $\Delta I = 2$ one, which is a result of the predicted kinematic suppression of the $\Delta I = 0$ transition [217], but again there is no hint for C violation in $\eta \to \pi^+\pi^-\pi^0$ as both BSM normalizations are consistent with zero.

A more rigorous construction of the BSM amplitudes consistent with the fundamental principles of analyticity (a mathematical description of causality) and unitarity (a consequence of probability conservation) can be achieved with techniques from dispersion theory, using the so-called Khuri–Treiman representations [106]. As Sutherland's theorem [275, 276], a statement of current algebra, and χPT calculations [272, 277] proved that electromagnetic effects are tiny compared to isospin breaking due to the light quark mass difference $m_u - m_d$, modern dispersion-theoretical studies of the SM contribution $\eta \to 3\pi$ [278–284] focus on a consistent, non-perturbative description of the final-state interactions with the goal to provide information on these fundamental SM parameters. Such a treatment of final-state interactions can also be incorporated in the C-violating amplitudes by establishing the corresponding dispersion relations for the $\Delta I = 0, 2$ transitions. As a by-product, such dispersive amplitude representations allow us to argue more rigorously why the dependence on yet unknown short-distance operators can be subsumed in a single unknown multiplicative

[1] As discussed at a later stage, we would already like to emphasize at this point that these normalization of Ref. [62] neither respect hermiticity nor do they account for the correct T transformation.

constant for each isospin. This non-perturbative approach has to be clearly distinguished from the formalism of ToPeχPT in Ch. 6 and can act as a supplement of the latter, as already shown in Sect. 6.3.1.2.

The opportunity to investigate C-odd effects as an interference in a Dalitz plot exists similarly for the decay $\eta' \to \eta\pi^+\pi^-$ (although without the potential benefit of the SM decay being suppressed by isospin). This is particularly interesting as the possible asymmetry in the distribution of the charged pions in this decay is sensitive to a different class of C-violating operators from those constrained in $\eta \to \pi^+\pi^-\pi^0$, namely the ones with $\Delta I = 1$. Both decays therefore provide orthogonal probes as far as the isospin structure of the C-violating operators is concerned. For $\eta' \to \eta\pi^+\pi^-$ such an operator must include two derivatives and explicitly reads

$$X_1^{\not C} \sim \epsilon_{ij3}\, \pi^i\, (\partial_\mu \pi^j)(\partial^\mu \eta)\, \eta' \,. \tag{8.2}$$

The experimental limits on the left-right asymmetry A_{LR} and the C-odd contributions of the phenomenological Dalitz-plot expansion measured by the BESIII collaboration [219] vanish again within one standard deviation. Prior to that, measurements by VES [285] as well as an earlier BESIII result [286] came to the same conclusion, albeit with much lower accuracy. While the theoretical description of the SM contribution relying on a sophisticated dispersion-theoretical approach was first established in Refs. [82, 287], the incorporation of C-violating effects is missing so far.

In this chapter we generalize the dispersion-theoretical analysis of C-conserving SM $\eta \to 3\pi$ and $\eta' \to \eta\pi\pi$ decays to additional C- and T-violating BSM contributions. Accordingly, the presented dispersive representations account for a consistent resummation of the respective three-particle final-state interactions in all allowed isospin transitions. To establish dispersion relations for the new C-violating contributions we split our analysis into two parts, Sect. 8.1 dealing with $\eta \to 3\pi$ and Sect. 8.2 with $\eta' \to \eta\pi\pi$, and follow the same general strategy in both of them. We start with the definition of the T-matrix elements and the general kinematics of the respective process in Sects. 8.1.1 and 8.2.1. In Sects. 8.1.2 and 8.2.2 we decompose the amplitudes into ones depending on one Mandelstam variable only, tremendously simplifying the evaluation. These single-variable amplitudes (SVA) are constrained by elastic unitarity as described in Sects. 8.1.3 and 8.2.3. Sections 8.1.5 and 8.2.5 describe how to extract coupling constants for the effective BSM operators in terms of the subtraction constants. The latter are the free parameters of our dispersive representation, which are fixed by a χ^2-fit to data in Sects. 8.1.6 and 8.2.6. Afterwards we compare our representations of the three-body amplitudes to measurements of the corresponding Dalitz-plot distributions and theoretical constraints in Sects. 8.1.7 and 8.2.7. Section 8.1.8 contains a brief comment on how to generalize the analysis for $\eta \to \pi^+\pi^-\pi^0$ to $\eta' \to \pi^+\pi^-\pi^0$. We conclude our study with a summary covering both parts in Sect. 8.3.

8.1 | Dispersive representation of $\eta \to 3\pi$

To investigate ToPe forces in $\eta \to \pi^+\pi^-\pi^0$ we rely on the sophisticated and well-established Khuri–Treiman framework [106], in which a set of integral equations for the scattering process $\eta\pi \to \pi\pi$ is established. For the corresponding dispersion relations we only take the dominant elastic pion–pion rescattering into account. With an analytic continuation of the decay mass as well as the Mandelstam variables one can project onto the physical realm of the decay, thereby taking final-state interactions to all orders in perturbation theory into account, and at the same time obtain a manifestly unitary amplitude. This formalism builds on the inhomogeneous Omnès problem discussed in Sect. 3.4.3.

Before going into more detail, let us have a look at the general properties of the $\eta \to \pi^+\pi^-\pi^0$ amplitude. Regarding the involved quantum numbers, Bose symmetry demands that $C = (-1)^{I+1}$ [264], where I is the total isospin of the three-body final state, which has to be distinguished from the isospin of the decaying meson. In analyses consistent with the symmetries of the Standard Model [273, 274, 278–284, 288–293], the decay amplitude is exclusively driven by isospin-breaking effects. The reason for this lies in the fact that this decay breaks G-parity, whose prerequisite is that either isospin or charge conjugation symmetry is broken, or both. As Standard-Model analyses consider the latter the more cherished symmetry (disregarding the weak interactions), the corresponding amplitudes solely contain $\Delta I = 1$ transitions.[2] On the contrary, in this work we allow for even isospin transitions $\Delta I = 0, 2$ and hence imply C violation. Moreover, considering that all involved particles are pseudoscalars, the decay at hand preserves parity and one can conclude that CP has to be violated, too. In summary, the C-violating mechanisms are driven by isoscalar $\Delta I = 0$ or isotensor $\Delta I = 2$ operators [217, 221, 264, 265], such that the generalized $\eta \to \pi^+\pi^-\pi^0$ amplitude has to be of the form [62]

$$\mathcal{M}_c(s,t,u) = \mathcal{M}_0^{\not C}(s,t,u) + \xi\,\mathcal{M}_1^{C}(s,t,u) + \mathcal{M}_2^{\not C}(s,t,u), \tag{8.3}$$

which is split into a contribution for each total isospin denoted by the respective index. In accordance with Refs. [281, 283], we factorized out the isospin-breaking normalization of the SM amplitude

$$\xi = \frac{\hat{M}_{K^+}^2 - \hat{M}_{K^0}^2}{3\sqrt{3}F_\pi^2} = -0.140(9) \tag{8.4}$$

in terms of the pion decay constant F_π and the QCD kaon-mass difference. The isoscalar amplitude $\mathcal{M}_0^{\not C}$ is isospin-conserving but C-violating, the Standard-Model amplitude $\mathcal{M}_1^{C}$ is isospin-violating but C-conserving, and the isotensor contribution $\mathcal{M}_2^{\not C}$ violates both quantum numbers. Note that isospin symmetry is an accidental (approximate) symmetry of the strong interactions due to the smallness of the two lightest quark masses (as well as their difference) on typical hadronic scales; as we do not know anything about the isospin structure of the BSM operators, there is no reason to assume isospin to be a useful symmetry for them, too, and hence imply any kind of hierarchy between isoscalar and isotensor C

[2] The C-conserving $\Delta I = 3$ transition is strongly suppressed.

violation on the underlying, fundamental level.
As a further consequence of Bose symmetry, the C-violating operators can only contribute to the charged decay mode, but not to $\eta \to 3\pi^0$. The latter is thus solely given in terms of $\mathcal{M}_1^C$ and explicitly reads

$$\mathcal{M}_n(s,t,u) = \xi \left[\mathcal{M}_1^C(s,t,u) + \mathcal{M}_1^C(t,u,s) + \mathcal{M}_1^C(u,s,t)\right], \tag{8.5}$$

as demanded by isospin symmetry. Corrections to Eq. (8.5) arise only due to higher-order corrections such as virtual-photon effects or the charged-to-neutral pion mass difference [272, 273].
As the Standard-Model contribution $\mathcal{M}_1^C$ has already been extensively studied using Khuri–Treiman equations in Refs. [278–284, 289, 290], in this section we generalize the dispersive analysis by elaborating on the C- and CP-odd amplitudes $\mathcal{M}_0^{\not C}$ and $\mathcal{M}_2^{\not C}$.

8.1.1 | Kinematics

Let us define the $\eta \to \pi^+\pi^-\pi^0$ transition amplitude in the common manner

$$\left\langle \pi^+(p_+)\,\pi^-(p_-)\,\pi^0(p_0)\middle|iT\middle|\eta(P_\eta)\right\rangle = i\,(2\pi)^4\,\delta^{(4)}(P_\eta - p_+ - p_- - p_0)\,\mathcal{M}_c(s,t,u)\,. \tag{8.6}$$

Up to the overall isospin-breaking normalization, we work in the isospin limit, i.e., $M_\pi \equiv M_{\pi^\pm} = M_{\pi^0}$, and conventionally write the corresponding Mandelstam variables as

$$s = (P_\eta - p_0)^2\,, \qquad t = (P_\eta - p_+)^2\,, \qquad u = (P_\eta - p_-)^2\,, \tag{8.7}$$

fulfilling the relation

$$s + t + u = M_\eta^2 + 3M_\pi^2 \equiv 3r\,. \tag{8.8}$$

Note that the amplitude $\mathcal{M}_1^C$ is symmetric under $t \leftrightarrow u$, while $\mathcal{M}_0^{\not C}$ and $\mathcal{M}_2^{\not C}$ are both antisymmetric under the exchange of these two Mandelstam variables. In the two-pion center-of-mass system, t and u can be expressed in terms of s and the s-channel scattering angle z_s by

$$t(s,z_s) = u(s,-z_s) = \frac{1}{2}\big(3r - s + \kappa(s) z_s\big)\,, \tag{8.9}$$

with

$$z_s = \cos\theta_s = \frac{t-u}{\kappa(s)}\,, \qquad \kappa(s) = \sigma(s)\,\lambda^{1/2}(M_\eta^2, M_\pi^2, s)\,, \tag{8.10}$$

where $\sigma(s) = \sqrt{1-4M_\pi^2/s}$ and $\lambda(x,y,z) = x^2+y^2+z^2-2(xy+xz+yz)$ denotes the Källén function. Analogously, the scattering angles in the t and u channels are $z_t = (u-s)/\kappa(t)$ and $z_u = (s-t)/\kappa(u)$, respectively.

8.1.2 | Reconstruction theorem

To avoid the intricate analysis of complex functions depending on multiple variables one can exploit a decomposition of the amplitude into single-variable functions. Such a de-

composition is commonly referred to as *reconstruction theorem*. It was first proven that the latter holds exactly up to and including two-loop order in the framework of χPT for $\pi\pi$ scattering [98], followed by generalizations for unequal masses [100] and scattering of mesons belonging to the pseudoscalar octet [101].

We already encountered a reconstruction theorem in Sect. 3.3.1. Instead of repeating the rather complicated derivation outlined there including additional contributions of different two-body isospins and the expected symmetrization in the Mandelstam variables, let us sketch how to derive the reconstruction theorem for the decay at hand in a much easier (but maybe less rigorous) fashion. To this end, we start by considering the s-, t-, and u-channel discontinuities for the according two-particle scattering amplitudes, i.e., $\eta\pi^0 \to \pi^+\pi^-$, $\eta\pi^+ \to \pi^+\pi^0$, and $\eta\pi^- \to \pi^-\pi^0$ respectively, for the SM contribution $\mathcal{M}_1^C$. Employing the partial-wave expansion from Eq. (B.19) for the angular momentum ℓ of the two-body state and summing over all allowed two-body isospins I, we can express these discontinuities in terms of partial-wave amplitudes $f_\ell^I(x)$. For this purpose, note that the pions in the s-channel cannot couple to $I = 1$, neither can t- and u-channels include a state of $I = 0$. Furthermore, due to Bose symmetry,[3] odd partial waves must be accompanied by an odd isospin of the $\pi\pi$ state. Combining these considerations and neglecting the discontinuities of D- and higher partial waves, one may write for each channel [88]

$$\begin{aligned}
\operatorname{disc}_s \mathcal{M}_1^C(s,z_s) &= \operatorname{disc} f_0^0(s) - \frac{2}{3}\operatorname{disc} f_0^2(s) &&\longrightarrow \quad \mathcal{F}_0^0(s) - \frac{2}{3}\mathcal{F}_0^2(s)\,,\\
\operatorname{disc}_t \mathcal{M}_1^C(t,z_t) &= \operatorname{disc} f_0^2(t) - z_t\kappa(t)\operatorname{disc} f_1^1(t) &&\longrightarrow \quad \mathcal{F}_0^2(t) + (s-u)\mathcal{F}_1^1(t)\,,\\
\operatorname{disc}_u \mathcal{M}_1^C(u,z_u) &= \operatorname{disc} f_0^2(u) + z_u\kappa(u)\operatorname{disc} f_1^1(u) &&\longrightarrow \quad \mathcal{F}_0^2(u) + (s-t)\mathcal{F}_1^1(u)\,,
\end{aligned} \tag{8.11}$$

where the single-variable functions $\mathcal{F}_\ell^I$ on the right, which we elaborate on in the next section, denote the contribution of each discontinuity to the reconstruction theorem. Note that when summing up the partial waves with different isospin we considered isospin factors, which can be calculated from corresponding Clebsch–Gordon coefficients [13]. These relative factors are a result of the Wigner–Eckart theorem [294, 295] and account for combinations of the different incoming and outgoing isospin states. More information on how to extract these isospin coefficients may be found for instance in Refs. [282, 283].[4] On the right-hand side, we moreover replaced $z_x\kappa(x)$ by the respective difference of Mandelstam variables, cf. Sect. 8.1.1. We can proceed analogously for the C-violating contributions. For $\mathcal{M}_0^{\not C}$ with

[3] As the strong interaction does not distinguish between the electromagnetic charges, π^0, π^+, and π^- can indeed be treated as identical particles, such that each $\pi\pi$ wave function has to be symmetric according to Bose statistics.

[4] Conventionally, constant factors are absorbed in the definition of the partial waves to obtain more handy results.

partial waves g_ℓ^I we obtain

$$\begin{aligned}
\operatorname{disc}_s \mathcal{M}_0^{\mathscr{C}}(s,z_s) &= z_s\kappa(s)\operatorname{disc} g_1^1(s) \quad &\longrightarrow \quad (t-u)\mathcal{G}_1^1(s)\,,\\
\operatorname{disc}_t \mathcal{M}_0^{\mathscr{C}}(t,z_t) &= z_t\kappa(t)\operatorname{disc} g_1^1(t) \quad &\longrightarrow \quad (u-s)\mathcal{G}_1^1(t)\,,\\
\operatorname{disc}_u \mathcal{M}_0^{\mathscr{C}}(u,z_u) &= z_u\kappa(u)\operatorname{disc} g_1^1(u) \quad &\longrightarrow \quad (s-t)\mathcal{G}_1^1(u)\,,
\end{aligned} \tag{8.12}$$

and the discontinuities for $\mathcal{M}_2^{\mathscr{C}}$, whose partial waves are denoted by h_ℓ^I, yield

$$\begin{aligned}
\operatorname{disc}_s \mathcal{M}_2^{\mathscr{C}}(s,z_s) &= -2z_s\kappa(s)\operatorname{disc} h_1^1(s) \quad &\longrightarrow \quad 2(u-t)\mathcal{H}_1^1(s)\,,\\
\operatorname{disc}_t \mathcal{M}_2^{\mathscr{C}}(t,z_t) &= -\operatorname{disc} h_0^2(t) + z_t\kappa(t)\operatorname{disc} h_1^1(t) \quad &\longrightarrow \quad -\mathcal{H}_0^2(t) + (u-s)\mathcal{H}_1^1(t)\,,\\
\operatorname{disc}_u \mathcal{M}_2^{\mathscr{C}}(u,z_u) &= \operatorname{disc} h_0^2(u) + z_u\kappa(u)\operatorname{disc} h_1^1(u) \quad &\longrightarrow \quad \mathcal{H}_0^2(u) + (s-t)\mathcal{H}_1^1(u)\,.
\end{aligned} \tag{8.13}$$

Hence, we can finally express each amplitude of *total* isospin, on the right-hand side of Eq. (8.3), in terms of functions depending on only one kinematic variable, the relative angular momentum and isospin of the $\pi\pi$ intermediate state [62, 289, 290]:

$$\begin{aligned}
\mathcal{M}_1^C(s,t,u) &= \mathcal{F}_0(s) + (s-u)\,\mathcal{F}_1(t) + (s-t)\,\mathcal{F}_1(u) + \mathcal{F}_2(t) + \mathcal{F}_2(u) - \frac{2}{3}\mathcal{F}_2(s)\,,\\
\mathcal{M}_0^{\mathscr{C}}(s,t,u) &= (t-u)\,\mathcal{G}_1(s) + (u-s)\,\mathcal{G}_1(t) + (s-t)\,\mathcal{G}_1(u)\,,\\
\mathcal{M}_2^{\mathscr{C}}(s,t,u) &= 2(u-t)\,\mathcal{H}_1(s) + (u-s)\,\mathcal{H}_1(t) + (s-t)\,\mathcal{H}_1(u) - \mathcal{H}_2(t) + \mathcal{H}_2(u)\,.
\end{aligned} \tag{8.14}$$

Here we simplified the notation using that the isospin I of the two-pion state fixes the partial wave ℓ unambiguously by means of $\mathcal{A}_{0,2} \equiv \mathcal{A}_{I=0,2}^{\ell=0}$ and $\mathcal{A}_1 \equiv \mathcal{A}_{I=1}^{\ell=1}$, with $\mathcal{A} \in \{\mathcal{F},\mathcal{G},\mathcal{H}\}$. Note that the single-variable functions $\mathcal{F}$, $\mathcal{G}$, and $\mathcal{H}$ are completely decoupled and can be evaluated independently. Furthermore, each single-variable function $\mathcal{A}_I(s)$ has only a right-hand cut. At this point the charge asymmetry in the C-odd contributions, stemming from the exchange $t \leftrightarrow u$, becomes evident. It is worth noting that the decomposition into single-variable functions presented here is not unique. The relation between the Mandelstam variables given in Eq. (8.8) allows us to shift the amplitude by polynomials in s, t, and u, i.e., $\mathcal{A}_I \to \mathcal{A}_I + \Delta\mathcal{A}_I$, without affecting the reconstruction theorems. The five-parameter ambiguity for the Standard Model reads [283]

$$\begin{aligned}
\Delta\mathcal{F}_0(s) &= -4a_1 + b_1\,(5s-9r) - 3c_1\,(s-r) - 27d_1\,r\,(s-r)\\
&\qquad + 4d_1\,s^2 - 162e_1\,r^2\,(s-r) - 4e_1\,s^2\,,\\
\Delta\mathcal{F}_1(s) &= c_1 + 3d_1\,s + 9e_1\,s^2\,,\\
\Delta\mathcal{F}_2(s) &= 3a_1 + 3b_1\,s - 3d_1 s^2 + 3e_1\,s^2\,(s-9r)\,,
\end{aligned} \tag{8.15}$$

while for the C-odd contributions we find

$$\begin{aligned}\Delta\mathcal{G}_1(s) &= a_0 + b_0\, s + c_0\, s^2\,(3r - s)\,,\\ \Delta\mathcal{H}_1(s) &= a_2 + b_2\, s + c_2\, s^2\,,\\ \Delta\mathcal{H}_2(s) &= d_2 - 3a_2\, s + 3b_2\, s\,(s - 3r) + 9c_2\, r\, s\,(s - 2r) - c_2\, s^3\,.\end{aligned} \tag{8.16}$$

The invariance groups of the amplitudes $\mathcal{M}_1^C$, $\mathcal{M}_0^{\not C}$, and $\mathcal{M}_2^{\not C}$, given by polynomial ambiguities, are different and independent of each other (in contrast to the erroneous assumption made in Ref. [62]).

Finally, we would like to address the issue of corrections to the reconstruction theorems for $\mathcal{M}_1^C$, $\mathcal{M}_0^{\not C}$, and $\mathcal{M}_2^{\not C}$ stated in Eq. (8.14). The next discontinuities, beyond those in S- and P-waves, would come from D- (for even isospin) and F-waves (for odd isospin). Since the symmetry structure of the isoscalar amplitude does not allow for even partial waves, it is obvious that its reconstruction theorem actually holds up to corrections due to F- and higher (odd) partial waves. Moreover, possible D-wave contributions to the discontinuity of the isotensor amplitude are only allowed to have $I = 2$, which is a nonresonant and extremely small partial wave at low energies. As the validity of the reconstruction theorem for the C-conserving amplitude $\mathcal{M}_1^C$, which neglects discontinuities due to $I = 0$ D-wave pion–pion rescattering, is well-established and tested against very accurate data, we conclude that corrections to the decomposition of the C-violating amplitudes $\mathcal{M}_0^{\not C}$ and $\mathcal{M}_2^{\not C}$ are necessarily even smaller and therefore entirely negligible.

8.1.3 | Elastic unitarity

Within the scope of this work we will exclusively study the dominant elastic rescattering effects, i.e., we restrict the evaluation of the single-variable functions to $\pi\pi$ intermediate states only. Due to the simplification of the reconstruction theorem, we are left with the evaluation of a scalar $2 \to 2$ scattering amplitude for fixed isospin and partial wave, i.e., our single-variable functions $\mathcal{A}_I$. As we are dealing with an inhomogenous Omnès problem we refer the reader to Sect. 3.4.3 for the derivations of formulas given below.

In order to obtain an amplitude with manifest unitarity, each single-variable function has to obey the discontinuity relation

$$\operatorname{disc}\mathcal{A}_I(s) = 2i\,\theta(s - 4M_\pi^2)\left[\mathcal{A}_I(s) + \hat{\mathcal{A}}_I(s)\right]\,\sin\delta_I(s)\,e^{-i\delta_I(s)}\,, \tag{8.17}$$

Here we introduced the so-called *inhomogeneities* $\hat{\mathcal{A}}_I(s)$ that do not have a discontinuity along the right-hand cut and can be evaluated by a projection onto the respective partial wave with fixed isospin

$$a_I(s) = \mathcal{A}_I(s) + \hat{\mathcal{A}}_I(s)\,. \tag{8.18}$$

Note that the full information about the discontinuity of the partial wave along the right-hand cut is contained in the respective $\mathcal{A}_I(s)$. Let us now, for the sake of simplicity, define

the angular average

$$\langle z_s^n \, \mathcal{A}_I \rangle \equiv \frac{1}{2} \int_{-1}^{1} \mathrm{d}z_s \, z_s^n \, \mathcal{A}_I\big(t(s,z_s)\big) \,. \tag{8.19}$$

This allows to write the inhomogeneities for the Standard-Model amplitude in the shortened form

$$\begin{aligned}
\hat{\mathcal{F}}_0(s) &= \frac{2}{9}\big[3\langle \mathcal{F}_0\rangle + 9(s-r)\,\langle \mathcal{F}_1\rangle + 3\kappa\,\langle z_s\,\mathcal{F}_1\rangle + 10\langle \mathcal{F}_2\rangle\big] \,, \\
\hat{\mathcal{F}}_1(s) &= \frac{1}{2\kappa}\big[6\langle z_s\,\mathcal{F}_0\rangle + 9(s-r)\,\langle z_s\,\mathcal{F}_1\rangle + 3\kappa\,\langle z_s^2\,\mathcal{F}_1\rangle - 10\langle z_s\,\mathcal{F}_2\rangle\big] \,, \\
\hat{\mathcal{F}}_2(s) &= \frac{1}{6}\big[6\langle \mathcal{F}_0\rangle - 9(s-r)\,\langle \mathcal{F}_1\rangle - 3\kappa\,\langle z_s\,\mathcal{F}_1\rangle + 2\langle \mathcal{F}_2\rangle\big] \,,
\end{aligned} \tag{8.20}$$

and the ones for the C-violating contributions as

$$\begin{aligned}
\hat{\mathcal{G}}_1(s) &= -\frac{3}{\kappa}\big[3(s-r)\,\langle z_s\,\mathcal{G}_1\rangle + \kappa\,\langle z_s^2\,\mathcal{G}_1\rangle\big] \,, \\
\hat{\mathcal{H}}_1(s) &= \frac{3}{2\kappa}\big[3(s-r)\,\langle z_s\,\mathcal{H}_1\rangle + \kappa\,\langle z_s^2\,\mathcal{H}_1\rangle + 2\langle z_s\,\mathcal{H}_2\rangle\big] \,, \\
\hat{\mathcal{H}}_2(s) &= \frac{1}{2}\big[9(s-r)\,\langle \mathcal{H}_1\rangle + 3\kappa\,\langle z_s\,\mathcal{H}_1\rangle - 2\langle \mathcal{H}_2\rangle\big] \,.
\end{aligned} \tag{8.21}$$

Note that the argument of $\mathcal{A}_I$ in Eq. (8.19) is Mandelstam t, meaning that the inhomogeneity in the s-channel single-variable function is determined by contributions of the crossed channels. In other words, $\hat{\mathcal{A}}(s)$ contains left-hand-cut contributions to the respective partial wave.

In order to obtain a unique solution for the discontinuity relation in Eq. (8.17) it is appealing to first consider the homogeneous case by setting $\hat{\mathcal{A}}_I(s) = 0$.[5] The homogeneous solution corresponds to the one of a pion form factor (of the appropriate quantum numbers) and is given in terms of the Omnès function [105]

$$\Omega(s) = \exp\left(\frac{s}{\pi}\int_{4M_\pi^2}^{\infty}\frac{\mathrm{d}x}{x}\,\frac{\delta(x)}{(x-s)}\right) . \tag{8.22}$$

Using the latter, the general solution becomes

$$\mathcal{A}_I(s) = \Omega_I(s)\left(P_{n-1}(s) + \frac{s^n}{\pi}\int_{4M_\pi^2}^{\infty}\frac{\mathrm{d}x}{x^n}\,\frac{\sin\delta_I(x)\,\hat{\mathcal{A}}_I(x)}{|\Omega_I(x)|\,(x-s)}\right) , \tag{8.23}$$

where $P_{n-1}(s)$ is a polynomial in s of order $n-1$. Its coefficients are known as subtraction constants, which are the only free parameters of our amplitude. The order of the subtraction polynomial is fixed by the asymptotics imposed on the single-variable functions and phase shifts, as worked out in the following section.

Throughout this section, we will assume all subtraction constants within the same decay

[5] This scenario is consistent with Watson's final-state theorem, which states that the phase of $\mathcal{A}_I$ coincides with the phase shift of elastic $\pi\pi$ rescattering.

amplitude representation to be *relatively real*. This is not rigorously true to arbitrary precision, as the SVAs do not fulfill the Schwarz' reflection principle, and their discontinuities are complex. However, the potential imaginary parts of the subtraction constants scale with the available three-body phase space, and therefore are tiny for decays such as $\eta \to 3\pi$ or $\eta' \to \eta\pi\pi$. This has been tested explicitly for $\eta \to 3\pi$ [283], making use of the two-loop representation in chiral perturbation theory [293], with the result that imaginary parts in the dispersive subtractions are entirely negligible. This is, however, not true any more for Khuri–Treiman representations of three-body decays with larger energy releases, see $\phi \to 3\pi$ [107] or certain D-meson decays [296, 297].

Besides these degrees of freedoms, which have to be fixed by data regression or matching to effective theories, the only input for the dispersive $\eta \to 3\pi$ amplitude are the $\pi\pi$ scattering phase shifts $\delta_I(s)$.

8.1.4 | Subtraction scheme

Choosing the number of subtraction constants n is a rather sensitive issue. Having a purely mathematical look at the dispersion integral in Eq. (8.23), the minimal number is the one at which convergence is ensured. Any additional subtraction just leads to a rearrangement of the equation. The thereby introduced subtraction constants have to fulfill the corresponding sum rule, such that the minimally and higher subtracted integrals are analytically the same. Any deviation from the respective sum rule violates the initially assumed high-energy behavior and is inconsistent as a matter of principle. But allowing the additional subtraction constants to vary from the sum rule suppresses the hardly-constrained high-energy behavior of the dispersion integral and introduces additional degrees of freedom in a fit to experimental data.

Past studies in the same Khuri–Treiman framework as presented here [281, 283] put their main focus on maximal precision of the low-energy representation of the $\eta \to 3\pi$ Standard-Model decay amplitude, and therefore incorporated a rather generous number of subtraction constants. Our aim here is slightly different: we will demonstrate that with rigorous assumptions on the high-energy behavior, and accordingly a minimal number of free parameters, we are still able to describe the Dalitz plot data sufficiently well. Subsequently, we impose the *same* high-energy asymptotics on the two C-violating amplitudes, and show that as a result, they can be written in terms of one single subtraction constant each. In this manner, we can prove that the mere assumption to describe the BSM amplitudes in terms of a multiplicative normalization only [62] can be justified more rigorously in terms of their analytic properties.

In order to investigate the convergence of the dispersion integral, some assumptions have to be made for the asymptotics of $\delta_I(s)$ and $\mathcal{A}_I(s)$. We rely on a Roy equation analysis [298, 299] to fix our phase shifts very precisely in the low-energy range, i.e., below about 1GeV^2, as shown in Fig. 8.1. Unfortunately the high-energy behavior is not severely restricted by these equations. Therefore we suppose that in the limit $s \to \infty$ the phase shifts approximate

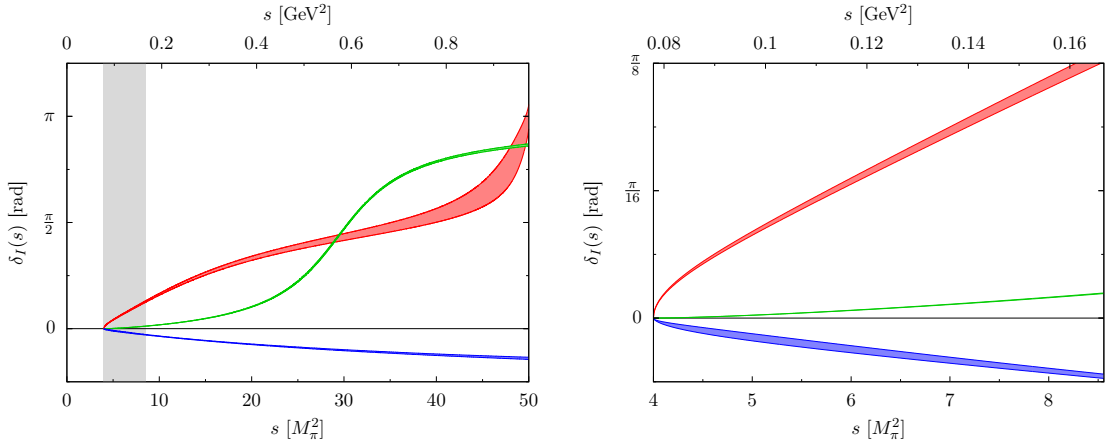

Figure 8.1: The S- and P-wave $\pi\pi$ scattering phase shifts δ_0 (red), δ_1 (green), and δ_2 (blue) covering low-energy uncertainty bands as determined by Roy equation analysis [298, 299]. Left panel: behavior of the phase shifts in the low-energy region below the $K\bar{K}$-threshold at about $50M_\pi^2$. The phase space for $\eta \to 3\pi$ is indicated by the gray region. Right panel: magnification of the physical decay region.

constants

$$\delta_0(s) \to \pi\,, \qquad \delta_1(s) \to \pi\,, \qquad \delta_2(s) \to 0\,, \tag{8.24}$$

and analytically continue them accordingly. These limits directly fix the asymptotics of the Omnès functions, which behave for $s \to \infty$ like s^{-k} if $\delta_I(s) \to k\pi$. Further, in order to use the minimal number of subtraction constants, we assume that our amplitudes scale in the limit of large momenta as

$$\mathcal{A}_0(s) = \mathcal{O}(s^0)\,, \qquad \mathcal{A}_1(s) = \mathcal{O}(s^{-1})\,, \qquad \mathcal{A}_2(s) = \mathcal{O}(s^0)\,, \tag{8.25}$$

and are thus even more restrictive than suggested by the Froissart–Martin bound [102]. Finally, with our minimal subtraction scheme we can obtain for the C-conserving Standard-Model amplitude

$$\begin{aligned}
\mathcal{F}_0(s) &= \Omega_0(s)\left(\alpha + \beta\, s + \frac{s^2}{\pi}\int_{4M_\pi^2}^{\infty}\frac{\mathrm{d}x}{x^2}\,\frac{\sin\delta_0(x)\,\hat{\mathcal{F}}_0(x)}{|\Omega_0(x)|\,(x-s)}\right),\\
\mathcal{F}_1(s) &= \Omega_1(s)\left(\gamma + \frac{s}{\pi}\int_{4M_\pi^2}^{\infty}\frac{\mathrm{d}x}{x}\,\frac{\sin\delta_1(x)\,\hat{\mathcal{F}}_1(x)}{|\Omega_1(x)|\,(x-s)}\right),\\
\mathcal{F}_2(s) &= \Omega_2(s)\left(\frac{s}{\pi}\int_{4M_\pi^2}^{\infty}\frac{\mathrm{d}x}{x}\,\frac{\sin\delta_2(x)\,\hat{\mathcal{F}}_2(x)}{|\Omega_2(x)|\,(x-s)}\right).
\end{aligned} \tag{8.26}$$

This representation hence depends on three free parameters (all of which are chosen to be real), where Refs. [281, 283] employed six. Similarly rigorous schemes with few parameters have previously been suggested in Refs. [279, 280, 282]. Analogously the C-violating

contributions become

$$\begin{aligned}
\mathcal{G}_1(s) &= \Omega_1(s)\left(\varepsilon + \frac{s}{\pi}\int_{4M_\pi^2}^{\infty}\frac{\mathrm{d}x}{x}\,\frac{\sin\delta_1(x)\,\hat{\mathcal{G}}_1(x)}{|\Omega_1(x)|\,(x-s)}\right),\\
\mathcal{H}_1(s) &= \Omega_1(s)\left(\vartheta + \frac{s}{\pi}\int_{4M_\pi^2}^{\infty}\frac{\mathrm{d}x}{x}\,\frac{\sin\delta_1(x)\,\hat{\mathcal{H}}_1(x)}{|\Omega_1(x)|\,(x-s)}\right),\\
\mathcal{H}_2(s) &= \Omega_2(s)\left(\frac{s}{\pi}\int_{4M_\pi^2}^{\infty}\frac{\mathrm{d}x}{x}\,\frac{\sin\delta_2(x)\hat{\mathcal{H}}_2(x)}{|\Omega_2(x)|\,(x-s)}\right).
\end{aligned} \tag{8.27}$$

Note that these representations are not unique. We exploited the ambiguity of the dispersive representation, as given in Eqs. (8.15) and (8.16), to express the single-variable functions in terms of independent subtraction constants only. Conventionally, we shifted the polynomials $\Delta\mathcal{A}_I$ such that the $I = 2$ amplitudes do not contain subtraction constants. Further, we would like to remark that the normalization of each amplitude of total isospin in Eq. (8.3) has a phase that is fixed unambiguously by T violation and hermiticity. Hence, the subtraction constants ε and ϑ, which absorb these normalizations, are complex quantities with a fixed phase, resulting in a total of five degrees of freedom for $\mathcal{M}$. We furthermore note that, were it not for strong rescattering phases, interference between the (then purely real) Standard-Model and the (purely imaginary) C-violating amplitudes would vanish altogether, and no Dalitz-plot asymmetries would be generated at all. This further increases the importance to implement these rescattering effects via the corresponding phase shifts exactly, using dispersion theory.[6]

The fact that these two subtraction constants indeed merely serve as overall normalizations of the BSM contributions becomes evident when realizing that the dispersive representation is linear in the subtraction constants. This very powerful property allows us to write

$$\mathcal{M}(s,t,u) = \sum_\nu \nu\,\mathcal{M}^\nu(s,t,u)\,, \qquad \mathcal{M}^\nu(s,t,u) = \mathcal{M}(s,t,u)|_{\nu=1,\,\mu=0,\,\ldots}\,, \tag{8.28}$$

where ν and μ denote generic subtraction constants and $\mathcal{M} \in \{\mathcal{M}_0^{\mathscr{C}}, \mathcal{M}_1^{C}, \mathcal{M}_2^{\mathscr{C}}\}$. The newly introduced functions $\mathcal{M}^\nu$ have their own *basis amplitudes* $\mathcal{A}_I^\nu$ defined by

$$\mathcal{A}_I(s) = \sum_\nu \nu\,\mathcal{A}_I^\nu(s)\,, \qquad \mathcal{A}_I^\nu(s) = \mathcal{A}_I(s)|_{\nu=1,\,\mu=0,\,\ldots}\,, \tag{8.29}$$

each of those fulfilling the respective reconstruction theorem separately. The great advantage of paraphrasing the amplitudes in this way is that instead of solving the Khuri–Treiman equations for $\mathcal{A}_I$, we can calculate the $\mathcal{A}_I^\nu$ once and for all before fixing the subtraction constants by data regression, thus simplifying the numerical evaluation tremendously. The number of subtraction constants and the contributing isospins in each reconstruction theo-

[6] At this point we note the erroneous assumption made in Ref. [62] and the first version of Ref. [1], who both allowed for arbitrary phases between the normalizations of the SM decay amplitudes and the C- and CP-violating ones.

rem amount to a total of twelve single-variable functions $\mathcal{A}_I^\nu$ to evaluate. Nonetheless, the numerical implementation is not as easy, because the treatment of the angular averages and the dispersion integrals is a quite delicate matter and is discussed in full detail in App. E. At this stage we shortly point out these intricacies as follows: first, one has to ensure that within the angular integration in Eq. (8.19) one does not cross the singularities generated by the unitarity cut, which in turn arises by the analytic continuation to the decay region. This issue can be handled by a suitable deformation of the complex integration contour. The second complication arises in the evaluation of the dispersion integrals, which have additional singularities for physical values of the Mandelstam variables as demanded by unitarity. These can be remedied by appropriate algebraic manipulations of the respective integrands.

8.1.5 | Taylor invariants

Any interpretation of subtraction constants, which do not have any physical meaning on their own, should be made with caution, as they depend on the chosen subtraction scheme, on the ambiguities of the dispersive representation, and on the not-well-restricted high-energy behavior of the dispersion integrals. Changes in any of the listed aspects are absorbed in the subtraction constants when fitting to data. Even a simple estimation of the relative and overall size of the two C-odd amplitudes from the subtraction constants ε and ϑ, as in similar fashion assumed by Ref. [62], may be misleading. Notice that an apparent difference in these coefficients can be due to the compensation of the relative, arbitrary normalization of the basis solutions $\mathcal{G}_I^\varepsilon$ and $\mathcal{H}_I^\vartheta$ when comparing to data.
To overcome these issues we follow the idea of Refs. [281, 283], where certain linear combinations of the subtraction constants for the SM contribution were introduced, which are identified as so-called Taylor invariants. To access those, the single-variable amplitudes $\mathcal{A}_I \in \{\mathcal{F}_I, \mathcal{G}_I, \mathcal{H}_I\}$ are expanded around $s = 0$, i.e.,

$$\mathcal{A}_I(s) = A_I^\mathcal{A} + B_I^\mathcal{A}\, s + C_I^\mathcal{A}\, s^2 + D_I^\mathcal{A}\, s^3 + \dots \,. \tag{8.30}$$

Inserting the series into the reconstruction theorem for the SM amplitude, cf. Eq. (8.14), one obtains[7]

$$\mathcal{M}_1^C(s,t,u) = F_0 + F_1\,(2s - t - u) + F_2\, s^2 + F_3\,\big[(s-t)\,u + (s-u)\,t\big] + \mathcal{O}(p^6)\,, \tag{8.31}$$

with the Taylor invariants

$$\begin{aligned} F_0 &= A_0^\mathcal{F} + r\,B_0^\mathcal{F} + \frac{4}{3}\big(A_2^\mathcal{F} + r\,B_2^\mathcal{F}\big)\,, & F_1 &= \frac{1}{3}B_0^\mathcal{F} + A_1^\mathcal{F} - \frac{5}{9}B_2^\mathcal{F} - 3r\,C_2^\mathcal{F}\,, \\ F_2 &= C_0^\mathcal{F} + \frac{4}{3}C_2^\mathcal{F}\,, & F_3 &= B_1^\mathcal{F} + C_2^\mathcal{F}\,. \end{aligned} \tag{8.32}$$

[7] For simplicity, here and in the following we denote the order of neglected higher-order polynomial terms by $\mathcal{O}(p^{2n})$, which should not be confused with the counting scheme of the chiral expansion that may include nonanalytic dependencies on quark masses etc.

These can be used as theory constraints to the SM amplitude when considering that one-loop χPT [274, 283] predicts them to be

$$F_0 = 1.176(53)\,, \quad f_1 = 4.52(29)\,\text{GeV}^{-2}\,, \quad f_2 = 16.4(4.9)\,\text{GeV}^{-4}\,, \quad f_3 = 6.3(2.0)\,\text{GeV}^{-4}\,, \tag{8.33}$$

where F_0 was used as an overall normalization by means of $f_i \equiv F_i/F_0$ and will furthermore serve to normalize $\mathcal{M}_1^C$.[8]

We now apply the same strategy to the C-odd contributions. The effective BSM operators of Eq. (8.1), which arise from elementary considerations such as crossing symmetry and the correct behavior under time reversal, demand the amplitudes for the $\Delta I = 0$ and $\Delta I = 2$ transitions at lowest contributing order to be of the form

$$\begin{aligned} \mathcal{M}_0^{\mathscr{C}}(s,t,u) &= i\,g_0\,(s-t)(u-s)(t-u) + \mathcal{O}(p^8)\,, \\ \mathcal{M}_2^{\mathscr{C}}(s,t,u) &= i\,g_2\,(t-u) + \mathcal{O}(p^4)\,, \end{aligned} \tag{8.34}$$

where the couplings have the dimensions $[g_0] = \text{GeV}^{-6}$ and $[g_2] = \text{GeV}^{-2}$, respectively. It has to be remarked that this simple polynomial expansion is by far less accurate than the full dispersive representation, but allows one to match the couplings in a convenient way. Reproducing the structure in Eq. (8.34) with the Taylor series from above we obtain

$$g_0 = i\,\varepsilon\left(C_1^{\mathcal{G}^\varepsilon} + 3r\,D_1^{\mathcal{G}^\varepsilon}\right), \qquad g_2 = i\,\vartheta\left(3A_1^{\mathcal{H}^\vartheta} + 3r\,B_1^{\mathcal{H}^\vartheta} + B_2^{\mathcal{H}^\vartheta} + 2r\,C_2^{\mathcal{H}^\vartheta}\right), \tag{8.35}$$

which we wrote in explicit dependence on the subtraction constants using the Taylor invariants for the basis amplitudes from Eq. (8.29), by means of $C_1^{\mathcal{G}} = \varepsilon\,C_1^{\mathcal{G}^\varepsilon}$ etc. In this form, T violation demands the coupling constants g_0 and g_2 to be *real*-valued. To satisfy this condition, the subtraction constants must be proportional to the complex conjugate of the linear combinations of Taylor invariants, by means of

$$i\,\varepsilon \stackrel{!}{=} c_\varepsilon\left(C_1^{\mathcal{G}^\varepsilon} + 3r\,D_1^{\mathcal{G}^\varepsilon}\right)^*, \quad \text{with} \quad c_\varepsilon \in \mathbb{R}\,, \tag{8.36}$$

as an example for ε. While this condition fixes the phase of ε, the constant c_ε is left as the only degree of freedom. We proceed analogously with ϑ. As we extract the Taylor invariants by an expansion of the single-variable amplitudes around $s = 0$, we are well below the dipion threshold, such that the contributions of the dispersion integrals are negligible for the decay at hand. Consequently, we can drop the real part of the subtraction constants, which have no visible effects on observables.

[8] In principle one can also define Taylor invariants for the SM amplitude at the two-loop level in χPT [284, 293]. However, as demonstrated in the analysis of Ref. [283], a high-precision matching requires a more flexible dispersive amplitude (i.e., more than three subtraction constants). Aside of this small flaw, we will demonstrate that our dispersive representation of the SM amplitude describes both the experimental Dalitz-plot distribution and the one-loop chiral constraints very well.

8.1.6 | Fixing the subtraction constants

Once the basis solutions $\mathcal{A}_I^\nu$ for the Khuri–Treiman coupled integral equations are evaluated numerically, one can determine the free parameters of our dispersive representation for $\eta \to 3\pi$. In summary we have the subtraction constants α, β, γ for the SM amplitude, where one of these can be seen as an overall normalization, as well as $\mathrm{Re}\,\varepsilon$, $\mathrm{Im}\,\varepsilon$ fixing the C-violating isoscalar contribution and $\mathrm{Re}\,\vartheta$, $\mathrm{Im}\,\vartheta$ for the isotensor one.

To determine these degrees of freedom we employ a χ^2-regression to three different data sets:

- the Dalitz-plot distribution of $\eta \to \pi^+\pi^-\pi^0$ from the KLOE-2 collaboration [215],
- the Dalitz-plot distribution of $\eta \to 3\pi^0$ from the A2 collaboration [300], and
- the Taylor invariants of $\mathcal{M}_1^C$ from one-loop χPT.

Note that the latter two only address the three free parameters of the SM amplitude. However, these two data sets help to fix the relative phases between the contributions of different total isospins, and furthermore any shift in $\mathcal{M}_1^C$ may affect the BSM contributions when additionally comparing to the data of Ref. [215].

Let us first turn our attention to the experimental data sets from the KLOE-2 and A2 collaborations. The KLOE-2 collaboration provides the world's highest statistics for the measurement of the Dalitz-plot distribution in $\eta \to \pi^+\pi^-\pi^0$. The data distributes about $4.6 \cdot 10^6$ events over 371 bins, where all bins overlapping with the physical boundaries were discarded. On the other hand, the A2 collaboration provides altogether 441 bins for a single Dalitz-plot sextant, exploiting the symmetry of $\eta \to 3\pi^0$, and accepts bins overlapping with the phase space boundary. It supersedes many earlier experiments on $\eta \to 3\pi^0$, which mostly concentrated on the leading nontrivial Dalitz-plot slope parameter [270, 301–305].

Let us refer to the experimental Dalitz-plot distributions by $\mathcal{D}_{c,n}^{\mathrm{exp}}$, where the index denotes the charged or neutral channel, respectively. The binning is given, as commonly done, in terms of the dimensionless and symmetrized coordinates $x_{c,n}^i, y_{c,n}^i$, where the additional index denotes the i-th bin at its center. These explicitly read

$$x_{c,n} = \frac{\sqrt{3}}{2M_\eta Q_{c,n}}(u_{c,n} - t_{c,n})\,, \qquad y_{c,n} = \frac{3}{2M_\eta Q_{c,n}}\left[(M_\eta - M_{\pi^0})^2 - s_{c,n}\right] - 1\,, \tag{8.37}$$

where $Q_c = M_\eta - 2M_{\pi^+} - M_{\pi^0}$ and $Q_n = M_\eta - 3M_{\pi^0}$. The indices labeling the Mandelstam variables correspond to the respective kinematic map given in Ref. [283].

We compare the experimental measurements to the dispersive Dalitz-plot distributions by integrating our amplitudes $\mathcal{M}_{c,n}$ over the respective bin

$$\mathcal{D}_{c,n}^{\mathrm{DR}}(x_{c,n}^i, y_{c,n}^i) = \int_{\mathrm{bin}\,\#i} \mathrm{d}x_{c,n}\,\mathrm{d}y_{c,n}\,|\mathcal{M}_{c,n}(x_{c,n}, y_{c,n})|^2\,. \tag{8.38}$$

The discrepancy functions $\chi^2_{c,n}$ for the charged and neutral data sets are then defined by

$$\chi^2_{c,n} = \sum_i \left(\frac{\mathcal{D}^{\text{exp}}_{c,n}(x^i_{c,n}, y^i_{c,n}) - |\mathcal{M}_{c,n}(x^i_{c,n}, y^i_{c,n})|^2}{\Delta\mathcal{D}^{\text{exp}}_{c,n}(x^i_{c,n}, y^i_{c,n})} \right)^2 . \tag{8.39}$$

To build in theory constraints on the Taylor invariants of the SM amplitude from one-loop χPT we introduce [283]

$$\chi^2_0 = \sum_{i=1}^{3} \left(\frac{f_i^{\chi\text{PT}} - \text{Re}\, f_i}{\Delta f_i^{\chi\text{PT}}} \right)^2 , \tag{8.40}$$

where the $f_i^{\chi\text{PT}}$ denote the theoretical predictions listed in Eq. (8.33). To define a real-valued discrepancy function we restrict our analysis to the real parts of the f_i and discuss the effects of their imaginary parts in Sect. 8.1.7.1.
When carrying out the combined regression to all three data sets we minimize the combined discrepancy function

$$\chi^2_{\text{tot}} = \chi^2_0 + \chi^2_c + \chi^2_n \tag{8.41}$$

and fix the normalization of $\mathcal{M}_c$ such that it reproduces the Taylor invariant F_0 from Eq. (8.33). Before fixing the subtraction constants, one has to consider higher-order isospin corrections due to the mass difference of the neutral and charged pions in the final state to obtain an accurate description of the experimental measurements. To this end, we follow the same strategy as proposed in Ref. [283], which shall serve as a reference for explicit formulas. The dominant isospin-breaking contribution can be taken into account by a kinematic map, such that the boundaries of the Dalitz plot in the isospin limit are mapped to the ones for physical masses. All remaining isospin-breaking effects are assumed to be mostly absorbed by electromagnetic correction factors $\mathcal{K}_{c,n}$ for the charged and neutral decay modes of $\eta \to 3\pi$ resulting from one-loop representations in χPT [272]. While the kinematic map will be applied to both the C-even and C-odd amplitudes, $\mathcal{K}_{c,n}$ only enter the SM amplitudes, as we are yet missing any effective theory to account for analogous corrections in the C-violating amplitudes. Due to the absence of $I = 0$ S-wave contributions, in general we expect such electromagnetic effects to be even smaller in that case.
When minimizing the χ^2 as described above, we distinguish between the four scenarios

- SM_c: exclusively minimize χ^2_c with $\mathcal{M}^{\not C}_{0,2} = 0$,
- BSM_c: exclusively minimize χ^2_c with the full amplitude $\mathcal{M}_c$,
- SM_{tot}: minimize χ^2_{tot} with $\mathcal{M}^{\not C}_{0,2} = 0$,
- BSM_{tot}: minimize χ^2_{tot} with the full amplitude $\mathcal{M}_c$.

A summary of the individual χ^2 contributions to the four scenarios is given in Table 8.1. We find for all fit scenarios considered a good agreement of our dispersive amplitude with data. Overall the individual parts of the discrepancy function χ^2_0, χ^2_c, and χ^2_n in the four different scenarios are almost identical. In fact, the dispersive representation is already

	χ^2_0	χ^2_c	χ^2_n	dof	χ^2_{tot}/dof	p-value
SM_c	(1.222)	387.8	(509.5)	368	1.054	22.9%
BSM_c	(1.222)	383.5	(509.5)	366	1.048	25.1%
SM_{tot}	1.247	387.9	509.3	811	1.108	1.7%
BSM_{tot}	1.247	383.6	509.3	809	1.105	2.0%

Table 8.1: Summary of the four considered fit scenarios: SM_c (exclusive, C-conserving), BSM_c (exclusive, C-violating), SM_{tot} (combined, C-conserving), BSM_{tot} (combined, C-violating). For fits obtained by dropping the contributions of χ^2_0 and χ^2_n to the total discrepancy function χ^2_{tot}, their values are put in brackets. All values refer to fit results of our central solution.

perfectly fixed by the KLOE-2 data on $\eta \to \pi^+\pi^-\pi^0$ alone, with the $\eta \to 3\pi^0$ Dalitz-plot distribution and the Taylor invariants for $\mathcal{M}_1^C$ being a prediction in excellent agreement with data. Accordingly, the differences between the results for the exclusive and combined fits are marginal, i.e., comparing SM_c vs. SM_{tot} and BSM_c vs. BSM_{tot}. Taking the C-violating contributions into account and comparing SM_c vs. BSM_c or SM_{tot} vs. BSM_{tot} respectively, we find a minor improvement of χ^2_c by about 1.1%, whereas χ^2_0 and χ^2_n do not change at all at the given level of accuracy. Furthermore, comparing the resulting discrepancy functions of the KLOE-2 and A2 data sets, we notice a slightly worse description of the Dalitz-plot distribution for the neutral $\eta \to 3\pi^0$ mode. This small tension of the dispersive representation for $\mathcal{M}_n$ and the experimental measurement from A2 has also been observed in Ref. [283]. Nevertheless, the experimental data of both the charged and neutral mode together are well described. Consequently, adding the contributions of $\mathcal{M}_0^{\not C}$ and $\mathcal{M}_2^{\not C}$ to our dispersive representation for $\mathcal{M}_c$ has no visible effect on the determination of $\mathcal{M}_1^C$.

Let us now elaborate on the error analysis. For the latter we consider the experimental uncertainties from the KLOE-2 and A2 Dalitz-plot distributions,[9] the uncertainty originating from χPT constraints including the Taylor invariants for $\mathcal{M}_1^C$ (8.33) and the electromagnetic correction factors $\mathcal{K}_{c,n}$ from Ref. [283], and the uncertainty resulting from the variation of the phase shift input in the low- and high-energy region, cf. Fig. 8.1. We will treat all these sources of error as symmetric and Gaussian distributed. Accordingly, the combined total uncertainties are found by adding the individual contributions in quadrature and the presented correlation matrices are calculated from the respective total covariance matrices of the investigated quantities.

For the sake of completeness we quote the subtraction constants determined with the combined regressions SM_{tot} and BSM_{tot} in Table 8.2, which underline the findings pointed out in the previous paragraphs, and illustrate the corresponding comparison to the KLOE-2

[9] The A2 collaboration provided us with three independent sets of their data, allowing us to assess the statistical and systematical uncertainties of their analysis. In case of the KLOE-2 data set we will consider only the statistical errors.

	α	$\beta \cdot M_\pi^2$	$\gamma \cdot M_\pi^2$	$\mathrm{Im}\,\varepsilon \cdot M_\pi^2$	$\mathrm{Im}\,\vartheta \cdot 10^3 M_\pi^2$
$\mathrm{SM}_{\mathrm{tot}}$	0.92(4)	−0.026(3)	0.096(4)	–	–
$\mathrm{BSM}_{\mathrm{tot}}$	0.92(4)	−0.026(3)	0.096(4)	0.014(22)	0.068(34)

Table 8.2: Results for the subtraction constants of the SM amplitude in the first row and the full BSM representation in the second row for the fit scenarios $\mathrm{SM}_{\mathrm{tot}}$ and $\mathrm{BSM}_{\mathrm{tot}}$.

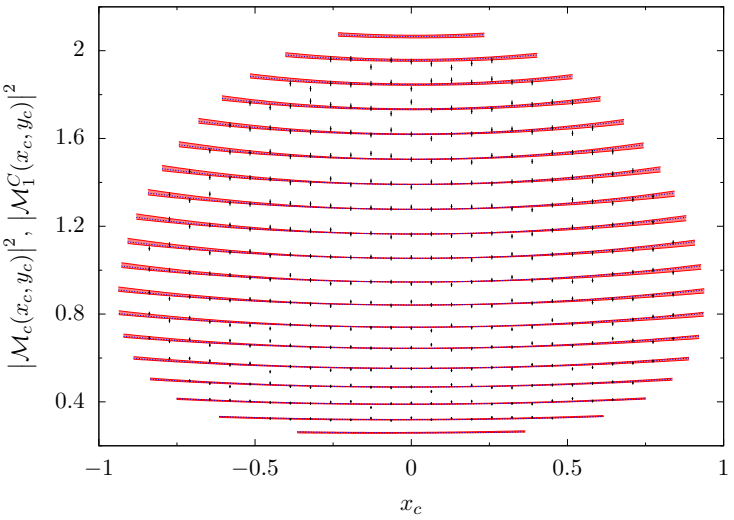

Figure 8.2: Comparison of the dispersive Dalitz-plot distribution for $\eta \to \pi^+\pi^-\pi^0$ to experimental data. The distributions are normalized to one at the Dalitz-plot center $x_c = y_c = 0$. From top to bottom we depict slices through the Dalitz plot given for $y_c^{\min} = -0.95$ to $y_c^{\max} = 0.85$ at distances of $\Delta y_c = 0.1$. We show the modulus square of the full amplitude $|\mathcal{M}_c|^2$ with its uncertainty band covering the statistical and systematical errors added in quadrature (red) as well as the central solution for the C-conserving part $|\mathcal{M}_1^C|^2$ (blue). The 371 data points with error bars (black) were provided by the KLOE-2 collaboration [215].

Dalitz plot in Fig. 8.2. Due to the reasons stated in Sect. 8.1.5 we will refrain from any further discussion of the subtraction constants and instead have a look at actual observables in the following sections. Based on the observations discussed above, we will henceforth exclusively refer to the results obtained with the scenario $\mathrm{BSM}_{\mathrm{tot}}$.

After fixing the C-conserving contribution with the subtraction constants listed in Table 8.2 we can compare the three contributions $\mathcal{M}_1^C$, $\mathcal{M}_0^{\mathcal{C}}$, and $\mathcal{M}_2^{\mathcal{C}}$ on the level of SVAs $\mathcal{F}_I$, $\mathcal{G}_I$, and $\mathcal{H}_I$. For this purpose we depict the respective normalized P-wave SVAs in Fig. 8.3. With the shown extrapolation to the region of the $\rho(770)$ resonance, we observe that the isovector and isotensor contributions, i.e., $\mathcal{F}_1$ and $\mathcal{H}_1$, are in good agreement with each other over an energy range exceeding the physical decay region. On the contrary, these

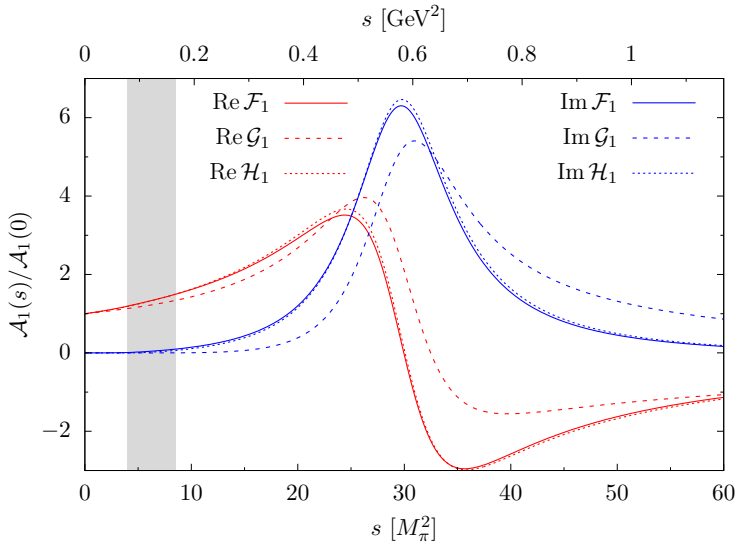

Figure 8.3: P-wave single-variable amplitudes as defined in Eqs. (8.26) and (8.27). Each amplitude is normalized to 1 at $s = 0$ and $\mathcal{F}_1$ is fixed by the central values of the respective subtraction constants from Table 8.2. The phase space for $\eta \to 3\pi$ is indicated by the gray region.

SVAs are significantly different from the isoscalar one, i.e., $\mathcal{G}_1$.[10] Hence the approximation that $\mathcal{F}_I(s) = \mathcal{G}_I(s) = \mathcal{H}_I(s)$ as assumed in Ref. [62] may not be accurate enough to investigate possible future measurements of C-violating effects in $\eta \to \pi^+\pi^-\pi^0$.

8.1.7 | Extraction of observables

In this section we present the numerical results for several observables that can be extracted from our dispersive representation of the $\eta \to 3\pi$ amplitudes. We start our discussion by first investigating theoretical and experimental constraints imposed on the SM amplitude and focus on a comparison of our results to the established analysis of Ref. [283], which shall serve as a consistency check of our dispersive representation. We show that our minimal subtraction scheme for the SM amplitude meets these requirements and can thus argue that the application of this subtraction scheme to the BSM amplitude, cf. Eq. (8.27), is justified. Subsequently we have a closer look at C-violating observables of the $\eta \to \pi^+\pi^-\pi^0$ Dalitz-plot distribution, the occurring asymmetries, and the coupling strength of effective BSM operators with isospins $\Delta I = 0$ and $\Delta I = 2$.

8.1.7.1 | Standard Model constraints

Let us start the discussion concerning the validity of our SM amplitude $\mathcal{M}_1^C$ by having a look at theoretical constraints from one-loop χPT. For this purpose we extract the Taylor

[10] Although the effects on the physical decay range might be smaller than the extrapolations in the figure suggest.

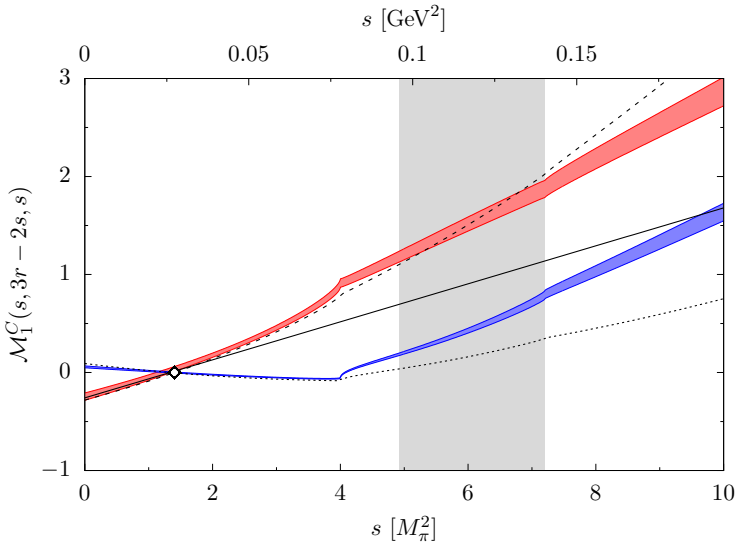

Figure 8.4: Comparison of the dispersive amplitude $\mathcal{M}_1^C$ with the respective tree and one-loop level expressions obtained from χPT along the critical line $s = u$. The real and imaginary parts of the dispersive amplitude are given by the red and blue bands, which cover the range of statistical and systematical uncertainties added in quadrature. The tree level result is depicted by the solid black line, while the one-loop real part is given by the dashed and the imaginary part by the dotted black lines. The black open diamond denotes the position of the Adler zero in one-loop χPT. The physically allowed region for the $\eta \to 3\pi$ decay is depicted by the gray area.

invariants as described in Sect. 8.1.5. Our value for the normalization of the Taylor invariants yields $F_0 = 1.176(53) - 0.0094(14)\, i$. As stated previously we fixed the normalization of $\mathcal{M}_1^C$ so that it reproduces $\mathrm{Re}\, F_0$ from Eq. (8.33), but allowed $\mathrm{Im}\, F_0$ to vary. Since the latter is exclusively generated by contributions of the dispersion integrals to Eq. (8.26) it is roughly two orders of magnitude smaller than $\mathrm{Re}\, F_0$ and will be neglected from now on. For the real parts of the reduced coefficients f_i and their correlation we hence find

$$\begin{array}{lr|ccc} \mathrm{Re}\, f_1/\,\mathrm{GeV}^{-2} = & 4.34(15) & 1.00 & 0.24 & -0.13 \\ \mathrm{Re}\, f_2/\,\mathrm{GeV}^{-4} = & 12.99(52) & & 1.00 & 0.03 \\ \mathrm{Re}\, f_3/\,\mathrm{GeV}^{-4} = & 7.54(59) & & & 1.00 \end{array} , \tag{8.42}$$

which are in good agreement with the prediction of one-loop χPT as quoted in Eq. (8.33). In contrast to the dispersive representation of Ref. [283], which uses a subtraction scheme for $\mathcal{M}_1^C$ involving six independent subtraction constants, our minimalist scheme (8.26) is extremely stiff. Therefore it does not allow for a large variation of the reduced Taylor invariants, cf. Table 8.1. Similar to $\mathrm{Im}\, F_0$ the imaginary parts of the reduced invariants $\mathrm{Im}\, f_1 = 0.193(29)\,\mathrm{GeV}^{-2}$, $\mathrm{Im}\, f_2 = -0.006(85)\,\mathrm{GeV}^{-4}$, and $\mathrm{Im}\, f_3 = -0.128(39)\,\mathrm{GeV}^{-4}$ are found to be small. Next, we want to consider the behavior of $\mathcal{M}_1^C$ at its soft-pion point, i.e., in the limit where the four-momentum of one of the pions vanishes. As current algebra

dictates, the amplitude $\mathcal{M}_1^C$ must exhibit a zero at this point. In terms of the Mandelstam variables we will find two of these so-called *Adler zeros* at $s_A = t_A = 0$ and $s_A = u_A = 0$ related by crossing symmetry. These zeros are protected by chiral $\mathrm{SU}(2)_L \times \mathrm{SU}(2)_R$ flavor symmetry, hence their positions are only subject to corrections of $\mathcal{O}(M_\pi^2)$ if the pion mass is turned on again. At tree level the amplitude exhibits a zero crossing at $s_A = \frac{4}{3}M_\pi^2$ [288]. A study of one-loop χPT yields a slight shift of the Adler zero to $s_A \approx 1.4 M_\pi^2$ [274]. In Fig. 8.4 the behavior of our dispersive representation for $\mathcal{M}_1^C$ along the critical line $s = u$ is compared to the tree level and one-loop predictions of χPT. We extract the zero crossing of the dispersive representation at

$$\begin{array}{rr|cc} s_A/M_\pi^2 = & 1.29(13) & 1.00 & -0.85 \\ (s_A - t_A)/M_\pi^2 = & -0.057(15) & & 1.00 \end{array} , \tag{8.43}$$

which is in perfect agreement with the χPT prediction. Nevertheless, we want to mention that the Adler zeros are shifted slightly away from the critical lines $s = t$ and $s = u$. The dominating error source in Eq. (8.43) stems from the low- and high-energy uncertainties of the phase shift input, cf. Fig. 8.1.

One last consistency check regards the observables of the neutral channel $\eta \to 3\pi^0$. Due to the symmetry under exchange of any two Mandelstam variables we stick to the common phenomenological parameterization in terms of the polar coordinates z_n and ϕ_n given by

$$|\mathcal{M}_n(z_n, \phi_n)|^2 \sim 1 + 2\alpha\, z_n + 2\beta\, z_n^{3/2} \sin 3\phi_n + \dots . \tag{8.44}$$

Performing a two-dimensional Taylor expansion of our amplitude results in

$$\begin{array}{rr|cc} \alpha = & -0.0293(31) & 1.00 & -0.77 \\ \beta = & -0.0043(8) & & 1.00 \end{array} , \tag{8.45}$$

where the slope α agrees well with the Particle Data Group (PDG) world average [13] and the parameter β is compatible with the findings of the A2 collaboration [300] as well as with the dispersive analysis of Ref. [283]. The extraction of higher parameters is beyond the scope of this work.

Finally, we can also calculate the ratio $\mathrm{BR}(\eta \to 3\pi^0)/\mathrm{BR}(\eta \to \pi^+\pi^-\pi^0)$, which can be computed from partial decay widths $\Gamma_{c,n}$ defined by

$$\Gamma_{c,n}(\eta \to 3\pi) = \frac{Q_{c,n}^2}{384\sqrt{3}\pi^3 M_\eta} \frac{\mathcal{D}_{c,n}}{S_{c,n}} , \qquad \mathcal{D}_{c,n} = \int \mathrm{d}x_{c,n}\, \mathrm{d}y_{c,n}\, |\mathcal{M}_{c,n}(x_{c,n}, y_{c,n})|^2 , \tag{8.46}$$

where $S_c = 1$ and $S_n = 6$ denoting the symmetry factors and $\mathcal{D}_{c,n}$ the integrals of the Dalitz-plot distributions over the full phase space. Since contributions antisymmetric under $t \leftrightarrow u$ cancel, $\mathcal{D}_c$ is determined entirely by $|\mathcal{M}_1^C|^2$ up to corrections quadratic in the BSM

couplings. We extract

$$\frac{\mathrm{BR}(\eta \to 3\pi^0)}{\mathrm{BR}(\eta \to \pi^+\pi^-\pi^0)} = 1.423(48) \tag{8.47}$$

in perfect agreement with the PDG world average [13]. Note that the uncertainty quoted in Eq. (8.47) is totally dominated by the errors on the electromagnetic correction factor $\mathcal{K}_{c,n}$ from Ref. [283].

As our minimal subtraction scheme meets all the presented constraints imposed on the SM amplitude, we conclude that there is no objection when applying it to the BSM contributions.

8.1.7.2 | Dalitz-plot distributions

We now turn our focus to the determination of C-violating observables in the $\eta \to \pi^+\pi^-\pi^0$ Dalitz-plot distribution. As already observed in Sect. 8.1.6, patterns arising from ToPe forces have a vanishingly small influence on the goodness of the regression. Nevertheless, we show to which order of magnitude C-and CP-violating signals in $\eta \to \pi^+\pi^-\pi^0$, as predicted by our dispersive representation, can be restricted with the currently most precise measurement of the respective Dalitz plot [215]. For this purpose, it may be advantageous to decompose the Dalitz-plot distribution of the total amplitude in Eq. (8.3) into its constituents by means of

$$\left|\mathcal{M}_c\right|^2 \approx \left|\xi\,\mathcal{M}_1^C\right|^2 + 2\mathrm{Re}\left[\xi\,\mathcal{M}_1^C\,(\mathcal{M}_0^{\not C})^*\right] + 2\mathrm{Re}\left[\xi\,\mathcal{M}_1^C\,(\mathcal{M}_2^{\not C})^*\right], \tag{8.48}$$

where we neglected all contributions that are quadratic in C-violating amplitudes, i.e., $|\mathcal{M}_0^{\not C}|^2$, $|\mathcal{M}_2^{\not C}|^2$, as well as $2\mathrm{Re}\,[\mathcal{M}_0^{\not C}\,(\mathcal{M}_2^{\not C})^*]$, and dropped the dependence on the dimensionless coordinates x_c and y_c for simplicity. Since we have full control on the amplitudes $\mathcal{M}_1^C$, $\mathcal{M}_0^{\not C}$, and $\mathcal{M}_2^{\not C}$ appearing in Eq. (8.48), we can study their disentangled contributions to the Dalitz-plot distribution for our central fit results individually, cf. Fig. 8.5. Obviously, the C-conserving SM part determined by $\mathcal{M}_1^C$ is dominating, while the two terms linear in the C-violating amplitudes $\mathcal{M}_0^{\not C}$ and $\mathcal{M}_2^{\not C}$ are suppressed by three orders of magnitude. We remark that all remaining terms quadratic in C-violating amplitudes not shown in the figure are suppressed by five to six orders of magnitude and are hence indeed totally negligible. Having a look at the two contributions linear in the C-violating effects, which determine the size of the mirror symmetry breaking of the Dalitz-plot distribution under $t \leftrightarrow u$, we find both contributions to be of similar size, i.e., the interference effect of $\mathcal{M}_1^C$ with $\mathcal{M}_0^{\not C}$ compared to the interference $\mathcal{M}_1^C$ with $\mathcal{M}_2^{\not C}$. Accordingly, $\mathcal{M}_0^{\not C}$ and $\mathcal{M}_2^{\not C}$ are of the same order of magnitude. Like the SM contribution $|\mathcal{M}_1^C|^2$, all effects quadratic in C violation are symmetric under $t \leftrightarrow u$ and will therefore not contribute to the mirror symmetry breaking.

Due to the small phase space of the decay at hand the Dalitz plot is typically parameterized

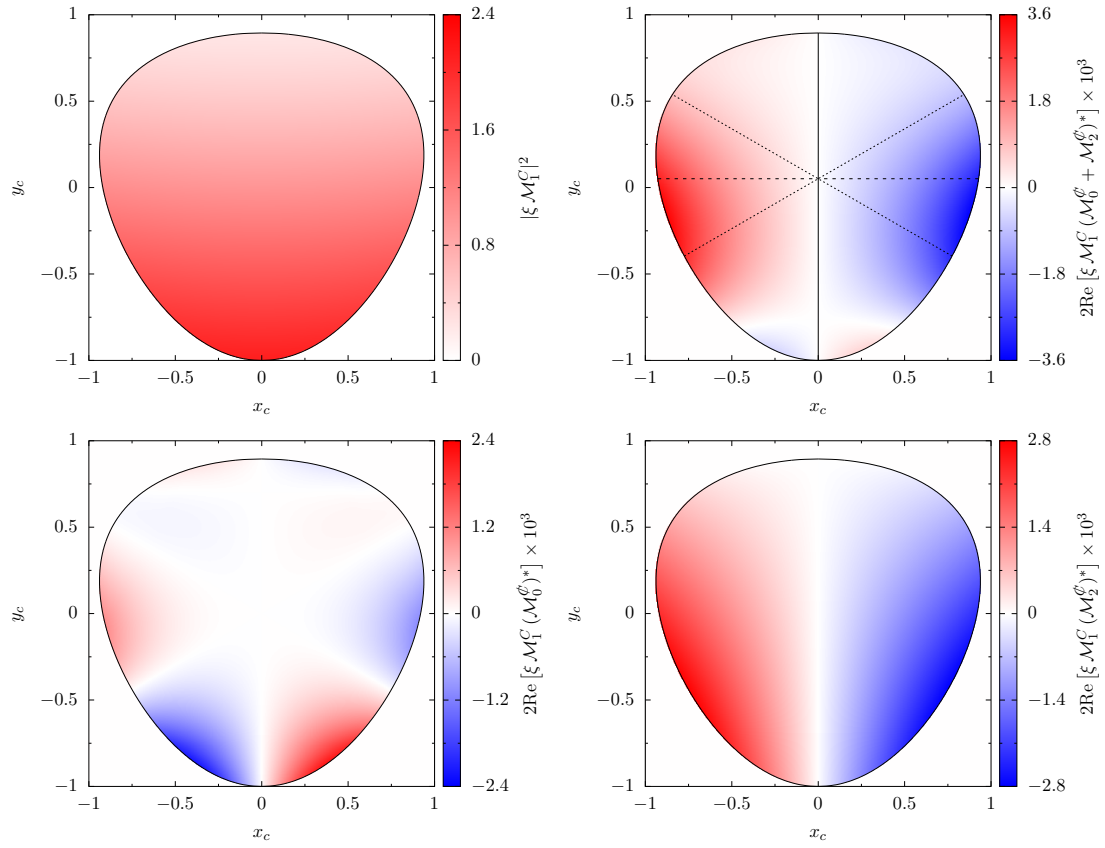

Figure 8.5: Decomposition of the Dalitz-plot distribution for $\eta \to \pi^+\pi^-\pi^0$ as given in Eq. (8.48) for the central fit result. The normalization is chosen such that $|\xi\mathcal{M}_1^C|^2$ (top left) is one in the center. Note the individual scales of each contribution. The interferences of $\mathcal{M}_1^C$ with $\mathcal{M}_0^{\mathscr{C}}$ (bottom left) and $\mathcal{M}_2^{\mathscr{C}}$ (bottom right) give rise to mirror symmetry breaking in the Dalitz plot. The total C-violating contributions to the full Dalitz plot is shown in the upper right, including the symmetry axes to define asymmetry parameters. The left-right asymmetry A_{LR} compares the population of the left and right halves divided by the line $t_c = u_c$ (solid vertical line), A_Q the quadrants divided by $t_c = u_c$ and $s_c = r_c$ (solid vertical and dashed horizontal lines), and A_S the sextants divided by $t_c = u_c$, $s_c = t_c$, and $s_c = u_c$ (solid vertical and dotted diagonal lines). The most significant impacts of the C-violating amplitudes are located in the vicinity of the kinematic boundary.

by a polynomial expansion around its center, by means of

$$|\mathcal{M}_c(x_c, y_c)|^2 \sim 1 + a\, y_c + b\, y_c^2 + c\, x_c + d\, x_c^2 + e\, x_c\, y_c + f\, y_c^3 + g\, x_c^2\, y_c + h\, x_c\, y_c^2 + l\, x_c^3 + \dots\,, \tag{8.49}$$

where the coefficients a, b, etc., are called Dalitz-plot parameters. By now, the first seven coefficients of this phenomenological parameterization have been studied by the KLOE-2 collaboration [215]. Note that non-vanishing values of the coefficients c, e, h, and l odd in x_c would directly implicate C violation in $\eta \to \pi^+\pi^-\pi^0$ decays. We first access the Dalitz-plot parameters for the C-conserving contribution, generated exclusively by $\mathcal{M}_1^C$, by employing a two-dimensional Taylor expansion of our amplitude $\mathcal{M}_1^C$, resulting in

$$\begin{array}{rr|rrrrr} a = & -1.0819(14) & 1.00 & -0.06 & 0.39 & -0.47 & -0.37 \\ b = & 0.1487(34) & & 1.00 & 0.57 & -0.66 & -0.60 \\ d = & 0.088(13) & & & 1.00 & -0.92 & -0.99 \\ f = & 0.1131(47) & & & & 1.00 & 0.90 \\ g = & -0.068(15) & & & & & 1.00 \end{array}\,. \tag{8.50}$$

The uncertainties of the parameters b, d, and g are completely driven by the variation of the phase shift input, while the uncertainties of a and f gain sizeable contributions from all sources of error. Similarly, for the C-violating Dalitz-plot parameters generated by the interference effects of $\mathcal{M}_1^C$ with $\mathcal{M}_0^{\not C}$ and $\mathcal{M}_2^{\not C}$ we find

$$\begin{array}{rr|rrrr} c = & -0.0024(12) & 1.00 & -1.00 & 0.01 & 0.05 \\ e = & 0.0026(13) & & 1.00 & -0.01 & -0.05 \\ h = & 0.0034(60) & & & 1.00 & -1.00 \\ l = & -0.0014(21) & & & & 1.00 \end{array}\,. \tag{8.51}$$

The uncertainties of these four parameters are dominated by the statistical error of the KLOE-2 data, while all other sources of uncertainty do not yield any significant contribution to the error budget.[11] Accordingly, we can confirm that all C-violating parameters vanish within 2σ at most. Furthermore, the C-violating parameters turn out to be at least one order of magnitude smaller than d and g, which are the smallest coefficients of the C-conserving part of the parameterization (8.50). Separating the individual contributions to the central values of c, e, h, and l originating from the interference effect of $\mathcal{M}_1^C$ with $\mathcal{M}_0^{\not C}$ we find

$$c = +0.0000\,, \qquad e = +0.0000\,, \qquad h = +0.0037\,, \qquad l = -0.0013\,, \tag{8.52}$$

[11] Note that the estimated correlations between the C-conserving and C-violating parameters given in Eqs. (8.50) and (8.51) are below 1%.

	$-a$	b	$-c$	d	e	f	$-g$	h	l
KLOE-2	1.095(3)	0.145(3)	0.004(3)	0.081(3)	0.003(3)	0.141(7)	0.044(9)	0.011(9)	0.001(7)
DR Orsay	1.142	0.172	-	0.097	-	0.122	0.089	-	-
DR Bern	1.081(2)	0.144(4)	-	0.081(3)	-	0.118(4)	0.069(4)	-	-
this work	1.082(1)	0.149(3)	0.002(1)	0.088(13)	0.003(1)	0.113(5)	0.068(15)	0.003(6)	−0.001(2)

Table 8.3: Comparison of the Dalitz-plot parameters obtained in different analyses of the KLOE-2 data [215]. The values given in the first row are obtained by a direct fit of Eq. (8.49) to data. The dispersive analyses from the Orsay [282] and Bern groups [283] consider the C-conserving amplitude $\mathcal{M}_1^C$ only.

whereas the interference of $\mathcal{M}_1^C$ with $\mathcal{M}_2^{\not{C}}$ yields

$$c = -0.0024\,, \qquad e = +0.0026\,, \qquad h = -0.0003\,, \qquad l = -0.0002\,. \tag{8.53}$$

A comparison of the extracted Dalitz-plot parameters with the results from KLOE-2 as well as the two most recent dispersive analyses on C-conserving $\eta \to 3\pi$ decays [282, 283] are summarized in Table 8.3.

8.1.7.3 | Asymmetries and BSM couplings

Besides these coefficients, we can also investigate three asymmetry parameters to quantify C-violating effects in the $\eta \to \pi^+\pi^-\pi^0$ Dalitz-plot distribution: the left-right A_{LR}, the quadrant A_Q, and sextant A_S asymmetry parameters [263–265]. These asymmetries compare the population of the Dalitz-plot distribution in the different sectors defined by the Dalitz-plot geometry, cf. Fig. 8.5. To quantify these asymmetries we follow Ref. [62] by defining

$$\begin{aligned} A_{LR} &= \frac{N_R - N_L}{N}\,, \qquad A_Q = \frac{N_A - N_B + N_C - N_D}{N}\,, \\ A_S &= \frac{N_{\rm I} - N_{\rm II} + N_{\rm III} - N_{\rm IV} + N_{\rm V} - N_{\rm VI}}{N}\,, \end{aligned} \tag{8.54}$$

with $N = N_R + N_L$ and

$$N_{\mathcal{C}} = \int_{\mathcal{C}} \mathrm{d}x_c\, \mathrm{d}y_c\, |\mathcal{M}_c(x_c, y_c)|^2 \tag{8.55}$$

denoting the normalized number of events for the total amplitude within each region $\mathcal{C}$. In our notation, N_R and N_L belong to the population for positive and negative values of x_c, respectively. The regions A, B, C, D and I to VI denote the quadrants and sextants, respectively, in clockwise ordering, where A is the quadrant for $x_c > 0$, $y_c > 0$ and I the sextant completely contained in A; cf. Fig. 8.5. Carrying out each integral for our dispersive

representation of $\mathcal{M}_c$ we obtain

$$\begin{array}{rr|ccc} A_{LR} = & -7.9(4.5) & 1.00 & -0.82 & 0.34 \\ A_Q = & 1.9(2.5) & & 1.00 & -0.82 \\ A_S = & 2.0(3.8) & & & 1.00 \end{array} , \tag{8.56}$$

where all three asymmetry parameters are given in units of 10^{-4}. We find A_{LR}, A_Q, and A_S in good agreement with the results reported by the KLOE-2 collaboration [215]. Again, there is no hint for C violation as all three asymmetries are compatible with zero in not more than 1.8σ. Note that the error budget in Eq. (8.56) is completely dominated by the statistical uncertainties of the KLOE-2 data.[12]

In contrast to experimental studies of C-violating effects in the $\eta \to \pi^+\pi^-\pi^0$ Dalitz-plot distribution, which are limited to the investigation of x_c-odd coefficients of the phenomenological parameterization (8.49) or the probe of the Dalitz-plot asymmetries, our dispersion-theoretical analysis provides us with the tools to disentangle the individual contributions of $\mathcal{M}_0^{\not C}$ and $\mathcal{M}_2^{\not C}$. Furthermore, we are in the position to extract coupling strengths g_0 and g_2 of the underlying isoscalar and isotensor BSM operators as defined Eq. (8.35). For our dispersive representation we obtain

$$\begin{array}{rr|cc} g_0/\text{GeV}^{-6} = & -2.8(4.5) & 1.00 & 0.01 \\ g_2/10^{-3}\,\text{GeV}^{-2} = & -9.3(4.6) & & 1.00 \end{array} . \tag{8.57}$$

Note that for the central values we find a ratio of $g_0/g_2 \approx 10^3\,\text{GeV}^{-4}$. This can be understood as follows. Generically, as we have remarked above, the operator $X_0^{\not C}$ is kinematically suppressed compared to $X_2^{\not C}$ by 4 orders in the chiral expansion; this means that we would expect their coefficients to behave as $|g_0/g_2| \sim (1\,\text{GeV})^{-4}$, the scale given by the chiral symmetry breaking scale $4\pi F_0 \approx 1.16\,\text{GeV}$. As the momenta throughout the $\eta \to 3\pi$ Dalitz plot are of order M_π (note the available phase space $M_\eta - 3M_\pi \approx M_\pi$), this would lead to a relative suppression of the isoscalar transition with respect to the isotensor one of roughly $(M_\pi/1\,\text{GeV})^4 \approx 4 \times 10^{-4}$. In fact, however, the data constrains both amplitudes including their respective coupling constants about equally, cf. Fig. 8.5, which means that the experimental sensitivities rather behave like $|g_0/g_2| \sim M_\pi^{-4} \approx 2.6 \times 10^3\,\text{GeV}^{-4}$, in good agreement with what we observe. This behavior of the amplitudes $\mathcal{M}_0^{\not C}$ and $\mathcal{M}_2^{\not C}$ has also been observed in Ref. [62].

Furthermore we can utilize these coupling strengths to obtain a more general representation of the Dalitz-plot asymmetries. Carrying out the phase space integrals individually for contributions involving interference effects of $\mathcal{M}_0^{\not C}$ or $\mathcal{M}_2^{\not C}$ in the Dalitz-plot distribution, we find that the asymmetry parameters (8.56) given in units of 10^{-4} are related to the BSM

[12] In fact, KLOE-2 reports that the systematic uncertainty of A_{LR} dominates the statistical one. Like the results for A_Q and A_S, A_{LR} is therefore compatible with zero in less than 1σ if systematic effects are taken into account.

couplings g_0 and g_2 by

$$\begin{aligned} A_{LR} &= -0.300\, g_0 + 0.936\, g_2\,, \\ A_Q &= 0.443\, g_0 - 0.336\, g_2\,, \\ A_S &= -0.850\, g_0 + 0.043\, g_2\,. \end{aligned} \tag{8.58}$$

In these relations g_0 and g_2 enter in units of $1\,\text{GeV}^{-6}$ and $10^{-3}\,\text{GeV}^{-2}$, respectively. Equation (8.58) reveals that especially the sextant asymmetry parameter A_S is sensitive to contributions generated by $\mathcal{M}_0^{\not C}$, while effects of $\mathcal{M}_2^{\not C}$ are suppressed.[13] Separating for contributions of $\mathcal{M}_0^{\not C}$ or $\mathcal{M}_2^{\not C}$ to the central values of the asymmetry parameters, we find

$$A_{LR} = 0.8\,, \qquad A_Q = -1.2\,, \qquad A_S = 2.4\,, \tag{8.59}$$

for interference effects of $\mathcal{M}_1^C$ with $\mathcal{M}_0^{\not C}$, whereas the interference of $\mathcal{M}_1^C$ with $\mathcal{M}_2^{\not C}$ yields

$$A_{LR} = -8.7\,, \qquad A_Q = 3.1\,, \qquad A_S = -0.4\,. \tag{8.60}$$

Once more, all asymmetry parameters are given in units of 10^{-4}.

To conclude the discussion of $\eta \to 3\pi$, we would like to comment on the future experimental focus to set more severe bounds on C and CP violation. We disrecommend using the polynomial parameterization of the Dalitz plot from Eq. (8.49), which is too inaccurate for this purpose, mostly because the order of the polynomial, i.e., the number of degrees of freedom, is not known a priori and depends strongly on the precision of the measurement. On the other hand, the measurement of two out of the three Dalitz-plot asymmetries is in principle sufficient to fix the two degrees of freedom in our amplitude representation of C and CP violation. Note however that we predict strong correlations between the three asymmetries, which would become even more significant if, as naturalness suggests, the isoscalar contribution is strongly suppressed compared to the isotensor one therein. We therefore advocate the use of the more physical decay amplitudes with proper phase behavior in future experimental analyses.

8.1.8 | Generalization to $\eta' \to 3\pi$

As η and η' have largely the same quantum numbers and differ mainly due to their masses, the fundamental decay mechanisms into the 3π final states are also identical. In the Standard Model, $\eta' \to 3\pi$ is also almost exclusively due to the light-quark-mass difference, and the classification in terms of isospin amplitudes works in exactly the same way as for $\eta \to 3\pi$. Consequently, the same goes for C-violating decay mechanisms. To be more precise, in Sect. 6.3.1 we have already shown that $\eta \to 3\pi$ and $\eta' \to 3\pi$ are maximally correlated at leading order in the large-N_c extension of ToPeχPT. A major difference concerns only the total widths of η and η': while the partial widths of both mesons into three pions

[13] Note, however, that this would cease to be true as soon as $g_{0/2}$ turned out to be of comparable natural order as suggested by the chiral power counting, i.e., $g_0/g_2 = \mathcal{O}(1\,\text{GeV}^{-4})$, in which case even the sextant asymmetry would be dominated by the isotensor contribution.

are of comparable size, the lifetime of the η' is shorter by about a factor of 150, and hence the branching ratios make $\eta' \to 3\pi$ relatively rare decay modes. As a result, high-precision investigations of the corresponding Dalitz plots on the same level as for $\eta \to 3\pi$, with the goal to put limits on C-odd effects therein, will most likely remain extremely difficult in the near future. To date, the BESIII collaboration has investigated the decay dynamics in $\eta' \to 3\pi$ most precisely, with a determination of the respective branching ratios [306], a measurement of the $\eta' \to 3\pi^0$ Dalitz plot [270], and the first amplitude analysis for both charged and neutral final states [218].

Here, we merely intend to estimate the relative size between isoscalar and isotensor C-violating transitions in $\eta' \to \pi^+\pi^-\pi^0$: due to the significantly larger available phase space, we suspect the strong kinematic or chiral suppression of the isoscalar amplitude in $\eta \to \pi^+\pi^-\pi^0$ to be lifted to a certain extent; an expectation that will be borne out below. As a result, despite the experimental difficulty due to the smaller branching ratio, as a matter of principle $\eta' \to \pi^+\pi^-\pi^0$ will be much more sensitive to the isoscalar C-odd operators. For the purpose of this qualitative investigation, it is sufficient to consider a dispersive representation of the $\eta' \to \pi^+\pi^-\pi^0$ decay amplitude as a rescaled version of $\eta \to \pi^+\pi^-\pi^0$, with the mass of the η replaced by the one for its heavier version η', hence increasing the available phase space. We omit the incorporation of any inelasticities, like via the dominant decay channel $\eta' \to \eta\pi\pi$.

For the purposes of our rather qualitative argument, we only investigate the phase space distributions of the C-odd contributions, because both amplitudes $\mathcal{M}_0^{\not C}$ and $\mathcal{M}_2^{\not C}$ only depend on one complex subtraction constant each.

In Sect. 6.3.1 we have seen that at leading order in large-N_c the normalizations of the decays $\eta \to \pi^+\pi^-\pi^0$ and $\eta' \to \pi^+\pi^-\pi^0$ differ for the isotensor transition by a factor $\sqrt{2}$. For the isoscalar contribution we cannot make such an argument unless we derive the corresponding full set of ToPeχPT operators at $\mathcal{O}(p^6)$. However, we can still argue with NDA that isoscalar coupling in the decays of η and η' are of the same order of magnitude. To be consistent we therefore suppose for our qualitative estimation that the respective coupling constants g_0 and g_2 are equal in both decays. Under this assumption we adjust the normalization of $\mathcal{M}_0^{\not C}$ and $\mathcal{M}_2^{\not C}$ in $\eta' \to \pi^+\pi^-\pi^0$ in terms of the subtraction constants ε and ϑ to g_0 and g_2 as extracted from the central results of the BSM couplings in Eq. (8.57). Note that the contribution of the dispersion integral to the real part of the subtraction constants is in this case not negligible due to the increased phase space. Hence we fix the subtraction constants according to Eq. (8.36).

The thereby generated distributions of the real and imaginary parts of the C-odd amplitudes in Fig. 8.6 show that the chiral suppression of the isoscalar transition with respect to the isotensor one is attenuated significantly by the increased phase space, such that $\mathcal{M}_0^{\not C}$ dominates $\mathcal{M}_2^{\not C}$ by roughly two orders of magnitude. More precisely, we predict that the relative sensitivity to the isoscalar transition is increased by about two orders of magnitude in comparison to the analogous η decay. This scaling can be qualitatively understood: we have emphasized that the isoscalar C-odd operators are suppressed by four orders in

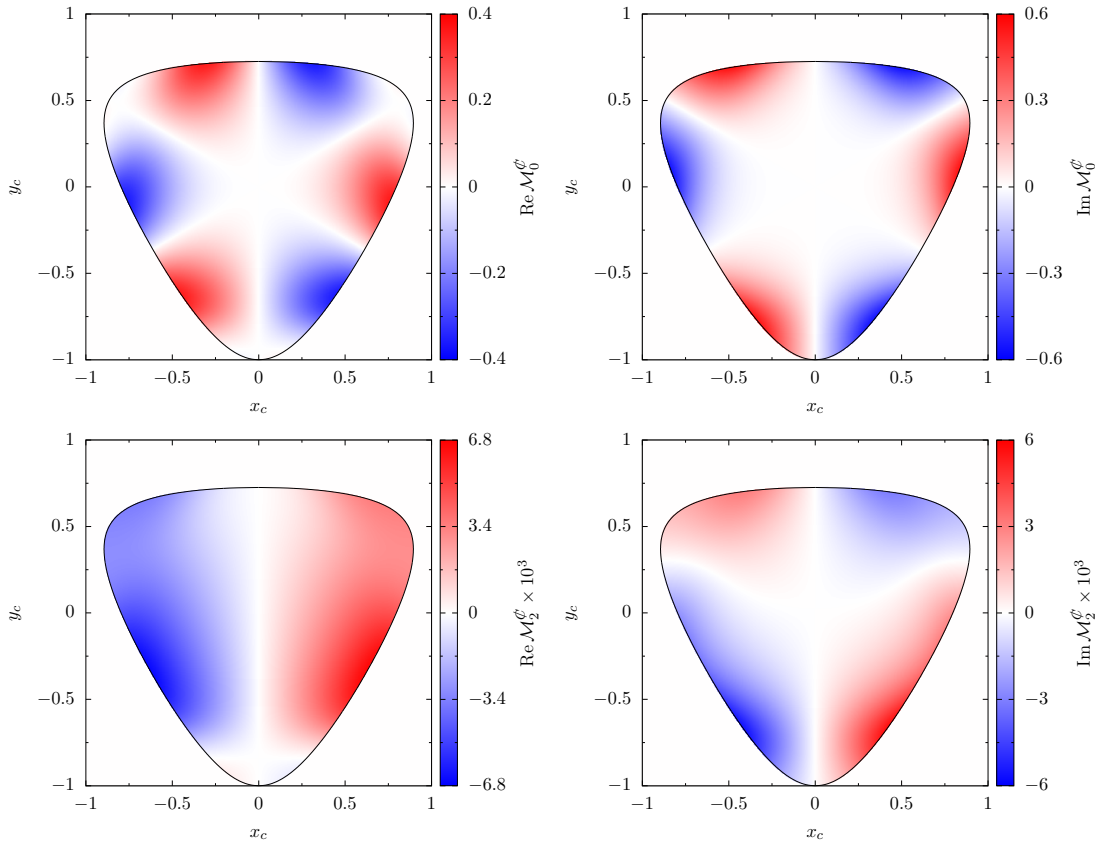

Figure 8.6: Estimation for the distribution of the real (left) and imaginary (right) parts of $\mathcal{M}_0^{\mathscr{C}}$ (top) and $\mathcal{M}_2^{\mathscr{C}}$ (bottom) in $\eta' \to \pi^+\pi^-\pi^0$ over the allowed phase space. As a rough estimation, the normalizations of each amplitude are fixed by the central fit result obtained for $\eta \to \pi^+\pi^-\pi^0$ in Table 8.2. In contrast to Fig. 8.5 additional zero lines occur as a consequence of the interference with the ρ-resonance, which lies in the kinematically accessible region.

the chiral expansion with respect to the isotensor ones. However, the η' decay into three pions is far less a low-energy decay: the available phase space is larger by about a factor of $(M_{\eta'} - 3M_\pi)/(M_\eta - 3M_\pi) \approx 4$. Taking this to the fourth power correctly predicts an increased relative sensitivity by roughly a factor of 250.
A more rigorous analysis of C-odd effects can be performed once a dispersion-theoretical fit to $\eta' \to 3\pi$ Dalitz plots within the Standard Model is accomplished [307].

8.2 | Dispersive representation of $\eta' \to \eta\pi\pi$

In this section we turn our attention to another class of ToPe forces by studying the decay $\eta' \to \eta\pi^+\pi^-$. Considering the quantum numbers of the involved mesons, one can argue in a similar manner as previously in Sect. 8.1: as the decay at hand preserves G-parity, transitions of even isospin $\Delta I = 0, 2$ conserve C, while odd ones violate the latter. Thus we can write the most general amplitude up to linear order in isospin breaking as

$$\mathcal{M}(s,t,u) = \mathcal{M}_0^C(s,t,u) + \mathcal{M}_1^{\not C}(s,t,u), \tag{8.61}$$

where for this decay, as opposed to $\eta^{(\prime)} \to 3\pi$, the isoscalar amplitude $\mathcal{M}_0^C$ is isospin- and C-conserving, whereas the $\mathcal{M}_1^{\not C}$ violates both quantum numbers. Note that the decay $\eta' \to \eta\pi^+\pi^-$ is sensitive to a different class of C- and CP-violating operators from those tested in $\eta^{(\prime)} \to \pi^+\pi^-\pi^0$, namely the ones for transitions with $\Delta I = 1$.
For the evaluation of the overall amplitudes we again rely on the Khuri–Treiman framework, which was already applied to the Standard-Model contribution $\mathcal{M}_0^C$ in Ref. [287]. The set of dispersion relations is built from the two scattering processes $\eta'\eta \to \pi\pi$ (s-channel) and $\eta'\pi \to \eta\pi$ (t-channel). Once more, we allow only for elastic rescattering. In order to determine the C-odd amplitude we follow the same agenda as laid out in Sect. 8.1.

8.2.1 | Kinematics

Define the $\eta' \to \eta\pi^+\pi^-$ transition amplitude as usual by

$$\big\langle \pi^+(p_+)\,\pi^-(p_-)\,\eta(p_\eta)\big|iT\big|\eta(P_{\eta'})\big\rangle = i\,(2\pi)^4\,\delta^{(4)}(P_{\eta'} - p_+ - p_- - p_\eta)\,\mathcal{M}(s,t,u)\,. \tag{8.62}$$

For the invariant masses we stick to the convention

$$s = \big(P_{\eta'} - p_\eta\big)^2\,, \qquad t = \big(P_{\eta'} - p_{\pi^+}\big)^2\,, \qquad u = \big(P_{\eta'} - p_{\pi^-}\big)^2\,. \tag{8.63}$$

These Mandelstam variables satisfy the relation

$$s + t + u = M_{\eta'}^2 + M_\eta^2 + 2M_\pi^2 \equiv 3r\,. \tag{8.64}$$

For the s-channel scattering amplitude $\eta'\eta \to \pi\pi$ one may write

$$t(s,z_s) = u(s,-z_s) = \frac{1}{2}\big(3r - s + z_s\,\kappa_{\pi\pi}(s)\big)\,, \tag{8.65}$$

with

$$z_s \equiv \cos\theta_s = \frac{t-u}{\kappa_{\pi\pi}(s)}\,, \qquad \kappa_{\pi\pi}(s) = \sigma(s)\,\lambda^{1/2}(s, M_{\eta'}^2, M_\eta^2)\,. \tag{8.66}$$

For the t-channel $\eta'\pi \to \eta\pi$ we have

$$s(t, z_t),\, u(t, z_t) = \frac{1}{2}\Big(3r - t \mp \frac{\Delta}{t} \mp z_t\,\kappa_{\pi\eta}(t)\Big)\,, \tag{8.67}$$

with $\Delta \equiv (M_{\eta'}^2 - M_\pi^2)(M_\eta^2 - M_\pi^2)$. Using the kinematic function

$$\kappa_{\pi\eta}(t) = \frac{\lambda^{1/2}(t, M_{\eta'}^2, M_\pi^2)\,\lambda^{1/2}(t, M_\eta^2, M_\pi^2)}{t} \tag{8.68}$$

we can express the t-channel scattering angle as

$$z_t \equiv \cos\theta_t = \frac{t\,(u-s) - \Delta}{t\,\kappa_{\pi\eta}(t)}\,. \tag{8.69}$$

As a consequence of crossing symmetry the corresponding relations for the u-channel can be obtained by exchanging the variables $t \leftrightarrow u$ and $z_t \leftrightarrow -z_u$. The scattering channels have the physical thresholds

$$s_{\rm th} = 4M_\pi^2, \qquad t_{\rm th} = u_{\rm th} = (M_\eta + M_\pi)^2\,. \tag{8.70}$$

8.2.2 | Reconstruction theorem

In the ongoing, we restrict our amplitude to discontinuities in the lowest contributing partial waves, i.e., to $\ell = 0$ for $\pi\pi$ states with isospin $I = 0$, or $\ell = 1$ for those with $I = 1$, and to $\ell = 0$ for the $\eta\pi$ system with $I = 1$. We neglect the phase of the $\eta\pi$ P-wave, which has exotic quantum numbers (i.e., no resonances are expected in the quark model), and is as suppressed at low energies in the chiral expansion as D- and higher partial waves [308]. With these approximations the decomposition of the Standard-Model amplitude in terms of single-variable functions takes the simple form [287]

$$\mathcal{M}_0^C(s,t,u) = \mathcal{F}_{\pi\pi}(s) + \mathcal{F}_{\eta\pi}(t) + \mathcal{F}_{\eta\pi}(u)\,, \tag{8.71}$$

with the abbreviations $\mathcal{F}_{\pi\pi}(s) \equiv \mathcal{F}^{\ell=0}_{I=0\,\pi\pi}(s)$ and $\mathcal{F}_{\eta\pi}(t) \equiv \mathcal{F}^{\ell=0}_{I=1\,\eta\pi}(t)$. In this notation the indices $\pi\pi$ and $\eta\pi$ denote the two-particle final state of the respective scattering process. In a similar fashion we obtain the reconstruction theorem for the C-violating amplitude

$$\mathcal{M}_1^{\not C}(s,t,u) = (t-u)\,\mathcal{G}_{\pi\pi}(s) + \mathcal{G}_{\eta\pi}(t) - \mathcal{G}_{\eta\pi}(u)\,, \tag{8.72}$$

which can be read off along the lines of Ref. [88]. In this equation we use the short form $\mathcal{G}_{\pi\pi}(s) \equiv \mathcal{G}^1_{1\,\pi\pi}(s)$ and $\mathcal{G}_{\eta\pi}(s) \equiv \mathcal{G}^0_{1\,\eta\pi}(s)$. Both reconstruction theorems can also be derived in complete analogy to the ones quoted in Sect. 8.1.2. The ambiguities of these representa-

tions are given by the transformations

$$\begin{aligned} \mathcal{F}_{\eta\pi}(t) &\to \mathcal{F}_{\eta\pi}(t) - \frac{1}{2}a_0 + b_0\,(t-r)\,, & \mathcal{F}_{\pi\pi}(s) &\to \mathcal{F}_{\pi\pi}(s) + a_0 + b_0\,(s-r)\,, \\ \mathcal{G}_{\eta\pi}(t) &\to \mathcal{G}_{\eta\pi}(t) + a_1 - b_1\,t + c_1\,t\,(t-3r)\,, & \mathcal{G}_{\pi\pi}(s) &\to \mathcal{G}_{\pi\pi}(s) + b_1 + c_1\,s\,, \end{aligned} \tag{8.73}$$

which leave the full amplitudes unaffected.

8.2.3 | Elastic unitarity

To ensure the conservation of probability, the single-variable functions have to obey

$$\begin{aligned} \operatorname{disc}\mathcal{A}_{\pi\pi}(s) &= 2i\,\theta(s-4M_\pi^2)\left[\mathcal{A}_{\pi\pi}(s) + \hat{\mathcal{A}}_{\pi\pi}(s)\right]\,\sin\delta_{\pi\pi}(s)\,e^{-i\delta_{\pi\pi}(s)}\,, \\ \operatorname{disc}\mathcal{A}_{\eta\pi}(t) &= 2i\,\theta\big(t-(M_\eta+M_\pi)^2\big)\left[\mathcal{A}_{\eta\pi}(t) + \hat{\mathcal{A}}_{\eta\pi}(t)\right]\,\sin\delta_{\eta\pi}(t)\,e^{-i\delta_{\eta\pi}(t)}\,, \end{aligned} \tag{8.74}$$

with $\mathcal{A} \in \{\mathcal{F},\mathcal{G}\}$ and the indices of the phase shifts labeling the respective two-particle intermediate states. Note that in case of $\mathcal{M}_0$ the $\pi\pi$ state has isospin $I=0$, such that $\delta_{\pi\pi} = \delta_{\pi\pi}^{I=0}$ for $\mathcal{A}=\mathcal{F}$. Analogously, the C-odd contribution $\mathcal{M}_1^{\not C}$ is driven by a dipion state that has isospin $I=1$, i.e., $\delta_{\pi\pi} = \delta_{\pi\pi}^{I=1}$ for $\mathcal{A}=\mathcal{G}$. Introducing the abbreviations

$$\begin{aligned} \langle z_s^n\,\mathcal{A}\rangle &\equiv \frac{1}{2}\int_{-1}^{1}\mathrm{d}z_s\,z_s^n\,\mathcal{A}\big(t(s,z_s)\big)\,, \\ \langle z_t^n\,\mathcal{A}\rangle^+ \equiv \frac{1}{2}\int_{-1}^{1}\mathrm{d}z_t\,z_t^n\,\mathcal{A}\big(u(t,z_t)\big)\,, &\qquad \langle z_t^n\,\mathcal{A}\rangle^- \equiv \frac{1}{2}\int_{-1}^{1}\mathrm{d}z_t\,z_t^n\,\mathcal{A}\big(s(t,-z_t)\big)\,, \end{aligned} \tag{8.75}$$

the inhomogeneities for the Standard-Model amplitude, obtained by a partial-wave projection as described in Sect. 8.1.3, become

$$\hat{\mathcal{F}}_{\pi\pi}(s) = 2\langle\mathcal{F}_{\eta\pi}\rangle\,, \qquad \hat{\mathcal{F}}_{\eta\pi}(t) = \langle\mathcal{F}_{\pi\pi}\rangle^- + \langle\mathcal{F}_{\eta\pi}\rangle^+\,, \tag{8.76}$$

and the ones entering the C-violating amplitude yield

$$\begin{aligned} \hat{\mathcal{G}}_{\pi\pi}(s) &= \frac{6}{\kappa_{\pi\pi}}\,\langle z_s\,\mathcal{G}_{\eta\pi}\rangle\,, \\ \hat{\mathcal{G}}_{\eta\pi}(t) &= -\langle\mathcal{G}_{\eta\pi}\rangle^+ - \frac{3}{2}\left(r-t+\frac{\Delta}{3t}\right)\langle\mathcal{G}_{\pi\pi}\rangle^- + \frac{1}{2}\kappa_{\eta\pi}\,\langle z_t\,\mathcal{G}_{\pi\pi}\rangle^-\,. \end{aligned} \tag{8.77}$$

Analogously to Eq. (8.23) we can write the general solutions as

$$\begin{aligned} \mathcal{A}_{\pi\pi}(s) &= \Omega_{\pi\pi}(s)\left(P_{\pi\pi}^{n-1}(s) + \frac{s^n}{\pi}\int_{s_\mathrm{th}}^{\infty}\frac{\mathrm{d}x}{x^n}\,\frac{\sin\delta_{\pi\pi}(x)\,\hat{\mathcal{A}}_{\pi\pi}(x)}{|\Omega_{\pi\pi}(x)|\,(x-s)}\right), \\ \mathcal{A}_{\eta\pi}(t) &= \Omega_{\eta\pi}(t)\left(P_{\eta\pi}^{n-1}(t) + \frac{t^n}{\pi}\int_{t_\mathrm{th}}^{\infty}\frac{\mathrm{d}x}{x^n}\,\frac{\sin\delta_{\eta\pi}(x)\,\hat{\mathcal{A}}_{\eta\pi}(x)}{|\Omega_{\eta\pi}(x)|\,(x-t)}\right), \end{aligned} \tag{8.78}$$

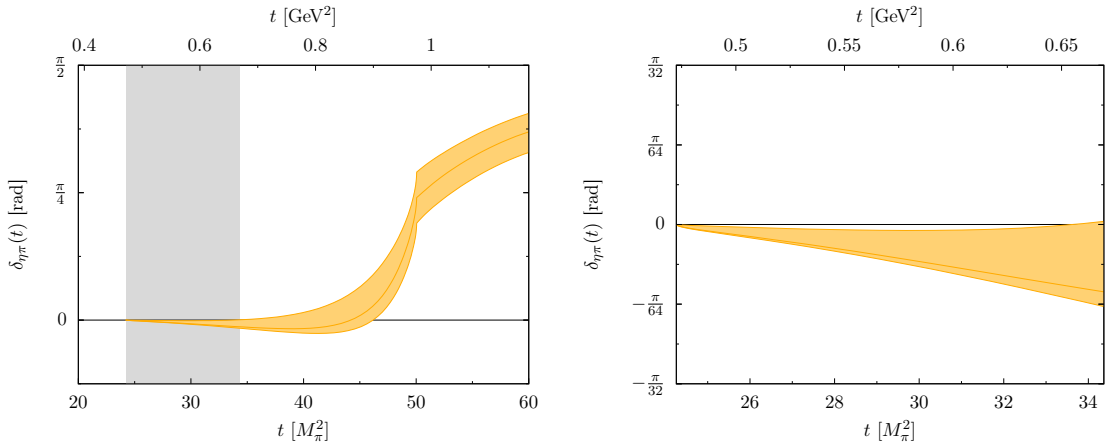

Figure 8.7: S-wave $\eta\pi$ phase shift extracted from Refs. [258, 309] including its uncertainty band. Left panel: behavior of the phase shift in the low- and intermediate-energy region. The $K\bar{K}$-cusp is clearly visible at about $50M_\pi^2$. The phase space for $\eta' \to \eta\pi\pi$ is indicated by the gray region. Right panel: magnification of the physical decay region.

with two distinct subtraction polynomials $P_{\pi\pi}^{n-1}$ and $P_{\eta\pi}^{n-1}$ of order $n-1$. The index of each Omnès function decides which scattering phase shift is used according to Eq. (8.22). In addition to that, one has to differentiate the case $\Omega_{\pi\pi} = \Omega_{\pi\pi}^{I=0}$ for $\mathcal{A} = \mathcal{F}$ from $\Omega_{\pi\pi} = \Omega_{\pi\pi}^{I=1}$ for $\mathcal{A} = \mathcal{G}$.

As our numerical input, we use the same $\pi\pi$ phase shifts as detailed in the discussion of $\eta \to 3\pi$ in Sect. 8.1.4. For the $\eta\pi$ S-wave, we employ the phase of the corresponding scalar form factor constructed in Ref. [309], further refined by imposing constraints from $\gamma\gamma \to \eta\pi^0$ [258]. This phase, including the associated uncertainties, is shown in Fig. 8.7.

8.2.4 | Subtraction scheme

In this section we proceed in the same fashion as in Sect. 8.1.4 to fix the yet undetermined number of subtractions entering the dispersive representation in Eq. (8.78). We assume that the involved phase shifts behave in the limits $s \to \infty$ or $t \to \infty$, respectively, as

$$\delta_{\pi\pi}^0(s) \to \pi\,, \qquad \delta_{\pi\pi}^1(s) \to \pi\,, \qquad \delta_{\eta\pi}(t) \to \pi\,. \tag{8.79}$$

Furthermore, we demand the asymptotics of the single-variable functions $\mathcal{F}_{\pi\pi}$ and $\mathcal{F}_{\eta\pi}$ resulting from the Froissart–Martin bound [102]

$$\mathcal{F}_{\pi\pi}(s) = \mathcal{O}(s)\,, \qquad \mathcal{F}_{\eta\pi}(t) = \mathcal{O}(t)\,. \tag{8.80}$$

This results in a representation of the corresponding SVAs involving four (real) subtraction constants,

$$\begin{aligned}\mathcal{F}_{\pi\pi}(s) &= \Omega^0_{\pi\pi}(s)\left(\alpha+\beta\,s+\gamma\,s^2+\frac{s^3}{\pi}\int_{s_\text{th}}^\infty \frac{\mathrm{d}x}{x^3}\,\frac{\sin\delta^0_{\pi\pi}(x)\,\hat{\mathcal{F}}_{\pi\pi}(x)}{|\Omega^0_{\pi\pi}(s')|\,(x-s)}\right),\\ \mathcal{F}_{\eta\pi}(t) &= \Omega_{\eta\pi}(t)\left(\lambda\,t^2+\frac{t^3}{\pi}\int_{t_\text{th}}^\infty \frac{\mathrm{d}x}{x^3}\,\frac{\sin\delta_{\eta\pi}(x)\,\hat{\mathcal{F}}_{\eta\pi}(x)}{|\Omega_{\eta\pi}(x)|\,(x-t)}\right).\end{aligned} \tag{8.81}$$

In Ref. [287], a more rigorous scheme with asymptotics analogous to those discussed for $\eta \to 3\pi$ in Sect. 8.1.4 and, correspondingly, less subtractions was employed in parallel, and found to describe the Dalitz plot data similarly well, while being more susceptible to sizeable uncertainties due to high-energy input to the dispersion integrals. With the adjusted input for $\eta\pi$ scattering [258], this reduced scheme ceases to work well [307]. We regard this partly as an artifact of the extremely slow asymptotic rise of the $\eta\pi$ phase shift, cf. Fig. 8.7, and therefore decide to stick to the more restrictive asymptotics for the C-odd contribution all the same, in order to avoid a proliferation of subtraction constants therein. The assumptions for $\mathcal{G}_{\pi\pi}$ and $\mathcal{G}_{\eta\pi}$ hence are

$$\mathcal{G}_{\pi\pi}(s) = \mathcal{O}(s^{-1})\,, \qquad \mathcal{G}_{\eta\pi}(t) = \mathcal{O}(t^0)\,, \tag{8.82}$$

such that the resulting C-violating SVAs are given by

$$\begin{aligned}\mathcal{G}_{\pi\pi}(s) &= \Omega^1_{\pi\pi}(s)\left(\varrho+\frac{s}{\pi}\int_{s_\text{th}}^\infty \frac{\mathrm{d}x}{x}\,\frac{\sin\delta^1_{\pi\pi}(x)\,\hat{\mathcal{G}}_{\pi\pi}(x)}{|\Omega^1_{\pi\pi}(x)|\,(x-s)}\right),\\ \mathcal{G}_{\eta\pi}(t) &= \Omega_{\eta\pi}(t)\left(\zeta\,t+\frac{t^2}{\pi}\int_{t_\text{th}}^\infty \frac{\mathrm{d}x}{x^2}\,\frac{\sin\delta_{\eta\pi}(x)\,\hat{\mathcal{G}}_{\eta\pi}(x)}{|\Omega_{\eta\pi}(x)|\,(x-t)}\right).\end{aligned} \tag{8.83}$$

Conventionally, the polynomial ambiguities from Eq. (8.73) were shifted such that a minimal number of subtraction constants contributes to the $\mathcal{A}_{\eta\pi}$. Again, the phase of the subtraction constants ϱ and ζ is fixed by T violation, so that $\mathcal{M}_1^{\not C}$ has two *real*-valued degrees of freedom, in contrast to the C-violating isoscalar and isotensor contributions in $\eta \to 3\pi$ which are fixed by a single normalization each. The numerical implementation proceeds in analogy to the strategy presented in Sect. 8.1.4.

8.2.5 | Taylor invariants

As pointed out in Sect. 8.1.5, the subtraction constants fixing our dispersive representation are no suitable observables. Therefore we again introduce their linear combinations as ambiguity-free Taylor invariants obtained by an expansion of the SVAs around $s,t=0$, i.e.,

$$\begin{aligned}\mathcal{A}_{\pi\pi}(s) &= A^{\mathcal{A}}_{\pi\pi}+B^{\mathcal{A}}_{\pi\pi}\,s+C^{\mathcal{A}}_{\pi\pi}\,s^2+D^{\mathcal{A}}_{\pi\pi}\,s^3+\dots\,,\\ \mathcal{A}_{\eta\pi}(t) &= A^{\mathcal{A}}_{\eta\pi}+B^{\mathcal{A}}_{\eta\pi}\,t+C^{\mathcal{A}}_{\eta\pi}\,t^2+D^{\mathcal{A}}_{\eta\pi}\,t^3+\dots\,.\end{aligned} \tag{8.84}$$

Of course the series coefficients take different values for SM and BSM contributions. Applying these expansions to the reconstruction theorem (8.71) allows us to express the SM amplitude by

$$\mathcal{M}_0^C(s,t,u) = F_0 + F_1\,(2s-t-u) + F_2\,s^2 + F_3\,(t^2+u^2) + \mathcal{O}(p^6) \tag{8.85}$$

with

$$F_0 = A_{\pi\pi}^{\mathcal{F}} + r\,B_{\pi\pi}^{\mathcal{F}} + 2(A_{\eta\pi}^{\mathcal{F}} + r\,B_{\eta\pi}^{\mathcal{F}})\,, \quad F_1 = \frac{1}{3}\left(B_{\pi\pi}^{\mathcal{F}} - B_{\eta\pi}^{\mathcal{F}}\right)\,, \quad F_2 = C_{\pi\pi}^{\mathcal{F}}\,, \quad F_3 = C_{\eta\pi}^{\mathcal{F}}\,, \tag{8.86}$$

where we dropped terms of cubic order in the Mandelstam variables and higher. The BSM operator driving the $\Delta I = 1$ transition as introduced in Eq. (8.2) demands that the matrix element takes the form

$$\mathcal{M}_1^{\mathcal{Q}}(s,t,u) = i\,g_1\,(t-u)\,(1+s\,\delta g_1) + \mathcal{O}(p^6)\,, \tag{8.87}$$

where in addition to the effective isovector coupling g_1, we also consider the leading s-dependent correction δg_1. In terms of the Taylor coefficients these quantities read

$$g_1 = -i\left(A_{\pi\pi}^{\mathcal{G}} + B_{\eta\pi}^{\mathcal{G}} + 3r\,C_{\eta\pi}^{\mathcal{G}}\right), \qquad \delta g_1 = -i\left(B_{\pi\pi}^{\mathcal{G}} - C_{\eta\pi}^{\mathcal{G}}\right)/g_1\,. \tag{8.88}$$

Note that the additional parameter δg_1 ensures that the degrees of freedom of the Taylor expansion match the ones of the dispersive representation for $\mathcal{M}_1^{\mathcal{Q}}$. Both couplings are real-valued as demanded by T violation and give rise to the phases of the subtraction constants ϱ and ζ. Anyway, the latter can be considered as purely imaginary due to the small available phase space.

8.2.6 | Fixing the subtraction constants

According to the subtraction scheme chosen in Sect. 8.2.4, the dispersive representation of the SM amplitude $\mathcal{M}_0^C$ contains the four degrees of freedom α, β, γ, λ, where again one subtraction constant can be chosen to fix the overall normalization. The C-violating isovector contribution $\mathcal{M}_1^{\mathcal{Q}}$ has a total of three parameters ϱ, ζ, and φ, where the latter fixes the complex phase between $\mathcal{M}_0^C$ and $\mathcal{M}_1^{\mathcal{Q}}$. After solving for the basis solutions of the dispersive representation in Eqs. (8.81) and (8.83), these subtraction constants can be determined by a comparison to data.

In contrast to Sect. 8.1.6, we only consider one single data set, i.e., the Dalitz-plot distribution $\mathcal{D}$ of $\eta' \to \eta\pi^+\pi^-$ from the BESIII collaboration [219]. The latter provides the currently most precise measurement including 3.51×10^5 events extracted from J/ψ decays in terms of the symmetrized coordinates

$$x = \frac{\sqrt{3}}{2M_{\eta'}Q_{\eta'}}(u-t)\,, \qquad y = \frac{(M_\eta + 2M_\pi)}{2M_\pi M_{\eta'}Q_{\eta'}}\left[(M_{\eta'}-M_\eta)^2 - s\right] - 1\,, \tag{8.89}$$

	χ^2	dof	χ^2/dof	p-value
FIT_{SM}	10720	10790	0.994	68%
FIT_{BSM}	10718	10788	0.994	68%

Table 8.4: Goodness of the central fit results for the SM amplitude $\mathcal{M}_0^C$ (FIT_{SM}) and the full one $\mathcal{M}_1^{\not C}$ (FIT_{BSM}) obtained by comparison with the BESIII data set [219].

	α	$\beta \cdot M_\pi^2$	$\gamma \cdot M_\pi^4$	$\lambda \cdot M_\pi^4$	$\text{Im}\,\varrho \cdot M_\pi^2$	$\text{Im}\,\zeta \cdot M_\pi^2$
FIT_{SM}	−19.0(8)	1.27(7)	0.0016(30)	0.0060(3)	–	–
FIT_{BSM}	−19.0(8)	1.27(7)	0.0016(30)	0.0060(3)	−0.04(12)	0.05(12)

Table 8.5: Results for the subtraction constants of the Standard-Model amplitude in the first row and the full C- and CP-odd dispersive representation in the second row.

with $Q_{\eta'} = M_{\eta'} - M_\eta - 2M_\pi$. We refrain from including data sets on $\eta' \to \eta\pi^0\pi^0$ [219, 310, 311] in the analysis, as, in contrast to the case of $\eta \to 3\pi^0$, they do not provide truly independent information on the SM amplitude, but rather probe subtle isospin-breaking effects [287, 312]. We determine the subtraction constants by minimizing the discrepancy function

$$\chi^2 = \sum_i \left(\frac{\mathcal{D}(x_i, y_i) - |\mathcal{M}(x_i, y_i)|^2}{\Delta\mathcal{D}(x_i, y_i)} \right)^2 , \tag{8.90}$$

for which we compute our dispersive amplitude $\mathcal{M}$ on the discrete grid covering the centers of all measured bins. and normalize $\mathcal{M}$ to reproduce the according experimental decay width $\Gamma(\eta' \to \eta\pi^+\pi^-) = 79.9(2.7)\,\text{keV}$ taken from the PDG [13].

We proceed by carrying out the regression using the pure SM amplitude $\mathcal{M}_0^C$ as well as the one for the full BSM contribution $\mathcal{M} = \mathcal{M}_0^C + \mathcal{M}_1^{\not C}$. The results for these fit scenarios, denoted as FIT_{SM} and FIT_{BSM}, are listed in Table 8.4 and the corresponding subtraction constants can be found in Table 8.5. We observe that the additional inclusion of the C-violating $\Delta I = 1$ transition does not have any visible influence on the overall goodness of the regression. As an illustration of the latter we show the phase space corrected x- and y-projections of the Dalitz plot in Fig. 8.8. Note that the small effects of mirror symmetry breaking are apparent in the x-projection.

Due to the fact that the current constraints for the $\eta' \to \eta\pi^+\pi^-$ SM amplitude are by far less restrictive than the ones pointed out for $\eta \to 3\pi$ in Sect. 8.1.7.1, we omit an elaborate analysis of the asymmetric systematical errors when varying the input for the $\eta\pi$ phase shift shown in Fig. 8.7 [307]. However, we remark that these systematical errors for the SM amplitude may increase up to the same order of magnitude as the corresponding statistical ones. In either way, the C-violating observables in the central scope of this analysis are

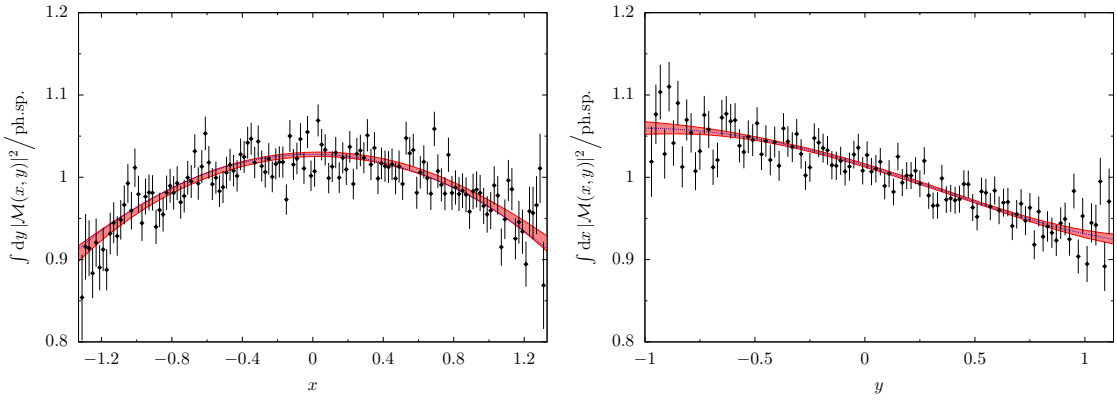

Figure 8.8: Dalitz-plot projections in x- and y-direction, which are divided by the corresponding phase space. We show the measurement of Ref. [219] overlayed with our dispersive representations covered by the red error bands. Note that the theoretical x-projection on the left is not perfectly symmetric, due to C-violating contributions. In both panels we depict our central solution for the C-conserving part $|\mathcal{M}_0^C|^2$ by the dotted blue line.

dominated by their statistical uncertainties.

8.2.7 | Extraction of observables

In this section we work out the numerical results of our dispersive representation for various C-violating observables in the $\eta' \to \eta\pi^+\pi^-$ amplitudes. Similar to Sect. 8.1.7 we first discuss the validity of our SM amplitude. To this end we extract the Adler zeros and the Taylor invariants in Sect. 8.2.7.1. Thereafter we extract patterns of C violation in the Dalitz-plot distribution, investigate the occurring asymmetries, and compute the coupling strength of an effective isovector BSM operator $X_1^{\not C}$.

8.2.7.1 | Standard Model constraints

The Taylor invariants F_i defined in Sect. 8.2.5 allow us to extract coefficients that can be compared to theoretical analyses for the $\eta' \to \eta\pi^+\pi^-$ SM contribution as for instance large-N_c χPT or RχT [313, 314].
As described in Sect. 8.2.4, we use four real-valued subtraction constants to fix the SM amplitude. These can be translated to the Taylor invariants

$$\begin{array}{rcr|cccc} F_0 & = & -13.0(7) & 1.00 & -0.67 & 0.91 & -0.49 \\ f_1/\mathrm{GeV}^{-2} & = & -0.3(1) & & 1.00 & -0.86 & 0.97 \\ f_2/\mathrm{GeV}^{-4} & = & 3.0(4) & & & 1.00 & -0.72 \\ f_3/\mathrm{GeV}^{-4} & = & -1.2(1) & & & & 1.00 \end{array} , \tag{8.91}$$

where F_0 serves as an overall normalization by means of $f_i \equiv F_i/F_0$. Possible imaginary parts of the Taylor invariants are exclusively generated by the dispersion integrals (8.81)

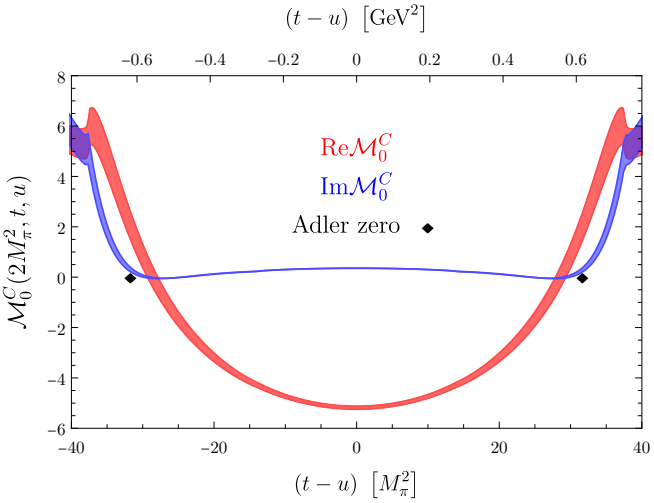

Figure 8.9: Standard-Model amplitude $\mathcal{M}_0^C$ for $\eta' \to \eta\pi^+\pi^-$ evaluated along the line $s = 2M_\pi^2$. The prediction for the real (imaginary) part of our dispersive amplitude is colored in red (blue). The naively expected Adler zeros from chiral symmetry at $(t-u) = \pm(M_{\eta'}^2 - M_\eta^2)$ are marked by the black diamonds. In this picture the normalization of the amplitude M_0^C is chosen such that it reproduces the physical decay width.

and are disregarded in the following.

Furthermore we want to study the behavior of the SM amplitude outside the physical region at its soft-pion points. Chiral $SU(2)_R \times SU(2)_L$ symmetry expects two Adler zeros to show up at $(t-u) = \pm(M_{\eta'}^2 - M_\eta^2)$ along the line $s = 0$ in the limit of massless pions [315–317]. Therefore, in analogy to Ref. [287] we study our dispersive amplitude for on-shell pions along the critical line $s = 2M_\pi^2$. Ref. [318] claimed that the incorporation of the scalar $a_0(980)$ propagator renders the amplitude free of Adler zeros. The fact that Adler zeros are immanent in our dispersive representation, but slightly shifted from their soft-pion points to smaller values of $|t-u|$ as can be seen in Fig. 8.9, refutes the statement. This behavior was also found by the first dispersive analysis of $\eta' \to \eta\pi^+\pi^-$ in Ref. [287]. We find that the two zeros are located at

$$(t_A - u_A)/(M_{\eta'}^2 - M_\eta^2) = \pm 0.902(23)\,. \tag{8.92}$$

An updated analysis of the SM $\eta' \to \eta\pi\pi$ decay presented in Ref. [287] is currently in progress [307], based on the latest high-statistics Dalitz-plot measurements from A2 [311] and BESIII [219] for the charged and neutral decay modes.

8.2.7.2 | Dalitz-plot distribution

Let us continue our discussion on C-violating patterns arising from the $\Delta I = 1$ transition $\eta' \to \eta\pi^+\pi^-$ Dalitz-plot distribution and quantify corresponding observables. Dropping the dependencies on the coordinates x and y and neglecting the contribution of $|\mathcal{M}_1^{\not C}|^2$, the

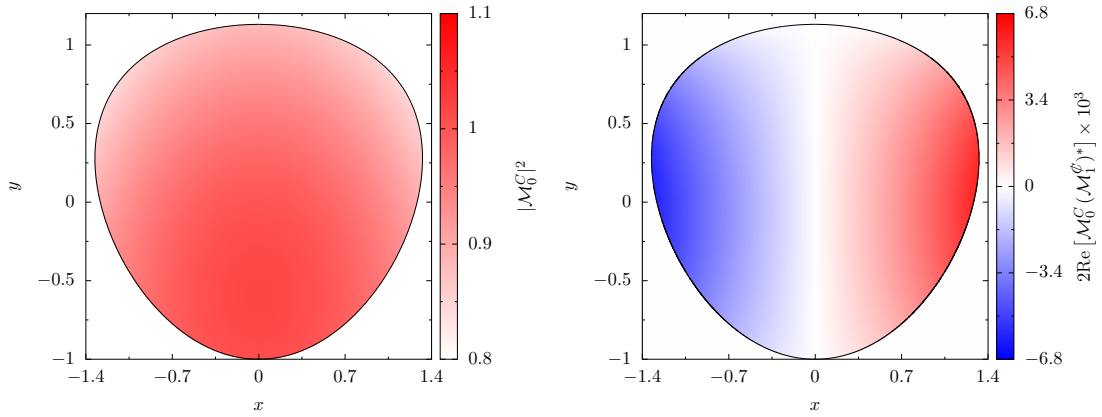

Figure 8.10: Dalitz-plots decomposition for $\eta' \to \eta\pi^+\pi^-$ as given in Eq. (8.93) for our central solution. The normalization is chosen such that the full amplitude $|\mathcal{M}|^2$ is one in its center. The interference term of $\mathcal{M}_0^C$ and $\mathcal{M}_1^{\not C}$ gives rise to the breaking of mirror symmetry. Note the relative order of magnitudes between the individual contributions.

Dalitz-plot distribution arising from Eq. (8.61) can be written as

$$|\mathcal{M}|^2 \approx |\mathcal{M}_0^C|^2 + 2\,\mathrm{Re}\left[\mathcal{M}_0^C\,(\mathcal{M}_1^{\not C})^*\right]\,, \tag{8.93}$$

which is depicted in Fig. 8.10. We observe a similar, however slightly flattened, hierarchy as in the case of $\eta \to 3\pi$ worked out in Sect. 8.1.7.2. The interference term giving rise to the Dalitz-plot asymmetry is constrained to be three orders of magnitude smaller than the SM contribution $|\mathcal{M}_0^C|^2$, whereas the pure $\Delta I = 1$ contribution $|\mathcal{M}_1^{\not C}|^2$ is suppressed by four orders of magnitude. We furthermore conclude that the current state of precision for the $\eta' \to \eta\pi^+\pi^-$ Dalitz plot merely restricts the effects of the C-violating isovector transition to the relative per mille level.

Given the small phase space of the process, the momentum distribution is quite smooth and commonly approximated by the same expansion as introduced in Eq. (8.49), but with adapted coordinates x and y from Eq. (8.89). The BESIII collaboration finds that the first three C-even coefficients a, b, and d of this expansion are sufficient to parameterize the Dalitz plot, as all other parameters of higher orders in x and y, as well as all parameters odd in x indicating C violation, are found to be compatible with zero within less than one standard deviation. A two dimensional Taylor expansion around the center of our dispersive representation of the Dalitz plot gives rise to the parameters

$$\begin{array}{rr|rrrrr} a = & -0.058(4) & 1.00 & -0.32 & -0.01 & -0.21 & -0.02 \\ b = & -0.050(7) & & 1.00 & 0.00 & 0.32 & -0.01 \\ c = & 0.004(3) & & & 1.00 & 0.00 & -0.16 \\ d = & -0.063(4) & & & & 1.00 & -0.02 \\ e = & 0.000(7) & & & & & 1.00 \end{array}\,. \tag{8.94}$$

where we neglect correlations smaller than 1% on the right-hand side. Considering the respective errors we find a perfect agreement of all our parameters with the experiment [219]. In particular there is no indication for C violation as c and e are effectively zero.

8.2.7.3 | Asymmetry and BSM coupling

To finalize our analysis we quantify the asymmetry and the coupling strength of the $\Delta I = 1$ transition in $\eta' \to \eta\pi^+\pi^-$ and apply the same procedure as in Sect. 8.1.7.3. We find the left-right asymmetry in units of 10^{-3} to be

$$A_{LR} = 2.1(1.5). \tag{8.95}$$

Thus the mirror symmetry breaking vanishes within roughly 1.4σ. Furthermore, we can parameterize A_{LR} in terms of the Taylor invariants

$$\begin{array}{rr|cc} g_1/\text{GeV}^{-2} = & 0.7(1.0) & 1.00 & -0.89 \\ \delta g_1/\text{GeV}^{-2} = & -5.5(7.3) & & 1.00 \end{array} , \tag{8.96}$$

which were introduced in Eq. (8.88) as the effective isovector coupling g_1 and its leading s-dependent correction δg_1, respectively. This allows us to write the left-right asymmetry, again in units of 10^{-3}, in the compact form

$$A_{LR} = 6.6\, g_1 \big(1 + 0.10\, \delta g_1\big)\,, \tag{8.97}$$

where g_1 and δg_1 enter in units of GeV^{-2}.

8.3 | Summary

In this study, we have put the pioneering work of Ref. [62] for C- and CP-violating amplitude representations in the decay $\eta \to \pi^+\pi^-\pi^0$ into a rigorous dispersion-theoretical framework, and extended the formalism to the analysis of C and CP violation in the hadronic three-body decays of the η'. Strictly relying on the fundamental principles of analyticity and unitarity, we constructed all three $\eta \to \pi^+\pi^-\pi^0$ amplitudes of distinct total isospin, i.e., the SM amplitude $\mathcal{M}_1^C$ as well as the C-violating isoscalar and isotensor contributions $\mathcal{M}_0^{\not C}$ and $\mathcal{M}_2^{\not C}$, non-perturbatively based on $\pi\pi$ phase shifts. We demonstrated that the same constraints—all amplitudes are not allowed to grow asymptotically for large energies—allow us to describe the experimental data by the KLOE-2 collaboration [215], fulfill constraints from chiral perturbation theory on $\mathcal{M}_1^C$, and reduce the freedom in the C-violating amplitudes to only one single complex normalization constant each. The phase of the latter is fixed by hermiticity and T violation, resulting in one *real*-valued free parameter for the isoscalar and isotensor transition, respectively. Ensuring that the Standard-Model contribution is in good accordance with the dispersive representation of Ref. [283], we extracted the contributions of $\mathcal{M}_0^{\not C}$ and $\mathcal{M}_2^{\not C}$, whose interference with $\mathcal{M}_1^C$ give rise to the

breaking of mirror symmetry in the $\eta \to \pi^+\pi^-\pi^0$ Dalitz-plot distribution. We confirmed that the currently most precise measurement of the latter restricts the C-violating effects to a relative per mille level. Due to the strong kinematic suppression of $\mathcal{M}_0^{\not C}$—the corresponding operator is smaller by four orders in the chiral expansion compared to $\mathcal{M}_2^{\not C}$—the accompanying effective coupling constant g_0 is far less rigorously constrained than g_2, by about three orders of magnitude.

Although there is no sufficiently precise Dalitz-plot measurement for $\eta' \to \pi^+\pi^-\pi^0$ yet, we have demonstrated that, in principle, the larger available phase space lifts the suppression of the isoscalar C-odd amplitude to a large extent, making a potential mirror-symmetry breaking therein more sensitive to $\mathcal{M}_0^{\not C}$ by roughly two orders of magnitude than in $\eta \to \pi^+\pi^-\pi^0$.

In a similar manner, we established a framework to analyze the decay $\eta' \to \eta\pi^+\pi^-$, which is sensitive to another class of C- and CP-violating operators with isospin $I = 1$. In this decay the amplitude decomposes into the isoscalar SM amplitude $\mathcal{M}_0^{C}$ and a C-violating isovector contribution $\mathcal{M}_1^{\not C}$. A regression to the Dalitz plot of the BESIII collaboration [219] yields again no evidence for C-violating effects and limits their patterns to a relative per mille level.

Chapter 9

Correlations of C and CP violation in $\eta \to \pi^0\ell^+\ell^-$ and $\eta' \to \eta\ell^+\ell^-$

In this chapter we reconsider the C- and CP-violating radiative decays $\eta \to \pi^0\gamma^{(*)}$ and $\eta' \to \eta\gamma^{(*)}$ and the corresponding semi-leptonic channels after pair production. Given that $\eta^{(\prime)}$ as well as π^0 have the eigenvalue $C = +1$ but photons have $C = -1$, C is violated in general if $\eta^{(\prime)}$ decays into an arbitrary number of uncharged pions and an odd number of photons. This consideration also holds for radiative decays of the η' into an η. To shorten the notation we will refer to both processes collectively by $X \to Y\gamma^{(*)}$. Regarding the involved angular momenta, $Y(S = 0)$ and $\gamma^{(*)}(S = 1)$ have to be in a relative P-wave in order to couple to $X(S = 0)$. The parity of the $Y\gamma^{(*)}$ state $P_{Y\gamma} = P_Y P_\gamma \cdot (-1)^L = -1$ is thus the same as the parity of X. Consequently, parity is conserved and the decays at hand additionally violate CP, thus offering an opportunity to investigate ToPe forces. The decay into a real, transverse photon violates both gauge invariance and the conservation of angular momentum [34, 220]. Therefore, the focus shall be laid on $X \to Y\gamma^* \to Y\ell^+\ell^-$, where the off-shell photon decays subsequently into a pair of charged leptons. At the theoretical front, the investigation of this BSM one-photon exchange urgently requires an update [221, 319] in comparison to analyses of the SM contribution, cf. Refs. [226, 228, 259–261, 320, 321], as well as studies of other BSM effects in these decays [34, 322]. From an experimental point of view, bounds on all the leptonic channels have already been set [203–205] and may become more stringent in future measurements [38–41, 323–325].
Assuming that the underlying new physics generating the C- and CP-odd decays $X \to Y\ell^+\ell^-$ originates from sources at some high-energy scale Λ, there are in principle three dominant mechanisms to consider:

1. short-distance contributions to the dilepton final state,

2. long-distance contributions caused by C- and CP-odd photon–hadron couplings,

3. long-distance contributions induced by hadronic intermediate states.

For the first two classes we rely on ToPeχPT as proposed in Ref. [2]. One intricacy of the contribution by hadronic intermediate states is that the subsequent photon is allowed to have both isoscalar and isovector components. To predict the involved isovector transitions in a model-independent way, one can utilize the $X \to Y\pi^+\pi^-$ amplitudes derived non-perturbatively in the Khuri–Treiman framework [1] and establish dispersion relations for the respective transition form factors. Analogous relations have previously been derived for the decays ω, ϕ, $J/\psi \to \pi^0\gamma^*$ [262, 326–329], which are compatible with conservation of

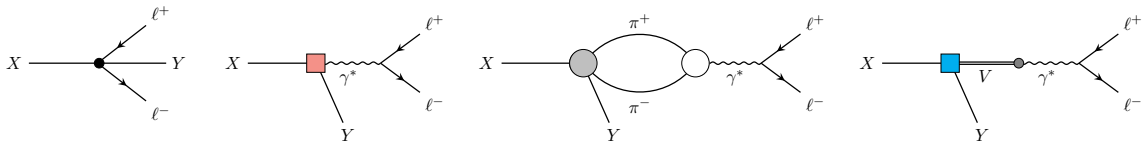

Figure 9.1: Contributions to the C- and CP-odd decay $X \to Y\ell^+\ell^-$. The first diagram describes a short-range semi-leptonic four-point vertex, the second one includes a long-range hadron–photon coupling, while the last two diagrams account for possible hadronic intermediate states. Among the latter, the pion loop corresponds to an isovector transition while the vector-meson conversion respects the isoscalar part of the virtual photon. The black dot, the red box, the gray circle, and the blue box refer to different C- and CP-violating vertices, while the white circle is C- and CP-conserving.

all discrete symmetries. In addition, we sketch an idea of how to evaluate the isoscalar contribution of the photon, employing a less sophisticated, but still symmetry-driven, vector-meson-dominance (VMD) model for the decay $X \to Y\gamma^*$. By an analytic continuation of the three-body amplitudes $X \to Y\pi^+\pi^-$ to the second Riemann sheet we can extract ρYX couplings, which can be related to the relevant ones with the same total isospin in the VMD model using $SU(3)$ symmetry and naive dimensional analysis (NDA).
To extract observables of the C- and CP-violating contribution in $X \to Y\ell^+\ell^-$ driven by a one-photon exchange we pursue the following strategy. First, we consider the phenomenology behind the three mechanisms mentioned above in Sect. 9.1. For this purpose we lay out the basic definitions of kinematics and relate the amplitude to the (differential) decay widths in Sect. 9.1.1. We discuss the short-range semi-leptonic operators, the long-range direct photon–hadron couplings, and the long-range hadronic contributions on a general level in Sects. 9.1.2–9.1.4, respectively. Subsequently, Sect. 9.1.5 includes a discussion of the feasibility of these contributions. The remainder of the article solely focuses on long-distance contributions with hadronic intermediate states. In Sect. 9.2 we investigate the isovector contributions to these hadronic long-range effects. For this purpose, we first sketch the C- and CP-odd contributions to the decays $X \to Y\pi^+\pi^-$ in Sect. 9.2.1, which serve as input to the respective transition form factors. The computation of the latter is discussed in Sect. 9.2.2. In Sect. 9.2.3, we extract the corresponding C-odd couplings of the $\rho(770)$ resonance to $\eta\pi^0$ and $\eta'\eta$ by analytic continuation in the complex-energy plane. Subsequently, we estimate the size of the hadronic long-range effects in the isoscalar parts in Sect. 9.3. Finally, we present the predicted upper limits on the branching ratios in Sect. 9.4 and close with a short summary and outlook in Sect. 9.5.

9.1 | Phenomenology

In this section we discuss the phenomenological importance of the three mechanisms driving $X \to Y\ell^+\ell^-$ and provide the model-independent expressions for them. As an illustration

we depict the different contributions in Fig. 9.1. For simplicity we adapt the notation and conventions introduced for the construction of operators in ToPeχPT in Ref. [2] without further details.

9.1.1 | Kinematics

Consider the transition amplitude $X(P) \to Y(p)\ell^+(p_{\ell^+})\ell^-(p_{\ell^-})$, with two pseudoscalars X and Y of masses $M_X > M_Y$. Conventionally, we describe the three-body decay in terms of the Lorentz invariants

$$s = (P-p)^2, \qquad t_\ell = (P-p_{\ell^+})^2, \qquad u_\ell = (P-p_{\ell^-})^2. \tag{9.1}$$

Throughout we use the electromagnetic quark current

$$J_\mu = \sum_f Q_f \bar{q}_f \gamma_\mu q_f \,, \tag{9.2}$$

where Q_f indicates the electric charge of the respective quarks with flavor f and is conventionally used in units of the proton charge e. In order to define a singularity-free electromagnetic transition form factor for $X \to Y\gamma^*$ we proceed as follows. Similar to Sect. 3.4.2 we can employ Poincaré invariance to write

$$\langle Y(p)|J_\mu(0)|X(P)\rangle = -i\left[(P+p)_\mu A(s) + q_\mu B(s)\right], \tag{9.3}$$

where the imaginary unit accounts for T-violation, the photon momentum is indicated by $q_\mu = (P-p)_\mu$, and A, B denote scalar functions. Both sides of this equation have to obey the Ward identity

$$\langle Y(p)|q^\mu J_\mu(0)|X(P)\rangle = -i\left[(M_X^2 - M_Y^2)A(s) + s\,B(s)\right] \stackrel{!}{=} 0. \tag{9.4}$$

To render the $X \to Y\gamma^*$ amplitude free of singularities,[1] we introduce the electromagnetic transition form factor F_{XY} as

$$A(s) \equiv s \cdot F_{XY}(s). \tag{9.5}$$

Combining the preceding equations we obtain

$$\langle Y(p)|J_\mu(0)|X(P)\rangle = -i\left[s(P+p)_\mu - (P^2-p^2)q_\mu\right] F_{XY}(s) \equiv -iQ_\mu F_{XY}(s)\,.^{[2]} \tag{9.6}$$

[1] Analogous considerations have been made for the kaon decay $K \to \pi\gamma$ in Ref. [223].

[2] This exercise can be repeated for real photons, with the only distinction that a polarization vector $\varepsilon_\mu(q)$ contracting with Q_μ is added. Due to the on-shell condition $s = 0$, the first term in Q_μ vanishes. The remaining contribution is proportional to $q_\mu \varepsilon^\mu(q) = 0$. Consequently, the decay into a real, transverse photon violates gauge invariance and the conservation of angular momentum. See also Ref. [220] for more information.

Note that $F_{XY}(s)$ thus defined is real at leading order in ToPeχPT. Upon contraction with the lepton current the full decay amplitude becomes

$$i\mathcal{M}(X \to Y\ell^+\ell^-) = e^2\,(P+p)_\mu F_{XY}(s)\,\bar{u}_r(p_{\ell^-})\gamma^\mu v_{r'}(p_{\ell^+}), \tag{9.7}$$

where the term proportional to q_μ drops out due to current conservation [319]. In the course of this work, we will see explicitly that the amplitude of each mechanism restores this functional form. Taking the squared absolute value and summing over the lepton spins, one may obtain the doubly differential decay width [229]

$$\frac{\mathrm{d}\Gamma(X \to Y\ell^+\ell^-)}{\mathrm{d}s\,\mathrm{d}\tau} = \frac{\alpha^2}{16\pi M_X^3}\,\big(\lambda\big(s, M_X^2, M_Y^2\big) - \tau^2\big)\,|F_{XY}(s)|^2, \tag{9.8}$$

in terms of the electromagnetic fine-structure constant $\alpha = e^2/4\pi$, the Källén function $\lambda(x,y,z) = x^2+y^2+z^2-2(xy+xz+yz)$, and the Lorentz invariant $\tau = t_\ell - u_\ell$. The τ-integration can be carried out analytically, giving

$$\frac{\mathrm{d}\Gamma(X \to Y\ell^+\ell^-)}{\mathrm{d}s} = \frac{\alpha^2}{8\pi M_X^3}\,\lambda^{3/2}\big(s, M_X^2, M_Y^2\big)\,\sigma_\ell(s)\left(1 - \frac{\sigma_\ell^2(s)}{3}\right)|F_{XY}(s)|^2, \tag{9.9}$$

where $\sigma_\ell(s) = \sqrt{1-4m_\ell^2/s}$ and the physical range is restricted to $s \in \big(4m_\ell^2, (M_X - M_Y)^2\big)$. Throughout, we use the masses $m_e = 0.51\,\mathrm{MeV}$, $m_\mu = 105.66\,\mathrm{MeV}$, $M_\eta = 547.86\,\mathrm{MeV}$, $M_{\eta'} = 957.78\,\mathrm{MeV}$, $M_{\pi^\pm} = 139.57\,\mathrm{MeV}$, and $M_{\pi^0} = 134.98\,\mathrm{MeV}$ [13]. For later use, we also quote the vector-meson masses $M_\rho = 775\,\mathrm{MeV}$ and $M_\omega = 782.66\,\mathrm{MeV}$ [13]. The errors and additional decimal digits on all of these masses are negligible in our analysis.

9.1.2 | Direct semi-leptonic contributions to $X \to Y\ell^+\ell^-$

In Ref. [2] it was shown that the only C-odd, P-even semi-leptonic four-point vertex to $\eta \to \pi^0\ell^+\ell^-$ at lowest order in the QED fine-structure constant and soft momenta originates from the dimension-8 LEFT operator

$$\mathcal{O}_{\ell\psi}^{(u)} \equiv \frac{c_{\ell\psi}^{(u)}}{\Lambda^4}\,\bar{\ell}\gamma^\mu\ell\bar{\psi}\gamma^\nu T^a\psi G^a_{\mu\nu}\,, \tag{9.10}$$

where $c_{\ell\psi}^{(u)}$ denotes flavor-dependent Wilson coefficients.[3] The choice of the high-energy scale Λ depends on the interpretation of the ToPe operators: in the picture of LEFT, Λ can be in the order of the electroweak scale, while in the spirit of the Standard Model effective field theory Λ is a typical BSM scale. The respective leading ToPeχPT operators in the

[3] In contrast, CP-violating quark–lepton operators that contribute to these decays but are C-even and P-odd already appear at dimension 6 [44, 322].

large-N_c limit read [2]

$$\bar{X}^{(u)}_{\ell\psi} \supset \frac{c^{(u)}_{\ell\psi}}{\Lambda^4}\,\bar{g}^{(u)}_1\, i\varphi\big\langle \lambda_L \partial_\mu \bar{U}^\dagger \bar{U} - \lambda_R \partial_\mu \bar{U}\bar{U}^\dagger\big\rangle \bar{\ell}\gamma^\mu \ell\,, \tag{9.11}$$

where we employ the simple single-angle η-η' mixing scheme [330], for which the singlet component corresponds to

$$\varphi = \frac{\sqrt{2}}{3\sqrt{3}F_0}\,\eta + \frac{4}{3\sqrt{3}F_0}\,\eta'\,. \tag{9.12}$$

The meson matrix in the large-N_c limit is then given by

$$\bar{U} = \exp\left(\frac{i\bar{\Phi}}{F_0}\right)\,, \quad \text{where} \quad \bar{\Phi} = \begin{pmatrix} \frac{1}{\sqrt{3}}\eta' + \sqrt{\frac{2}{3}}\eta + \pi^0 & \sqrt{2}\pi^+ & \sqrt{2}K^+ \\ \sqrt{2}\pi^- & \frac{1}{\sqrt{3}}\eta' + \sqrt{\frac{2}{3}}\eta - \pi^0 & \sqrt{2}K^0 \\ \sqrt{2}K^- & \sqrt{2}\bar{K}^0 & \frac{2}{\sqrt{3}}\eta' - \sqrt{\frac{2}{3}}\eta \end{pmatrix}. \tag{9.13}$$

Furthermore, in relation (9.11) we have introduced the spurion matrices $\lambda_{L,R}$ in flavor space, which were defined in Ref. [2] and acquire the same physical values, namely $\lambda_{L,R} \in \{\mathrm{diag}(1,0,0), \mathrm{diag}(0,1,0), \mathrm{diag}(0,0,1)\}$ for the quark flavor $\psi = u,d,s$, respectively. Besides, F_0 denotes the common meson decay constant in the combined chiral and large-N_c limit, $F_0 \lesssim F_\pi \approx 92.3\,\mathrm{MeV}$. Summing over ψ and only picking the interactions relevant for our interests, the operator $\bar{X}^{(u)}_{\ell\psi}$ gives rise to the leading-order Lagrangians

$$\mathcal{L}_{XY\ell^+\ell^-} = \frac{1}{\Lambda^4 F_0^2}\,\mathcal{N}_{X\to Y\ell^+\ell^-}\,\bar{\ell}\gamma^\mu \ell X \partial_\mu Y \tag{9.14}$$

with the normalizations

$$\mathcal{N}_{\eta\to\pi^0\ell^+\ell^-} \equiv \frac{2\sqrt{2}}{3\sqrt{3}}\,\bar{g}^{(u)}_1\big(c^{(u)}_{\ell u} - c^{(u)}_{\ell d}\big)\,, \qquad \mathcal{N}_{\eta'\to\eta\ell^+\ell^-} \equiv \frac{2\sqrt{2}}{3}\,\bar{g}^{(u)}_1\big(c^{(u)}_{\ell u} + c^{(u)}_{\ell d} - 2c^{(u)}_{\ell s}\big)\,. \tag{9.15}$$

Both processes are uncorrelated as their normalizations are linearly independent; the flavor combinations reflect the isospin and $SU(3)$ structure of the transitions. Making use of the Dirac equation for the leptons, the corresponding matrix element yields

$$i\mathcal{M} = e^2(P+p)_\mu F_1(s)\,\bar{u}_r(p_{\ell^-})\gamma^\mu v_{r'}(p_{\ell^+})\,, \tag{9.16}$$

with

$$F_1(s) \equiv -\frac{1}{2e^2\Lambda^4 F_0^2}\,\mathcal{N}_{X\to Y\ell^+\ell^-} \sim -\frac{1}{\Lambda^4}\frac{2\pi F_0^2}{e^2} = -\frac{F_0^2}{2\alpha\Lambda^4}\,. \tag{9.17}$$

In the last step we applied the NDA assumption $\mathcal{N}_{X\to Y\ell^+\ell^-} \sim 4\pi F_0^4$. Note, however, that the sign of the normalization is not fixed by NDA.

9.1.3 | Direct photonic contributions to $X \to Y\gamma^*$

The leading-order contribution to the effective Lagrangian of $X \to Y\gamma^*$ reads [2]

$$\mathcal{L}_{X\to Y\gamma^*} = \frac{1}{\Lambda^4 F_0^2}\mathcal{N}_{X\to Y\gamma^*}\partial_\mu X \partial_\nu Y F^{\mu\nu} + \mathcal{O}(p^6). \tag{9.18}$$

We may access the normalization $\mathcal{N}_{X\to Y\gamma^*}$ using NDA, by regarding the possible sources on the level of LEFT, cf. Ref. [2]. In this discussion we can directly ignore LEFT sources whose leading-order contributions in ToPeχPT are proportional to the ϵ-tensor and can thus not generate an even number of pseudoscalars and at the same time preserve parity. The NDA estimate of $\mathcal{N}_{X\to Y\gamma^*}$ for the chirality-breaking dimension-7 LEFT quark-quadrilinear [109–112, 158]

$$\mathcal{O}^{(a)}_{\psi\chi} = \frac{v}{\Lambda^4} c^{(a)}_{\psi\chi}\, \bar\psi \overleftrightarrow{D}_\mu \gamma_5 \psi \bar\chi \gamma^\mu \gamma_5 \chi\,, \tag{9.19}$$

which is in the focus of Ref. [2], yields $evF_0^3/4\pi$, with Higgs vev v. For the C- and CP-odd dimension-8 operators listed in this reference with two quarks and two gluon field strengths, four quarks and one gluon field strength, four quarks and one photon field strength, we have $\mathcal{N}_{X\to Y\gamma^*} \sim eF_0^4$, $eF_0^4/(4\pi)$, F_0^4, respectively. It has to be underlined that *each* of these estimates may differ by one order of magnitude, possibly rendering all of these operators to the same numerical size. However, in the scope of these NDA estimations, we assume the normalization of the dimension-7 LEFT operator to dominate the remaining ones.
Using $\mathcal{L}_{X\to Y\gamma^*}$ to evaluate the C-odd vertex in the second diagram of Fig. 9.1, we obtain the matrix element [2]

$$i\mathcal{M} = e^2 (P+p)_\nu F_2(s)\, \bar u_r(p_{\ell^-})\gamma^\nu v_{r'}(p_{\ell^+})\,, \tag{9.20}$$

with

$$F_2(s) \equiv \frac{1}{2e\Lambda^4 F_0^2}\mathcal{N}_{X\to Y\gamma^*} \sim \frac{vF_0}{8\pi\Lambda^4}\,. \tag{9.21}$$

Again, NDA does not provide any information on the sign of the amplitude. Comparing Eqs. (9.17) and (9.21), we note $F_2(s)/F_1(s) \sim \alpha v/(4\pi F_0) \approx 1.5$, hence both contributions are really expected to be of comparable size.

9.1.4 | Hadronic long-range effects

The hadronic long-range contributions to the transition form factor can be constructed with knowledge about ToPe forces in $X \to Y\pi^+\pi^-$ [1]. As we cannot assume isospin to be a good symmetry for this kind of BSM physics, we consider in the following sections both the isovector and isoscalar part of the photon.

9.1.4.1 | The isovector contribution

In this section we establish dispersion relations for hadronic contributions of the C- and CP-odd transition form factor F_{XY} and restrict the calculation to the isovector part of

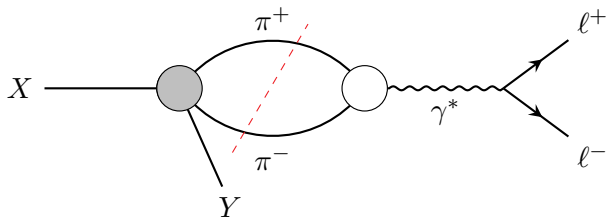

Figure 9.2: Discontinuity of the $X \to Y\gamma^*$ transition form factors, representative for the decays $\eta \to \pi^0\gamma^*$ and $\eta' \to \eta\gamma^*$. The white blob denotes the pion vector form factor and the gray one the C-violating contributions to the $\eta \to \pi^0\pi^+\pi^-$ and $\eta' \to \eta\pi^+\pi^-$ amplitudes, respectively. The dashed line illustrates the unitarity cut.

the photon. The discontinuity of $X \to Y\gamma^*$, as depicted in Fig. 9.2, can be calculated by applying a unitarity cut on the dominant intermediate state, i.e., two charged pions, allowing us to access the transition form factor in a non-perturbative fashion. The first ingredient to the discontinuity in Fig. 9.2 is indicated by the gray blob and describes the C- and CP-odd contributions to the hadronic $X \to Y\pi^+\pi^-$ decay amplitude defined by

$$\big\langle Y(p)\,\pi^+(p_+)\,\pi^-(p_-)\big|iT\big|X(P)\big\rangle = (2\pi)^4\,\delta^{(4)}(P-p-p_+-p_-)\,i\mathcal{M}^{XY}(s,t,u)\,. \tag{9.22}$$

These amplitudes will be discussed in detail for the different cases in Sect. 9.2. The remaining contribution is the pion vector form factor defined via the current[4]

$$\langle\pi^+(p_+)\pi^-(p_-)|J_\mu(0)|0\rangle = (p_+-p_-)_\mu F_\pi^V(s)\,. \tag{9.23}$$

Note that this equation and Eq. (9.6) differ, beside the respective momentum configuration, by an explicit imaginary unit as demanded by their different behavior under time reversal. With only elastic rescattering taken into account, the pion vector form factor obeys the discontinuity relation

$$\operatorname{disc} F_\pi^V(s) = 2i\,F_\pi^V(s)\sin\delta_1(s)e^{-i\delta_1(s)}\theta(s-4M_\pi^2)\,, \tag{9.24}$$

where $\delta_1(s)$ denotes the P-wave $\pi\pi$ phase shift with two-body isospin $I_{\pi\pi}=1$. The most general solution to this equation is given in terms of the Omnès function [105]

$$F_\pi^V(s) = P_n(s)\,\Omega_1(s) = P_n(s)\exp\left(\frac{s}{\pi}\int\limits_{4M_\pi^2}^{\infty}\frac{\delta_1(x)}{x(x-s)}\,\mathrm{d}x\right), \tag{9.25}$$

with a real-valued subtraction polynomial P_n of order n. The index of the Omnès function indicates the isospin $I_{\pi\pi}$ of the dipion state. The pion vector form factor is expected to behave as $F_\pi^V(s) \asymp 1/s$ for large energies [331–338] (up to logarithmic corrections), and to

[4] In the isospin limit, which we will employ for the pion form factor in the following, only the isovector contribution of the current contributes, i.e., $J_\mu^{(1)} = \frac{1}{2}\big(\bar{u}\gamma_\mu u - \bar{d}\gamma_\mu d\big)$.

be free of zeros [338, 339]. Thus, P_n is a constant and can be set to 1 due to gauge invariance, such that $F_\pi^V(s) = \Omega_1(s)$. For consistency we waive the incorporation of inelastic effects, which we do not consider in $X \to Y\pi^+\pi^-$ either. In the region of the $\rho(770)$ resonance dominating $F_\pi^V(s)$, these are known to affect the form factor by no more than 6%, depending on the phase shift used as input [233]. Given other sources of uncertainty in the present study, we consider this error negligible.

When we cut the dipion intermediate state in Fig. 9.2, the discontinuity of the isovector contribution $F_{XY}^{(1)}$ to the transition form factor F_{XY} becomes

$$Q_\mu \text{disc} F_{XY}^{(1)}(s) = \int \frac{\mathrm{d}^4 k}{(2\pi)^2}\, \delta(k^2 - M_\pi^2)\, \delta\left((q-k^2) - M_\pi^2\right)\, \mathcal{M}^{XY}(s,t,u)\, (q-2k)_\mu F_\pi^{V*}(s)\,, \tag{9.26}$$

where $t = (P - p_+)^2$ and $u = (P - p_-)^2$. Carrying out the trivial momentum integration over the delta distributions we obtain

$$Q_\mu \text{disc} F_{XY}^{(1)}(s) = \frac{i}{32\pi^2}\sigma_\pi(s) F_\pi^{V*}(s) \int \mathrm{d}\Omega_k\, \mathcal{M}^{XY}(s,t,u)(q-2k)_\mu, \tag{9.27}$$

with $\mathrm{d}\Omega_k = \mathrm{d}\phi\, \mathrm{d}z$. In order to handle the k_μ dependence of the integrand we express it in terms of the remaining momenta. For this purpose we use (again in analogy to Sect. 3.4.2) the ansatz

$$\int \mathrm{d}\Omega_k\, \mathcal{M}^{XY}(s,t,u)(q-2k)_\mu \stackrel{!}{=} (P+p)_\mu I_1 + q_\mu I_2\,, \tag{9.28}$$

with two yet undetermined integrals $I_{1,2}$. We contract each side of this equation with q^μ and $(P+p)^\mu$ to obtain the system of linear equations

$$\begin{aligned} 0 &= (M_X^2 - M_Y^2)\, I_1 + s\, I_2, \\ \int \mathrm{d}\Omega_k\, \kappa(s) z\, \mathcal{M}^{XY}(s,t,u) &= (2M_X^2 + 2M_Y^2 - s)\, I_1 + (M_X^2 - M_Y^2)\, I_2\,, \end{aligned} \tag{9.29}$$

with

$$z = \frac{t-u}{\kappa(s)}\,, \qquad \kappa(s) = \sigma_\pi(s)\lambda^{1/2}(s, M_X^2, M_Y^2)\,, \qquad \text{and} \qquad \sigma_\pi(s) = \sqrt{1 - \frac{4M_\pi^2}{s}}\,. \tag{9.30}$$

From this we obtain

$$I_1 = -\sigma_\pi^2(s)\frac{s}{\kappa(s)} \int \mathrm{d}\Omega_k\, z\, \mathcal{M}^{XY}(s,t,u) = -\frac{s}{M_X^2 - M_Y^2}\, I_2\,. \tag{9.31}$$

Hence, the angular integral can be rewritten as

$$\int \mathrm{d}\Omega_k\, \mathcal{M}^{XY}(s,t,u)(q-2k)_\mu = \left[q_\mu \frac{M_X^2 - M_Y^2}{s} - (P+p)_\mu\right] \frac{s\sigma_\pi^2(s)}{\kappa(s)} \int \mathrm{d}\Omega_k\, z\, \mathcal{M}^{XY}(s,t,u). \tag{9.32}$$

Identifying the expression in brackets as $(-Q_\mu/s)$, carrying out the trivial integration over

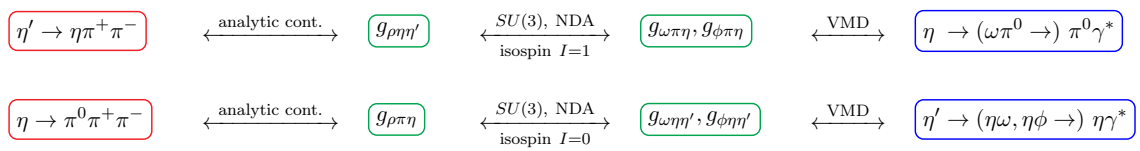

Figure 9.3: Schematic sketch of the strategy to extract the isoscalar contribution of the $\eta \to \pi^0\gamma^*$ ($\eta' \to \eta\gamma^*$) transition form factor (blue) from the C- and CP-odd $\eta' \to \eta\pi^+\pi^-$ ($\eta \to \pi^0\pi^+\pi^-$) amplitude (red) using vector-meson couplings (green).

the azimuthal angle ϕ, and inserting the result in Eq. (9.27), we find that

$$\mathrm{disc}F_{XY}^{(1)}(s) = -\frac{1}{24\pi}\sigma_\pi^3(s)F_\pi^{V*}(s)\, f_{XY}(s)\,\theta(s-4M_\pi^2)\,, \tag{9.33}$$

where $\sigma_\pi(s) = \sqrt{1-4M_\pi^2/s}$. In this discontinuity relation the quantity f_{XY} denotes the P-wave projection of the hadronic decay amplitude given by

$$f_{XY}(s) \equiv \frac{3}{2\kappa(s)}\int_{-1}^{1}\mathrm{d}z\, z\,\mathcal{M}^{XY}(s,t,u), \tag{9.34}$$

with

$$z = \frac{t-u}{\kappa(s)} \quad \text{and} \quad \kappa(s) = \sigma_\pi(s)\lambda^{1/2}\big(s, M_X^2, M_Y^2\big)\,. \tag{9.35}$$

Adapting the high-energy behavior of f_{XY} and δ_1 from Ref. [1], an unsubtracted dispersion relation is sufficient to ensure convergence of the remaining integral over the discontinuity, such that the form factor can be evaluated with

$$F_{XY}^{(1)}(s) = \frac{i}{48\pi^2}\int_{4M_\pi^2}^{\infty}\mathrm{d}x\,\sigma_\pi^3(x)F_\pi^{V*}(x)\,\frac{f_{XY}(x)}{x-s}. \tag{9.36}$$

9.1.4.2 | The isoscalar contribution

In order to estimate the isoscalar contribution, we apply a VMD pole approximation and consider a vector-meson conversion of γ^* to v_μ, with $v \in \{\omega, \phi\}$, cf. the very right diagram in Fig. 9.1. While this strategy is not as model-independent and sophisticated as the dispersive analysis of the isovector part of γ^*, it serves as a good approximation to at least estimate the relative size of this contribution, not least due to the narrowness of the ω and ϕ resonances dominating isoscalar vector spectral functions at low energies. Furthermore, this ansatz even correlates the decay $\eta \to \pi^0\gamma^*$ to $\eta' \to \eta\pi^+\pi^-$ and $\eta' \to \eta\gamma^*$ to $\eta \to \pi^0\pi^+\pi^-$ by following the strategy sketched in Fig. 9.3 to relate the decays of same total isospin.
The combination of vector mesons with χPT was extensively worked out for instance in Refs. [340–345] and references therein. The number of free parameters can be reduced most efficiently, cf. Ref. [342], by coupling uncharged vector mesons to uncharged pseudoscalars via the field-strength tensor $V_{L,R}^{\mu\nu}$. The latter is the analog to the photonic one with the same

discrete symmetries and transformations under $SU(3)_L \times SU(3)_R$. If we only consider the relevant degrees of freedom, i.e., treating $\bar{U}$ and $V^\mu_{L,R}$ as diagonal matrices, we can effectively write

$$V^{\mu\nu}_{L,R} = \partial^\mu V^\nu_{L,R} - \partial^\nu V^\mu_{L,R} \,. \tag{9.37}$$

The physical value of this chiral building block can be evaluated with $V^\mu_L = V^\mu_R = \mathrm{diag}(\rho + \omega, -\rho + \omega, \sqrt{2}\phi)^\mu + \ldots$, where the ellipsis indicates terms without vector mesons. At the mesonic level, we can deduce the desired interaction from the leading-order $XY\gamma^*$ operator, cf. Ref. [221], and hence write

$$\mathcal{L}_{vYX} = g_{vYX} \partial_\mu X \partial_\nu Y v^{\mu\nu} \,, \tag{9.38}$$

with $v_{\mu\nu} \equiv \partial_\mu v_\nu - \partial_\nu v_\mu$. The ToPe$\chi$PT operators that can generate this mesonic interaction at leading order in the large-N_c power counting, i.e., $\mathcal{O}(p^4, \delta^2)$ (see Ref. [2] for further details), and originate from the LEFT operator in Eq. (9.19) are

$$\begin{aligned} \bar{X}^{(a)}_{\psi\chi} \supset \frac{v}{\Lambda^4} c^{(a)}_{\psi\chi} \Big(& \bar{g}^{(a)}_{V_1} \big\langle \lambda_L \partial_\nu \bar{U}^\dagger \bar{U} - \lambda_R \partial_\nu \bar{U} \bar{U}^\dagger \big\rangle \big\langle \big(\lambda V^{\mu\nu}_L \partial_\mu \bar{U}^\dagger - \lambda^\dagger V^{\mu\nu}_R \partial_\mu \bar{U} \big) - \text{h.c.} \big\rangle \\ & + \bar{g}^{(a)}_{V_2} \big\langle \lambda \partial_\mu \bar{U}^\dagger - \lambda^\dagger \partial_\mu \bar{U} \big\rangle \big\langle \big(\lambda_L V^{\mu\nu}_L \partial_\nu \bar{U}^\dagger \bar{U} - \lambda_R V^{\mu\nu}_R \partial_\nu \bar{U} \bar{U}^\dagger \big) - \text{h.c.} \big\rangle \\ & + \bar{g}^{(a)}_{V_3} \partial_\nu \varphi \big\langle \big(\lambda \lambda_L V^{\mu\nu}_L \partial_\mu \bar{U}^\dagger - \lambda^\dagger \lambda_R V^{\mu\nu}_R \partial_\mu \bar{U} \big) - \text{h.c.} \big\rangle \Big) \,. \end{aligned} \tag{9.39}$$

Here, we only list the operators leading to distinct, non-vanishing, expressions after we set $\lambda^{(\dagger)}$, $\lambda_{L,R}$, and $V^{\mu\nu}_{L,R}$ to their physical values and use the fact that in our application all appearing matrices are diagonal and therefore commute. Evaluating the flavor traces of the operator in the first line and labeling the vector-meson couplings with a corresponding superscript (V_1), we end up with

$$\begin{aligned} g^{(V_1)}_{\rho\pi\eta} &= \frac{16v}{\Lambda^4 F_0^2} \sqrt{\frac{2}{3}} \big(c^{(a)}_{ud} + c^{(a)}_{du} \big) \bar{g}^{(a)}_{V_1} - \frac{1}{\sqrt{3}} g^{(V_1)}_{\omega\eta\eta'} \,, & g^{(V_1)}_{\rho\eta\eta'} &= \frac{8\sqrt{2}v}{\Lambda^4 F_0^2} \big(c^{(a)}_{us} - c^{(a)}_{ds} \big) \bar{g}^{(a)}_{V_1} \,, \\ g^{(V_1)}_{\omega\pi\eta} &= \frac{16v}{\Lambda^4 F_0^2} \sqrt{\frac{2}{3}} \big(c^{(a)}_{ud} - c^{(a)}_{du} \big) \bar{g}^{(a)}_{V_1} - \frac{1}{\sqrt{3}} g^{(V_1)}_{\rho\eta\eta'} \,, & g^{(V_1)}_{\omega\eta\eta'} &= \frac{8\sqrt{2}v}{\Lambda^4 F_0^2} \big(c^{(a)}_{us} + c^{(a)}_{ds} \big) \bar{g}^{(a)}_{V_1} \,, \\ g^{(V_1)}_{\phi\pi\eta} &= \frac{16v}{\sqrt{3}\Lambda^4 F_0^2} \big(c^{(a)}_{su} - c^{(a)}_{sd} \big) \, \bar{g}^{(a)}_{V_1} \,, & g^{(V_1)}_{\phi\eta\eta'} &= -\frac{16v}{\Lambda^4 F_0^2} \big(c^{(a)}_{su} + c^{(a)}_{sd} \big) \bar{g}^{(a)}_{V_1} \,. \end{aligned} \tag{9.40}$$

For the second operator in Eq. (9.39) we observe that the resulting vector meson couplings $g^{(V_2)}_{vYX}$ equal the $g^{(V_1)}_{vYX}$ from Eq. (9.40) if $c^{(a)}_{\psi\chi} \bar{g}^{(a)}_{V_2} = -c^{(a)}_{\chi\psi} \bar{g}^{(a)}_{V_1}$. The third operator in $\bar{X}^{(a)}_{\psi\chi}$ yields

$$\begin{aligned} g^{(V_3)}_{\rho\pi\eta} &= \frac{1}{\sqrt{3}} g^{(V_3)}_{\omega\eta\eta'} \,, & g^{(V_3)}_{\rho\eta\eta'} &= -\frac{4\sqrt{2}v}{3\Lambda^4 F_0^2} \big(c^{(a)}_{uu} - c^{(a)}_{dd} \big) \bar{g}^{(a)}_{V_3} \,, \\ g^{(V_3)}_{\omega\pi\eta} &= \frac{1}{\sqrt{3}} g^{(V_3)}_{\rho\eta\eta'} \,, & g^{(V_3)}_{\omega\eta\eta'} &= -\frac{4\sqrt{2}v}{3\Lambda^4 F_0^2} \big(c^{(a)}_{uu} + c^{(a)}_{dd} \big) \bar{g}^{(a)}_{V_3} \,, \\ g^{(V_3)}_{\phi\pi\eta} &= 0 \,, & g^{(V_3)}_{\phi\eta\eta'} &= \frac{16v}{3\Lambda^4 F_0^2} c^{(a)}_{ss} \bar{g}^{(a)}_{V_3} \,. \end{aligned} \tag{9.41}$$

Both Eqs. (9.40) and (9.41) suggest that there is a correlation between $g_{\rho\pi\eta}$ and $g_{\omega\eta\eta'}$ as well as between $g_{\rho\pi\eta}$ and $g_{\omega\eta\eta'}$, but none of $g_{\phi\pi\eta}$ or $g_{\phi\eta\eta'}$ with the ρ couplings. However, this observation does not necessarily hold for higher orders in ToPeχPT or for operators derived from other LEFT sources. We continue with the couplings in Eq. (9.41) as our central estimates and make use of the flavor relations implied therein.

Next, we consider the Lagrangian

$$\mathcal{L}_{v\gamma} = -\frac{eM_v^2}{g_{v\gamma}} A_\nu v^\nu \tag{9.42}$$

for the vector-meson conversion with known coupling constants $g_{v\gamma}$. As Eq. (9.42) employs the photon field instead of the field strength tensor, it is not manifestly gauge invariant. In the end, this is a necessity to implement *strict* VMD for the isoscalar part of the form factor, avoiding an additional direct photon coupling. We can now evaluate the isoscalar contribution illustrated on the very right in Fig. 9.1, which, in agreement with Eq. (9.7), gives rise to the matrix element

$$i\mathcal{M}_{XY}^{(0)} = e^2\,(P+p)_\mu\, F_{XY}^{(0)}(s)\,\bar{u}_r(p_{\ell^-})\gamma^\mu v_{r'}(p_{\ell^+})\,. \tag{9.43}$$

The corresponding isoscalar form factor, which is consistent with the high-energy behavior of the isovector part in Eq. (9.36), finally reads

$$F_{XY}^{(0)}(s) \equiv \frac{\tilde{g}}{2g_{v\gamma}} \frac{M_v^2}{M_v^2 - s}\,, \tag{9.44}$$

where $\tilde{g}$ equals $g_{v\pi\eta}$ for $X = \eta$, $Y = \pi^0$ and $g_{v\eta\eta'}$ for $X = \eta'$, $Y = \eta$.

9.1.5 | Discussion

With the results worked out in the previous sections we can evaluate the full contribution of the $X \to Y\gamma^*$ transition form factors by

$$F_{XY}(s) = F_1(s) + F_2(s) + F_{XY}^{(1)}(s) + F_{XY}^{(0)}(s)\,, \tag{9.45}$$

where each summand corresponds to one diagram in Fig. 9.1. Note that there is no way to distinguish between the four contributions in a sole measurement of the $X \to Y\ell^+\ell^-$ branching ratio.

Regarding F_1 and F_2, we observe that their NDA estimates in Eqs. (9.17) and (9.21) yield roughly the same result, even without accounting for the uncertainty of NDA. Hence, there is no clear hierarchy between direct semi-leptonic contributions and C- and CP-violating photon–hadron couplings contributing to $X \to Y\ell^+\ell^-$. In future analyses, the sum $F_1 + F_2$ (which does not depend on s at leading order in ToPeχPT) may be replaced by a single constant parameter in a regression to hypothetical measurements of respective singly- or doubly-differential momentum distributions.

We remark in passing that *all* transition form factor contributions could be expected to undergo further hadronic corrections due to "initial-state interactions" of $\eta\pi$ and $\eta'\eta$ P-wave type, respectively. However, all corresponding phase shifts are expected to be tiny and the resulting effects to be hence utterly negligible: the $\eta\pi$ P-wave is strongly suppressed in the chiral expansion at low energies relative to $\eta\pi$ S-wave or $\pi\pi$ rescattering [308, 312], and resonances with quark-model-exotic quantum numbers $J^{PC} = 1^{-+}$ due to their C-odd nature will have a rather large mass [**?**]. We therefore do not consider any such corrections in this article.

Given the currently accessible experimental data and the missing information on the normalizations of F_1 and F_2, we henceforth focus on the contributions of $F_{XY}^{(1)}$ and $F_{XY}^{(0)}$. On the one hand, we are in a position to predict the latter with the input discussed in Sect. 9.1.4. On the other hand, they provide new conceptual insights by directly relating ToPe forces in $X \to Y\pi^+\pi^-$ with $X \to Y\gamma^*$. Moreover, we assume no significant cancellations among the individual contributions in Eq. (9.45) throughout this manuscript.

9.2 | Hadronic long-range effects: the isovector contribution

In this section we investigate the isovector contribution to the transition form factor $X \to Y\gamma^*$ based on the dispersive representations derived in Sect. 9.1.4.1. Thus, we focus on C- and CP-odd contributions of the lowest-lying hadronic intermediate state, i.e., on the decay chain $X \to Y\pi^+\pi^- \to Y\gamma^*$.

9.2.1 | The dispersive C- and CP-odd $X \to Y\pi^+\pi^-$ partial-wave amplitude

The formalism, results, and most of the notation are adopted from Ref. [1]. The latter uses a dispersive framework known as Khuri–Treiman equations [106] to access the three-body amplitude $X \to Y\pi^+\pi^-$ including its C- and CP-odd contributions. In this approach, a coupled set of integral equations is set up for the two-body scattering process and analytically continued to the physical realm of the three-body decay.

9.2.1.1 | $\eta \to \pi^0\pi^+\pi^-$

The C- and CP-odd contributions to $\eta \to \pi^0\pi^+\pi^-$ read

$$\mathcal{M}^{\eta\pi}(s,t,u) = \mathcal{M}_0^{\eta\pi}(s,t,u) + \mathcal{M}_2^{\eta\pi}(s,t,u), \tag{9.46}$$

where the lower index denotes the *total* isospin of the three-body final state. Neglecting D- and higher partial waves, we can decompose these amplitudes in the sense of a reconstruction theorem [98, 100, 101] into single-variable functions $\mathcal{G}_{I_{\pi\pi}}(s)$, $\mathcal{H}_{I_{\pi\pi}}(s)$ with fixed *two-body*

isospin $I_{\pi\pi}$ and relative angular momentum ℓ of the $\pi^+\pi^-$ state:

$$\begin{aligned}\mathcal{M}_0^{\eta\pi}(s,t,u) &= (t-u)\mathcal{G}_1(s) + (u-s)\mathcal{G}_1(t) + (s-t)\mathcal{G}_1(u),\\ \mathcal{M}_2^{\eta\pi}(s,t,u) &= 2(u-t)\mathcal{H}_1(s) + (u-s)\mathcal{H}_1(t) + (s-t)\mathcal{H}_1(u) - \mathcal{H}_2(t) + \mathcal{H}_2(u).\end{aligned} \tag{9.47}$$

Due to Bose symmetry the $I_{\pi\pi} = 1$ single-variable functions have $\ell = 1$ while the ones with $I_{\pi\pi} = 2$ have $\ell = 0$. Unitarity demands the single-variable functions to obey

$$\operatorname{disc}\mathcal{A}_{I_{\pi\pi}}(s) = 2i\,\sin\delta_{I_{\pi\pi}}(s)e^{-i\delta_{I_{\pi\pi}}(s)}\left(\mathcal{A}_{I_{\pi\pi}}(s) + \hat{\mathcal{A}}_{I_{\pi\pi}}(s)\right)\theta(s-4M_\pi^2), \tag{9.48}$$

with $\mathcal{A}_{I_{\pi\pi}} \in \{\mathcal{G}_{I_{\pi\pi}}, \mathcal{H}_{I_{\pi\pi}}\}$ and the $\pi\pi$ scattering phase shift $\delta_{I_{\pi\pi}}(s)$. The inhomogeneity $\hat{\mathcal{A}}_{I_{\pi\pi}}(s)$ contains left-hand-cut contributions induced by crossed-channel rescattering effects. In terms of the angular average

$$\langle z^n f\rangle := \frac{1}{2}\int_{-1}^{1}\mathrm{d}z\, z^n f\left(\tfrac{3r-s+z\kappa(s)}{2}\right), \tag{9.49}$$

with $3r \equiv s+t+u$, the $\hat{\mathcal{A}}_{I_{\pi\pi}}(s)$ explicitly read

$$\begin{aligned}\hat{\mathcal{G}}_1(s) &= -\frac{3}{\kappa(s)}\left(3(s-r)\langle z\mathcal{G}_1\rangle + \kappa(s)\langle z^2\mathcal{G}_1\rangle\right),\\ \hat{\mathcal{H}}_1(s) &= \frac{3}{2\kappa(s)}\left(3(s-r)\langle z\mathcal{H}_1\rangle + \kappa(s)\langle z^2\mathcal{H}_1\rangle + 2\langle z\mathcal{H}_2\rangle\right),\\ \hat{\mathcal{H}}_2(s) &= \frac{1}{2}\left(9(s-r)\langle\mathcal{H}_1\rangle + 3\kappa(s)\langle z\mathcal{H}_1\rangle - 2\langle\mathcal{H}_2\rangle\right).\end{aligned} \tag{9.50}$$

For the $\mathcal{A}_{I_{\pi\pi}}(s)$ we employ dispersion relations with a minimal number of subtractions to ensure convergence. Assuming that in the limit of infinite s the phase shifts scale like $\delta_1(s) \to \pi$, $\delta_2(s) \to 0$ and the single-variable functions as $\mathcal{A}_1(s) = \mathcal{O}(s^{-1})$, $\mathcal{A}_2(s) = \mathcal{O}(s^0)$, we obtain

$$\begin{aligned}\mathcal{G}_1(s) &= \Omega_1(s)\left(\varepsilon + \frac{s}{\pi}\int\limits_{4M_\pi^2}^{\infty}\frac{\mathrm{d}x}{x}\,\frac{\sin\delta_1(x)\hat{\mathcal{G}}_1(x)}{|\Omega_1(x)|\,(x-s)}\right),\\ \mathcal{H}_1(s) &= \Omega_1(s)\left(\vartheta + \frac{s}{\pi}\int\limits_{4M_\pi^2}^{\infty}\frac{\mathrm{d}x}{x}\,\frac{\sin\delta_1(x)\hat{\mathcal{H}}_1(x)}{|\Omega_1(x)|\,(x-s)}\right),\\ \mathcal{H}_2(s) &= \Omega_2(s)\frac{s}{\pi}\int\limits_{4M_\pi^2}^{\infty}\frac{\mathrm{d}x}{x}\,\frac{\sin\delta_2(x)\hat{\mathcal{H}}_2(x)}{|\Omega_2(x)|\,(x-s)},\end{aligned} \tag{9.51}$$

where here and in the following $M_\pi \equiv M_{\pi^\pm}$. The C-conserving SM amplitude for $\eta \to \pi^+\pi^-\pi^0$ is similarly described in terms of Khuri–Treiman amplitudes; these have been discussed extensively in the literature, see Ref. [283] and references therein. The subtraction

constants obtained by a fit to the Dalitz-plot distributions[5] of $X \to Y\pi^+\pi^-$ [215] yield [1]

$$\varepsilon = i\,0.014(22)\,M_\pi^{-2}\,, \qquad \vartheta = i\,0.068(34)\times 10^{-3}\,M_\pi^{-2}\,. \tag{9.52}$$

These subtraction constants give rise to the real-valued isoscalar and isotensor couplings $g_0 = -2.8(4.5)\,\text{GeV}^{-6}$ and $g_2 = -9.3(4.6)\cdot 10^{-3}\,\text{GeV}^{-2}$ [1], using

$$\varepsilon = -0.25i\,\text{GeV}^4\,g_0\,, \qquad \vartheta = -0.38i\,g_2\,. \tag{9.53}$$

With the $\mathcal{A}_{I_{\pi\pi}}(s)$ defined above, the P-wave amplitude necessary to evaluate the $\eta \to \pi^0\gamma^*$ transition form factor is by definition, cf. Eq. (9.34), given as

$$f_{\eta\pi}(s) = \mathcal{G}_1(s) + \hat{\mathcal{G}}_1(s) + \mathcal{H}_1(s) + \hat{\mathcal{H}}_1(s)\,, \tag{9.54}$$

whose dependence on $\mathcal{H}_2$ and $\hat{\mathcal{H}}_2$ is rather subtle and enters the definition of $\hat{\mathcal{H}}_1$ in Eq. (9.50).

The transition form factor is fully determined by knowledge about the partial-wave amplitude $f_{XY}(s)$ and the pion vector form factor $F_\pi^V(s)$. These quantities are in turn fixed by the subtraction constants ε, ϑ, the S-wave $\pi\pi$ scattering phase shift δ_2 with isospin 2, and the P-wave $\pi\pi$ scattering phase shift δ_1 [299], respectively. The latter has to be used consistently in $f_{XY}(s)$ and $F_\pi^V(s)$, i.e., we use the same continuation to asymptotic s and omit the incorporation of inelasticities, which is beyond the scope of this work.

9.2.1.2 | $\eta' \to \eta\pi^+\pi^-$

In the C-and CP-violating contribution to $\eta' \to \eta\pi^+\pi^-$ the three-body final state carries total three-body isospin 1. The respective amplitude can be decomposed as

$$\mathcal{M}^{\eta'\eta}(s,t,u) = (t-u)\mathcal{G}_{\pi\pi}(s) + \mathcal{G}_{\eta\pi}(t) - \mathcal{G}_{\eta\pi}(u); \tag{9.55}$$

see Ref. [287] for the corresponding SM amplitude. The indices labeling the single-variable functions indicate which two particles contribute to the intermediate state of the scattering process. While the $\pi\pi$ intermediate state has the quantum numbers $I_{\pi\pi} = 1$, $\ell = 1$, $\eta\pi$ has $I_{\eta\pi} = 1$, $\ell = 0$. Both $\mathcal{G}_{\pi\pi}(s)$ and $\mathcal{G}_{\eta\pi}(s)$ fulfill the discontinuity equation as quoted in Eq. (9.48). The inhomogeneities in this case are

$$\begin{aligned}
\hat{\mathcal{G}}_{\pi\pi}(s) &= \frac{6}{\kappa_{\pi\pi}}\,\langle z_s\mathcal{G}_{\eta\pi}\rangle,\\
\hat{\mathcal{G}}_{\eta\pi}(t) &= -\langle\mathcal{G}_{\eta\pi}\rangle^+ - \frac{3}{2}\left(r - t + \frac{\Delta}{3t}\right)\langle\mathcal{G}_{\pi\pi}\rangle^- + \frac{1}{2}\kappa_{\eta\pi}\langle z_t\mathcal{G}_{\pi\pi}\rangle^-,
\end{aligned} \tag{9.56}$$

[5] The latest BESIII data for $\eta \to \pi^+\pi^-\pi^0$ [346] is not included in Ref. [1] yet and has also not been added to our present analysis, as the statistical accuracy does not supersede that of Ref. [215].

where the cosine of the scattering angles in the s-channel is still given by the general expression Eq. (9.35), $z_s \equiv z$, while the one in the t-channel reads

$$z_t = \frac{t\,(u-s)-\Delta}{t\,\kappa_{\pi\eta}(t)} \quad \text{with} \quad \kappa_{\pi\eta}(t) = \frac{\lambda^{1/2}(t,M_{\eta'}^2,M_\pi^2)\,\lambda^{1/2}(t,M_\eta^2,M_\pi^2)}{t}\,. \tag{9.57}$$

In these equations we used the notation $\Delta \equiv (M_{\eta'}^2 - M_\pi^2)(M_\eta^2 - M_\pi^2)$. We additionally introduced two new types of angular averages, namely

$$\langle z^n f\rangle^\pm := \frac{1}{2}\int_{-1}^{1} \mathrm{d}z\, z^n f\Big(\tfrac{3r-t+z\kappa_{\eta\pi}(t)\pm\Delta/t}{2}\Big)\,. \tag{9.58}$$

Assuming the asymptotics $\delta_{\eta\pi}(t) \to \pi$ and $\mathcal{G}_{\pi\pi}(s) = \mathcal{O}(1/s)$, $\mathcal{G}_{\eta\pi}(t) = \mathcal{O}(t^0)$, the single-variable functions can be evaluated by

$$\begin{aligned}
\mathcal{G}_{\pi\pi}(s) &= \Omega_{\pi\pi}(s)\left(\varrho + \frac{s}{\pi}\int_{s_\text{th}}^{\infty}\frac{\mathrm{d}x}{x}\frac{\sin\delta_{\pi\pi}(x)\hat{\mathcal{G}}_{\pi\pi}(x)}{|\Omega_{\pi\pi}(x)|\,(x-s)}\right),\\
\mathcal{G}_{\eta\pi}(t) &= \Omega_{\eta\pi}(t)\left(\zeta\,t + \frac{t^2}{\pi}\int_{t_\text{th}}^{\infty}\frac{\mathrm{d}x}{x^2}\frac{\sin\delta_{\eta\pi}(x)\hat{\mathcal{G}}_{\eta\pi}(x)}{|\Omega_{\eta\pi}(x)|\,(x-t)}\right).
\end{aligned} \tag{9.59}$$

Here, the $\eta\pi$ S-wave phase shift from Refs. [258, 309] has been employed. For the subtraction constants, the values

$$\varrho = -i\,0.04(12)\,M_\pi^{-2}\,, \qquad \zeta = i\,0.05(12)\,M_\pi^{-2}\,, \tag{9.60}$$

have been obtained by a regression to the Dalitz-plot distribution of $\eta' \to \eta\pi^+\pi^-$ [219]. In terms of the real-valued isovector coupling $g_1 = 0.7(1.0)\,\text{GeV}^{-2}$ and its leading correction $\delta g_1 = -5.5(7.3)\,\text{GeV}^{-2}$ [1], the subtraction constants read

$$\varrho = -3.5\cdot 10^{-3}\,i g_1\left(1 - 166.5\,\text{GeV}^2\,\delta g_1\right)\,, \qquad \zeta = 0.76\,i g_1\left(1 - 0.65\,\text{GeV}^2\,\delta g_1\right)\,. \tag{9.61}$$

Finally, the P-wave entering the $\eta' \to \eta\gamma^*$ transition form factor is given by

$$f_{\eta'\eta}(s) = \mathcal{G}_{\pi\pi}(s) + \hat{\mathcal{G}}_{\pi\pi}(s). \tag{9.62}$$

The dependence of $f_{\eta'\eta}$ on the S-wave amplitude $\mathcal{G}_{\eta\pi}$ is encoded in the angular averages in Eq. (9.56).

9.2.2 | Computation of the isovector form factor $X \to Y\gamma^*$

When computing the transition form factors $F_{XY}^{(1)}$, it is advantageous to exploit the linearity of the three-body decay amplitudes $\mathcal{M}^{XY}$ in the subtraction constants. As mentioned in Ref. [1], the solutions of the Khuri–Treiman amplitudes can be represented by so-called

basis solutions, which are independent of the subtraction constants and can be fixed once and for all before even carrying out a regression to data.

9.2.2.1 | $\eta \to \pi^0\gamma^*$

The basis solutions for the P-wave amplitude $f_{\eta\pi}$ are defined by

$$f^{\varepsilon}_{\eta\pi}(s) \equiv \left[\mathcal{G}_1(s) + \hat{\mathcal{G}}_1(s)\right]\Big|_{\varepsilon=1}, \qquad f^{\vartheta}_{\eta\pi}(s) \equiv \left[\mathcal{H}_1(s) + \hat{\mathcal{H}}_1(s)\right]\Big|_{\vartheta=1}, \tag{9.63}$$

and illustrated in Fig. 9.4(top). The dimensionless $f^{\varepsilon}_{\eta\pi}$ corresponds to the isoscalar amplitude $\mathcal{M}_0^{\eta\pi}$, while $f^{\vartheta}_{\eta\pi}$ belongs to the isotensor one, i.e., to $\mathcal{M}_2^{\eta\pi}$. The partial waves have a singular character at pseudothreshold, i.e., the upper limit in s of the physical region in the $\eta \to \pi^0\pi^+\pi^-$ decay, which is contained in the inhomogeneities describing left-hand-cut contributions to the respective partial wave. Note that the form factor, after performing the dispersion integral over the discontinuity as in Eq. (9.36), is perfectly regular at that point. Based on Eq. (9.63), we can calculate the corresponding *basis form factors*

$$F^{\nu}_{\eta\pi}(s) = F^{(1)}_{\eta\pi}(s)|_{f_{\eta\pi}=f^{\nu}_{\eta\pi}} \quad \text{with} \quad \nu \in \{\varepsilon, \vartheta\}, \tag{9.64}$$

which allow us to linearly decompose $F^{(1)}_{\eta\pi}$ according to

$$F^{(1)}_{\eta\pi}(s) = \varepsilon F^{\varepsilon}_{\eta\pi}(s) + \vartheta F^{\vartheta}_{\eta\pi}(s). \tag{9.65}$$

The $F^{\nu}_{\eta\pi}$ are pure predictions of our dispersive representation, independent of the subtraction constants. Our results for the basis solutions for the form factors are depicted in Fig. 9.4(bottom).

Let us have a look at the hierarchy of the two amplitudes contributing to $F^{(1)}_{\eta\pi}$. The plots in Fig. 9.4 show that the basis solutions for the isoscalar and isotensor contributions to the $\eta \to \pi^0\pi^+\pi^-$ P-wave amplitude are of the same order of magnitude, and so are, as a result, the corresponding basis form factors. But due to the vast difference in their normalizing subtraction constants, the term $\vartheta F^{\vartheta}_{\eta\pi}(s)$ is negligibly small in comparison to $\varepsilon F^{\varepsilon}_{\eta\pi}(s)$. The origin of this discrepancy is well understood [1, 62]. The totally antisymmetric combination of P-wave single-variable functions in the isoscalar amplitude $\mathcal{M}_0^{\eta\pi}$, cf. Eq. (9.47), leads to a strong kinematic suppression inside the Dalitz plot; for symmetry reasons alone, the amplitude is required to vanish along the three lines $s = t$, $t = u$, and $u = s$. As a result, the corresponding normalization ε is far less rigorously constrained from fits to experimental data [215] than the isotensor amplitude, which only vanishes for $t = u$. No such suppression occurs for the individual partial waves, or the transition form factors, be it in the ρ-resonance region or below, in the kinematic range relevant for the semi-leptonic decays studied here, where isoscalar and isotensor contributions show non-negligible, but moderate corrections to a ρ-dominance picture. We also remark that this subtle interplay demonstrates that the model-independent connection between Dalitz plots and transition form factors absolutely requires the use of dispersion-theoretical methods—a low-energy

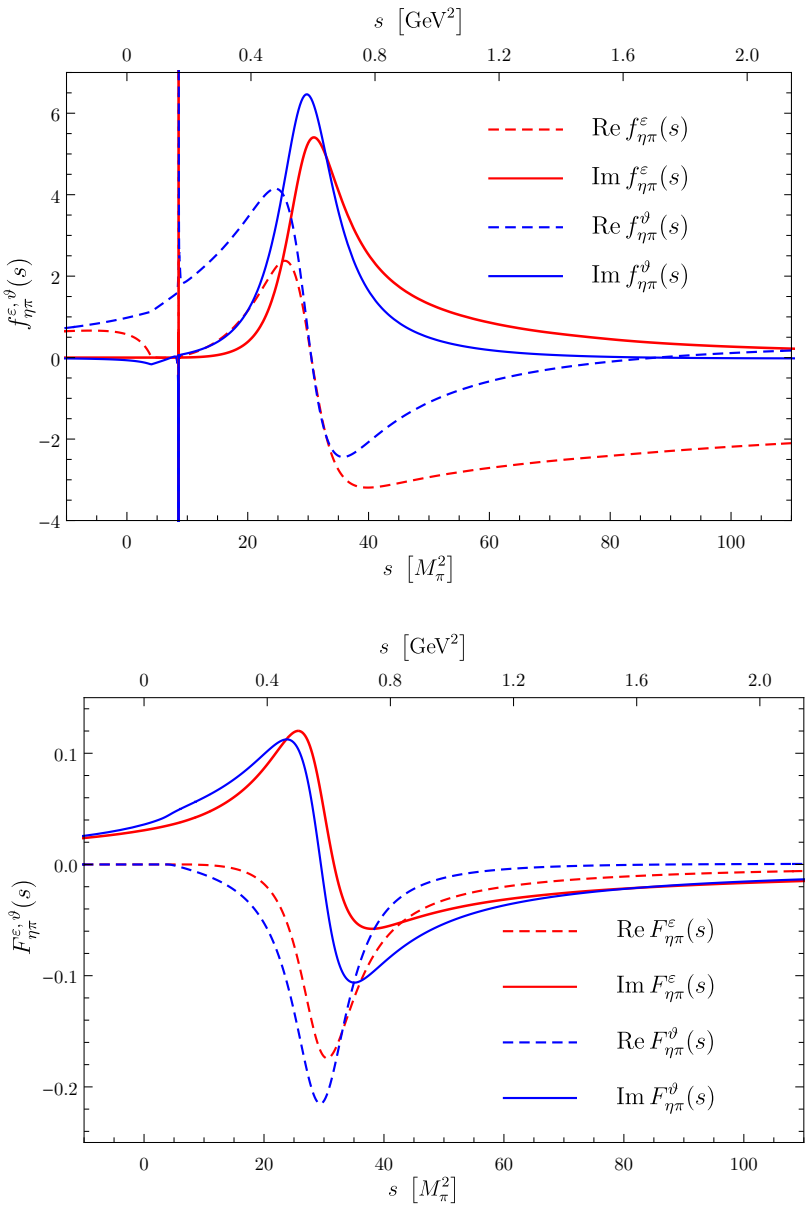

Figure 9.4: Basis solutions for the partial waves and form factors for the $\eta \to \pi^0$ transition. The partial-wave amplitudes $f^{\nu}_{\eta\pi}$ from Eq. (9.63) are depicted in the upper panel; the singularity at the pseudothreshold $s = (M_\eta - M_{\pi^0})^2$ is clearly visible. These serve as an input to calculate the basis solutions of the transition form factors $F^{\nu}_{\eta\pi}(s)$ as defined in Eq. (9.64) and shown in the lower panel.

effective theory such as chiral perturbation theory is insufficient for such extrapolations. For the numerical evaluation of $F^{(1)}_{\eta\pi}$ we only consider the by far dominant source of error, i.e., the uncertainty of the subtraction constants entering the partial wave. As their errors are of the same order of magnitude as their corresponding central values, it is a good approximation to neglect all other sources of uncertainties, such as the variation of phase-

shift input.

9.2.2.2 | $\eta' \to \eta\gamma^*$

We now turn the focus on the transition form factor $f_{\eta'\eta}$, whose basis solutions in terms of partial waves are defined as

$$f^{\varrho}_{\eta'\eta}(s) = \left[\mathcal{G}_{\pi\pi}(s) + \hat{\mathcal{G}}_{\pi\pi}(s)\right]\Big|_{\varrho=1,\,\zeta=0}\,, \qquad f^{\zeta}_{\eta'\eta}(s) = \left[\mathcal{G}_{\pi\pi}(s) + \hat{\mathcal{G}}_{\pi\pi}(s)\right]\Big|_{\varrho=0,\,\zeta=1}\,. \tag{9.66}$$

Using the $f^{\nu}_{\eta'\eta}$ we can define the basis from factors

$$F^{\nu}_{\eta'\eta}(s) = F^{(1)}_{\eta'\eta}(s)|_{f_{\eta'\eta}=f^{\nu}_{\eta'\eta}} \quad \text{with} \quad \nu \in \{\varrho,\zeta\}\,, \tag{9.67}$$

and finally obtain the complete isovector form factor in explicit dependence on the subtraction constants by means of

$$F^{(1)}_{\eta'\eta}(s) = \varrho F^{\varrho}_{\eta'\eta}(s) + \zeta F^{\zeta}_{\eta'\eta}(s)\,. \tag{9.68}$$

The basis solutions for both partial waves and transition form factors are shown in Fig. 9.5.

9.2.3 | Resonance couplings from analytic continuation

As both the partial waves $f_{XY}(s)$ and the resulting transition form factors $F^{(1)}_{XY}(s)$ have been constructed with the correct analytic properties, we can analytically continue them into the complex plane and onto the second Riemann sheet to extract resonance pole residues. The resonance in question is the $\rho(770)$; its residues can be interpreted as model-independent definitions of C-violating $\rho \to XY$ coupling constants. To this end, we recapitulate aspects of Refs. [347, 348]. First, consider the discontinuity of the transition form factor in Eq. (9.33) on the first Riemann sheet

$$F^{(1),\mathrm{I}}_{XY}(s+i\epsilon) - F^{(1),\mathrm{I}}_{XY}(s-i\epsilon) = \frac{i}{24\pi}\big(\sigma^{\pi}(s+i\epsilon)\big)^3\left(F^{V,\mathrm{I}}_{\pi}(s+i\epsilon)\right)^* f^{\mathrm{I}}_{XY}(s+i\epsilon), \tag{9.69}$$

with

$$\sigma^{\pi}(s) \equiv \sqrt{\frac{4M_\pi^2}{s} - 1}\,, \qquad \sigma^{\pi}(s \pm i\epsilon) = \mp i\,\sigma_{\pi}(s)\,. \tag{9.70}$$

Using that the pion vector form factor fulfills Schwarz' reflection principle and demanding continuity of the scattering amplitudes when moving from one Riemann sheet to another, i.e.,

$$F^{(1),\mathrm{I}}_{XY}(s-i\epsilon) = F^{(1),\mathrm{II}}_{XY}(s+i\epsilon) \quad \text{and} \quad F^{V,\mathrm{I}}_{\pi}(s-i\epsilon) = F^{V,\mathrm{II}}_{\pi}(s+i\epsilon), \tag{9.71}$$

we obtain

$$F^{(1),\mathrm{II}}_{XY}(s+i\epsilon) = F^{(1),\mathrm{I}}_{XY}(s+i\epsilon) - \frac{i}{24\pi}\big(\sigma^{\pi}(s+i\epsilon)\big)^3 F^{V,\mathrm{II}}_{\pi}(s+i\epsilon)\, f^{\mathrm{I}}_{XY}(s+i\epsilon)\,. \tag{9.72}$$

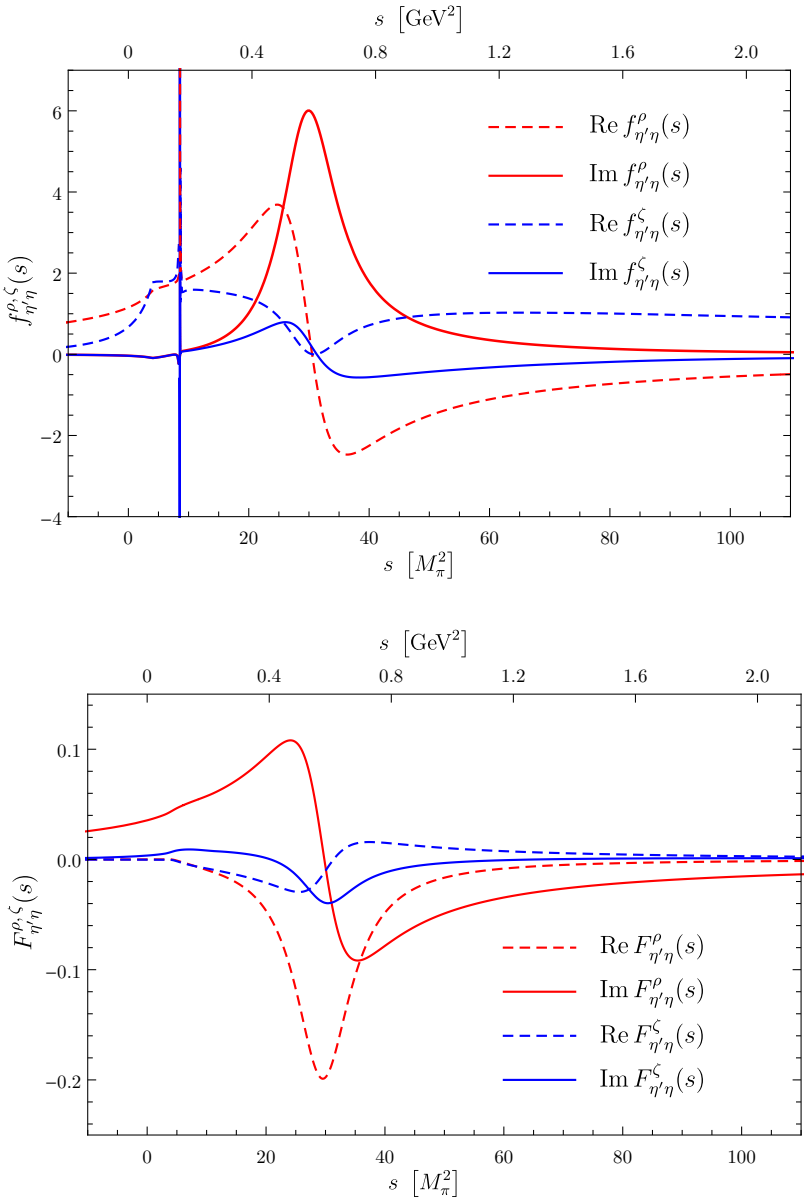

Figure 9.5: Basis solutions for the partial waves and form factors for the $\eta' \to \eta$ transition. The partial-wave amplitudes $f^{\nu}_{\eta'\eta}$ from Ref. [1] are depicted in the upper panel; again, the singularity at the pseudothreshold $s = (M_{\eta'} - M_\eta)^2$ can be seen. These serve as an input to calculate the basis solutions of the transition form factors $F^{\nu}_{\eta'\eta}(s)$ as defined in Eq. (9.67) and shown in the lower panel.

In the vicinity of the $\rho(770)$ pole, the transition form factors as well as the pion form factor on the second Riemann sheet behave as

$$F^{(1),\mathrm{II}}_{XY}(s)\,,\;\; F^{V,\mathrm{II}}_{\pi}(s) \propto \frac{1}{s_\rho - s} \quad \text{with} \quad s_\rho = \left(\tilde{M}_\rho - i\frac{\Gamma_\rho}{2}\right)^2 . \tag{9.73}$$

The pole position s_ρ has been determined most accurately in Ref. [349], using Roy-like equations for pion–pion scattering: $\tilde{M}_\rho = 763.7\,\text{MeV}$, $\Gamma_\rho = 146.4\,\text{MeV}$ (cf. also Ref. [298]); for later use, we also quote the coupling constant to $\pi\pi$, $|g_{\rho\pi\pi}| = 6.01$, $\arg(g_{\rho\pi\pi}) = -5.3°$. We neglect the uncertainties in these parameters, as they are small compared to the ones fixing the partial waves f_{XY}. While $F_\pi^{V,\text{II}}$ is explicitly given in Ref. [348], we can match $F_{XY}^{(1),\text{II}}$ to a VMD-type form factor similar to Eq. (9.44), but with $g_{\rho YX}$, $g_{\rho\gamma}$, and M_ρ^2 instead of $\tilde{g}$, $g_{v\gamma}$, and M_v^2. Thus, in sufficient vicinity to the pole, we can write

$$F_\pi^{V,\text{II}}(s) = \frac{g_{\rho\pi\pi}}{g_{\rho\gamma}}\frac{s_\rho}{s_\rho - s} \quad \text{and} \quad F_{XY}^{(1),\text{II}}(s) = \frac{g_{\rho YX}}{2g_{\rho\gamma}}\frac{M_\rho^2}{s_\rho - s}. \tag{9.74}$$

If we evaluate Eq. (9.72) near the pole s_ρ and insert Eq. (9.74), we can compute the desired C-odd ρ-meson couplings by

$$g_{\rho YX} = \frac{g_{\rho\pi\pi}}{12\pi}\frac{s_\rho}{M_\rho^2}\sigma_\pi^3(s_\rho)\, f_{XY}^{\text{I}}(s_\rho)\,. \tag{9.75}$$

The problem is therefore reduced to evaluating the partial wave f_{XY}^{I} on the first Riemann sheet at the pole position, a task for which the dispersive representations are perfectly suited. To clarify the dependence on subtractions or effective coupling constants and therefore separate the uncertainty in these from the precisely calculable dispersive aspects, we will once more make use of the decomposition in terms of basis functions.

We begin with the $\eta \to \pi^0$ transition form factor. The basis functions of the partial wave $f_{\eta\pi}$, evaluated at the ρ pole, result in

$$f_{\eta\pi}^{\varepsilon}(s_\rho) = -0.02 - 2.76i\,, \qquad f_{\eta\pi}^{\vartheta}(s_\rho) = 0.87 - 3.05i\,, \tag{9.76}$$

so that we obtain

$$f_{\eta\pi}(s_\rho) = \varepsilon f_{\eta\pi}^{\varepsilon}(s_\rho) + \vartheta f_{\eta\pi}^{\vartheta}(s_\rho) = \left[(-0.704 + i\,0.005)\,\text{GeV}^4\, g_0 - (1.149 + i\,0.330) g_2\right], \tag{9.77}$$

where we made use of Eq. (9.53). Employing of Eq. (9.75) and finally inserting the values for the coupling constants g_0 and g_2 as extracted from the $\eta \to \pi^0\pi^+\pi^-$ Dalitz-plot asymmetry then yields

$$\begin{aligned} g_{\rho\pi\eta} &= \left[(-0.087 + i\,0.021)\,\text{GeV}^4\, g_0 - (0.151 + i\,0.007)\, g_2\right] \\ &= \left[0.24(0.39) - i\,0.06(0.10)\right]\text{GeV}^{-2}\,. \end{aligned} \tag{9.78}$$

Note that the isotensor contribution g_2 is negligible in the coupling $g_{\rho\pi\eta}$.

The analytic continuation of the basis partial wave for $f_{\eta'\eta}$ to the pole position of the ρ meson yields

$$f_{\eta'\eta}^{\varrho}(s_\rho) = 0.44 - 2.95i\,, \qquad f_{\eta'\eta}^{\zeta}(s_\rho) = -0.45 - 0.17i\,. \tag{9.79}$$

With Eq. (9.61) we can hence express the analytically continued partial wave at the ρ pole

by

$$f_{\eta'\eta}(s_\rho) = \varrho f^{\varrho}_{\eta'\eta}(s_\rho) + \zeta f^{\zeta}_{\eta'\eta}(s_\rho) = g_1 \left[(0.12 - i\,0.34) + (1.63 + i\,0.48)\,\mathrm{GeV}^2\,\delta g_1\right] . \quad (9.80)$$

In terms of this result, the ρ-meson coupling from Eq. (9.75) results in

$$\begin{aligned} g_{\rho\eta\eta'} &= g_1 \left[(0.005 - i\,0.046) + (0.215 + i\,0.011)\,\mathrm{GeV}^2\,\delta g_1\right] \\ &= -\left[0.82(2.25) + i\,0.07(0.16)\right] \mathrm{GeV}^{-2} , \end{aligned} \quad (9.81)$$

where we considered correlated Gaussian errors for the couplings g_1 and δg_1.

Note that the coupling constants in Eq. (9.75) become inevitably complex-valued, thus spoiling the well-defined transformation under time reversal when compared to the tree-level coupling constants from ToPeχPT. This is neither surprising nor specific to the context of symmetry violation studied here: in the strong interactions, resonance couplings that are real in the narrow-width limit necessarily turn complex when defined model-independently via pole residues in the complex plane. However, this points towards the reason why these complex phases will be irrelevant when using symmetry arguments to estimate isoscalar contributions in the next section: for the narrow ω and ϕ resonances, they are negligible to far better accuracy; symmetry arguments within the vector-meson nonet are not applicable to their total widths. We will therefore simply omit the imaginary parts in the next section and relate the C-odd ω couplings required for the model of the isoscalar parts of the form factors to the real parts of the ρ coupling (of the same total isospin) only. Note furthermore that Eqs. (9.78) and (9.81) still suggest the imaginary parts of $g_{\rho\pi\eta}$ and $g_{\rho\eta\eta'}$ to be rather small, such that the difference between real part and modulus, e.g., is negligible for our purposes.

9.3 | Hadronic long-range effects: the isoscalar contribution

We now attempt to combine the findings of Sects. 9.1.4.2 and 9.2.3. We wish to access the couplings $\tilde{g}$, cf. Eq. (9.44), by linking them to the $g_{\rho YX}$ discussed in the last section. In Sect. 9.1.4.2 we found a ToPeχPT operator that, when considered separately, allows us—according to Eq. (9.41)—to relate these couplings by $SU(3)$ symmetry. The vector-meson couplings with the same total isospin are found to be related by $g_{\omega\pi\eta} = 1/\sqrt{3}\, g_{\rho\eta\eta'}$ and $g_{\omega\eta\eta'} = \sqrt{3}\, g_{\rho\pi\eta}$, while $g_{\phi\pi\eta} = 0$ and $g_{\phi\eta\eta'}$ does *not* correlate with respective ρ couplings. However, the predictive power of flavor symmetry arguments does not hold in general for all operators. This leads to the shortcoming that we cannot fix the relative sign of the couplings, which becomes evident when comparing Eqs. (9.40) and (9.41), and have to rely on NDA arguments to consider that there may be additional contributions to the couplings from linear combinations of Wilson coefficients, cf. Eq. (9.40). An alternative approach would be to use NDA right away and drop the relative factors of $1/\sqrt{3}$ and $\sqrt{3}$, respectively, but this still leads to the same caveats.

9.3.1 | $\eta \to \pi\ell^+\ell^-$

Possible contributions to the isoscalar form factor in $\eta \to \pi^0\ell^+\ell^-$ can originate from an ω or a ϕ intermediate state. In accordance with Sect. 9.1.4.2, these enter the form factor in the linear combination

$$F^{(0)}_{\eta\pi}(s) \equiv \frac{g_{\omega\pi\eta}}{2g_{\omega\gamma}}\frac{M_\omega^2}{M_\omega^2 - s} + \frac{g_{\phi\pi\eta}}{2g_{\phi\gamma}}\frac{M_\phi^2}{M_\phi^2 - s}\,. \tag{9.82}$$

With our $SU(3)$ estimate $g_{\phi\pi\eta} = 0$ we can ignore the contribution of the ϕ. Dropping the latter is also justified from an NDA point of view: the difference of the two summands in Eq. (9.82) is negligible compared to the uncertainty of NDA if $F^{(0)}_{\eta\pi}(s)$ is evaluated within the physical range. Therefore, we continue the estimation of the isoscalar contribution with the ω intermediate state only, for which we use $|g_{\omega\gamma}| = 16.7(2)$ [348].

Relating $g_{\omega\pi\eta}$ to the ρ coupling of the same total isospin $I = 1$ and omitting the imaginary part for the reasons given above, we find

$$g_{\omega\pi\eta} \approx \frac{1}{\sqrt{3}}\mathrm{Re}\, g_{\rho\eta\eta'} = -0.47(1.30)\,\mathrm{GeV}^{-2} \quad \text{or} \quad |g_{\omega\pi\eta}| \lesssim 1.8\,\mathrm{GeV}^{-2}\,. \tag{9.83}$$

Throughout this manuscript we do not account for the numerically intangible uncertainties from our $SU(3)$ estimates or NDA. As neither of the latter fixes the sign of $|g_{\omega\pi\eta}|$, we have to content ourselves with its absolute value. Note that retaining the imaginary part of $g_{\rho\eta\eta'}$ would have a negligible effect on the upper limit for $|g_{\omega\pi\eta}|$.

On the other hand, we can also place a bound on $|g_{\omega\pi\eta}|$ using the upper limit on the branching ratio of $\omega \to \eta\pi^0$ as determined by the Crystal Ball multiphoton spectrometer at the Mainz Microtron (MAMI) [350] and the Lagrangian in Eq. (9.38). The partial decay width is found to be

$$\Gamma(\omega \to \eta\pi^0) = \frac{1}{192\pi M_\omega}\,|g_{\omega\pi\eta}|^2\,\lambda^{3/2}\big(M_\omega^2, M_\eta^2, M_{\pi^0}^2\big)\,. \tag{9.84}$$

With $\mathrm{BR}(\omega \to \eta\pi^0) < 2.3 \cdot 10^{-4}$ [350] and $\Gamma_\omega = 8.68$ MeV [13], we obtain the bound

$$|g_{\omega\pi\eta}| < 0.24\,\mathrm{GeV}^{-2}\,, \tag{9.85}$$

which is significantly more restrictive than the theoretical estimate for the bound on the coupling inferred from $g_{\rho\eta\eta'}$.

9.3.2 | $\eta' \to \eta\ell^+\ell^-$

Similarly to the previous section, the isoscalar part of the form factor in $\eta' \to \eta\ell^+\ell^-$ can be written as

$$F^{(0)}_{\eta'\eta}(s) \equiv \frac{g_{\omega\eta\eta'}}{2g_{\omega\gamma}}\frac{M_\omega^2}{M_\omega^2 - s} + \frac{g_{\phi\eta\eta'}}{2g_{\phi\gamma}}\frac{M_\phi^2}{M_\phi^2 - s}\,. \tag{9.86}$$

With the same reasoning as above we henceforth drop the contribution of the ϕ and only take the ω into account. The numerical result for the corresponding vector meson coupling, which has total isospin $I = 0$, is

$$g_{\omega\eta\eta'} \approx \sqrt{3}\,\mathrm{Re}\,g_{\rho\pi\eta} = 0.42(0.68)\,\mathrm{GeV}^{-2} \quad \text{or} \quad |g_{\omega\eta\eta'}| \lesssim 1.1\,\mathrm{GeV}^{-2}\,. \tag{9.87}$$

Once more, the imaginary part of $g_{\rho\pi\eta}$ would yield just a minor contribution to the upper limit on $|g_{\omega\eta\eta'}|$ and can be neglected. We furthermore remark that the $\rho\pi\eta$ coupling also has an isotensor component, which, however, has a negligible effect, cf. Eq. (9.78).

9.4 | Results

With the theoretical apparatus at hand we are now able to predict upper limits on the decay widths

$$\Gamma(X \to Y\ell^+\ell^-) = \frac{\alpha^2}{8\pi M_X^3} \int_{4m_\ell^2}^{(M_X-M_Y)^2} \mathrm{d}s\, \lambda^{3/2}\big(s, M_X^2, M_Y^2\big)\, \sigma_\ell(s) \left(1 - \frac{\sigma_\ell^2(s)}{3}\right) |F_{XY}(s)|^2\,, \tag{9.88}$$

relying on the Dalitz-plot asymmetries in $X \to Y\pi^+\pi^-$ as the main input. As argued in Sect. 9.1.5, we focus on the long-range contributions via hadronic intermediate states only, i.e., we set

$$F_{XY}(s) = F_{XY}^{(1)}(s) + F_{XY}^{(0)}(s)\,. \tag{9.89}$$

We disregard the contributions analyzed in Sects. 9.1.2 and 9.1.3 according to the discussion in Sect. 9.1.5: these do not show interesting correlations with other ToPe processes, and absent significant cancellations, we can study the consequences of limit setting for the long-range hadronic effects alone. The corresponding transition form factors for the isovector and isoscalar contributions to $\eta \to \pi^0\gamma^*$ read

$$F_{\eta\pi}^{(1)}(s) = \varepsilon F_{\eta\pi}^{\varepsilon}(s) + \vartheta F_{\eta\pi}^{\vartheta}(s)\,, \qquad F_{\eta\pi}^{(0)}(s) = \frac{g_{\omega\pi\eta}}{2g_{\omega\gamma}} \frac{M_\omega^2}{M_\omega^2 - s}\,, \tag{9.90}$$

while the ones contributing to $\eta' \to \eta\gamma^*$ are

$$F_{\eta'\eta}^{(1)}(s) = \varrho F_{\eta'\eta}^{\varrho}(s) + \zeta F_{\eta'\eta}^{\zeta}(s)\,, \qquad F_{\eta'\eta}^{(0)}(s) = \frac{g_{\omega\eta\eta'}}{2g_{\omega\gamma}} \frac{M_\omega^2}{M_\omega^2 - s}\,. \tag{9.91}$$

The subtraction constants fixing the $F_{XY}^{(1)}$ are given in Eqs. (9.52) and (9.60), the respective basis solutions F_{XY}^{ν} are depicted in Figs. 9.4 and 9.5, and the coupling constants $g_{\omega YX}$ entering the $F_{XY}^{(0)}$ are quoted in Eqs. (9.85) and (9.87), respectively.
We have pointed out above that we have no means to assess the relative sign of the isoscalar contribution. To determine theoretical upper bounds, we therefore employ

$$|F_{\eta\pi}|^2 \leq |F_{\eta\pi}^{(0)}|^2 + |F_{\eta\pi}^{(1)}|^2 + 2\,|F_{\eta\pi}^{(0)}|\,|F_{\eta\pi}^{(1)}| \tag{9.92}$$

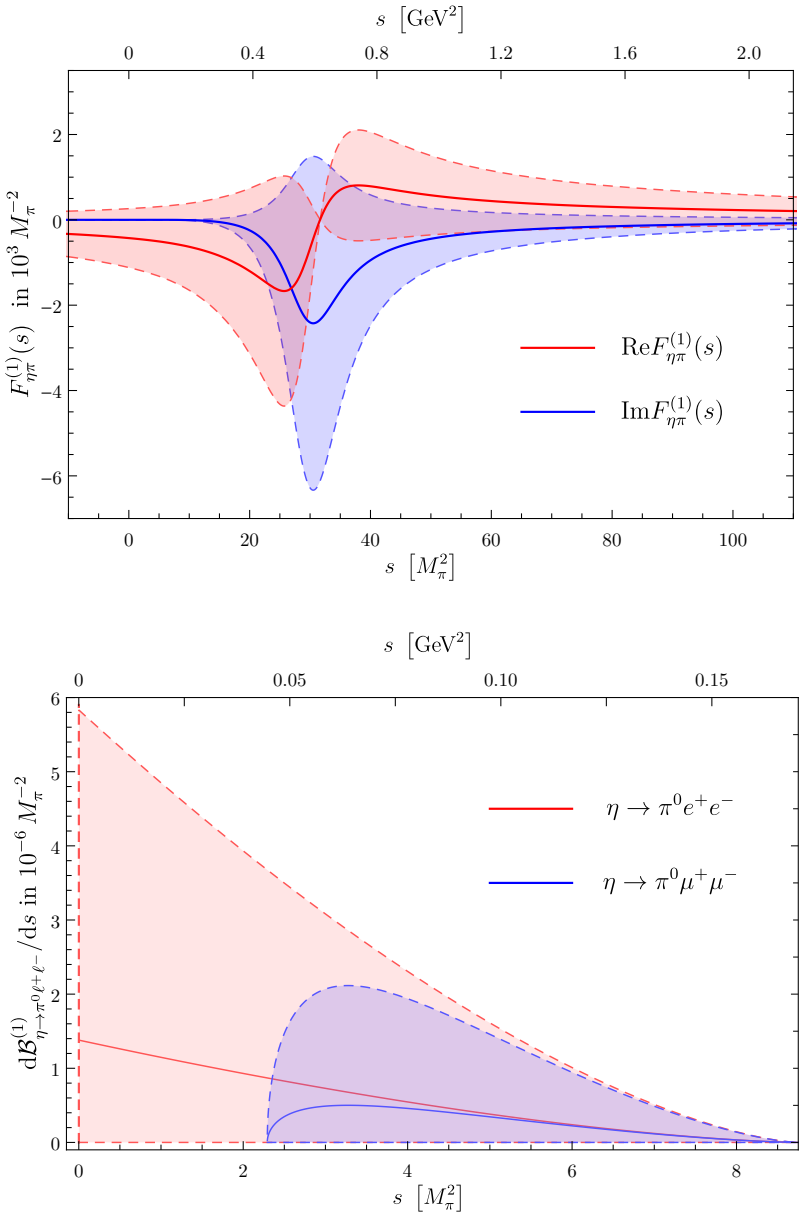

Figure 9.6: Spectrum of the isovector contribution to the form factor (top) and the corresponding differential decay distribution (bottom) for $\eta \to \pi^0\ell^+\ell^-$. The dashed lines mark the respective upper and lower limits stemming from the uncertainties of the subtraction constants in Eq. (9.52). The physical ranges are in both cases restricted by $4m_\ell^2 \leq s \leq (M_\eta - M_\pi)^2$.

and similarly for $F_{\eta'\eta}$, which possibly overestimates the interference term.

9.4.1 | $\eta \to \pi\ell^+\ell^-$

We depict the isovector contributions to the respective form factors and differential decay widths for the decay $\eta \to \pi\ell^+\ell^-$ in Fig. 9.6. Integrating the region enclosed by the error bands of the differential decay distribution, we obtain the limits

$$\begin{aligned}
&\mathcal{B}^{(1)}_{\eta\to\pi^0 e^+e^-} < 20\cdot 10^{-6}, \qquad \mathcal{B}_{\eta\to\pi^0 e^+e^-} < 29\cdot 10^{-6}, \qquad \mathcal{B}^{\text{exp}}_{\eta\to\pi^0 e^+e^-} < 7.5\cdot 10^{-6}\,,\\
&\mathcal{B}^{(1)}_{\eta\to\pi^0 \mu^+\mu^-} < 7.2\cdot 10^{-6}, \qquad \mathcal{B}_{\eta\to\pi^0 \mu^+\mu^-} < 10\cdot 10^{-6}, \qquad \mathcal{B}^{\text{exp}}_{\eta\to\pi^0 \mu^+\mu^-} < 5\cdot 10^{-6}\,,
\end{aligned} \tag{9.93}$$

where the first entry in each line corresponds to the isovector contribution and the second includes the isoscalar one in addition. Finally, the experimental results [203, 205], to be understood at 90% C.L., are quoted last, which are of similar order of magnitude as our findings. This observation shows that the considered experiments for $\eta \to \pi^0\pi^+\pi^-$ and $\eta \to \pi^0\ell^+\ell^-$ have a very similar sensitivity for ToPe forces, despite the fact that asymmetries in the former are based on C-odd interferences and therefore scale *linearly* with a (small) BSM coupling [2, 62], while the latter is a rate that is suppressed to second order in a similar coupling. Comparing $\mathcal{B}^{(1)}_{\eta\to\pi^0\ell^+\ell^-}$ to $\mathcal{B}_{\eta\to\pi^0\ell^+\ell^-}$, our analysis suggests that the isoscalar form factor contributes roughly one third to the overall branching ratio, however again with the caveat of the imprecise NDA normalization of $F^{(0)}_{\eta\pi}$.

As the experimental limits turn out to be more restrictive than our theoretical predictions for $\mathcal{B}^{(1)}_{\eta\to\pi^0\ell^+\ell^-}$, the $\eta \to \pi^0\ell^+\ell^-$ decay widths [203, 205] can be used to refine the fit to the $\eta \to \pi^0\pi^+\pi^-$ Dalitz plot [215]. As long as the latter constrains the corresponding BSM couplings in a way that the form factor is dominated by the contribution of g_0, an improved regression to the full Dalitz plot is redundant. Instead we note that isoscalar (g_0) and isotensor (g_2) couplings in $\eta \to \pi^0\pi^+\pi^-$ are nearly uncorrelated [1] and turn the experimental limit for $\mathcal{B}^{(1)}_{\eta\to\pi^0 e^+e^-}$ into the upper bound

$$|g_0| < 4.4\,\text{GeV}^{-6}, \tag{9.94}$$

to be compared to the previous constraint $g_0 = -2.8(4.5)\,\text{GeV}^{-6}$ [1].

9.4.2 | $\eta' \to \eta\ell^+\ell^-$

Proceeding in analogy to Sect. 9.4.1, we obtain the following upper limits on the decays $\eta' \to \eta\ell^+\ell^-$ (the experimental ones [204, 205] again to be understood at 90% C.L.):[6]

$$\begin{aligned}
&\mathcal{B}^{(1)}_{\eta'\to\eta e^+e^-} < 4.1\cdot 10^{-6}, \qquad \mathcal{B}_{\eta'\to\eta e^+e^-} < 9.0\cdot 10^{-6}, \qquad \mathcal{B}^{\text{exp}}_{\eta'\to\eta e^+e^-} < 2.4\cdot 10^{-3}\,,\\
&\mathcal{B}^{(1)}_{\eta'\to\eta\mu^+\mu^-} < 1.6\cdot 10^{-6}, \qquad \mathcal{B}_{\eta'\to\eta\mu^+\mu^-} < 3.8\cdot 10^{-6}, \qquad \mathcal{B}^{\text{exp}}_{\eta'\to\eta\mu^+\mu^-} < 15\cdot 10^{-6}\,.
\end{aligned} \tag{9.95}$$

A depiction of the isovector contribution to the form factor and differential decay width is given in Fig. 9.7. For these decays, our approximation for the isoscalar form factor loosens

[6] For these branching ratios we use the total width $\Gamma_{\eta'} = 0.23\,\text{MeV}$ listed as *PDG average* in Ref. [13].

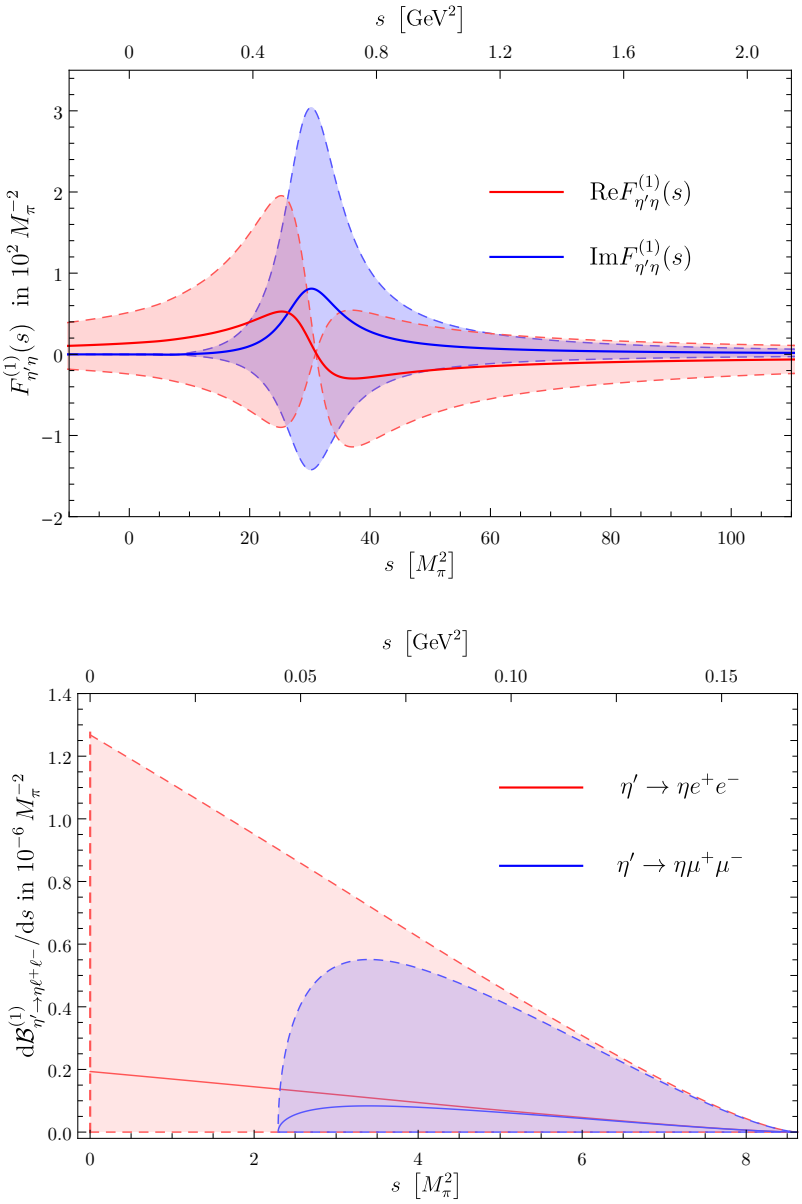

Figure 9.7: Spectrum of the isovector contribution to the form factor (top) and the corresponding differential decay distribution (bottom) for $\eta' \to \eta\ell^+\ell^-$. The dashed lines mark the respective upper and lower limits stemming from the uncertainties of the subtraction constants in Eq. (9.60). The physical ranges are in both cases restricted by $4m_\ell^2 \leq s \leq (M_{\eta'} - M_\eta)^2$.

the limit on the isovector contribution alone by roughly a factor of 2. In contrast to the findings for $\mathcal{B}_{\eta\to\pi^0\ell^+\ell^-}$, our limits on $\mathcal{B}_{\eta'\to\eta\ell^+\ell^-}$ are more restrictive than the respective experimental ones.

9.5 | Summary and outlook

In this work, we have studied the C- and CP-violating decays $\eta \to \pi^0\ell^+\ell^-$ and $\eta' \to \eta\ell^+\ell^-$, which can—from a phenomenological point of view—be driven by three different mechanisms. The first two of these are short-distance contributions induced by semi-leptonic four-point vertices and long-distance contributions caused by C- and CP-odd photon–hadron couplings. The only statements we can make about them is that they contribute as constants to respective transition form factors at leading order in ToPeχPT [2], that they cannot be distinguished by a sole measurement of the semi-leptonic decay widths, and that NDA estimates them to be of the same order of magnitude.

In contrast, the third mechanism, i.e., long-distance contributions induced by hadronic intermediate states, is conceptually more insightful. To access these contributions we have established dispersion relations for the isovector contribution to the transition form factors $\eta(\to \pi^0\pi^+\pi^-) \to \pi^0\gamma^*$ and $\eta'(\to \eta\pi^+\pi^-) \to \eta\gamma^*$. By construction, these form factors meet the fundamental requirements of analyticity and unitarity, solely relying on the dominant hadronic contribution of the P-waves in the C- and CP-odd $\eta \to \pi^0\pi^+\pi^-$ and $\eta' \to \eta\pi^+\pi^-$ amplitudes, which have been worked out in Ref. [1]. The non-perturbative predictions thereby obtained allow us to directly investigate the correlation between C-violating signals in different decays in a model-independent manner. By an analytic continuation of the C-odd $\eta \to \pi^0\pi^+\pi^-$ and $\eta' \to \eta\pi^+\pi^-$ P-wave amplitudes to the second Riemann sheet, we have extracted C-odd ρ-meson couplings to $\eta\pi^0$ and $\eta'\eta$. Furthermore, the latter can be related by total isospin and NDA to coupling constants entering the isoscalar contribution in a VMD model for $\eta' \to \eta\omega \to \eta\gamma^*$ and $\eta \to \pi^0\omega \to \pi^0\gamma^*$, respectively.

Accounting for these hadronic long-range effects only, we have predicted the corresponding upper limits on the semi-leptonic decay widths, relying on ToPe forces in the respective purely hadronic three-body decays as input. We observed that the currently most precise measurements of $\eta \to \pi^0\ell^+\ell^-$ and $\eta' \to \eta\ell^+\ell^-$ have a similar sensitivity to ToPe interactions as the measured Dalitz-plot asymmetries in $\eta \to \pi^0\pi^+\pi^-$ and $\eta' \to \eta\pi^+\pi^-$, despite their different scaling with small BSM couplings. As we found the experimental limits for $\eta \to \pi^0\ell^+\ell^-$ to be more restrictive than our theoretically predicted ones, we were able to use the respective transition form factor as a constraint to sharpen the bounds on C violation in $\eta \to \pi^0\pi^+\pi^-$.

Further perspectives on the decays $\eta \to \pi^0\ell^+\ell^-$ and $\eta' \to \eta\ell^+\ell^-$ could be opened by possible future measurements of the respective Dalitz-plot distributions. This would allow us to investigate actual C- and CP-odd observables, the Dalitz-plot asymmetries arising from the interference with the respective SM contributions. Such interference effects would, as the asymmetries in the hadronic η and η' decays, scale linearly with BSM couplings, however with likely less advantage in sensitivity due to the strongly suppressed SM amplitudes. Still, due to synergy effects with other BSM searches in these decays, such as for weakly coupled light scalars [34], renewed experimental efforts are strongly encouraged.

Epilogue

Chapter 10

Summary, conclusion, and outlook

This thesis is devoted to a model-independent parameterization of a simultaneous violation of C and CP in light-meson decays, which has hitherto been largely excluded from theoretical considerations. The decays of the η and η' mesons provide an ideal stage for this endeavour: not only due to their strongly reduced Standard Model background, but more importantly as they allow us to investigate C and CP violation in the absence of the weak interaction, so that corresponding signals are direct implications for BSM physics. Assuming that the Standard Model is an effective low-energy approximation of a yet unknown, more fundamental theory and that C- and CP-violating forces enter above some high-energy scale Λ, we investigated new interactions among the verified degrees of freedom of the SM in the spirit of effective field theories and dispersion theory.

In this sense, we first worked out a complete set of fundamental C- and CP-odd quark-level operators in LEFT up to and including mass dimension 8 that can give rise to neutrinoless flavor-conserving transitions respecting lepton- and baryon-number conservation. We found that these operators appear as chirality-conserving ones at dimension 7 or as chirality-violating ones at dimension 8 in LEFT, which scale as $1/\Lambda^4$ and v/Λ^4, respectively, and can numerically be of the same order of magnitude. A translation of these operators into (large-N_c) χPT shows that the ToPe forces in our analysis of over 20 η and η' decays, which exhibit clear hierarchies in the chiral power counting, are mostly uncorrelated. With SMEFT as the UV completion of LEFT, we applied naive dimensional analysis to estimate respective observables in explicit dependence on Λ. We found that current experiments merely restrict Λ to the few GeV range and that a more realistic scenario of $\Lambda \gtrsim 1\,\text{TeV}$ requires future experiments to be at least a factor of roughly 10^7 more restrictive regarding corresponding C- and CP-odd observables.

Among the investigated decays, the hadronic three-body decays $\eta^{(\prime)} \to \pi^+\pi^-\pi^0$ and $\eta' \to \eta\pi^+\pi^-$ provide the best prospects to find indications for C and CP violation. The dispersive Khuri–Treiman framework allowed us to fix the C- and CP-violating isoscalar and isotensor transitions in $\eta^{(\prime)} \to \pi^+\pi^-\pi^0$ by just one real-valued degree of freedom each and the isovector one in $\eta' \to \eta\pi^+\pi^-$ by two. Moreover, we matched the parameters of each of these transitions with definite isospin to a leading-order coupling constant in ToPeχPT. Studying the respective Dalitz-plot asymmetries, which arise from the interference of SM and BSM contributions only in presence of strong rescattering phases, we found that the currently most precise measurements restrict C and CP violation in the decays at hand to the relative per mille level and that these signals are consistent with zero within at most 2σ. To further study the correlation between different ToPe signals, we used the C- and CP-odd P-waves of $\eta \to \pi^+\pi^-\pi^0$ and $\eta' \to \eta\pi^+\pi^-$ to establish dispersion relations for the

transition form factors $\eta \to \pi^0\gamma^*$ and $\eta' \to \eta\gamma^*$. This allowed us to predict hadronic long-range contributions to the decays $\eta \to \pi^0\ell^+\ell^-$ and $\eta' \to \eta\ell^+\ell^-$. We observed that the most recent measurements of branching ratios of these semi-leptonic decays share a similar sensitivity to ToPe forces as the ones for the aforementioned hadronic Dalitz-plots, despite their different scaling in Λ, and were able to sharpen the bounds on the C- and CP-odd isoscalar coupling in $\eta \to \pi^+\pi^-\pi^0$.

As this thesis opens a new and innovative window to a model-independent and systematic approach on the parameterization of C and CP violation in light-meson decays, one could consider the following extensions in future analyses.

- On the one hand, one could analyze remaining decays that have not been considered in this thesis, as $\eta^{(\prime)} \to \ell^+\ell^-\gamma$ or $\eta^{(\prime)} \to \pi^+\pi^-\ell^+\ell^-$, cf. Ref. [351], or adapt the considerations made for η mesons to heavy quark physics.

- The investigation of flavor-changing processes may yield more promising limits for future measurements, as the underlying LEFT operators can already appear at dimension 6 and thus coming with a suppression of $1/\Lambda^2$. However, it is not clear which observables would be most appropriate for testing these operators, especially when considering non-negligible C- *or* CP-violating contributions from the weak interaction that complicate the identification of corresponding symmetry violations as clear BSM signals.

- Furthermore, we suggest to reconsider the limits on the BSM scale Λ, which are set indirectly by EDM analyses of elementary fermions like in Ref. [112], who assumed a suppression of the dimension-7 LEFT operators by $1/\Lambda^3$. However, we have shown that—with SMEFT as the UV completion of LEFT—the suppression of these operators is rather given as v/Λ^4. Consequently, the limits of Ref. [112] reduce to roughly $\Lambda \gtrsim 10\,\text{TeV}$, yielding a more promising scale for prospective measurements. This follows even regardless of the fact that operators at dimension-8 LEFT, or flavor-violating ones at dimension-6 LEFT, were not considered at all in the cited references.

- We have found that the direct limits on ToPe forces in the light-meson sector from current experiments, which are roughly three orders of magnitude less restrictive than the indirect limits on Λ via elementary fermion EDMs, are not as rigorous as initially believed. Therefore, it remains the question whether direct constraints on ToPe forces from the nucleon sector are indeed less rigorous than the ones from light-meson physics, as assumed by Ref. [34] and references therein. For this purpose, we recommend an analysis of nucleon interactions in the spirit of ToPeχPT. Embedding these results in loops with a Z^0-exchange additionally allows us to extract corresponding indirect limits from nucleon EDMs.

- Once suitable decays in these different sectors are identified, more accurate dispersion-theoretical analyses as thoroughly described in this thesis may follow.

- On the experimental side, new measurements, for instance taken by the REDTOP [38–40] and JEF [41–43] collaborations, can provide important insights into comprehending the origin of a possible simultaneous violation of C and CP. One implication of such measurements could be, besides new hypothetical light degrees of freedom, that there is another yet unknown mechanism that circumvents the SMEFT and/or LEFT power counting, so that our results from ToPeχPT have to be adapted accordingly.

But in all these extensions it needs to be emphasized that—although we have provided a systematic approach to describe ToPe forces in the low-energy range and to access the high-energy scale Λ—it still remains unclear how a corresponding BSM theory at the quark-level above the scale Λ explicitly looks like. This underlines the importance of connecting the high-precision and high-energy frontiers of physics in future works.

Appendices

Appendix A

Kinematics

This appendix serves as an overview of kinematic relations used throughout this work. We focus on generic three- and four-point functions in Sects. A.1 and A.2, respectively, and especially derive the corresponding decay rates

$$\mathrm{d}\Gamma = \frac{S}{2M}\,\mathrm{d}\Pi_{\mathrm{LIPS}} \sum_{\mathrm{pol.}} |\mathcal{M}|^2\,, \tag{A.1}$$

with the Lorentz -invariant phase space defined via

$$\mathrm{d}\Pi_{\mathrm{LIPS}} = (2\pi)^4\delta^4\left(P - \sum_i p_i\right) \prod_i \frac{\mathrm{d}^3 p_i}{(2\pi)^3 2E_i}\,. \tag{A.2}$$

In these equations, M indicates the mass of the decaying particle, the p_i are the outgoing momenta, S is a symmetry factor accounting for identical particles in the final state, and $\sum_{\mathrm{pol.}}$ is meant to average over initial particle polarizations and sum over outgoing ones. For simplicity we consider purely scalar processes of distinct particles, so that we can set $S = 1$ and drop the polarization sum. More information about relativistic kinematics of particle interactions can for instance be found in Refs. [13, 352, 353].

A.1 | Three-point functions

In this section we consider a generic two-body decay. In the center-of-mass system (cms) we denote the four-momenta by

$$P = \begin{pmatrix} M \\ \mathbf{0} \end{pmatrix}\,, \qquad p_1 = \begin{pmatrix} E_1 \\ \boldsymbol{p}_1 \end{pmatrix}\,, \qquad p_2 = \begin{pmatrix} E_2 \\ \boldsymbol{p}_2 \end{pmatrix}\,, \tag{A.3}$$

with P belonging to the decaying particle and $p_{1,2}$ to the two particles in the final state. While three-momentum conservation demands $\boldsymbol{p}_1 = -\boldsymbol{p}_2 \equiv \boldsymbol{p}$, energy conservation predicts

$$M = E_1 + E_2 = \sqrt{m_1^2 + |\boldsymbol{p}|^2} + \sqrt{m_2^2 + |\boldsymbol{p}|^2}\,. \tag{A.4}$$

In the second step we applied the relativistic energy-momentum relation. The respective solution of this equation for $|\boldsymbol{p}|$, E_1, and E_2 can be written as

$$|\boldsymbol{p}| = \frac{\lambda^{1/2}(M^2, m_1^2, m_2^2)}{2M}\,, \qquad E_1 = \frac{M^2 + m_1^2 - m_2^2}{2M}\,, \qquad E_2 = \frac{M^2 - m_1^2 + m_2^2}{2M}\,, \tag{A.5}$$

where we introduced the Källén function

$$\lambda(x,y,z) = x^2 + y^2 + z^2 - 2(xy + xz + yz)\,. \tag{A.6}$$

A.1.1 | Phase space

With the notations from above we evaluate the Lorentz -invariant phase space for a two-body decay in the cms by

$$\begin{aligned}\int \mathrm{d}\Pi_{\mathrm{LIPS}} &= \int \frac{\mathrm{d}^3p_1}{(2\pi)^3 2E_1}\frac{\mathrm{d}^3p_2}{(2\pi)^3 2E_2}(2\pi)^4\delta^3\Big(\sum_{i=1}^{2}\boldsymbol{p}_i\Big)\delta\Big(M - \sum_{i=1}^{2}E_i\Big) \\ &= \frac{1}{4(2\pi)^2}\int \mathrm{d}|\boldsymbol{p}|\mathrm{d}\Omega_p \frac{|\boldsymbol{p}|^2}{E_1E_2}\,\delta\big(M - E_1 - E_2\big)\,.\end{aligned} \tag{A.7}$$

The remaining delta distribution can be reformulated using

$$\delta(f(x)) = \sum_{i=1}^{n}\frac{\delta(x-x_i)}{|f'(x_i)|}\,, \tag{A.8}$$

with x_i as zeros of $f(x)$, so that

$$\delta\big(M - E_1 - E_2\big) = \frac{E_1E_2}{M|\boldsymbol{p}|}\delta\Big(|\boldsymbol{p}| - \frac{\lambda^{1/2}(M^2,m_1^2,m_2^2)}{2M}\Big)\,. \tag{A.9}$$

After the momentum integration we hence obtain the decay width

$$\Gamma = \frac{1}{32\pi^2}\frac{|\boldsymbol{p}|}{M^2}\int \mathrm{d}\Omega_p|\mathcal{M}|^2\,. \tag{A.10}$$

Note that the two-body decay amplitude $\mathcal{M}$ can always be expressed in terms of just one independent variable, so that one of the angular integrals encoded in the solid angle $\mathrm{d}\Omega_p = \mathrm{d}\phi_p\mathrm{d}\theta_p$ can always be carried out trivially.

A.2 | Four-point functions

We now focus on the kinematics of four-point functions for spinless particles, which include in general $2 \to 2$ scattering and $1 \to 3$ decay processes. We will start our discussion with the scattering process and apply crossing symmetry to relate the kinematics to the three-body decay. Some of the following considerations are closely related to Refs. [82, 88].

From a kinematic point of view, processes involving four particles have in general 16 degrees of freedom (dof), i.e., one Minkowski-four-vector for each particle. However, not all of them are independent. Upon imposing four-momentum conservation (4 dof), using the relativistic energy-momentum relation with known masses of each particle (4 dof), choosing a coordinate axis for the three-dimensional euclidean space (3 dof), and finally going to a

suitable frame like the cms (3 dof), one can describe the whole kinematics by just two independent variables.

For a process of the type $p_1 + p_2 = p_3 + p_4$ we conveniently introduce the Lorentz-covariant Mandelstam variables

$$\begin{aligned} s &= (p_1 + p_2)^2 = (p_3 + p_4)^2 \,, \\ t &= (p_1 - p_3)^2 = (p_2 - p_4)^2 \,, \\ u &= (p_1 - p_4)^2 = (p_2 - p_3)^2 \,. \end{aligned} \tag{A.11}$$

Regarding that energy-momentum conservation demands

$$s + t + u = \sum_{i=1}^{4} m_i^2 \equiv 3r \,, \tag{A.12}$$

we can choose any two of the Mandelstam variables as the kinematic degrees of freedom, in agreement with the consideration made above. The momenta in the s-channel cms, for which $\boldsymbol{p}_1 + \boldsymbol{p}_2 = 0 = \boldsymbol{p}_3 + \boldsymbol{p}_4$ holds, are given by

$$|\boldsymbol{p}_{1,2}| = \frac{\lambda^{1/2}(s, m_1^2, m_2^2)}{2\sqrt{s}} \,, \qquad |\boldsymbol{p}_{3,4}| = \frac{\lambda^{1/2}(s, m_3^2, m_4^2)}{2\sqrt{s}} \,, \tag{A.13}$$

while the corresponding energies are

$$E_1 = \frac{s + m_1^2 - m_2^2}{2\sqrt{s}} \,, \quad E_2 = \frac{s - m_1^2 + m_2^2}{2\sqrt{s}} \,, \quad E_3 = \frac{s + m_3^2 - m_4^2}{2\sqrt{s}} \,, \quad E_4 = \frac{s - m_1^2 - m_4^2}{2\sqrt{s}} \,. \tag{A.14}$$

Depending on the explicit form of the amplitude, it may be convenient to express the Mandelstam variables in terms of $z_{s,t,u} \equiv \cos\theta_{s,t,u}$, i.e., the cosine of scattering angle in the s, t or u cms, or vice versa. We start with the s-channel cms. The corresponding cosine of the scattering angle θ_s spanned by $\boldsymbol{p}_1$ and $\boldsymbol{p}_3$ is

$$z_s = \frac{s(t-u) + \Delta_s}{\lambda^{1/2}(s, m_1^2, m_2^2)\lambda^{1/2}(s, m_3^2, m_4^2)} \equiv \frac{(t-u) + \Delta_s/s}{\kappa_s(s)} \,, \tag{A.15}$$

with $\Delta_s \equiv (m_1^2 - m_2^2)(m_3^2 - m_4^2)$, and can be derived from

$$\begin{aligned} t &= \frac{1}{2}\left(3r - s - \frac{\Delta_s}{s} + \kappa_s(s)\, z_s\right) , \\ u &= \frac{1}{2}\left(3r - s + \frac{\Delta_s}{s} - \kappa_s(s)\, z_s\right) . \end{aligned} \tag{A.16}$$

Applying crossing symmetry, i.e., exchanging $p_2 \leftrightarrow -p_3$, the scattering angle in the t-channel cms and variabels s and u are described by

$$\begin{aligned} z_t &= \frac{t(u-s)-\Delta_t}{\lambda^{1/2}(t,m_1^2,m_3^2)\lambda^{1/2}(t,m_2^2,m_4^2)} \equiv \frac{(u-s)-\Delta_t/t}{\kappa_t(t)}\,, \\ u &= \frac{1}{2}\left(3r - t + \frac{\Delta_t}{t} + \kappa_t(t)\, z_t\right), \\ s &= \frac{1}{2}\left(3r - t - \frac{\Delta_t}{t} - \kappa_t(t)\, z_t\right), \end{aligned} \tag{A.17}$$

where $\Delta_t \equiv (m_1^2 - m_3^2)(m_2^2 - m_4^2)$. Similarly, the interchange $p_2 \leftrightarrow -p_4$ yields

$$\begin{aligned} z_u &= \frac{u(s-t)+\Delta_u}{\lambda^{1/2}(u,m_1^2,m_4^2)\lambda^{1/2}(u,m_2^2,m_3^2)} \equiv \frac{(s-t)+\Delta_u/u}{\kappa_u(u)}\,, \\ s &= \frac{1}{2}\left(3r - u - \frac{\Delta_u}{u} + \kappa_u(u)\, z_u\right), \\ t &= \frac{1}{2}\left(3r - u + \frac{\Delta_u}{u} - \kappa_u(u)\, z_u\right), \end{aligned} \tag{A.18}$$

where $\Delta_u \equiv (m_1^2 - m_4^2)(m_2^2 - m_3^2)$. The kinematic limits on the scattering angles read

$$-1 \leq z_{s,t,u} \leq 1\,, \tag{A.19}$$

while the Mandelstam variables are bounded from below in their respective scattering channel by

$$\begin{aligned} s &\geq \max\left((m_1+m_2)^2, (m_3+m_4)^2\right), \\ t &\geq \max\left((m_1+m_3)^2, (m_2+m_4)^2\right), \\ u &\geq \max\left((m_1+m_4)^2, (m_2+m_3)^2\right). \end{aligned} \tag{A.20}$$

A.2.1 | Phase space

We now move to the scenario of a three-body decay and consider a process with momentum assignment $p_1 = p_2 + p_3 + p_4$, where $m_1 > m_2 + m_3 + m_4$ with the aim to derive a formula for the corresponding phase-space integral. According to crossing symmetry, this case is related to our previous considerations by the shift $p_2 \to -p_2$ in Eq. (A.11), meaning that

$$\begin{aligned} s &= (p_1 - p_2)^2 = (p_3 + p_4)^2\,, \\ t &= (p_1 - p_3)^2 = (p_2 + p_4)^2\,, \\ u &= (p_1 - p_4)^2 = (p_2 + p_3)^2\,. \end{aligned} \tag{A.21}$$

We can now restrict s by the mass of the decaying particle, i.e.,

$$(m_3 + m_4)^2 \leq s \leq (m_1 - m_2)^2\,, \tag{A.22}$$

and fix the upper and lower limits of t, denoted by t_+ and t_-, with [353]

$$t_\pm(s) = m_2^2+m_3^2+\frac{1}{2s}\left(\left(m_1^2-m_2^2-s\right)\left(m_3^2-m_4^2+s\right)\pm\lambda^{1/2}\left(s,m_1^2,m_2^2\right)\lambda^{1/2}\left(s,m_3^2,m_4^2\right)\right). \tag{A.23}$$

The phase-space integral of a generic three-body decay in the rest frame of the inital state is given by

$$\int \mathrm{d}\Pi_{\mathrm{LIPS}} = \int \frac{\mathrm{d}^3p_2}{(2\pi)^3 2E_2}\frac{\mathrm{d}^3p_3}{(2\pi)^3 2E_3}\frac{\mathrm{d}^3p_4}{(2\pi)^3 2E_4}(2\pi)^4\delta^3\Big(\sum_{i=2}^{4}\boldsymbol{p}_i\Big)\delta\Big(m_1-\sum_{i=2}^{4}E_i\Big). \tag{A.24}$$

Integrating over d^3p_4 one can eliminate the first delta distribution and set $\boldsymbol{p}_4=-(\boldsymbol{p}_3+\boldsymbol{p}_2)$ and thus $E_4=\sqrt{m_4^2+\boldsymbol{p}_3^2+\boldsymbol{p}_2^2+2|\boldsymbol{p}_2||\boldsymbol{p}_3|z_s}$, where z_s is the cosine of the angle between $\boldsymbol{p}_2$ and $\boldsymbol{p}_3$. With this, the phase space simplifies to

$$\int \mathrm{d}\Pi_{\mathrm{LIPS}} = 2\pi\int \frac{\mathrm{d}|\boldsymbol{p}_2|\;\boldsymbol{p}_2^2}{(2\pi)^3 2E_2}\frac{\mathrm{d}|\boldsymbol{p}_3|\;\boldsymbol{p}_3^2}{(2\pi)^3 2E_3}\,\mathrm{d}\Omega_2\,\mathrm{d}\Omega_3\frac{1}{2E_4}\delta\Big(m_1-\sum_{i=2}^{4}E_i\Big) \tag{A.25}$$

and the remaining delta distribution becomes

$$\begin{aligned}\delta\Big(m_1-\sum_{i=2}^{4}E_i\Big) &= \delta\left(m_1-E_3-E_2-\sqrt{m_4^2+\boldsymbol{p}_2^2+\boldsymbol{p}_3^2+2|\boldsymbol{p}_3||\boldsymbol{p}_2|z_s}\right)\\ &= \frac{E_4}{|\boldsymbol{p}_2||\boldsymbol{p}_3|}\,\delta\left(z_s-\frac{\left((m_1-E_2-E_3)^2-m_4^2-|\boldsymbol{p}_2|^2-|\boldsymbol{p}_3|^2\right)}{2|\boldsymbol{p}_3||\boldsymbol{p}_2|}\right).\end{aligned} \tag{A.26}$$

Since the latter fixes the integration over $\mathrm{d}z_s$ and the momenta of the particles in the final state are aligned in one plane,[1] every angular integration can be carried out trivially, such that

$$\int \mathrm{d}\Pi_{\mathrm{LIPS}} = \frac{1}{32\pi^3}\int \mathrm{d}|\boldsymbol{p}_2|\mathrm{d}|\boldsymbol{p}_3|\;\frac{|\boldsymbol{p}_2||\boldsymbol{p}_3|}{E_2E_3}\,. \tag{A.27}$$

To substitute the integration elements $\mathrm{d}|\boldsymbol{p}_2|$ and $\mathrm{d}|\boldsymbol{p}_3|$ in terms of the Lorentz invariants s and t we can employ the respective Jacobian

$$\mathcal{J}=\begin{pmatrix}-\frac{E_2}{2m_1|\boldsymbol{p}_2|} & 0\\ 0 & -\frac{E_3}{2m_1|\boldsymbol{p}_3|}\end{pmatrix}\quad\text{with determinant}\quad |\mathcal{J}|=\frac{1}{4m_1^2}\frac{E_2E_3}{|\boldsymbol{p}_2||\boldsymbol{p}_3|}\,, \tag{A.28}$$

so that we end up with the decay width

$$\Gamma=\frac{1}{32(2\pi)^3m_1^3}\int_{(m_3+m_4)^2}^{(m_1-m_2)^2}\mathrm{d}s\int_{t_-(s)}^{t_+(s)}\mathrm{d}t\,|\mathcal{M}|^2\,. \tag{A.29}$$

[1] This is a direct consequence of three-momentum conservation and the fact that we consider the rest frame of the decaying particle.

Alternatively, we can express the phase space in terms of the scattering angle by means of

$$\Gamma = \frac{1}{64(2\pi)^3 m_1^3} \int_{(m_3+m_4)^2}^{(m_1-m_2)^2} \mathrm{d}s\, \kappa_s(s) \int_{-1}^{1} \mathrm{d}z_s\, |\mathcal{M}|^2 \,, \tag{A.30}$$

where we used the relation between t and z_s as given in Eq. (A.16). Note that this substitution shifted the dependence of the integration limits on s, cf. $t_\pm(s)$ in Eq. (A.29), to the integrand by introducing an additional function $\kappa_s(s)$.
An observable derived from these representations of the phase space is the corresponding Mandelstam plane. We illustrate an example for a symmetrized version of the Dalitz plot with the kinematic ranges for the scattering and decay processes in Fig. A.1. The latter shows a homogeneous distribution, i.e., the trivial case for a constant matrix element. Additionally respecting relativistic momentum conservation results in the smooth distribution shown by the orange plane in Fig. A.1. In the non-relativistic limit, the Dalitz plot would become a circle within the equilateral triangle. Note the $2\pi/3$-rotational symmetry of this specific representation.

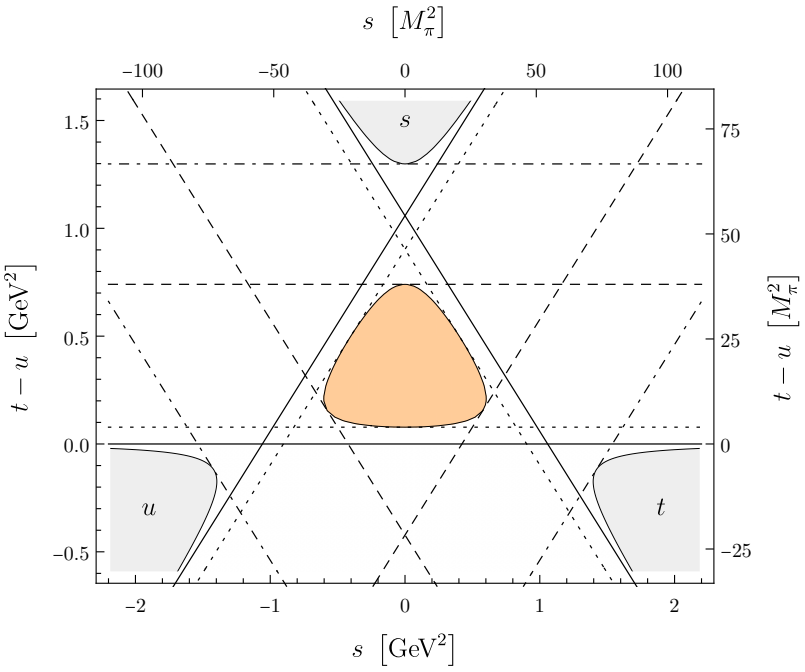

Figure A.1: Mandelstam plane created for a particle with mass $m_1 = 1\,\mathrm{GeV}$ and three light particles with equal masses, which are chosen to be $m_{2,3,4} = M_\pi$. The inner shape in orange denotes the allowed kinematic region for the three-body decay $1 \to 2+3+4$. The scattering process $1+2 \to 3+4$ is described by the outer planes in gray corresponding to one channel (s, t, or u) each. The solid lines denote the cases $s = 0$, $t = 0$, and $u = 0$, respectively. The dashed lines correspond to the upper limit on each Mandelstam variable in the decay process at pseudo-threshold $(m_1 - M_\pi)^2$. Similarly, the dotted lines indicate the values at threshold $4M_\pi^2$ and finally the dashed-dotted ones denote the threshold of each scattering channel at $(m_1 + M_\pi)^2$.

Appendix B

Partial-wave formalism

This appendix serves as an introduction to the partial-wave formalism as used in all dispersive approaches in this thesis (see for instance the examples in Sect. 3.4). The presented technique allows us to separate the angular dependence of each amplitude using a series expansion in terms of fixed angular momenta. The smaller the characteristic momenta of the involved particles are the earlier we can truncate the partial-wave expansion at finite order.

We start our considerations by introducing two different bases for a general amplitude in terms of helicity and angular-momentum in Sect. B.1. Subsequently, we perform a corresponding basis transformation in order to derive the partial-wave expansion of $2 \to 2$ scattering in Sect. B.2. More details about the formalism presented below can for instance be found in Refs. [239, 354].[1]

B.1 | Helicity and angular-momentum bases

We refer to the helicity basis whenever a matrix element is expressed in terms of momenta and spins. This goes back to the fact that the helicity λ is given by the projection of the spin S to the direction of momentum $\hat{p}$ by means of

$$\lambda = \hat{p} \cdot \boldsymbol{S}. \tag{B.1}$$

Henceforth, we denote a helicity state of one particle moving along the z-direction as $\psi_{p\lambda}$. With the angular momentum operator J_i, arbitrary directions of this state can be expressed in terms of Euler angles by

$$R_{\alpha\beta\gamma} = e^{-i\alpha J_z} e^{-i\beta J_y} e^{-i\gamma J_z}. \tag{B.2}$$

As $\psi_{p\lambda}$ has an axial symmetry, two angles are sufficient to rotate the helicity state to arbitrary directions. We can hence express a helicity state with absolute value of three-momentum p, $\alpha = \theta$, and $\beta = \phi$ in arbitrary direction by

$$|p\,\theta\phi;\lambda\rangle \equiv R_{\phi\theta-\phi}\psi_{p\lambda}\,, \tag{B.3}$$

where we chose the third angle as $\gamma = -\phi$ [239, 355]. Note that one can in principle also stick to the alternative convention $\gamma = 0$ [356, 357], which will result in a physically unimportant overall phase compared to our choice.

[1] Moreover, parts of this appendix were very similarly presented in Ref. [87].

We now continue with two-particle states and consider the two single-particle states $\psi_{p_1\lambda_1}$ and $\chi_{p_2\lambda_2}$. In the center-of-mass frame we have $\boldsymbol{p}_1 = -\boldsymbol{p}_2 \equiv \boldsymbol{p}$, with $\boldsymbol{p}$ pointing in positive z-direction. We can hence define a direct product that gives rise to the two-particle state [239]

$$\psi_{p\lambda_1\lambda_2} \equiv \psi_{p\lambda_1} \odot \chi_{p\lambda_2} \,. \tag{B.4}$$

Applying the same rotations as before, arbitrary two-particle states can be written as

$$|p\,\theta\phi;\lambda_1\lambda_2\rangle \equiv R_{\phi\theta-\phi}\psi_{p\lambda_1\lambda_2}. \tag{B.5}$$

In order to construct helicity states with definite angular momentum J out of these two-particle states, we introduce the Wigner-D function

$$\mathfrak{D}^J_{m'm}(\alpha,\beta,\gamma) = \langle Jm'|R_{\alpha\beta\gamma}|Jm\rangle = e^{-im'\alpha} d^J_{m'm}(\beta) e^{-im\gamma} \,, \tag{B.6}$$

with the small Wigner-d defined as

$$d^J_{m'm}(\beta) = \langle Jm'|e^{-i\beta J_y}|Jm\rangle \,. \tag{B.7}$$

With these definitions the partial-wave expansion of a two-particle helicity state becomes [354]

$$|p\,\theta\phi;\lambda_1\lambda_2\rangle = \sum_{J,M} \sqrt{\frac{2J+1}{4\pi}} \mathfrak{D}^J_{M\lambda}(\phi,\theta,-\phi)|p\;JM;\lambda_1\lambda_2\rangle \,, \tag{B.8}$$

while the corresponding inverse transformation reads

$$|p\;JM;\lambda_1\lambda_2\rangle = \sqrt{\frac{2J+1}{4\pi}} \int \mathrm{d}\Omega\, \mathfrak{D}^{J*}_{M\lambda}(\phi,\theta,-\phi)|p\,\theta\phi;\lambda_1\lambda_2\rangle \,, \tag{B.9}$$

where M indicates the z-component of the total angular momentum J, $\lambda \equiv \lambda_1 - \lambda_2$, and $\mathrm{d}\Omega = \mathrm{d}\phi\,\mathrm{d}\cos\theta$. Thus, instead of describing two-particle states by the angles θ and ϕ we can express it in terms of the angular momenta J and M.

B.2 | $2 \to 2$ scattering

We can now apply the shift from the helicity to the angular-momentum basis to a general amplitude $\mathcal{M}$ describing $2 \to 2$ scattering. The respective partial-wave expansion reads

$$\begin{aligned}\langle q\,\theta'\phi';\lambda_1'\lambda_2'|\mathcal{M}|p\,\theta\phi;\lambda_1\lambda_2\rangle \\ = \sum_{J',M'} \sqrt{\frac{2J'+1}{4\pi}} \mathfrak{D}^{J'*}_{M'\lambda'}(\phi',\theta',-\phi') \sum_{J,M} \sqrt{\frac{2J+1}{4\pi}} \mathfrak{D}^J_{M\lambda}(\phi,\theta,-\phi) \\ \times \langle q\;J'M';\lambda_1'\lambda_2'|\mathcal{M}|p\;JM;\lambda_1\lambda_2\rangle,\end{aligned} \tag{B.10}$$

with $\lambda' = \lambda_1' - \lambda_2'$. The conservation of angular momentum allows us to simplify this expression to

$$\begin{aligned}&\langle q\,\theta'\phi';\lambda_1'\lambda_2'|\mathcal{M}|p\,\theta\phi;\lambda_1\lambda_2\rangle \\ &\quad= \sum_{J,M} \frac{2J+1}{4\pi} \mathfrak{D}^{J*}_{M\lambda'}(\phi',\theta',-\phi') \mathfrak{D}^{J}_{M\lambda}(\phi,\theta,-\phi) \langle q\;JM;\lambda_1'\lambda_2'|\mathcal{M}|p\;JM;\lambda_1\lambda_2\rangle .\end{aligned} \tag{B.11}$$

For initial states moving along the z-direction one can set $\phi = \theta = 0$, such that $\mathfrak{D}^{J}_{M\lambda}(\phi,\theta,-\phi)$ reduces to $\delta_{M\lambda}$ and hence

$$\begin{aligned}&\langle q\,\theta'\phi';\lambda_1'\lambda_2'|\mathcal{M}|p\,0\,0;\lambda_1\lambda_2\rangle \\ &\qquad= \sum_{J,M} \frac{2J+1}{4\pi} \mathfrak{D}^{J*}_{\lambda\lambda'}(\phi',\theta',-\phi') \langle q\;JM;\lambda_1'\lambda_2'|\mathcal{M}|p\;JM;\lambda_1\lambda_2\rangle \,.\end{aligned} \tag{B.12}$$

We can evaluate the inverse of the latter two equations with the orthogonality relation

$$\int_0^{2\pi} \mathrm{d}\alpha \int_{-1}^{1} \mathrm{d}\cos(\beta)\, \mathfrak{D}^{J*}_{\lambda_1\lambda_2}(\alpha,\beta,-\alpha)\, \mathfrak{D}^{J'}_{\lambda_1'\lambda_2'}(\alpha,\beta,-\alpha) = \frac{4\pi}{2J+1} \delta_{JJ'} \delta_{\lambda_1\lambda_1'} \delta_{\lambda_2\lambda_2'} \,. \tag{B.13}$$

For this purpose, we first multiply the respective equation with a Wigner-D, carry out the integration over the Euler angles, and apply the orthogonality relation. With these steps the inverse of Eq. (B.11) becomes

$$\begin{aligned}&\langle q\;JM;\lambda_1'\lambda_2'|\mathcal{M}|p\;JM;\lambda_1\lambda_2\rangle \\ &\quad= \frac{2J+1}{4\pi} \int \mathrm{d}\Omega' \mathrm{d}\Omega\, \mathfrak{D}^{J}_{M\lambda'}(\phi',\theta',-\phi') \mathfrak{D}^{J*}_{M\lambda}(\phi,\theta,-\phi) \langle q\,\theta'\phi';\lambda_1'\lambda_2'|\mathcal{M}|p\,\theta\phi;\lambda_1\lambda_2\rangle \,,\end{aligned} \tag{B.14}$$

while the inverse of Eq. (B.12) reads

$$\langle q\;JM;\lambda_1'\lambda_2'|\mathcal{M}|p\;JM;\lambda_1\lambda_2\rangle = \int \mathrm{d}\Omega'\, \mathfrak{D}^{J}_{\lambda\lambda'}(\phi',\theta',-\phi') \langle q\,\theta'\phi';\lambda_1'\lambda_2'|\mathcal{M}|p\,0\,0;\lambda_1\lambda_2\rangle . \tag{B.15}$$

B.2.1 | Scalar $2 \to 2$ scattering

In the simplified case of scalar $2 \to 2$ scattering, J equals the relative angular momentum ℓ between the particles in the initial (or final) state. Hence, the Wigner-D reduces to Legendre polynomials by means of $\mathfrak{D}^{\ell}_{00}(\alpha,\beta,\gamma) = P_\ell(\cos\beta)$. Abbreviating the scalar amplitudes by $\mathcal{M}(s,z_s) \equiv \langle q\,\theta'0;00|\mathcal{M}|p\,0\,0;00\rangle$ and $f_\ell(s) \equiv \langle q\;\ell 0;00|\mathcal{M}|p\;\ell 0;00\rangle$, where s and $z_s = \cos\beta$ are defined as in Sect. A.2, the partial-wave expansion and its inverse become

$$\boxed{\mathcal{M}(s,z_s) = \sum_{\ell} \frac{2\ell+1}{4\pi} P_\ell(z_s)\, f_\ell(s) \quad \text{and} \quad f_\ell(s) = \int \mathrm{d}\Omega\, P_\ell(z_s)\, \mathcal{M}(s,z_s) \,.} \tag{B.16}$$

Note that one can in principle directly carry out the trivial azimuthal integration on the right-hand side, as stated in Sect. A.1.1, which contributes with a factor of 2π.
A concern regarding the expansion in Eq. (B.16) arises if we allow the Legendre polynomials to take complex values and may become apparent if we consider analytic continuations of $\mathcal{M}(s, z_s)$ to three-body decays. To elaborate on this point, we consider the *discontinuity* as introduced in Eq. (3.18) and for simplicity set the masses in the final state equal. Neglecting the suppressed contributions from discontinuities of D-waves and higher partial waves we can for instance write the s-channel discontinuity of $\mathcal{M}$ according to Eq. (B.16) as

$$\text{disc}_s \, \mathcal{M}(s, z_s) = \frac{1}{4\pi} \text{disc}_s \, f_0(s) + \frac{3}{4\pi} \text{disc}_s \left(z_s f_1(s) \right) . \tag{B.17}$$

The issue with this expression is that, according to Eq. (A.15), z_s is proportional to a kinematic function $1/\kappa(s)$ containing right-hand cuts, cf. Sect. 3.1, or in other words $\kappa(s)$ could become complex after analytic continuations. To avoid the thus arising complications when evaluating $\text{disc}_s \left(z_s f_1(s) \right)$ we instead consider the re-scaled partial-wave amplitude

$$f_\ell(s) \to \frac{4\pi}{2\ell + 1} \, \kappa^\ell(s) \, f_\ell(s) \, , \tag{B.18}$$

where we additionally absorbed all appearing constants for convenience. Unless stated otherwise, we henceforth restrict the sum of partial waves for scalar $2 \to 2$ amplitudes only to S- and P-waves without further notice. We use the transformations

$$\boxed{\mathcal{M}(s, z_s) = \sum_\ell \kappa^\ell(s) P_\ell(z_s) f_\ell(s) \quad \text{and} \quad f_\ell(s) = \frac{2\ell + 1}{2\kappa^\ell(s)} \int_{-1}^{1} \mathrm{d}z_s \, P_\ell(z_s) \mathcal{M}(s, z_s)} \tag{B.19}$$

whenever we want to analytically continue our amplitude such that the respective Legendre polynomials become complex. Hence, we can decompose the s-channel discontinuity of $\mathcal{M}(s, z_s)$ as

$$\text{disc}_s \, \mathcal{M}(s, z_s) = \text{disc} \, f_0(s) + z_s \kappa(s) \, \text{disc} \, f_1(s). \tag{B.20}$$

Appendix C

C and CP violation in LEFT up to dimension 8

In this appendix we comment on our classification of C- and CP-violating LEFT operators presented in Ch. 5, based on the complete sets from Ref. [146] up to and including mass dimension 6, Ref. [150] for dimension 7, and Ref. [136] for dimension-8 operators. For simplicity we do not quote all of the numerous contributing operators in these bases, but go directly to their characterization in terms of C-, P-, and T-eigenstates. The genuine LEFT operators are written in terms of chiral projectors, i.e.,

$$\psi_{L/R} \equiv P_{L/R}\psi \quad \text{with} \quad P_L = \frac{1-\gamma_5}{2}\,, \quad P_R = \frac{1+\gamma_5}{2}\,, \tag{C.1}$$

and thus include in general superpositions of states with different discrete symmetries. Our C- and CP-odd operators will be identified as linear combinations of these LEFT operators, such that the separated (pseudo)scalar, (axial)vector, and (pseudo)tensor contributions have definite eigenvalues under C, P, and T. Technically, we merely write each projector explicitly in terms of Dirac matrices and separate the summands with different discrete symmetries. We will rephrase the quark portion of each LEFT operator in this way and drop possible field-strength tensors and $SU(3)$ generators in the first place, which can be restored in most cases straightforwardly.

To keep the notation as short and simple as possible we use a rather sloppy notation and refer to generic Wilson coefficients by $c \in \mathbb{C}$, whose numerical value may be different in each operator. This abuse of notation shall not bother us, as we are solely interested in LEFT and not in any matching between operators in SMEFT and LEFT. The notes on the following pages are all restricted to the flavor-conserving case. However, flavor-violating LEFT operators that may contribute to ToPe forces, which are less relevant for our analysis of η decays, can be derived in a similar manner. Other than that, we will follow the strategy already sketched in Ch. 5.

The outline of this appendix is as follows. In Sect. C.1 we explicitly confirm at hand of well-known operator bases of LEFT that there are no ToPe interactions of dimension ≤ 6. Subsequently we investigate the operators at dimension 7 and 8 LEFT in Sects. C.2 and C.3, respectively, and carefully distinguish between the ones that are chirality-violating and chirality-conserving.

C.1 | Dimension ≤ 6 LEFT

In this section we consider LEFT operators carefully worked out by Ref. [146] and explicitly show that there are indeed no ToPe operators below dimension 7 in LEFT. We directly

discard the dimension-3 operators, which are solely given by neutrino bilinears [146].

C.1.1 | Dimension 5 LEFT

The modest number of dimension-5 operators only allows for quarks with the sole Dirac structure $\bar{\psi}_L \sigma_{\mu\nu} \psi_R$. We can multiply this structure with the Wilson coefficient and respect hermiticity, to obtain

$$c\,\bar{\psi}\sigma_{\mu\nu}P_R\psi + \text{h.c.} = \text{Re}\,c\,\bar{\psi}\sigma_{\mu\nu}\psi + i\,\text{Im}\,c\,\bar{\psi}\sigma_{\mu\nu}\gamma_5\psi\,. \tag{C.2}$$

After contracting with the gluon or photon field-strength tensor, we can read from Table 5.1 that the resulting terms preserve C.

C.1.2 | Dimension 6 LEFT

In dimension 6 LEFT we encounter operators including the quadrilinear

$$\begin{aligned} c\,\bar{\psi}\gamma_\mu P_{\text{R/L}}\psi\bar{\chi}\gamma^\mu P_{\text{R/L}}\chi + \text{h.c.} = \frac{1}{2}\text{Re}\,c\,\big[&\bar{\psi}\gamma_\mu\psi\bar{\chi}\gamma^\mu\chi + \bar{\psi}\gamma_\mu\gamma_5\psi\bar{\chi}\gamma^\mu\gamma_5\chi \\ &\pm\bar{\psi}\gamma_\mu\gamma_5\psi\bar{\chi}\gamma^\mu\chi \pm \bar{\psi}\gamma_\mu\psi\bar{\chi}\gamma^\mu\gamma_5\chi\big]\,. \end{aligned} \tag{C.3}$$

While the first two summands have the signature $CPT = +++$, the last two have the eigenvalues $CPT = --+$. Therefore these cannot contribute to ToPe interactions. The same holds for $\bar{\psi}\gamma_\mu P_\text{L}\psi\bar{\chi}\gamma^\mu P_\text{R}\chi$, which just distinguishes by relative signs from the case discussed above. Next, consider

$$c\,\bar{\psi}P_\text{R}\chi\bar{\chi}P_\text{R}\psi + \text{h.c.} = \frac{1}{2}\text{Re}\,c\,\big[\bar{\psi}\chi\bar{\chi}\psi + \bar{\psi}\gamma_5\chi\bar{\chi}\gamma_5\psi\big] + \frac{i}{2}\text{Im}\,c\big[\bar{\psi}\gamma_5\chi\bar{\chi}\psi + \bar{\psi}\chi\bar{\chi}\gamma_5\psi\big]\,. \tag{C.4}$$

While the summand scaling with $\text{Re}\,c$ has $CPT = +++$ the one proportional to $\text{Im}\,c$ is $CPT = +--$. Analogously, this is also true for $\bar{\psi}P_\text{L}\psi\bar{\chi}P_\text{L}\chi$.
Using $\sigma^\dagger_{\mu\nu} = \gamma_0\sigma_{\mu\nu}\gamma_0$ we can easily derive

$$\begin{aligned} c\,\bar{\psi}\sigma_{\mu\nu}P_\text{R}\chi\bar{\chi}\sigma^{\mu\nu}P_\text{R}\psi + \text{h.c.} = \frac{1}{2}\text{Re}\,c\,\big[&\bar{\psi}\sigma_{\mu\nu}\chi\bar{\chi}\sigma^{\mu\nu}\psi + \bar{\psi}\sigma_{\mu\nu}\gamma_5\chi\bar{\chi}\sigma^{\mu\nu}\gamma_5\psi\big] \\ &+ \frac{i}{2}\text{Im}\,c\big[\bar{\psi}\sigma_{\mu\nu}\gamma_5\chi\bar{\chi}\sigma^{\mu\nu}\psi + \bar{\psi}\sigma_{\mu\nu}\chi\bar{\chi}\sigma^{\mu\nu}\gamma_5\psi\big]\,, \end{aligned} \tag{C.5}$$

where the two summands have $CPT = +++$ and $CPT = +--$, respectively. Again, the term $\bar{\psi}\sigma_{\mu\nu}P_\text{L}\psi\bar{\chi}\sigma^{\mu\nu}P_\text{L}\chi$ proceeds in the same manner. The remaining dimension-6 operators under consideration are the triple gauge terms

$$f_{abc}G^{\nu a}_\mu G^{\rho b}_\nu G^{\mu c}_\rho \quad \text{and} \quad f_{abc}\tilde{G}^{\nu a}_\mu G^{\rho b}_\nu G^{\mu c}_\rho\,, \tag{C.6}$$

which, according to Table 5.1, have the symmetries $CPT = +++$ and $CPT = +--$, respectively.

Thus, none of the considered operators in dimension-6 LEFT can create ToPe effects. Furthermore, note that one can neither build a loop consisting of two of these dimension-6 LEFT operators that results in a C- and CP-odd transition.
If we relax the condition of flavor-conservation, i.e., if we consider flavor-*violating* operators, we can indeed find terms with the signature $CPT = - + -$, as pointed out in Refs. [156, 157]. However, these do not contribute to the physics we are interested in and do not necessarily allow for an unambiguous identification of BSM signals, due to C- *or* CP-violating contributions from the weak interaction.

C.2 | Dimension-7 LEFT

Considering the—for our purposes relevant—lepton- and baryon-number-conserving operators, there occur two different types of fermion bilinears: $\bar{\psi}_R\psi_L$ and $\bar{\psi}_R\sigma_{\mu\nu}\psi_L$. Let us again neglect the (hermitian) product of field-strength tensors accompanying these bilinears for now. Accounting for the respective Wilson coefficients, the hermitian bilinears can be rewritten as

$$c\,\bar{\psi}_R\psi_L + \text{h.c.} = \text{Re}\,c\;\bar{\psi}\psi - \text{Im}\,c\;\bar{\psi}i\gamma_5\psi \tag{C.7}$$

and

$$c\,\bar{\psi}_R\sigma_{\mu\nu}\psi_L + \text{h.c.} = \text{Re}\,c\;\bar{\psi}\sigma_{\mu\nu}\psi - \text{Im}\,c\;\bar{\psi}i\sigma_{\mu\nu}\gamma_5\psi\,. \tag{C.8}$$

In complete analogy, the two types of fermion quadrilinears $(\bar{\psi}_L\gamma^\mu\psi_L)(\bar{\chi}_L i\overleftrightarrow{D}_\mu\chi_R)$ and $(\bar{\psi}_R\gamma^\mu\psi_R)(\bar{\chi}_L i\overleftrightarrow{D}_\mu\chi_R)$ become

$$\begin{aligned} c\,(\bar{\psi}_L\gamma^\mu\psi_L)(\bar{\chi}_L i\overleftrightarrow{D}_\mu\chi_R) + \text{h.c.} = \frac{1}{2}\text{Re}\,c\;&\left[(\bar{\chi}i\overleftrightarrow{D}_\mu\chi)(\bar{\psi}\gamma^\mu\psi) - (\bar{\chi}i\overleftrightarrow{D}_\mu\chi)(\bar{\psi}\gamma^\mu\gamma_5\psi)\right] \\ - \frac{1}{2}\text{Im}\,c\;&\left[(\bar{\chi}\overleftrightarrow{D}_\mu\gamma_5\chi)(\bar{\psi}\gamma^\mu\psi) - (\bar{\chi}\overleftrightarrow{D}_\mu\gamma_5\chi)(\bar{\psi}\gamma^\mu\gamma_5\psi)\right]\,, \end{aligned} \tag{C.9}$$

where in the second step $P_L + P_R = 1$ and $P_R - P_L = \gamma_5$ were applied. Similarly, we obtain

$$\begin{aligned} c\,(\bar{\psi}_R\gamma^\mu\psi_R)(\bar{\chi}_L i\overleftrightarrow{D}_\mu\chi_R) + \text{h.c.} = \frac{1}{2}\text{Re}\,c\;&\left[(\bar{\chi}i\overleftrightarrow{D}_\mu\chi)(\bar{\psi}\gamma^\mu\psi) + (\bar{\chi}i\overleftrightarrow{D}_\mu\chi)(\bar{\psi}\gamma^\mu\gamma_5\psi)\right] \\ - \frac{1}{2}\text{Im}\,c\;&\left[(\bar{\chi}\overleftrightarrow{D}_\mu\gamma_5\chi)(\bar{\psi}\gamma^\mu\psi) + (\bar{\chi}\overleftrightarrow{D}_\mu\gamma_5\chi)(\bar{\psi}\gamma^\mu\gamma_5\psi)\right]\,, \end{aligned} \tag{C.10}$$

with the same operators as Eq. (C.9), but with different real-valued prefactors. Note that the factor i from the Wilson coefficients flips the sign of time reversal, while γ_5 changes the one of parity. Attaching the products of field-strength tensors to the fermion bilinears, like explicitly done in Table C.1, we can formulate the operators of Ref. [150] in a way that allows us to directly read off the transformation properties under the discrete symmetries

C, P, and T. According to Table C.1, there are only two operators at dimension 7 in LEFT which violate C and CP, namely

$$\begin{aligned} &\bar{\psi} T^A \sigma^{\mu\nu} \psi F_{\mu\rho} G_\nu^{A\rho} \,, \\ &\bar{\chi} \overleftrightarrow{D}_\mu \gamma_5 \chi \bar{\psi} \gamma^\mu \gamma_5 \psi \,, \end{aligned} \tag{C.11}$$

with the same form as already proposed decades ago, cf. Eq. (5.4). There is in principle also another color contraction for the quark quadrilinear allowed, but we refrain from quoting it explicitly because it leads to the same effective operator on the mesonic level and in this way we are as consistent as possible with the original operators from Eq. (5.4). Furthermore, as already stated in Sect. 5.3.1, in this work we do not consider corrections due to QCD running, which arise from possible mixing of different color contractions.

C.3 | Dimension-8 LEFT

We proceed with the classification of dimension-8 operators from Ref. [136]. For the sake of simplicity, we categorize the operators according to the number n of contributing quarks (ψ^n), derivatives (D^n), and gauge field-strength tensors (X^n). Once more, we first focus on the Dirac structure of each operator and characterize different combinations (given in the original basis of LEFT operators) with X^n, structure constants d_{abc}, f_{abc}, and $SU(3)$ generators T^a in Tables C.2–C.10. Operators that are not listed in these tables do either not appear in the original LEFT basis of Ref. [136] or are beforehand identified as irrelevant for our analysis, cf. Ch. 5. The results, i.e., chirality-conserving and -violating dimension-8 LEFT operators, are summarized in Sect. C.3.5.

C.3.1 | Operator class X^4

Each field-strength tensor $X_{\mu\nu}$ has the signature $CPT = -+-$, while the ones in dual space, i.e., $\tilde{X}_{\mu\nu}$, obey $CPT = --+$. Hence any combination of four field-strength tensors with no or trivial color contractions, i.e., contractions without structure constants f_{abc} or d_{abc}, conserves C. Having a look at these non-trivial color structures, there appear either terms including three gluons and one photon or four gluons and no photon. In the LEFT basis under consideration the former always involve the symmetric structure constant d_{abc}, so that terms of the form

$$d_{abc} G^a_{\mu\nu} G^{b\mu\nu} G^c_{\alpha\beta} F^{\alpha\beta} \tag{C.12}$$

are always C-even, as can be read off from Table 5.1. The possible four-gluon operators include structures like

$$d_{abe} d_{cde} G^a_{\mu\nu} G^{b\mu\nu} G^c_{\alpha\beta} G^{d\alpha\beta} \,, \tag{C.13}$$

which conserve each of the three fundamental discrete symmetries separately. This can easily be checked analogously to the example given in Sect. 5.2. The exchange of any of these field-strength tensors with its dual representation preserves the C-even nature of the operators. Thus there is no C-violating operator in this class.

		C	P	T
1a)	$\bar{\psi}\psi F_{\mu\nu}F^{\mu\nu}$	+	+	+
1b)	$\bar{\psi}i\gamma_5\psi F_{\mu\nu}F^{\mu\nu}$	+	−	−
2a)	$\bar{\psi}T^A\psi F^{\mu\nu}G^A_{\mu\nu}$	+	+	+
2b)	$\bar{\psi}T^Ai\gamma_5\psi F^{\mu\nu}G^A_{\mu\nu}$	+	−	−
3a)	$\bar{\psi}T^A\sigma^{\mu\nu}\psi F_{\mu\rho}G^{A\rho}_{\nu}$	−	+	−
3b)	$\bar{\psi}T^A\sigma^{\mu\nu}i\gamma_5\psi F_{\mu\rho}G^{A\rho}_{\nu}$	−	−	+
4a)	$d_{abc}\bar{\psi}T^A\psi G^B_{\mu\nu}G^{C\mu\nu}$	+	+	+
4b)	$d_{abc}\bar{\psi}T^Ai\gamma_5\psi G^B_{\mu\nu}G^{C\mu\nu}$	+	−	−
5a)	$f_{abc}\bar{\psi}T^A\sigma^{\mu\nu}\psi G^B_{\mu\rho}G^{C\rho}_{\nu}$	+	+	+
5b)	$f_{abc}\bar{\psi}T^A\sigma^{\mu\nu}i\gamma_5\psi G^B_{\mu\rho}G^{C\rho}_{\nu}$	+	−	−
6a)	$\bar{\psi}\psi F_{\mu\nu}\tilde{F}^{\mu\nu}$	+	−	−
6b)	$\bar{\psi}i\gamma_5\psi F_{\mu\nu}\tilde{F}^{\mu\nu}$	+	+	+
7a)	$\bar{\psi}T^A\psi F^{\mu\nu}\tilde{G}^A_{\mu\nu}$	+	−	−
7b)	$\bar{\psi}T^Ai\gamma_5\psi F^{\mu\nu}\tilde{G}^A_{\mu\nu}$	+	+	+
8a)	$d_{abc}\bar{\psi}T^A\psi G^B_{\mu\nu}\tilde{G}^{C\mu\nu}$	+	−	−
8b)	$d_{abc}\bar{\psi}T^Ai\gamma_5\psi G^B_{\mu\nu}\tilde{G}^{C\mu\nu}$	+	+	+
9)	$(\bar{\chi}i\overleftrightarrow{D}_\mu\chi)(\bar{\psi}\gamma^\mu\psi)$	+	+	+
10)	$(\bar{\chi}\overleftrightarrow{D}_\mu\gamma_5\chi)(\bar{\psi}\gamma^\mu\psi)$	+	−	−
11)	$(\bar{\chi}i\overleftrightarrow{D}_\mu\chi)(\bar{\psi}\gamma^\mu\gamma_5\psi)$	−	−	+
12)	$(\bar{\chi}\overleftrightarrow{D}_\mu\gamma_5\chi)(\bar{\psi}\gamma^\mu\gamma_5\psi)$	−	+	−

Table C.1: Operators in dimension 7 LEFT with well defined discrete space-time symmetries. All operators listed are hermitian and have to be multiplied by a real-valued coefficient corresponding to real or imaginary parts of the respective Wilson coefficents. This table covers the operators that are not discarded beforehand, as described in Ch. 5, and can be generalized in future analyses. The operators 3a) and 12) are C- and CP-odd.

C.3.2 | Operator class $\psi^2 X^2 D$

In this operator class we encounter

$$c\,\bar{\psi}\gamma_\mu i\overleftrightarrow{D}_\nu P_{\mathrm{R/L}}\psi + \text{h.c.} = \mathrm{Re}\,c\left(\bar{\psi}\gamma_\mu i\overleftrightarrow{D}_\nu\psi \pm \bar{\psi}\gamma_\mu\gamma_5 i\overleftrightarrow{D}_\nu\psi\right). \tag{C.14}$$

Taking appropriate linear combinations, these Dirac structures can be reduced to

$$\bar{\psi}\gamma_\mu i\overleftrightarrow{D}_\nu\psi \quad \text{and} \quad \bar{\psi}\gamma_\mu\gamma_5 i\overleftrightarrow{D}_\nu\psi\,, \tag{C.15}$$

which have to be multiplied with a real-valued linear combination of Wilson coefficients that can be absorbed in a single overall normalization for each of these two operators. All combinations with attached field strengths are listed in Table C.2.

C.3.3 | Operator class $\psi^4 X$

The simplest quadrilinears occurring in the class $\psi^4 X$ read

$$\begin{aligned} c\,\bar{\psi}\gamma^\mu P_{\mathrm{L}}\psi\bar{\chi}\gamma^\nu P_{\mathrm{R}}\chi + \text{h.c.} = \frac{1}{2}\mathrm{Re}\,c\,\big(&\bar{\psi}\gamma^\mu\psi\bar{\chi}\gamma^\nu\chi - \bar{\psi}\gamma^\mu\gamma_5\psi\bar{\chi}\gamma^\nu\gamma_5\chi \\ &- \bar{\psi}\gamma^\mu\gamma_5\psi\bar{\chi}\gamma^\nu\chi + \bar{\psi}\gamma^\mu\psi\bar{\chi}\gamma^\nu\gamma_5\chi\big) \end{aligned} \tag{C.16}$$

and

$$\begin{aligned} c\,\bar{\psi}\gamma^\mu P_{\mathrm{R/L}}\psi\bar{\chi}\gamma^\nu P_{\mathrm{R/L}}\chi + \text{h.c.} = \frac{1}{2}\mathrm{Re}\,c\,\big(&\bar{\psi}\gamma^\mu\psi\bar{\chi}\gamma^\nu\chi + \bar{\psi}\gamma^\mu\gamma_5\psi\bar{\chi}\gamma^\nu\gamma_5\chi \\ &\pm \bar{\psi}\gamma^\mu\gamma_5\psi\bar{\chi}\gamma^\nu\chi \pm \bar{\psi}\gamma^\mu\psi\bar{\chi}\gamma^\nu\gamma_5\chi\big)\,. \end{aligned} \tag{C.17}$$

Note that the expression $\bar{\psi}\gamma^\mu P_{\mathrm{L}}\psi\bar{\chi}\gamma^\nu P_{\mathrm{R}}\chi$ is (up to a sign) the same as $\bar{\psi}\gamma^\mu P_{\mathrm{R}}\psi\bar{\chi}\gamma^\nu P_{\mathrm{L}}\chi$ after a contraction with the field-strength tensor and a re-labelling $\psi \leftrightarrow \chi$. Therefore it suffices to consider only one of them. In analogy to Eq. (C.15) we can write these operators as linearly independent combinations with the same eigenvalue of C by means of

$$\bar{\psi}\gamma^\mu\psi\bar{\chi}\gamma^\nu\chi \pm \bar{\psi}\gamma^\mu\gamma_5\psi\bar{\chi}\gamma^\nu\gamma_5\chi \quad \text{and} \quad \bar{\psi}\gamma^\mu\gamma_5\psi\bar{\chi}\gamma^\nu\chi \pm \bar{\psi}\gamma^\mu\psi\bar{\chi}\gamma^\nu\gamma_5\chi\,. \tag{C.18}$$

After contracting with $F_{\mu\nu}$ or $G^a_{\mu\nu}$ and attaching the respective color structures, the discrete symmetries of these operators can be read off straightforwardly.

Next, we have a look at

$$\begin{aligned} c\,\bar{\psi}\gamma^\mu P_{\mathrm{L}}\chi\bar{\chi}\gamma^\nu P_{\mathrm{R}}\psi + \text{h.c.} = &\,\mathrm{Re}\,c\left(\bar{\psi}\gamma^\mu P_{\mathrm{L}}\chi\bar{\chi}\gamma^\nu P_{\mathrm{R}}\psi + \bar{\psi}\gamma^\nu P_{\mathrm{R}}\chi\bar{\chi}\gamma^\mu P_{\mathrm{L}}\psi\right) \\ &+ i\,\mathrm{Im}\,c\left(\bar{\psi}\gamma^\mu P_{\mathrm{L}}\chi\bar{\chi}\gamma^\nu P_{\mathrm{R}}\psi - \bar{\psi}\gamma^\nu P_{\mathrm{R}}\chi\bar{\chi}\gamma^\mu P_{\mathrm{L}}\psi\right). \end{aligned} \tag{C.19}$$

To simplify the expression after expanding the projectors, we need to contract the operator with the field-strength tensors. The antisymmetry of $F_{\mu\nu}$ under interchange of the Lorentz

indices leads to

$$\begin{aligned}\big(c\,\bar\psi\gamma^\mu P_\mathrm{L}\chi\bar\chi\gamma^\nu P_\mathrm{R}\psi + \mathrm{h.c.}\big)F_{\mu\nu} = \frac{1}{2}\mathrm{Re}\,c\,\big(\bar\psi\gamma^\mu\chi\bar\chi\gamma^\nu\gamma_5\psi - \bar\psi\gamma^\mu\gamma_5\chi\bar\chi\gamma^\nu\psi\big)F_{\mu\nu}\\ + \frac{i}{2}\mathrm{Im}\,c\,\big(\bar\psi\gamma^\mu\chi\bar\chi\gamma^\nu\psi - \bar\psi\gamma^\mu\gamma_5\chi\bar\chi\gamma^\nu\gamma_5\psi\big)F_{\mu\nu}\,.\end{aligned} \tag{C.20}$$

Special care has to be taking when working out the C-transformation of operators mixing different flavors in a single bilinear, as is the case for the operator above. The charge conjugate of the first summand in Eq. (C.20) reads

$$\begin{aligned}C\left[\big(\bar\psi\gamma^\mu\chi\bar\chi\gamma^\nu\gamma_5\psi - \bar\psi\gamma^\mu\gamma_5\chi\bar\chi\gamma^\nu\psi\big)F_{\mu\nu}\right] &= \big(\bar\psi\gamma^\nu\gamma_5\chi\bar\chi\gamma^\mu\psi - \bar\psi\gamma^\nu\chi\bar\chi\gamma^\mu\gamma_5\psi\big)F_{\mu\nu}\\ &= \big(-\bar\psi\gamma^\mu\gamma_5\chi\bar\chi\gamma^\nu\psi + \bar\psi\gamma^\mu\chi\bar\chi\gamma^\nu\gamma_5\psi\big)F_{\mu\nu}\,,\end{aligned} \tag{C.21}$$

where, in the last step, we renamed $\mu \leftrightarrow \nu$ and again used the antisymmetry of $F_{\mu\nu}$. For the second summand one can proceed analogously. Hence the operator in Eq. (C.20) is C-even. The case when contracting the quadrilinear with $G^a_{\mu\nu}$ instead of $F_{\mu\nu}$ is slightly more intricate, as we need to account for the $SU(3)$ color generator T^a:

$$\begin{aligned}&c\,\bar\psi\gamma^\mu P_\mathrm{L}T^a\chi\bar\chi\gamma^\nu P_\mathrm{R}\psi G^a_{\mu\nu} + \mathrm{h.c.} =\\ &\quad\frac{1}{4}\mathrm{Re}\,c\,\big[\bar\psi\gamma^\mu T^a\chi\bar\chi\gamma^\nu\psi + \bar\psi\gamma^\mu T^a\chi\bar\chi\gamma^\nu\gamma_5\psi - \bar\psi\gamma^\mu\gamma_5 T^a\chi\bar\chi\gamma^\nu\psi\\ &\qquad\qquad - \bar\psi\gamma^\mu\gamma_5 T^a\chi\bar\chi\gamma^\nu\gamma_5\psi + (\psi\leftrightarrow\chi)\big]G^a_{\mu\nu}\\ &\quad+\frac{i}{4}\mathrm{Im}\,c\,\big[\bar\psi\gamma^\mu T^a\chi\bar\chi\gamma^\nu\psi + \bar\psi\gamma^\mu T^a\chi\bar\chi\gamma^\nu\gamma_5\psi - \bar\psi\gamma^\mu\gamma_5 T^a\chi\bar\chi\gamma^\nu\psi\\ &\qquad\qquad - \bar\psi\gamma^\mu\gamma_5 T^a\chi\bar\chi\gamma^\nu\gamma_5\psi - (\psi\leftrightarrow\chi)\big]G^a_{\mu\nu}\,.\end{aligned} \tag{C.22}$$

As already done several times, one can conveniently split this operator into its C-even and C-odd eigenstates. In complete analogy, we now evaluate

$$\begin{aligned}&c\,f_{abc}\,\bar\psi\gamma^\mu P_\mathrm{L}T^a\chi\bar\chi\gamma^\nu P_\mathrm{R}T^b\psi G^c_{\mu\nu} + \mathrm{h.c.} =\\ &\qquad\frac{1}{2}\mathrm{Re}\,c\,f_{abc}\,\big[\bar\psi\gamma^\mu T^a\chi\bar\chi\gamma^\nu T^b\psi - \bar\psi\gamma^\mu\gamma_5 T^a\chi\bar\chi\gamma^\nu\gamma_5 T^b\psi\big]G^c_{\mu\nu}\\ &\qquad+\frac{i}{2}\mathrm{Im}\,c\,f_{abc}\,\big[\bar\psi\gamma^\mu T^a\chi\bar\chi\gamma^\nu T^b\gamma_5\psi - \bar\psi\gamma^\mu\gamma_5 T^a\chi\bar\chi\gamma^\nu T^b\psi\big]G^c_{\mu\nu}\,,\end{aligned} \tag{C.23}$$

where we simplified the expression using the antisymmetry of the structure constant f_{abc} and $G^c_{\mu\nu}$. Similarly, we find

$$\begin{aligned}&c\,d_{abc}\,\bar\psi\gamma^\mu P_\mathrm{L}T^a\chi\bar\chi\gamma^\nu P_\mathrm{R}T^b\psi G^c_{\mu\nu} + \mathrm{h.c.}\\ &\qquad= \frac{1}{2}\mathrm{Re}\,c\,d_{abc}\,\big[\bar\psi\gamma^\mu T^a\chi\bar\chi\gamma^\nu\gamma_5 T^b\psi - \bar\psi\gamma^\mu\gamma_5 T^a\chi\bar\chi\gamma^\nu T^b\psi\big]G^c_{\mu\nu}\,,\end{aligned} \tag{C.24}$$

where terms symmetric under $\psi \leftrightarrow \chi$ drop out, because the operator is symmetric under $a \leftrightarrow b$ and antisymmetric under $\mu \leftrightarrow \nu$. We continue with

$$\begin{aligned} c\,\bar{\psi}P_{\mathrm{R}}\psi\bar{\chi}\sigma^{\mu\nu}P_{\mathrm{R}}\chi + \mathrm{h.c.} = \frac{1}{2}\mathrm{Re}\,c\left(\bar{\psi}\psi\bar{\chi}\sigma^{\mu\nu}\chi + \bar{\psi}\gamma_5\psi\bar{\chi}\sigma^{\mu\nu}\gamma_5\chi\right) \\ + \frac{i}{2}\mathrm{Im}\,c\left(\bar{\psi}\gamma_5\psi\bar{\chi}\sigma^{\mu\nu}\chi + \bar{\psi}\psi\bar{\chi}\sigma^{\mu\nu}\gamma_5\chi\right). \end{aligned} \tag{C.25}$$

The next quadrilinear under consideration has the form

$$\begin{aligned} & c\,\bar{\psi}P_{\mathrm{R}}\chi\bar{\chi}\sigma^{\mu\nu}P_{\mathrm{R}}\psi + \mathrm{h.c.} \\ & \quad = \mathrm{Re}\,c\left(\bar{\psi}P_{\mathrm{R}}\chi\bar{\chi}\sigma^{\mu\nu}P_{\mathrm{R}}\psi + \bar{\chi}P_{\mathrm{L}}\psi\bar{\psi}\sigma^{\mu\nu}P_{\mathrm{L}}\chi\right) \\ & \qquad + i\mathrm{Im}\,c\left(\bar{\psi}P_{\mathrm{R}}\chi\bar{\chi}\sigma^{\mu\nu}P_{\mathrm{R}}\psi - \bar{\chi}P_{\mathrm{L}}\psi\bar{\psi}\sigma^{\mu\nu}P_{\mathrm{L}}\chi\right) \\ & \quad = \frac{1}{4}\mathrm{Re}\,c\,\Big[\left(\bar{\psi}\chi\bar{\chi}\sigma^{\mu\nu}\psi + \bar{\chi}\psi\bar{\psi}\sigma^{\mu\nu}\chi + \bar{\psi}\gamma_5\chi\bar{\chi}\sigma^{\mu\nu}\gamma_5\psi + \bar{\chi}\gamma_5\psi\bar{\chi}\sigma^{\mu\nu}\gamma_5\chi\right) \\ & \qquad\qquad + \left(\bar{\psi}\gamma_5\chi\bar{\chi}\sigma^{\mu\nu}\psi + \bar{\psi}\chi\bar{\chi}\sigma^{\mu\nu}\gamma_5\psi - \bar{\chi}\gamma_5\psi\bar{\chi}\sigma^{\mu\nu}\chi - \bar{\chi}\psi\bar{\psi}\sigma^{\mu\nu}\gamma_5\chi\right)\Big] \\ & \qquad + \frac{i}{4}\mathrm{Im}\,c\,\Big[\left(\bar{\psi}\chi\bar{\chi}\sigma^{\mu\nu}\psi - \bar{\chi}\psi\bar{\psi}\sigma^{\mu\nu}\chi + \bar{\psi}\gamma_5\chi\bar{\chi}\sigma^{\mu\nu}\gamma_5\psi - \bar{\chi}\gamma_5\psi\bar{\chi}\sigma^{\mu\nu}\gamma_5\chi\right) \\ & \qquad\qquad + \left(\bar{\psi}\gamma_5\chi\bar{\chi}\sigma^{\mu\nu}\psi + \bar{\psi}\chi\bar{\chi}\sigma^{\mu\nu}\gamma_5\psi + \bar{\chi}\gamma_5\psi\bar{\chi}\sigma^{\mu\nu}\chi + \bar{\chi}\psi\bar{\psi}\sigma^{\mu\nu}\gamma_5\chi\right)\Big]\,. \end{aligned} \tag{C.26}$$

In this equation, the terms are ordered such that each expression in parenthesis has the same eigenvalue under charge conjugation. In the same manner, the last operator occurring in this class is

$$\begin{aligned} & c\,\bar{\psi}\sigma^{\mu}{}_{\lambda}P_{\mathrm{R}}\chi\bar{\chi}\sigma^{\lambda\nu}P_{\mathrm{R}}\psi + \mathrm{h.c.} \\ & = \mathrm{Re}\,c\big(\bar{\psi}\sigma^{\mu}{}_{\lambda}P_{\mathrm{R}}\chi\bar{\chi}\sigma^{\lambda\nu}P_{\mathrm{R}}\psi + \bar{\psi}\sigma^{\mu}{}_{\lambda}P_{\mathrm{L}}\chi\bar{\chi}\sigma^{\lambda\nu}P_{\mathrm{L}}\psi\big) \\ & \quad + i\mathrm{Im}\,c\left(\bar{\psi}\sigma^{\mu}{}_{\lambda}P_{\mathrm{R}}\chi\bar{\chi}\sigma^{\lambda\nu}P_{\mathrm{R}}\psi - \bar{\psi}\sigma^{\mu}{}_{\lambda}P_{\mathrm{L}}\chi\bar{\chi}\sigma^{\lambda\nu}P_{\mathrm{L}}\psi\right) \\ & = \frac{1}{4}\mathrm{Re}\,c\,\Big[\left(\bar{\psi}\sigma^{\mu}{}_{\lambda}\chi\bar{\chi}\sigma^{\lambda\nu}\psi + \bar{\chi}\sigma^{\mu}{}_{\lambda}\psi\bar{\psi}\sigma^{\lambda\nu}\chi + \bar{\psi}\sigma^{\mu}{}_{\lambda}\gamma_5\chi\bar{\chi}\sigma^{\lambda\nu}\gamma_5\psi + \bar{\chi}\sigma^{\mu}{}_{\lambda}\gamma_5\psi\bar{\chi}\sigma^{\lambda\nu}\gamma_5\chi\right) \\ & \qquad + \left(\bar{\psi}\sigma^{\mu}{}_{\lambda}\gamma_5\chi\bar{\chi}\sigma^{\lambda\nu}\psi + \bar{\psi}\sigma^{\mu}{}_{\lambda}\chi\bar{\chi}\sigma^{\lambda\nu}\gamma_5\psi - \bar{\chi}\sigma^{\mu}{}_{\lambda}\gamma_5\psi\bar{\chi}\sigma^{\lambda\nu}\chi - \bar{\chi}\sigma^{\mu}{}_{\lambda}\psi\bar{\psi}\sigma^{\lambda\nu}\gamma_5\chi\right)\Big] \\ & \quad + \frac{i}{4}\mathrm{Im}\,c\,\Big[\left(\bar{\psi}\sigma^{\mu}{}_{\lambda}\chi\bar{\chi}\sigma^{\lambda\nu}\psi - \bar{\chi}\sigma^{\mu}{}_{\lambda}\psi\bar{\psi}\sigma^{\lambda\nu}\chi + \bar{\psi}\sigma^{\mu}{}_{\lambda}\gamma_5\chi\bar{\chi}\sigma^{\lambda\nu}\gamma_5\psi - \bar{\chi}\sigma^{\mu}{}_{\lambda}\gamma_5\psi\bar{\chi}\sigma^{\lambda\nu}\gamma_5\chi\right) \\ & \qquad + \left(\bar{\psi}\sigma^{\mu}{}_{\lambda}\gamma_5\chi\bar{\chi}\sigma^{\lambda\nu}\psi + \bar{\psi}\sigma^{\mu}{}_{\lambda}\chi\bar{\chi}\sigma^{\lambda\nu}\gamma_5\psi + \bar{\chi}\sigma^{\mu}{}_{\lambda}\gamma_5\psi\bar{\chi}\sigma^{\lambda\nu}\chi + \bar{\chi}\sigma^{\mu}{}_{\lambda}\psi\bar{\psi}\sigma^{\lambda\nu}\gamma_5\chi\right)\Big]\,. \end{aligned} \tag{C.27}$$

Once multiplied with the field-strength tensors, many operators of this class simplify depending on their color contractions. We list the operators presented in this section with all allowed (non-vanishing) contractions with field-strength tensors in Tables C.3–C.6.

C.3.4 | Operator class $\psi^4 D^2$

The fermion multilinears in the class $\psi^4 D^2$ have the simplest structure and (ignoring the derivatives for now) either appear as quadrilinears consisting of two quark currents, i.e.,

$$\begin{aligned} c\,\bar\psi\gamma^\mu P_{\rm L}\psi\bar\chi\gamma_\mu P_{\rm R}\chi + \text{h.c.} = \frac{1}{2}\text{Re}\,c\,\big(&\bar\psi\gamma^\mu\psi\bar\chi\gamma_\mu\chi - \bar\psi\gamma^\mu\gamma_5\psi\bar\chi\gamma_\mu\gamma_5\chi \\ &- \bar\psi\gamma^\mu\gamma_5\psi\bar\chi\gamma_\mu\chi + \bar\psi\gamma^\mu\psi\bar\chi\gamma_\mu\gamma_5\chi\big)\,, \end{aligned} \tag{C.28}$$

$$\begin{aligned} c\,\bar\psi\gamma^\mu P_{\rm R/L}\psi\bar\chi\gamma_\mu P_{\rm R/L}\chi + \text{h.c.} = \frac{1}{2}\text{Re}\,c\,\big(&\bar\psi\gamma^\mu\psi\bar\chi\gamma_\mu\chi + \bar\psi\gamma^\mu\gamma_5\psi\bar\chi\gamma_\mu\gamma_5\chi \\ &\pm \bar\psi\gamma^\mu\gamma_5\psi\bar\chi\gamma_\mu\chi \pm \bar\psi\gamma^\mu\psi\bar\chi\gamma_\mu\gamma_5\chi\big)\,, \end{aligned} \tag{C.29}$$

and

$$\begin{aligned} c\,\bar\psi\gamma_\mu P_{\rm L}\chi\bar\chi\gamma^\mu P_{\rm R}\psi + \text{h.c.} = &\frac{1}{2}\text{Re}\,c\,\big(\bar\psi\gamma_\mu\chi\bar\chi\gamma^\mu\psi - \bar\psi\gamma_\mu\gamma_5\chi\bar\chi\gamma^\mu\gamma_5\psi\big) \\ &+ \frac{i}{2}\text{Im}\,c\,\big(\bar\psi\gamma_\mu\chi\bar\chi\gamma^\mu\gamma_5\psi - \bar\psi\gamma_\mu\gamma_5\chi\bar\chi\gamma^\mu\psi\big)\,, \end{aligned} \tag{C.30}$$

or as a product of two densities like

$$c\,\bar\psi P_{\rm R}\chi\bar\chi P_{\rm R}\psi + \text{h.c.} = \frac{1}{2}\text{Re}\,c\,\big(\bar\psi\chi\bar\chi\psi + \bar\psi\gamma_5\chi\bar\chi\gamma_5\psi\big) + \frac{i}{2}\text{Im}\,c\,\big(\bar\psi\chi\bar\chi\gamma_5\psi + \bar\psi\gamma_5\chi\bar\chi\psi\big) \tag{C.31}$$

and

$$c\,\bar\psi P_{\rm R}\psi\bar\chi P_{\rm R}\chi + \text{h.c.} = \frac{1}{2}\text{Re}\,c\,\big(\bar\psi\psi\bar\chi\chi + \bar\psi\gamma_5\psi\bar\chi\gamma_5\chi\big) + \frac{i}{2}\text{Im}\,c\,\big(\bar\psi\psi\bar\chi\gamma_5\chi + \bar\psi\gamma_5\psi\bar\chi\chi\big)\,. \tag{C.32}$$

These Dirac structures are categorized with all allowed combinations of derivatives in Tables C.7–C.10.

C.3.5 | Summary of C- and CP-odd operators

For LEFT dimension-8 ToPe operators that are chirality-breaking, i.e., they do *not* arise at dimension 8 in SMEFT and are hence suppressed with respect to the chirality-breaking dimension-7 LEFT and chirality-conserving dimension-8 LEFT operators by at least one additional inverse power of the new-physics scale Λ, we find (note that all these operators vanish for $\psi = \chi$)

$$\begin{aligned} &\big[\bar\psi\gamma^\mu\chi\bar\chi\gamma^\nu T^a\psi - \bar\psi\gamma^\mu\gamma_5\chi\bar\chi\gamma^\nu T^a\gamma_5\psi + (\psi\leftrightarrow\chi)\big]G^a_{\mu\nu}\,, \\ &i\big[\bar\psi\gamma^\mu\gamma_5\chi\bar\chi\gamma^\nu T^a\psi - \bar\psi\gamma^\mu\chi\bar\chi\gamma^\nu T^a\gamma_5\psi - (\psi\leftrightarrow\chi)\big]\tilde G^a_{\mu\nu}\,, \\ &i\big[\bar\psi T^a\chi\bar\chi\sigma^{\mu\nu}T^a\psi + \bar\psi\gamma_5 T^a\chi\bar\chi\sigma^{\mu\nu}\gamma_5 T^a\psi - (\psi\leftrightarrow\chi)\big]F_{\mu\nu}\,, \\ &id_{abc}\big[\bar\psi T^a\chi\bar\chi\sigma^{\mu\nu}T^b\psi + \bar\psi\gamma_5 T^a\chi\bar\chi\sigma^{\mu\nu}\gamma_5 T^b\psi - (\psi\leftrightarrow\chi)\big]G^c_{\mu\nu}\,, \\ &f_{abc}\big[\bar\psi T^a\chi\bar\chi\sigma^{\mu\nu}T^b\psi + \bar\psi\gamma_5 T^a\chi\bar\chi\sigma^{\mu\nu}\gamma_5 T^b\psi + (\psi\leftrightarrow\chi)\big]G^c_{\mu\nu}\,. \end{aligned} \tag{C.33}$$

The fact that these operators are indeed chirality-violating can also be understood as follows. Quark quadrilinears in which both bilinears contain an $SU(3)_C$ generator cannot originate from a coupling to a W-boson as described in detail in Sect. 5.3. Although less obvious, the same holds for the first two operators in Eq. (C.33) as they both arise from quadrilinears with the handedness $\bar{\psi}_L\gamma^\mu\chi_L\bar{\chi}_R\gamma^\nu\psi_R$. Thus, all of the operators listed above are point interactions that convert left-handed ψ and χ to respective right-handed ones.
Our results for LEFT dimension-8 ToPe operators that are chirality-conserving and a priori not necessarily suppressed by the chirality-violating dimension-7 ToPe operators read

$$
\begin{aligned}
&f_{abc}\bar{\psi}\gamma^\mu i\overleftrightarrow{D}^\nu T^a\psi\, G^b_{\mu\rho}G^{c\,\rho}_{\nu}\,,\\
&\bar{\psi}\gamma^\mu i\overleftrightarrow{D}^\nu T^a\gamma_5\psi\left(F_{\mu\rho}\tilde{G}^{a\,\rho}_{\nu}\pm F_{\nu\rho}\tilde{G}^{a\,\rho}_{\mu}\right),\\
&\left(\bar{\psi}\gamma^\mu\psi\bar{\chi}\gamma^\nu\chi\pm\bar{\psi}\gamma^\mu\gamma_5\psi\bar{\chi}\gamma^\nu\gamma_5\chi\right)F_{\mu\nu}\,,\\
&\left(\bar{\psi}\gamma^\mu T^a\psi\bar{\chi}\gamma^\nu T^a\chi\pm\bar{\psi}\gamma^\mu\gamma_5 T^a\psi\bar{\chi}\gamma^\nu\gamma_5 T^a\chi\right)F_{\mu\nu}\,,\\
&\left(\bar{\psi}\gamma^\mu\psi\bar{\chi}\gamma^\nu T^a\chi\pm\bar{\psi}\gamma^\mu\gamma_5\psi\bar{\chi}\gamma^\nu\gamma_5 T^a\chi\right)G^a_{\mu\nu}\,,\\
&f_{abc}\left(\bar{\psi}\gamma^\mu\gamma_5 T^a\psi\bar{\chi}\gamma^\nu T^b\chi\pm\bar{\psi}\gamma^\mu T^a\psi\bar{\chi}\gamma^\nu\gamma_5 T^b\chi\right)\tilde{G}^c_{\mu\nu}\,,\\
&d_{abc}\left(\bar{\psi}\gamma^\mu T^a\psi\bar{\chi}\gamma^\nu T^b\chi\pm\bar{\psi}\gamma^\mu\gamma_5 T^a\psi\bar{\chi}\gamma^\nu\gamma_5 T^b\chi\right)G^c_{\mu\nu}\,,\\
&i\left[\bar{\psi}\chi\bar{\chi}\sigma^{\mu\nu}\psi+\bar{\psi}\gamma_5\chi\bar{\chi}\sigma^{\mu\nu}\gamma_5\psi-(\psi\leftrightarrow\chi)\right]F_{\mu\nu}\,,\\
&i\left[\bar{\psi}T^a\chi\bar{\chi}\sigma^{\mu\nu}\psi+\bar{\psi}\gamma_5 T^a\chi\bar{\chi}\sigma^{\mu\nu}\gamma_5\psi-(\psi\leftrightarrow\chi)\right]G^a_{\mu\nu}\,,\\
&i\left[\bar{\psi}\chi\bar{\chi}\sigma^{\mu\nu}T^a\psi+\bar{\psi}\gamma_5\chi\bar{\chi}\sigma^{\mu\nu}\gamma_5 T^a\psi-(\psi\leftrightarrow\chi)\right]G^a_{\mu\nu}\,,\\
&\left[\bar{\psi}\sigma^{\lambda\mu}T^a\chi\bar{\chi}\sigma_{\mu\nu}\psi+\bar{\psi}\sigma^{\lambda\mu}\gamma_5 T^a\chi\bar{\chi}\sigma_{\mu\nu}\gamma_5\psi+(\psi\leftrightarrow\chi)\right]G^{a\,\nu}_{\lambda}\,,\\
&\left[\bar{\psi}\sigma^{\lambda\mu}\chi\bar{\chi}\sigma_{\mu\nu}T^a\psi+\bar{\psi}\sigma^{\lambda\mu}\gamma_5\chi\bar{\chi}\sigma_{\mu\nu}\gamma_5 T^a\psi+(\psi\leftrightarrow\chi)\right]G^{a\,\nu}_{\lambda}\,.
\end{aligned}
\tag{C.34}
$$

Note that these operators are not unique, as they depend on the LEFT operator basis and the linear combinations chosen to group respective operators together with an appropriate redefinition of the Wilson coefficients. For example, the last two operators in Eq. (C.34) are linearly dependent, which can be shown using the antisymmetry of $\sigma_{\mu\nu}$ and $G^{a\,\nu}_{\lambda}$, so that they can be understood as only one operator with an appropriately redefined Wilson coefficient. In a similar manner one can decompose all LEFT operators with '$\pm$' into two linearly independent operators each. Moreover, we remark that operators that only differ (up to an overall sign) in the interchange of ψ and χ can be summarized as one operator by adding flavor indices.

	$\bar{\psi}_{L/R}\gamma^\mu i\overleftrightarrow{D}^\nu\psi_{L/R}$	C	P	T
1a)	$\bar{\psi}\gamma^\mu i\overleftrightarrow{D}^\nu\psi\, F_{\mu\rho}F^\rho_\nu$	$+$	$+$	$+$
1b)	$\bar{\psi}\gamma^\mu i\overleftrightarrow{D}^\nu\gamma_5\psi\, F_{\mu\rho}F^\rho_\nu$	$-$	$-$	$+$
2a)	$\bar{\psi}\gamma^\mu i\overleftrightarrow{D}^\nu\psi\, G^a_{\mu\rho}G^{a\,\rho}_\nu$	$+$	$+$	$+$
2b)	$\bar{\psi}\gamma^\mu i\overleftrightarrow{D}^\nu\gamma_5\psi\, G^a_{\mu\rho}G^{a\,\rho}_\nu$	$-$	$-$	$+$
3a)	$f_{abc}\bar{\psi}\gamma^\mu i\overleftrightarrow{D}^\nu T^a\psi\, G^b_{\mu\rho}G^{c\,\rho}_\nu$	$-$	$+$	$-$
3b)	$f_{abc}\bar{\psi}\gamma^\mu i\overleftrightarrow{D}^\nu T^a\gamma_5\psi\, G^b_{\mu\rho}G^{c\,\rho}_\nu$	$+$	$-$	$-$
4a)	$d_{abc}\bar{\psi}\gamma^\mu i\overleftrightarrow{D}^\nu T^a\psi\, G^b_{\mu\rho}G^{c\,\rho}_\nu$	$+$	$+$	$+$
4b)	$d_{abc}\bar{\psi}\gamma^\mu i\overleftrightarrow{D}^\nu T^a\gamma_5\psi\, G^b_{\mu\rho}G^{c\,\rho}_\nu$	$-$	$-$	$+$
5a)	$\bar{\psi}\gamma^\mu i\overleftrightarrow{D}^\nu T^a\psi\left(F_{\mu\rho}G^{a\,\rho}_\nu \pm F_{\nu\rho}G^{a\,\rho}_\mu\right)$	$+$	$+$	$+$
5b)	$\bar{\psi}\gamma^\mu i\overleftrightarrow{D}^\nu T^a\gamma_5\psi\left(F_{\mu\rho}G^{a\,\rho}_\nu \pm F_{\nu\rho}G^{a\,\rho}_\mu\right)$	$-$	$-$	$+$
6a)	$\bar{\psi}\gamma^\mu i\overleftrightarrow{D}^\nu T^a\psi\left(F_{\mu\rho}\tilde{G}^{a\,\rho}_\nu \pm F_{\nu\rho}\tilde{G}^{a\,\rho}_\mu\right)$	$+$	$-$	$-$
6b)	$\bar{\psi}\gamma^\mu i\overleftrightarrow{D}^\nu T^a\gamma_5\psi\left(F_{\mu\rho}\tilde{G}^{a\,\rho}_\nu \pm F_{\nu\rho}\tilde{G}^{a\,\rho}_\mu\right)$	$-$	$+$	$-$
7a)	$f_{abc}\bar{\psi}\gamma^\mu i\overleftrightarrow{D}^\nu T^a\psi\left(G^b_{\mu\rho}\tilde{G}^{c\,\rho}_\nu \pm \tilde{G}^b_{\nu\rho}G^{c\,\rho}_\mu\right)$	$-$	$-$	$+$
7b)	$f_{abc}\bar{\psi}\gamma^\mu i\overleftrightarrow{D}^\nu T^a\gamma_5\psi\left(G^b_{\mu\rho}\tilde{G}^{c\,\rho}_\nu \pm \tilde{G}^b_{\nu\rho}G^{c\,\rho}_\mu\right)$	$+$	$+$	$+$

Table C.2: Operators of the class ψ^2X^2D with well defined discrete space-time symmetries. All operators follow the description given in Table C.1. The operators 3a) and 6b) are C- and CP-odd. Note that for the cases 1a) to 4b) there are no operators with the dual field-strength tensor $\tilde{X}^\rho_\nu$ in the considered LEFT basis of Ref. [136].

	$\bar{\psi}_{L/R}\gamma^\mu\psi_{L/R}\bar{\chi}_{L/R}\gamma^\nu\chi_{L/R}$ & $\bar{\psi}_L\gamma^\mu\psi_L\bar{\chi}_R\gamma^\nu\chi_R$	C	P	T
1a)	$\left(\bar{\psi}\gamma^\mu\psi\bar{\chi}\gamma^\nu\chi \pm \bar{\psi}\gamma^\mu\gamma_5\psi\bar{\chi}\gamma^\nu\gamma_5\chi\right)F_{\mu\nu}$	$-$	$+$	$-$
1b)	$\left(\bar{\psi}\gamma^\mu\gamma_5\psi\bar{\chi}\gamma^\nu\chi \pm \bar{\psi}\gamma^\mu\psi\bar{\chi}\gamma^\nu\gamma_5\chi\right)F_{\mu\nu}$	$+$	$-$	$-$
2a)	$\left(\bar{\psi}\gamma^\mu\psi\bar{\chi}\gamma^\nu\chi \pm \bar{\psi}\gamma^\mu\gamma_5\psi\bar{\chi}\gamma^\nu\gamma_5\chi\right)\tilde{F}_{\mu\nu}$	$-$	$-$	$+$
2b)	$\left(\bar{\psi}\gamma^\mu\gamma_5\psi\bar{\chi}\gamma^\nu\chi \pm \bar{\psi}\gamma^\mu\psi\bar{\chi}\gamma^\nu\gamma_5\chi\right)\tilde{F}_{\mu\nu}$	$+$	$+$	$+$
3a)	$\left(\bar{\psi}\gamma^\mu T^a\psi\bar{\chi}\gamma^\nu T^a\chi \pm \bar{\psi}\gamma^\mu\gamma_5 T^a\psi\bar{\chi}\gamma^\nu\gamma_5 T^a\chi\right)F_{\mu\nu}$	$-$	$+$	$-$
3b)	$\left(\bar{\psi}\gamma^\mu\gamma_5 T^a\psi\bar{\chi}\gamma^\nu T^a\chi \pm \bar{\psi}\gamma^\mu T^a\psi\bar{\chi}\gamma^\nu\gamma_5 T^a\chi\right)F_{\mu\nu}$	$+$	$-$	$-$
4a)	$\left(\bar{\psi}\gamma^\mu T^a\psi\bar{\chi}\gamma^\nu T^a\chi \pm \bar{\psi}\gamma^\mu\gamma_5 T^a\psi\bar{\chi}\gamma^\nu\gamma_5 T^a\chi\right)\tilde{F}_{\mu\nu}$	$-$	$-$	$+$
4b)	$\left(\bar{\psi}\gamma^\mu\gamma_5 T^a\psi\bar{\chi}\gamma^\nu T^a\chi \pm \bar{\psi}\gamma^\mu T^a\psi\bar{\chi}\gamma^\nu\gamma_5 T^a\chi\right)\tilde{F}_{\mu\nu}$	$+$	$+$	$+$
5a)	$\left(\bar{\psi}\gamma^\mu\psi\bar{\chi}\gamma^\nu T^a\chi \pm \bar{\psi}\gamma^\mu\gamma_5\psi\bar{\chi}\gamma^\nu\gamma_5 T^a\chi\right)G^a_{\mu\nu}$	$-$	$+$	$-$
5b)	$\left(\bar{\psi}\gamma^\mu\gamma_5\psi\bar{\chi}\gamma^\nu T^a\chi \pm \bar{\psi}\gamma^\mu\psi\bar{\chi}\gamma^\nu\gamma_5 T^a\chi\right)G^a_{\mu\nu}$	$+$	$-$	$-$
6a)	$\left(\bar{\psi}\gamma^\mu\psi\bar{\chi}\gamma^\nu T^a\chi \pm \bar{\psi}\gamma^\mu\gamma_5\psi\bar{\chi}\gamma^\nu\gamma_5 T^a\chi\right)\tilde{G}^a_{\mu\nu}$	$-$	$-$	$+$
6b)	$\left(\bar{\psi}\gamma^\mu\gamma_5\psi\bar{\chi}\gamma^\nu T^a\chi \pm \bar{\psi}\gamma^\mu\psi\bar{\chi}\gamma^\nu\gamma_5 T^a\chi\right)\tilde{G}^a_{\mu\nu}$	$+$	$+$	$+$
7a)	$f_{abc}\left(\bar{\psi}\gamma^\mu T^a\psi\bar{\chi}\gamma^\nu T^b\chi \pm \bar{\psi}\gamma^\mu\gamma_5 T^a\psi\bar{\chi}\gamma^\nu\gamma_5 T^b\chi\right)G^c_{\mu\nu}$	$+$	$+$	$+$
7b)	$f_{abc}\left(\bar{\psi}\gamma^\mu\gamma_5 T^a\psi\bar{\chi}\gamma^\nu T^b\chi \pm \bar{\psi}\gamma^\mu T^a\psi\bar{\chi}\gamma^\nu\gamma_5 T^b\chi\right)G^c_{\mu\nu}$	$-$	$-$	$+$
8a)	$f_{abc}\left(\bar{\psi}\gamma^\mu T^a\psi\bar{\chi}\gamma^\nu T^b\chi \pm \bar{\psi}\gamma^\mu\gamma_5 T^a\psi\bar{\chi}\gamma^\nu\gamma_5 T^b\chi\right)\tilde{G}^c_{\mu\nu}$	$+$	$-$	$-$
8b)	$f_{abc}\left(\bar{\psi}\gamma^\mu\gamma_5 T^a\psi\bar{\chi}\gamma^\nu T^b\chi \pm \bar{\psi}\gamma^\mu T^a\psi\bar{\chi}\gamma^\nu\gamma_5 T^b\chi\right)\tilde{G}^c_{\mu\nu}$	$-$	$+$	$-$
9a)	$d_{abc}\left(\bar{\psi}\gamma^\mu T^a\psi\bar{\chi}\gamma^\nu T^b\chi \pm \bar{\psi}\gamma^\mu\gamma_5 T^a\psi\bar{\chi}\gamma^\nu\gamma_5 T^b\chi\right)G^c_{\mu\nu}$	$-$	$+$	$-$
9b)	$d_{abc}\left(\bar{\psi}\gamma^\mu\gamma_5 T^a\psi\bar{\chi}\gamma^\nu T^b\chi \pm \bar{\psi}\gamma^\mu T^a\psi\bar{\chi}\gamma^\nu\gamma_5 T^b\chi\right)G^c_{\mu\nu}$	$+$	$-$	$-$
10a)	$d_{abc}\left(\bar{\psi}\gamma^\mu T^a\psi\bar{\chi}\gamma^\nu T^b\chi \pm \bar{\psi}\gamma^\mu\gamma_5 T^a\psi\bar{\chi}\gamma^\nu\gamma_5 T^b\chi\right)\tilde{G}^c_{\mu\nu}$	$-$	$-$	$+$
10b)	$d_{abc}\left(\bar{\psi}\gamma^\mu\gamma_5 T^a\psi\bar{\chi}\gamma^\nu T^b\chi \pm \bar{\psi}\gamma^\mu T^a\psi\bar{\chi}\gamma^\nu\gamma_5 T^b\chi\right)\tilde{G}^c_{\mu\nu}$	$+$	$+$	$+$

Table C.3: Operators of the class $\psi^4 X$ with well defined discrete space-time symmetries. All operators follow the description given in Table C.1. The operators 1a), 3a), 5a), 8b), and 9a) are C- and CP-odd.

	$\bar{\psi}_L\gamma^\mu\chi_L\bar{\chi}_R\gamma^\nu\psi_R$	C	P	T
1a)	$(\bar{\psi}\gamma^\mu\gamma_5\chi\bar{\chi}\gamma^\nu\psi - \bar{\psi}\gamma^\mu\chi\bar{\chi}\gamma^\nu\gamma_5\psi)F_{\mu\nu}$	+	−	−
1b)	$i(\bar{\psi}\gamma^\mu\chi\bar{\chi}\gamma^\nu\psi - \bar{\psi}\gamma^\mu\gamma_5\chi\bar{\chi}\gamma^\nu\gamma_5\psi)F_{\mu\nu}$	+	+	+
2a)	$(\bar{\psi}\gamma^\mu\gamma_5\chi\bar{\chi}\gamma^\nu\psi - \bar{\psi}\gamma^\mu\chi\bar{\chi}\gamma^\nu\gamma_5\psi)\tilde{F}_{\mu\nu}$	+	+	+
2b)	$i(\bar{\psi}\gamma^\mu\chi\bar{\chi}\gamma^\nu\psi - \bar{\psi}\gamma^\mu\gamma_5\chi\bar{\chi}\gamma^\nu\gamma_5\psi)\tilde{F}_{\mu\nu}$	+	−	−
3a)	$(\bar{\psi}\gamma^\mu\gamma_5 T^a\chi\bar{\chi}\gamma^\nu T^a\psi - \bar{\psi}\gamma^\mu T^a\chi\bar{\chi}\gamma^\nu\gamma_5 T^a\psi)F_{\mu\nu}$	+	−	−
3b)	$i(\bar{\psi}\gamma^\mu T^a\chi\bar{\chi}\gamma^\nu T^a\psi - \bar{\psi}\gamma^\mu\gamma_5 T^a\chi\bar{\chi}\gamma^\nu\gamma_5 T^a\psi)F_{\mu\nu}$	+	+	+
4a)	$(\bar{\psi}\gamma^\mu\gamma_5 T^a\chi\bar{\chi}\gamma^\nu T^a\psi - \bar{\psi}\gamma^\mu T^a\chi\bar{\chi}\gamma^\nu\gamma_5 T^a\psi)\tilde{F}_{\mu\nu}$	+	+	+
4b)	$i(\bar{\psi}\gamma^\mu T^a\chi\bar{\chi}\gamma^\nu T^a\psi - \bar{\psi}\gamma^\mu\gamma_5 T^a\chi\bar{\chi}\gamma^\nu\gamma_5 T^a\psi)\tilde{F}_{\mu\nu}$	+	−	−
5a)	$\big[\bar{\psi}\gamma^\mu\chi\bar{\chi}\gamma^\nu T^a\psi - \bar{\psi}\gamma^\mu\gamma_5\chi\bar{\chi}\gamma^\nu T^a\gamma_5\psi + (\psi\leftrightarrow\chi)\big]G^a_{\mu\nu}$	−	+	−
5b)	$\big[\bar{\psi}\gamma^\mu\gamma_5\chi\bar{\chi}\gamma^\nu T^a\psi - \bar{\psi}\gamma^\mu\chi\bar{\chi}\gamma^\nu T^a\gamma_5\psi + (\psi\leftrightarrow\chi)\big]G^a_{\mu\nu}$	+	−	−
5c)	$i\big[\bar{\psi}\gamma^\mu\chi\bar{\chi}\gamma^\nu T^a\psi - \bar{\psi}\gamma^\mu\gamma_5\chi\bar{\chi}\gamma^\nu T^a\gamma_5\psi - (\psi\leftrightarrow\chi)\big]G^a_{\mu\nu}$	+	+	+
5d)	$i\big[\bar{\psi}\gamma^\mu\gamma_5\chi\bar{\chi}\gamma^\nu T^a\psi - \bar{\psi}\gamma^\mu\chi\bar{\chi}\gamma^\nu T^a\gamma_5\psi - (\psi\leftrightarrow\chi)\big]G^a_{\mu\nu}$	−	−	+
6a)	$\big[\bar{\psi}\gamma^\mu\chi\bar{\chi}\gamma^\nu T^a\psi - \bar{\psi}\gamma^\mu\gamma_5\chi\bar{\chi}\gamma^\nu T^a\gamma_5\psi + (\psi\leftrightarrow\chi)\big]\tilde{G}^a_{\mu\nu}$	−	−	+
6b)	$\big[\bar{\psi}\gamma^\mu\gamma_5\chi\bar{\chi}\gamma^\nu T^a\psi - \bar{\psi}\gamma^\mu\chi\bar{\chi}\gamma^\nu T^a\gamma_5\psi + (\psi\leftrightarrow\chi)\big]\tilde{G}^a_{\mu\nu}$	+	+	+
6c)	$i\big[\bar{\psi}\gamma^\mu\chi\bar{\chi}\gamma^\nu T^a\psi - \bar{\psi}\gamma^\mu\gamma_5\chi\bar{\chi}\gamma^\nu T^a\gamma_5\psi - (\psi\leftrightarrow\chi)\big]\tilde{G}^a_{\mu\nu}$	+	−	−
6d)	$i\big[\bar{\psi}\gamma^\mu\gamma_5\chi\bar{\chi}\gamma^\nu T^a\psi - \bar{\psi}\gamma^\mu\chi\bar{\chi}\gamma^\nu T^a\gamma_5\psi - (\psi\leftrightarrow\chi)\big]\tilde{G}^a_{\mu\nu}$	−	+	−
7a)	$if_{abc}(\bar{\psi}\gamma^\mu T^a\chi\bar{\chi}\gamma^\nu T^b\gamma_5\psi - \bar{\psi}\gamma^\mu T^a\gamma_5\chi\bar{\chi}\gamma^\nu T^b\psi)G^c_{\mu\nu}$	+	−	−
7b)	$f_{abc}(\bar{\psi}\gamma^\mu T^a\chi\bar{\chi}\gamma^\nu T^b\psi - \bar{\psi}\gamma^\mu T^a\gamma_5\chi\bar{\chi}\gamma^\nu T^b\gamma_5\psi)G^c_{\mu\nu}$	+	+	+
8a)	$if_{abc}(\bar{\psi}\gamma^\mu T^a\chi\bar{\chi}\gamma^\nu T^b\gamma_5\psi - \bar{\psi}\gamma^\mu T^a\gamma_5\chi\bar{\chi}\gamma^\nu T^b\psi)\tilde{G}^c_{\mu\nu}$	+	+	+
8b)	$f_{abc}(\bar{\psi}\gamma^\mu T^a\chi\bar{\chi}\gamma^\nu T^b\psi - \bar{\psi}\gamma^\mu T^a\gamma_5\chi\bar{\chi}\gamma^\nu T^b\gamma_5\psi)\tilde{G}^c_{\mu\nu}$	+	−	−
9)	$d_{abc}(\bar{\psi}\gamma^\mu T^a\chi\bar{\chi}\gamma^\nu T^b\gamma_5\psi - \bar{\psi}\gamma^\mu T^a\gamma_5\chi\bar{\chi}\gamma^\nu T^b\psi)G^c_{\mu\nu}$	+	−	−
10)	$d_{abc}(\bar{\psi}\gamma^\mu T^a\chi\bar{\chi}\gamma^\nu T^b\gamma_5\psi - \bar{\psi}\gamma^\mu T^a\gamma_5\chi\bar{\chi}\gamma^\nu T^b\psi)\tilde{G}^c_{\mu\nu}$	+	+	+

Table C.4: Operators of the class ψ^4X with well defined discrete space-time symmetries. All operators follow the description given in Table C.1. The operators 5a) and 6d) are C- and CP-odd.

	$\bar{\psi}_L\chi_R\bar{\chi}_L\sigma^{\mu\nu}\psi_R$	C	P	T
1a)	$i\big[\bar{\psi}\chi\bar{\chi}\sigma^{\mu\nu}\psi + \bar{\psi}\gamma_5\chi\bar{\chi}\sigma^{\mu\nu}\gamma_5\psi - (\psi \leftrightarrow \chi)\big]F_{\mu\nu}$	$-$	$+$	$-$
1b)	$i\big[\bar{\psi}\gamma_5\chi\bar{\chi}\sigma^{\mu\nu}\psi + \bar{\psi}\chi\bar{\chi}\sigma^{\mu\nu}\gamma_5\psi + (\psi \leftrightarrow \chi)\big]F_{\mu\nu}$	$+$	$-$	$-$
1c)	$\big[\bar{\psi}\chi\bar{\chi}\sigma^{\mu\nu}\psi + \bar{\psi}\gamma_5\chi\bar{\chi}\sigma^{\mu\nu}\gamma_5\psi + (\psi \leftrightarrow \chi)\big]F_{\mu\nu}$	$+$	$+$	$+$
1d)	$\big[\bar{\psi}\gamma_5\chi\bar{\chi}\sigma^{\mu\nu}\psi + \bar{\psi}\chi\bar{\chi}\sigma^{\mu\nu}\gamma_5\psi - (\psi \leftrightarrow \chi)\big]F_{\mu\nu}$	$-$	$-$	$+$
2a)	$i\big[\bar{\psi}T^a\chi\bar{\chi}\sigma^{\mu\nu}T^a\psi + \bar{\psi}\gamma_5T^a\chi\bar{\chi}\sigma^{\mu\nu}\gamma_5T^a\psi - (\psi \leftrightarrow \chi)\big]F_{\mu\nu}$	$-$	$+$	$-$
2b)	$i\big[\bar{\psi}\gamma_5T^a\chi\bar{\chi}\sigma^{\mu\nu}T^a\psi + \bar{\psi}T^a\chi\bar{\chi}\sigma^{\mu\nu}\gamma_5T^a\psi + (\psi \leftrightarrow \chi)\big]F_{\mu\nu}$	$+$	$-$	$-$
2c)	$\big[\bar{\psi}T^a\chi\bar{\chi}\sigma^{\mu\nu}T^a\psi + \bar{\psi}\gamma_5T^a\chi\bar{\chi}\sigma^{\mu\nu}\gamma_5T^a\psi + (\psi \leftrightarrow \chi)\big]F_{\mu\nu}$	$+$	$+$	$+$
2d)	$\big[\bar{\psi}\gamma_5T^a\chi\bar{\chi}\sigma^{\mu\nu}T^a\psi + \bar{\psi}T^a\chi\bar{\chi}\sigma^{\mu\nu}\gamma_5T^a\psi - (\psi \leftrightarrow \chi)\big]F_{\mu\nu}$	$-$	$-$	$+$
3a)	$i\big[\bar{\psi}T^a\chi\bar{\chi}\sigma^{\mu\nu}\psi + \bar{\psi}\gamma_5T^a\chi\bar{\chi}\sigma^{\mu\nu}\gamma_5\psi - (\psi \leftrightarrow \chi)\big]G^a_{\mu\nu}$	$-$	$+$	$-$
3b)	$i\big[\bar{\psi}\gamma_5T^a\chi\bar{\chi}\sigma^{\mu\nu}\psi + \bar{\psi}T^a\chi\bar{\chi}\sigma^{\mu\nu}\gamma_5\psi + (\psi \leftrightarrow \chi)\big]G^a_{\mu\nu}$	$+$	$-$	$-$
3c)	$\big[\bar{\psi}T^a\chi\bar{\chi}\sigma^{\mu\nu}\psi + \bar{\psi}\gamma_5T^a\chi\bar{\chi}\sigma^{\mu\nu}\gamma_5\psi + (\psi \leftrightarrow \chi)\big]G^a_{\mu\nu}$	$+$	$+$	$+$
3d)	$\big[\bar{\psi}\gamma_5T^a\chi\bar{\chi}\sigma^{\mu\nu}\psi + \bar{\psi}T^a\chi\bar{\chi}\sigma^{\mu\nu}\gamma_5\psi - (\psi \leftrightarrow \chi)\big]G^a_{\mu\nu}$	$-$	$-$	$+$
4a)	$i\big[\bar{\psi}\chi\bar{\chi}\sigma^{\mu\nu}T^a\psi + \bar{\psi}\gamma_5\chi\bar{\chi}\sigma^{\mu\nu}\gamma_5T^a\psi - (\psi \leftrightarrow \chi)\big]G^a_{\mu\nu}$	$-$	$+$	$-$
4b)	$i\big[\bar{\psi}\gamma_5\chi\bar{\chi}\sigma^{\mu\nu}T^a\psi + \bar{\psi}\chi\bar{\chi}\sigma^{\mu\nu}\gamma_5T^a\psi + (\psi \leftrightarrow \chi)\big]G^a_{\mu\nu}$	$+$	$-$	$-$
4c)	$\big[\bar{\psi}\chi\bar{\chi}\sigma^{\mu\nu}T^a\psi + \bar{\psi}\gamma_5\chi\bar{\chi}\sigma^{\mu\nu}\gamma_5T^a\psi + (\psi \leftrightarrow \chi)\big]G^a_{\mu\nu}$	$+$	$+$	$+$
4d)	$\big[\bar{\psi}\gamma_5\chi\bar{\chi}\sigma^{\mu\nu}T^a\psi + \bar{\psi}\chi\bar{\chi}\sigma^{\mu\nu}\gamma_5T^a\psi - (\psi \leftrightarrow \chi)\big]G^a_{\mu\nu}$	$-$	$-$	$+$
5a)	$id_{abc}\big[\bar{\psi}T^a\chi\bar{\chi}\sigma^{\mu\nu}T^b\psi + \bar{\psi}\gamma_5T^a\chi\bar{\chi}\sigma^{\mu\nu}\gamma_5T^b\psi - (\psi \leftrightarrow \chi)\big]G^c_{\mu\nu}$	$-$	$+$	$-$
5b)	$id_{abc}\big[\bar{\psi}\gamma_5T^a\chi\bar{\chi}\sigma^{\mu\nu}T^b\psi + \bar{\psi}T^a\chi\bar{\chi}\sigma^{\mu\nu}\gamma_5T^b\psi + (\psi \leftrightarrow \chi)\big]G^c_{\mu\nu}$	$+$	$-$	$-$
5c)	$d_{abc}\big[\bar{\psi}T^a\chi\bar{\chi}\sigma^{\mu\nu}T^b\psi + \bar{\psi}\gamma_5T^a\chi\bar{\chi}\sigma^{\mu\nu}\gamma_5T^b\psi + (\psi \leftrightarrow \chi)\big]G^c_{\mu\nu}$	$+$	$+$	$+$
5d)	$d_{abc}\big[\bar{\psi}\gamma_5T^a\chi\bar{\chi}\sigma^{\mu\nu}T^b\psi + \bar{\psi}T^a\chi\bar{\chi}\sigma^{\mu\nu}\gamma_5T^b\psi - (\psi \leftrightarrow \chi)\big]G^c_{\mu\nu}$	$-$	$-$	$+$
6a)	$if_{abc}\big[\bar{\psi}T^a\chi\bar{\chi}\sigma^{\mu\nu}T^b\psi + \bar{\psi}\gamma_5T^a\chi\bar{\chi}\sigma^{\mu\nu}\gamma_5T^b\psi - (\psi \leftrightarrow \chi)\big]G^c_{\mu\nu}$	$+$	$+$	$+$
6b)	$if_{abc}\big[\bar{\psi}\gamma_5T^a\chi\bar{\chi}\sigma^{\mu\nu}T^b\psi + \bar{\psi}T^a\chi\bar{\chi}\sigma^{\mu\nu}\gamma_5T^b\psi + (\psi \leftrightarrow \chi)\big]G^c_{\mu\nu}$	$-$	$-$	$+$
6c)	$f_{abc}\big[\bar{\psi}T^a\chi\bar{\chi}\sigma^{\mu\nu}T^b\psi + \bar{\psi}\gamma_5T^a\chi\bar{\chi}\sigma^{\mu\nu}\gamma_5T^b\psi + (\psi \leftrightarrow \chi)\big]G^c_{\mu\nu}$	$-$	$+$	$-$
6d)	$f_{abc}\big[\bar{\psi}\gamma_5T^a\chi\bar{\chi}\sigma^{\mu\nu}T^b\psi + \bar{\psi}T^a\chi\bar{\chi}\sigma^{\mu\nu}\gamma_5T^b\psi - (\psi \leftrightarrow \chi)\big]G^c_{\mu\nu}$	$+$	$-$	$-$

Table C.5: Operators of the class ψ^4X with well-defined discrete space-time symmetries. All operators follow the description given in Table C.1. The operators 1a), 2a), 3a), 4a), 5a), and 6c) are C- and CP-odd. Note that there are no operators with the dual field-strength tensor $\tilde{X}^\rho_\nu$ in the considered LEFT basis of Ref. [136].

	$\bar{\psi}_L\sigma^{\lambda\mu}\chi_R\bar{\chi}_L\sigma_{\mu\nu}\psi_R$	C	P	T
1a)	$i\big[\bar{\psi}\sigma^{\lambda\mu}\chi\bar{\chi}\sigma_{\mu\nu}\psi + \bar{\psi}\sigma^{\lambda\mu}\gamma_5\chi\bar{\chi}\sigma_{\mu\nu}\gamma_5\psi)\big]F^\nu_\lambda$	+	+	+
1b)	$\big[\bar{\psi}\sigma^{\lambda\mu}\gamma_5\chi\bar{\chi}\sigma_{\mu\nu}\psi + \bar{\psi}\sigma^{\lambda\mu}\chi\bar{\chi}\sigma_{\mu\nu}\gamma_5\psi\big]F^\nu_\lambda$	+	−	−
2a)	$i\big[\bar{\psi}\sigma^{\lambda\mu}T^a\chi\bar{\chi}\sigma_{\mu\nu}T^a\psi + \bar{\psi}\sigma^{\lambda\mu}\gamma_5T^a\chi\bar{\chi}\sigma_{\mu\nu}\gamma_5T^a\psi\big]F^\nu_\lambda$	+	+	+
2b)	$\big[\bar{\psi}\sigma^{\lambda\mu}\gamma_5T^a\chi\bar{\chi}\sigma_{\mu\nu}T^a\psi + \bar{\psi}\sigma^{\lambda\mu}T^a\chi\bar{\chi}\sigma_{\mu\nu}\gamma_5T^a\psi\big]F^\nu_\lambda$	+	−	−
3a)	$i\big[\bar{\psi}\sigma^{\lambda\mu}T^a\chi\bar{\chi}\sigma_{\mu\nu}\psi + \bar{\psi}\sigma^{\lambda\mu}\gamma_5T^a\chi\bar{\chi}\sigma_{\mu\nu}\gamma_5\psi - (\psi\leftrightarrow\chi)\big]G^{a\,\nu}_\lambda$	+	+	+
3b)	$i\big[\bar{\psi}\sigma^{\lambda\mu}\gamma_5T^a\chi\bar{\chi}\sigma_{\mu\nu}\psi + \bar{\psi}\sigma^{\lambda\mu}T^a\chi\bar{\chi}\sigma_{\mu\nu}\gamma_5\psi + (\psi\leftrightarrow\chi)\big]G^{a\,\nu}_\lambda$	−	−	+
3c)	$\big[\bar{\psi}\sigma^{\lambda\mu}T^a\chi\bar{\chi}\sigma_{\mu\nu}\psi + \bar{\psi}\sigma^{\lambda\mu}\gamma_5T^a\chi\bar{\chi}\sigma_{\mu\nu}\gamma_5\psi + (\psi\leftrightarrow\chi)\big]G^{a\,\nu}_\lambda$	−	+	−
3d)	$\big[\bar{\psi}\sigma^{\lambda\mu}\gamma_5T^a\chi\bar{\chi}\sigma_{\mu\nu}\psi + \bar{\psi}\sigma^{\lambda\mu}T^a\chi\bar{\chi}\sigma_{\mu\nu}\gamma_5\psi - (\psi\leftrightarrow\chi)\big]G^{a\,\nu}_\lambda$	+	−	−
4a)	$i\big[\bar{\psi}\sigma^{\lambda\mu}\chi\bar{\chi}\sigma_{\mu\nu}T^a\psi + \bar{\psi}\sigma^{\lambda\mu}\gamma_5\chi\bar{\chi}\sigma_{\mu\nu}\gamma_5T^a\psi - (\psi\leftrightarrow\chi)\big]G^{a\,\nu}_\lambda$	+	+	+
4b)	$i\big[\bar{\psi}\sigma^{\lambda\mu}\gamma_5\chi\bar{\chi}\sigma_{\mu\nu}T^a\psi + \bar{\psi}\sigma^{\lambda\mu}\chi\bar{\chi}\sigma_{\mu\nu}\gamma_5T^a\psi + (\psi\leftrightarrow\chi)\big]G^{a\,\nu}_\lambda$	−	−	+
4c)	$\big[\bar{\psi}\sigma^{\lambda\mu}\chi\bar{\chi}\sigma_{\mu\nu}T^a\psi + \bar{\psi}\gamma_5\chi\bar{\chi}\sigma_{\mu\nu}\gamma_5T^a\psi + (\psi\leftrightarrow\chi)\big]G^{a\,\nu}_\lambda$	−	+	−
4d)	$\big[\bar{\psi}\sigma^{\lambda\mu}\gamma_5\chi\bar{\chi}\sigma_{\mu\nu}T^a\psi + \bar{\psi}\sigma^{\lambda\mu}\chi\bar{\chi}\sigma_{\mu\nu}\gamma_5T^a\psi - (\psi\leftrightarrow\chi)\big]G^{a\,\nu}_\lambda$	+	−	−
5a)	$id_{abc}\big[\bar{\psi}\sigma^{\lambda\mu}T^a\chi\bar{\chi}\sigma_{\mu\nu}T^b\psi + \bar{\psi}\sigma^{\lambda\mu}\gamma_5T^a\chi\bar{\chi}\sigma_{\mu\nu}\gamma_5T^b\psi\big]G^{c\,\nu}_\lambda$	+	+	+
5b)	$d_{abc}\big[\bar{\psi}\sigma^{\lambda\mu}\gamma_5T^a\chi\bar{\chi}\sigma_{\mu\nu}T^b\psi + \bar{\psi}\sigma^{\lambda\mu}T^a\chi\bar{\chi}\sigma_{\mu\nu}\gamma_5T^b\psi\big]G^{c\,\nu}_\lambda$	+	−	−
6a)	$if_{abc}\big[\bar{\psi}\sigma^{\lambda\mu}\gamma_5T^a\chi\bar{\chi}\sigma_{\mu\nu}T^b\psi + \bar{\psi}\sigma^{\lambda\mu}T^a\chi\bar{\chi}\sigma_{\mu\nu}\gamma_5T^b\psi)\big]G^{c\,\nu}_\lambda$	+	−	−
6b)	$f_{abc}\big[\bar{\psi}\sigma^{\lambda\mu}T^a\chi\bar{\chi}\sigma_{\mu\nu}T^b\psi + \bar{\psi}\sigma^{\lambda\mu}\gamma_5T^a\chi\bar{\chi}\sigma_{\mu\nu}\gamma_5T^b\psi\big]G^{c\,\nu}_\lambda$	+	+	+

Table C.6: Operators of the class ψ^4X with well defined discrete space-time symmetries. All operators follow the description given in Table C.1. The operators 3c) and 4c) are C- and CP-odd. Note that there are no operators with the dual field-strength tensor $\tilde{X}^\rho_\nu$ in the considered LEFT basis of Ref. [136].

	$\bar{\psi}_{L/R}\gamma_\mu\psi_{L/R}\bar{\chi}_{L/R}\gamma^\mu\chi_{L/R}$ & $\bar{\psi}_{L/R}\gamma_\mu\psi_{L/R}\bar{\chi}_{R/L}\gamma^\mu\chi_{R/L}$	C	P	T
1a)	$D_\nu(\bar{\psi}\gamma_\mu\psi)D^\nu(\bar{\chi}\gamma^\mu\chi) \pm D_\nu(\bar{\psi}\gamma_\mu\gamma_5\psi)D^\nu(\bar{\chi}\gamma^\mu\gamma_5\chi)$	+	+	+
1b)	$D_\nu(\bar{\psi}\gamma_\mu\psi)D^\nu(\bar{\chi}\gamma^\mu\gamma_5\chi) \pm D_\nu(\bar{\psi}\gamma_\mu\gamma_5\psi)D^\nu(\bar{\chi}\gamma^\mu\chi)$	−	−	+
2a)	$\bar{\psi}\gamma_\mu\overleftrightarrow{D}_\nu\psi\bar{\chi}\gamma^\mu\overleftrightarrow{D}^\nu\chi \pm \bar{\psi}\gamma_\mu\gamma_5\overleftrightarrow{D}_\nu\psi\bar{\chi}\gamma^\mu\gamma_5\overleftrightarrow{D}^\nu\chi$	+	+	+
2b)	$\bar{\psi}\gamma_\mu\overleftrightarrow{D}_\nu\psi\bar{\chi}\gamma^\mu\overleftrightarrow{D}^\nu\gamma_5\chi \pm \bar{\psi}\gamma_\mu\gamma_5\overleftrightarrow{D}_\nu\psi\bar{\chi}\gamma^\mu\overleftrightarrow{D}^\nu\chi$	−	−	+
3a)	$D_\nu(\bar{\psi}\gamma_\mu T^a\psi)D^\nu(\bar{\chi}\gamma^\mu T^a\chi) \pm D_\nu(\bar{\psi}\gamma_\mu\gamma_5 T^a\psi)D^\nu(\bar{\chi}\gamma^\mu\gamma_5 T^a\chi)$	+	+	+
3b)	$D_\nu(\bar{\psi}\gamma_\mu T^a\psi)D^\nu(\bar{\chi}\gamma^\mu\gamma_5 T^a\chi) \pm D_\nu(\bar{\psi}\gamma_\mu\gamma_5 T^a\psi)D^\nu(\bar{\chi}\gamma^\mu T^a\chi)$	−	−	+
4a)	$\bar{\psi}\gamma_\mu\overleftrightarrow{D}_\nu T^a\psi\bar{\chi}\gamma^\mu\overleftrightarrow{D}^\nu T^a\chi \pm \bar{\psi}\gamma_\mu\gamma_5\overleftrightarrow{D}_\nu T^a\psi\bar{\chi}\gamma^\mu\gamma_5\overleftrightarrow{D}^\nu T^a\chi$	+	+	+
4b)	$\bar{\psi}\gamma_\mu\overleftrightarrow{D}_\nu T^a\psi\bar{\chi}\gamma^\mu\overleftrightarrow{D}^\nu\gamma_5 T^a\chi \pm \bar{\psi}\gamma_\mu\gamma_5\overleftrightarrow{D}_\nu T^a\psi\bar{\chi}\gamma^\mu\overleftrightarrow{D}^\nu T^a\chi$	−	−	+

Table C.7: Operators of the class ψ^4D^2 with well defined discrete space-time symmetries. All operators follow the description given in Table C.1. None of these operators is C- and CP-odd.

	$\bar{\psi}_L\gamma_\mu\chi_L\bar{\chi}_R\gamma^\mu\psi_R$	C	P	T
1a)	$D_\nu(\bar{\psi}\gamma_\mu\chi)D^\nu(\bar{\chi}\gamma^\mu\psi) - D_\nu(\bar{\psi}\gamma_\mu\gamma_5\chi)D^\nu(\bar{\chi}\gamma^\mu\gamma_5\psi)$	+	+	+
1b)	$i\big[D_\nu(\bar{\psi}\gamma_\mu\chi)D^\nu(\bar{\chi}\gamma^\mu\gamma_5\psi) - D_\nu(\bar{\psi}\gamma_\mu\gamma_5\chi)D^\nu(\bar{\chi}\gamma^\mu\psi)\big]$	+	−	−
2a)	$\bar{\psi}\gamma_\mu\overleftrightarrow{D}_\nu\chi\bar{\chi}\gamma^\mu\overleftrightarrow{D}^\nu\psi - \bar{\psi}\gamma_\mu\gamma_5\overleftrightarrow{D}_\nu\chi\bar{\chi}\gamma^\mu\gamma_5\overleftrightarrow{D}^\nu\psi$	+	+	+
2b)	$i\big[\bar{\psi}\gamma_\mu\overleftrightarrow{D}_\nu\chi\bar{\chi}\gamma^\mu\overleftrightarrow{D}^\nu\gamma_5\psi - \bar{\psi}\gamma_\mu\gamma_5\overleftrightarrow{D}_\nu\chi\bar{\chi}\gamma^\mu\overleftrightarrow{D}^\nu\psi\big]$	+	−	−
3a)	$D_\nu(\bar{\psi}\gamma_\mu T^a\chi)D^\nu(\bar{\chi}\gamma^\mu T^a\psi) - D_\nu(\bar{\psi}\gamma_\mu\gamma_5 T^a\chi)D^\nu(\bar{\chi}\gamma^\mu\gamma_5 T^a\psi)$	+	+	+
3b)	$i\big[D_\nu(\bar{\psi}\gamma_\mu T^a\chi)D^\nu(\bar{\chi}\gamma^\mu\gamma_5 T^a\psi) - D_\nu(\bar{\psi}\gamma_\mu\gamma_5 T^a\chi)D^\nu(\bar{\chi}\gamma^\mu T^a\psi)\big]$	+	−	−
4a)	$\bar{\psi}\gamma_\mu\overleftrightarrow{D}_\nu T^a\chi\bar{\chi}\gamma^\mu\overleftrightarrow{D}^\nu T^a\psi - \bar{\psi}\gamma_\mu\gamma_5\overleftrightarrow{D}_\nu T^a\chi\bar{\chi}\gamma^\mu\gamma_5\overleftrightarrow{D}^\nu T^a\psi$	+	+	+
4b)	$i\big[\bar{\psi}\gamma_\mu\overleftrightarrow{D}_\nu T^a\chi\bar{\chi}\gamma^\mu\overleftrightarrow{D}^\nu\gamma_5 T^a\psi - \bar{\psi}\gamma_\mu\gamma_5\overleftrightarrow{D}_\nu T^a\chi\bar{\chi}\gamma^\mu\overleftrightarrow{D}^\nu T^a\psi\big]$	+	−	−

Table C.8: Operators of the class ψ^4D^2 with well defined discrete space-time symmetries. All operators follow the description given in Table C.1. None of these operators is C- and CP-odd.

	$\bar{\psi}_L\chi_R\bar{\chi}_L\psi_R$	C	P	T
1a)	$D_\mu(\bar{\psi}\chi)D^\mu(\bar{\chi}\psi) + D_\mu(\bar{\psi}\gamma_5\chi)D^\mu(\bar{\chi}\gamma_5\psi)$	+	+	+
1b)	$i\big[D_\mu(\bar{\psi}\chi)D^\mu(\bar{\chi}\gamma_5\psi) + D_\mu(\bar{\psi}\gamma_5\chi)D^\mu(\bar{\chi}\psi)\big]$	+	−	−
2a)	$\bar{\psi}\overleftrightarrow{D}_\mu\chi\bar{\chi}\overleftrightarrow{D}^\mu\psi + \bar{\psi}\gamma_5\overleftrightarrow{D}_\mu\chi\bar{\chi}\gamma_5\overleftrightarrow{D}^\mu\psi$	+	+	+
2b)	$i\big[\bar{\psi}\overleftrightarrow{D}_\mu\chi\bar{\chi}\overleftrightarrow{D}^\mu\gamma_5\psi + \bar{\psi}\gamma_5\overleftrightarrow{D}_\mu\chi\bar{\chi}\overleftrightarrow{D}^\mu\psi\big]$	+	−	−
3a)	$D_\mu(\bar{\psi}T^a\chi)D^\mu(\bar{\chi}T^a\psi) + D_\mu(\bar{\psi}\gamma_5T^a\chi)D^\mu(\bar{\chi}\gamma_5T^a\psi)$	+	+	+
3b)	$i\big[D_\mu(\bar{\psi}T^a\chi)D^\mu(\bar{\chi}\gamma_5T^a\psi) + D_\mu(\bar{\psi}\gamma_5T^a\chi)D^\mu(\bar{\chi}T^a\psi)\big]$	+	−	−
4a)	$\bar{\psi}\overleftrightarrow{D}_\mu T^a\chi\bar{\chi}\overleftrightarrow{D}^\mu T^a\psi + \bar{\psi}\gamma_5\overleftrightarrow{D}_\mu T^a\chi\bar{\chi}\gamma_5\overleftrightarrow{D}^\mu T^a\psi$	+	+	+
4b)	$i\big[\bar{\psi}\overleftrightarrow{D}_\mu T^a\chi\bar{\chi}\overleftrightarrow{D}^\mu\gamma_5T^a\psi + \bar{\psi}\gamma_5\overleftrightarrow{D}_\mu T^a\chi\bar{\chi}\overleftrightarrow{D}^\mu T^a\psi\big]$	+	−	−

Table C.9: Operators of the class ψ^4D^2 with well defined discrete space-time symmetries. All operators follow the description given in Table C.1. None of these operators is C- and CP-odd.

	$\bar{\psi}_L\psi_R\bar{\chi}_L\chi_R$	C	P	T
1a)	$D_\mu(\bar{\psi}\psi)D^\mu(\bar{\chi}\chi) + D_\mu(\bar{\psi}\gamma_5\psi)D^\mu(\bar{\chi}\gamma_5\chi)$	+	+	+
1b)	$i\big[D_\mu(\bar{\psi}\psi)D^\mu(\bar{\chi}\gamma_5\chi) + D_\mu(\bar{\psi}\gamma_5\psi)D^\mu(\bar{\chi}\chi)\big]$	+	−	−
2a)	$\bar{\psi}\overleftrightarrow{D}_\mu\psi\bar{\chi}\overleftrightarrow{D}^\mu\chi + \bar{\psi}\gamma_5\overleftrightarrow{D}_\mu\psi\bar{\chi}\gamma_5\overleftrightarrow{D}^\mu\chi$	+	+	+
2b)	$i\big[\bar{\psi}\overleftrightarrow{D}_\mu\psi\bar{\chi}\overleftrightarrow{D}^\mu\gamma_5\chi + \bar{\psi}\gamma_5\overleftrightarrow{D}_\mu\psi\bar{\chi}\overleftrightarrow{D}^\mu\chi\big]$	+	−	−
3a)	$D_\mu(\bar{\psi}T^a\psi)D^\mu(\bar{\chi}T^a\chi) + D_\mu(\bar{\psi}\gamma_5T^a\psi)D^\mu(\bar{\chi}\gamma_5T^a\chi)$	+	+	+
3b)	$i\big[D_\mu(\bar{\psi}T^a\psi)D^\mu(\bar{\chi}\gamma_5T^a\chi) + D_\mu(\bar{\psi}\gamma_5T^a\psi)D^\mu(\bar{\chi}T^a\chi)\big]$	+	−	−
4a)	$\bar{\psi}\overleftrightarrow{D}_\mu T^a\psi\bar{\chi}\overleftrightarrow{D}^\mu T^a\chi + \bar{\psi}\gamma_5\overleftrightarrow{D}_\mu T^a\psi\bar{\chi}\gamma_5\overleftrightarrow{D}^\mu T^a\chi$	+	+	+
4b)	$i\big[\bar{\psi}\overleftrightarrow{D}_\mu T^a\psi\bar{\chi}\overleftrightarrow{D}^\mu\gamma_5T^a\chi + \bar{\psi}\gamma_5\overleftrightarrow{D}_\mu T^a\psi\bar{\chi}\overleftrightarrow{D}^\mu T^a\chi\big]$	+	−	−

Table C.10: Operators of the class ψ^4D^2 with well defined discrete space-time symmetries. All operators follow the description given in Table C.1. None of these operators is C- and CP-odd.

Appendix D

Irreducible representations of $SU(3)_L \times SU(3)_R$

Although it turned out that the decomposition of LEFT operators into explicit irreducible representations of $SU(3)_L \times SU(3)_R$ is not necessary to derive the corresponding ToPeχPT operators, we still would like to comment on the derivation of Eq. (6.19) and related expressions. The following considerations are taken from Refs. [358, 359].

We denote quark triplets (they belong to the representation $\mathbf{3}$) by u^i, v^i and use lower indices for antiquark triplets (they belong to the representation $\bar{\mathbf{3}}$), i.e., u_i, v_i. The decompositions we show below apply to $SU(3)_L$ and $SU(3)_R$ separately, i.e., these groups act in different spaces and do not interfere. Hence, we consider generic irreducible representations of $SU(3)$, which are obtained by (anti)symmetrizing the tensor products according to the respective Young tableaux and subtracting possible occurring traces. For this purpose, one may raise and lower indices with the tensors $\delta^i_j, \epsilon^{ijk}, \epsilon_{ijk}$ that are invariant under $SU(3)$.

Start with the simple example of $\mathbf{3} \otimes \mathbf{3}$, which reads

$$u^i v^i = \frac{1}{2}\big(u^i v^j + u^j v^i\big) + \frac{1}{2}\big(u^i v^j - u^j v^i\big) = \frac{1}{2}\big(u^i v^j + u^j v^i\big) + \frac{1}{2}\epsilon^{ijk}\epsilon_{klm} u^l v^m \,. \tag{D.1}$$

We can now read off the dimension of each summand, i.e., the number of independent non-vanishing components. Hence, the symmetric part belongs to the irrep $\mathbf{6}$, while the antisymmetric term $\epsilon_{klm} u^l v^m$ with one lower index corresponds to $\bar{\mathbf{3}}$. We can therefore write

$$\mathbf{3} \otimes \mathbf{3} = \mathbf{6} \oplus \bar{\mathbf{3}} \,. \tag{D.2}$$

Analogously, the tensor product $\bar{\mathbf{3}} \otimes \bar{\mathbf{3}}$ yields

$$u_i v_i = \frac{1}{2}\big(u_i v_j + u_j v_i\big) + \frac{1}{2}\big(u_i v_j - u_j v_i\big) = \frac{1}{2}\big(u_i v_j + u_j v_i\big) + \frac{1}{2}\epsilon_{ijk}\epsilon^{klm} u_l v_m \tag{D.3}$$

and thus

$$\bar{\mathbf{3}} \otimes \bar{\mathbf{3}} = \bar{\mathbf{6}} \oplus \mathbf{3} \,, \tag{D.4}$$

while $\mathbf{3} \otimes \bar{\mathbf{3}}$ decomposes as

$$u^i v_j = \big(u^i v_j - \frac{1}{3}\delta^i_j u^k v_k\big) + \frac{1}{3}\delta^i_j u^k v_k = u^i_j + \frac{1}{3}\delta^i_j u^k v_k, \tag{D.5}$$

which means

$$\mathbf{3} \otimes \bar{\mathbf{3}} = \mathbf{8} \oplus \mathbf{1} \,. \tag{D.6}$$

Note that these three cases represent all combinations of any quark bilinear.

In order to work out the tensor product of operators with more than two quarks, we

introduce for certain combinations of different quarks, which are associated with $u, v, \tilde{u}, \tilde{v}$, the shorthand notations

$$u^i_j \equiv u^i v_j - \frac{1}{3}(u\cdot v)\,, \quad v^i_j \equiv \tilde{u}^i \tilde{v}_j - \frac{1}{3}(\tilde{u}\cdot\tilde{v})\,, \quad u\cdot v \equiv u^k v_k\,, \qquad \tilde{u}\cdot\tilde{v} \equiv \tilde{u}^k\tilde{v}_k\,. \tag{D.7}$$

With this we can for instance calculate $\mathbf{3}\otimes\mathbf{8}$, yielding

$$\begin{aligned} u^i v^j_k =& \frac{1}{2}\big(u^i v^j_k + u^j v^i_k - \frac{1}{4}\delta^i_k u^l v^j_l - \frac{1}{4}\delta^j_k u^l v^i_l\big) + \frac{1}{4}\epsilon^{ijl}\big(\epsilon_{lmn}u^m v^n_k + \epsilon_{kmn}u^m v^n_l\big) \\ &+ \frac{1}{8}\big(3\delta^i_k u^l v^j_l - \delta^j_k u^l v^i_l\big)\,, \end{aligned} \tag{D.8}$$

i.e.,

$$\mathbf{3}\otimes\mathbf{8} = \mathbf{15}\oplus\bar{\mathbf{6}}\oplus\mathbf{3}\,, \tag{D.9}$$

or

$$\begin{aligned} u_i v^j_k =& \frac{1}{2}\big(u_i v^j_k + u_k v^j_i - \frac{1}{4}\delta^j_i u_l v^l_k - \frac{1}{4}\delta^j_k u_l v^l_i\big) + \frac{1}{4}\epsilon_{ikl}\big(\epsilon_{lmn}u_m v^j_n + \epsilon_{jmn}u_m v^l_n\big) \\ &+ \frac{1}{8}\big(3\delta^j_i u_l v^l_k - \delta^j_k u_l v^l_i\big)\,, \end{aligned} \tag{D.10}$$

indicating

$$\bar{\mathbf{3}}\otimes\mathbf{8} = \overline{\mathbf{15}}\oplus\mathbf{6}\oplus\bar{\mathbf{3}}\,. \tag{D.11}$$

The two decompositions in Eqs. (D.9) and (D.11) give rise to Eq. (6.19). For the latter the $\mathbf{6}$ and $\bar{\mathbf{6}}$ contributions drop out because the considered operator is symmetric in the quark triplets forming the $\mathbf{8}$. As a last example, we consider the tensor product $\mathbf{8}\otimes\mathbf{8}$, including four free indices in total. We simplify the results indicating symmetric pairs of indices by parentheses, e.g., $u^{(i}v^{j)} = u^i v^j + u^j v^i$, and antisymmetric ones by brackets, e.g., $u^{[i}v^{j]} = u^i v^j - u^j v^i$. The corresponding decomposition is

$$u^i_j v^k_l = \frac{1}{2}\big(u^i_j v^k_l + u^k_l v^i_j\big) + \frac{1}{2}\big(u^i_j v^k_l - u^k_l v^i_j\big) \equiv S^{ik}_{jl} + A^{ik}_{jl}\,. \tag{D.12}$$

This gives rise to

$$\mathbf{8}\otimes\mathbf{8} = \mathbf{27}\oplus\mathbf{8}_\mathrm{S}\oplus\mathbf{1}\oplus\mathbf{10}\oplus\overline{\mathbf{10}}\oplus\mathbf{8}_\mathrm{A}\,, \tag{D.13}$$

where the first three summands $\mathbf{27}\oplus\mathbf{8}_\mathrm{S}\oplus\mathbf{1}$ contribute to a symmetric tensor $S^{ik}_{jl} = S^{ki}_{lj}$, while the direct sum $\mathbf{10}\oplus\overline{\mathbf{10}}\oplus\mathbf{8}_\mathrm{A}$ yields an antisymmetric tensor $A^{ik}_{jl} = -A^{ki}_{lj}$ [360]. A rather tedious computation of each irrep reveals [359]

$$\begin{aligned} \mathbf{27} &= \frac{1}{4}u^{(i}_{(j}v^{k)}_{l)} - \frac{1}{20}\Big[\delta^{(i}_{(j}u^{k)}_{m}v^{m}_{l)} + \delta^{(i}_{(j}u^{m}_{l)}v^{k)}_{m}\Big] + \frac{1}{40}\delta^{(i}_{(j}\delta^{k)}_{l)}(u\cdot v)\,, \\ \mathbf{8}_\mathrm{S} &= \frac{1}{4}u^{[i}_{[j}v^{k]}_{l]} + \frac{1}{20}\Big[\delta^{(i}_{(j}u^{k)}_{m}v^{m}_{l)} + \delta^{(i}_{(j}u^{m}_{l)}v^{k)}_{m}\Big] - \frac{1}{15}\delta^{(i}_{(j}\delta^{k)}_{l)}(u\cdot v) + \frac{1}{12}\delta^{[i}_{[j}\delta^{k]}_{l]}(u\cdot v)\,, \\ \mathbf{1} &= \frac{1}{24}\delta^{(i}_{(j}\delta^{k)}_{l)}(u\cdot v) - \frac{1}{12}\delta^{[i}_{[j}\delta^{k]}_{l]}(u\cdot v) \end{aligned} \tag{D.14}$$

for the contributions adding up to the symmetric tensor $S^{ik}_{jl} = \frac{1}{2}\big(u^i_j v^k_l + u^k_l v^i_j\big)$ and

$$\begin{aligned}
\mathbf{10} &= \frac{1}{4} u^{(i}_{[j} v^{k)}_{l]} - \frac{1}{12} \delta^{(i}_{[j} u^{k)}_{m} v^{m}_{l]} + \frac{1}{12} \delta^{(i}_{[j} u^{m}_{l]} v^{k)}_{m} \,, \\
\overline{\mathbf{10}} &= \frac{1}{4} u^{[i}_{(j} v^{k]}_{l)} + \frac{1}{12} \delta^{[i}_{(j} u^{k]}_{m} v^{m}_{l)} - \frac{1}{12} \delta^{[i}_{(j} u^{m}_{l)} v^{k]}_{m} \,, \\
\mathbf{8}_{\mathrm{A}} &= \frac{1}{12} \Big[\delta^{(i}_{[j} u^{k)}_{m} v^{m}_{l]} - \delta^{(i}_{[j} u^{m}_{l]} v^{k)}_{m} - \delta^{[i}_{(j} u^{k]}_{m} v^{m}_{l)} + \delta^{[i}_{(j} u^{m}_{l)} v^{k]}_{m} \Big]
\end{aligned} \tag{D.15}$$

for the contributions adding up to the antisymmetric tensor $A^{ik}_{jl} = \frac{1}{2}\big(u^i_j v^k_l - u^k_l v^i_j\big)$.

Appendix E

Numerical implementation of dispersive integrals

This appendix summarizes important aspects considering the numerical implementation of the Khuri–Treiman-type dispersion relations. Most concepts of the implementation strategies presented below follow the previous works in Refs. [82, 84, 87, 88], however, for the sake of readability, we refrain from citing these references in every section.[1]

Before we dive straight into the technical details, would like to emphasize two intricacies in the evaluation of the KT equations that have to be taken into account. First, we need a complex deformation of the integration contour to avoid crossing the unitarity cut when evaluating the angular averages from Eqs. (3.106) and (3.107). Secondly, the dispersion integrals in Eq. (3.103) themselves have poles for physical values of the Mandelstam variables as demanded by unitarity, which can be handled by appropriate algebraic reformulations of the respective integrands.

This appendix is structured in the following way. First, we show a numerically stable integration of the Omnès function in Sect. E.1. The required contour deformation for the evaluation of the inhomogeneities proceeds in Sect. E.2 for the examples of the $\eta^{(\prime)} \to 3\pi$ and $\eta' \to \eta\pi\pi$. Subsequently, we discuss the implementation of the respective dispersion integrals in Sect. E.3. A discussion about the numerically stable implementation of occurring removable singularities can be found in Sect. E.4. Finally, we introduce the iterative strategy to solve the coupled integral equations and provide explicit plots for the solutions of the single-variable functions and respective inhomogenities in Sect. E.5.

E.1 | Omnès function

As a warm up, let us start with the implementation of the Omnès function

$$\Omega(s \pm i\epsilon) = \exp\left(\frac{s}{\pi}\int_{s_{\text{th}}}^{\infty} \frac{\delta(x)}{x(x - s \mp i\epsilon)}\,\mathrm{d}x\right) \tag{E.1}$$

as given in Eq. (3.86). For simplicity we drop indices denoting the isospin and partial wave. A naive numerical evaluation of the dispersion integral is doomed to fail, because the integral has poles for physical s along the right-hand cut, as demanded by unitarity, known as *Cauchy singularities*. In other words, we encounter one singularity for each value of $s > s_{\text{th}}$ and none for $s < s_{\text{th}}$ and $s \in \mathbb{C}$.

[1] Note that in this chapter we also correct some typographical errors and notational abuses occurring in some of the cited references.

To evaluate the dispersion integral for $s > s_{\text{th}}$, we add $0 = \delta(s) - \delta(s)$ in the numerator to rewrite the Omnès function as

$$\Omega(s \pm i\epsilon) = \exp\left(\frac{s}{\pi}\int_{s_{\text{th}}}^{\infty} \frac{\delta(x)-\delta(s)}{x(x-s\mp i\epsilon)}\,\mathrm{d}x + \frac{s}{\pi}\int_{s_{\text{th}}}^{\infty}\frac{\delta(s)}{x(x-s\mp i\epsilon)}\,\mathrm{d}x\right). \tag{E.2}$$

This simple trick leads to a removable singularity in the first integral, which can now be carried out numerically. The second integral, in turn, can be evaluated analytically with the Sokhotski–Plemelj theorem stating that

$$\lim_{\epsilon\to 0^+}\int \frac{f(x)}{x-s\pm i\epsilon}\,\mathrm{d}x = \fint \frac{f(x)}{x-s}\,\mathrm{d}x \mp i\pi\int f(x)\,\delta(x-s)\,\mathrm{d}x \tag{E.3}$$

holds for any holomorphic function $f(x)$. The first integral on the right-hand side denotes the respective Cauchy principal value. The latter is defined as

$$\fint_a^c g(x)\,\mathrm{d}x = \lim_{\epsilon\to 0}\left(\int_a^{b-\epsilon} g(x)\,\mathrm{d}x + \int_{b+\epsilon}^c g(x)\,\mathrm{d}x\right), \tag{E.4}$$

where a singularity occurs at $g(b)$. Using this and a subsequent partial-fraction decomposition, we can evaluate the second summand in Eq. (E.2) and obtain

$$\Omega(s\pm i\epsilon) = \exp\left(\frac{s}{\pi}\int_{s_{\text{th}}}^{\infty}\frac{\delta(x)-\delta(s)}{x(x-s)}\,\mathrm{d}x + \frac{\delta(s)}{\pi}\,\ln\left(\left|\frac{s_{\text{th}}}{s_{\text{th}}-s}\right|\right) \pm i\delta(s)\right), \tag{E.5}$$

which can now be computed by numerical integration. Note that the evaluation of the Omnès function above or below the cut changes the sign of $i\delta(s)$ in the exponential.
This expression is also useful to work out the asymptotic behaviour of the Omnès function. As the phase shift $\delta(s)$ is supposed to converge we can set $\lim_{s\to\infty}\delta(s) = k\pi$, with some constant $k \in \mathbb{R}$. Consequently, the high-energy behaviour of the Omnès function is

$$\lim_{s\to\infty}\Omega(s\pm i\epsilon) = \exp\Bigg(\underbrace{\lim_{s\to\infty}\frac{s}{\pi}\int_{s_{\text{th}}}^{\infty}\frac{\delta(x)-\delta(s)}{x(x-s\mp i\epsilon)}\,\mathrm{d}x \pm i\,k\pi}_{\text{constant}} + k\,\ln\left(\frac{s_{\text{th}}}{s}\right)\Bigg) \sim s^{-k}. \tag{E.6}$$

Finally, we depict the Omnès functions that enter the $\eta \to 3\pi$ and $\eta' \to \eta\pi\pi$ amplitudes in Sect. 8.1 and 8.2, respectively, evaluated at arguments infinitesimally *above* the real axis in Fig. E.1. As the Omnès function fulfills Schwarz' reflection principle, which can directly be read from Eq. (E.5), the plots for an evaluation infinitesimally *below* the real axis are obtained by flipping the sign of the respective imaginary part.

E.2 | Inhomogeneities

In the following we discuss the implementation of the angular averages that drive the inhomogeneities and focus on the case of three equal masses in the final state, as in $\eta^{(\prime)} \to 3\pi$,

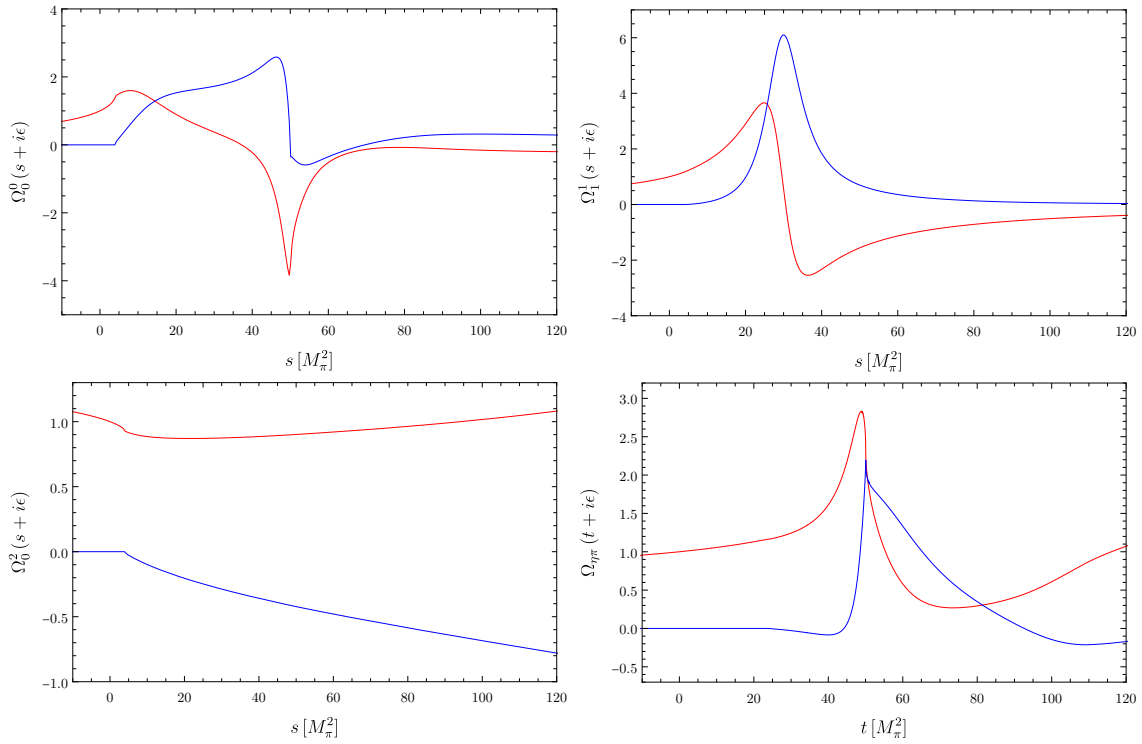

Figure E.1: Omnès functions $\Omega_\ell^I(s+i\epsilon)$ and $\Omega_{\eta\pi}(t+i\epsilon)$ with the phase input described in Sect. 8.1.4 and 8.2.4. The red curves belong to the respective real parts while the blue ones denote the imaginary parts.

and the more intricate one with two distinct masses in the final state, as in $\eta' \to \eta\pi\pi$.

Let us work with a generic inhomogeneity $\hat{\mathcal{A}}$ and drop the indices denoting partial waves and isospin. As noted in Sect. 3.4.3.2 and explicitly shown in Sects. 8.1.3 and 8.2.3, these inhomogeneities are given in terms of angular averages. We encounter three of those angular integrals, namely

$$\langle z^n \mathcal{A}(s)\rangle = \frac{1}{2}\int_{-1}^{1} \mathrm{d}z\, z^n \mathcal{A}\left(\frac{3r - s + z\kappa_{\pi\pi}(s)}{2}\right) \tag{E.7}$$

in $\eta^{(\prime)} \to 3\pi$ and $\eta' \to \eta\pi\pi$, whereas the latter additionally includes

$$\langle z^n \mathcal{A}(t)\rangle^{\pm} = \frac{1}{2}\int_{-1}^{1} \mathrm{d}z\, z^n \mathcal{A}\left(\frac{3r - t + z\kappa_{\pi\eta}(t) \pm \Delta/t}{2}\right) . \tag{E.8}$$

It is appealing to shift the information about the three-particle cut from the argument of

$\mathcal{A}$ to the integration limits by substituting[2]

$$t' = \frac{3r - s + z\kappa_{\pi\pi}(s)}{2}\,, \quad s' = \frac{3r - t + z\kappa_{\pi\eta}(t) - \Delta/t}{2}\,, \quad u' = \frac{3r - t + z\kappa_{\pi\eta}(t) + \Delta/t}{2}\,, \tag{E.9}$$

such that the angular averages become

$$\begin{aligned}
\langle z^n \mathcal{A}(s)\rangle &= \frac{1}{\kappa_{\pi\pi}^{n+1}(s)} \int_{t_-(s)}^{t_+(s)} \mathrm{d}t' \; (2t' - t_0')^n \; \mathcal{A}\left(t'\right), \\
\langle z^n \mathcal{A}(t)\rangle^- &= \frac{1}{\kappa_{\pi\eta}^{n+1}(t)} \int_{s_-(t)}^{s_+(t)} \mathrm{d}s' \; (2s' - s_0')^n \, \mathcal{A}\left(s'\right), \\
\langle z^n \mathcal{A}(t)\rangle^+ &= \frac{1}{\kappa_{\pi\eta}^{n+1}(t)} \int_{u_-(t)}^{u_+(t)} \mathrm{d}u' \, (2u' - u_0')^n \mathcal{A}\left(u'\right).
\end{aligned} \tag{E.10}$$

Here the notation was simplified by introducing $t_0' \equiv 3r - s$, $s_0' \equiv 3r - t - \Delta/t$, and $u_0' \equiv 3r - t + \Delta/t$. Remember that $3r$ equals the sum over all squared masses occurring in the decay and has to be adjusted for the respective process. With $-1 \leq z \leq +1$ the integration limits can be read off from Eq. (E.9). With this procedure we can for instance write the inhomogeneities of $\eta^{(\prime)} \to 3\pi$ for the $\Delta I = 2$ transition, cf. Eq. (8.21), as

$$\begin{aligned}
\hat{\mathcal{H}}_1(s) = \frac{1}{\kappa_{\pi\pi}^3(s)} \int_{t_-(s)}^{t_+(s)} \mathrm{d}t' \Bigg(&\frac{9}{2}(s - r)(2t' - t_0')\mathcal{H}_1(t') \\
&+ \frac{3}{2}(2t' - t_0')^2 \mathcal{H}_1(t') + 3(2t' - t_0')\mathcal{H}_2(t') \Bigg), \\
\hat{\mathcal{H}}_2(s) = \frac{1}{\kappa_{\pi\pi}(s)} \int_{t_-(s)}^{t_+(s)} \mathrm{d}t' \left(\frac{9}{2}(s - r)\mathcal{H}_1(t') + \frac{3}{2}(2t' - t_0')\mathcal{H}_1(t') - \mathcal{H}_2(t') \right),
\end{aligned} \tag{E.11}$$

and analogously for all other inhomogeneities in our dispersive representation of $\eta^{(\prime)} \to 3\pi$ and $\eta' \to \eta\pi\pi$. Note that in our applications the inhomogeneities of all S-waves are proportional to $1/\kappa$ and the ones for all P-waves are proportional to $1/\kappa^3$. At this point we omit the critical singularites arising from the zeros of κ, which will be handled later in the dispersion integral, and instead focus on the functions

$$\tilde{\mathcal{A}}(x) \equiv \kappa^{2\ell+1}(x)\hat{\mathcal{A}}(x) = \int_{y_-(x)}^{y_+(x)} \mathrm{d}y' \, \mathcal{I}(y'), \tag{E.12}$$

where $\hat{\mathcal{A}}$ is some generic inhomogeneity, κ stands for $\kappa_{\pi\pi}$ or $\kappa_{\pi\eta}$ respectively, x and y denote the respective Mandelstam variables, and $\mathcal{I}$ is the corresponding integrand, as for example given in Eq. (E.11). Still, a naive integration results in non-analyticities when crossing the three-particle cut.

[2]Note that t' and u' correspond to the definitions of the respective Mandelstam variables, but not s' (the sign of z is flipped).

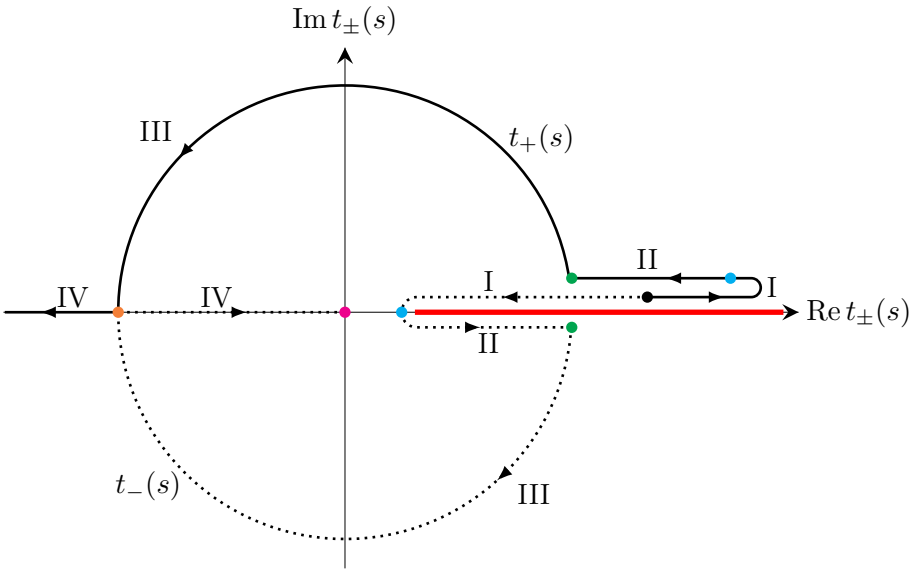

Figure E.2: Trajectories of the integration limits $t_\pm(s)$, i.e., the real and imaginary part of $t_\pm$ for varying s, which occur in the angular average $\langle z^n A(s)\rangle$. The solid (dotted) line indicates how $t_+(t_-)$ moves for increasing $s \in \mathbb{R}$. As discussed in the main text, the colored dots correspond to the start and end points of the four different integration regions.

A possible contour deformation in which the integration end points do not cross the cut is depicted in Fig. E.2 and discussed in detail below.[3] Note that the choice of complex contour is not unique, see for instance the method of Ref. [361], who even managed to carry out the angular averages trivially by instead deforming the contour of the dispersion integral, or the *horseshoe* integration in Ref. [81]. However, we stick to the strategy described in the following, which is a cumbersome but generally valid procedure ensuring for instance well-behaved analytic properties (necessary for possible analytic continuations of the single-variable amplitude, e.g. to complex values of the Mandelstam variables) and on the other hand allowing that we can directly insert analytic, or interpolated numeric expressions, for the scattering phase shifts without adapting them.

E.2.1 | $\eta^{(\prime)} \to 3\pi$

Let us break down the complex contour shown in Fig. E.2 for the decays $\eta^{(\prime)} \to 3\pi$ into four regions characterized in terms of

$$s_{\rm I} = 4M_\pi^2\,, \qquad s_{\rm II} = \frac{1}{2}(M_{\eta^{(\prime)}}^2 - M_\pi^2)\,, \qquad s_{\rm III} = (M_{\eta^{(\prime)}} - M_\pi)^2\,, \qquad s_{\rm IV} = (M_{\eta^{(\prime)}} + M_\pi)^2 \tag{E.13}$$

[3] Due to its prominent shape, physicists sometimes refer to this specific integration path as the *Pinocchio contour*. Note that the turning point at the tip of the *nose* arises naturally from the kinematic function $\kappa(s)$. For reasons of illustration we equipped the *nose* with a finite height, although it completely lies infinitesimally above the cut.

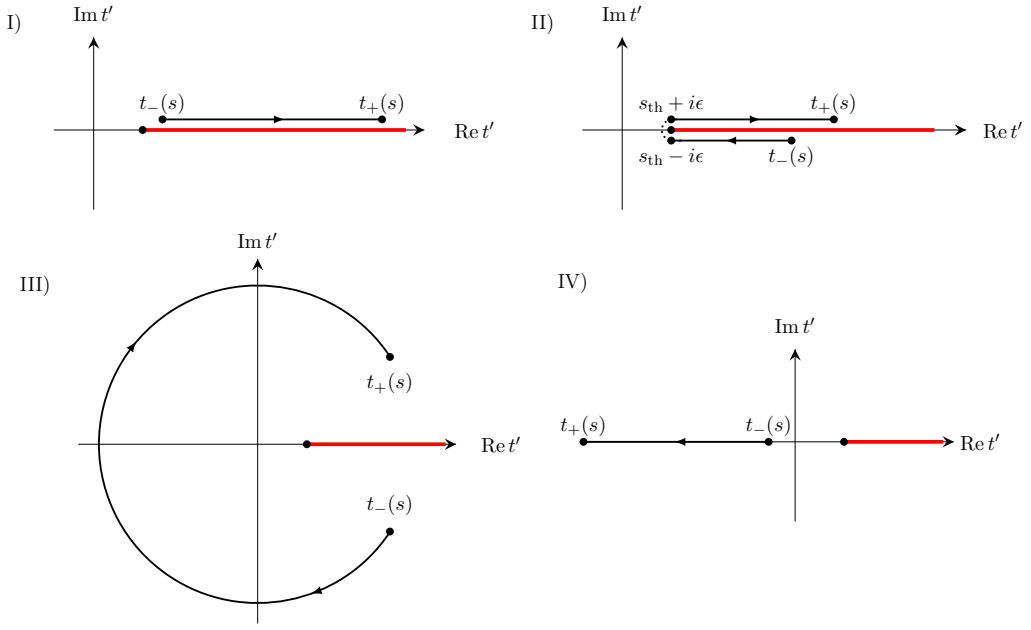

Figure E.3: Integration limits $t_\pm(s)$ in the complex t' plane for each of the four integration regions. The unitarity cut is shown by the red line. Note the different axes compared to Fig. E.2.

and have a look at the explicit formulas for $\tilde{A}$ in each region. Note that $s_{\text{I}} = s_{\text{th}}$. It is important to remark that we only need to evaluate the $\tilde{\mathcal{A}}(s)$ within the integration limits of the dispersion integral, i.e., in the interval $s \in [s_{\text{th}}, \infty)$.

For each region, we provide, based on Ref. [107], a prescription for the trajectories of $t_\pm$ from Fig. E.2. Note that the correct analytic structure requires that we implicitly treat $M_{\eta^{(\prime)}}$ as $M_{\eta^{(\prime)}} + i\epsilon$, as for instance mentioned in Refs. [84, 107, 108]. Additionally, we quote the explicit formulas we use to carry out the numeric integrations. The corresponding continuous integration contours, i.e., $t_\pm(s)$ in the complex t' plane, for each separate region is shown in Fig. E.3.

I) $\underline{s_{\text{I}} \leq s \leq s_{\text{II}}:}$
For these values of s we are in the physical decay region with $\kappa_{\pi\pi}(s) \in \mathbb{R}$. Both t_+ and t_- start at the black dot $s = s_{\text{I}}$ in Fig. E.2 and move towards the blue dots for increasing s. In the case of $s = s_{\text{II}}$ we integrate counterclockwise from the blue dot on the dashed line to the blue dot on the solid line. The endpoints in this region obey

$$\begin{aligned} t_+(s) &= \frac{1}{2}(t_0' + |\kappa_{\pi\pi}(s)|) + i\epsilon\,, \\ t_-(s) &= \frac{1}{2}(t_0' - |\kappa_{\pi\pi}(s)|) + i\epsilon\,. \end{aligned} \tag{E.14}$$

Thus an integration along a straight line from $t_-(s)$ to $t_+(s)$ does not cross the cut

and we can simply implement

$$\tilde{\mathcal{A}}(s) = \int_{t_-(s)}^{t_+(s)} \mathrm{d}t' \, \mathcal{I}\left(t' + i\epsilon\right) \,, \tag{E.15}$$

as shown in the upper left corner of Fig. E.3.

II) $\underline{s_{\mathrm{II}} < s \leq s_{\mathrm{III}} :}$
Also in this region we have $\kappa_{\pi\pi}(s) \in \mathbb{R}$. While t_+ continues its journey on the upper complex half-plane, t_- bends smoothly around the cut into the lower plane. Here we integrate for $s = s_{\mathrm{III}}$ from the green dot below the cut to the blue dot at the zero line and from the blue dot above the cut to the green dot above the cut, both in counterclockwise orientation. This behaviour is described by

$$\begin{aligned} t_+(s) &= \frac{1}{2}(t_0' + |\kappa_{\pi\pi}(s)|) + i\epsilon \,, \\ t_-(s) &= \frac{1}{2}(t_0' - |\kappa_{\pi\pi}(s)|) - i\epsilon \,. \end{aligned} \tag{E.16}$$

This time an integration along a straight line from $t_-(s)$ to $t_+(s)$ will cross the cut. Hence we need to split the integration over t' into two parts and choose

$$\tilde{\mathcal{A}}(s) = \int_{t_-(s)}^{s_{\mathrm{I}}} \mathrm{d}t' \, \mathcal{I}\left(t' - i\epsilon\right) + \int_{s_{\mathrm{I}}}^{t_+(s)} \mathrm{d}t' \, \mathcal{I}\left(t' + i\epsilon\right) \,. \tag{E.17}$$

Note that this integration still has a continuous contour. This can be seen by the fact that the integration path is point-like at threshold s_{I}, because ϵ is infinitesimally small, and therefore vanishes. This fact is illustrated by the dotted line in upper right panel of Fig. E.3.

III) $\underline{s_{\mathrm{III}} < s \leq s_{\mathrm{IV}} :}$
For these values of s we enter the unphysical region, in which $\mathrm{Re}\,\kappa_{\pi\pi}(s) = 0$. For $s = s_{\mathrm{IV}}$ we integrate counterclockwise from the orange dot to the green one below the real axis and from green dot above the real axis to the same orange dot. The trajectories in the complex $t_\pm$ plane are

$$\begin{aligned} t_+(s) &= \frac{1}{2}(t_0' + i|\kappa_{\pi\pi}(s)|) \,, \\ t_-(s) &= \frac{1}{2}(t_0' - i|\kappa_{\pi\pi}(s)|) \,. \end{aligned} \tag{E.18}$$

For a suitable parameterization of the corresponding complex arcs we stick to Ref. [83], who proposed

$$t' = t'(\varphi) \equiv R(\varphi) e^{i\varphi}. \tag{E.19}$$

Applying this contour to Eq. (E.18) we obtain

$$\begin{aligned} R(s) &= \frac{M_\pi}{\sqrt{s}}(M_{\eta^{(\prime)}} - M_\pi)(M_{\eta^{(\prime)}} + M_\pi)\,, \\ \cos\varphi(s) &= \frac{3r - s}{2M_\pi(M_{\eta^{(\prime)}} - M_\pi)(M_{\eta^{(\prime)}} + M_\pi)}\sqrt{s}\,. \end{aligned} \tag{E.20}$$

With $z_\varphi \equiv \cos\varphi$ and

$$\theta_n(z_\varphi) \equiv \frac{1}{3}\left(\arccos\left(2\frac{M_\pi^2(M_{\eta^{(\prime)}} - M_\pi)^2)(M_{\eta^{(\prime)}} + M_\pi)^2}{r^3}z_\varphi^2 - 1\right) + n\pi\right), \tag{E.21}$$

these two equations demand

$$2z_\varphi R^3 - 3rR^2 + M_\pi(M_{\eta^{(\prime)}} - M_\pi)^2(M_{\eta^{(\prime)}} + M_\pi)^2 = 0 \tag{E.22}$$

and hence

$$R(z_\varphi) = \begin{cases} \frac{r}{2z_\varphi}(1 - 2\cos\theta_0(z_\varphi)), & z_\varphi \in [-1, 0) \\ \frac{M_\pi}{\sqrt{3r}}(M_{\eta^{(\prime)}} - M_\pi)(M_{\eta^{(\prime)}} + M_\pi), & z_\varphi = 0 \\ \frac{r}{2z_\varphi}(1 + 2\cos\theta_1(z_\varphi)), & z_\varphi \in (0, 1]. \end{cases} \tag{E.23}$$

With these considerations we obtain the explicit form of the contour by

$$\tilde{\mathcal{A}} = \int\limits_{\varphi_-(s)}^{\varphi_+(s)} \mathrm{d}\varphi \frac{\mathrm{d}t'(\varphi)}{\mathrm{d}\varphi}\,\mathcal{I}(t'(\varphi))\,, \tag{E.24}$$

which is shown in the lower left of Fig. E.3. The integration limits yield[4]

$$\varphi_+(s) = \arccos\varphi(s) \quad \text{and} \quad \varphi_-(s) = 2\pi - \varphi_+(s). \tag{E.25}$$

The advantage of this parameterization is that, in this simple case of three equal masses in the final state, the contour can be describe by a single real-valued curve parameter φ.

IV) $\underline{s_{\mathrm{IV}} < s < \infty :}$
Finally we enter the physical region of scattering and have thus $\kappa_{\pi\pi}(s) \in \mathbb{R}$. In this case both integration limits are located infinitesimally above the cut, so that we drop the $i\epsilon$ prescription. We integrate for asymptotic s counterclockwise from the magenta dot to the orange one and from the orange one along the negative real axis. The

[4]Note the erroneous limits quoted in Ref. [83].

integration endpoints are[5]

$$t_+(s) = \frac{1}{2}(t_0' - |\kappa_{\pi\pi}(s)|)\,,$$
$$t_-(s) = \frac{1}{2}(t_0' + |\kappa_{\pi\pi}(s)|)\,. \tag{E.26}$$

As an integration along a straight line does not cross the cut, we evaluate

$$\tilde{\mathcal{A}}(s) = \int_{t_-(s)}^{t_+(s)} \mathrm{d}t'\, \mathcal{I}\left(t' + i\epsilon\right). \tag{E.27}$$

E.2.2 | $\eta' \to \eta\pi\pi$

The treatment of $\eta' \to \eta\pi\pi$ is more complicated than for $\eta^{(\prime)} \to 3\pi$. Due to the two different intermediate states, namely $\pi\pi$ and $\pi\eta$, we have two distinct masses in the final state and need to handle three different types of angular averages.

E.2.2.1 | s-channel

The s-channel angular averages, with $\pi\pi$ intermediate states, are of the type $\langle z^n \mathcal{A}\rangle$. Here we have to consider the integration regions marked by

$$s_{\text{th}} = 4M_\pi^2, \qquad s_{\text{II}} = M_\pi \frac{M_{\eta'}^2 - M_\eta^2}{M_\eta + M_\pi}, \qquad s_{\text{III}} = (M_{\eta'} - M_\eta)^2, \qquad s_{\text{IV}} = (M_{\eta'} + M_\eta)^2. \tag{E.28}$$

The integrations in regions I, II, and IV are completely analogous to the ones presented for $\eta^{(\prime)} \to 3\pi$, just with adjusted endpoints. However, special care has to be taken for the unphysical region III, as the previous parameterization of the arc with a single curve parameter fails in the case of two distinct masses in the final state. Instead, we follow Ref. [82], which provides a parameterization in terms of the trajectories $t_\pm(s)$ in Eq. (E.18) avoiding endpoint singularities at $s = s_{\text{III}}$ and $s = s_{\text{IV}}$.[6] These endpoint singularities occur in the Jacobian of the parameterization $\gamma(t') = t_\pm(t')$, i.e., at the points s_{III} and s_{IV} the path opens square root-like, leading to a diverging derivative at these specific values. Instead, we parameterize the complex arcs by

$$\gamma(t'(y)) = t_\pm(t'(y)) \in \mathbb{C} \quad \text{with} \quad t', y \in \mathbb{R} \tag{E.29}$$

and further subdivide the integration into two more regions.

[5] The signs in front of the $\kappa_{\pi\pi}$ are chosen conventionally as in Refs. [82, 84], in contrast to Ref. [83] who uses different signs. Both parameterizations are valid.

[6] Note that we correct the erroneous mathematical notation used in Ref. [82].

$\underline{(s_{\rm III}+s_{\rm IV})/2 < s < s_{\rm IV}}$:

For these values of s we only need to take the two left quadrants of the complex plane with negative real part into account. We introduce the curve parameter

$$y_b(t') = \sqrt{\frac{\sqrt{s_{\rm III}}+\sqrt{t'}}{2}} - \sqrt{\frac{\sqrt{s_{\rm III}}-\sqrt{t'}}{2}} \tag{E.30}$$

and thus

$$t'(y_b) = y_b^2(2M_\eta + 2M_{\eta'} - y_b^2). \tag{E.31}$$

To shorten the notation, we define $y_b^\pm \equiv t_\pm(t'(y_b))$. The integration within this region is then given by

$$\tilde{\mathcal{A}}(s) = \int\limits_{y_b(s)}^{y_b(s_{\rm IV})} \mathrm{d}y_b \, \frac{\mathrm{d}y_b^-}{\mathrm{d}y_b} \mathcal{I}(y_b^-) + \int\limits_{y_b(s_{\rm IV})}^{y_b(s)} \mathrm{d}y_b \, \frac{\mathrm{d}y_b^+}{\mathrm{d}y_b} \mathcal{I}(y_b^+), \tag{E.32}$$

where each integral considers one of the aforementioned quadrants.

$\underline{s_{\rm III} < s < (s_{\rm III}+s_{\rm IV})/2}$:

In this region the arcs extend across all quadrants of the complex plane. To handle this integration we substitute

$$y_a(t') = \sqrt{\frac{\sqrt{t'}+\sqrt{s_{\rm IV}}}{2}} - \sqrt{\frac{\sqrt{t'}-\sqrt{s_{\rm IV}}}{2}} \tag{E.33}$$

and obtain

$$t'(y_a) = \frac{\left((M_{\eta'}-M_\eta)^2 + y_a^4\right)^2}{4y_a^4}. \tag{E.34}$$

Again, define the short form $y_a^\pm \equiv t_\pm(t'(y_a))$, so that $\tilde{A}$ in this region becomes

$$\begin{aligned}\tilde{\mathcal{A}}(s) = &\int\limits_{y_a(s)}^{y_a(\frac{s_{\rm III}+s_{\rm IV}}{2})} \mathrm{d}y_a \, \frac{\mathrm{d}y_a^-}{\mathrm{d}y_a} \mathcal{I}(y_a^-) + \int\limits_{y_a(\frac{s_{\rm III}+s_{\rm IV}}{2})}^{y_a(s)} \mathrm{d}y_a \, \frac{\mathrm{d}y_a^+}{\mathrm{d}y_a} \mathcal{I}(y_a^+) \\ &+ \int\limits_{y_b(\frac{s_{\rm III}+s_{\rm IV}}{2})}^{y_b(s_{\rm IV})} \mathrm{d}y_b \, \frac{\mathrm{d}y_b^-}{\mathrm{d}y_b} \mathcal{I}(y_b^-) + \int\limits_{y_b(s_{\rm IV})}^{y_b(\frac{s_{\rm III}+s_{\rm IV}}{2})} \mathrm{d}y_b \, \frac{\mathrm{d}y_b^+}{\mathrm{d}y_b} \mathcal{I}(y_b^+),\end{aligned} \tag{E.35}$$

with one integral for each quadrant.

With this procedure the endpoint singularites are not included in the respective integration intervals and the remaining integrals can be carried out numerically.

E.2.2.2 | *t*-channel

In the t-channel with $\pi\eta$ intermediate states we encounter the angular averages $\langle z^n \mathcal{A}\rangle^-$ and $\langle z^n \mathcal{A}\rangle^+$. Let us first have a look at the average of the kind $\langle z^n \mathcal{A}\rangle^-$. The characteristic points of the contour are this time given by

$$t_{\rm I} = (M_\eta + M_\pi)^2\,, \quad t_{\rm II} = \frac{M_{\eta'}^2 + M_\eta^2 - 2M_\pi^2}{2}\,, \quad t_{\rm III} = (M_{\eta'} - M_\pi)^2\,, \quad t_{\rm IV} = (M_{\eta'} + M_\pi)^2\,. \tag{E.36}$$

Compared with the s-channel angular average, we just have to replace $t_\pm(s) \to s_\pm(t)$, $t_0' \to s_0'$, and $s_{\rm I,II,III,IV} \to t_{\rm I,II,III,IV}$ in order to obtain the correct analytic continuation. The remaining implementation follows exactly the same prescription given for the s-channel.[7] Concerning the average $\langle z^n \mathcal{A}\rangle^+$ we have

$$\begin{aligned} u_{\rm I} &= (M_\eta + M_\pi)^2\,, \quad u_{\rm II} = \frac{M_\eta(M_{\eta'}^2 - M_\pi^2) - M_\pi(M_\eta^2 - M_\pi^2)}{M_\eta + M_\pi}\,, \\ u_{\rm III} &= (M_{\eta'} - M_\pi)^2\,, \quad u_{\rm IV} = (M_{\eta'} + M_\pi)^2\,. \end{aligned} \tag{E.37}$$

This type of angular average can be evaluated upon replacing $t_\pm(s) \to u_\pm(t)$, $t_0' \to u_0'$, as well as $s_{\rm I,II,III,IV} \to u_{\rm I,II,III,IV}$ within the implementation for the s-channel.

[7] Note the corrected factors and signs compared to Ref. [82].

E.3 | Dispersion integral

In this section we work out a numerically stable representation of the dispersion integrals we have first encountered in Eq. (3.103) and then applied to the decays of interest in Sects. 8.1.4 and 8.2.4. Consider a generic n-times subtracted dispersion integral of the form

$$\mathcal{I}(s \pm i\epsilon) \equiv \int_{s_\mathrm{I}}^{\infty} \frac{\mathrm{d}x}{x^n} \frac{\sin\delta(x)\tilde{\mathcal{A}}(x)}{\kappa^{2\ell+1}(x)\,|\Omega(x)|\,(x - s \mp i\epsilon)}\,, \tag{E.38}$$

in which we replaced the inhomogneity $\hat{\mathcal{A}}$ according to Eq. (E.12) by $\tilde{\mathcal{A}}$ and again dropped isospin indices to keep the notation as short as possible. Confusions with the integrand $\mathcal{I}$ used in Sect. E.2 shall be excluded from the context. Some non-trivial issues of this integral are the singularities caused by the roots of κ.[8] To break down the problem, we first factorize κ in terms of its zeros, by means of

$$\kappa(s) = \sqrt{1 - \frac{s_\mathrm{I}}{s}}\sqrt{1 - \frac{s_\mathrm{x}}{s}}\,\sqrt{s_\mathrm{III} - s}\,\sqrt{s_\mathrm{IV} - s}\,, \tag{E.39}$$

with s_I, s_III, and s_IV as introduced in the last section and $s_\mathrm{x} = 0$ for $\kappa_{\pi\pi}$. In case of $\kappa_{\pi\eta}$ we have to replace the $s_{\mathrm{I,III,IV}}$ by $t_{\mathrm{I,III,IV}}$ and s_x by $t_\mathrm{x} = (M_\eta - M_\pi)^2$. Since our following discussion is the same for both $\kappa_{\pi\pi}$ and $\kappa_{\pi\eta}$, let us for simplicity continue with the s-channel. The value s_x does not bother us at all, as it lies outside the integration region. The singularites arising at the scattering thresholds s_I and s_IV are also less concerning, because at these values for s the integration path of the angular average is point-like. Thus, $\tilde{\mathcal{A}}$ vanishes at these values, leading to removable singularities. In order to avoid a numerical troublesome evaluation of the resulting ratio of zeros, we use an expansion for $\tilde{\mathcal{A}}$ in the vicinity of s_I and s_IV and cancel the singularities by hand. This procedure is detailed in section E.4. From now on we will therefore work with the numerically stable function

$$\bar{\mathcal{A}} \equiv \tilde{\mathcal{A}}/\nu^{2\ell+1} \quad \text{with} \quad \nu(s) = \begin{cases} \sqrt{1 - s_\mathrm{I}/s}\,\sqrt{1 - s_\mathrm{x}/s}\,\sqrt{s_\mathrm{IV} - s}, & \text{for } s < s_\mathrm{IV} \\ i\sqrt{1 - s_\mathrm{I}/s}\,\sqrt{1 - s_\mathrm{x}/s}\,\sqrt{s - s_\mathrm{IV}}, & \text{for } s > s_\mathrm{IV} \end{cases}. \tag{E.40}$$

The sign of i in the lower line depends on how the analytic continuation depicted in Fig. E.2 is chosen for $s > s_\mathrm{IV}$. If we swap the lower and upper limits of the angular integral in this region, as for instance done in Ref. [83, 362], we would have to pick up an additional minus sign. Unfortunately, $\tilde{\mathcal{A}}$ does not vanish at the remaining root of κ, i.e., at pseudo-threshold s_III, which therefore needs to be handled with special care. Although the singularity at this point is integrable, it will need a special numerical treatment, which will be evaluated below.

Furthermore, we have to elaborate on the Cauchy singularities at $s = x$ in Eq. (E.38).

[8] Note that these issus are not apparent when using the alternative integration method presented in Ref. [361].

To this end, we rely on Hadamard regularization—also known as Hadamard finite-part integration—which can be regarded as a generalized version of Cauchy's principal value to handle hypersingular integrals. More information about the involved mathematical concepts can be found in Refs. [363–365].

Having identified the critical singularities, we can absorb all unproblematic parts of the integrand in

$$\mathcal{P}(s) \equiv \frac{\sin\delta(s)\bar{\mathcal{A}}(s)}{s^n\,|\Omega(s)|}\,, \tag{E.41}$$

so that the dispersion integral acquires the more compact form

$$\mathcal{I}(s \pm i\epsilon) = \int_{s_\mathrm{I}}^{\infty} \mathrm{d}x \frac{\mathcal{P}(x)}{\sqrt{s_\mathrm{III}-x}^{2\ell+1}\,(x - s \mp i\epsilon)}. \tag{E.42}$$

In the following we present a procedure to handle both the Cauchy singularity and the one at pseudo-threshold—which are determined by the expressions $(x-s)$ and $\sqrt{s_\mathrm{III}-x}^{2\ell+1}$, in the denominator, respectively—for partial S- and P-waves. The main idea is to split the dispersion integral into parts that can be calculated analytically and integrals containing removable singularites, similar to the basic example of the Omnès function in Sect. E.1. The implementation shown below follows Ref. [83] and provides only one possible way to treat the dispersion integral.

E.3.1 | *S*-wave

Starting with S-waves, it is appealing to break down the integration range to shift the critical points out of the integration interval. We distinguish between the following two cases.

1. $s \in \mathbb{R} \wedge s < s_\mathrm{th}$ or $s \in \mathbb{C}$:
   In this scenario no value of s can hit the Cauchy singularity, as the latter lies outside the integration limits. To handle the integration at the critical point $x = s_\mathrm{III}$, we add $0 = \mathcal{P}(s_\mathrm{III}) - \mathcal{P}(s_\mathrm{III})$ to the numerator in Eq. (E.42) to obtain

$$\mathcal{I}(s) = \int_{s_\mathrm{I}}^{\Lambda^2} \mathrm{d}x\, \frac{\mathcal{P}(x) - \mathcal{P}(s_\mathrm{III})}{\sqrt{s_\mathrm{III}-x}\,(x-s)} + \mathcal{P}(s_\mathrm{III})\,\mathcal{Q}_{1/2}(s, s_\mathrm{I}, \Lambda^2)\,. \tag{E.43}$$

   The integration to ∞ is implemented by a numeric cutoff Λ^2 that we choose sufficiently large. Empirically, a value of $\Lambda^2 \approx 20\,\mathrm{GeV}^2$ leads to negligible systematic errors.

The analytic part of Eq. (E.43) yields

$$\begin{aligned}\mathcal{Q}_{1/2}(s,x,y) &= \int_x^y \frac{\mathrm{d}x}{\sqrt{s_{\mathrm{III}}-x}\,(x-s)} \\ &= \frac{1}{\sqrt{s_{\mathrm{III}}-s}}\left[\log\frac{\sqrt{s_{\mathrm{III}}-s}+\sqrt{s_{\mathrm{III}}-x}}{\sqrt{s_{\mathrm{III}}-s}-\sqrt{s_{\mathrm{III}}-x}} - 2i\arctan\frac{\sqrt{y-s_{\mathrm{III}}}}{\sqrt{s_{\mathrm{III}}-s}}\right].\end{aligned} \tag{E.44}$$

2. $\underline{s\in\mathbb{R}\wedge s>s_{\mathrm{I}}}$:
For this case we have to account for both singularities at $s=s_{\mathrm{III}}$ and $x=s$. We define $p=(s_{\mathrm{III}}+s)/2$ and divide the integral into two parts by

$$\int_{s_{\mathrm{I}}}^{\Lambda^2} = \int_{s_{\mathrm{I}}}^{p} + \int_{p}^{\Lambda^2}. \tag{E.45}$$

With this convenient choice the singularities are now located in two separate integrals. We now have to differentiate between the cases $s<s_{\mathrm{III}}$, for which $p<s_{\mathrm{III}}$, and $s>s_{\mathrm{III}}$, for which $p>s_{\mathrm{III}}$.

(a) $\underline{s<s_{\mathrm{III}}}$:
For these values, the Cauchy singularity occurs in the first integral with limits s_{I} and p, while the one at pseudo-threshold appears in the integral with limits p and Λ^2. Hence we analytically rewrite the dispersion integral as

$$\begin{aligned}\mathcal{I}(s) = &\int_{s_{\mathrm{I}}}^{p}\mathrm{d}x\frac{\mathcal{P}(x)-\mathcal{P}(s)}{\sqrt{s_{\mathrm{III}}-x}\,(x-s)} + \int_{p}^{\Lambda^2}\mathrm{d}x\frac{\mathcal{P}(x)-\mathcal{P}(s_{\mathrm{III}})}{\sqrt{s_{\mathrm{III}}-x}\,(x-s)} \\ &+\mathcal{P}(s)\,\mathcal{R}_{1/2}(s,s_{\mathrm{I}},p)+\mathcal{P}(s_{\mathrm{III}})\,\mathcal{Q}_{1/2}(s,p,\Lambda^2)\,,\end{aligned} \tag{E.46}$$

where we again added zeros to the numerators in the respective integrals as done in Eq. (E.43). The new analytic function $R_{1/2}$ is defined as

$$\begin{aligned}\mathcal{R}_{1/2}(s,x,y) &= \int_x^y \frac{\mathrm{d}x}{(s_{\mathrm{III}}-x)^{1/2}\,(x-s\mp i\epsilon)} \\ &= \frac{1}{\sqrt{s_{\mathrm{III}}-s}}\left[\log\frac{\sqrt{s_{\mathrm{III}}-x}+\sqrt{s_{\mathrm{III}}-s}}{\sqrt{s_{\mathrm{III}}-x}-\sqrt{s_{\mathrm{III}}-s}} + \log\frac{\sqrt{s_{\mathrm{III}}-s}-\sqrt{s_{\mathrm{III}}-y}}{\sqrt{s_{\mathrm{III}}-s}+\sqrt{s_{\mathrm{III}}-y}} \pm i\pi\right].\end{aligned} \tag{E.47}$$

Although the remaining integrals in Eq. (E.46) can in principle be evaluated numerically, we should avoid a numeric evaluation of ratios of zeros. Such a ratio appears at $x=s_{\mathrm{III}}$ in the integration with limits p and Λ^2. To solve this

issue we first expand $\mathcal{P}(x)$ in vicinity of s_{III} as

$$\mathcal{P}(x) \approx \mathcal{P}(s_{\mathrm{III}}) + b_S\sqrt{s_{\mathrm{III}} - s} + c_S\,(s_{\mathrm{III}} - s) + d_S\,(s_{\mathrm{III}} - s)^{3/2} + \dots\,. \tag{E.48}$$

The coefficients b_S, c_S, and d_S are fixed by the continuity of $\mathcal{P}$, its first, and its second derivative at s_{III}. More information can be found in Sect. E.4.3. The considered expansion can now be rewritten as

$$\frac{\mathcal{P}(x) - \mathcal{P}(s_{\mathrm{III}})}{\sqrt{s_{\mathrm{III}} - x}} \approx b_S + c_S\,\sqrt{s_{\mathrm{III}} - x} + d_S(s_{\mathrm{III}} - x) + \dots\,. \tag{E.49}$$

Evidently, this procedure allows us to analytically replace the ratio of zeros on the left-hand side by a numerically stable expression that can be inserted in Eq. (E.46). Note that this expansion for the integrand is only used in a small range around s_{III}, otherwise the uncertainty of this approximation gets non-negligible.

(b) $\underline{s > s_{\mathrm{III}}}$:
These values of s swap the places of the singularities, i.e., the Cauchy singularity lies between p and Λ^2 and the one at pseudo-threshold between s_{I} and p. Similar to the considerations made above, we write the dispersive integral in the numerically stable form

$$\begin{aligned}\mathcal{I}(s) = &\int_{s_{\mathrm{I}}}^{p} \mathrm{d}x\,\frac{\mathcal{P}(x) - \mathcal{P}(s_{\mathrm{III}})}{\sqrt{s_{\mathrm{III}} - x}\,(x - s)} + \int_{p}^{\Lambda^2} \mathrm{d}x\,\frac{\mathcal{P}(x) - \mathcal{P}(s)}{\sqrt{s_{\mathrm{III}} - x}\,(x - s)} \\ &+ \mathcal{P}(s_{\mathrm{III}})\,\mathcal{Q}_{1/2}(s, s_{\mathrm{I}}, p) + \mathcal{P}(s)\,\mathcal{R}_{1/2}(s, p, \Lambda^2)\,.\end{aligned} \tag{E.50}$$

The remaining integrals can now be evaluated numerically.

E.3.2 | *P*-wave

The considerations made for the S-wave can be adapted to the P-wave as shown in the following.

1. $\underline{s \in \mathbb{R} \wedge s < s_{\mathrm{th}} \;\text{ or }\; s \in \mathbb{C}}$:
We add $0 = \mathcal{P}(s_{\mathrm{III}}) + (s_{\mathrm{III}} - x)\,\mathcal{P}'(s_{\mathrm{III}}) - \mathcal{P}(s_{\mathrm{III}}) - (s_{\mathrm{III}} - x)\,\mathcal{P}'(s_{\mathrm{III}})$ to the numerator in Eq. (E.42) to write

$$\begin{aligned}\mathcal{I}(s) = &\int_{s_{\mathrm{I}}}^{\Lambda^2} \mathrm{d}x\,\frac{\mathcal{P}(x) - \mathcal{P}(s_{\mathrm{III}}) - (s_{\mathrm{III}} - x)\,\mathcal{P}'(s_{\mathrm{III}})}{(s_{\mathrm{III}} - x)^{3/2}\,(x - s)} \\ &+ \mathcal{P}'(s_{\mathrm{III}})\,\mathcal{Q}_{1/2}(s, s_{\mathrm{I}}, \Lambda^2) + \mathcal{P}(s_{\mathrm{III}})\,\mathcal{Q}_{3/2}(s, s_{\mathrm{I}}, \Lambda^2),\end{aligned} \tag{E.51}$$

where $\mathcal{P}'(s)$ denotes the first derivative and the newly introduced analytic function $\mathcal{Q}_{3/2}$ reads

$$\begin{aligned}\mathcal{Q}_{3/2}(s,x,y) &= \int_x^y \frac{\mathrm{d}x}{(s_{\mathrm{III}}-x)^{3/2}\,(x-s)} \\ &= \frac{1}{s_{\mathrm{III}}-s}\left[-2\left(\frac{i}{\sqrt{y-s_{\mathrm{III}}}}+\frac{1}{\sqrt{s_{\mathrm{III}}-x}}\right)+\mathcal{Q}_{1/2}(s,x,y)\right].\end{aligned} \tag{E.52}$$

2. $\underline{s \in \mathbb{R} \wedge s > s_{\mathrm{I}}}$:
For s within the integration limits, we again split the integral in the following way.

   (a) $\underline{s < s_{\mathrm{III}}}$:
   Applying Eq. (E.45) and again blowing up the numerators with zeros leaves us with

$$\begin{aligned}\mathcal{I}(s) = &\int_{s_{\mathrm{I}}}^{p} \mathrm{d}x \frac{\mathcal{P}(x)-\mathcal{P}(s)}{(s_{\mathrm{III}}-x)^{3/2}\,(x-s)} + \int_{p}^{\Lambda^2} \mathrm{d}x \frac{\mathcal{P}(x)-\mathcal{P}(s_{\mathrm{III}})-(s_{\mathrm{III}}-x)\,\mathcal{P}'(s_{\mathrm{III}})}{(s_{\mathrm{III}}-x)^{3/2}\,(x-s)} \\ &+ \mathcal{P}(s)\,\mathcal{R}_{3/2}(s,s_{\mathrm{I}},p) + \mathcal{P}(s_{\mathrm{III}})\,\mathcal{Q}_{3/2}(s,p,\Lambda^2) + \mathcal{P}'(s_{\mathrm{III}})\,\mathcal{Q}_{1/2}(s,p,\Lambda^2),\end{aligned} \tag{E.53}$$

   where

$$\begin{aligned}\mathcal{R}_{3/2}(s,x,y) &= \int_x^y \frac{\mathrm{d}x}{(s_{\mathrm{III}}-x)^{3/2}\,(x-s\mp i\epsilon)} \\ &= \frac{1}{s_{\mathrm{III}}-s}\left[2\left(\frac{1}{\sqrt{s_{\mathrm{III}}-y}}-\frac{1}{\sqrt{s_{\mathrm{III}}-x}}\right)+\mathcal{R}_{1/2}(s,x,y)\right].\end{aligned} \tag{E.54}$$

   Now we again apply a series expansion of the integrand including the pseudo-threshold singularity, which reads

$$\mathcal{P}(x) \approx \mathcal{P}(s_{\mathrm{III}}) + (s_{\mathrm{III}}-x)\mathcal{P}'(s_{\mathrm{III}}) + c_P(s_{\mathrm{III}}-x)^{3/2} + d_P(s_{\mathrm{III}}-x)^2 + \dots\,. \tag{E.55}$$

   Section E.4.3 explains how to determine the coefficients c_P, d_P and for simplicity also $\mathcal{P}'(s_{\mathrm{III}})$. Hence, we can write

$$\frac{\mathcal{P}(x)-\mathcal{P}(s_{\mathrm{III}})-(s_{\mathrm{III}}-x)\,\mathcal{P}'(s_{\mathrm{III}})}{(s_{\mathrm{III}}-x)^{3/2}} \approx c_P + d_P\sqrt{s_{\mathrm{III}}-x} + \dots \tag{E.56}$$

   in vicinity of s_{III}.[9]

[9] One can additionally consider one more term in the expansion, which would for instance be especially

(b) $s > s_{\mathrm{III}}$:
Applying the same techniques as discussed above, the dispersion integral in this region becomes

$$\mathcal{I}(s) = \int_{s_{\mathrm{I}}}^{p} \mathrm{d}x \, \frac{\mathcal{P}(x) - \mathcal{P}(s_{\mathrm{III}}) - (s_{\mathrm{III}} - x)\,\mathcal{P}'(s_{\mathrm{III}})}{(s_{\mathrm{III}} - x)^{3/2}\,(x - s)} + \int_{p}^{\Lambda^2} \mathrm{d}x \, \frac{\mathcal{P}(x) - \mathcal{P}(s)}{(s_{\mathrm{III}} - x)^{3/2}\,(x - s)} + \mathcal{P}(s_{\mathrm{III}})\,\mathcal{Q}_{3/2}(s, s_{\mathrm{I}}, p) + \mathcal{P}'(s_{\mathrm{III}})\,\mathcal{Q}_{1/2}(s, s_{\mathrm{I}}, p) + \mathcal{P}(s)\,\mathcal{R}_{3/2}(s, p, \Lambda^2). \tag{E.57}$$

It shall be remarked that $\mathcal{P}'(s_{\mathrm{III}})$ is not well-defined, due to the square root-like opening of $\bar{\mathcal{A}}$ at pseudo-threshold. Therefore, instead attempting to calculate the derivative of $\mathcal{P}$ one should use the corresponding coefficient of the series expansion in Eq. (E.55). This holds for all $\mathcal{P}'(s_{\mathrm{III}})$ appearing in the presented implementation. Furthermore notice that the P-wave is much more sensible to numerical uncertainties than the S-wave, as the singularity at pseudo-threshold scales is of order 3/2 instead of 1/2.[10]

E.4 | Matching conditions

In this section we discuss an accurate way to avoid the problematic numerical evaluation of ratios of zeros that occur in the evaluation of the dispersion integral. Due to the division by zero, smallest uncertainties in the numerator can result in large numerical uncertainties of the ratio, which do not allow for an accurate computation of the integrals we are dealing with. This fact was already pointed out in Ref. [81]. Moreover, the resulting uncertainties propagate during the iterative solution algorithm, which is discussed in Sect. E.5, leading to distortions and numerical instabilities over the whole energy range.
Based on Ref. [367], the following shows how to expand the numerators of such ratios in a series around the zeros of κ in Eq. (E.39) and how to match the series coefficients accordingly. In the course of this work we have to match two different functions to an appropriate series expansion. On the one hand we need to match $\tilde{\mathcal{A}}_I$ in order to analytically cancel the removable singularities in Eq. (E.40) at the points s_{I} and s_{IV}, while an expansion of $\mathcal{P}$ is required to obtain the numerically stable expressions at pseudo-threshold s_{III} given in Eq. (E.49) and (E.56).
Note that we can build in two parameters that can be adjusted by hand, such that the matched functions become as smooth as possible around each zero of κ: the matching point that lies ϵ next to these zeros and the range of validity within which we use the matched

important fort analyses aiming at the numerical stable computation of D-waves. For this purpose, the then occurring additional parameter should not be fixed by a derivative of order three, as one would suggest from the matching conditions explained in Sect. E.4.3, because this would introduce even more numerical inaccuracies. As an alternative, we suggest that one could instead evaluate $\mathcal{P}$ at some additional point that does not enter the matching conditions in Sect. E.4.3. Note that the conditions with derivatives presented in the latter guarantees smoothness of the applied expansion.

[10] For an application with D-waves we refer to Refs. [296, 297, 366].

expressions. The latter should be at least as large as ϵ. Empirically, a good starting point for ϵ is $0.5M_\pi^2$. Going too close to the zeros of κ makes the whole matching pointless, while the approximations used in this section become inaccurate if we stay to far away from these values of s.

Again, we lay out the concepts for the $\pi\pi$ intermediate states, for $\pi\eta$ intermediate states one can proceed completely analogously by just replacing $s_{\mathrm{I,III,IV}} \to t_{\mathrm{I,III,IV}}$. We furthermore restore the indices denoting the two-body isospin and partial wave, i.e., $\tilde{\mathcal{A}} \equiv \tilde{\mathcal{A}}_I^\ell$ and $\mathcal{P} \equiv \mathcal{P}_I^\ell$, which help us to keep the following considerations more general.

E.4.1 | Matching in vicinity of s_I

We start by expanding $\tilde{\mathcal{A}}_I^\ell$ in κ by means of

$$\begin{aligned}\tilde{\mathcal{A}}_I^0(s) &\approx \kappa(s)\,(a_S + b_S\,\kappa^2(s) + c_S\,\kappa^4(s) + \ldots)\,,\\ \tilde{\mathcal{A}}_I^1(s) &\approx \kappa^3(s)\,(a_P + b_P\kappa^2(s) + c_P\,\kappa^4(s) + \ldots)\,.\end{aligned} \tag{E.58}$$

If the expansion is used in a sufficiently small range around s_I the other roots of κ, i.e., s_III and s_IV, are in a good approximation constant, simplifying the further evaluation tremendously. Hence, it is sufficient to use the expansion

$$\begin{aligned}\tilde{\mathcal{A}}_I^0(s) &\approx \sqrt{s-s_\mathrm{I}}\,(a_S + b_S(s-s_\mathrm{I}) + c_S\,(s-s_\mathrm{I})^2 + \ldots)\,,\\ \tilde{\mathcal{A}}_I^1(s) &\approx \sqrt{s-s_\mathrm{I}}^3\,(a_P + b_P(s-s_\mathrm{I}) + c_P\,(s-s_\mathrm{I})^2 + \ldots)\,.\end{aligned} \tag{E.59}$$

Note that this expansion is consistent with the previous considerations made in Sect. E.3: the function $\tilde{\mathcal{A}}_I^\ell$ vanishes at s_I. This has the great advantage that we can now cancel the factors $\sqrt{s-s_\mathrm{I}}$ and $\sqrt{s-s_\mathrm{I}}^3$ appearing in the denominator of $\bar{\mathcal{A}}_I$ in Eq. (E.40) by hand.

To match the appearing coefficients, we evaluate the $\tilde{\mathcal{A}}_I^\ell$, their first, and their second derivative at a suitable chosen matching point $x = s_\mathrm{I}+\epsilon$ close to s_I and solve the three-dimensional system of equations. The resulting matching conditions for S-waves are

$$\begin{aligned}a_S &= -\frac{-15\tilde{\mathcal{A}}_I^0(x) + 12\epsilon\,\tilde{\mathcal{A}}_I^{0\prime}(x) - 4\epsilon^2\tilde{\mathcal{A}}_I^{0\prime\prime}(x)}{8\sqrt{\epsilon}}\Big|_{x=(s_\mathrm{I}+\epsilon)}\,,\\ b_S &= -\frac{5\tilde{\mathcal{A}}_I^0(x) - 8\epsilon\,\tilde{\mathcal{A}}_I^{0\prime}(x) + 4\epsilon^2\tilde{\mathcal{A}}_I^{0\prime\prime}(x)}{4\sqrt{\epsilon}^3}\Big|_{x=(s_\mathrm{I}+\epsilon)}\,,\\ c_S &= -\frac{-3\tilde{\mathcal{A}}_I^0(x) + 4\epsilon\,\tilde{\mathcal{A}}_I^{0\prime}(x) - 4\epsilon^2\tilde{\mathcal{A}}_I^{0\prime\prime}(x)}{8\sqrt{\epsilon}^5}\Big|_{x=(s_\mathrm{I}+\epsilon)}\,,\end{aligned} \tag{E.60}$$

and the ones for P-waves yield

$$\begin{aligned} a_P &= -\frac{-35\tilde{\mathcal{A}}_I^1(x) + 20\epsilon\,\tilde{\mathcal{A}}_I^{1\prime}(x) - 4\epsilon^2\tilde{\mathcal{A}}_I^{1\prime\prime}(x)}{8\sqrt{\epsilon}^3}\Big|_{x=(s_\mathrm{I}+\epsilon)}\,, \\ b_P &= -\frac{21\tilde{\mathcal{A}}_I^1(x) - 16\epsilon\,\tilde{\mathcal{A}}_I^{1\prime}(x) + 4\epsilon^2\tilde{\mathcal{A}}_I^{1\prime\prime}(x)}{4\sqrt{\epsilon}^5}\Big|_{x=(s_\mathrm{I}+\epsilon)}\,, \\ c_P &= -\frac{-15\tilde{\mathcal{A}}_I^1(x) + 12\epsilon\,\tilde{\mathcal{A}}_I^{1\prime}(x) - 4\epsilon^2\tilde{\mathcal{A}}_I^{1\prime\prime}(x)}{8\sqrt{\epsilon}^7}\Big|_{x=(s_\mathrm{I}+\epsilon)}\,. \end{aligned} \tag{E.61}$$

Within the limits of the dispersion integral s is always larger than s_I, therefore there is no need for a further differentiation of cases.

E.4.2 | Matching in vicinity of s_IV

In analogy to the scattering threshold s_I, the expansion around s_IV reads

$$\begin{aligned} \tilde{\mathcal{A}}_I^0(s) &\approx \sqrt{s_\mathrm{IV}-s}\,(a_S + b_S(s_\mathrm{IV}-s) + c_S\,(s_\mathrm{IV}-s)^2 + \ldots)\,, \\ \tilde{\mathcal{A}}_I^1(s) &\approx \sqrt{s_\mathrm{IV}-s}^3\,(a_P + b_P(s_\mathrm{IV}-s) + c_P\,(s_\mathrm{IV}-s)^2 + \ldots)\,. \end{aligned} \tag{E.62}$$

The overall factors $\sqrt{s_\mathrm{IV}-s}$ and $\sqrt{s_\mathrm{IV}-s}^3$, respectively, can now be cancelled analytically against the corresponding ones from $\nu(s)$ in Eq. (E.40).

This time we have to match separately above and below s_IV. For S-waves with $s < s_\mathrm{IV}$ we obtain

$$\begin{aligned} a_S &= -\frac{-15\tilde{\mathcal{A}}_I^0(x) - 12\epsilon\,\tilde{\mathcal{A}}_I^{0\prime}(x) - 4\epsilon^2\tilde{\mathcal{A}}_I^{0\prime\prime}(x)}{8\sqrt{\epsilon}}\Big|_{x=(s_\mathrm{IV}-\epsilon)}\,, \\ b_S &= -\frac{5\tilde{\mathcal{A}}_I^0(x) + 8\epsilon\,\tilde{\mathcal{A}}_I^{0\prime}(x) + 4\epsilon^2\tilde{\mathcal{A}}_I^{0\prime\prime}(x)}{4\sqrt{\epsilon}^3}\Big|_{x=(s_\mathrm{IV}-\epsilon)}\,, \\ c_S &= -\frac{-3\tilde{\mathcal{A}}_I^0(x) - 4\epsilon\,\tilde{\mathcal{A}}_I^{0\prime}(x) - 4\epsilon^2\tilde{\mathcal{A}}_I^{0\prime\prime}(x)}{8\sqrt{\epsilon}^5}\Big|_{x=(s_\mathrm{IV}-\epsilon)}\,, \end{aligned} \tag{E.63}$$

and for the corresponding P-waves

$$\begin{aligned} a_P &= -\frac{-35\tilde{\mathcal{A}}_I^1(x) - 20\epsilon\,\tilde{\mathcal{A}}_I^{1\prime}(x) - 4\epsilon^2\tilde{\mathcal{A}}_I^{1\prime\prime}(x)}{8\sqrt{\epsilon}^3}\Big|_{x=(s_\mathrm{IV}-\epsilon)}\,, \\ b_P &= -\frac{21\tilde{\mathcal{A}}_I^1(x) + 16\epsilon\,\tilde{\mathcal{A}}_I^{1\prime}(x) + 4\epsilon^2\tilde{\mathcal{A}}_I^{1\prime\prime}(x)}{4\sqrt{\epsilon}^5}\Big|_{x=(s_\mathrm{IV}-\epsilon)}\,, \\ c_P &= -\frac{-15\tilde{\mathcal{A}}_I^1(x) - 12\epsilon\,\tilde{\mathcal{A}}_I^{1\prime}(x) - 4\epsilon^2\tilde{\mathcal{A}}_I^{1\prime\prime}(x)}{8\sqrt{\epsilon}^7}\Big|_{x=(s_\mathrm{IV}-\epsilon)}\,. \end{aligned} \tag{E.64}$$

Similarly, the S-wave parameters for $s > s_{\rm IV}$ obey

$$\begin{aligned} a_S &= -\left.\frac{15\tilde{\mathcal{A}}_I^0(x) - 12\epsilon\,\tilde{\mathcal{A}}_I^{0\prime}(x) + 4\epsilon^2\tilde{\mathcal{A}}_I^{0\prime\prime}(x)}{8\sqrt{\epsilon}}\right|_{x=(s_{\rm IV}+\epsilon)}, \\ b_S &= -\left.\frac{5\tilde{\mathcal{A}}_I^0(x) - 8\epsilon\,\tilde{\mathcal{A}}_I^{0\prime}(x) + 4\epsilon^2\tilde{\mathcal{A}}_I^{0\prime\prime}(x)}{4\sqrt{\epsilon}^3}\right|_{x=(s_{\rm IV}+\epsilon)}, \\ c_S &= -\left.\frac{3\tilde{\mathcal{A}}_I^0(x) - 4\epsilon\,\tilde{\mathcal{A}}_I^{0\prime}(x) + 4\epsilon^2\tilde{\mathcal{A}}_I^{0\prime\prime}(x)}{8\sqrt{\epsilon}^5}\right|_{x=(s_{\rm IV}+\epsilon)}, \end{aligned} \tag{E.65}$$

while the respective ones for the P-wave are

$$\begin{aligned} a_P &= \left.\frac{35\tilde{\mathcal{A}}_I^1(x) - 20\epsilon\,\tilde{\mathcal{A}}_I^{1\prime}(x) + 4\epsilon^2\tilde{\mathcal{A}}_I^{1\prime\prime}(x)}{8\sqrt{\epsilon}^3}\right|_{x=(s_{\rm IV}+\epsilon)}, \\ b_P &= \left.\frac{21\tilde{\mathcal{A}}_I^1(x) - 16\epsilon\,\tilde{\mathcal{A}}_I^{1\prime}(x) + 4\epsilon^2\tilde{\mathcal{A}}_I^{1\prime\prime}(x)}{4\sqrt{\epsilon}^5}\right|_{x=(s_{\rm IV}+\epsilon)}, \\ c_P &= \left.\frac{15\tilde{\mathcal{A}}_I^1(x) - 12\epsilon\,\tilde{\mathcal{A}}_I^{1\prime}(x) + 4\epsilon^2\tilde{\mathcal{A}}_I^{1\prime\prime}(x)}{8\sqrt{\epsilon}^7}\right|_{x=(s_{\rm IV}+\epsilon)}. \end{aligned} \tag{E.66}$$

Note that the matching point does not have to chosen symmetrically, i.e., we could as well use different ϵ for s below or above $s_{\rm IV}$.

E.4.3 | Matching in vicinity of $s_{\rm III}$

Finally, we need an expansion of the $\mathcal{P}_I^\ell$ around pseudo-threshold, i.e.,

$$\begin{aligned} \mathcal{P}_I^0(s) &\approx a_S + b_S\kappa(s) + c_S\kappa(s)^2 + d_S\kappa(s)^3 + \dots, \\ \mathcal{P}_I^1(s) &\approx a_P + b_P\kappa(s)^2 + c_P\kappa(s)^3 + d_P\kappa(s)^4 + \dots, \end{aligned} \tag{E.67}$$

which do not vanish at $s_{\rm III}$, because $\tilde{\mathcal{A}}_I$ does not. In vicinity of $s_{\rm III}$ we can write

$$\begin{aligned} \mathcal{P}_I^0(s) &\approx a_S + b_S\sqrt{s_{\rm III} - s} + c_S\,(s_{\rm III} - s) + d_S\,(s_{\rm III} - s)^{3/2} + \dots, \\ \mathcal{P}_I^1(s) &\approx a_P + b_P\,(s_{\rm III} - s) + c_P\,(s_{\rm III} - s)^{3/2} + d_P\,(s_{\rm III} - s)^2 + \dots. \end{aligned} \tag{E.68}$$

The parameters $a_{S,P}$ can easily obtained by evaluating the amplitude at pseudo-threshold, while $b_{S,P}$, $c_{S,P}$, and $d_{S,P}$ are matched in the same way as done previously. In this sense,

the matching conditions for S- and P-waves with $s < s_{\rm III}$ become

$$\begin{aligned} a_S =& \quad \mathcal{P}_I^0(s_{\rm III})\,, \\ b_S =& -\frac{3\mathcal{P}_I^0\left(s_{\rm III}\right) - 3\mathcal{P}_I^0(x) - 3\epsilon\mathcal{P}_I^{0\prime}(x) - 2\epsilon^2\mathcal{P}_I^{0\prime\prime}(x)}{\sqrt{\epsilon}}\Big|_{x=(s_{\rm III}-\epsilon)}\,, \\ c_S =& -\frac{-3\mathcal{P}_I^0\left(s_{\rm III}\right) + 3\mathcal{P}_I^0(x) + 4\epsilon\mathcal{P}_I^{0\prime}(x) + 4\epsilon^2\mathcal{P}_I^{0\prime\prime}(x)}{\epsilon}\Big|_{x=(s_{\rm III}-\epsilon)}\,, \\ d_S =& -\frac{\mathcal{P}_I^0\left(s_{\rm III}\right) - \mathcal{P}_I^0(x) - \epsilon\mathcal{P}_I^{0\prime}(x) - 2\epsilon^2\mathcal{P}_I^{0\prime\prime}(x)}{\epsilon^{3/2}}\Big|_{x=(s_{\rm III}-\epsilon)}\,, \end{aligned} \tag{E.69}$$

and

$$\begin{aligned} a_P =& \quad \mathcal{P}_I^1(s_{\rm III})\,, \\ b_P =& -\frac{6\mathcal{P}_I^1\left(s_{\rm III}\right) - 6\mathcal{P}_I^1(x) - 5\epsilon\mathcal{P}_I^{1\prime}(x) - 2\epsilon^2\mathcal{P}_I^{1\prime\prime}(x)}{\epsilon}\Big|_{x=(s_{\rm III}-\epsilon)}\,, \\ c_P =& -\frac{-8\mathcal{P}_I^1\left(s_{\rm III}\right) + 8\mathcal{P}_I^1(x) + 8\epsilon\mathcal{P}_I^{1\prime}(x) + 4\epsilon^2\mathcal{P}_I^{1\prime\prime}(x)}{\sqrt{\epsilon}^3}\Big|_{x=(s_{\rm III}-\epsilon)}\,, \\ d_P =& -\frac{3\mathcal{P}_I^1\left(s_{\rm III}\right) - 3\mathcal{P}_I^1(x) - 3\epsilon\mathcal{P}_I^{1\prime}(x) - 2\epsilon^2\mathcal{P}_I^{1\prime\prime}(x)}{\epsilon^2}\Big|_{x=(s_{\rm III}-\epsilon)}\,, \end{aligned} \tag{E.70}$$

respectively. For $s > s_{\rm III}$ we find the coefficients for the S-wave to be

$$\begin{aligned} a_S =& \quad \mathcal{P}_I^0(s_{\rm III})\,, \\ b_S =& -\frac{-3\mathcal{P}_I^0\left(s_{\rm III}\right) + 3\mathcal{P}_I^0(x) - 3\epsilon\mathcal{P}_I^{0\prime}(x) + 2\epsilon^2\mathcal{P}_I^{0\prime\prime}(x)}{\sqrt{\epsilon}}\Big|_{x=(s_{\rm III}+\epsilon)}\,, \\ c_S =& -\frac{3\mathcal{P}_I^0\left(s_{\rm III}\right) - 3\mathcal{P}_I^0(x) + 4\epsilon\mathcal{P}_I^{0\prime}(x) - 4\epsilon^2\mathcal{P}_I^{0\prime\prime}(x)}{\epsilon}\Big|_{x=(s_{\rm III}+\epsilon)}\,, \\ d_S =& -\frac{\mathcal{P}_I^0\left(s_{\rm III}\right) - \mathcal{P}_I^0(x) + \epsilon\mathcal{P}_I^{0\prime}(x) - 2\epsilon^2\mathcal{P}_I^{0\prime\prime}(x)}{\epsilon^{3/2}}\Big|_{x=(s_{\rm III}+\epsilon)}\,, \end{aligned} \tag{E.71}$$

and the P-wave parameters as

$$\begin{aligned} a_P =& \quad \mathcal{P}_I^1(s_{\rm III})\,, \\ b_P =& -\frac{-6\mathcal{P}_I^1\left(s_{\rm III}\right) + 6\mathcal{P}_I^1(x) - 5\epsilon\mathcal{P}_I^{1\prime}(x) + 2\epsilon^2\mathcal{P}_I^{1\prime\prime}(x)}{\epsilon}\Big|_{x=(s_{\rm III}+\epsilon)}\,, \\ c_P =& -\frac{-8\mathcal{P}_I^1\left(s_{\rm III}\right) + 8\mathcal{P}_I^1(x) - 8\epsilon\mathcal{P}_I^{1\prime}(x) + 4\epsilon^2\mathcal{P}_I^{1\prime\prime}(x)}{\sqrt{\epsilon}^3}\Big|_{x=(s_{\rm III}+\epsilon)}\,, \\ d_P =& -\frac{3\mathcal{P}_I^1\left(s_{\rm III}\right) - 3\mathcal{P}_I^1(x) + 3\epsilon\mathcal{P}_I^{1\prime}(x) - 2\epsilon^2\mathcal{P}_I^{1\prime\prime}(x)}{\epsilon^2}\Big|_{x=(s_{\rm III}+\epsilon)}\,. \end{aligned} \tag{E.72}$$

E.5 | Iterative solution

Finally, as all numerical subtleties on our way to evaluate the angular averages and the dispersion integrals are dealt with, we can solve the system of coupled integral equations. For this purpose we consider the basis functions $\mathcal{A}_I^\nu$ and $\hat{\mathcal{A}}_I^\nu = \kappa^{2\ell+1}\tilde{\mathcal{A}}_I^\nu$ as introduced in Sect. 8.1.4, which can be fixed once and for all even before fitting the subtraction constants to data. We decide to use the simplest solution method, i.e., an iterative algorithm. The idea is to initialize the algorithm with an arbitrary starting value for $\mathcal{A}_I^\nu$ as an input for the inhomogeneity $\hat{\mathcal{A}}_I^\nu$. Note that the final result does not depend on this starting value, which can in principle be arbitrary. However, it is appealing to choose the homogeneous solution of the unitarity equation in Eq. (3.97), i.e., the Omnès function $\Omega(s)$ multiplied by the corresponding order of the subtraction polynomial, as the initial guess for the amplitude $\mathcal{A}_I^\nu$. This reduces the number of iterations. Once $\hat{\mathcal{A}}_I^\nu$ is evaluated with this input, the inhomogeneity can be used to compute $\mathcal{A}_I^\nu$, which can be used as a new input for $\hat{\mathcal{A}}_I^\nu$. This procedure can be iterated until the desired convergence is achieved, cf. Fig. E.4. Note that this iterative algorithm does not always converge. In such cases one has to resort to a more complicated matrix inversion as used in Ref. [296]. Empirical observations have shown that the convergence of the iteration procedure depends on the available phase space and the chosen subtraction scheme for the dispersion integrals. The smaller the available phase space and the fewer the number of basis functions, the better the convergence of the iterative algorithm. Anyway, for the considered decays and the chosen subtraction schemes the iterative method converges.

Before we present the numerical results, we would like to emphasize that in order to finish the computation in a reasonable amount of time, one should evaluate both the single-variable functions as well as the inhomogeneities along an array for each distinct *real-valued* curve parameter, i.e., for each real-valued variable that fixes the argument of $\mathcal{A}_I$ or $\hat{\mathcal{A}}_I$ occurring in the integrands, and interpolate them afterwards. In this way, each integration is performed only once, leading to an immense reduce of computation cost.[11] Otherwise, every single function call of the dispersion integral would start a whole new numeric integration of the angular averages and vice versa. A suitable method of interpolation are *cubic splines* [368]. Particular care should be taken near cusps or scattering thresholds. Close to these values of s or t, respectively, the number of points used in each array should increase significantly. Depending on how good the presented strategies to overcome the numerical difficulties work for the specific process, subtraction scheme, applied integration routines, etc., it might still be advisable to leave out the values in each array that are in immediate vicinity of these critical points. Thus, the arrays must sometimes be readjusted empirically.

In the following we present the numerical solutions of the basis functions and their inhomogeneities and show how they evolve during the iteration procedure.

[11] Also, any integral or function that is used more than once and is more complicated than a simple polynomial should be interpolated in this manner to optimize the computation time.

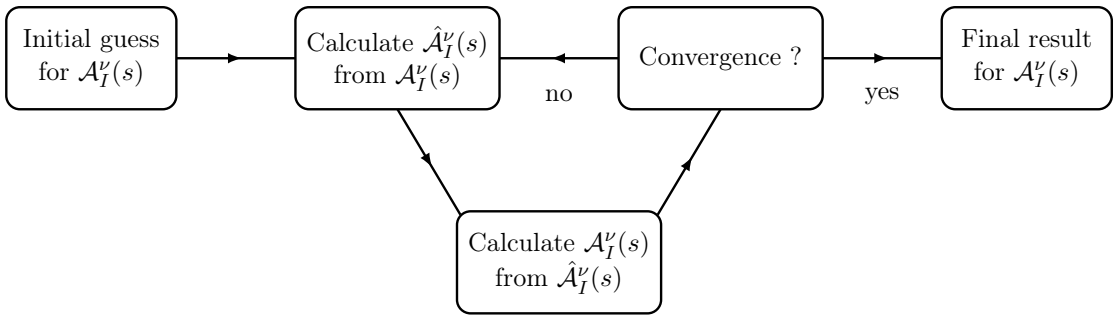

Figure E.4: Depiction of an iterative solution algorithm to obtain the single variable amplitudes corresponding to each basis amplitude.

E.5.1 | Inhomogeneities

The numerical results for all $\tilde{\mathcal{A}}_I^\nu$ used in this, which are related to the respective inhomogeneities of Sects. 8.1.3 and 8.2.3 by Eq. (E.12), are depicted in Figs. E.5–E.10. Note that the $\tilde{\mathcal{A}}_I^\nu$ must only be evaluated from the respective scattering threshold onward. In the diagrams one can clearly see cusps occurring at the zeroths of κ, which were previously denoted by $s_\mathrm{I}, s_\mathrm{III}, s_\mathrm{IV}$ and $t_\mathrm{I}, t_\mathrm{III}, t_\mathrm{IV}$, respectively. Another interesting aspect to mention is that in the first iteration all $\tilde{\mathcal{A}}_I^\nu$ show certain zero lines in the real and imaginary parts. This is due to the fact that we initialize the iteration procedure with the Omnès function $\Omega(s)$, which fulfills Schwarz' reflection principle from Eq. (3.20). But during the iteration this attribute gets spoiled, such that the basis functions $\mathcal{A}_I^\nu$, used to calculate the $\tilde{\mathcal{A}}_I^\nu$, get a complex-valued discontinuity smearing the zero lines.

$\eta \to 3\pi$

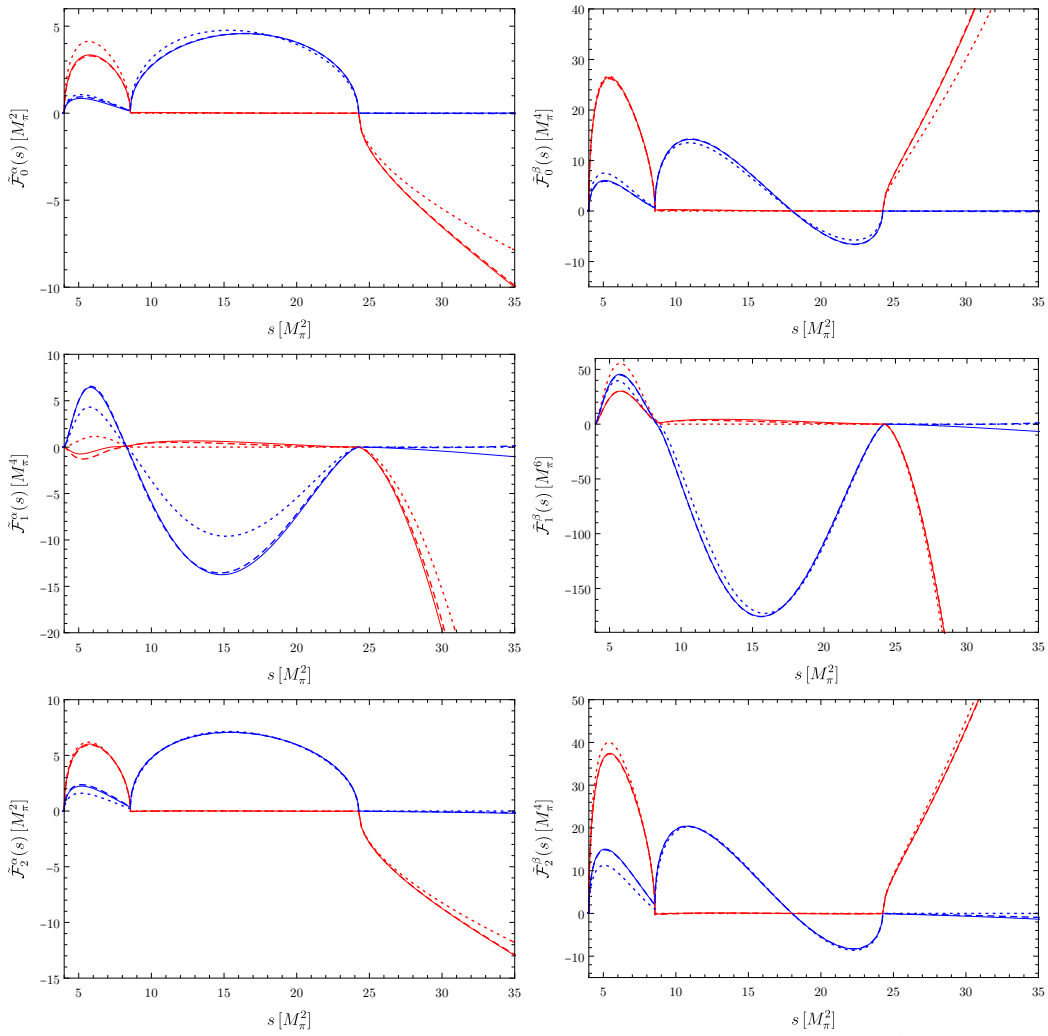

Figure E.5: Inhomogeneities without singular character, i.e., $\tilde{\mathcal{A}}_I^\nu = \kappa^{2\ell+1}\hat{\mathcal{A}}_I^\nu$, for the basis functions $\tilde{\mathcal{F}}_I^\alpha$ and $\tilde{\mathcal{F}}_I^\beta$ in $\eta \to 3\pi$ The real parts are colored in red, the imaginary ones in blue. Dotted lines denote the first iteration, dashed lines the second one, and solid lines the final solution (after 5 iterations).

$\eta \to 3\pi$

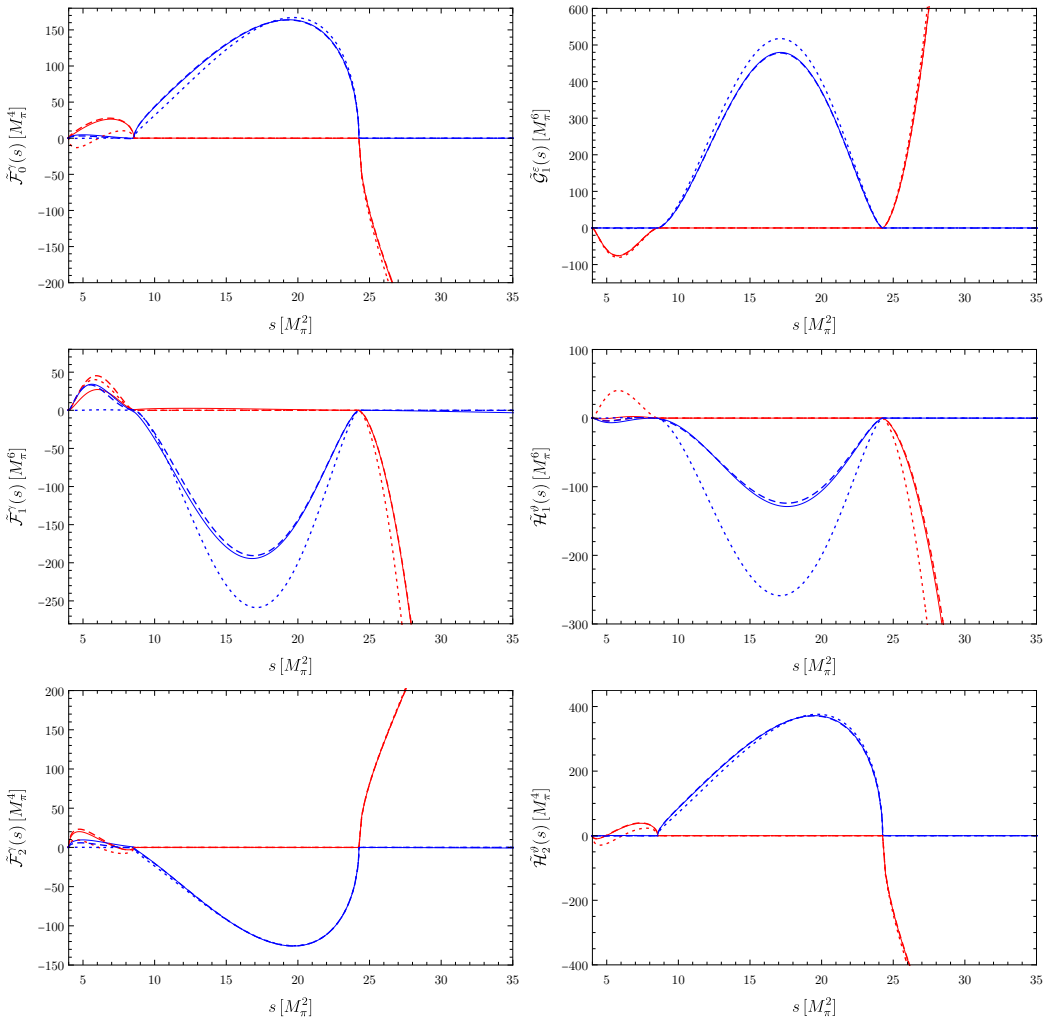

Figure E.6: Inhomogeneities without singular character, i.e., $\tilde{\mathcal{A}}_I^\nu = \kappa^{2\ell+1}\hat{\mathcal{A}}_I^\nu$, for the basis functions $\tilde{\mathcal{F}}_I^\gamma$, $\tilde{\mathcal{G}}_I^\varepsilon$, and $\tilde{\mathcal{H}}_I^\vartheta$ in $\eta \to 3\pi$. The real parts are colored in red, the imaginary ones in blue. Dotted lines denote the first iteration, dashed lines the second one, and solid lines the final solution (after 5 iterations).

$\eta' \to 3\pi$

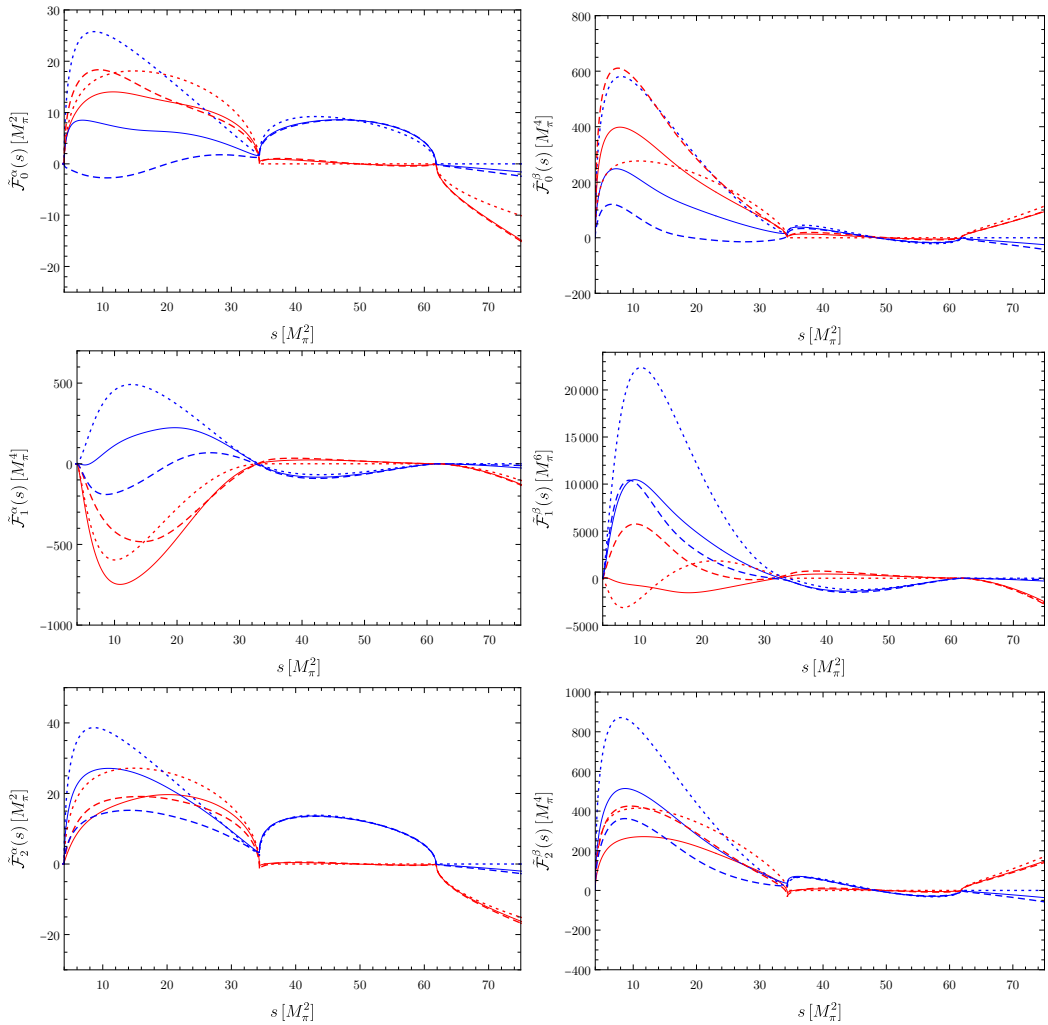

Figure E.7: Inhomogeneities without singular character, i.e., $\tilde{\mathcal{A}}_I^\nu = \kappa^{2\ell+1}\hat{\mathcal{A}}_I^\nu$, for the basis functions $\tilde{\mathcal{F}}_I^\alpha$ and $\tilde{\mathcal{F}}_I^\beta$ in $\eta' \to 3\pi$. The real parts are colored in red, the imaginary ones in blue. Dotted lines denote the first iteration, dashed lines the second one, and solid lines the final solution (after 10 iterations).

$\eta' \to 3\pi$

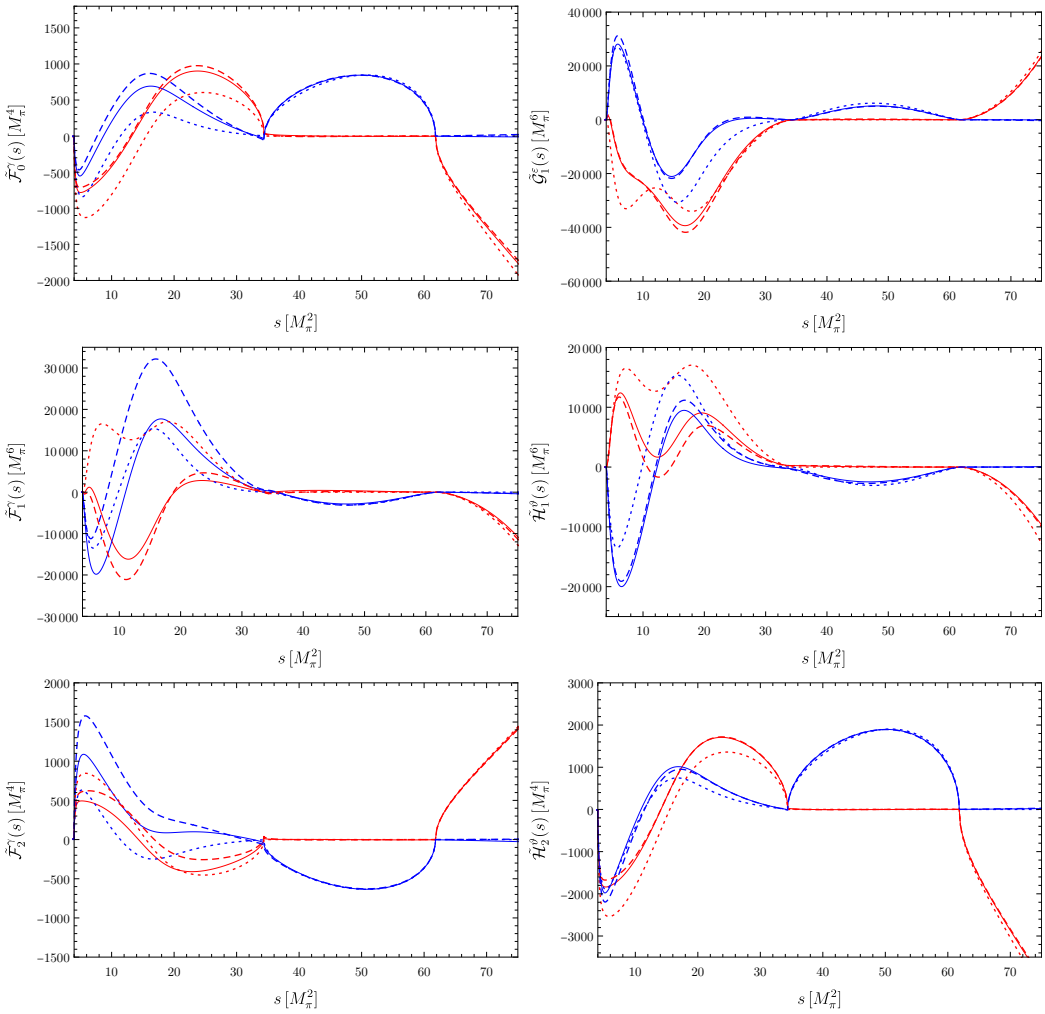

Figure E.8: Inhomogeneities without singular character, i.e., $\tilde{\mathcal{A}}_I^\nu = \kappa^{2\ell+1}\hat{\mathcal{A}}_I^\nu$, for the basis functions $\tilde{\mathcal{F}}_I^\gamma$, $\tilde{\mathcal{G}}_I^\varepsilon$, and $\tilde{\mathcal{H}}_I^\vartheta$ in $\eta' \to 3\pi$. The real parts are colored in red, the imaginary ones in blue. Dotted lines denote the first iteration, dashed lines the second one, and solid lines the final solution (after 10 iterations).

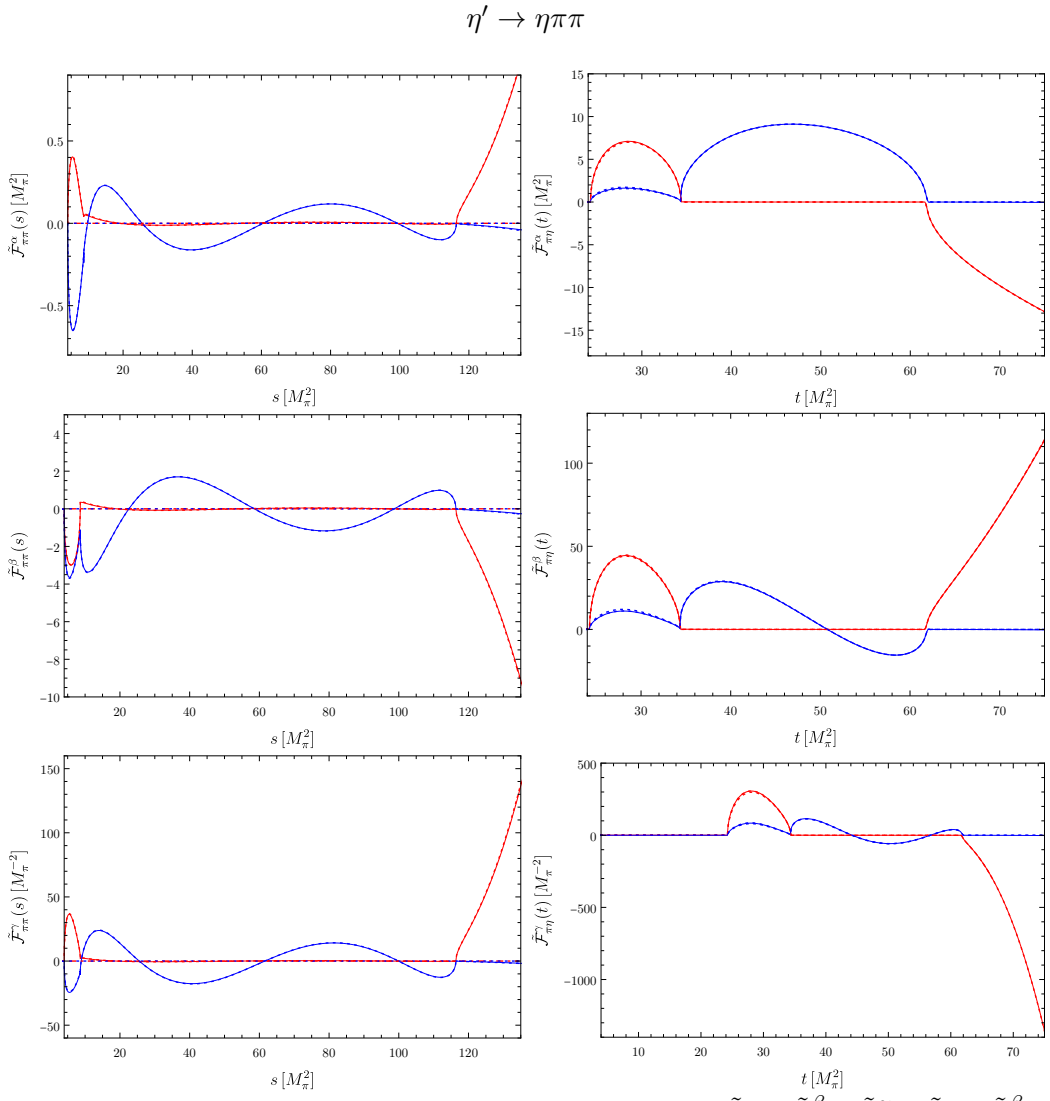

Figure E.9: Inhomogeneities without singular character, i.e., $\tilde{\mathcal{F}}^{\alpha}_{\pi\pi}$, $\tilde{\mathcal{F}}^{\beta}_{\pi\pi}$, $\tilde{\mathcal{F}}^{\gamma}_{\pi\pi}$, $\tilde{\mathcal{F}}^{\alpha}_{\pi\eta}$, $\tilde{\mathcal{F}}^{\beta}_{\pi\eta}$, and $\tilde{\mathcal{F}}^{\gamma}_{\pi\eta}$, for $\eta' \to \eta\pi\pi$. The real parts are colored in red, the imaginary ones in blue. Dotted lines denote the first iteration, dashed lines the second one, and solid lines the final solution (after 3 iterations).

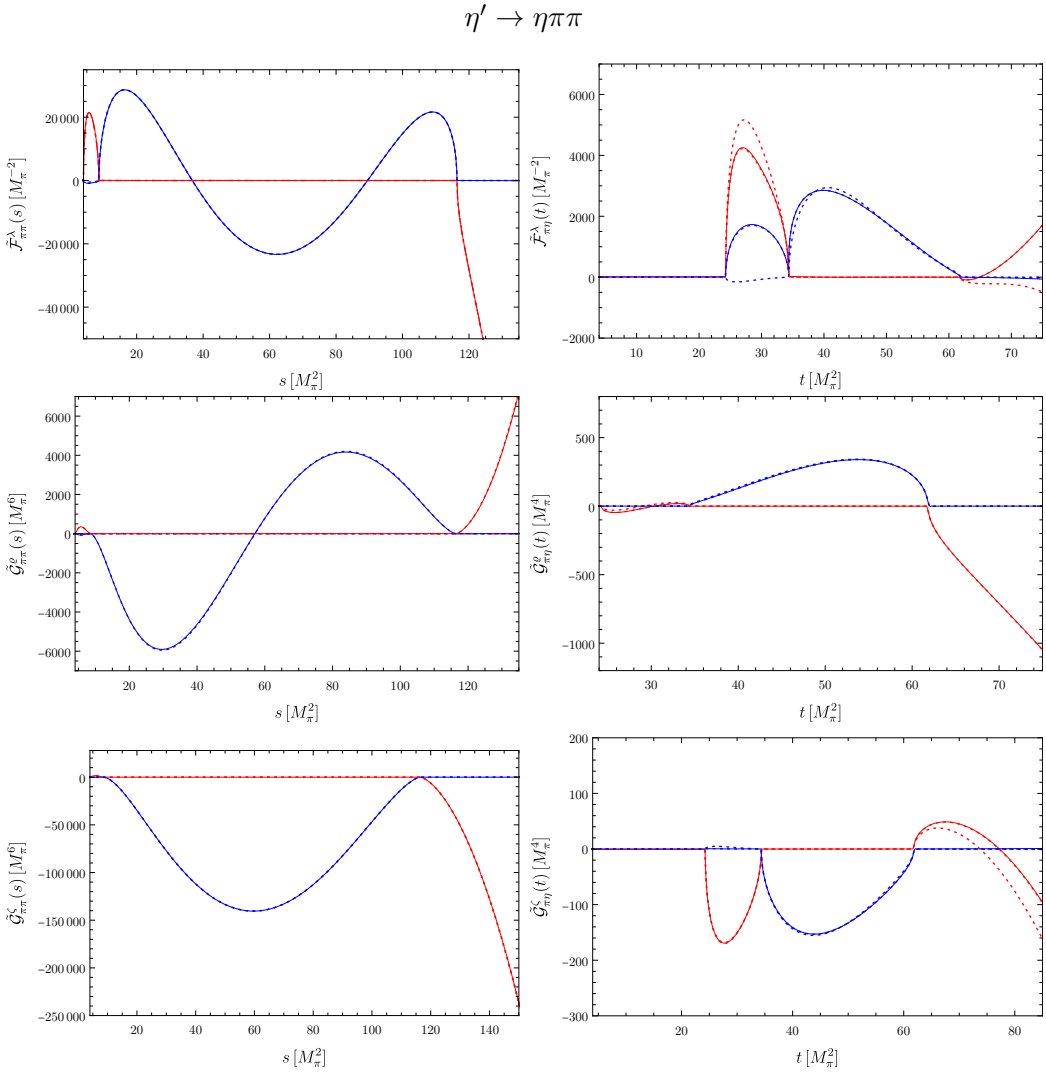

Figure E.10: Inhomogeneities without singular character, i.e., $\tilde{\mathcal{F}}^{\lambda}_{\pi\pi}$, $\tilde{\mathcal{F}}^{\lambda}_{\eta\pi}$, $\tilde{\mathcal{G}}^{\varrho}_{\pi\pi}$, $\tilde{\mathcal{G}}^{\varrho}_{\eta\pi}$, $\tilde{\mathcal{G}}^{\zeta}_{\pi\pi}$, and $\tilde{\mathcal{G}}^{\zeta}_{\eta\pi}$, for $\eta' \to \eta\pi\pi$. The real parts are colored in red, the imaginary ones in blue. Dotted lines denote the first iteration, dashed lines the second one, and solid lines the final solution (after 3 iterations).

E.5.2 | Dispersion integral

The solutions for the basis amplitudes $\mathcal{A}_I^\nu$, which are mainly determined by the respective Omnès functions and the dispersion integrals in Sects. 8.1.4 and 8.2.4, are shown in Figs. E.11–E.16. One can see that the solutions for $\eta \to 3\pi$ and $\eta' \to \eta\pi\pi$ converge already after a few iterations, are quite smooth within the physical range, and exhibit their prominent functional structure far outside the decay region. In contrast, the solutions for $\eta' \to 3\pi$ include for example a non-negligible influence of the resonance due to the enlarged phase space. Another interesting aspect to mention is the relative scale between the basis solutions. The relative size of the latter changes drastically in several orders of magnitude when changing the applied subtraction schemes. These scales do not have a physical meaning at all and are absorbed by the subtraction constants when fitting to data. Lastly, we note the cusps at roughly $50M_\pi^2$ marking the $K\bar{K}$-threshold in the S-wave scattering phase shifts.

$\eta \to 3\pi$

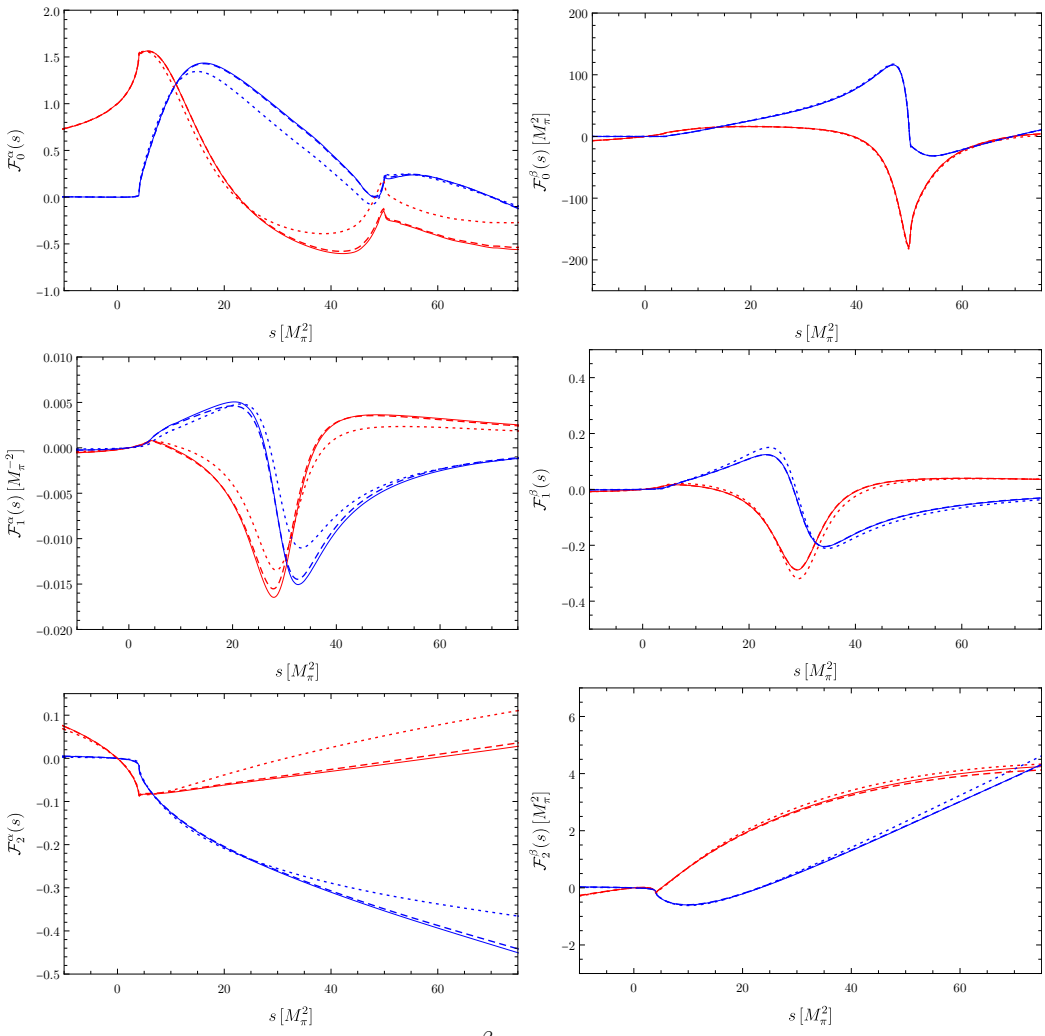

Figure E.11: Basis amplitudes $\mathcal{F}_I^{\alpha}$ and $\mathcal{F}_I^{\beta}$ for $\eta \to 3\pi$. The real parts are colored in red, the imaginary ones in blue. Dotted lines denote the first iteration, dashed lines the second one, and solid lines the final solution (after 5 iterations).

$\eta \to 3\pi$

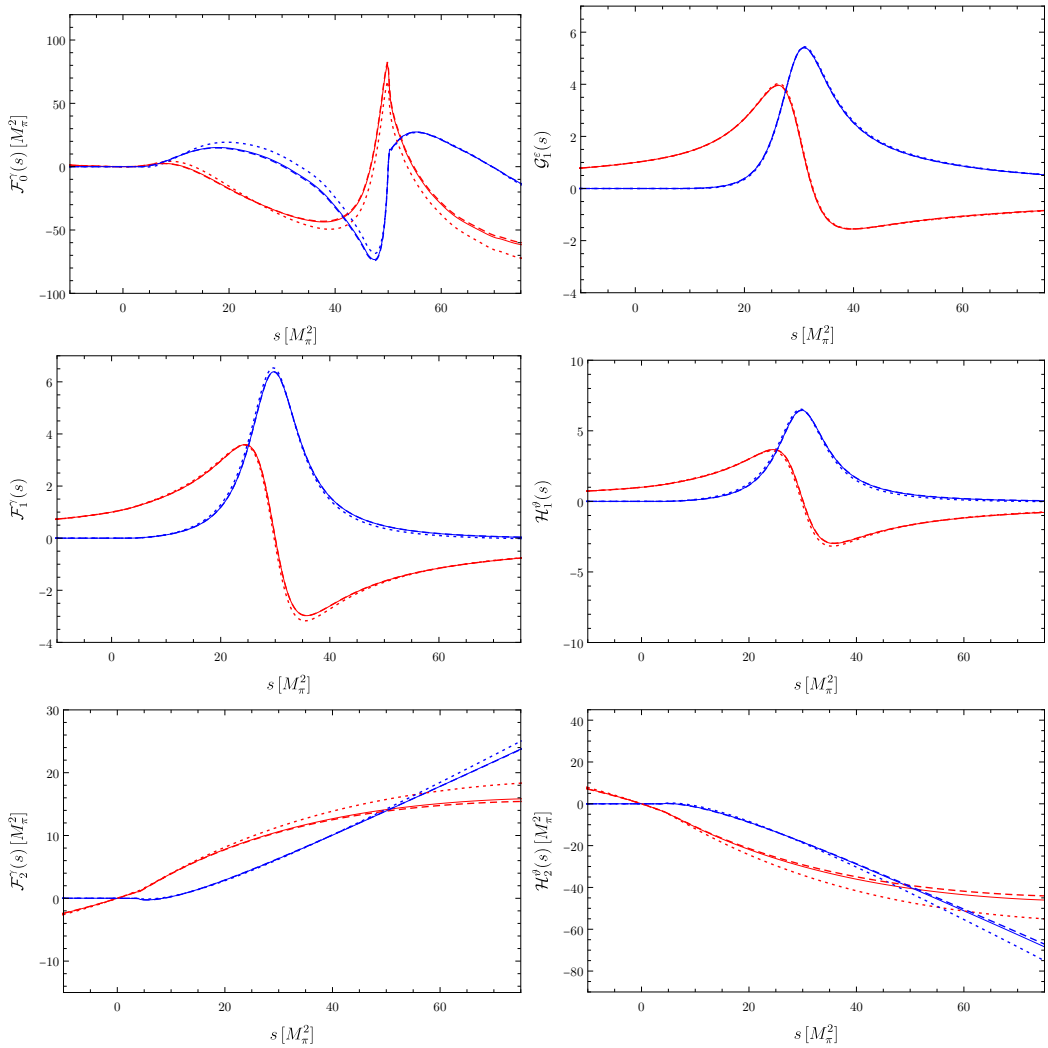

Figure E.12: Basis amplitudes $\mathcal{F}_I^\gamma$, $\mathcal{G}_I^\varepsilon$, and $\mathcal{H}_I^\vartheta$ for $\eta \to 3\pi$. The real parts are colored in red, the imaginary ones in blue. Dotted lines denote the first iteration, dashed lines the second one, and solid lines the final solution (after 5 iterations).

$\eta' \to 3\pi$

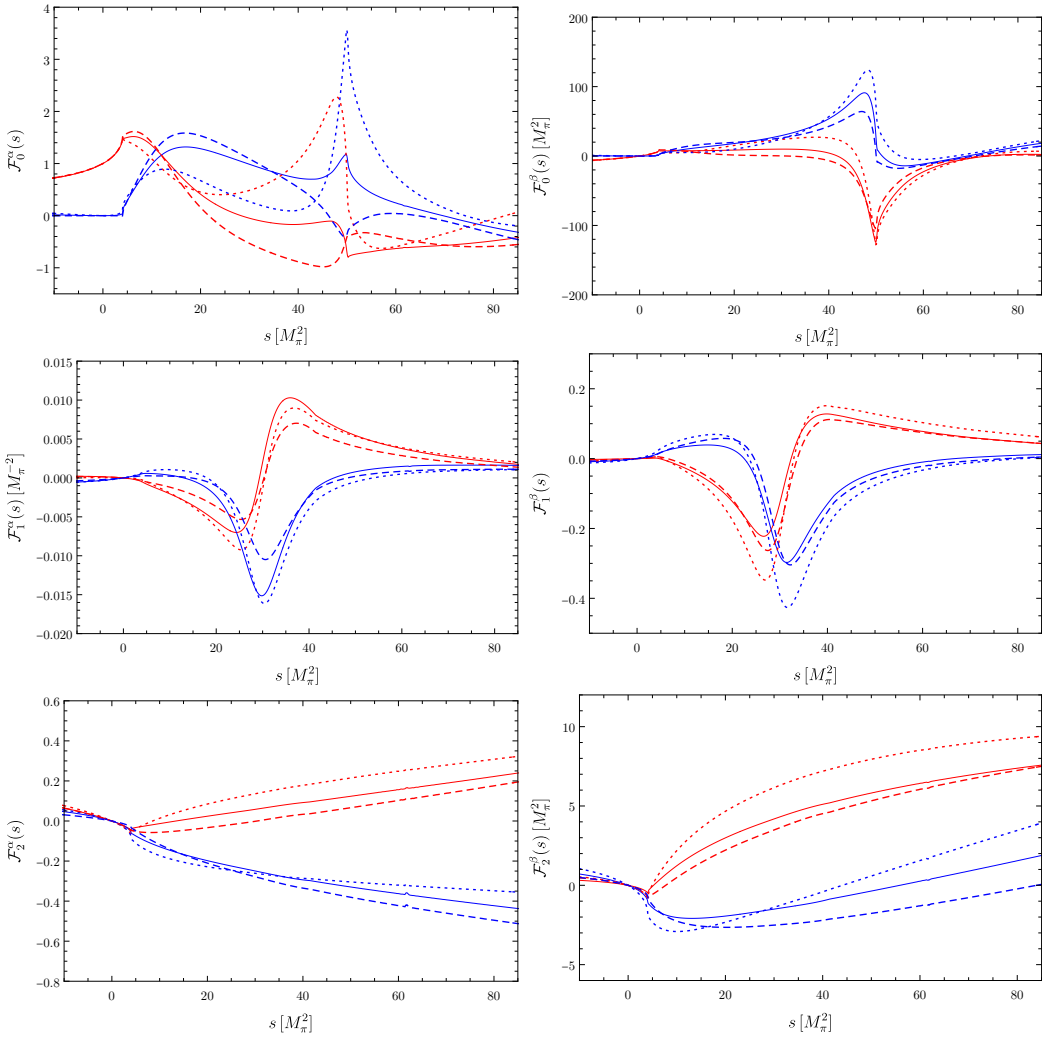

Figure E.13: Basis amplitudes $\mathcal{F}_I^\alpha$ and $\mathcal{F}_I^\beta$ for $\eta' \to 3\pi$. The real parts are colored in red, the imaginary ones in blue. Dotted lines denote the first iteration, dashed lines the second one, and solid lines the final solution (after 10 iterations).

$\eta' \to 3\pi$

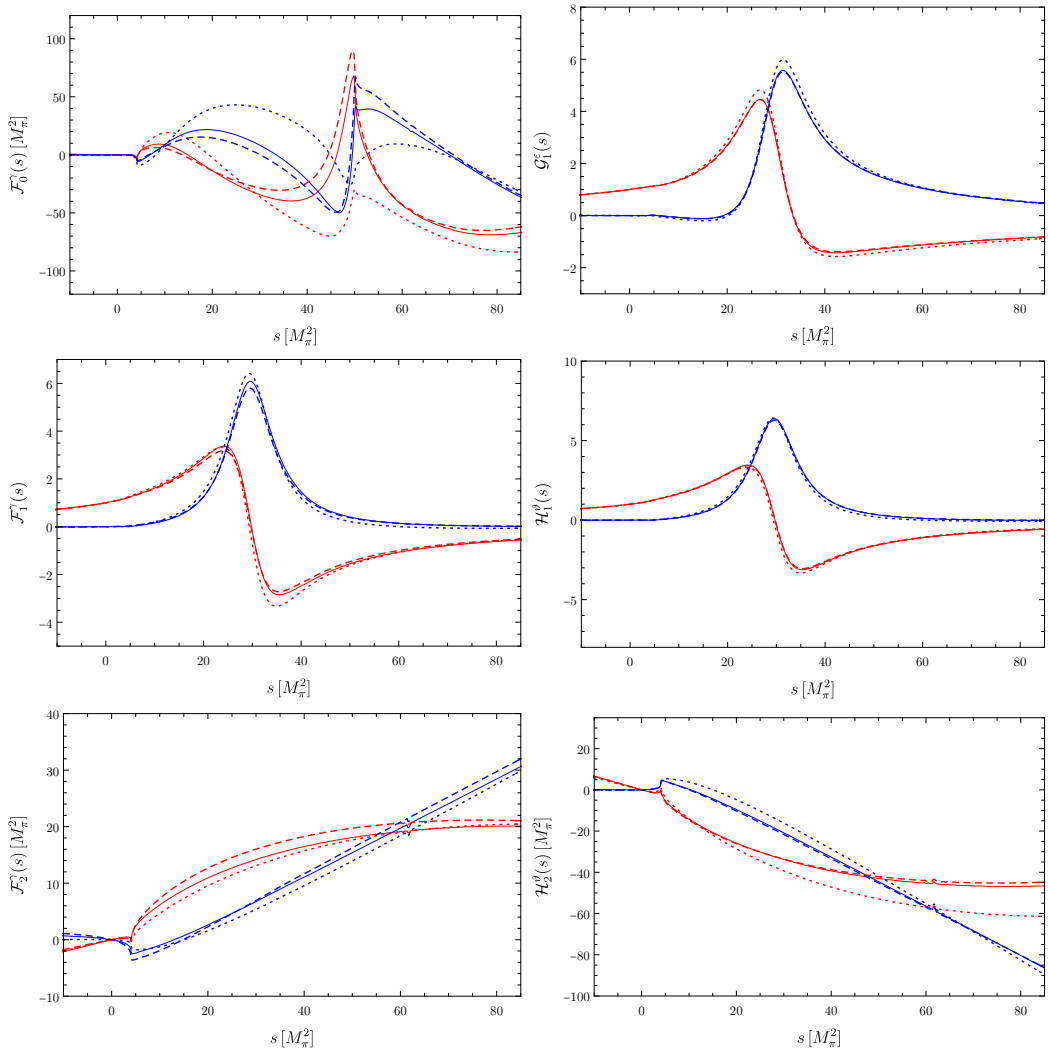

Figure E.14: Basis amplitudes $\mathcal{F}_I^\gamma$, $\mathcal{G}_I^\varepsilon$, and $\mathcal{H}_I^\vartheta$ for $\eta' \to 3\pi$. The real parts are colored in red, the imaginary ones in blue. Dotted lines denote the first iteration, dashed lines the second one, and solid lines the final solution (after 10 iterations).

$\eta' \to \eta\pi\pi$

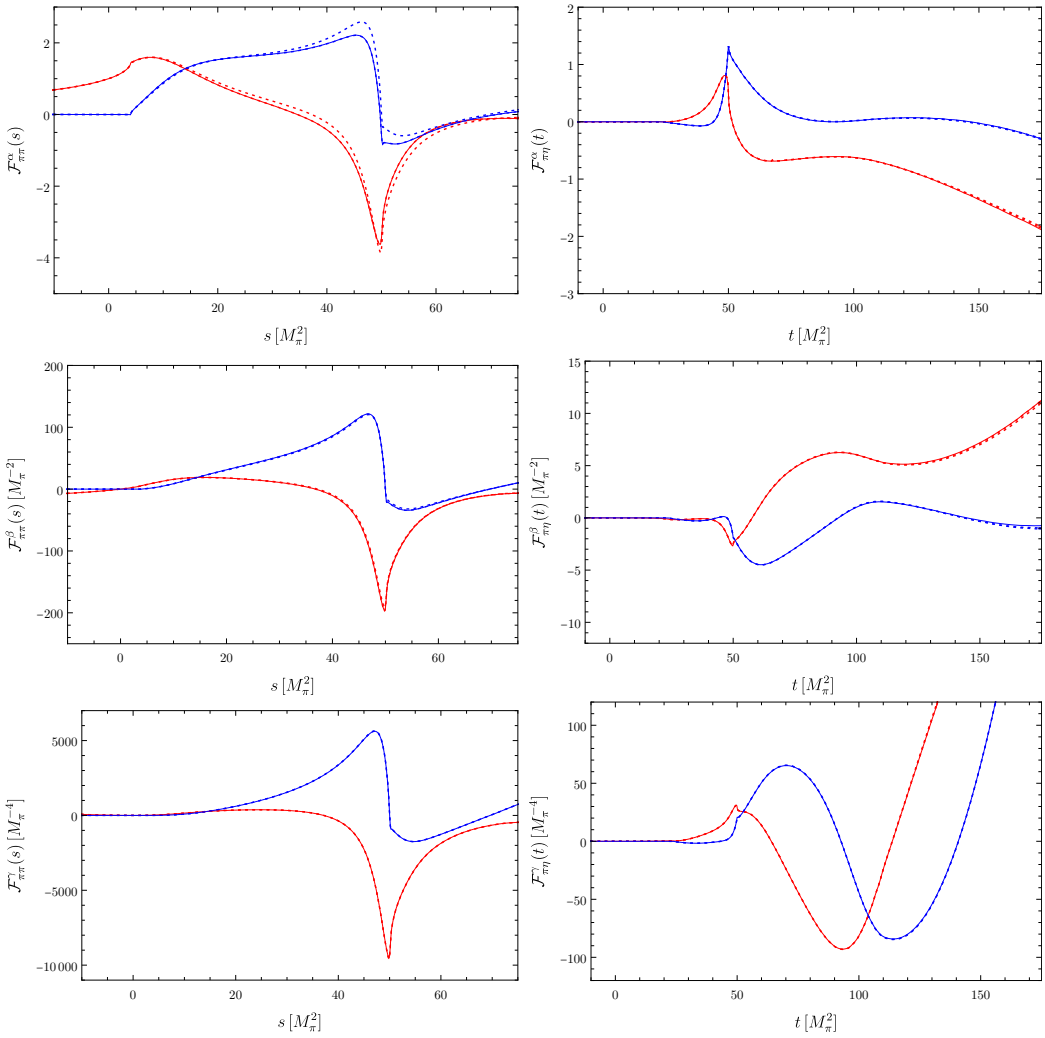

Figure E.15: Basis amplitudes $\mathcal{F}^{\alpha}_{\pi\pi}$, $\mathcal{F}^{\beta}_{\pi\pi}$, $\mathcal{F}^{\gamma}_{\pi\pi}$, $\mathcal{F}^{\alpha}_{\pi\eta}$, $\mathcal{F}^{\beta}_{\pi\eta}$, and $\mathcal{F}^{\gamma}_{\pi\eta}$ for $\eta' \to \eta\pi\pi$. The real parts are colored in red, the imaginary ones in blue. Dotted lines denote the first iteration, dashed lines the second one, and solid lines the final solution (after 3 iterations).

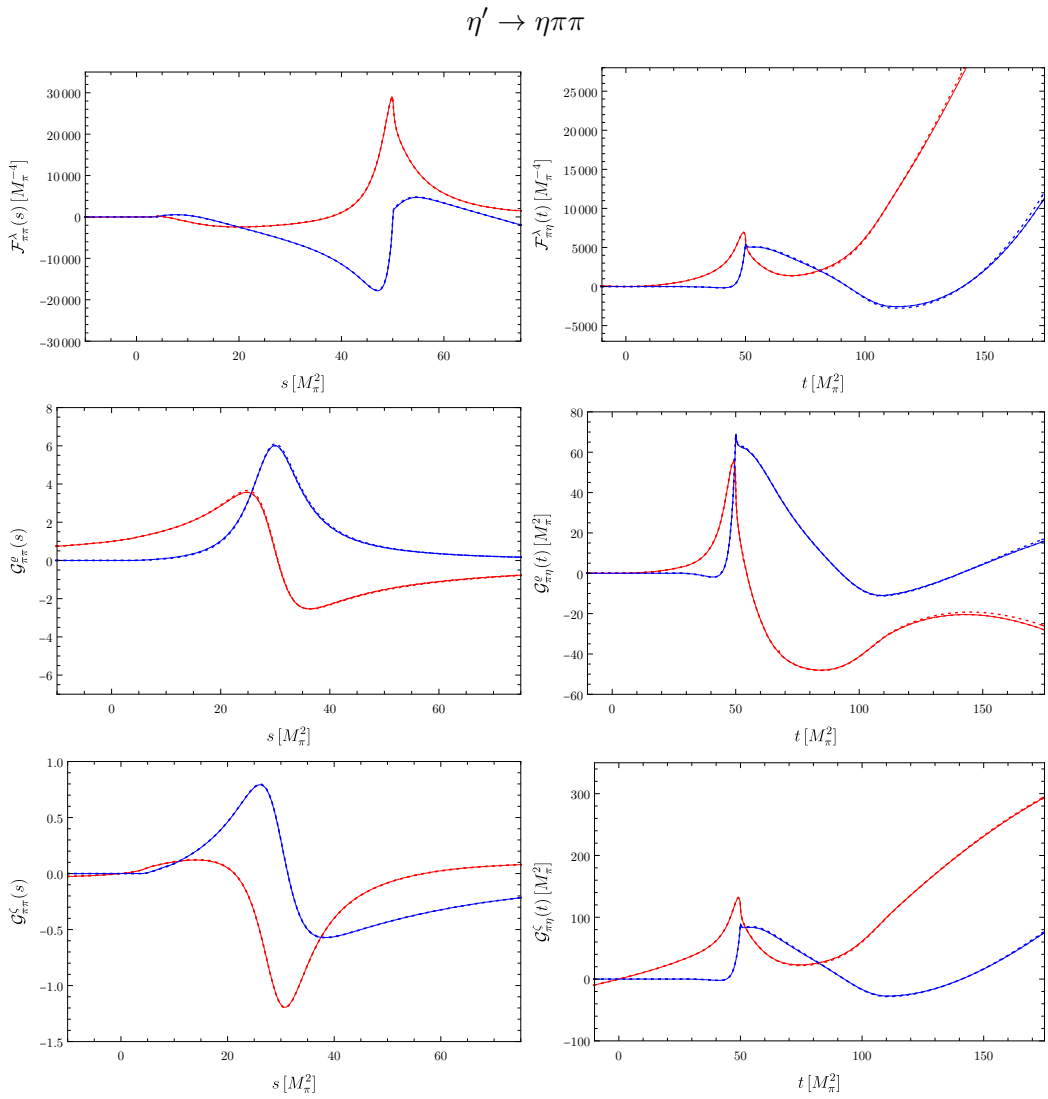

Figure E.16: Basis amplitudes $\mathcal{F}^{\lambda}_{\pi\pi}$, $\mathcal{F}^{\lambda}_{\eta\pi}$, $\mathcal{G}^{\varrho}_{\pi\pi}$, $\mathcal{G}^{\varrho}_{\eta\pi}$, $\mathcal{G}^{\zeta}_{\pi\pi}$, and $\mathcal{G}^{\zeta}_{\eta\pi}$ for $\eta' \to \eta\pi\pi$. The real parts are colored in red, the imaginary ones in blue. Dotted lines denote the first iteration, dashed lines the second one, and solid lines the final solution (after 3 iterations).

Bibliography

[1] H. Akdag, T. Isken and B. Kubis, *Patterns of C- and CP-violation in hadronic η and η' three-body decays*, *JHEP* **02** (2022) 137 [2111.02417].

[2] H. Akdag, B. Kubis and A. Wirzba, *C and CP violation in effective field theories*, *JHEP* **06** (2023) 154 [2212.07794].

[3] H. Akdag, B. Kubis and A. Wirzba, *Correlations of C and CP violation in $\eta \to \pi^0 \ell^+ \ell^-$ and $\eta' \to \eta \ell^+ \ell^-$*, 2307.02533.

[4] H. Akdag, T. Isken and B. Kubis, *Dispersive representation of C- and CP-violation in η and η' decays*, .

[5] D. Sadasivan, M. Mai, H. Akdag and M. Döring, *Dalitz plots and lineshape of $a_1(1260)$ from a relativistic three-body unitary approach*, *Phys. Rev. D* **101** (2020) 094018 [2002.12431].

[6] D. Sadasivan, A. Alexandru, H. Akdag, F. Amorim, R. Brett, C. Culver et al., *Pole position of the $a_1(1260)$ resonance in a three-body unitary framework*, *Phys. Rev. D* **105** (2022) 054020 [2112.03355].

[7] S.L. Glashow, *Partial Symmetries of Weak Interactions*, *Nucl. Phys.* **22** (1961) 579.

[8] A. Salam and J.C. Ward, *Electromagnetic and weak interactions*, *Phys. Lett.* **13** (1964) 168.

[9] P.W. Higgs, *Broken Symmetries and the Masses of Gauge Bosons*, *Phys. Rev. Lett.* **13** (1964) 508.

[10] S. Weinberg, *A Model of Leptons*, *Phys. Rev. Lett.* **19** (1967) 1264.

[11] G. 't Hooft and M.J.G. Veltman, *Regularization and Renormalization of Gauge Fields*, *Nucl. Phys. B* **44** (1972) 189.

[12] H. Fritzsch, M. Gell-Mann and H. Leutwyler, *Advantages of the Color Octet Gluon Picture*, *Phys. Lett. B* **47** (1973) 365.

[13] Particle Data Group collaboration, *Review of Particle Physics*, *PTEP* **2022** (2022) 083C01.

[14] F. Englert and R. Brout, *Broken Symmetry and the Mass of Gauge Vector Mesons*, *Phys. Rev. Lett.* **13** (1964) 321.

[15] ATLAS collaboration, *Observation of a new particle in the search for the Standard Model Higgs boson with the ATLAS detector at the LHC*, *Phys. Lett. B* **716** (2012) 1 [1207.7214].

[16] CMS collaboration, *Combined results of searches for the standard model Higgs boson in pp collisions at* $\sqrt{s} = 7$ *TeV*, *Phys. Lett. B* **710** (2012) 26 [1202.1488].

[17] Super-Kamiokande collaboration, *Evidence for oscillation of atmospheric neutrinos*, *Phys. Rev. Lett.* **81** (1998) 1562 [hep-ex/9807003].

[18] S. Singh, *Big bang: The origin of the universe (1st us ed.)*, *New York: Fourth Estate.* (2004) .

[19] A.D. Sakharov, *Violation of CP invariance, C asymmetry, and baryon asymmetry of the universe*, *Pisma Zh. Eksp. Teor. Fiz.* **5** (1967) 32.

[20] C.S. Wu, E. Ambler, R.W. Hayward, D.D. Hoppes and R.P. Hudson, *Experimental Test of Parity Conservation in* β *Decay*, *Phys. Rev.* **105** (1957) 1413.

[21] J.H. Christenson, J.W. Cronin, V.L. Fitch and R. Turlay, *Evidence for the* 2π *Decay of the* K_2^0 *Meson*, *Phys. Rev. Lett.* **13** (1964) 138.

[22] J.S. Schwinger, *The Theory of quantized fields. 1.*, *Phys. Rev.* **82** (1951) 914.

[23] G. Luders, *On the Equivalence of Invariance under Time Reversal and under Particle-Antiparticle Conjugation for Relativistic Field Theories*, *Kong. Dan. Vid. Sel. Mat. Fys. Med.* **28N5** (1954) 1.

[24] W. Pauli, L. Rosenfeld and V. Weisskopf, *Niels bohr and the development of physics*, *British Journal for the Philosophy of Science* **7** (1957) .

[25] E.M. Purcell and N.F. Ramsey, *On the Possibility of Electric Dipole Moments for Elementary Particles and Nuclei*, *Phys. Rev.* **78** (1950) 807.

[26] M.A. Shifman, A.I. Vainshtein and V.I. Zakharov, *Can Confinement Ensure Natural CP Invariance of Strong Interactions?*, *Nucl. Phys. B* **166** (1980) 493.

[27] R.J. Crewther, P. Di Vecchia, G. Veneziano and E. Witten, *Chiral Estimate of the Electric Dipole Moment of the Neutron in Quantum Chromodynamics*, *Phys. Lett. B* **88** (1979) 123.

[28] A. Pich and E. de Rafael, *Strong CP violation in an effective chiral Lagrangian approach*, *Nucl. Phys. B* **367** (1991) 313.

[29] M. Gorchtein, *Nucleon EDM and rare decays of* η *and* η' *mesons*, 0803.2906.

[30] T. Gutsche, A.N. Hiller Blin, S. Kovalenko, S. Kuleshov, V.E. Lyubovitskij, M.J. Vicente Vacas et al., *CP-violating decays of the pseudoscalars η and η' and their connection to the electric dipole moment of the neutron*, *Phys. Rev. D* **95** (2017) 036022 [1612.02276].

[31] A.S. Zhevlakov, M. Gorchtein, A.N. Hiller Blin, T. Gutsche and V.E. Lyubovitskij, *Bounds on rare decays of η and η' mesons from the neutron EDM*, *Phys. Rev. D* **99** (2019) 031703 [1812.00171].

[32] A.S. Zhevlakov, T. Gutsche and V.E. Lyubovitskij, *Updated limits on the CP violating $\eta\pi\pi$ and $\eta'\pi\pi$ couplings derived from the neutron EDM*, *Phys. Rev. D* **99** (2019) 115004 [1904.08154].

[33] A.S. Zhevlakov and V.E. Lyubovitskij, *Deuteron EDM induced by CP violating couplings of pseudoscalar mesons*, *Phys. Rev. D* **101** (2020) 115041 [2003.12217].

[34] L. Gan, B. Kubis, E. Passemar and S. Tulin, *Precision tests of fundamental physics with η and η' mesons*, *Phys. Rept.* **945** (2022) 1 [2007.00664].

[35] M. Pospelov and A. Ritz, *Electric dipole moments as probes of new physics*, *Annals Phys.* **318** (2005) 119 [hep-ph/0504231].

[36] WMAP collaboration, *Nine-Year Wilkinson Microwave Anisotropy Probe (WMAP) Observations: Cosmological Parameter Results*, *Astrophys. J. Suppl.* **208** (2013) 19 [1212.5226].

[37] M. Simonius, *On Time Reversal Violation in the Nucleon–Nucleon System*, *Phys. Lett. B* **58** (1975) 147.

[38] REDTOP collaboration, *The REDTOP project: Rare Eta Decays with a TPC for Optical Photons*, *PoS* **ICHEP2016** (2016) 812.

[39] REDTOP collaboration, *The REDTOP experiment*, 1910.08505.

[40] REDTOP collaboration, *The REDTOP experiment: Rare η/η' Decays To Probe New Physics*, 2203.07651.

[41] L. Gan, *Probes for Fundamental QCD Symmetries and a Dark Gauge Boson via Light Meson Decays*, *PoS* **CD15** (2015) 017.

[42] GlueX collaboration, L. Gan and *et al.*, "*Eta Decays with Emphasis on Rare Neutral Modes: The JLab Eta Factory (JEF) Experiment.*" https://www.jlab.org/exp_prog/proposals/14/PR12-14-004.pdf, 2014.

[43] L. Gan, *Test Fundamental Symmetries via Precision Measurements of π^0, η, and η' Decays*, *JPS Conf. Proc.* **13** (2017) 020063.

[44] P. Sánchez-Puertas, *CP violation in η muonic decays*, *JHEP* **01** (2019) 031 [1810.13228].

[45] R. Escribano, E. Royo and P. Sánchez-Puertas, *New-physics signatures via CP violation in $\eta^{(\prime)} \to \pi^0\mu^+\mu^-$ and $\eta' \to \eta\mu^+\mu^-$ decays*, *JHEP* **05** (2022) 147 [2202.04886].

[46] M. Zillinger, B. Kubis and P. Sánchez-Puertas, *CP violation in $\eta^{(\prime)} \to \pi^+\pi^-\mu^+\mu^-$ decays*, *JHEP* **12** (2022) 001 [2210.14925].

[47] M.J. Ramsey-Musolf and S. Su, *Low Energy Precision Test of Supersymmetry*, *Phys. Rept.* **456** (2008) 1 [hep-ph/0612057].

[48] J.C. Pati and A. Salam, *Lepton Number as the Fourth Color*, *Phys. Rev. D* **10** (1974) 275 [*Erratum Phys. Rev. D* **11** (1975) 703].

[49] R.N. Mohapatra and J.C. Pati, *Left-Right Gauge Symmetry and an Isoconjugate Model of CP Violation*, *Phys. Rev. D* **11** (1975) 566.

[50] R.N. Mohapatra and J.C. Pati, *A Natural Left-Right Symmetry*, *Phys. Rev. D* **11** (1975) 2558.

[51] R.N. Mohapatra and G. Senjanovic, *Neutrino Mass and Spontaneous Parity Nonconservation*, *Phys. Rev. Lett.* **44** (1980) 912.

[52] R.N. Mohapatra and G. Senjanovic, *Neutrino Masses and Mixings in Gauge Models with Spontaneous Parity Violation*, *Phys. Rev. D* **23** (1981) 165.

[53] G. Senjanovic and R.N. Mohapatra, *Exact Left-Right Symmetry and Spontaneous Violation of Parity*, *Phys. Rev. D* **12** (1975) 1502.

[54] G. Senjanovic, *Spontaneous Breakdown of Parity in a Class of Gauge Theories*, *Nucl. Phys. B* **153** (1979) 334.

[55] G.C. Branco, L. Lavoura and J.P. Silva, *CP Violation*, vol. 103 (1999).

[56] I.I. Bigi and A.I. Sanda, *CP Violation*, Cambridge University Press, 2 ed. (2009), 10.1017/CBO9780511581014.

[57] T.D. Lee, *A Theory of Spontaneous T Violation*, *Phys. Rev. D* **8** (1973) 1226.

[58] T.D. Lee, *CP Nonconservation and Spontaneous Symmetry Breaking*, *Phys. Rept.* **9** (1974) 143.

[59] P. Fayet, *A Gauge Theory of Weak and Electromagnetic Interactions with Spontaneous Parity Breaking*, *Nucl. Phys. B* **78** (1974) 14.

[60] R.A. Flores and M. Sher, *Higgs Masses in the Standard, Multi-Higgs and Supersymmetric Models*, *Annals Phys.* **148** (1983) 95.

[61] S. Weinberg, *Larger Higgs Exchange Terms in the Neutron Electric Dipole Moment*, *Phys. Rev. Lett.* **63** (1989) 2333.

[62] S. Gardner and J. Shi, *Patterns of CP violation from mirror symmetry breaking in the $\eta \to \pi^+\pi^-\pi^0$ Dalitz plot*, *Phys. Rev. D* **101** (2020) 115038 [1903.11617].

[63] S. Weinberg, *Phenomenological Lagrangians*, *Physica* **A96** (1979) 327.

[64] J. Goldstone, A. Salam and S. Weinberg, *Broken Symmetries*, *Phys. Rev.* **127** (1962) 965.

[65] C.A. Baker et al., *An Improved experimental limit on the electric dipole moment of the neutron*, *Phys. Rev. Lett.* **97** (2006) 131801 [hep-ex/0602020].

[66] J.E. Kim and G. Carosi, *Axions and the Strong CP Problem*, *Rev. Mod. Phys.* **82** (2010) 557 [0807.3125].

[67] J.M. Pendlebury et al., *Revised experimental upper limit on the electric dipole moment of the neutron*, *Phys. Rev. D* **92** (2015) 092003 [1509.04411].

[68] B. Graner, Y. Chen, E.G. Lindahl and B.R. Heckel, *Reduced Limit on the Permanent Electric Dipole Moment of Hg199*, *Phys. Rev. Lett.* **116** (2016) 161601 [1601.04339].

[69] C.G. Callan, Jr., R.F. Dashen and D.J. Gross, *The Structure of the Gauge Theory Vacuum*, *Phys. Lett. B* **63** (1976) 334.

[70] M.D. Schwartz, *Quantum Field Theory and the Standard Model*, Cambridge University Press (3, 2014).

[71] J.D. Bjorken and S.D. Drell, *Relativistic quantum fields*, .

[72] C. Itzykson and J.B. Zuber, *Quantum Field Theory*, International Series In Pure and Applied Physics, McGraw-Hill, New York (1980).

[73] S. Weinberg, *The Quantum theory of fields. Vol. 1: Foundations*, Cambridge University Press (6, 2005), 10.1017/CBO9781139644167.

[74] M.E. Peskin and D.V. Schroeder, *An Introduction to quantum field theory*, Addison-Wesley, Reading, USA (1995).

[75] I.I. Bigi and A.I. Sanda, *CP violation*, vol. 9, Cambridge University Press (9, 2009), 10.1017/CBO9780511581014.

[76] S. Scherer, *Introduction to chiral perturbation theory*, *Adv. Nucl. Phys.* **27** (2003) 277 [hep-ph/0210398].

[77] S. Scherer and M.R. Schindler, *A Primer for Chiral Perturbation Theory*, vol. 830, Springer (2012), 10.1007/978-3-642-19254-8.

[78] G. 't Hooft, *Symmetry Breaking Through Bell-Jackiw Anomalies*, *Phys. Rev. Lett.* **37** (1976) 8.

[79] H.K. Dreiner, H.E. Haber and S.P. Martin, *Two-component spinor techniques and Feynman rules for quantum field theory and supersymmetry*, *Phys. Rept.* **494** (2010) 1 [0812.1594].

[80] A. Jaffe and E. Witten, *Quantum yang-mills theory*, *The millennium prize problems* **1** (2006) 129.

[81] S. Lanz, *Determination of the quark mass ratio Q from $\eta \to 3\pi$*, Ph.D. thesis, Bern U., 2011. 1809.10110.

[82] S.P. Schneider, *Analysis tools for precision studies of hadronic three-body decays and transition form factors*, Ph.D. thesis, Bonn U., HISKP, 2012. https://hdl.handle.net/20.500.11811/5628.

[83] T. Isken, *Dispersive analysis of $\eta' \to 3\pi$ decays*, Master's thesis, Bonn U., HISKP, 2015.

[84] F. Niecknig, *Dispersive analysis of charmed meson decays*, Ph.D. thesis, Bonn U., HISKP, 2016.

[85] M. Niehus, *Quark mass dependence of $\gamma\pi \to \pi\pi$*, Master's thesis, Bonn U., HISKP, 2017.

[86] S. Holz, *Factorization breaking effects in the doubly-virtual η' transition form factor*, Master's thesis, Bonn U., HISKP, 2018.

[87] H. Akdag, *Comparative Analysis of Three-Body Unitarity in $\omega/\phi \to 3\pi$*, Master's thesis, Bonn U., HISKP, 2020.

[88] T. Isken, *Dispersive-theoretical analysis of $\pi\pi$ and $\pi\eta$ rescattering effects in strong three-body decays*, Ph.D. thesis, Bonn U., HISKP, 2021.

[89] S. Holz, *The Quest for the η and η' Transition Form Factors: A Stroll on the Precision Frontier*, Ph.D. thesis, Bonn U., HISKP, 2022.

[90] G. Barton, *Introduction to dispersion techniques in field theory*, W. A. Benjamin Inc., New York City (NY), United States (1965).

[91] R.J. Eden, P.V. Landshoff, D.I. Olive and J.C. Polkinghorne, *The analytic S-matrix*, Cambridge Univ. Press, Cambridge (1966).

[92] H.M. Nussenzveig, *Causality and dispersion relations*, vol. 95, Academic Press, New York, London (1972).

[93] N.M. Queen and G. Violini, *Dispersion theory in high-energy physics*, Macmillan Press Ltd., London, United Kingdom (1974).

[94] J.A. Oller, *A Brief Introduction to Dispersion Relations*, SpringerBriefs in Physics, Springer (2019), 10.1007/978-3-030-13582-9.

[95] B. Kubis, *Introduction to dispersion relations in hadron physics*, 2019.

[96] D. Olive, *Unitarity and the evaluation of discontinuities*, *Il Nuovo Cimento (1955-1965)* **26** (1962) 73.

[97] R.E. Cutkosky, *Singularities and discontinuities of Feynman amplitudes*, *J. Math. Phys.* **1** (1960) 429.

[98] J. Stern, H. Sazdjian and N.H. Fuchs, *What π-π scattering tells us about chiral perturbation theory*, *Phys. Rev. D* **47** (1993) 3814 [hep-ph/9301244].

[99] M. Knecht, B. Moussallam, J. Stern and N.H. Fuchs, *The Low-energy pi pi amplitude to one and two loops*, *Nucl. Phys. B* **457** (1995) 513 [hep-ph/9507319].

[100] B. Ananthanarayan and P. Büttiker, *Comparison of πK scattering in SU(3) chiral perturbation theory and dispersion relations*, *Eur. Phys. J. C* **19** (2001) 517 [hep-ph/0012023].

[101] M. Zdráhal and J. Novotný, *Dispersive Approach to Chiral Perturbation Theory*, *Phys. Rev. D* **78** (2008) 116016 [0806.4529].

[102] M. Froissart, *Asymptotic behavior and subtractions in the Mandelstam representation*, *Phys. Rev.* **123** (1961) 1053.

[103] S. Weinberg, *Pion scattering lengths*, *Phys. Rev. Lett.* **17** (1966) 616.

[104] K.M. Watson, *The Effect of final state interactions on reaction cross-sections*, *Phys. Rev.* **88** (1952) 1163.

[105] R. Omnès, *On the Solution of certain singular integral equations of quantum field theory*, *Nuovo Cim.* **8** (1958) 316.

[106] N.N. Khuri and S.B. Treiman, *Pion–Pion Scattering and $K^{\pm} \to 3\pi$ Decay*, *Phys. Rev.* **119** (1960) 1115.

[107] F. Niecknig, B. Kubis and S.P. Schneider, *Dispersive analysis of $\omega \to 3\pi$ and $\phi \to 3\pi$ decays*, *Eur. Phys. J.* **C72** (2012) 2014 [1203.2501].

[108] J.B. Bronzan and C. Kacser, *Khuri-Treiman Representation and Perturbation Theory*, *Phys. Rev.* **132** (1963) 2703.

[109] R.S. Conti and I.B. Khriplovich, *New limits on T odd, P even interactions*, *Phys. Rev. Lett.* **68** (1992) 3262.

[110] J. Engel, P.H. Frampton and R.P. Springer, *Effective Lagrangians and parity conserving time reversal violation at low-energies*, *Phys. Rev. D* **53** (1996) 5112 [nucl-th/9505026].

[111] M.J. Ramsey-Musolf, *Electric dipole moments and the mass scale of new T violating, P conserving interactions*, *Phys. Rev. Lett.* **83** (1999) 3997 [hep-ph/9905429].

[112] A. Kurylov, G.C. McLaughlin and M.J. Ramsey-Musolf, *Constraints on T odd, P even interactions from electric dipole moments, revisited*, *Phys. Rev. D* **63** (2001) 076007 [hep-ph/0011185].

[113] M. Hoferichter, *private communication*, 2021.

[114] J. Bsaisou, U.-G. Meißner, A. Nogga and A. Wirzba, *P- and T-Violating Lagrangians in Chiral Effective Field Theory and Nuclear Electric Dipole Moments*, *Annals Phys.* **359** (2015) 317 [1412.5471].

[115] J. Gasser and H. Leutwyler, *Chiral Perturbation Theory to One Loop*, *Annals Phys.* **158** (1984) 142.

[116] J. Gasser and H. Leutwyler, *Chiral Perturbation Theory: Expansions in the Mass of the Strange Quark*, *Nucl. Phys. B* **250** (1985) 465.

[117] W.R. Inc., "Mathematica, Version 13.2." Champaign, IL, 2022.

[118] T. Appelquist and J. Carazzone, *Infrared Singularities and Massive Fields*, *Phys. Rev. D* **11** (1975) 2856.

[119] C.W. Murphy, *Dimension-8 operators in the Standard Model Eective Field Theory*, *JHEP* **10** (2020) 174 [2005.00059].

[120] S. Weinberg, *Baryon and Lepton Nonconserving Processes*, *Phys. Rev. Lett.* **43** (1979) 1566.

[121] W. Buchmüller and D. Wyler, *Effective Lagrangian Analysis of New Interactions and Flavor Conservation*, *Nucl. Phys. B* **268** (1986) 621.

[122] B. Grzadkowski, M. Iskrzynski, M. Misiak and J. Rosiek, *Dimension-Six Terms in the Standard Model Lagrangian*, *JHEP* **10** (2010) 085 [1008.4884].

[123] L. Lehman, *Extending the Standard Model Effective Field Theory with the Complete Set of Dimension-7 Operators*, *Phys. Rev. D* **90** (2014) 125023 [1410.4193].

[124] B. Henning, X. Lu, T. Melia and H. Murayama, *2, 84, 30, 993, 560, 15456, 11962, 261485, ...: Higher dimension operators in the SM EFT*, *JHEP* **08** (2017) 016 [1512.03433].

[125] Y. Liao and X.-D. Ma, *Renormalization Group Evolution of Dimension-seven Baryon- and Lepton-number-violating Operators*, *JHEP* **11** (2016) 043 [1607.07309].

[126] H.-L. Li, Z. Ren, J. Shu, M.-L. Xiao, J.-H. Yu and Y.-H. Zheng, *Complete set of dimension-eight operators in the standard model effective field theory*, *Phys. Rev. D* **104** (2021) 015026 [2005.00008].

[127] Y. Liao and X.-D. Ma, *An explicit construction of the dimension-9 operator basis in the standard model effective field theory*, *JHEP* **11** (2020) 152 [2007.08125].

[128] H.-L. Li, Z. Ren, M.-L. Xiao, J.-H. Yu and Y.-H. Zheng, *Complete set of dimension-nine operators in the standard model effective field theory*, *Phys. Rev. D* **104** (2021) 015025 [2007.07899].

[129] F. del Aguila, S. Bar-Shalom, A. Soni and J. Wudka, *Heavy Majorana Neutrinos in the Effective Lagrangian Description: Application to Hadron Colliders*, *Phys. Lett. B* **670** (2009) 399 [0806.0876].

[130] A. Aparici, K. Kim, A. Santamaria and J. Wudka, *Right-handed neutrino magnetic moments*, *Phys. Rev. D* **80** (2009) 013010 [0904.3244].

[131] S. Bhattacharya and J. Wudka, *Dimension-seven operators in the standard model with right handed neutrinos*, *Phys. Rev. D* **94** (2016) 055022 [1505.05264].

[132] Y. Liao and X.-D. Ma, *Operators up to Dimension Seven in Standard Model Effective Field Theory Extended with Sterile Neutrinos*, *Phys. Rev. D* **96** (2017) 015012 [1612.04527].

[133] W. Dekens, J. de Vries, K. Fuyuto, E. Mereghetti and G. Zhou, *Sterile neutrinos and neutrinoless double beta decay in effective field theory*, *JHEP* **06** (2020) 097 [2002.07182].

[134] H.-L. Li, Z. Ren, M.-L. Xiao, J.-H. Yu and Y.-H. Zheng, *Operator bases in effective field theories with sterile neutrinos: $d \leq 9$*, *JHEP* **11** (2021) 003 [2105.09329].

[135] A.M. Galda, M. Neubert and S. Renner, *ALP — SMEFT interference*, *JHEP* **06** (2021) 135 [2105.01078].

[136] C.W. Murphy, *Low-Energy Effective Field Theory below the Electroweak Scale: Dimension-8 Operators*, *JHEP* **04** (2021) 101 [2012.13291].

[137] B. Grinstein and M. Trott, *A Higgs-Higgs bound state due to new physics at a TeV*, *Phys. Rev. D* **76** (2007) 073002 [0704.1505].

[138] R. Alonso, M.B. Gavela, L. Merlo, S. Rigolin and J. Yepes, *The Effective Chiral Lagrangian for a Light Dynamical "Higgs Particle"*, *Phys. Lett. B* **722** (2013) 330 [1212.3305].

[139] G. Buchalla, O. Catà and C. Krause, *Complete Electroweak Chiral Lagrangian with a Light Higgs at NLO*, *Nucl. Phys. B* **880** (2014) 552 [1307.5017].

[140] M.B. Gavela, K. Kanshin, P.A.N. Machado and S. Saa, *On the renormalization of the electroweak chiral Lagrangian with a Higgs*, *JHEP* **03** (2015) 043 [1409.1571].

[141] I. Brivio, J. Gonzalez-Fraile, M.C. Gonzalez-Garcia and L. Merlo, *The complete HEFT Lagrangian after the LHC Run I*, *Eur. Phys. J. C* **76** (2016) 416 [1604.06801].

[142] H. Sun, M.-L. Xiao and J.-H. Yu, *Complete NLO Operators in the Higgs Effective Field Theory*, 2206.07722.

[143] H. Sun, M.-L. Xiao and J.-H. Yu, *Complete NNLO Operator Bases in Higgs Effective Field Theory*, 2210.14939.

[144] H. Sun, Y.-N. Wang and J.-H. Yu, *Hilbert Series and Operator Counting on the Higgs Effective Field Theory*, 2211.11598.

[145] I. Brivio and M. Trott, *The Standard Model as an Effective Field Theory*, *Phys. Rept.* **793** (2019) 1 [1706.08945].

[146] E.E. Jenkins, A.V. Manohar and P. Stoffer, *Low-Energy Effective Field Theory below the Electroweak Scale: Operators and Matching*, *JHEP* **03** (2018) 016 [1709.04486].

[147] E.E. Jenkins, A.V. Manohar and P. Stoffer, *Low-Energy Effective Field Theory below the Electroweak Scale: Anomalous Dimensions*, *JHEP* **01** (2018) 084 [1711.05270].

[148] W. Dekens and P. Stoffer, *Low-energy effective field theory below the electroweak scale: matching at one loop*, *JHEP* **10** (2019) 197 [1908.05295].

[149] H.-L. Li, Z. Ren, M.-L. Xiao, J.-H. Yu and Y.-H. Zheng, *Low energy effective field theory operator basis at $d \leq 9$*, *JHEP* **06** (2021) 138 [2012.09188].

[150] Y. Liao, X.-D. Ma and Q.-Y. Wang, *Extending low energy effective field theory with a complete set of dimension-7 operators*, *JHEP* **08** (2020) 162 [2005.08013].

[151] T. Li, X.-D. Ma and M.A. Schmidt, *General neutrino interactions with sterile neutrinos in light of coherent neutrino-nucleus scattering and meson invisible decays*, *JHEP* **07** (2020) 152 [2005.01543].

[152] M. Chala and A. Titov, *One-loop matching in the SMEFT extended with a sterile neutrino*, *JHEP* **05** (2020) 139 [2001.07732].

[153] W. Dekens, J. de Vries and S. Shain, *CP-violating axion interactions in effective field theory*, 2203.11230.

[154] E. Fermi, *Tentativo di una Teoria Dei Raggi β*, *Nuovo Cim.* **11** (1934) 1.

[155] E. Fermi, *Versuch einer Theorie der β-Strahlen. I*, *Z. Phys.* **88** (1934) 161.

[156] J. Shi, *Theoretical Studies of C and CP Violation in $\eta \to \pi^+\pi^-\pi^0$ Decay*, Ph.D. thesis, Kentucky U., 2017. 10.13023/etd.2020.388.

[157] S. Gardner and J. Shi, *Leading-dimension, effective operators with CP and C or P violation in Standard Model effective field theory*, to be published, 2023.

[158] I.B. Khriplovich, *What do we know about T odd but P even interaction?*, *Nucl. Phys. B* **352** (1991) 385.

[159] C.M. Maekawa, E. Mereghetti, J. de Vries and U. van Kolck, *The Time-Reversal- and Parity-Violating Nuclear Potential in Chiral Effective Theory*, *Nucl. Phys. A* **872** (2011) 117 [1106.6119].

[160] J. de Vries, E. Mereghetti, R.G.E. Timmermans and U. van Kolck, *The Effective Chiral Lagrangian From Dimension-Six Parity and Time-Reversal Violation*, *Annals Phys.* **338** (2013) 50 [1212.0990].

[161] W. Dekens and J. de Vries, *Renormalization Group Running of Dimension-Six Sources of Parity and Time-Reversal Violation*, *JHEP* **05** (2013) 149 [1303.3156].

[162] J. Ng and S. Tulin, *D versus d: CP Violation in Beta Decay and Electric Dipole Moments*, *Phys. Rev. D* **85** (2012) 033001 [1111.0649].

[163] Y. Zhang, H. An, X. Ji and R.N. Mohapatra, *General CP Violation in Minimal Left-Right Symmetric Model and Constraints on the Right-Handed Scale*, *Nucl. Phys. B* **802** (2008) 247 [0712.4218].

[164] N.G. Deshpande, J.F. Gunion, B. Kayser and F.I. Olness, *Left-right symmetric electroweak models with triplet Higgs*, *Phys. Rev. D* **44** (1991) 837.

[165] F. Xu, H. An and X. Ji, *Neutron Electric Dipole Moment Constraint on Scale of Minimal Left-Right Symmetric Model*, *JHEP* **03** (2010) 088 [0910.2265].

[166] H. An, X. Ji and F. Xu, *P-odd and CP-odd Four-Quark Contributions to Neutron EDM*, *JHEP* **02** (2010) 043 [0908.2420].

[167] W. Dekens, J. de Vries, J. Bsaisou, W. Bernreuther, C. Hanhart, U.-G. Meißner et al., *Unraveling models of CP violation through electric dipole moments of light nuclei*, *JHEP* **07** (2014) 069 [1404.6082].

[168] G. Prezeau, M. Ramsey-Musolf and P. Vogel, *Neutrinoless double beta decay and effective field theory*, *Phys. Rev. D* **68** (2003) 034016 [hep-ph/0303205].

[169] M.L. Graesser, *An electroweak basis for neutrinoless double β decay*, *JHEP* **08** (2017) 099 [1606.04549].

[170] V. Cirigliano, W. Dekens, M. Graesser and E. Mereghetti, *Neutrinoless double beta decay and chiral $SU(3)$*, *Phys. Lett. B* **769** (2017) 460 [1701.01443].

[171] V. Cirigliano, W. Dekens, J. de Vries, M.L. Graesser and E. Mereghetti, *A neutrinoless double beta decay master formula from effective field theory*, *JHEP* **12** (2018) 097 [1806.02780].

[172] W. Dekens, E.E. Jenkins, A.V. Manohar and P. Stoffer, *Non-perturbative effects in $\mu \to e\gamma$*, *JHEP* **01** (2019) 088 [1810.05675].

[173] Y. Liao, X.-D. Ma and H.-L. Wang, *Effective field theory approach to lepton number violating decays $K^{\pm} \to \pi^{\mp} l^{\pm} l^{\pm}$: short-distance contribution*, *JHEP* **01** (2020) 127 [1909.06272].

[174] Y. Liao, X.-D. Ma and H.-L. Wang, *Effective field theory approach to lepton number violating decays $K^{\pm} \to \pi^{\mp} l_{\alpha}^{\pm} l_{\beta}^{\pm}$: long-distance contribution*, *JHEP* **03** (2020) 120 [2001.07378].

[175] X.-G. He, X.-D. Ma, J. Tandean and G. Valencia, *Evading the Grossman-Nir bound with $\Delta I = 3/2$ new physics*, *JHEP* **08** (2020) 034 [2005.02942].

[176] Y. Liao, X.-D. Ma and H.-L. Wang, *Effective field theory approach to lepton number violating τ decays*, *Chin. Phys. C* **45** (2021) 073102 [2102.03491].

[177] X.-G. He and X.-D. Ma, *An EFT toolbox for baryon and lepton number violating dinucleon to dilepton decays*, *JHEP* **06** (2021) 047 [2102.02562].

[178] J. Bijnens and E. Kofoed, *Chiral perturbation theory for neutron–antineutron oscillations*, *Eur. Phys. J. C* **77** (2017) 867 [1710.04383].

[179] J. de Vries, R.G.E. Timmermans, E. Mereghetti and U. van Kolck, *The Nucleon Electric Dipole Form Factor From Dimension-Six Time-Reversal Violation*, *Phys. Lett. B* **695** (2011) 268 [1006.2304].

[180] R. Kamand, B. Altschul and M.R. Schindler, *Hadronic Lorentz Violation in Chiral Perturbation Theory*, *Phys. Rev. D* **95** (2017) 056005 [1608.06503].

[181] R. Kamand, B. Altschul and M.R. Schindler, *Hadronic Lorentz Violation in Chiral Perturbation Theory Including the Coupling to External Fields*, *Phys. Rev. D* **97** (2018) 095027 [1712.00838].

[182] B. Altschul and M.R. Schindler, *Lorentz- and CPT -violating standard model extension in chiral perturbation theory*, *Phys. Rev. D* **100** (2019) 075031 [1907.02490].

[183] O. Cata and V. Mateu, *Chiral perturbation theory with tensor sources*, *JHEP* **09** (2007) 078 [0705.2948].

[184] U.-G. Meißner and A. Rusetsky, *Effective Field Theories*, Cambridge University Press (2022), 10.1017/9781108689038.

[185] H. Leutwyler, *On the foundations of chiral perturbation theory*, *Annals Phys.* **235** (1994) 165 [hep-ph/9311274].

[186] H.W. Fearing and S. Scherer, *Extension of the chiral perturbation theory meson Lagrangian to order p(6)*, *Phys. Rev. D* **53** (1996) 315 [hep-ph/9408346].

[187] J.A. Cronin, *Phenomenological model of strong and weak interactions in chiral U(3) x U(3)*, *Phys. Rev.* **161** (1967) 1483.

[188] J. Kambor, J.H. Missimer and D. Wyler, *The Chiral Loop Expansion of the Nonleptonic Weak Interactions of Mesons*, *Nucl. Phys. B* **346** (1990) 17.

[189] Y. Ünal, D. Severt, J. de Vries, C. Hanhart and U.-G. Meißner, *Electric dipole moments of baryons with bottom quarks*, *Phys. Rev. D* **105** (2022) 055026 [2111.13000].

[190] C. Rosenzweig, J. Schechter and C.G. Trahern, *Is the Effective Lagrangian for QCD a Sigma Model?*, *Phys. Rev. D* **21** (1980) 3388.

[191] P. Di Vecchia and G. Veneziano, *Chiral Dynamics in the Large n Limit*, *Nucl. Phys. B* **171** (1980) 253.

[192] E. Witten, *Large N Chiral Dynamics*, *Annals Phys.* **128** (1980) 363.

[193] K. Kawarabayashi and N. Ohta, *The Problem of η in the Large N Limit: Effective Lagrangian Approach*, *Nucl. Phys. B* **175** (1980) 477.

[194] P. Nath and R.L. Arnowitt, *The U(1) Problem: Current Algebra and the Theta Vacuum*, *Phys. Rev. D* **23** (1981) 473.

[195] H. Leutwyler, *On the 1/N expansion in chiral perturbation theory*, *Nucl. Phys. B Proc. Suppl.* **64** (1998) 223 [hep-ph/9709408].

[196] P. Herrera-Siklódy, J.I. Latorre, P. Pascual and J. Taron, *Chiral effective Lagrangian in the large N_c limit: The Nonet case*, *Nucl. Phys. B* **497** (1997) 345 [hep-ph/9610549].

[197] R. Kaiser and H. Leutwyler, *Large N_c in chiral perturbation theory*, *Eur. Phys. J. C* **17** (2000) 623 [hep-ph/0007101].

[198] P. Bickert, P. Masjuan and S. Scherer, *η-η' Mixing in Large-N_c Chiral Perturbation Theory*, *Phys. Rev. D* **95** (2017) 054023 [1612.05473].

[199] Serpukhov-Brussels-Los Alamos-Annecy(LAPP) collaboration, *Neutral Decays of η' (958)*, *Z. Phys. C* **36** (1987) 603.

[200] KLOE collaboration, *Upper limit on the $\eta \to \gamma\gamma\gamma$ branching ratio with the KLOE detector*, *Phys. Lett. B* **591** (2004) 49 [hep-ex/0402011].

[201] A.M. Blik et al., *Searches for rare and forbidden neutral decays of eta mesons at the GAMS-4pi facility*, *Phys. Atom. Nucl.* **70** (2007) 693.

[202] B.M.K. Nefkens et al., *Search for the forbidden decays $\eta \to 3\gamma$ and $\eta \to \pi^0\gamma$ and the rare decay $\eta \to \pi^0\pi^0\gamma\gamma$*, *Phys. Rev. C* **72** (2005) 035212.

[203] WASA-AT-COSY collaboration, *Search for C violation in the decay $\eta \to \pi^0 e^+ e^-$ with WASA-at-COSY*, *Phys. Lett. B* **784** (2018) 378 [1802.08642].

[204] CLEO collaboration, *Rare decays of the eta-prime*, *Phys. Rev. Lett.* **84** (2000) 26 [hep-ex/9907046].

[205] R.I. Dzhelyadin et al., *Search for Rare Decays of η and η' Mesons and for Light Higgs Particles*, *Phys. Lett. B* **105** (1981) 239.

[206] J.J. Thaler, J.A. Appel, A. Kotlewski, J.G. Layter, W.-Y. Lee and S. Stein, *Charge asymmetry in the decay $\eta \to \pi^+\pi^-\gamma$*, *Phys. Rev. Lett.* **29** (1972) 313.

[207] M. Gormley, E. Hyman, W.-Y. Lee, T. Nash, J. Peoples, C. Schultz et al., *Experimental determination of the Dalitz-plot distribution of the decays $\eta \to \pi^+\pi^-\pi^0$ and $\eta \to \pi^+\pi^-\gamma$, and the branching ratio $\eta \to \pi^+\pi^-\gamma/\eta \to \pi^+\pi^-\pi^0$*, *Phys. Rev. D* **2** (1970) 501.

[208] M.R. Jane et al., *A measurement of the charge asymmetry in the decay $\eta \to \pi^+\pi^-\gamma$*, *Phys. Lett. B* **48** (1974) 265.

[209] CRYSTAL BALL collaboration, *Test of Charge Conjugation Invariance*, *Phys. Rev. Lett.* **94** (2005) 041601.

[210] J. McDonough et al., *New Searches for the C Noninvariant Decay $\pi^0 \to 3\gamma$ and the Rare Decay $\pi^0 \to 4\gamma$*, *Phys. Rev. D* **38** (1988) 2121.

[211] A. Manohar and H. Georgi, *Chiral Quarks and the Nonrelativistic Quark Model*, *Nucl. Phys. B* **234** (1984) 189.

[212] H. Georgi, *Generalized dimensional analysis*, *Phys. Lett. B* **298** (1993) 187 [hep-ph/9207278].

[213] E.E. Jenkins, A.V. Manohar and M. Trott, *Naive Dimensional Analysis Counting of Gauge Theory Amplitudes and Anomalous Dimensions*, *Phys. Lett. B* **726** (2013) 697 [1309.0819].

[214] B.M. Gavela, E.E. Jenkins, A.V. Manohar and L. Merlo, *Analysis of General Power Counting Rules in Effective Field Theory*, *Eur. Phys. J. C* **76** (2016) 485 [1601.07551].

[215] KLOE-2 collaboration, *Precision measurement of the $\eta \to \pi^+\pi^-\pi^0$ Dalitz plot distribution with the KLOE detector*, *JHEP* **05** (2016) 019 [1601.06985].

[216] M. Gaspero, B. Meadows, K. Mishra and A. Soffer, *Isospin analysis of D0 decay to three pions*, *Phys. Rev. D* **78** (2008) 014015 [0805.4050].

[217] J. Prentki and M.J.G. Veltman, *Possibility of CP violation in semistrong interactions*, *Phys. Lett.* **15** (1965) 88.

[218] BESIII collaboration, *Amplitude Analysis of the Decays $\eta' \to \pi^+\pi^-\pi^0$ and $\eta' \to \pi^0\pi^0\pi^0$*, *Phys. Rev. Lett.* **118** (2017) 012001 [1606.03847].

[219] BESIII collaboration, *Measurement of the matrix elements for the decays $\eta' \to \eta\pi^+\pi^-$ and $\eta' \to \eta\pi^0\pi^0$*, *Phys. Rev. D* **97** (2018) 012003 [1709.04627].

[220] J.J. Sakurai, *Invariance principles and elementary particles*, Princeton University Press (1964).

[221] B. Barrett, M. Jacob, M. Nauenberg and T.N. Truong, *Consequences of C-Violating Interactions in η^0 and X^0 Decays*, *Phys. Rev.* **141** (1966) 1342.

[222] G. Ecker, A. Pich and E. de Rafael, *$K \to \pi\ell^+\ell^-$ decays in the effective chiral lagrangian of the standard model*, *Nucl. Phys. B* **291** (1987) 692.

[223] G. D'Ambrosio, G. Ecker, G. Isidori and J. Portoles, *The Decays $K \to \pi l^+ l^-$ beyond leading order in the chiral expansion*, *JHEP* **08** (1998) 004 [hep-ph/9808289].

[224] J. Bernstein, G. Feinberg and T.D. Lee, *Possible C, T Noninvariance in the Electromagnetic Interaction*, *Phys. Rev.* **139** (1965) B1650.

[225] M.J. Bazin, A.T. Goshaw, A.R. Zacher and C.R. Sun, *An Evaluation of Searches for C Nonconservation in eta Decay*, *Phys. Rev. Lett.* **20** (1968) 895.

[226] T.P. Cheng, *C-Conserving Decay $\eta \to \pi^0 e^+ e^-$ in a Vector-Meson-Dominant Model*, *Phys. Rev.* **162** (1967) 1734.

[227] J.N. Ng and D.J. Peters, *The Decay of the η meson into $\pi\mu^+\mu^-$*, *Phys. Rev. D* **46** (1992) 5034.

[228] R. Escribano and E. Royo, *A theoretical analysis of the semileptonic decays $\eta^{(\prime)} \to \pi^0 l^+ l^-$ and $\eta' \to \eta l^+ l^-$*, *Eur. Phys. J. C* **80** (2020) 1190 [2007.12467].

[229] B. Kubis and R. Schmidt, *Radiative corrections in $K \to \pi\ell^+\ell^-$ decays*, *Eur. Phys. J. C* **70** (2010) 219 [1007.1887].

[230] F. Stollenwerk, C. Hanhart, A. Kupść, U.-G. Meißner and A. Wirzba, *Model-independent approach to $\eta \to \pi^+\pi^-\gamma$ and $\eta' \to \pi^+\pi^-\gamma$*, *Phys. Lett. B* **707** (2012) 184 [1108.2419].

[231] C. Hanhart, A. Kupść, U.-G. Meißner, F. Stollenwerk and A. Wirzba, *Dispersive analysis for $\eta \to \gamma\gamma^*$*, *Eur. Phys. J. C* **73** (2013) 2668 [1307.5654].

[232] B. Kubis and J. Plenter, *Anomalous decay and scattering processes of the η meson*, *Eur. Phys. J. C* **75** (2015) 283 [1504.02588].

[233] C. Hanhart, S. Holz, B. Kubis, A. Kupść, A. Wirzba and C.-W. Xiao, *The branching ratio $\omega \to \pi^+\pi^-$ revisited*, *Eur. Phys. J. C* **77** (2017) 98 [1611.09359].

[234] S. Holz, J. Plenter, C.-W. Xiao, T. Dato, C. Hanhart, B. Kubis et al., *Towards an improved understanding of $\eta \to \gamma^*\gamma^*$*, *Eur. Phys. J. C* **81** (2021) 1002 [1509.02194].

[235] S. Holz, C. Hanhart, M. Hoferichter and B. Kubis, *A dispersive analysis of $\eta' \to \pi^+\pi^-\gamma$ and $\eta' \to \ell^+\ell^-\gamma$*, *Eur. Phys. J. C* **82** (2022) 434 [2202.05846].

[236] B. Barrett and T.N. Truong, *Analysis of η^0, $X^0 \to \pi^+\pi^-\gamma$ with a Possible C Violation*, *Phys. Rev.* **147** (1966) 1161.

[237] J. Wess and B. Zumino, *Consequences of anomalous Ward identities*, *Phys. Lett. B* **37** (1971) 95.

[238] E. Witten, *Global Aspects of Current Algebra*, *Nucl. Phys.* **B223** (1983) 422.

[239] M. Jacob and G.C. Wick, *On the General Theory of Collisions for Particles with Spin*, *Annals Phys.* **7** (1959) 404.

[240] R. García-Martín, R. Kamiński, J.R. Peláez, J. Ruiz de Elvira and F.J. Ynduráin, *The pion–pion scattering amplitude. IV: Improved analysis with once subtracted Roy-like equations up to 1100 MeV*, *Phys. Rev. D* **83** (2011) 074004 [1102.2183].

[241] H. Akdag, *Resonanzkopplungen in $\eta^{(\prime)} \to \pi^+\pi^-\gamma$*, 2018.

[242] B.M.K. Nefkens and J.W. Price, *The Neutral decay modes of the eta meson*, *Phys. Scripta T* **99** (2002) 114 [nucl-ex/0202008].

[243] C. Jarlskog and E. Shabalin, *On searches for CP, T, CPT and C violation in flavour-changing and flavour-conserving interactions*, *Phys. Scripta T* **99** (2002) 23.

[244] F.-K. Guo, B. Kubis and A. Wirzba, *Anomalous decays of η' and η into four pions*, *Phys. Rev. D* **85** (2012) 014014 [1111.5949].

[245] N. Cabibbo and A. Maksymowicz, *Angular Correlations in K_{e4} Decays and Determination of Low-Energy $\pi\pi$ Phase Shifts*, *Phys. Rev.* **137** (1965) B438.

[246] A.R. Barker, H. Huang, P.A. Toale and J. Engle, *Radiative corrections to double Dalitz decays: Effects on invariant mass distributions and angular correlations*, *Phys. Rev. D* **67** (2003) 033008 [hep-ph/0210174].

[247] K. Kampf, J. Novotný and P. Sánchez-Puertas, *Radiative corrections to double-Dalitz decays revisited*, *Phys. Rev. D* **97** (2018) 056010 [1801.06067].

[248] F.A. Berends, *The T violating decay of* $\pi^0 \to 3\gamma$, *Phys. Lett.* **16** (1965) 178.

[249] A.V. Tarasov, *3-photon decay of neutral pions*, *Sov. J. Nucl. Phys.* **5** (1967) 445.

[250] D.A. Dicus, *An Estimate of the Rate of the Rare Decay* $\pi^0 \to 3\gamma$, *Phys. Rev. D* **12** (1975) 2133.

[251] H.E. Conzett, *Null tests of time reversal invariance*, *Phys. Rev. C* **48** (1993) 423.

[252] M. Beyer, *Test of time reversal symmetry in the proton deuteron system*, *Nucl. Phys. A* **560** (1993) 895 [nucl-th/9302002].

[253] Y.N. Uzikov and A.A. Temerbayev, *Null-test signal for T-invariance violation in pd scattering*, *Phys. Rev. C* **92** (2015) 014002 [1506.08303].

[254] Y.N. Uzikov and J. Haidenbauer, *Polarized proton–deuteron scattering as a test of time-reversal invariance*, *Phys. Rev. C* **94** (2016) 035501 [1607.04409].

[255] D. Eversheim, Y. Valdau and B. Lorentz, *The Time Reversal Invariance Experiment at Cosy (TRIC)*, *PoS* **INPC2016** (2017) 177.

[256] PAX collaboration, *The Test of Time Reversal Invariance at Cosy (TRIC)*, *Acta Phys. Polon. B* **48** (2017) 1925.

[257] W.C. Haxton, A. Höring and M.J. Musolf, *Constraints on T-odd and P-even hadronic interactions from nucleon, nuclear, and atomic electric dipole moments*, *Phys. Rev. D* **50** (1994) 3422.

[258] J. Lu and B. Moussallam, *The* $\pi\eta$ *interaction and* a_0 *resonances in photon–photon scattering*, *Eur. Phys. J. C* **80** (2020) 436 [2002.04441].

[259] J. Smith, *C-Conserving Decay Modes* $\eta \to \pi^0 e^+ e^-$ *and* $\eta \to \pi^0 \mu^+ \mu^-$, *Phys. Rev.* **166** (1968) 1629.

[260] J.N. Ng and D.J. Peters, *Decay of the* η *meson into* $\pi\mu^+\mu^-$, *Phys. Rev. D* **46** (1992) 5034.

[261] J.N. Ng and D.J. Peters, *Study of* $\eta \to \pi^0\gamma\gamma$ *decay using the quark-box diagram*, *Phys. Rev. D* **47** (1993) 4939.

[262] S.P. Schneider, B. Kubis and F. Niecknig, *The* $\omega \to \pi^0\gamma^*$ *and* $\phi \to \pi^0\gamma^*$ *transition form factors in dispersion theory*, *Phys. Rev. D* **86** (2012) 054013 [1206.3098].

[263] J.G. Layter, J.A. Appel, A. Kotlewski, W.-Y. Lee, S. Stein and J.J. Thaler, *Measurement of the charge asymmetry in the decay* $\eta \to \pi^+\pi^-\pi^0$, *Phys. Rev. Lett.* **29** (1972) 316.

[264] T.D. Lee, *Possible C-Noninvariant Effects in the 3π Decay Modes of η^0 and ω^0*, *Phys. Rev.* **139** (1965) B1415.

[265] M. Nauenberg, *The $\eta \to \pi^+\pi^-\pi^0$ decay with C-violation*, *Phys. Lett.* **17** (1965) 329.

[266] M. Gormley, E. Hyman, W. Lee, T. Nash, J. Peoples, C. Schultz et al., *Experimental Test of C Invariance in $\eta \to \pi^+\pi^-\pi^0$*, *Phys. Rev. Lett.* **21** (1968) 402.

[267] M.R. Jane et al., *A Measurement of the Charge Asymmetry in the Decay $\eta \to \pi^+\pi^-\pi^0$*, *Phys. Lett. B* **48** (1974) 260.

[268] KLOE collaboration, *Determination of $\eta \to \pi^+\pi^-\pi^0$ Dalitz plot slopes and asymmetries with the KLOE detector*, *JHEP* **05** (2008) 006 [0801.2642].

[269] WASA-AT-COSY collaboration, *Measurement of the $\eta \to \pi^+\pi^-\pi^0$ Dalitz plot distribution*, *Phys. Rev. C* **90** (2014) 045207 [1406.2505].

[270] BESIII collaboration, *Measurement of the Matrix Elements for the Decays $\eta \to \pi^+\pi^-\pi^0$ and $\eta/\eta' \to \pi^0\pi^0\pi^0$*, *Phys. Rev. D* **92** (2015) 012014 [1506.05360].

[271] T.D. Lee and L. Wolfenstein, *Analysis of CP-Noninvariant Interactions and the K_1^0, K_2^0 System*, *Phys. Rev.* **138** (1965) B1490.

[272] C. Ditsche, B. Kubis and U.-G. Meißner, *Electromagnetic corrections in $\eta \to 3\pi$ decays*, *Eur. Phys. J. C* **60** (2009) 83 [0812.0344].

[273] S.P. Schneider, B. Kubis and C. Ditsche, *Rescattering effects in $\eta \to 3\pi$ decays*, *JHEP* **02** (2011) 028 [1010.3946].

[274] J. Gasser and H. Leutwyler, *$\eta \to 3\pi$ to One Loop*, *Nucl. Phys. B* **250** (1985) 539.

[275] D.G. Sutherland, *Current algebra and the decay $\eta \to 3\pi$*, *Phys. Lett.* **23** (1966) 384.

[276] J.S. Bell and D.G. Sutherland, *Current algebra and $\eta \to 3\pi$*, *Nucl. Phys. B* **4** (1968) 315.

[277] R. Baur, J. Kambor and D. Wyler, *Electromagnetic corrections to the decays $\eta \to 3\pi$*, *Nucl. Phys. B* **460** (1996) 127 [hep-ph/9510396].

[278] K. Kampf, M. Knecht, J. Novotný and M. Zdráhal, *Analytical dispersive construction of $\eta \to 3\pi$ amplitude: first order in isospin breaking*, *Phys. Rev. D* **84** (2011) 114015 [1103.0982].

[279] P. Guo, I.V. Danilkin, D. Schott, C. Fernández-Ramírez, V. Mathieu and A.P. Szczepaniak, *Three-body final state interaction in $\eta \to 3\pi$*, *Phys. Rev. D* **92** (2015) 054016 [1505.01715].

[280] P. Guo, I.V. Danilkin, C. Fernández-Ramírez, V. Mathieu and A.P. Szczepaniak, *Three-body final state interaction in $\eta \to 3\pi$ updated*, *Phys. Lett. B* **771** (2017) 497 [1608.01447].

[281] G. Colangelo, S. Lanz, H. Leutwyler and E. Passemar, *$\eta \to 3\pi$: Study of the Dalitz plot and extraction of the quark mass ratio Q*, *Phys. Rev. Lett.* **118** (2017) 022001 [1610.03494].

[282] M. Albaladejo and B. Moussallam, *Extended chiral Khuri–Treiman formalism for $\eta \to 3\pi$ and the role of the $a_0(980)$, $f_0(980)$ resonances*, *Eur. Phys. J. C* **77** (2017) 508 [1702.04931].

[283] G. Colangelo, S. Lanz, H. Leutwyler and E. Passemar, *Dispersive analysis of $\eta \to 3\pi$*, *Eur. Phys. J. C* **78** (2018) 947 [1807.11937].

[284] K. Kampf, M. Knecht, J. Novotný and M. Zdráhal, *Dispersive construction of two-loop $P \to \pi\pi\pi$ ($P = K, \eta$) amplitudes*, *Phys. Rev. D* **101** (2020) 074043 [1911.11762].

[285] V. Dorofeev et al., *Study of $\eta' \to \eta\pi^+\pi^-$ Dalitz plot*, *Phys. Lett. B* **651** (2007) 22 [hep-ph/0607044].

[286] BESIII collaboration, *Measurement of the Matrix Element for the Decay $\eta' \to \eta\pi^+\pi^-$*, *Phys. Rev. D* **83** (2011) 012003 [1012.1117].

[287] T. Isken, B. Kubis, S.P. Schneider and P. Stoffer, *Dispersion relations for $\eta' \to \eta\pi\pi$*, *Eur. Phys. J. C* **77** (2017) 489 [1705.04339].

[288] H. Osborn and D.J. Wallace, *$\eta - x$ mixing, $\eta \to 3\pi$ and chiral lagrangians*, *Nucl. Phys. B* **20** (1970) 23.

[289] J. Kambor, C. Wiesendanger and D. Wyler, *Final state interactions and Khuri–Treiman equations in $\eta \to 3\pi$ decays*, *Nucl. Phys. B* **465** (1996) 215 [hep-ph/9509374].

[290] A.V. Anisovich and H. Leutwyler, *Dispersive analysis of the decay $\eta \to 3\pi$*, *Phys. Lett. B* **375** (1996) 335 [hep-ph/9601237].

[291] J. Bijnens and J. Gasser, *Eta decays at and beyond p^4 in chiral perturbation theory*, *Phys. Scripta T* **99** (2002) 34 [hep-ph/0202242].

[292] B. Borasoy and R. Nißler, *Hadronic η and η' decays*, *Eur. Phys. J. A* **26** (2005) 383 [hep-ph/0510384].

[293] J. Bijnens and K. Ghorbani, *$\eta \to 3\pi$ at Two Loops In Chiral Perturbation Theory*, *JHEP* **11** (2007) 030 [0709.0230].

[294] E. Wigner, *Einige Folgerungen aus der Schrödingerschen Theorie für die Termstrukturen*, *Z. Phys.* **43** (1927) 624.

[295] C. Eckart, *The Application of Group Theory to the Quantum Dynamics of Monatomic Systems*, *Rev. Mod. Phys.* **2** (1930) 305.

[296] F. Niecknig and B. Kubis, *Dispersion-theoretical analysis of the $D^+ \to K^-\pi^+\pi^+$ Dalitz plot*, *JHEP* **10** (2015) 142 [1509.03188].

[297] F. Niecknig and B. Kubis, *Consistent Dalitz plot analysis of Cabibbo-favored $D^+ \to \bar{K}\pi\pi^+$ decays*, *Phys. Lett. B* **780** (2018) 471 [1708.00446].

[298] G. Colangelo, J. Gasser and H. Leutwyler, *$\pi\pi$ scattering*, *Nucl. Phys. B* **603** (2001) 125 [hep-ph/0103088].

[299] I. Caprini, G. Colangelo and H. Leutwyler, *Regge analysis of the $\pi\pi$ scattering amplitude*, *Eur. Phys. J. C* **72** (2012) 1860 [1111.7160].

[300] A2 collaboration, *High-statistics measurement of the $\eta \to 3\pi^0$ decay at the Mainz Microtron*, *Phys. Rev. C* **97** (2018) 065203 [1803.02502].

[301] M. Bashkanov et al., *Measurement of the slope parameter for the $\eta \to 3\pi^0$ decay in the $pp \to pp\eta$ reaction*, *Phys. Rev. C* **76** (2007) 048201 [0708.2014].

[302] WASA-at-COSY collaboration, *Measurement of the $\eta \to 3\pi^0$ Dalitz Plot Distribution with the WASA Detector at COSY*, *Phys. Lett. B* **677** (2009) 24 [0811.2763].

[303] Crystal Ball at MAMI, A2 collaboration, *Measurement of the Slope Parameter alpha for the $\eta \to 3\pi^0$ decay with the Crystal Ball at MAMI-C*, *Phys. Rev. C* **79** (2009) 035204 [0812.1999].

[304] Crystal Ball at MAMI, TAPS, A2 collaboration, *Determination of the Dalitz plot parameter alpha for the decay $\eta \to 3\pi^0$ with the Crystal Ball at MAMI-B*, *Eur. Phys. J. A* **39** (2009) 169 [0812.3324].

[305] KLOE collaboration, *Measurement of the $\eta \to 3\pi^0$ slope parameter α with the KLOE detector*, *Phys. Lett. B* **694** (2011) 16 [1004.1319].

[306] BESIII collaboration, *Observation of the isospin-violating decay $J/\psi \to \phi\pi^0 f_0(980)$*, *Phys. Rev. D* **92** (2015) 012007 [1505.06283].

[307] T. Isken, P. Stoffer, B. Kubis and A. Kupść, *Strong three-body decays of η and η' mesons*, to be published, 2023.

[308] V. Bernard, N. Kaiser and U.-G. Meißner, *$\pi\eta$ scattering in QCD*, *Phys. Rev. D* **44** (1991) 3698.

[309] M. Albaladejo and B. Moussallam, *Form factors of the isovector scalar current and the $\eta\pi$ scattering phase shifts*, *Eur. Phys. J. C* **75** (2015) 488 [1507.04526].

[310] A.M. Blik et al., *Measurement of the matrix element for the decay $\eta' \to \eta\pi^0\pi^0$ with the GAMS-4pi spectrometer*, *Phys. Atom. Nucl.* **72** (2009) 231.

[311] P. Adlarson et al., *Measurement of the decay $\eta' \to \pi^0\pi^0\eta$ at MAMI*, *Phys. Rev. D* **98** (2018) 012001 [1709.04230].

[312] B. Kubis and S.P. Schneider, *The Cusp effect in $\eta' \to \eta\pi\pi$ decays*, *Eur. Phys. J. C* **62** (2009) 511 [0904.1320].

[313] R. Escribano, P. Masjuan and J.J. Sanz-Cillero, *Chiral dynamics predictions for $\eta' \to \eta\pi\pi$*, *JHEP* **05** (2011) 094 [1011.5884].

[314] S. Gonzàlez-Solís and E. Passemar, *$\eta' \to \eta\pi\pi$ decays in unitarized resonance chiral theory*, *Eur. Phys. J. C* **78** (2018) 758 [1807.04313].

[315] S.L. Adler, *Consistency Conditions on the Strong Interactions Implied by a Partially Conserved Axial-Vector Current*, *Phys. Rev.* **137** (1965) B1022.

[316] S.L. Adler, *Consistency Conditions on the Strong Interactions Implied by a Partially Conserved Axial-Vector Current. II*, *Phys. Rev.* **139** (1965) B1638.

[317] Riazuddin and S. Oneda, *Some remarks on the $(3, 3^*) \bigoplus (3^*, 3)$ breaking of chiral symmetry*, *Phys. Rev. Lett.* **27** (1971) 548.

[318] N.G. Deshpande and T.N. Truong, *Resolution of the $\eta' \to \eta\pi\pi$ puzzle*, *Phys. Rev. Lett.* **41** (1978) 1579.

[319] J. Bernstein, G. Feinberg and T.D. Lee, *Possible C, T Noninvariance in the Electromagnetic Interaction*, *Phys. Rev.* **139** (1965) B1650.

[320] C.H. Llewellyn Smith, *The Decay $\eta \to \pi^0 e^+ e^-$ with C Conservation*, *Nuovo Cim. A* **48** (1967) 834 [*Erratum Nuovo Cim. A* **50** (1967) 374].

[321] H. Schäfer, M. Zanke, Y. Korte and B. Kubis, *The semileptonic decays $\eta^{(\prime)} \to \pi^0\ell^+\ell^-$ and $\eta' \to \eta\ell^+\ell^-$ in the standard model*, 2307.10357.

[322] R. Escribano, E. Royo and P. Sánchez-Puertas, *New-physics signatures via CP violation in $\eta^{(\prime)} \to \pi^0\mu^+\mu^-$ and $\eta' \to \eta\mu^+\mu^-$ decays*, *JHEP* **05** (2022) 147 [2202.04886].

[323] L. Gan and A. Gasparian, *Search of new physics via eta rare decays*, *PoS* **CD09** (2009) 048.

[324] GlueX collaboration, L. Gan et al., "*Eta Decays with Emphasis on Rare Neutral Modes: The JLab Eta Factory (JEF) Experiment.*" https://www.jlab.org/exp_prog/proposals/14/PR12-14-004.pdf, 2014.

[325] GlueX collaboration, L. Gan et al., "*Update to the JEF proposal.*" https://www.jlab.org/exp_prog/proposals/17/C12-14-004.pdf, 2017.

[326] G. Köpp, *Dispersion calculation of the transition form factor $f_{\pi\omega\gamma}(t)$ with cut contributions*, *Phys. Rev. D* **10** (1974) 932.

[327] I.V. Danilkin, C. Fernández-Ramírez, P. Guo, V. Mathieu, D. Schott, M. Shi et al., *Dispersive analysis of $\omega/\phi \to 3\pi, \pi^0\gamma$*, *Phys. Rev. D* **91** (2015) 094029 [1409.7708].

[328] B. Kubis and F. Niecknig, *Analysis of the $J/\psi \to \pi^0\gamma^*$ transition form factor*, *Phys. Rev. D* **91** (2015) 036004 [1412.5385].

[329] JPAC collaboration, *$\omega \to 3\pi$ and $\omega\pi^0$ transition form factor revisited*, *Eur. Phys. J. C* **80** (2020) 1107 [2006.01058].

[330] T. Feldmann, *Quark structure of pseudoscalar mesons*, *Int. J. Mod. Phys. A* **15** (2000) 159 [hep-ph/9907491].

[331] V.L. Chernyak and A.R. Zhitnitsky, *Asymptotic Behavior of Hadron Form-Factors in Quark Model. (In Russian)*, *JETP Lett.* **25** (1977) 510.

[332] V.L. Chernyak and A.R. Zhitnitsky, *Asymptotics of Hadronic Form-Factors in the Quantum Chromodynamics. (In Russian)*, *Sov. J. Nucl. Phys.* **31** (1980) 544.

[333] A.V. Efremov and A.V. Radyushkin, *Asymptotical Behavior of Pion Electromagnetic Form-Factor in QCD*, *Theor. Math. Phys.* **42** (1980) 97.

[334] A.V. Efremov and A.V. Radyushkin, *Factorization and Asymptotical Behavior of Pion Form-Factor in QCD*, *Phys. Lett. B* **94** (1980) 245.

[335] G.R. Farrar and D.R. Jackson, *The Pion Form-Factor*, *Phys. Rev. Lett.* **43** (1979) 246.

[336] G.P. Lepage and S.J. Brodsky, *Exclusive Processes in Quantum Chromodynamics: Evolution Equations for Hadronic Wave Functions and the Form-Factors of Mesons*, *Phys. Lett. B* **87** (1979) 359.

[337] G.P. Lepage and S.J. Brodsky, *Exclusive Processes in Perturbative Quantum Chromodynamics*, *Phys. Rev. D* **22** (1980) 2157.

[338] H. Leutwyler, *Electromagnetic form factor of the pion*, in *Continuous Advances in QCD 2002 / Arkadyfest (honoring the 60th birthday of Prof. Arkady Vainshtein)*, pp. 23–40, 12, 2002, DOI [hep-ph/0212324].

[339] B. Ananthanarayan, I. Caprini and I.S. Imsong, *Implications of the recent high statistics determination of the pion electromagnetic form factor in the timelike region*, *Phys. Rev. D* **83** (2011) 096002 [1102.3299].

[340] B. Lee, *Chiral dynamics*, *Cargese Lect. Phys.* **5** (1972) 119.

[341] O. Kaymakcalan and J. Schechter, *Chiral Lagrangian of Pseudoscalars and Vectors*, *Phys. Rev. D* **31** (1985) 1109.

[342] U.-G. Meißner, *Low-Energy Hadron Physics from Effective Chiral Lagrangians with Vector Mesons*, *Phys. Rept.* **161** (1988) 213.

[343] P. Jain, R. Johnson, U.-G. Meißner, N.W. Park and J. Schechter, *Realistic Pseudoscalar Vector Chiral Lagrangian and Its Soliton Excitations*, *Phys. Rev. D* **37** (1988) 3252.

[344] F. Klingl, N. Kaiser and W. Weise, *Effective Lagrangian approach to vector mesons, their structure and decays*, *Z. Phys. A* **356** (1996) 193 [hep-ph/9607431].

[345] M. Mai, U.-G. Meißner and C. Urbach, *Towards a theory of hadron resonances*, *Phys. Rept.* **1001** (2023) 1 [2206.01477].

[346] BESIII collaboration, *Precision measurement of the matrix elements for $\eta \to \pi^+\pi^-\pi^0$ and $\eta \to \pi^0\pi^0\pi^0$ decays*, *Phys. Rev. D* **107** (2023) 092007 [2302.08282].

[347] B. Moussallam, *Couplings of light $I = 0$ scalar mesons to simple operators in the complex plane*, *Eur. Phys. J. C* **71** (2011) 1814 [1110.6074].

[348] M. Hoferichter, B. Kubis and M. Zanke, *Radiative resonance couplings in $\gamma\pi \to \pi\pi$*, *Phys. Rev. D* **96** (2017) 114016 [1710.00824].

[349] R. García-Martín, R. Kamiński, J.R. Peláez and J. Ruiz de Elvira, *Precise determination of the $f_0(600)$ and $f_0(980)$ pole parameters from a dispersive data analysis*, *Phys. Rev. Lett.* **107** (2011) 072001 [1107.1635].

[350] A. Starostin et al., *Search for the charge-conjugation-forbidden decay $\omega \to \eta\pi^0$*, *Phys. Rev. C* **79** (2009) 065201.

[351] J. Herz, H. Akdag and B. Kubis, *C and CP violation in $\eta^{(\prime)} \to \gamma\ell^+\ell^-$ and $\eta^{(\prime)} \to \pi^+\pi^-\ell^+\ell^-$*, .

[352] E. Byckling and K. Kajantie, *Particle Kinematics: (Chapters I-VI, X)*, University of Jyvaskyla, Jyvaskyla, Finland (1971).

[353] W. von Schlippe, "*Relativistic kinematics of particle interactions*." https://web.physics.utah.edu/~jui/5110/hw/kin_rel.pdf, 2002.

[354] S.U. Chung, *SPIN FORMALISMS*, .

[355] P.A. Carruthers, *Spin and Isospin in Particle Physics*, Harwood Academic (Medical, Reference and Social Sc (1 Nov. 1971), Vermont (11, 1971).

[356] G. Wick, *Angular momentum states for three relativistic particles*, *Annals of Physics* **18** (1962) 65.

[357] E. Leader, *Spin in particle physics*, vol. 15 (2, 2011).

[358] H. Georgi, *Lie algebras in particle physics: From Isospin to Unified Theories*, CRC Press (1999), https://doi.org/10.1201/9780429499210.

[359] X.-D. Ma, *private communication*, 2022.

[360] A. Zee, *Group Theory in a Nutshell for Physicists*, Princeton University Press, USA (2016).

[361] J. Gasser and A. Rusetsky, *Solving integral equations in* $\eta \to 3\pi$, *Eur. Phys. J. C* **78** (2018) 906 [1809.06399].

[362] J. Plenter, *Decay of* η' *into four Pions and its Impact on the Doubly-virtual* η' *Transition Form Factor*, Master's thesis, Bonn U., HISKP, 2017.

[363] H. Kutt, *The numerical evaluation of principal value integrals by finite-part integration*, *Numerische Mathematik* **24** (1975) 205.

[364] N. Ioakimidis, *On the numerical evaluation of a class of finite-part integrals*, *ZAMM-Journal of Applied Mathematics and Mechanics/Zeitschrift für Angewandte Mathematik und Mechanik* **63** (1983) 572.

[365] G. Monegato, *Numerical evaluation of hypersingular integrals*, *Journal of Computational and Applied Mathematics* **50** (1994) 9.

[366] D. Stamen, T. Isken, B. Kubis, M. Mikhasenko and M. Niehus, *Analysis of rescattering effects in* 3π *final states*, *Eur. Phys. J. C* **83** (2023) 510 [2212.11767].

[367] T. Isken, *private communication*, 2020.

[368] R.H. Bartels, J.C. Beatty and B.A. Barsky, *An introduction to splines for use in computer graphics and geometric modeling*, Morgan Kaufmann (1995).

Acknowledgments

Physics is not a one-man show. In this sense, I would like to express my deepest gratitude to all the people without whom this thesis would not have been possible. As space on this page is limited, I apologize in advance to everyone I am not able to thank appropriately.
First and foremost, I am grateful for the outstanding support of my supervisor Bastian Kubis, who truly lives up to the term *Doktorvater*. Thank you for guiding me through the—metaphorically spoken—kindergarten of my bachelor's thesis, the high school of my master's thesis, and finally to scientific adulthood with the completion of this dissertation. Thank you for proposing this well-thought out topic for my thesis, for your patience in endless discussions, and for the heart-warming atmosphere you create in the research group. I am also grateful to you for helping me get several scholarships. At this point, I would also like to show my deepest thankfulness to you, Michael Döring, for your additional support to receive the scholarship of the Avicenna-Studienwerk e.V. that financed my doctoral studies and for your exceptional letter of recommendation, which I successfully used for my first job applications. I truly appreciate the time Andreas Wirzba—although (officially) already retired—has spent with me during countless discussions and our great collaboration. Without your outstanding support, our projects on ToPeχPT, as presented in this thesis, would not have been possible. I do not only thank you for all the effort you put in our projects but also for being the second referee of this thesis.
It was an honor to be part of the family-like AG Kubis. As such, I really enjoyed each minute I spent together with Dominik Stamen, Marvin Zanke, and Yannis Korte in the doubtlessly(!) best office the HISKP has ever seen; including the endless challenges and every redundant, but always amusing, dispute. I thank Simon Holz for the coffee breaks, which have continuously prevented us from working too much. My special thanks goes to Tobias Isken and Malwin Niehus. Thank you for your support with the implementation of the Khuri–Treiman formalism and teaching me how to code in C++. Additionally, I thank you, Tobi, for the great collaboration during our joined project on Dalitz-plot asymmetries in η decays and for all the explanations, tips, and tricks you have shown me since my bachelor's thesis. Furthermore, I thank Maxim Mai for teaching me how to bring my Mathematica skills to the next level and Daniel Severt, Jordy De Vries, and Peter Stoffer for encouraging discussions on the construction of new extensions of chiral perturbation theory. A very special *thanks* goes out to my study buddies Fabian Metzger, Jonas Rieder, Karl Flöthner, Lars Schall, Michael Kamenar, Pierre Seyb, and Tobias Kree. I am glad that I found friends like you. Especially, I would like to thank you, Karl and Lars, for all the fun and the great time we had since the very beginning of our studies. We rocked physics!
My siblings Melisa, Ali Can, and Tunahan always served as moral support. Thank you for being by my side. Lastly, and most importantly, I am deeply indebted to my parents, who have taught me so much more than could ever fit in this book. You never had the chance to go to university, but you did everything you could to give me that privilege. Therefore, this thesis is not just mine, it is ours.